Tethers in Space

A Propellantless Propulsion In-Orbit Demonstration

Kabels in de ruimte

Een demonstratie van stuwstofloze voortstuwing
in een baan om de aarde

PROEFSCHRIFT

ter verkrijging van de graad van doctor
aan de Technische Universiteit Delft
op gezag van de Rector Magnificus Prof. ir. K.Ch.A.M. Luyben;
voorzitter van het College voor Promoties
in het openbaar te verdedigen op maandag 30 mei 2011 om 10.00 uur
door

Michiel Kruijff
Ingenieur Lucht en Ruimtevaart
geboren te Den Helder.

Dit proefschrift is goedgekeurd door de promotoren:

Prof. dr. W.J. Ockels

Prof. dr. E.K.A. Gill

Samenstelling promotiecommissie:

Rector Magnificus	voorzitter
Prof. dr. W.J. Ockels	Technische Universiteit Delft, promotor
Prof. dr. E.K.A. Gill	Technische Universiteit Delft, promotor
Prof. dr. E. Lorenzini	Università di Padova
Prof. ir. B.A.C. Ambrosius	Technische Universiteit Delft
Prof. C. Nicollier	École Polytechnique Fédérale de Lausanne
Dr. P.A. Swan	Southwest Analytic Network
Dr. C. Menon	Simon Fraser University
Prof. dr. ir. J.A. Mulder	Technische Universiteit Delft, reservelid

Delta-Utec Space Research and Consultancy heeft in belangrijke mate financiëel bijgedragen aan de totstandkoming van dit proefschrift.

ISBN 978-90-8891-282-5

Cover:	By M. Kruijff & Proefschriftmaken.nl. The YES & YES2 space experiments and T-REX tether in orbit. YES image by M. Kruijff, YES2 image by ESA (S. Corvaja), T-REX image kindly provided by JAXA.
Printed by:	Proefschriftmaken.nl || Printyourthesis.com
Published by:	Uitgeverij BOXPress, Oisterwijk

Written in OpenOffice. Printed in The Netherlands.

For my father who only caught a glimpse and Maria who caught me

Contents

1 Introduction

Given ships or sails adapted to the breezes of heaven, there will be those who will not shrink from even that vast expanse.

— Johannes Kepler, letter to Galileo, 1610

Tether: a cord that secures something to something else

Tether propulsion systems: proposals to use long, very strong cables to change the orbits of spacecraft. Spaceflight using this form of spacecraft propulsion may be significantly less expensive than spaceflight using rocket engines.

— Definitions as found on Wikipedia, Jan. 2008

In this section the thesis objective is defined following a review that exposes the gap between potential tether applications, on one side, and the flight experience so far, on the other. A survey of the thesis structure is then provided.

1.1 Sustainability and the appeal of space tethers

Mankind's exploration of space has so far been severely limited by the difficulty to reach Earth orbit. Our way into space is much the same today as it was originally in 1957, when the first satellite Sputnik was carried into space by the R-7 rocket. The Soyuz rocket that delivers cosmonauts to the International Space Station today is a direct descendent of that original R-7 and still similar to a large degree. All rockets provide propulsion by expulsion of matter, and have proven so far to be a highly inefficient means of transport. Whereas a ship sailing an ocean is kept afloat by buoyancy alone, it requires a great deal of energy to get a rocket into orbit and balance the Earth's gravity during its ascent. Rocket science is to pre-pack all this energy into a drum and release it in a controlled manner. Whereas a sailing ship exploits the wind to propel itself, a rocket carries its energy along, plows through the atmosphere and hardly benefits from the opportunities that the environment provides. Worse, for this gargantuan and non-trivial task to succeed, a great deal of additional energy and effort is required to build up the infrastructure for design, production and transport of that rocket.

Once we are in space, for most purposes it becomes somewhat easier to travel around, and there are numerous concepts, proven or under development, to ride the 'breezes of heaven'. The same type of high-thrust (or 'impulsive') rocket engines could be employed once more. Alternatively, ion engines use the same principle of expulsion but they are characterized by continuous, low thrust levels. More literally, solar sails, or, indeed, space tethers can ride the breezes of heaven. Solar sails are propelled by the minute pressure exerted by the impact of

sunlight. They are especially promising for use in interplanetary space where, over time, low acceleration can accumulate to obtain significant changes in velocity. Space tethers are long thin cables, primal structures that, like solar sails, can be used for essentially propellantless propulsion, but also to build formations that would be very costly if created in another way. Space tethers provide a unique outlook for sustainable space transportation, because energy and momentum are not lost through exhaust gases. This may explain their perceived elegance and appeal.

Th resulting attractiveness has made tethers an academic favorite. As will be illustrated in the following sections, exciting concepts and the sometimes elusive tether dynamics have been closely studied for decades by a great many scientists. Yet despite all this effort, there is little flight experience and no tether application is in use today.

1.2 Examples of tether applications

The potential for space tethers to create a paradigm shift in the way we travel to and through space is probably best exemplified by the 'space elevator'. This still futuristic concept was created in 1960 by Yuri N. Artsutanov [Artsutanov 1960] when he proposed to physically connect Earth to space by tether. The idea was an improvement of the visionary orbital tower concept as conceptualized by Tsiolkovsky already in 1895 [Tsiolkovsky 1895]. A self-balancing connection would be necessary, i.e. a vertical tether in orbit around and co-rotating with Earth while just touching its surface. A large endmass on the “space” end of the tether, beyond geostationary orbit, could be used to achieve such a balance. Alternatively a tether of 144,000 km length and without endmass would fulfill these requirements [Pearson 1975].

In order to obtain access to space using the space elevator one would simply board a delivery vehicle on the Earth surface, exert some patience as the vehicle climbs the tether, then disembark at the altitude matching the desired orbit. The most popular orbits would likely be geostationary and interplanetary orbits, although elliptical ones approaching Earth in perigee would also be a possibility. The delivery vehicle would take on-board any returning cargo and descend back to the Earth surface to pick up the next passengers.

The space elevator should offer access to space at a cost orders of magnitude lower than possible today, changing the appearance and scope of space travel itself. The elevator has two major conceptual advantages over rockets that should lower operational cost. Firstly, the energy required to climb the tether does not have to be stored on-board of the delivery vehicle, but can be e.g. transmitted from the ground by laser or by electrical power through the cable. Secondly, the energy spent can be partially recovered as the delivery vehicle and its return cargo descends. As a result of the steep drop in cost, rapid developments could be expected, as have happened in recent years for personal computers and mobile communication. For large multi-stage rockets it would mean they would become all but obsolete. The use of satellites for any purpose would however become commonplace, and so would commercialization of space as well as human exploration of the solar system.

Many technical challenges are still to be dealt with before we can actually build the space elevator. Work is needed to cover dynamic issues, delivery vehicle concept, power supply and recovery, atmospheric interaction challenges, deployment and operational issues, and so on. Not the least of the developments required is that of high strength low-density tether materials such as carbon nanotubes [Edwards 2000, 2003].

Fortunately, tethers can also be used if they are much shorter and in orbit without a physical connection to Earth. A large number of applications for space tethers has in fact been proposed, ranging all the way from modest systems tailored for niche markets to grand enabling solutions [for an overview, see e.g. Cosmo 1997, Cartmell 2008, Pelt 2009]. Tether lengths range from hundreds of meters to hundreds of kilometers. These applications generally make use of the tether as long-distance mechanical connection, and they may exploit the ability of conductive tethers to interact with the Earth magnetic field.

One of the more futuristic of the proposed mechanical tether applications uses multiple rotating tether systems, or 'bolos', in orbit around Earth and the Moon or Mars to create an interplanetary transportation system. Permanent habitation of Mars or mining of the Moon for rare minerals and raw materials could then become a possibility. Each system would be a hundred kilometers or more in length and feature a tip velocity with respect to the system's center of mass of at least 1.0 km/s. The direction of tether rotation would be prograde, i.e. identical to that of the orbital direction. By careful timing a payload on a suborbital vehicle could be grabbed from the tip of a low orbiting tether as it approaches the Earth atmosphere and temporarily matches the suborbital vehicle's position and velocity. Half a turn of the tether system later the payload could be released and hurled into space. The system would provide the payload with an altitude increase of twice the distance between tip and system center of mass and with a velocity increase of twice the (relative) tip velocity. Next, a similar and synchronized system would capture the payload and hurl it onward. Eventually the payloads could be delivered all the way to the Moon or Mars. The same infrastructure would be used to return cargo from those remote celestial bodies to Earth. In this way, the energy balance would be largely maintained and a high degree of efficiency could be achieved, be it that significant initial investment would be required to develop the infrastructure [Hoyt 1999.I, Forward 1999].

Advanced mechanical tether concepts have also been recognized as some of the more feasible alternatives to “clean” the busy lower regions of space around Earth [Bade 1993, Bonnal 2005]. Hundreds of pieces of large debris, mostly spent stages, can be found in Low Earth Orbit (LEO). If not removed, such debris is likely to eventually break up in collision with a piece of the even more numerous smaller debris or, in some cases, with a functional satellite. Not only would a functional satellite be almost certainly destroyed by such an incident, the secondary debris generated in the collision would increase the incidence rate of further collisions. A traveling system with a swinging or rotating tether could move from debris to debris, capture each piece with the help of a suitable grapple system and deorbit it subsequently by momentum transfer.

The above concepts could be significantly enhanced by using also a conductive tether material. Within the Earth's magnetic field and plasmasphere it is possible to convert solar energy to orbital energy without the use of propellant. Using the electrical potential generated by e.g. solar panels a current can be driven through the tether: electrons can be collected from the Earth's plasma on one end and be expelled on the other end. In the magnetic field of the Earth a Lorentz thrust will result acting over the conducting part of the tether and creating an electrodynamic form of propulsion [Johnson 1998, Estes 2000.I]. The orbital lifetime of large rotating tethers in LEO could be increased by using this Lorentz thrust for atmospheric drag compensation. The MXER concept for example is an electrodynamically-enhanced bolo system [Sorensen 2001]. The above-mentioned debris-remover systems could be moved from one debris object without propellant by properly modulating the Lorentz thrust such that it would in a way sail the Earth's magnetic field [Pearson 2000].

Electrodynamic tether performance is dependent on the orbital, magnetic and plasma environment which provides a limitation but also creates opportunities. Around Jupiter or Saturn with their strong magnetic fields, high orbital energies and fast rotating, dense plasmas unique conditions exist in which a tether could effectively convert the planet's rotational energy into both orbital and electrical energy without the need for solar power [Gallagher 1998]. An electrodynamic tether could also be combined with an electric propulsion system, which would act as efficient provider of electrons, such that the dependency on the plasma density around the Earth would be reduced [Ockels 2004].

Such applications require significant investment in tether infrastructure. Furthermore, for most of them a reliable rendez-vous and docking system would have to be developed. The tether's orbit would have to be kept clear of debris and other satellites to avoid collisions. Although indeed carbon-nanotube materials could eventually offer extremely strong and lightweight tether solutions and reduce the mass overhead and thus the investment cost, the question remains whether emerging alternative technologies with equivalent capabilities will be developed first, at lower cost and risk. However, not all proposed tether applications are so remote.

For example, a rotating tether system with a baseline of about a kilometer is able to generate a comfortable level of artificial gravity through the (apparent) centrifugal force. Exposure to long periods of weightlessness has important reversible and irreversible effects on the human physique. Humans traveling to Mars for six months or more would benefit from an artificially generated gravity-like force to secure their physical fitness upon arrival. Little or no viable alternative exists to tethers for artificial gravity [Clark 1960, Stone 1973, Cramer 1985].

For orbital transfer less ambitious than the bolo systems one can avoid the requirement of spin-up that is inherent to a rotating tether system. A pendulum motion can be sufficient in some cases and it is readily achieved as a side-effect of deployment. A well-timed payload release from a swinging rather than rotating tether can be an effective way of changing orbit for both endmasses through the principle of momentum transfer. An example is the delivery

of samples from a Space Station back to Earth, or SpaceMail. Thin tethers of some kilometers to tens of kilometers could be used to frequently deorbit small capsules from a manned or unmanned station returning data, biological, medical or material samples for detailed investigation on the ground [Aerospatiale 1986, Ockels 1995, Heide 1996.I]. At the same time, the orbit of the Space Station would be raised and the amount of propellant required for its orbit maintenance would thus be reduced. A similar system could be used to efficiently remove waste from the International Space Station [Alenia Spazio 1995].

A vertically hanging tether without pendulum motion or momentum transfer could also be of use, e.g. to investigate the Earth's thermosphere in multiple, coordinated points, assisting scientists in advancing its three-dimensional understanding [Heelis 1998]. Such coordinated in-situ measurements for this altitude regime are very difficult or even impossible to obtain with conventional techniques such as (Earth Observation) satellites or balloons.

Electrodynamic tether applications also have been proposed for the short term. The Mir Electrodynamic Tether System (METS) has been designed to convert solar power into thrust and compensate for the Mir Station's atmospheric drag. It would have significantly reduced the station's orbit maintenance cost, and would have allowed Mir to orbit at lower altitude in a higher drag environment, reducing cost of access by conventional means [Levin 2007]. Although METS has reached an advanced state of development, it was never launched due to the decision to deorbit Mir in 2001. Nevertheless, the same system could be employed for future stations or other large objects in a high-atmospheric drag environment [Vas 2000, Blumer 2001].

An electrodynamic tether in LEO to which no electrical power is applied can still be equipped to conduct a current, fed by the Earth's plasma and driven by the electromotive force (emf), the latter induced by the orbital motion inside the Earth's magnetic field. This current would generate electrodynamic drag (and electrical power) rather than thrust. Such a simple "drag tail" or Terminator Tether could be used to deorbit a satellite after its nominal lifetime and help maintain the cleanliness of the orbital environment [Forward 1998, Hoyt 1999.II, Vannaroni 1999, Dobrowolny 2000].

What these various tether applications, mechanical or electrodynamic, distant or more short-term, have in common, is that with respect to conventional (rocket-based) solutions they would significantly reduce the need for propellant, as they tend to keep energy and momentum within the system of interest rather than lose those through expulsion of mass. In addition, for some cases tether technology may indeed be enabling, e.g. for artificial gravity, applications in high-drag environments, orbital debris removal or an operational interplanetary transport system. The physical principles these concepts are based on appear to be simple, whereas the cost of conventional alternatives has so far proven to be -and are likely to remain- prohibitive. The question naturally arises whether the real application of tether systems will be as elegant and technologically simple as their conceptual description appears to imply and therefore, whether the investments required to make them operational are indeed worth making.

1.3 Flight history of space tethers

Table 1 provides an overview of the major suborbital and orbital tether experiments that have been built and (in most cases) flown to date, as well as relevant references for each. For convenience the list includes the Young Engineers' Satellites, YES and YES2, which are subject of this work, as well as the recent T-REX experiment to which the author also participated.

The earliest experiments took place in the sixties. In two separate experiments in 1966, the Gemini 11 and 12 manned capsules were connected by a 36 m cable to their respective Agena upper stage. With considerable difficulty the astronauts manually controlled the tethered system they were a part of using cold gas thrusters, in order to bring the system first in a gravity gradient stabilized position and then in rotation. During the Gemini 11 mission about 1 mgee of artificial gravity was created by a 0.15 rpm rotation. The Gemini 12 crew succeeded to achieve a somewhat stabilized vertical orientation.

The complex dynamics encountered during these bold trials with short tethers may have been the reason it took 14 years before tethers were deployed in space again. Tether experimentation in the eighties and early nineties was dominated by modest short suborbital flights. Japanese, US and later also Canadian sounding rocket experiments used conducting tethers to investigate their interaction with the Earth ionosphere. The first Tethered Payload Experiments (TPE) suffered from deployment problems, but with assistance from cold gas thrusters the various CHARGE (Cooperative High Altitude Rocket Gun Experiment) and OEDIPUS (Observations of Electric-field Distribution in the Ionospheric Plasma – a Unique Strategy) missions were completed successfully, with tether lengths ranging from 400 m to 1174 m.

From these technically modest experiments it was a large step to the 19.6 km, 2 mm thick and layered electric cable that was deployed from the Space Shuttle in 1992 as part of the American-Italian Tethered Satellite System (TSS). Objective was to deploy the tether upward out of the Shuttle, collect electrons at the far end using a 1.6 m diameter endmass as anode and study the tether electrodynamics as a result of the current flowing through the tether. The complex, actively controlled reel system got stuck after 268 m of deployment, but the tethered satellite could be successfully retrieved and returned to Earth. In 1996, during the TSS-1R reflight of the same equipment 19.6 km of tether was deployed exposing the endmass to an emf of as much as 3500 V. A current of several Amperes caused significant dynamics in the tether, and a significant Lorentz drag force must have acted on the Space Shuttle. A clear skip-rope motion was observed in the tether. The experiment also provided a wealth of information concerning the electron collection behavior of large charged spheres in a plasma. Unfortunately, the tether was severed near the Shuttle end due to sparking after damage due to debris or meteroid impact [Chobotov 1999]. This cut provided the accidental opportunity to witness the dynamics of the free tether in space. It was seen to create its own, artificial, lower endmass due to tether recoil in the low-tension end. The

tether was tracked and re-entered within a few weeks, providing a first datapoint on tether orbital lifetime.

A less ambitious orbital electrodynamic tether experiment was performed in 1993, the Plasma Motor Generator (PMG), a 500 m tether attached to a Delta upper stage. PMG succeeded in demonstrating that the Lorentz drag force can be turned around into a thrust force, by actively sending electrons upward through the cable.

Highly successful mechanical tether experiments were NASA's Small Expendable Deployer System missions, SEDS-1 and SEDS-2. They each deployed downward 20 km of a 0.78 mm line braided from a special polyethylene fiber material, Spectra, again from a Delta upperstage. A small subsatellite as endmass transmitted dynamics data to the ground whereas the deployed length and tension were measured on the Delta side. SEDS-1 deployed the tether with an open-loop control and ended in a swing and subsequent release and re-entry of the tether and subsatellite. SEDS-2 took a step further with a closed-loop controlled deployment to a stable vertical position of the tether. Unexpectedly, the SEDS-2 tether was severed just 3.7 days after successful completion of the mission, most probably by a debris particle. Thanks to Spectra's high reflectivity, the SEDS-2 tether was observed from the ground with the bare eye [Carroll 1995.I], passing through the sky as a bright thin object with an angular dimension similar to that of the Moon.

The unexpected cut of the SEDS-2 tether increased concerns with regards to the limited in-orbit lifetime of tethers. Tethers Unlimited Inc. (TUI) provided a reaction with the concept of the Hoytether, a webbed tether believed to resist multiple impacts and securing very long lifetime in space [Forward 1995]. The last of the large US tether experiments flown so far, the ATeX (Advanced Tether eXperiment) by the National Reconaissance Office (NRO), intended to demonstrate a meteoroid-impact resistant tape-shaped tether. Unfortunately, the actively driven reel deployment of ATeX failed.

Recent data indicates however that the SEDS-2 cut must have been an anomaly. The Naval Research Lab's 4 km long, 2 mm thick tether of TiPS (Tether Physics and Survivability) was unwound in May 1996, using also SEDS deployer technology. It has been orbiting for over a decade in vertical orientation, with a slight oscillation, to be cut only in July 2006 [VSO 2010].

Nevertheless, especially the TSS-1R and SEDS-2 tether severings have resulted in the evidently false, but widely-held belief that tethers in space are severely prone to failure. Increasingly, the fear of accidentally severed tethers moving uncontrollably through space and colliding with other satellites or even the Space Station, lead to mission cancellations. In 1997, the Young Engineers' Satellite (YES) was launched, but the tether deployment was not initiated for fear of potential collision [Kruijff 1998]. The implementation of a tether as part of the Shuttle-based SEDSAT [Lorenzini 1995] was cancelled. The electrodynamic Propulsive SEDS experiment ProSEDS was built, but not launched [Vaughn 2004]. In their wake new tether proposals became less frequent and less ambitious. The work reported in this thesis was performed in this context.

Year	Experiment	Length [km]	Technology	Objective	Success	Remark	Ref.
1966	Gemini 11	0.036	Mechanical link between Gemini and	Artificial gravity	YES	Spin stable 0.15 rpm	NASA 1967
1966	Gemini 12	0.04	Athena upper stage	Gravity gradient stabilization	MOSTLY	Manned with manual control	
1980	TPE-1	0.04 of 0.4	Conductive	Plasma interaction	PARTLY	Suborbital	
1981	TPE-2	0.07 of 0.4		and VHF wave	PARTLY		Sasaki 1987
1983	Charge-1	0.418	Cold gas assisted	generation	MOSTLY		Sasaki 1994
1985	Charge-2	0.426			YES		
1992	Charge-2B	0.4			YES		
1989	Oedipus-A	0.959	Conductive	Ionospheric science	YES	Suborbital	Tyc 1995
1995	Oedipus-C	1.174	Cold gas assisted Passive reel		YES		Vigneron 1997
1992	TSS-1	0.268 of 19.6	Conductive, active reel deployment	Electrodynamic Power generation	NO	Shuttle missions. Tether jammed	Dobrowolny 1994
1996	TSS-1R	19.6			MOSTLY	Tether broke after science success	Gilchrist 1998
1993	PMG	0.5	Conductive insulated tether, passive spool	Power and thrust	YES	7 hrs experiment piggyback on Delta	McCoy 1995
1993	SEDS-1	20	Mechanical, brake + spool	Swing & cut	YES	SEDS-2 probably cut by debris after mission completion	Carroll 1993
1994	SEDS-2	19.7		Controlled deployment	YES		Carroll 1995.I
1996	TiPS	4	Mechanical, passive spool	Study survival and stability	YES	Cut after 1 decade in orbit	Barnds 1998
2005	ProSEDS	(13.1)	Bare conductive/ mechanical, brake + spool	Thrust	-	Cancelled for ISS safety	Johnson 2003
1997	YES	(35)	Mechanical, double-strand, brake + spool	Rotation, re-entry	-	GTO. Not deployed due to unsafe orbit	Kruijff 1999.II
2007	YES2	31.7	Mechanical, brake + spool	Accurate re-entry of a scientific capsule	MOSTLY	Full two-stage deployment. Overdeployed.	Kruijff 2009.I, II
1998	ATeX	0.02 of 6.2	Mechanical, tape, reel, active	Stability & control	NO	S/W stopped deployment	Zedd 1998
2000	METS	(5)	Bare conductive tape/mechanical, passive reel	Thrust (Mir station)	-	Cancelled as Mir was deorbited	Levin 2007
2007	MAST	0? of 1.0	Multistrand plus inspector crawler	Study tether survivability	NO	Minimal deployment	Hoyt 2003
2010	T-REX	0.3	Conductive bare tether tape, passive folded	Deployment and current collection demonstrator	MOSTLY	Suborbital Successfully deployed, video	Fujii 2009

Table 1. *Overview of major tether experiments to date, by chronology of experiment family. Experiments with length between brackets were not launched or deployment was not started.*

Only recently, nearly a decade after ATeX, new tether experiments have been launched, all developed in educational context, and with mixed results. The MAST university project (Multi-Application Survivable Tether) attempted in 2007 to deploy a tether between light-weight cubesats but apparently without success. In the same year, as reported in this thesis, the European Space Agency's 2nd Young Engineers' Satellite (YES2) deployed a 32 km tether in two stages as part of a SpaceMail demonstration. This success for mechanical tethers was complemented in 2010 as the Tethered Rocket Experiment (T-REX) of Tokyo Metropolitan University featured the first and so far only deployment of a bare electrodynamic tether. An innovative passive deployer system successfully unfolded a 300 m tape.

Of the 22 experiments listed in Table 1, 19 were in fact flown and a good majority, namely 14 of those, can be considered largely or fully successful. The flight experiments involved essentially four types of deployers: the active reel, the passive reel, the passive spool and the T-REX (passive) unfolding system. An active reel deployer unwinds the tether from a motorized drum, in a direction perpendicular to the drum shaft. This in contrast to the deployment from a passive spool, which is in axial direction over the head of the spool. The more complex experiments based on active reel deployers, TSS and ATeX, have encountered significant deployment problems. Virtually all the passive systems have lead to complete deployment so far, with a notably good track record for the company Tether Applications responsible for SEDS-1, SEDS-2, PMG and TiPS. The few spool failures (TPE and MAST) suffered from a shared problem, i.e. insufficient initial momentum in relation to the deployment friction. The importance of proper design choices is therefore apparent. Based on flight heritage there is a strong case to move forward with the more simple, passive deployment systems.

1.4 Objective of this thesis

Today, the concept of using tethers in space is still innovative but certainly not unexplored. True, considering the current state of tether materials and technologies, sustainable space transportation based on tether-assisted launch or bolo-based interplanetary infrastructures is certainly still remote. However, tethers have been studied for many years, fundamental principles have been demonstrated in orbit and several attractive applications have been identified for the short term. Small development steps along the lines of such applications could bring tether technology forward until a demand arises for more ambitious systems.

Nevertheless it has proven difficult to move beyond theory and concept demonstration towards a first true application. Partly this is because development and operational risks are generally judged to be high. There is a need to demonstrate that tether applications can be effective, affordable, predictable and safe. Due to the very nature of tethers their performance cannot be fully demonstrated in ground testing. Without a first in-orbit demonstration of an actual tether application it seems hard to make a convincing case.

Those perceived obstacles may be overcome through a systematic and targeted approach over the full width of the matter. This approach should include a suitable application selection, a solid mission analysis, a full system understanding and qualification, a thorough coverage of safety aspects and, enabled by the results, an affordable, application-oriented in-orbit demonstration. By going through this process, first a deeper insight is to be gained about the challenges currently faced by tether initiatives. That achieved insight should next allow to close the circle and shed light on the initial question regarding the effectiveness, affordability, predictability and safety of tether applications and lead to credible recommendations regarding near term tether initiatives on the road towards the first applications and, eventually, a sustainable space transportation.

The objective of this thesis is to achieve and exploit this insight accordingly. The approach can be thought to consist of three steps:

1. *definition* of the required tools and a suitable tether application for demonstration,
2. *development* of an adequate tether deployment system,
3. *evaluation* of its performance and extraction of lessons learned from the evaluation process and its results.

Following this logic, the remainder of this thesis is structured in three parts, one part for each of the above-mentioned steps.

1.5 Survey of this thesis

The three parts of this thesis consider respectively the definition, development and evaluation of a tether application.

Part I of this thesis, the definition, provides the physics background and an analysis of various concepts that could be candidate for a short term implementation. Chapter 2 first describes the principles of tethers in space, both mechanical and electrodynamic, providing insight into the physics behind their potential uses. In order to study potential applications more closely, an extensive tether mission simulator has been developed. Chapter 3 analyzes and discusses some of the candidate applications, their benefits and their limitations. Special attention is given to the seemingly ambiguous role that tethers may play both in creation and reduction of orbital debris. To take the step from concept to an application-oriented demonstration focus will be on technology that is both low-risk and low-cost, and for which significant heritage exists.

Part II, the development, therefore narrows down on the SpaceMail application. It focuses on the design, development and qualification of a tether system for a demonstration mission. Chapters 4 is concerned with the development and assessment of a suitable material and tether design. As tether-induced collision risk has been identified as a primary show stopper for past mission proposals, particular attention is paid to the design's implications for safety. Possibilities are explored to decrease risk both during and after

deployment, for example risk of entanglement with the deployment platform, and risk of collision with other satellites after tether release. With the tether design eventually consolidated, Chapter 5 continues by reporting on the development of the hardware and software required for controlled deployment of that tether. It includes the tether winding and unwinding facilities development, as well as SEDS-inspired designs for spool and brake. Furthermore the chapter describes the deployment control algorithms, simulations and ground-based deployment testing. Simulated performance versus actual deployment results are compared.

Part III, the evaluation, final part of this thesis, reports on the construction of two space tether experiments, the analysis of mission data and the extraction of lessons learned from the exercise of actual implementation and from the mission results. Chapters 6 and 7 describe respectively the process leading to the development of the Young Engineers' Satellite (YES) and the Second Young Engineers' Satellite (YES2). These space tether experiments demonstrate the feasibility of actually building, qualifying and, in case of YES2, operating the proposed system. Significant challenges had to be met, beyond the mere production of the tether and deployer, in order to bring the experiments into space, and to finally perform a tether deployment. An overview of the YES and YES2 systems and of the management processes followed provide insight into these challenges. The YES2 mission preparation, tether deployment results and problems encountered are analyzed and evaluated in Chapter 8. A comparison of the flight data is provided against simulation results, ground tests as well as the earlier SEDS missions. The suitability of the developed tether system for the SpaceMail application is analyzed. Finally, the work is placed in a broader context. In Chapter 9, conclusions are formulated and from the integrated findings, recommendations are derived for further development, as well as implications for tether applications in the near future that are to lead to a more sustainable transportation in space. The Epilogue touches upon the same items, but more from the author's personal perspective.

Following Chapter 9, a summary of the thesis is provided in both English and Dutch language.

Part I - *Tethers and their applications*

Ad astra per ligamentum.

— Robert Forward, science fiction author, engineer and tether advocate, at the bottom of his emails

Part I of this thesis provides a description of tether basics and a tether dynamics simulator that has been developed. Armed with these tools, a number of possible near-term tether applications is analyzed to finally make a statement on the safe niches that exist for tethers in space.

2 Tether Dynamics

bx + ay = ac

axx + byy = bcc

— Christiaan Huygens, on 29 October 1651, writes down what may be the first ever physics formulae, and will shortly after correctly define the conservation laws of momentum and energy in "De motu corporum ex percussione", 1652.

This chapter introduces the reader to the physical principles of tether dynamics in space. The fundamentals behind the applications of mechanical and electrodynamic tethers are worked out. A newly developed tool is finally described for simulation of detailed tether behavior and real-world aspects that are difficult to take into account in analytical models.

2.1 Deploying a tether in space

This section discusses basic models for the dynamics of a hypothetical tether that is massless, straight and non-conducting.

2.1.1 Gravity gradient tension for a hanging tether in circular orbit

The orbital period of an object orbiting a massive body depends on the orbit's semi-major axis a. A larger semi-major axis means a larger orbital period, as is e.g. obvious from the Moon's orbit around the Earth in about 28 days ($a \approx 384400$ km) as compared to that of the Space Shuttle, in approximately 90 minutes ($a \approx 6700$ km).

In the simple example of a circular orbit this can be easily understood. The motion of an object in an orbit with constant radius $r = a$, around a homogeneous spherical body with gravitational constant μ - if viewed in a co-rotating frame - can be thought to be subjected to a balance between a gravitational force $\mathbf{F}_g$ and a centrifugal force $\mathbf{F}_c$, which is apparent in that frame. Whereas the force of gravity decreases quadratically with increasing r, the centrifugal force is proportional with the product of r and the square of the angular velocity ω around the central body. In order to obtain said balance for an orbit with a larger radius, the angular velocity must therefore be decreased, see Eqs. (2.1) and (2.2).

$$\left|\mathbf{F}_g\right| = m\frac{\mu}{r^2} = \left|\mathbf{F}_c\right| = mr\omega^2 \tag{2.1}$$

$$\omega = \sqrt{\frac{\mu}{r^3}} \tag{2.2}$$

The implication is that if two objects are connected by a radially oriented tether, these so-called "endmasses" are each forced to orbit with an angular rate different from that belonging to the local circular orbit according to Eq. 2.2. Gravity force and centrifugal force

on the endmasses can thus not be in balance. Suppose two endmasses m_1 and m_2 in circular orbit at respective radii r_1 and r_2, with $r_2 > r_1$ as depicted in Figure 1. Endmass m_2 will orbit the Earth faster than its non-tethered companions at the same radius r_2, whereas similarly the lower mass m_1 will be moving slower at r_1 than its non-tethered companions there. Both endmasses will share the same angular rate Ω matching that of a circular orbit at a point between the masses, the center of orbit r_{CO},

$$r_{CO}^{\ 3} = \frac{\mu}{\Omega^2}, \tag{2.3}$$

where the term μ/Ω^2 can be derived from the balance between gravity force and centrifugal force for the system as a whole,

$$\mu \int_{r_1}^{r_2} \frac{\mathrm{d}m}{r^2} = \Omega^2 \int_{r_1}^{r_2} r \cdot \mathrm{d}m, \tag{2.4}$$

such that for a massless tether

$$r_{CO}^{\ 3} = \frac{m_1 r_1 + m_2 r_2}{m_1 / r_1^{\ 2} + m_2 / r_2^{\ 2}}. \tag{2.5}$$

For comparison, the radius of the center of mass r_{CM} is

$$r_{CM} = \frac{m_1 r_1 + m_2 r_2}{m_1 + m_2}. \tag{2.6}$$

For a vertical tether with length L, $r_1 = r_2 - L$, it follows that $r_{CO}^3 / r_{CM}^3 = 1 + O(L/r_2)^2$. Center of mass and center of orbit can therefore be assumed to coincide for a vertical tether, if the tether length is a mere fraction of the radius, $L \ll r_2$. This assumption remains true for a non-zero tether mass [Newlands 1994].

The force required to have the endmasses orbit at the angular rate of the center of orbit is the tether tension T. It can be expressed in terms of distance l from m_1 to that center of orbit, $l = r_{co} - r_1$ (see Figure 1). By substituting this definition of l and Eq. 2.3 into the force balance on the mass m one obtains for the tension in the tether an expression for T,

$$T = \left|\mathbf{F}_\mathbf{g} - \mathbf{F}_\mathbf{c}\right| = \frac{\mu m_1}{(r_{CO} - l)^2} - m_1 \Omega^2 (r_{CO} - l) = m_1 \Omega^2 \left(\frac{r_{CO}}{(1 - \frac{l}{r_{CO}})^2} - r_{CO}(1 - \frac{l}{r_{CO}}) \right) \tag{2.7}$$

$$= 3 m_1 l \Omega^2 + \mathrm{O}(\frac{l}{r_{CO}})^2 \Rightarrow T \approx 3 m_1 l \Omega^2$$

A similar result can be obtained for the tension on mass m_2. As a typical example, a 10 kg mass suspended from a massive platform ($m_2 \gg m_1$) orbiting at 400 km by a massless 10 km tether would generate a tension of 0.38 N. This tension is commonly but not fully descriptively known as the gravity gradient tension. In fact it results from the stability condition for a system for which with increasing radius not only the gravity force decreases, but also the centrifugal force *in*creases. In magnitude, the gravity gradient tension is

approximately equal to three times that part of the centrifugal force that results from the separation between endmass and center of orbit, under the orbital angular motion. The equivalent "gravity gradient" is responsible for the tendency for a tether in orbit to assume a vertical orientation and can help to drive a tether deployment, once an initial vertical separation between endmasses has been achieved.

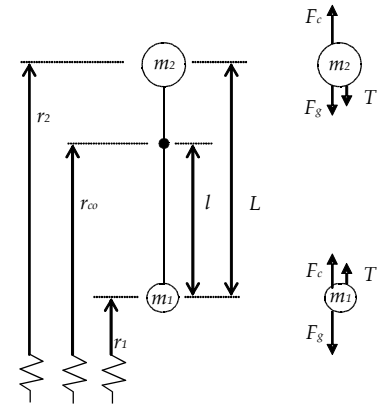

Figure 1. *Force balance in a vertical tether.*

2.1.2 Equations of motion

In order to obtain a first insight into mechanical tether dynamics and tether deployment, a set of simple equations suffices. For this purpose it is assumed here that m_2 is a massive platform M from which a much lighter endmass m is deployed in downward direction, or $m_2 = M \gg m_1 = m$. The orbit of M is not affected by the deployment. Such a platform coincides with the center of orbit, with constant radius $r_2 = r_{CO} = R$ and angular rate Ω. Furthermore, it is assumed the tether is a straight line without flexibility, and its mass can be ignored with respect to the endmass m. Finally it is assumed that the tether dynamics take place inside the orbital plane only. The dynamics of the system are thus defined by the endmass m, the tether length $L = l$ and its angle to the local nadir θ, as measured from M and depicted in Figure 2. The generalized force on this system in θ-direction is zero (no perpendicular forces are exerted by the tether), in l-direction it is the tension T.

Ignoring higher order terms, the following equations can be derived, for exampling using the Lagrangian $\mathscr{L}$ [e.g. Crellin 1994, Heide 1996.I]:

$$\ddot{\theta} + 2\frac{\dot{l}}{l}(\dot{\theta} - \Omega) + \frac{3}{2}\Omega^2 \sin 2\theta = 0 \tag{2.8}$$

$$\frac{T}{m} = -\ddot{l} + l\left((\dot{\theta} - \Omega)^2 - \Omega^2(1 - 3\cos^2\theta)\right) \tag{2.9}$$

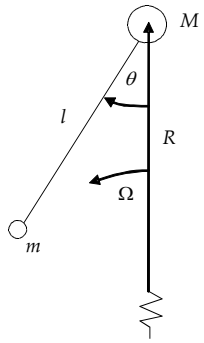

Figure 2. *Simple model for tether dynamics.*

These equations describe the relative motion of objects in orbit close together, expressed in polar coordinates, in the familiar form of the so-called rendez-vous equations [e.g. Lorenzini 1996] however with the only force of influence being the tension between the masses. In Eq. 2.8 a Coriolis term and a component of the gravity gradient perpendicular to the tether can be discerned. Note that from Eq. 2.9, for a non-deploying vertical tether $(\dot{l}=0,\ddot{l}=0,\dot{\theta}=0,\ddot{\theta}=0)$ Eq. 2.7 follows once more. The effect of rotation or swing on the tension in a non-deploying tether can be recognized in a term of Eq. 2.9 relating to the centrifugal force on the endmass. The gravity gradient contribution on tension can be seen to decrease with increasing θ due to the decreasing difference in radius between *m* and *M* and the reducing component of the gravity gradient force along the tether direction.

2.1.3 Pendulum motion of a swinging non-deploying tether

Eq. 2.8 describes the in-plane angular motion of the tether. The hanging tether of Section 2.1.1 is a special case, whereas, in absence of deployment, an oscillation around the local vertical represents a more general situation, be it intentionally or accidentally achieved. Such oscillation is driven by the gravity gradient force that acts to accelerate the tether towards a radial orientation.

For small angular deviations θ between tether and the local nadir direction, this oscillation follows closely a pendulum motion. If $\dot{l}=0,\ddot{l}=0,\theta<<1$, Eq. 2.8 becomes an expression for a harmonic oscillation, from which the tether's in-plane natural (radian) frequency ω_{IP} can be derived,

$$\ddot{\theta}+3\Omega^2\theta=0 \;\Rightarrow\; \omega_{IP}=\sqrt{3}\Omega\,. \tag{2.10}$$

In LEO, at an altitude of 400 km, $\Omega \approx 0.00113$ rad/s, and it takes about 800 s for a tether to swing from maximum (small) amplitude to the vertical. For larger angles, the difference in radius between endmasses decreases significantly, and so too the gravity gradient. Therefore the period of oscillation increases.

The swing amplitude θ_0 and the maximum angular rate $\dot{\theta}_{\max}$ at $\theta = 0$ are useful parameters that can be easily derived from any arbitrary state in the swing by integration of Eq. 2.8, taking the shape of an expression for conservation of energy:

$$\dot{\theta}^2 + 3\Omega^2 \sin^2\theta = const = \dot{\theta}_{\max}{}^2 = 3\Omega^2 \sin^2\theta_0 \,. \tag{2.11}$$

By integration of $\dot{\theta}$ in this expression the time t_{swing} to swing from an arbitrary maximum angle θ_0 to the vertical can be determined. The following approximation can be used to solve for the resulting integral [Heide 1996.I]:

$$t_{swing} = \frac{\pi}{2\sqrt{3}\Omega}\left(1 + \frac{\kappa^2}{4} + \frac{9}{64}\kappa^4 + \frac{225}{2304}\kappa^6 + \frac{(1\cdot 3\cdot 5\cdot 7)^2}{(2\cdot 4\cdot 6\cdot 8)^2}\kappa^8 + \ldots\right), \tag{2.12}$$
$$\kappa = \sin\theta_0$$

or $t_{swing} \approx 1200$ s for $\theta_0 = 60°$ in LEO. This result exceeds by 50% the earlier result for the duration of a swing from a small initial amplitude.

2.1.4 Tether deployment

The trajectory of a deploying tether can be controlled in either of two ways, depending on tether and deployer design:

1. by imposing a length profile *l(t),* or
2. by imposing a tension profile *T(t)* or torque

When designing a deployment trajectory, certain limitations are to be taken into account. At any point in time, the potential for deployment acceleration is restricted by the level of gravity gradient, whereas the in-plane angle development at a given tether length follows from the deployment velocity profile and can therefore not be arbitrarily shaped.

For a deployment controlled by length, the deployment trajectory is described by Eq. 2.8 alone and the resulting tension follows from Eq. 2.9. A risk is that too high deployment accelerations can lead to tether slackness ($T = 0$). As tension cannot be negative, a free orbital motion will follow. Above equations can still be used with the understanding that l now describes the distance between the masses, not the tether length. Control is only regained when the distance between platform M and endmass m increases enough to reach the deployed length, and tension will assume non-zero values again.

When controlling the deployment with tension, the length profile follows from Eq. 2.9. Next the in-plane angle can be determined from Eq. 2.8. Such a deployment control is less prone to slackness. However, if the tension is imposed through friction, there will generally be a minimal friction level inherent to the deployment system that, if not properly planned, can cause an early deployment stop. The tether then enters a pendulum motion. Tension is no longer imposed by the deployer but follows Eq. 2.9. Unless the deployer friction is reduced below the pendulum tension, deployment will not continue.

With regards to influencing the tether motion in θ-direction, a careful selection must be made of the initial conditions and of the applied deployment velocity profile, no matter the

selected means of deployment control. As shown in Eq. 2.8, for a given length and in-plane angle, it is the deployment velocity that determines whether the in-plane angle will increase or decrease, through the Coriolis-term. By controlling deployment velocity, the in-plane angle can be affected. In return, the in-plane angle influences how the deployment velocity develops, through Eq. 2.9. A particularly low tension will lead to an initially fast deployment, such that the Coriolis force pushes the endmass to a high angle from the vertical, where the gravity gradient is smaller and deployment will slow down. For a downward deploying endmass this angle will be in forward direction, as depicted in Figure 2. A tension maintained close to the gravity gradient force level would also lead to a slow deployment, this time along the local vertical. The maximum deployment velocity can be obtained at intermediate tension levels and angles. If a constant deployment angle is somehow maintained ($\dot{\theta} = 0, \ddot{\theta} = 0$ in Eq. 2.8), the gravity gradient force will increase with length and so will therefore the acceleration, resulting in an exponential deployment:

$$\frac{\dot{l}}{l} = \frac{3}{4}\Omega \sin 2\theta \,. \tag{2.13}$$

In this case the increase in gravity gradient force balances that of the Coriolis force. Minimum deployment time is obtained at an angle of 45°.

2.1.5 Impact of tether properties

Tether mass and flexibility have an impact on the tether dynamics described so far.

Real tethers have a finite mass m_t that may be significant compared to the endmasses. Tether mass density will lead to a variation of tension over the tether. Reconsider the case of Figure 1. If the tether has a finite and constant linear mass density ρ [kg/m] then according to d$m = \rho \cdot$ ds tension can be integrated along the tether to yield a quadratic dependency:

$$T = m_1\left(\frac{\mu}{r_1^{\,2}}\Omega^2 - \Omega^2 r_1\right) + \rho \cdot s\left(\frac{\mu}{r_1^{\,2}} \cdot \frac{r_1}{r_1 + s} - \Omega^2 r_1 \cdot \left(1 + \frac{1}{2}\frac{s}{r_1}\right)\right) \approx 3\left(m_1 + \rho s(1 - \frac{1}{2}\frac{s}{l})\right) \cdot l\Omega^2 \tag{2.14}$$

with s ranging from 0 to L. The maximum tension $T = 3(m_1 + \frac{1}{2}m_t)l\Omega^2$ occurs in the center of orbit where $s = l$. The center of orbit and Ω are determined according to Eq. 2.3 and Eq.2.4. Because the tether mass will shift the center of orbit in the direction of the halfway point on the tether, a finite tether density can have a negative impact on e.g. momentum transfer (Section 2.2.1).

Another relevant effect of tether mass density impacts deployment tension and thus deployment dynamics. Suppose a tether being pulled from a resting, untensioned pile (or coil or spool) a tension will be introduced in the moving part of the tether, which is called the *rocket term*. The discontinuity that a tether experiences when making the transition from being at rest on a spool to sudden deployment velocity causes a shock tension, equal to rate of change in momentum of the moving section with mass ρl and velocity dl/dt. If that velocity is constant the rocket term equals

$$T = \frac{\mathrm{d}}{\mathrm{d}t}(\rho l \cdot \dot{l}) = \rho \dot{l}^2 \,. \tag{2.15}$$

The tether will be tensioned even in absence of any gravity or deployer friction. This term will influence deployment dynamics especially if control friction F_{brake} exercised by the deployer is low. A tether of 0.001 kg/m deploying at 10 m/s from a spool without any friction will as a result still have a tension of 0.1 N.

For the simple case of Figure 2, i.e. a small endmass and light rigid tether being deployed from a large platform, the effect of the tether mass on the endmass dynamics can be taken into account in a simplified way, Eqs. 2.8 and 2.9 then become [Heide 1996.I],

$$\begin{aligned} &(m + \frac{1}{3}\rho l)\cdot\left(\ddot{\theta} + \frac{3}{2}\Omega^2 \sin 2\theta\right) + (m + \frac{1}{2}\rho l)\cdot 2\frac{\dot{l}}{l}\left(\dot{\theta} - \Omega\right) = 0 \\ &-\left(m + \rho l\right)\cdot\ddot{l} + \left(m + \frac{1}{2}\rho l\right)\cdot l \cdot \left[\left(\dot{\theta} - \Omega\right)^2 - \Omega^2\left(1 - 3\cos^2\theta\right)\right] = T = F_{brake} + \rho \dot{l}^2 \end{aligned} \tag{2.16}$$

This equation shows how the instantaneous tether mass $m_t = \rho l$ participates in different fractions to the various terms of the equation: linear and angular acceleration, Coriolis term, centrifugal term, gravity gradient and rocket term.

Another complication with impact is that tethers, even under tension, do not behave like rigid bars. Oscillations are relevant for tethers in space and they may have to be prevented or dampened. Three major oscillations are distinguished: spring-mass, longitudinal and transverse.

Sudden braking of the deploying tether may induce a longitudinal spring-mass oscillation, which is typically quite slow (tens of seconds) and can stretch the tether for a few percent of its length. The resulting oscillation in tension can influence deployment and cause slackness. The period depends on length, endmass and stiffness (product of elasticity modulus E and cross-sectional area A). By smooth braking, such oscillations can be avoided [Kruijff 1996]. For braided tethers, the stiffness should be taken for the braid rather than for the fiber (Section 4.1). Especially if loaded at low fractions of tensile strength, a tether's braid stiffness can be orders of magnitude lower than the fiber stiffness.

The longitudinal wave (or sound wave) is generally the fastest disturbance. It transports tension disturbances. The wave velocity depends on stiffness and tether density - not on tension itself. For a tether braided from uninterrupted fibers, these properties should be taken for the fibers within the braid.

Transverse wave modes are lateral disturbances traveling along the tether, e.g. after a period of slackness or bending when tether tension is regained. The period is determined by tension and tether density. Initial lateral disturbances can be created during deployment. Like the endmasses themselves, each segment of a deploying massive tether is susceptible to an apparent Coriolis force $\rho \cdot \mathrm{d}l \cdot 2\dot{l}\left(\dot{\theta} - \Omega\right)$, acting perpendicular to its motion. The distribution of this force over the length of the tether will lead to a concave bending in case of downward deployment from a platform. Upon subsequent deceleration of a bent tether transverse

oscillations are created. Transverse waves can therefore be avoided by maintaining sufficient tension in the tether, especially at high deployment velocities.

The first resonant mode periods for these three oscillations closely resemble those of the typical string and suspended mass [Yost 2002, Misra 1986]:

$$P_m = 2\pi\sqrt{\frac{L(m+0.34m_t)}{EA}}\,, \tag{2.17}$$

$$P_L = 2\sqrt{\frac{\rho L^2}{EA}}\,, \tag{2.18}$$

$$P_T = \frac{2\pi}{\sqrt{\pi^2(1+\frac{m_t}{3m})-\frac{m_t}{4m}}}\sqrt{\frac{\rho L^2}{T}}\,. \tag{2.19}$$

For a 10 km long tether of 0.1 kg/km under 1 N of tension, with an EA of 10000 N and a 10 kg endmass, the spring-mass period P_m is about 20 s, the longitudinal period P_L is 6 s (so it takes only 3 s for a tension disturbance to travel along the tether), the transverse period P_T is much slower (622 s). This range of two orders of magnitude for the various fundamental frequencies makes for a highly stiff system.

2.2 How the tether becomes useful

With the tether deployed and its dynamics under control, there is the opportunity to apply the newly obtained system properties such as length and tension to the benefit of the user. Two major applications are momentum transfer and electrodynamic thrust generation.

2.2.1 Momentum transfer

The tether tension is an internal force, so it does not affect the system's total momentum. As the tether tension acts on the system endmasses during deployment and angular motion, it however does affect the individual endmass motion and in this manner is able to redistribute, or transfer, the momentum from one endmass to the other. By the simple act of releasing the tether (or part of the endmass) this transfer is completed, and, if proper timed, the release can lead to a beneficial orbital change for the objects on both ends of the tether.

Consider, for example, a capsule that is to return to Earth from a heavy platform in circular orbit at 400 km altitude. It requires an impulsive deceleration by about 117 m/s in order to reduce its perigee altitude to zero. A tether can provide this change in perigee altitude through a combination of two mechanisms: the gravity gradient effect and the swing of the tether.

The gravity gradient effect is explained in Section 2.1.1. During tether deployment, the endmasses, platform and capsule, are forced by their mechanical connection to orbit the Earth with the same angular rate. While connected to the tether, the capsule - being the endmass with smaller radius - is kept artificially below the local circular velocity. If the

tether is cut it is no longer forced to remain in a circular orbit and the capsule's motion will assume an elliptical trajectory matching its momentary radius and velocity. In other words, its perigee will be reduced and the capsule will start to drop down. The upper endmass's apogee for the same reasons will be raised.

As explained in Section 2.1.4 the tether can be deployed at low tension to a forward angle with respect to the local vertical direction and orbital motion. By next increasing the tension, the tether and lower endmass can be brought into a swing back towards that vertical. Once deployment has stopped, swing velocity increases according to Eq. 2.20, reaching a maximum at the platform's local vertical. If the tether is cut near that vertical, the backward swing contributes significantly to the deceleration of the lower endmass (i.e. the capsule).

The beneficial effect of a momentum transfer in circular orbit is described by the difference between the initial circular orbit radius r_{CO}, i.e. the radius of the center of orbit, and, for the lower endmass, the perigee radius $r_{1,p}$ that results from the momentum transfer. This difference can be expressed in terms of the length l, referring to the distance between the center of orbit of the tethered system and that of the released object. It can be derived by substituting the expression for velocity $v_{1,a}$ of the lower endmass at tether release,

$$v_{1,a} = \Omega \cdot \mathrm{r}_{1,\mathrm{a}} - \dot{\theta}_{\max} l \,, \tag{2.21}$$

with $\dot{\theta}_{\max}$ from Eq. 2.11, Ω from Eq. 2.3 and $r_{1,a} = r_{CO} - l$, the apogee radius of the newly obtained orbit, into the equation for conservation of orbital energy,

$$-\frac{\mu}{2a} = \frac{v^2}{2r} - \frac{\mu}{r} \,, \tag{2.22}$$

in which a denotes the semi-major axis, here $a = (r_{1,a} + r_{1,p})/2$. Rewriting yields the desired result:

$$r_{1,p} = r_{CO} - (7 + 4\sqrt{3}\sin\theta_0 + O(\frac{l}{r_{CO}})) \cdot l \approx r_{CO} - (7 + 4\sqrt{3}\sin\theta_0) \cdot l \,. \tag{2.23}$$

The release of the lower endmass from a hanging tether impacts its perigee radius by seven times the (effective) tether length l. The impact of a release from a swinging tether passing through the local vertical depends on the initial swing angle θ_0. The maximal impact is achieved by a swing from 90°, equaling about 14 l. However, due to the impact of deployment friction on deployment dynamics (Section 2.1.4), a swing angle of about 60 degrees turns out to be more realistic, which would yield an effect of about 13 l [Heide 1996.I]. These results are sometimes referred to as the "*7l*-rule" for hanging tethers, and the "*13l*-rule" for swinging tethers.

Larger effectiveness can be obtained in eccentric orbits. Crellin has shown that in orbits with eccentricity exceeding 0.44, such as GTO, the gravity gradient and angular rate vary so much over one orbit that a tether is dynamically unstable and will start to rotate [Crellin 1996]. This feature can be exploited by a synchronized pumping strategy such that as much as 40l change in perigee or apogee radius can be achieved [Ockels 1996].

If required, the exchange of momentum can be boosted further by other means of increasing the tether's angular rate, such as by thrusters or tether retrieval [Lansdorp 2003.II] or by making use of a planetary magnetic field [Dijk 2003.I]. Eventually an untapered tether will break under its own weight at a limit given by the tether material properties. Suppose the simple case of a tether without any endmass, under centrifugal load only, with constant cross-sectional area A_t, tensile strength σ_b and volumetric density ρ_V. Its maximum allowable tip velocity $v_{tip,\max}$ can be expressed in terms of the "characteristic velocity" $v_{ch} = \sqrt{\frac{\sigma_b}{\rho_V}}$:

$$T_{\max} = \sigma_b A_t = \frac{v_{tip,\max}^2}{2} \rho_V A_t \Rightarrow v_{tip,\max} = \sqrt{\frac{2\sigma_b}{\rho_V}} = \sqrt{2} \cdot v_{ch} . \tag{2.24}$$

For modern materials, based purely on theoretical fiber strength, v_{ch} is in the order of 1 - 2 km/s (Table 18). If an endmass m is included, balancing centrifugal force and tether tension yields

$$v_{tip,\max} = \frac{v_{ch}}{\sqrt{\frac{m}{m_t} + \frac{1}{2}}} , \tag{2.25}$$

with m_t the tether mass from center of mass to tip.

A tether operating at the limit of its performance can launch only payloads that are relatively small with respect to its own mass, and therefore need to be used a large number of times to become beneficial from a launch cost point of view. An untapered spinning tether can be used for tip velocities up to $\sqrt{2}\, v_{ch}$, in which case the allowable endmass, and thus payload, has reduced to zero. By tether tapering the range can be extended, to obtain a tip velocity of 2 v_{ch}, the tether needs to outweigh the endmass by 18 times [Cosmo 1997].

For single-use applications, tethered momentum transfer can be more directly compared to conventional, rocket-based, propulsion. The required tether mass per unit of endmass m_t/m can be taken from Eq. 2.25 and compared to the equivalent ratio of propellant over payload mass m_p/m, based on the rocket equation,

$$\frac{m_p}{m} = e^{\frac{\Delta v}{w}} - 1 , \tag{2.26}$$

with w the rocket propellant exhaust velocity, and the velocity increment Δv equal to $v_{tip,\max}$. Figure 3 plots such a comparison for a Dyneema® tether. One of the Dyneema® curves is based on a theoretical v_{ch} = 1800 m/s, the other includes a safety factor on tensile strength F_S = 4 or, alternatively, v_{ch} = 900 m/s. Two curves representing rocket performance have been added, with typical values of specific impulse I_{sp} depending on the exhaust velocity according to I_{sp} = 9.81 w. Ignoring differences in system complexity and overhead, single-use momentum transfer tethers compare favorably against rocket propulsion for velocity increments below 200 - 400 m/s. If a tether is used for a velocity increment of 1000 m/s, mass benefits are obtained after about ten uses. The mass ratio curves as presented in Figure 3 are independent of endmass and do not take into account environmental factors. The

abundance of micrometeoroids in space however precludes the use of very thin tethers (typically below 0.3 mm) that would otherwise be attractive for very light endmasses (see Section 4.3.1). Still, in conclusion, disposable tether systems for single-use momentum transfer do have an application niche. They are currently mostly suitable for low Δv applications, such as orbit maintenance, circularization and re-entry, and with payloads heavy enough such that the tether is to be dimensioned primarily for strength.

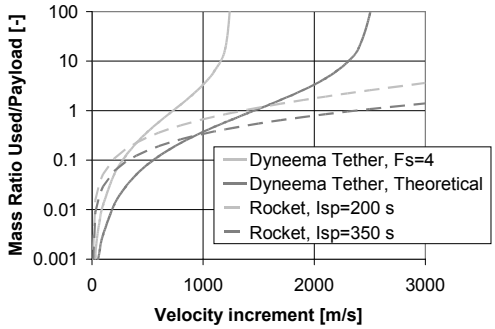

Figure 3. *Comparison between single-use tether mass and rocket propellant*

2.2.2 Electrodynamic tether principles

Another feature of long structures in space is exploited by conductive tethers for electrodynamic (ED) applications. An orbiting conductive tether crossing the Earth's magnetic field **B** with relative velocity **v** will be subjected to an induced potential or electromotive force (emf) V_{emf} varying over the tether length,

$$V_{emf} = \int (\mathbf{v} \times \mathbf{B}) \cdot \mathrm{d}\mathbf{l} \tag{2.27}$$

In low equatorial orbit the emf per unit length equals about 200 V/km, increasing in radial direction. The emf can therefore reach a kilovolt or more over a tether longer than 5 km. This emf can drive an interaction between the conductor and the Earth's plasma and enable an electrical current to flow through the tether. The presence of this current in the Earth magnetic field gives rise to an electrodynamic effect that can be put to use, i.e. the Lorentz force.

Electrons can be collected from the plasma by an anode at the end of the conductive tether that is positively charged by the emf. A large conductive body (e.g. an inflatable conductive balloon) can for example be used as collector [Dobrowolny 1994, Dobrowolny 2000]. Also a dedicated system like an ion-engine can generate electrons and thus has the benefit of being independent of ionospheric (plasma) electron density [Nicolini 2003]. If left uninsulated (or "bare") the conductive tether itself can function as anode to collect electrons from the plasma [Dobrowolny 1976].

At the cathodic end, electrons can be emitted back into the plasma. A special plasma contactor device can be used here that provides effective emission at low cathodic

potentials, typically below 100 V. Examples of plasma contactors are the Hollow Cathode (HC) and the Field Emitter Array Cathode (FEAC). For Hollow Cathodes the required potential is lower than for FEACs, but a small continuous flow of ionized gas is required. FEACs require no consumables, but the hardware is delicate and suffers from erosion [Williams 1992, Morris 2000]. Such a plasma contactor at the cathodic end essentially shorts one end of the tether to the plasma such that most of the V_{emf} can be utilized at the opposite end as anodic potential for electron collection. The emitted electrons follow the Earth's magnetic field lines to be eventually absorbed by the Earth's plasma reservoir.

The Lorentz-force $\mathbf{F}_L$ will result from integration along coordinate s over the tether according to Eq. 2.28. This force is transferred by tether tension to the endmasses and can be used as a propellantless form of thrust.

$$\mathbf{F}_L = \int_0^l I(s) \cdot (\mathrm{d}\mathbf{l}(s) \times \mathbf{B}) \tag{2.28}$$

For a passive conductive tether in Earth orbit, the emf-generated current and Lorentz force act to deorbit the tether and its endmasses. The induced current can be used as an electrical power source but at the expense of orbital energy and only as long as the tethered spacecraft remains in orbit. Alternatively, if a large enough voltage is actively applied over the tether, e.g. using solar cells, it is possible to drive the electrons in opposite direction, such that a propulsive thrust is produced that raises the satellite's orbit. In this way, solar energy can be converted into orbital energy. This is a powerful and promising application of tethers in low Earth orbit. For this case, the emf acts to reduce the system performance and must be overcome by the added power supply.

Bare tether performance model

The bare tether anode has a number of notable advantages over the mentioned alternatives. It allows for a system design without complex endmass and a more effective collection mechanism [Dobrowolny 1976, Sanmartin 1993]. Simply put, through its potential a thin tether exerts electrical influence within a cylindrical volume around the tether that is large compared to the tether's own dimensions. The charged bare tether can attract and collect much more electrons from the plasma than just those that happen to be in the path of the tether itself. A highly simplified performance model can be derived, from which some numbers on bare tether current collection and Lorentz force generation can be obtained and typical tether shapes (cylinder and tape) can be compared.

Suppose a cylindrical tether, biased positively with respect to the surrounding plasma and attracting electrons by a cylindrical force field. If the tether radius is smaller than a certain quality of the plasma called its *sheath thickness*, the electron flow from the plasma into the conductor can be expressed as a function of the conductor's bias through the so-called Orbital Motion Limited model (OML) [Schott 1968]. The OML is based on the conservation of energy and angular momentum of the attracted electrons, as they orbit magnetic field lines. According to the OML, the current increment $\mathrm{d}I_{OML}$ collected by a piece of tether at a constant bias reads:

$$\mathrm{d}I_{OML} = \mathrm{d}I_{th}\left(\frac{4}{\pi}\right)^{1/2}\left(1+\frac{e(V_t - V_{pl})}{kT_e}\right)^{1/2} \tag{2.29}$$

where $V_t - V_{pl}$ is the potential bias of the tether with respect to the plasma, $k = 1.3807 \cdot 10^{-23}\,m^2kgs^{-2}K^{-1}$ the Boltzmann constant, T_e the electron temperature (a typical value in LEO being $T_e = 2000$ K) and I_{th} is the random thermal current, according to

$$\mathrm{d}I_{th} = \frac{1}{4}\, e\, n_{pl}\left(\frac{8kT_e}{\pi m_e}\right)^{1/2} \pi d_{eff} \cdot \mathrm{d}l \tag{2.30}$$

with n_{pl} the plasma's electron density, $e = 1.6022 \cdot 10^{-19}\,C$ the elementary charge and $m_e = 9.1094 \cdot 10^{-31}$ kg the electron mass. Within the OML regime, for long tethers with concave cross-sections (i.e. without indentations), the collection of electrons is proportional to the exterior surface of the tether, which can be represented by the product of cross-sectional perimeter p and length increment dl [Sanmartin 1999]. Analogous to the diameter of a cylinder we can define for an arbitrary concave cross-section shape an "effective diameter" $d_{efff} = p/\pi$, such that the exterior surface is described in Eq. 2.30 as πd_{eff} dl.

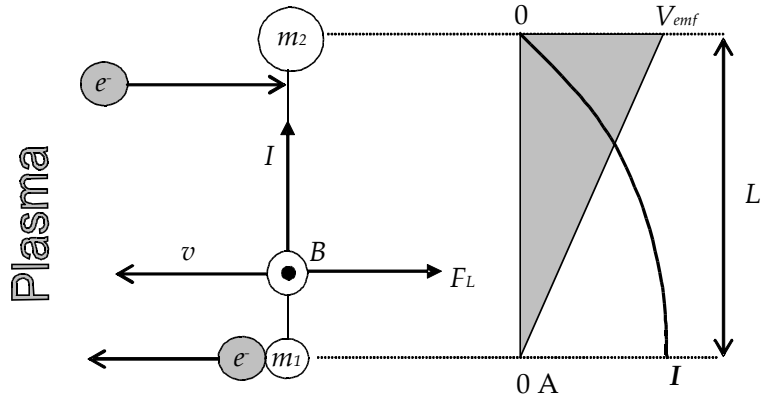

Figure 4. *Principle of bare conductive tether in orbit, plasma contactor in* m_1

Consider a vertically oriented bare tether around Earth, configured for deorbit. It is performing passively apart from a cathodic plasma contactor operating at plasma potential placed at the bottom of the tether, Figure 4. For simplicity, magnetic field and velocity are assumed horizontal, perpendicular and constant over the length of the tether. Also the plasma density n_{pl} is assumed constant. The tether itself is assumed straight and with negligible electrical resistance, such that the potential of the tether is constant. In this case, $V_t - V_{pl} = V_{emf}$. Finally the potential is assumed highly suprathermal ($V_{emf} \gg kT_e/e$), which will typically be true if the tether is much longer than 1 m, such that the unity in Eq. 2.29 can be ignored. In Figure 4, to the right of the system schematic, the development of plasma potential and current are plotted against the tether length. The positive potential of plasma with respect to the tether is shaded. The shaded area highlights the potential to be used in Eq. 2.29 to compute current collection. Integrating Eq. 2.29 over l we find for the maximum current:

$$I_{\max} = en_{pl}d_{eff}\sqrt{\frac{8evB}{9m_e}}L^{\frac{3}{2}}, \tag{2.31}$$

with B the amplitude of the magnetic field vector **B.** Similarly we can integrate for the Lorentz force and obtain an expression for its amplitude F_L,

$$F_L = \frac{3}{5}B^{\frac{3}{2}}en_{pl}d_{eff}\sqrt{\frac{8ev}{9m_e}}L^{\frac{5}{2}}. \tag{2.32}$$

It can be seen that both the current and thrust force are strongly dependent on the length of the tether. A typical system at $n_{pl} = 10^{11}$ m^{-3}, B = 26 μT, L = 10 km, d = 1 mm (cylindrical), at 400 km altitude results in an emf per unit length of 186 V/km, a current I = 2.7 A and a force F_L = 0.42 N acting against the orbital velocity vector. If the tether is made of aluminium, its mass is 21 kg. Magnetic field amplitude B decreases rapidly with radius. Apart from rather strong dependencies on solar cycle and diurnal variations, the plasma's electron density n_{pl} peaks around 300-400 km altitude at a level in the order of 10^{12} m^{-3} and decreases rapidly at higher altitudes to level off to around 10^{10} - 10^{11} m^{-3} (Figure 5). At altitudes higher than some 2000 km applications and designs for systems relying on these parameters are therefore much more restricted.

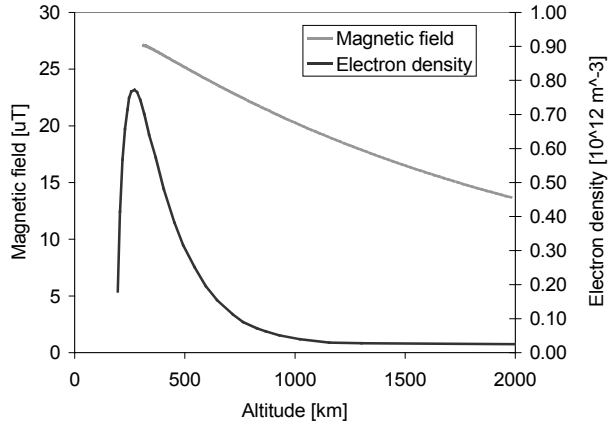

Figure 5. *Magnetic field and an occurrence of electron density in LEO (equatorial plane, IGRF and IRI95 models)*

Now suppose a plasma contactor is placed at the top of the tether and a relative potential $V_t - V_{plasma} = V_s$ is applied there, as shown in Figure 7. If the supply voltage is smaller than the total emf over the tether length L (or $V_s \leq V_{emf,L} = vBL$), only a fraction $V_s/V_{emf,L}$ will be at positive potential with respect to the plasma and collect electrons. Then similarly, the following equivalent relationships can be derived,

$$I_{\max} = en_{pl}d_{eff}\sqrt{\frac{8evB}{9m_e}}\left(\frac{V_s}{V_{emf,L}}\right)^{\frac{3}{2}}L^{\frac{3}{2}}, \tag{2.33}$$

$$F_L = \frac{2}{5} B^{\frac{3}{2}} e n_{pl} d_{eff} \sqrt{\frac{8ev}{9m_e}} \left(\frac{V_s}{V_{emf,L}} \right)^{\frac{5}{2}} L^{\frac{5}{2}} . \tag{2.34}$$

Such a tether configuration can make for a highly capable propulsion system. Suppose the supply is selected such that $V_s = V_{emf,L}$, then the same system as described above would yield a continuous thrust of $F_L = 0.28$ N along the orbital velocity vector tether. This thrust can be used to counteract atmospheric drag or to raise orbital altitude. The impact of continuous thrust on the orbit semi-major axis a of the total system with mass M_{total} can be quantified from the increase in orbital energy (Eq. 2.22) as a result of the power input $F_L \cdot v$ (ignoring the influence of atmospheric drag),

$$\frac{\mathrm{d}a}{\mathrm{d}t} = \frac{2a^2 F_L v}{M_{total} \mu} , \tag{2.35}$$

The above-mentioned tether would raise a system with $M_{total} = 10000$ kg by 4.3 km/day. At the expense of 5 kW electrical power consumption, this performance is comparable to that of contemporary ion engines [Saccoccia 2000]. Apart from some gas released for cathodic plasma contactor performance, the tether system requires no consumables. Furthermore, the system in this example can still be significantly enhanced by proper tether design.

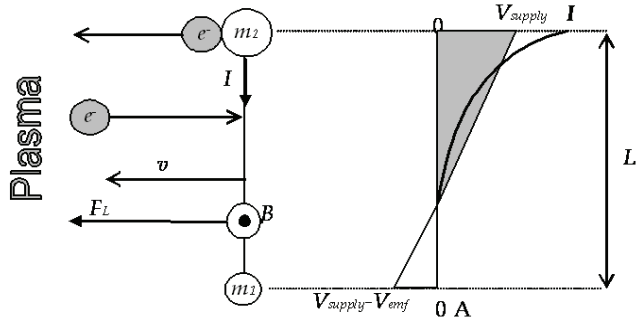

Figure 7. *Principle of bare conductive tether in orbit under supply voltage and plasma contactor at* m_2

Tape tethers

A tape tether offers a higher effective diameter than a cylindrical tether and thus higher collection surface per unit of mass. A tape can thus be an attractive design option. For a tape of dimensions $a \times b$, the effective diameter equals

$$d_{eff,tape} = \frac{2}{\pi}(a+b) . \tag{2.36}$$

The design limit for a tape is primarily the tape tickness b. Compared to an equal-mass cylindrical tether with diameter d, if $b \ll d$, a relative increase in effective diameter follows according to Eq. 2.37. Equivalently this ratio can be read to express a thin tape's reduction of tether mass for the same effective diameter.

$$\left(\frac{d_{eff,tape}}{d}\right)_{m_{tape}=m_{cylinder}} = \left(\frac{m_{cylinder}}{m_{tape}}\right)_{d_{eff,tape}=d} = \frac{d}{2b} \tag{2.37}$$

A 10 μm thick non-resistive conductive tether tape (about the thickness of aluminium kitchen foil) would ideally achieve the same thrust of 0.42 N from above example at only 2% of the cylindrical tether mass, representing a 50-fold efficiency increase (in terms of thrust per kilogram of tether).

In practise however, at high current density levels, so especially for a thin tape tether, Eqs. 2.32 and 2.34 turns out to be oversimplifications. Ohmic losses due or potential drop V_R due to the tether impedance must be taken into account. Dissipative tether heating further increases the tether's electrical resistance. The tether potential can no longer be assumed to remain constant. The resulting reduction in bias voltage of the tether with respect to the plasma can reduce the extent of the tape advantage significantly [Lorenzini 1999]. Furthermore, for tape widths outside the OML regime (typically much wider than a few centimeters), electron collection will become less effective than the OML model of Eq. 2.30 [Estes 2000.II].

Although these considerations may drive optimal tether tape design towards less extreme cross-sectional dimensions, a tape design does provide a mass-effective solution with significantly increased thrust levels as compared to a cylindrical tether. The ohmic losses are taken into account by the advanced simulator ETBSim described in the next section. For the deorbit configuration example described above, with a tape of 4 cm $\times$ 10 μm rather than the 1 mm diameter cylindrical tether, a thrust force of 2.0 N is obtained, compared to the 0.42 N for the cylindrical case. Furthermore, the tape tether has a mass of 11 kg versus the 21 kg of the cylindrical tether. All things considered therefore, the thin-tape design does not quite provide the 50-fold increase of efficiency over a cylindrical tether as predicted by Eq. 2.37, but still a respectable 9-fold improvement.

For the propulsive case of Figure 7, it is noted that the current level rises steeply near the cathodic end of the tether. Ohmic losses will therefore be concentrated here, and in a very thin tape only a small fraction of the tether, close to the cathode, will be charged positively with respect to the plasma and conduct current. Although this current will be very large, as the Lorentz force is generated only over that section of the tether that actually conducts a current, the ohmic losses will have a significant and negative impact on the generated Lorentz force. It is therefore suggested to limit the current but increase the length over which it flows and over which the Lorentz force is generated. This is achieved by inclusion of a large section of insulated, but highly conductive, tether between cathode and the exposed (bare) tether tape. The electron collection at the tape will then be reduced, but it will take place at much increased distance from the cathode. The full collected current will now flow through all of the insulated tether section and the Lorentz force will be generated over its full length (Figure 8). This design does not only improve tether efficiency for the propulsive case, but also is found to reduce the dependency of thrust level on plasma density [Johnson 1998, Lorenzini 1999.I, Estes 2000.III].

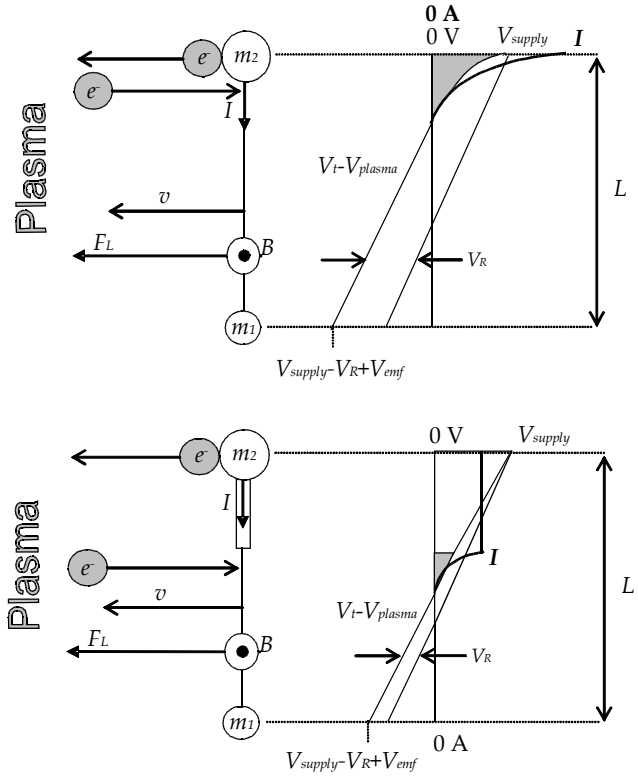

Figure 8. *Current collection for resistive tether, with and without insulated section*

2.3 Tether mission simulation

This section summarizes the rationale and features behind the development of a BeadSim tether mission simulator family (referred to in the following as MTBSim/ETBSim), Figure 9: Mechanical Tether Bead Simulator (MTBSim), the Real-time Tether Bead Simulator (RTBSim), the Young Engineers' Satellite mission Simulator (YESSim) and the Electrical Tether Bead Simulator (ETBSim). MTBSim has been developed to simulate mechanical tether deployment realistically but fast (i.e. computing hours of simulated time within minutes). From this starting point, the development is split into two directions. YESSim includes functions for momentum transfer, re-entry capsule dynamics, mission planning and post-flight data analysis. ETBSim also builds on MTBSim but focuses on electrodynamic performance and stability of already deployed electrodynamic tethers. The executable and source of these simulator tools is available for research purposes on request.

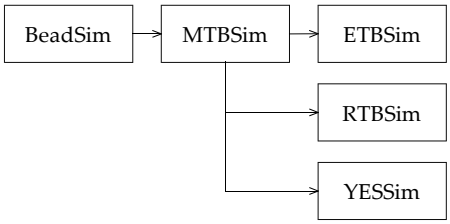

Figure 9. *Tether simulator evolution*

2.3.1 Advanced tether models

Without the simplifying assumptions and when taking into account real-tether properties such as finite stiffness, tether mass, tether bending, tether dynamics become naturally more complex than e.g. those described by Eqs. 2.8 and 2.9. For realistic simulation, particularly when designing an actual mission, non-circular orbits around the non-spherical Earth with proper environmental models are to be taken into account. As far as electrodynamic tether applications are concerned it was already mentioned that ohmic effects on the tether potential and dissipative heating of the tether have a significant impact on tether performance. The distributed forces on the tether will cause it to deform and remain neither vertical nor straight. In an inclined orbit, the magnetic field is no longer perpendicular to velocity, causing out-of-plane dynamics. The current collection and Lorentz force distribution depend on many parameters that in reality vary over a satellite's orbit and over the length of the tether in a non-trivial manner. These effects combined make real-life tether electrodynamics significantly more complex than described so far.

A multitude of tether dynamics models, each with its own strengths and limitations is available in literature [Misra 1986, Tyc 2001, Cartmell 2008]. Simulators are typically built on numeric integration of a discretization of the model, be it of the physical continuum of the tether (finite elements or lumped mass) or of the nonlinear partial diffential equations that jointly describe the various modes of the tether motion (e.g. by finite difference methods). Problems to be overcome by simulators are the non-linearity for large amplitudes and the large stiffness of the system (Section 2.1.5) [Schagerl 1998]. Some of the models and simulators that have been encountered and/or compared during the development of MTBSim/ETBsim are listed in Table 2.

Most of the encountered simulators that take into account complex environmental influences are based on lumped mass (or "bead") models that represent the tether as a chain of beads or pointmasses connected by massless springs or spring-damper elements. The validity of bead models has been demonstrated e.g. by Biesbroek and Crellin [Biesbroek 1999].

Simulation performance comparisons between various models are provided by Van der Heide & Kruijff [Heide 1996.I, Heide 1996.II]. These comparisons show that straight and inextensible tether models (e.g. Eqs. 2.8 and 2.9) can well represent deployment at medium tension levels, but in the cases of low tension deployment and heavy deceleration tether

flexibility can no longer be ignored. The various lumped mass models give comparable results although at significantly different computational times, (at the time) ranging from minutes to hours for a full deployment. BeadSim was found to be the fastest simulator, with no appreciable difference in predicted dynamics compared to the alternatives [Heide 1996.II]. No publicly available simulator was identified that handles bare electrodynamic (or hybrid) tethers.

Simulator	Model	Features and Assumptions	Reference
BeadSim	Lumped mass	Newtonian force and acceleration model, trapezoidal integrator with bead redistribution for larger stepsize, extensible massive tether, 2D, SEDS deployer friction, US standard 1976 atmosphere	Carroll 1993
Tether Simple Simulation	Endmass dynamics	Inextensible massive tether, free moving endmasses, 3D, differential equations derived from Lagrangian in matrix form	Crellin 1994
StarTrack matlab	Endmass dynamics	Inextensible massive tether, free moving endmasses, 2D, differential equations derived from Lagrangian in matrix form, Runge-Kutta integrator	Heide 1996
ACM/LRTeth	Lumped mass	Circular orbits, 3D, various environmental models, re-entry, finite differences discretization, various integrators	Sabath 1996
Matlab Blanksby	Lumped mass	Finite element discretization based on Kane's equations. 3D, various elasticity and environmental models, insulated electrodynamic tether	Blanksby 2000
Matlab Williams	Lumped mass	Based on Kane's equations. 3D, basic elasticity and environmental models	Williams 2009
Smirnov	Continuous	2D circular orbit, heavy platform, open loop tension control only, no environmental models, longitudinal wave propagation	Smirnov 2010

Table 2. *Some tether deployment models and simulators*

2.3.2 Simulator Overview

BeadSim

BeadSim, one of the simulators evaluated, has then been selected as the starting point for the MTBSim/ETBSim development. BeadSim is a basic tether simulator written in Turbo Pascal and developed and successfully used for SEDS-1 and SEDS-2 in the early 1990s by the San Diego company Tether Applications [Carroll 1993]. The model is limited to tether dynamics within the orbital plane (here referred to as "2D"), which has been shown to be a reasonable assumption for mechanical tethers [Crellin 1994]. The endmasses are regarded as pointmasses. The tether is approximated by the lumped mass model, with fixed-mass beads connected by massless springs. Damping between the beads is only taken into account when the tether is not deploying. Initial conditions are freely and conveniently definable in the local horizontal, local vertical frame. During deployment, additional beads are inserted at deployment velocity on the deployer side. For every bead inserted, deployer endmass is reduced. The deployment can be controlled in open loop by introducing a profile of

deployer friction (or more specifically, SEDS brake settings) versus deployment time or tether length. For each timestep, individual bead accelerations are derived directly from Newton's force balance in an inertial Cartesian frame. The ordinary differential equations are solved numerically using Heun's method. The timestep is automatically adapted based on a user-defined stability criterion. In this way it is straightforward to extend the model and add environmental forces and complex, nonlinear mechanical properties. For these reasons BeadSim is rather suitable to assess quickly various mission concepts and tether behavior.

A key feature of BeadSim as compared to other lumped-mass tether simulators is its approach to deal with the system's stiffness and enable large timesteps and fast integration. Conventional simulations of flexible structures like membranes or tethers using lumped mass models are computationally intensive. They require a large number of elements to realistically represent tension changes that move through the continuous flexible structure at very high speeds of potentially kilometers per second. For convergence of the solution very small timesteps are required, multiple orders of magnitude below the time it takes for such a tension change to traverse the distance between two mass elements (see also Eq. 2.18). BeadSim prevents unrealistic discontinuities also for large timesteps. Following each integration step, a redistribution of beads is applied, under the artificial assumption of a continuous tension distribution within the tether, taking into account the gravity gradient, much as it appears in Eq. 2.14. This approach essentially removes the fastest oscillation - the longitudinal or sound wave - from the tether behavior. Typical deployment dynamics and associated spring-mass, swing and transverse modes are hardly affected as they are much slower and are simulated in accordance with non-simplified models [Heide 1996.I].

MTBSim

In a first extension step, BeadSim has been developed into MTBSim, to perform end-to-end mechanical tether mission analysis, i.e. to study and design deployment and control of flexible tethers and understand the behavior of endmasses before and after release. The tool has been moved to the fully graphical environment of Borland Delphi Pascal, to allow better real-time visual evaluation of tether and orbital dynamics aspects. Features, inputs and outputs of MTBSim (combined with those of ETBSim) are presented in Figure 10, Table 3 and Table 4.

The two-dimensional (planar) BeadSim algorithms have been extended to three dimensions. In addition to the Cartesian inertial and Local Horizontal Local Vertical (LVLH) coordinates, the classical six orbital elements can now be used to describe the initial conditions and output states over a rotating Earth. This 3D approach is also a necessary step to include realistically out-of-plane dynamics and environmental influences. The Earth oblateness for example impacts inclined orbits through its J2 effect on gravity and through fluctuations in atmospheric drag – as around an oblate body orbital altitude varies even for circular orbits. Relative positions of the Sun and Moon are also calculated such that gravity effects, thermal heat input, lighting conditions and solar pressure forces can be taken into

account. For the study of deployment control and robustness, the tether deployer hardware has been modeled, including uncertainties and performance limitations.

A development environment is provided for design and evaluation of tether deployment. Like BeadSim, MTBSim includes a model of the SEDS-type static spool deployer and friction brake (see Sections 1.3,5.1.1). With this simple system deployment is passive, by inertia and gravity gradient, controlled by an adjustable friction (translating into tether tension following Eq. 2.16). Unwinding length or rate cannot be controlled directly (such as with a motorized reel) and retrieval is not possible. Tables specifying the nominal (target) tension or friction brake settings as a function of length or time can be used as input for the simulated control, as well as reference profiles for deployment length and velocity against deployment time. As in BeadSim, deployment to other angles can be developed manually with some level of intuition, by adjusting the spool and brake hardware parameters and the brake reference profile. One common need for trajectory optimizaton is provided by MTBSim, namely to obtain a robust deployment to a stable vertical state, based on a control algorithm method devised by Beletski & Levin [Beletski 1993]. Due to the large number of variables and effects to be taken into account, the parameter optimizer is based on genetic algorithms [Biesbroek 1996]. In order to develop other (optimal) reference profiles, off-line Matlab tools are available [Williams 2009]. Trajectories resulting from such optimization tools typically are verified in MTBSim in order to evaluate flexible tether behavior, impact of environmental effects and control hardware performance. Any of a variety of feedback control algorithms with variable or constant parameters can be selected. The impact of the numerous parameters mentioned above and robustness against environmental and hardware parameter unknowns and disturbances can be investigated stochastically using the Monte Carlo feature. This feature allows a large number of simulations to be performed autonomously with the required parameters disturbed in each simulation according to a user-defined probability distribution. In Section 5.5 a detailed description is provided of the described control and analysis features.

RTBSim

A real-time version of MTBSim, dubbed RTBSim, has been created to be used in a hardware-in-the-loop set-up. RTBSim takes actual measured deployer friction measurements as input, rather than using a simulated deployer performance. The resulting deployment can be studied, and the simulated velocity can be communicated to the deployment test facility such that closed-loop deployment control can be tested realistically on the ground (Section 5.2.2).

YESSim

In addition, MTBSim has been further extended to YESSim in the context of the Second Young Engineers' Satellite project [Kruijff 2003.I, Kruijff 2007], particularly with regards to endmass attitude dynamics, integrated re-entry simulation and extended environmental models. Apart from dynamics simulation, a number of mission support features have been added to YESSim, such as ground track and ground station contacts and tether visibility opportunities from the ground [Stelzer 2006].

The YESSim Deimos module [Stelzer 2006] propagates the attitude for the tethered endmasses based on pre-ejection initial conditions, ejection system induced pitch-off rates and tether torques after ejection. Euler angles with respect to an inertial frame are computed, as well as relative angles of the endmass with respect to the attached tether. Through the arm from tether attachment point to endmass center of mass, the tether tension applies a torque and thus affects the endmass dynamics. Knowledge of the attitude of the deployer with respect to the tether improves tether tension estimates: a different bending of the tether around the deployer exit will cause a different level of deployment friction (Section 5.4.1). Attitude simulation of the second, suspended endmass during deployment is also relevant, namely to identify the conditions at which the endmass will start to rotate and potentially wrap itself into the tether. MTBSim does not yet take into account the inverse influence of how dynamics of the suspended endmass may affect the tether tension. Fast endmass oscillations may introduce tension fluctuations propagating through the tether, just as it does in a rope on Earth from which a dangling stick is suspended. Due to the low stiffness of long tethers, this effect is relevant only when the tether is short compared to the torque's arm (Eq. 2.17). Nevertheless, based on an observed discrepancy between YES2 mission results and simulation (Section 8.3) this interaction may have significant impact on early deployment .

YESSim can be used to simulate SpaceMail-type capsule re-entry by endmass release from a tether. YESSim's integrated Re-Entry Simulator Tool (or REST) is an extensive re-entry module that tracks the endmass trajectory as it enters the atmosphere, as well as attitude, external and internal temperature. Apart from the already present US 1976 atmospheric model [U.S. 1976], sophisticated atmospheric models were included through dynamic link libraries (*dll* files) to study seasonal and diurnal effects on the re-entry capsule landing area: MSISE-00 for density [Picone 2002], the horizontal wind model HWM93 for average winds [Hedin 1996] and the Naval Research Laboratory's Ground to Space model G2S [Drob 2007], the latter for the inclusion of meteorological predictions at a resolution of 60 km, kindly made available by NRL. For the purpose of validation against other tools, the (Russian) standard atmospheric density model GOST [Cefola 2004] has been added to the already present NASA standard. REST includes a Monte Carlo mode to calculate the landing area. Detailed investigations using these models are reported by Calzada [Calzada 2004]. Furthermore REST takes as input a 2D or 3D (panel) model of the re-entry capsule, and computes (hypersonic) drag and lift coefficients and the impact on trajectory, as well as aerodynamic torques using the modified Newton approach [Calzada 2004, Lyaskin 2004]. REST attitude propagation can be used e.g. to determine at which altitude in the atmosphere a re-entering endmass (or capsule) will stop rotating and what will be the amplitude of its oscillation around the velocity vector during peak heating. To this purpose REST includes shockwave and heatflux models valid in the stagnation point, and heat transport computation inside a 2D capsule (panel model, integrated) and a 3D capsule model (finite elements model, off-line) based on the heatshield design and materials' properties [Lyaskin 2004, De Pascale 2006, De Pascale 2008, Asma 2008]. REST thus supports heatshield and capsule design in addition to landing area determination.

ETBSim

A development from MTBSim parallel to that of YESSim is ETBSim. This tool aims to study performance and dynamics of complex, user-defined designs of electrodynamic tethers [Kruijff 2001.I, Dijk 2003.I]. This tool extension is as yet limited to non-deploying electrodynamic tethers.

The user can combine three different types of tether segments: insulated, bare and mechanical. The insulated part serves to conduct a constant current, and obtain a significant Lorentz force acting over a large distance (Figure 8). The bare part acts as a collector surface for electrons and/or ions. The mechanical part can be added to ease initial deployment and to increase the distance between the endmasses and thus improve gravity gradient stabilization of the tether as it is subjected to the lateral and distributed Lorentz force. Each segment has its own dimensions, electrical properties such as ohmic resistance and thermal dependancy of the ohmic resistance, as well as mechanical properties such as stiffness and mass density. The cross-sectional shape of these segments can be chosen to be either round or flat (tape-shaped). Cross-section shape impacts not only collection of charged particles, but also atmospheric drag and reflection of sunlight.

In addition to the cylindrical or tape-shaped bare tether elements that act as anodic electron collectors, a spherical anode can be inserted into the tether system design, similar for example to the TSS-1R satellite [Dobrowolny 1994, Vannaroni 1998]. Spherical anode electron collection is modeled according to [Dobrowolny 2000].

At the cathodic end of the tether a Hollow Cathode or FEAC plasma contactor can be added to emit electrons back into the plasma (Section 2.2.2). Such devices have a certain current-voltage characteristic to accelerate the electrons away from the tether. For hollow cathodes the required voltage is low and little dependent on current. It is modeled in ETBSim with a fixed voltage drop relative to the plasma. FEACs are more complex and have a strong dependency of ejected current on voltage. It is modeled using a typical exponential dependency [Dobrowolny 2000].

Additional environmental models included into ETBSim are the International Reference Ionosphere 1995 [Bilitza 1997], the International Geomagnetic Reference Field (IGRF) and the T96 External Magnetic Field model [Tsyganenko 1995].

The computation of current and Lorentz force in ETBSim follows the approach suggested by Dobrowolny & Vannaroni [Dobrowolny 2000]. An estimate of the current in a bare tether with ohmic resistance can be obtained iteratively through a discrete tether model with a high number of individually straight elements. Each element is biased with respect to the plasma by the combination of local emf, ohmic losses and, if applicable, the applied voltage, as sketched for example in Figure 8.

The initial current profile estimate for a bare tether is produced by the assumption of a non-resistive, straight tether. If an active cathodic device is present, the dominating contributor to the current will be electron collection. Each positively charged segment of bare wire supplies to the tether an increment in current that is computed by Eq. 2.29. A simple

representation as in Figure 4 or Figure 6 can be used to derive the initial estimate of the current profile through the tether. The bias estimate can then be improved. In the following iterative steps, the ohmic losses are more and more refined until convergence is achieved.

For a floating bare tether without active cathodic device, ion collection on the cathodic side of the tether cannot be ignored. Current in the tether then results from the balance between ion and electron collection. Because ions are much heavier and more difficult to divert from their paths towards the tether, they are much less efficiently collected. The current will be rather limited and ohmic losses can typically be neglected. Ions are collected over a much larger part of the length than electrons [Estes 2000.III].

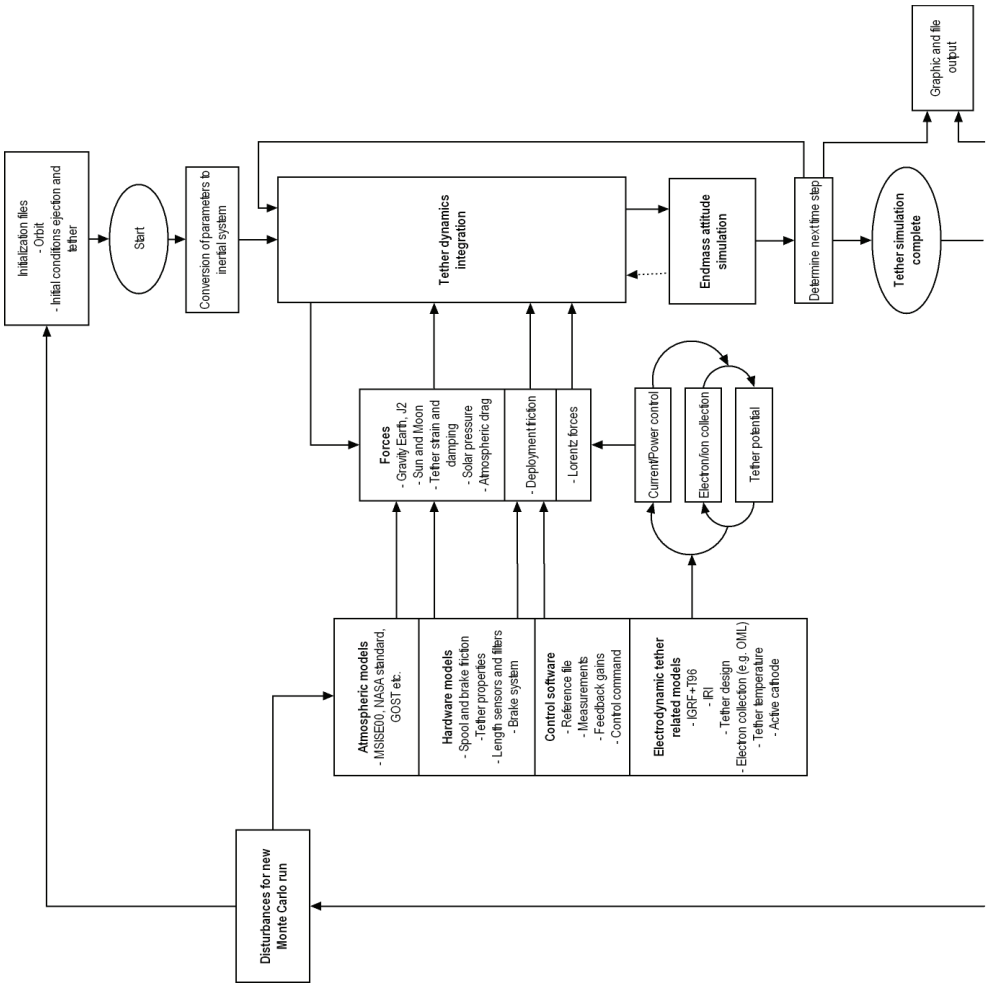

Figure 10. *MTBSim/ETBSim flow diagram (combined for simplicity)*

Effective yield can differ by a few percent from that predicted by the OML model, e.g. due to secondary emission of electrons on impact of the ions [Estes 2000.III], but such second order effects are ignored by the model. Under the simplifying assumption of a straight tether and constant environmental conditions, a closed solution can then be used as initial estimate [Dijk 2003.I].

The ETBSim user can define any of various types of control laws for the system, through a text file. A maximum in applied power or voltage can be applied, or the cathodic current can be forced to track a predefined level versus time. This control is assumed to be effectuated by an adjustable resistor in series with the cathodic device. A second iterative loop adjusts the level of the applied resistance to match the control target.

The forces on the tether segments and dynamic behavior of the generally non-straight tether in complex environmental conditions is determined after these two layers of iteration have converged.

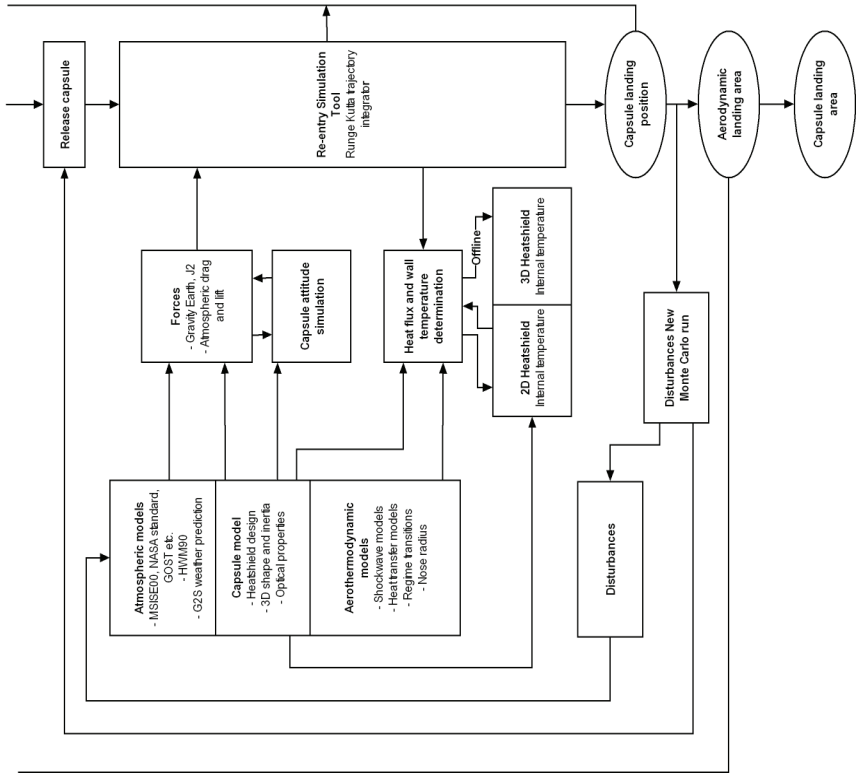

Main features	Impact on behavior	Model	Features
Tether modeling	Dynamics	Spring-mass elements, damping during bounces	Unlimited segments, typically 50-200 used.
Integration	Integration stiffness	Newton's law in inertial coordinates, constant acceleration assumed per interval	Self-adjusting time step. Smoothing using infinite speed of sound assumption
Electrodynamic tethers	Propellantless thrust, instability	OML collection	Complex tethers (bare, insulated, mechanical), types of cathodes. Control laws. Temperature dependent electrical resistance
Tether temperature	Electrical resistance, melting, expansion	Optical properties, radiation balance, aerodynamic heating, resistive heating	Sun, Earth, albedo, thermal radiation, reflection models,
End mass attitude	Stability of deployment and end mass	Tether torques during tether phase, 3D aerodynamic torques during entry. Impact attitude back on deployment and tension, drag etc.	3D endmass panel model. Possibility to include thrusting schemes.
Hardware and controller	Tension, resonance, robustness	Barberpole brake, spool deployment, feedback controller.	Feedback uses optical loop detection simulation, velocity filter, reference file of time, length, velocity etc. with variable feedback gains
Re-entry	Capsule	Drag and lift (modified Newton), heatflux (using Fay-Riddle based Stanton number, Chang dissociation, Rankine-Hugoniot shockwave, Sutherland viscosity), thermal propagation inside capsule	3D capsule model, drag and lift integrated with attitude simulation
Error models	Robustness	Configurable standard deviations and noise distribution on all parameters	See Table 50 for typical disturbed parameters. Monte Carlo runs. Simulation of control/hardware failures. Typically normal distribution used.
Other	-	-	Day/night, groundtrack, ground station visibility, 3D graphics, tether geometry and brightness as seen from ground. Run modes: controlled deployment, reference file maker, manual control, trajectory optimiser, Monte Carlo, real-time hardware-in-the-loop etc.

Table 3. *MTBSim/ETBSim dynamic and interface features*

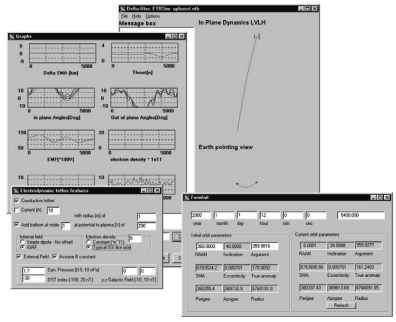

Figure 11. *ETBSim sample output*

Environmental factor	Impact on behavior	Model	Features
Gravity potential of Earth	Out of plane motion, altitude variation	First harmonic	Newtonian + J2-J4
Gravity of Sun and Moon	Tidal effects on orbit, lifetime	Newtonian	-
Earth bulge	Altitude variation	Ellipsoid	Distinction between geodetic and geocentric coordinates
Atmosphere	Lifetime, tether dynamics, capsule trajectory	Exponential US standard '76 GOST MSISE 2000	US and GOST have solar activity dependency, MSISE also includes seasonal, diurnal, and long term trend
Wind	Capsule trajectory	HWM 93	Horizontal wind averages
Weather	Capsule trajectory	G2S	100 km resolution daily weather prediction
Magnetic field	Potential and Lorentz force on tether	Dipole IGRF T-96	-
Ionosphere	Electron/ion collection affecting potential and current, neutral temperature affecting atmospheric density	Simple model IRI-95	Day/night, seasonal effects, longitude, latitude, altitude effects.

Table 4. *MTBSim/ETBSim environmental models*

2.3.3 Validation and comparison to other models

Early MTBSim developments have been validated against reference cases from a dynamics and integrator point of view. For a fully deployed tether, frequencies of oscillations and swing period have been verified against the simplified equations (Section 2.1.5) and other simulators [Heide 1996.I, Heide 1996.II]. Deployment dynamics were compared against those predicted by three alternative simulators in the context of the StarTrack SpaceMail study:

1. Simplified equations of motion for a straight 2D tether based on Lagrangian models by Heide & Kruijff [Heide 1996.I]
2. The LRTeth simulator by Sabath [Sabath 1996.I] and Heide [Heide 1996.I]
3. The simulator of Royal Melbourne Institute of Technology, based on Kane's equations, by Blanksby [Heide 1999, Blanksby 2000].

In all cases, deviations of only 0.01-0.1% were recorded in length and time parameters, which is well within the targeted accuracy range of about 1% (Section 5.5).

In the context of the YES2 mission, independent comparative works were commissioned by the European Space Agency and the Russian design bureau TsSKB in order to further boost the confidence in the proposed deployment and control based on YESSim. These analyses

by Ishkov & Naumov, Sazonov, Crellin, Smirnov and Yolkin[1] generally were based on open loop rather than closed-loop control laws but all resulted in positive recommendations [Ishkov 2006, YES2 2006, Smirnov 2010].

For ETBSim, the electron collection performance has been confirmed by exact duplication of results published by Dobrowoly & Vannaroni [Dobrowolny 2000], using also the same input conditions. Long term dynamics and the occurrence of instability in the tether motion has been qualitatively compared with analytical work in [Kruijff 2001.I] and ProSEDS simulations [Estes 2000.IV].

YESSim re-entry dynamics were successfully verified for a spherical capsule in the context of the YES2 mission by TsSKB [Stelzer 2006, TsSKB 2006], using the GOST atmospheric model, and for the T-Series project by the French space agency CNES [Hyslop 2006]. Heatflux estimates were found to coincide with those of Computational Fluid Dynamics (CFD) results, for continuum conditions, and Direct Simulations using Monte Carlo (DSMC) for the rarefied regime [Lyaskin 2004, Asma 2008].

Although it has not been possible to do a full verification of some of the more advanced features also due to lack of comparison material, sufficient confidence has been obtained for the primary simulator functionalities. In Section 8.5.3, the applicability of simulator results to mission planning will be further evaluated, based on comparison against flight results.

[1] YES2 datapackage, containing technical reports and notes from Prof. Ishkov (SSAU, 2003), Prof. Sazonov (KIAM, for TsSKB, 2006), Prof. Yolkin (TsNIIMASh, 2006), Prof. Smirnov (Moscow M.V. Lomonosov State University, for ESA, 2007), Dr. E. Crellin (ESA, 2007).

3 Analysis of Tether Applications

Any good engineer can build a mechanical tether system and it will work as planned. But an electrodynamic tether is a different story. You may have done everything right and it still won't work.

— Joseph A. Carroll, builder of four successful space tether experiments

In co-operation with several co-authors, a number of technical investigations has been performed into possible near-term applications that provides a taste of their potential, particular challenges and concerns. The original, referenced work has been re-evaluated and elaborated, the results are summarized in this Chapter. An overview of the investigations is provided in Table 5.

Tether Application	**Question investigated**	**Reference**
SpaceMail	Is there a feasible tethered alternative to the retro-rocket option?	Ockels 1996 Heide 1996.I
Launch assist & spent stage deorbit	Is there an application niche for mechanical tether-assisted launch of small payloads and deorbit of upper stages?	Hyslop 2006 Heide 2001.I
Multipoint sensing	What options exist for low-cost lower thermospheric missions?	Heide 2001.II
Artificial gravity	Would the tether system mass be a prohibiting factor for a manned demonstrator in Low Earth Orbit?	Lansdorp 2003 Lansdorp 2004
Electrodynamic tether deboost	Can OML electron collection be confirmed for a realistic tether application environment?	Kruijff 2001
	How does system design affect dynamic instability?	Kruijff 2001
	Can electrodynamic tethers contribute to a mitigated debris environment?	Heide 2001.I
	How could a simple passive tether system be put to use - around Jupiter?	Van Dijk 2003.I
All applications	Which are the safe orbital regimes that should be observed for tether mission design?	Heide 2001.I

Table 5. *Analysis performed for a selection of near-term tether applications*

3.1 Mechanical tether applications

3.1.1 SpaceMail and waste disposal from a Space Station

The case for tethered SpaceMail

SpaceMail is a frequent sample return capability from Low Earth Orbit that aims to enable in-space research to progress at a significantly higher rate. It is particularly applicable to an orbital space station. The 1986 SpaceMail study for Columbus [Aerospatiale 1986], performed in the context of the (then) International Space Station Alpha (ISSA), foresaw that in-orbit research would require a bi-weekly sample-return capability, involving a re-entry capsule of 88 kg. Payload of a sample-return capsule might consist of e.g. research samples (for on-orbit iteration after ground based analysis), data carriers with large amounts of video, or blood samples of astronauts for medical examination.

It has been proposed that a solution involving tether assisted re-entry through momentum transfer could provide a simpler, safer and lower-cost solution than the conventional retro-rocket or cold-gas propelled deorbit system, through the following advantages:

- If the re-entry of a capsule could be achieved by a transfer of momentum to the station this would provide an elegant, propellant-efficient solution. A re-entry is achieved by taking away orbital momentum from the system that is to be deorbited. At the same time, the station itself will be supplied with (much of) that momentum. This is beneficial since a Station in Low Earth Orbit loses orbital energy gradually but continuously through atmospheric drag. Apart from SpaceMail capsules also heavy cargo vehicles can be deorbited by the same system to the benefit of station altitude. In the case of the International Space Station, several times per year a vehicle such as Progress or ATV is deorbited.
- Capsule and deorbit system design requirements will be more relaxed compared to a conventional system. The latter requires dedicated safety measures for on-station storage of solid propellant or pressurized gas. With a tether system, multiple capsules can be conveniently stored within the manned environment, such that astronauts can easily access and load a capsule when necessary.
- The energy requirement for the initial separation system can be reduced by about an order of magnitude when comparing to the conventional system. The same holds for the shock disturbance that results from the system's activation. Before a rocket deboost system could be activated, for safety, sufficient initial separation with the station needs to be secured for which an initial ejection velocity of about 4 m/s is required, about 700 J for an 88 kg capsule [Aerospatiale 1986]. For a tether deployment an ejection energy of about 40 J suffices, equivalent to about 1 m/s for the same capsule (see also Section 4.2.1).
- The tethered capsule can be ballistic and completely passive or, for reduced g-loads and increased landing precision, can have a certain amount of lift controlled by an aerodynamic guidance system. A retro-rocket or cold-gas firing would require

thrust vector control and an attitude determination and control system. A capsule deorbited by a tether obtains its velocity vector and orientation through the control of tether dynamics which naturally take place inside the orbital plane [Crellin 1994].

A consideration against the use of tethers on a space station may be the disturbance of the microgravity environment on the station as a result of tether tension and, possibly, station attitude control torques during the several hours of deployment. With a typical maximum tension of 20 N and a station mass of 200,000 kg the disturbance will however remain below 10 μg. This level is still compatible with the best available research environments today. However, in order to limit the consumables required to maintain the attitude of the station, the tether system may need to be placed close to the station's center of mass.

Swinging tether approach

A number of SpaceMail studies have been performed in the United States [Carroll 1995.II], as already discussed, but also in Europe.

Following the Aerospatiale study in which the tethered SpaceMail option has first been identified, design work towards a tethered SpaceMail system was done for the European Space Agency by the TATS/TARGET study team under the lead of Alenia Spazio [Alenia Spazio 1995]. This study aimed for a demonstration using a Raduga capsule deployed from the Progress vehicle. It also looked into the deployment of a Raduga capsule, Progress or ATV directly from the International Space Station Alpha. A swinging tether was proposed to decrease tether length. As part of this study a hybrid spool-reel system breadboard and a deployment test facility were produced [Licata 1995].

Performed in support of TATS, the StarTrack study (Swinging Tether Assisted re-entry Through Robust Actively Controlled Kinetics) contains innovations intended to overcome basic concerns with respect to tether dynamics and capsule landing accuracy, as achievable with a swinging tether [Ockels 1995, Heide 1996.I]:

1. A two-stage deployment, for improved landing accuracy and control.
2. A non-linear tension feedback control, based on length measurements only, towards a reference deployment profile.
3. The Flex-End Brake, a method to stop the deployment, at a large in-plane deployment angle and without residual spring-mass oscillations.
4. A release time optimized for minimal landing error, based on end-to-end evaluation of sensitivity of deployment and re-entry to disturbances.

The two-stage deployment is perhaps the most defining element of the StarTrack approach. It is recognized that during the first, inertia-driven stage of deployment, for some hundreds of meters, tether tension must be low to maintain deployment velocity. Typically, tension will approach the system's minimal friction level. As a result, large errors in the deployment profile can be introduced in case of off-nominal friction levels or errors in initial (ejection) velocity. Those early errors in length and in-plane angle can significantly impact gravity

gradient levels compared to those foreseen. Off-nominal levels of acceleration will then result, and, if the deployment is performed in only one (single) stage, the deviation builds up further over time. If, however, a stage limited to a few kilometers of tether is first deployed and stabilized around the vertical, its control would not be time-critical. Time is available to achieve the proper length, dampen any residual oscillations as necessary and assess the achieved state. Then, at the appropriate time, and now with a well-known gravity gradient level, which is also much larger than the system friction, the second stage of the tether can be deployed quickly and robustly. In this way, the sensitivity of the overall deployment to initial disturbances is strongly reduced.

The deployment is controlled towards the desired final state with the help of the Energy Feedback. This non-linear feedback, as proposed by StarTrack, is based on estimation of the system's kinetic and potential energy from length measurements. Excess energy is then dissipated using a friction brake (Section 5.5). The second stage of deployment lasts less than one hour, and in this time, sufficient in-plane angle is to be achieved for an effective momentum transfer.

The deployment is completed by a Flex End Brake [Kruijff 1996], a rapid deceleration performed in such a way as to avoid residual spring-mass oscillation. The full length of the tether is about 25-35 kilometers. The exact required length depends on the station altitude, target swing angle and the required entry angle, the latter typically in the range from 1.3-1.8 degrees. By decelerating quickly, much of the built-up in-plane angle is maintained and available for the swing back, such that a shorter tether is required (Section 2.2.1), whereas mission duration is minimized. Using the Flex End Brake profile, the intensity of the braking can be set with a free parameter, $\sigma > 1$. For this method, the minimal length increment between final length l_e and initial length l_0 when decelerating from initial deployment velocity $\dot{l}_0$ down to zero can be determined to be:

$$l_e - l_0 = 1.45761 \cdot \sigma \frac{\dot{l}_0}{\sqrt{k}} \tag{3.1}$$

with $\sigma = 1$ for maximum brake intensity, and k is the tether stiffness, $k = EA/l_0$. The Flex End Brake deceleration strategy brings the deployment velocity down within a few minutes from a maximum of 15-25 m/s to zero, after which the swing towards the vertical is initiated.

Release from a swinging tether is best performed around the first passage of the vertical. In subsequent passages the error in phasing can build up due to the integrated effect of initial errors and transverse and longitudinal tether oscillations. Also the tether can get slack during the retrograde part of the swing, which would lead to unstable endmass behavior and further uncertainties in the endmass trajectory [Heide 1996.I].

The optimal time of release during the swing is determined through end-to-end Monte Carlo simulations, covering the complete mission from capsule separation from the station to its landing on Earth. This end-to-end approach can be contrasted against a segmented optimization of multiple mission stages towards intermediate but rather arbitrary targets, for example an accurate achievement of the capsule's atmospheric entry point, which

happens to be a well-defined target but has no clear relevance. The end-to-end approach however optimizes towards a single and final parameter of undisputed relevance, in this case, landing accuracy. The end-to-end approach obtains its benefit from the fact that some disturbance sources may be coupled such that their effects cancel each other out when integrated over all stages of the mission.

An optimal in-plane angle for capsule release is found to be several degrees before the vertical [Heide 1996.I], the exact value depending on the magnitude of the errors expected. A striking example of a cancellation of effects occurs at this optimum. Consider for comparison the case of a retro-rocket deorbit system. If the deorbit burn is delayed by one second, due to the orbital velocity, the position of the landing site is consequently affected by about 8 kilometer. For the tether case however, if the release of the capsule from the tether is delayed by one second, in that second the tether swings further towards the vertical. Swing velocity and gravity gradient both increase. A steeper entry angle results, which cancels out much of the progression over the one second due to the orbital velocity of the system. The remaining sensitivity is only about 1 km per second of delay (Section 5.5.2).

StarTrack performance evaluation

Sabath has compared the StarTrack approach to his concept of a hanging tether release [Sabath 1996.I]. The advantage of the hanging tether is that once the vertical state has been achieved, the landing accuracy is mostly determined by release timing. It is also suitable for multiple release applications (see e.g. Section 3.1.3). The hanging tether is heavier than the swinging equivalent. Tether exposure to meteoroids and debris, as expressed in kilometer-hours (Section 4.3.1), is increased significantly, therefore a larger diameter may be necessary. Although the loads encountered for hanging and swinging tethers are comparable, the hanging tether is significantly longer (Eq. 2.23).

In the uncontrolled ballistic entry case, the StarTrack 3σ landing accuracy will typically remain below two hundred kilometers, comparable to a retro-rocket deboost [Schonenborg 2000]. Heide & Kruijff describe various methods to improve the landing accuracy further, e.g. by adjusting the second stage start time or by real-time selection of the release time based on a look-up table and GNSS measurements at the endmass [Heide 1996.I].

System operation on the space station

Most of the system complexity and cost of any SpaceMail system will lie in the effort to load the capsule, inside the station, and next to place the readied system outside. A typical operational procedure could run as follows.

Astronauts on the station load up to 5 kg of samples in a container which may be thermally isolated or cooled depending on the contents. The container is placed inside a small re-entry capsule that the astronaut may pick from a storage rack inside the station. The size of the capsule is limited by the dimension of the available airlock hatch, typically about 70 cm. An inflatable or deployable capsule can be used if larger payloads need to be returned to Earth. There are several options for integration of the capsule with the tether system.

A mass effective option involves a reusable deployer system with a retrievable tether installed beneath the station, including an autonomous system for arming and release of a spring-loaded ejection platform Figure 12a. The astronaut delivers the capsule to the airlock, from where it is picked up by a robotic arm and mounted to the ejection platform. The ejection platform is designed to be deployed together with the capsule and includes a functionality to release the capsule at the required time. It is equipped with a GNSS and communication system. The tether is stored on a reel and deployed to a hanging tether configuration for capsule release and controlled retrieval afterwards. From many perspectives this is a complex system that will require significant flight experience before start of service.

An alternative concept reuses the deployer, but expends the tether. In this scenario, the astronaut mounts both a tether spool and a capsule onto the deployer system. In an ideal situation, the station module design takes into account the necessity of these manual operations, and the tether can be deployed directly from the airlock, Figure 12b.

A retro-rocket or cold gas system deboost would typically require a configuration as in a., however for each capsule deorbited, a retro-rocket orientation system, the retro-rocket itself and possibly a cold-gas separation system would be disposed. In terms of operational complexity the two systems are therefore, at first glance, comparable.

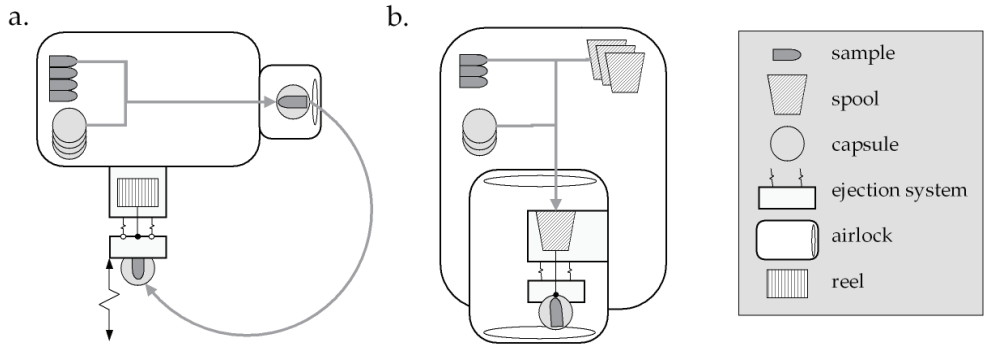

Figure 12. *Sample configurations for a SpaceMail system on a Space Station (see text). Deployer: left (a.) - retrievable tether on reel; right (b.) - expendable tether spools.*

Mass comparison

The StarTrack study [Heide 1996.I] compares the system mass of the proposed tether system (configuration b.) to the retro-rocket case, based on the 1986 SpaceMail study [Aerospatiale 1986], taking into account expendables (propellant, tether, retro-rocket & GNC systems) and reusables (deployer, ejection system), for an 84 kg re-entry capsule. The reusable systems are comparable in mass. For the swinging tether option, a mass savings of 23 kg on system expendables is quoted, per (ballistic) re-entry. For a hanging tether, this advantage reduces to 8 kg. In addition however, for each tethered re-entry, about 4 kg of propellant for station altitude maintenance is saved. A retrievable tether would save a further 10 kg per sample return (configuration a.).

Various projects and studies since have suggested that indeed a ballistic capsule can be simple and lightweight, if it relies on the tether system for safe separation, orientation and accurate deorbit [Carroll 1995.II, De Pascale 2008]. For more complex (controllable, non-ballistic) capsules that already contain active guidance systems, the mass advantage is likely to be smaller. In any case, only if the sample return is indeed frequent, and the station is adapted for use of tethers (as in Figure 12), the quoted mass advantages become significant compared to the operational cost.

Much more significant benefits in terms of saved propellant mass can be obtained if heavy cargo vehicles would be returned using a tether. According to the TATS study, a tethered re-entry of 2-3 Progress and 1-2 ATV by tether could be foreseen for the ISSA, and would save about 3 ton of propellant cargo to the ISSA [Alenia Spazio 1995] per year, compared to the 4.7 ton propellant cargo capacity and 8 ton total cargo of a single ATV or the 1.95 ton propellant cargo and 2.2 ton of total cargo capacity for Progress M1. These data include both the propellant savings for Progress/ATV deorbit and for ISSA orbit maintenance. During a typical operation of the ISSA a tether system therefore saves about one in two Progress launches or, alternatively one in four ATV's. In order to reduce required tether length, deployment tension, tether diameter as well as the amount of energy to be dissipated by the brake system, such a heavy vehicle would be deployed at low velocity towards a large forward angle, close to 80° (Section 2.1.4), and in a single stage.

Challenges of tethered SpaceMail

Although a retro-rocket may pose a risk for storage, tether operations are not without safety issues. Unimpeded deployment must be secured. A contingency action (due to e.g. tether jam) or unexpected cut can leave a tether in space, free to collide with other spacecraft (Section 3.3). Reliability of tether deployment is not easily confirmed based on limited the flight data and ground-tests only.

In light of the current reality of International Space Station operations, with goods transport and crew activity heavily reduced as compared to the ISSA planning, the call for a frequent sample return has all but disappeared. It could be sufficient for a sample return system to hitch a ride on an ATV or Progress and decouple before re-entry. It may however still be of interest to deorbit ATV or Progress itself by tether.

3.1.2 Tethered upper stage for a launch assist and upper stage deorbit.

The SpaceMail tethered momentum transfer, with some adaptations, can be used in the opposite direction, as a means of assist for launch rather than re-entry. As an added benefit, the rocket upper stage, acting as a countermass, can at the same time be deorbited in a controlled manner, thus contributing to best practice in debris mitigation [ESA 2000, IADC 2002, NASA 2007, Jablonsky 2008]. The T-Series case study involving a yet-to-be developed micro-launcher indicates that a tethered upper stage can indeed service an increased payload mass when compared to a conventional liquid upper stage alternative [Hyslop 2006]. A detailed analysis is here summarized that highlights the peculiarities, possibilities and limitations of such a system. In addition, a first analysis is reported of the

existing launcher market to gain insight into the wider potential for such a mechanical tether application [Heide 2001.II].

Analysis approach T-Series case study

The T-Series case study starts from a simple and low-cost micro-launcher concept under development at CNES, as shown in Figure 13. This micro-launcher aims to deliver a payload of 150-175 kg into a circular highly inclined Sun Synchronous Orbit (SSO) at an altitude of 600 km. The launcher is based on three solid stages (designated by P9-P9-P2, the numeral describes the amount of propellant in tons). The third stage, a P2, can bring the payload into an elliptical orbit with 100-200 km perigee altitude, and apogee within LEO as required. From there, a tether system placed on the P2 can deploy and release the payload into its circular destination orbit. At the same time it delivers, through momentum transfer, a controlled deorbit of the P2. The tether system will provide the required ΔV for payload circularization, and can be used to correct for the solid stage orbit insertion error.

Conventional alternatives would need to include a re-ignitable liquid stage and would be more complex. Possible conventional solutions are a P9-P9-P2-L0.02 using a small fourth stage of 50-100 kg with about 20-30 kg of hydrazine propellant, or a P9-P9-L2 design replacing the P2 (and tether) completely by a capable L2 liquid stage (2 tons of N_2O_4/MMH).

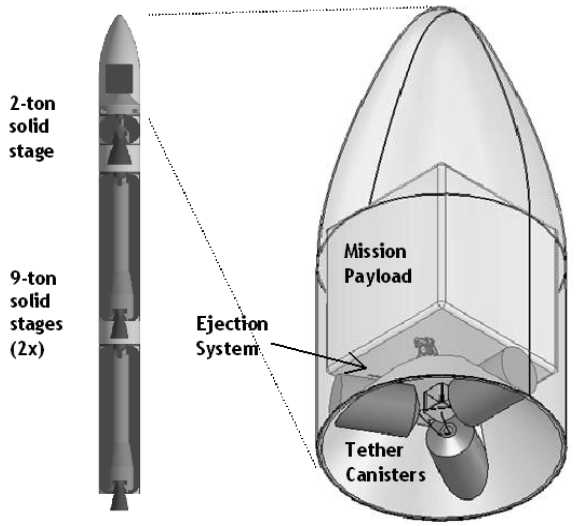

Figure 13. *T-Series suggested configuration*

The difference in the launch process for the conventional and tethered alternatives is illustrated in the following example (Figure 125). Starting from the same initial orbit (here 150x560 km) the conventional system would require three burns to reach a target orbit of 600x600 km, with a total of 138 m/s. The tether system would achieve the same final situation in a different manner. It would be deployed between payload and P2 third stage, and release the payload in apogee, 40 km above the system's center of mass. The P2, below the center of mass, would be deorbited. One could say the tether applies to the payload first

a change in apogee altitude of 40 km, then a ΔV of 95 m/s with respect to the center of mass of the tether system to circularize.

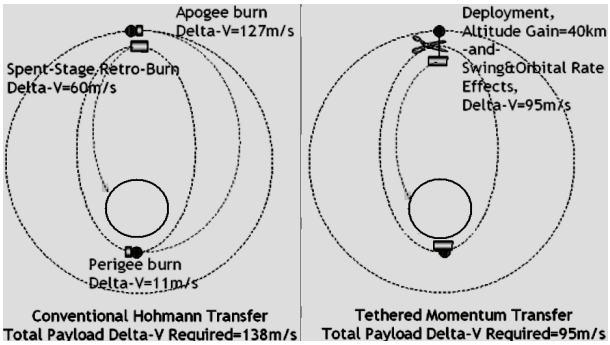

Figure 14. *Comparison between conventional and tethered payload circularization*

The proposed system is to be dimensioned such that mission payload mass is maximized and nominal P2 perigee is minimized. The mass of the empty P2 is 287 kg.

A number of system parameters can be determined straightforwardly. Following a certain launch, the tether length that needs to be deployed depends on the difference between target altitude (600 km) and the apogee altitude h_a obtained by the third stage, in combination with the mass ratio of payload and P2. With higher payload mass a longer tether is required to achieve the same effective length from the center of mass and put the payload at target altitude (Figure 15). From the *13-L rule* (Eq. 2.23), the +3σ allowable extreme of h_a can next be determined ($h_{a,max}$), above which the tether would be too short to deorbit the upper stage. The P2's 3σ burn-out accuracy was analyzed to be –32/+24 km on apogee, from which the nominal ($h_{a,max}$ -24 km) and minimal altitude ($h_{a,max}$ -56 km) can now be derived. For a perigee of 150-200 km and 150-175 kg payload, the maximum feasible altitude is about 560 km. Following this reasoning, a typical tether length range that covers the quoted launch uncertainties is between 60-150 km. At perigees below about 175 km however, MTBSim simulations show that the atmospheric drag on the tether will bring the system down significantly during deployment. To compensate for this altitude loss, a tether longer by some ten(s) of kilometers is then required.

Correction of off-nominal orbit insertion by the P2 is performed using two controls. Firstly, the deployed length of the tether is selected to bring the payload to the altitude of the target circular orbit. Secondly, the deployment is controlled in such a way that at apogee, where the payload will be released, the proper swing velocity for circularization is achieved. A proper deployment profile and start-time of deployment have to be selected to make sure the desired state of the tether system is obtained exactly at the apogee of the tethered system's center of mass (Figure 14). The +3σ apogee-error case features the shorter deployed tether length, selected such that only a maximum swing can deliver the required ΔV for circularization. For the -3σ case, the tether must be deployed much more, just to reach apogee altitude, in fact to such a length that even release from a hanging tether would

increase the payload perigee above the target circular altitude. Therefore, the payload must be released only on the return swing, when the tether rotates against orbital direction (514.5 km case in Figure 17).

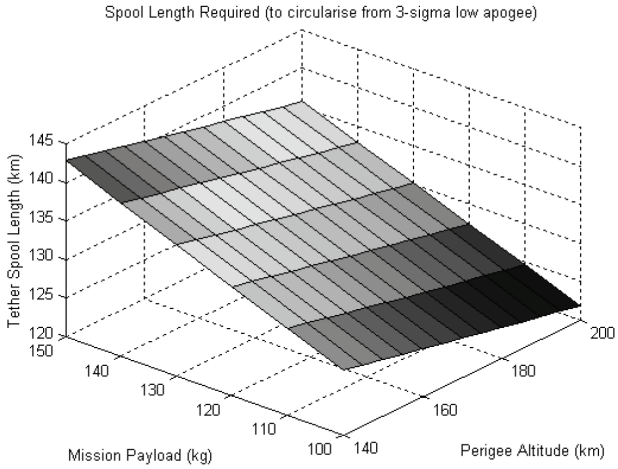

Figure 15. *Tether length required vs. payload and perigee*

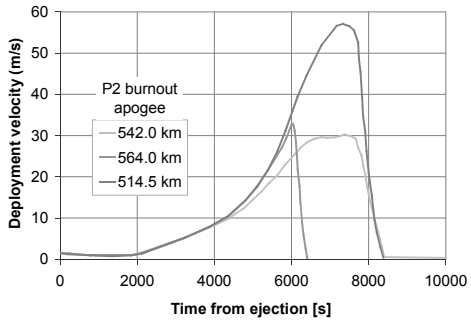

Figure 16. *Deployment velocity profile for three cases*

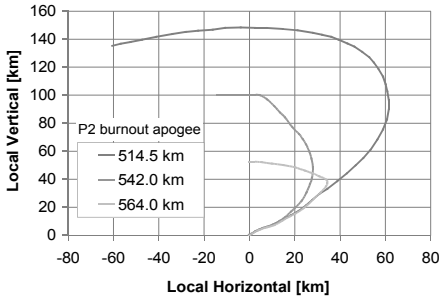

Figure 17. In-plane trajectory for the same three cases

Matching deployment profiles can now be determined (Figure 16 and Figure 17**).** Deployments are performed in single stage rather than two-stage for several reasons. Atmospheric drag and eccentricity prevent a properly hanging tether, required as part of the two-stage approach. Furthermore, a single stage deployment is faster and can achieve a higher deployment angle, at lower tension levels and with a more effective swing [Ockels 1995]. There are further constraints to deployment design. Firstly, ejection cannot take place shortly before perigee, in the true anomaly range of 345-355 degrees, because in that case drag will dominate over the gravity gradient and a proper deployment becomes impossible. Secondly, the deployable tether length before perigee passage is limited, as the P2 should not be dipped into the dense atmospheric region below about 145 km. Such a situation would cause excessive drag losses, heavy tether bending and even melting. Finally,

after perigee, only an additional 30 km of tether can be deployed due to the constraint that deployment shall be completed in apogee. As a result, if the required tether length is to be successfully deployed for the -3σ case, there is an upper limit to payload mass and a lower limit to initial perigee altitude.

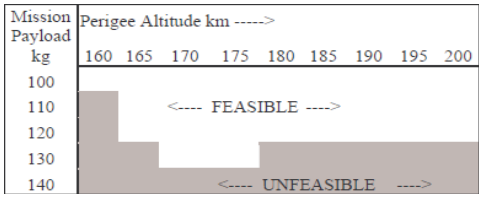

Figure 18. *Feasibility envelope for T-Series (287 kg P2, 600 km target orbit)*

For a given tether length requirement, deployment profile, survivability and safety factor, the tether system can be designed (including deployer and brake) and its mass estimated. In order to obtain the useful payload mass, the tether system mass is subtracted from the launcher performance.

From these performance limits, the resulting feasibility envelope for the P9-P9-P2 plus T-Series can be derived, as shown in Figure 18. Table 6 lists the optimal system design parameters as they were identified in the study.

Parameter	**Value**
Mission payload	127 kg
Target orbit	600x600 km, i = 97.79°
Tethered stage total mass	YES2 type, 34.65 kg of which 17.9 kg tether
Tether	1 spool Dyneema: Ø0.4 mm 2 spools Zylon: Ø0.35 & 0.3 mm, all 6 kg Zylon is heat resistant, required during braking phase
Tether safety factor	-3σ tensile strength as measured (1450 MPa - 3x130 MPa) must be larger than 1.25 x stress from +3σ tension level, as simulated (100 N)
Tether survivability	99.10%
Reliability insertion from Monte Carlo	eccentricity < 0.002 : 99.52% SMA error < 12 km : 98.94%
P2-burnout perigee/apogee	175 (±4) km x 542 (-32,+24) km
Tether length	47-159 km (nominal 81 km)
Deployment duration	typically 7000-10200 s
Max. deployment velocity	typically 30-57 m/s
True anomaly of ejection	typically 232° (nominal or lower apogee), 25-84° (higher apogee)
Spent stage re-entry	1.78±0.13° entry angle, dispersion area 2200x350 km over mid-Pacific (Kourou launch)

Table 6. *T-Series design parameters for a 600x600 km target using P9-P9-P2 launcher.*

Applicability range for T-Series

As far as the payload target orbit is concerned, the proposed concept is shown to be valid for circular orbits from 300 to 1800 km altitude (Figure 19). A lower limit is provided by atmospheric drag interfering too heavily with the tether dynamics. High target apogees can be served by long tethers, at the expense of payload mass. The upper limit is provided by the decrease in payload mass below the level of commercial interest (set to 100 kg in this study).

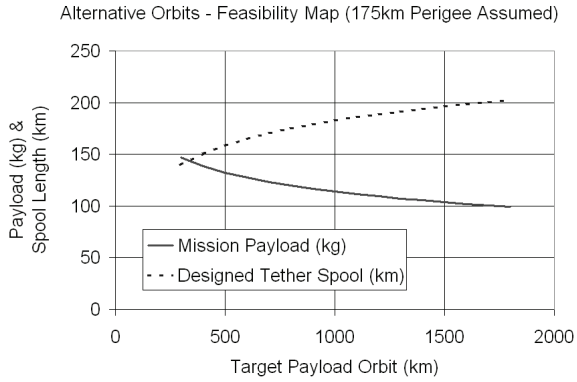

Figure 19. *Tether length and payload vs. circular orbit altitude*

The tether system can in principle be used also for heavier rockets and consequently, larger payloads. These systems will be less affected by atmospheric drag, but there will be significant additional engineering challenges, such as high brake tension and high heat dissipation levels.

Extension to existing upper stages

Spent stages are considered to have a prime share in catastrophic collisions and the future debris environment [Anselmo 1999]. If the spent stage deorbit for debris mitigation purposes is the primary objective, and if the payload has its own means of obtaining its (exact) target orbit, the mechanical tether application will be less restrictive than for the T-Series case.

A mechanical tether for spent stage deorbit has some advantages over deorbit by electrodynamic tether (Section 3.2). Mechanical tether deployment and momentum transfer can be completed within hours, the dynamics are bound within the orbital plane. The deorbit can be controlled straightforwardly and accurately. The tether will be designed to deorbit with the debris, limiting collision risk.

A rough analysis has been performed to compare estimated tether system mass to the fuel mass saved for a representative population of launchers [Anselmo 1999]. Assumed is a specific impulse of I_{sp} = 300 s, a Dyneema® swinging tether, deorbit of the spent stage to 60 km perigee and a safety factor on tether strength of 6. The assumed tether system is using

a SEDS type deployer as a starting point. An approximate mass relation is assumed by curve-fitting through a small number of rough system design points [Heide 2001.II].

Based on the available launch data, about 28% of all launches to (near-)circular Low Earth Orbits are found to be good candidates for tethered deorbit, with on the average about 3% of mass reduction (or increase in available payload mass). These are upper stages that are relatively light compared to the payload mass, at relatively low altitudes, using relatively short tethers. For more extreme cases, the situation is generally not favorable (Table 7). Tethered momentum transfer can thus be seen as a candidate for reducing low LEO debris, if the payloads find advantage in the extra orbital height or (perhaps alternatively) mass budget. On the other hand, spent stages in such orbits often have already a sufficiently short lifetime to meet the current international standard of 25 years.

Also spent stages in Geostationary Transfer Orbit (GTO) might be deorbited via a tether system [Ockels 1996]. Of the investigated upper stages 30% are a candidate for this type of deorbit. Stage deorbiting is of special interest for Ariane 5, since it has a very high perigee of 620 km (lifetime of hundreds of years) and will be the major contributor to space debris in GTO. The tethered spent stage deorbit from GTO has been investigated for all upper stages [Heide 2000.I]. A deployment on the arc towards apogee has been assumed at 2 m/s, with a release in the second apogee passage. The safety factor on the tether design is assumed here as 4, which is considered conservative, because of the less demanding deployment in a highly elliptical orbit [Kruijff 1998]. It is found that the advantages of a tether are only significant for Ariane 5, mostly because other upper stages in GTO have a perigee altitude of only about 200 km. Controlled excitation of the rotation [Ockels 1996] almost doubles tether performance, equivalent to a further payload gain of about 60 kg. However, this gain comes at the considerable cost of an additional 3 days or more of launcher operations and delay for the payload.

A more exotic use of mechanical tethers for debris mitigation could also be considered. A large traveling system has been proposed, that would rendez-vous with existing debris using conventional propulsion, whereas a tethered momentum exchange between the system and the debris is then used to deorbit the debris [Bonnal 2005]. The system would not necessarily have to make very large orbital changes to make a noticeable impact. About half of the debris mass in LEO is clustered in a 83 degree inclination at around 1000 km altitude [Carroll 2002]. One of the advantages of using a mechanical tether system could be the possibility of docking even at significant distance and relative velocity between the system and the debris (i.e. harpooning). This would greatly reduce the mission complexity and duration.

For the near term however it can be concluded that, although for many upper stages in LEO a mass benefit can be obtained from mechanical tether deorbit, only for a fraction of those there is a need from a debris mitigation point of view. Spent stage deorbit is certainly of importance to Ariane 5 GTO launches, but a mechanical tether provides relatively little gain considering the impact on system, operations and payload. The T-Series is an example

where the requirement for deorbit is imposed by the developer and where a suitable tether solution has been worked out in more detail.

	All suitable	***Zenit***	***NewElint***	***Delta-II***	***Tselina-2***	***Ariane 5***
Case	*Circular* Scaled average	*Circular* Lowest orbit	*Circular* Highest orbit	*Circular* Lowest stage mass	*Circular* Highest stage mass	*GTO* single launch, Best case
Mass upper stage	1954	1976	4185	924	8300	3138
& payload [kg]	3678	6500	5000	1050	3250	6800
Perigee altitude [km]	642	275	2125	1000	850	620
Tether length [km]	69	22	292	136	216	20
Payload target perigee	951	340	3853	1827	2868	35869
& apogee altitude	666	280	2258	1064	1005	878
Fuel savings stage	113	43	760	83	638	62
& payload [kg]	110	45	601	77	574	60
Est. tether system mass [kg]	111	20	2978	161	1696	28
Est. advantage tether [kg]	***112***	***68***	-1617	-1	-484	***94***

Table 7. *Tethered momentum transfer statistics for common spent stage deorbit: scaled average and extreme cases. Mass advantage, if present, indicated in bold italics.*

3.1.3 Multipoint sensing in the lower thermosphere

There is a gap in our access to the Earth's atmosphere. The mesosphere (50-90 km) and the lower ranges of the thermosphere (90-250 km) have hardly been accessed. Although satellites can perform in-situ research above 250 km, at lower altitudes atmospheric drag severely limits satellite lifetime. Prolonged access from below is precluded as neither airplanes nor high altitude balloons can reach these layers. Our knowledge of this atmospheric region is poor and based only on incidental measurements from sounding rockets or remote sensing.

The thermosphere for one is of considerable relevance to atmospheric processes. It represents the upper layers of the atmosphere, from about 90 to 2000 km altitude, and is named so because the gases here are heated by solar radiation to temperatures of up to thousands of Kelvin. Its behavior and structure is highly dynamic and heavily influenced by solar activity, diurnal and tidal variations. The gases are also ionized, leading to effects such as the aurora, which occurs where Earth's magnetic field lines concentrate and penetrate the thermosphere. The thermosphere is the final barrier to the exosphere from where (mostly light) molecules, atoms, ions are able to escape into space. Throughout the thermosphere there is little mixing of the different species of gas. Each species features its own scale height, causing a layered structure with the heaviest species concentrated in the lower thermosphere. These processes and interactions have a directly observable impact, such as when ionized gases affect radio signals that are passing through, but may also have a more intricate influence, e.g. on weather and climate. Such effects are not all equally well

understood. In particular there is a need to study in-situ the relationship between the ion and neutral dynamics, as well as composition variations in the charged and neutral atmosphere [Heelis 1998].

From a scientific point of view, it is advantageous to have multiple atmospheric measurements at the same instant, spread in altitude along a certain multi-kilometer profile. Although it is possible to infer such a profile using penetrating remote sensing techniques, a multi-satellite mission would provide in-situ measurements. Compared to a single satellite at low altitude, a constellation provides the possibility for faster revisits and resolve better for thermosphere dynamics. Even low-cost satellites could provide significant scientific return [Muylaert 2010]. Data with significant added value can be collected for the scientific community even inside a time-frame of days, especially if global coverage is achieved. For such short mission durations a dedicated launch may not be attainable, instead a piggy-back opportunity may be considered [e.g. Kruijff 1999.III].

Heide, Carroll & Kruijff report of three piggy-back concepts for synchronized multi-point measurements over tens of kilometers in the lower thermosphere. Two of those use a tether. For each, the use of multiple 30-40 kg research probes is proposed with a selected set of instruments [Heide 2001.I]. The first concept, the Dynamic Wheel, uses a single 35 km tether to drop many research satellites into eccentric co-planar orbits with complementary perigee altitudes and phases. The second concept, LADDERS, consists of a vertical string with small satellites distributed along the length. The combined tether provides passive station-keeping and 2-axis attitude control. In both cases the tether technology can be fully based on SEDS or SpaceMail technologies. These tether options are compared to a third concept, without a tether, that involves the release of multiple satellites at the apogee of a geostationary transfer orbit (GTO) into orbits with different perigee heights.

Dynamic wheel tether concept

In the dynamic wheel tether concept, a dispenser of small satellites is deployed by tether from a massive host, such as an upper stage, in circular Low Earth Orbit at about 400 km altitude. The dispenser is stabilized to a vertical, 35 km below the host. From there, it drops the satellites one by one into eccentric co-planar orbits with a perigee altitude of about 150 km, and complementary argument of perigee and true anomaly. The tether deployment is very similar to that of SEDS-2 [Carroll 1995.I]. Figure 20 depicts the concept.

Consider the case of a total of 6 satellites that are released 200 seconds after each other. Figure 21 shows the altitude of the research satellites as a function of a planar angle for the first orbital period of the mission, referenced to the true anomaly of the satellite that was first released. Each angle value represents a specific vertical column in the Earth atmosphere. The vertical spacings of the sub-satellites at the angle of –60 degrees are 2, 7, 14, 20 and 25 km respectively. This atmospheric column is crossed by the subsequent satellites within 60 s of each other. In this example, two subsequent measurements at a single inertial angle will have a variance in time that is less then 14 seconds. Assuming an atmosphere co-rotating with the Earth, this time interval will induce a horizontal atmospheric spacing between the measurements. For example in a (worst-case) polar orbit, at the equator the

horizontal spacing between the two measurements amounts to 6 km. The horizontal spacing between the first and last satellite will thus remain below 5x6 km = 30 km. During half of their orbital period, the satellites are in the interesting region between 150 km and 250 km altitude. Due to the rotation of the atmosphere along with the Earth every new orbit another slice of atmosphere will be mapped. In several weeks a large part of the atmosphere can be mapped in three dimensions which is in line with the expected orbital lifetime.

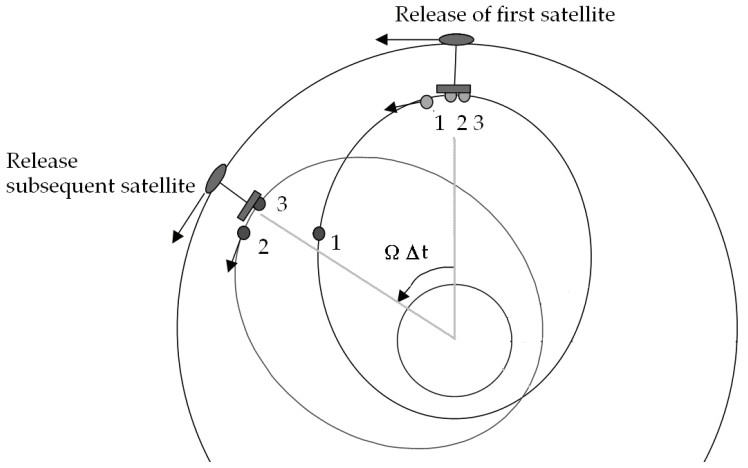

Figure 20. *Dynamic wheel concept*

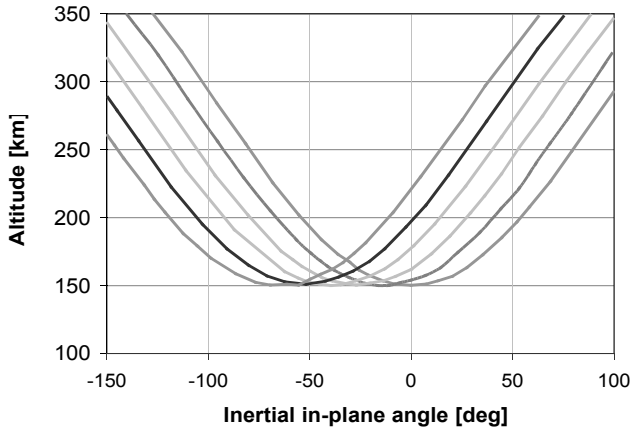

Figure 21.*Passage of atmospheric probes released by Dynamic Wheel*

It will be necessary to include active control to maintain synchronization of the orbits during the decay. This is partly due to finite tether control precision, partly due to finite host mass (causing the system to rise after each release), and partly the result of atmospheric bulges due to the diurnal effect and the Earth flattening. In particular, the Earth flattening creates a

significant altitude difference at equator versus pole of 21 km at the same radius, three times the Earth atmosphere's characteristic height. Ground control or on-board GNSS will be required, as well as a drag control system or thrusters for drag compensation.

The LADDERS concept

LADDERS, or Low-Altitude Daisychain-Deployed Expendable Research Satellites, is an alternative concept brought forward by J.A. Carroll in [Heide 2001.I]. In the LADDERS concept, a series of probes is connected to the next by a vertical tether, with a spacing between the probes of 5-15 km, i.e. in the order of the atmospheric density scale height yet finer at the bottom in the higher density regions.

The LADDERS is deployed in stages from a central massive platform, possibly an upper stage or interface cone. From the platform, a full set of probes is deployed downward using a tether. Each probe is equipped with its own small and passive tether deployer. Once the first tether is deployed, the remaining probes decouple from a first operational probe, and, as a group, they are lowered further using the tether and deployer that is inside this first probe. This process repeats until all probes of the first set have deployed their tether and a vertical daisy chain configuration has been achieved. A second set of probes could then be deployed upward in the same manner. With the platform centrally located, the maximum tension level, occurring in the tether attached to the platform, is minimized.

Deployment of the full system will take several hours. The platform-mounted tether deployer is designed for low friction. The deployment is actively controlled when gravity gradient levels are still small. In contrast, the deployers on the probes would be simple and similar, with a mass below 1 kg. The tether mass per probe would be 1-2 kg. Deployment velocity is passively kept below 5 m/s, making use of the spool's tendency to increase friction with deployment velocity (Section 5.3.5). A thicker tether near the end and built-in damping system in the tether (Section 4.2.3) could be used to terminate the deployment in a smooth manner.

The total tether length might be between 40 km and 100 km with 4-8 probes. The useful lower altitude limit is 120-130 km, below which atmospheric heating and drag threaten the integrity and stability of the system. The lower ~15 km of tether will experience over 85% of the total atmospheric drag and will govern the exponential decay of system altitude. If the initial altitude of the lowest probe is 150 km, and the platform mass is 1000 kg, MTBSim predicts a lifetime of 2 days, just sufficient to obtain a rough global coverage with a ground track spacing of about 1250 km. Lifetime can be somewhat increased to about 3 days, if the lowest tether segment is released every time the bottom probe has reached an altitude of 120-130 km. The reduced daisy-chain system will then get an upboost due to momentum exchange. Active drag cancellation by a thruster on the platform would require about 100 kg propellant per day of mission extension. Alternatively, an electrodynamic tether system on the top probe, including solar panels and power supply with a mass of about 300 kg could provide sufficient Lorentz thrust to maintain altitude and can extend the mission by months (Section 2.2.2).

A preliminary trade-off has been made to select tether diameter and material. The trade-off takes into account survivability for the tether exposed to atomic oxygen and micrometeoroids, lifetime in the presence of atmospheric drag, while limiting mass and complexity. The lower tether segments should be very thin yet resilient. They could consist of a single strand 0.3-0.5 mm tether of oriented PTFE (Teflon) or quartz. For the upper tether segments a Kevlar or Dyneema double-strand caduceus tether could be used (Section 4.3.1).

The main advantage of LADDERS over the Daisy Wheel is that the probes can be very simple. Instrumentation can be oriented in yaw direction towards the gas flow using aerodynamic torques, assisted by magneto-torquers. Pitch and roll can be handled by the torque from tether tension.

Solution without tethers: probing from GTO

From a highly elliptic orbit it is possible to enter the lower atmosphere region multiple times over a sustained period. A suitable orbit to make deep dips into the Earth thermosphere is the Soyuz GTO (200 x 35786 km). Contrary to the dynamic wheel concept there will be virtually no planar phase shift for subsequently released satellites. However, the perigee height, and linked to that the orbital period, can be selected differently for each satellite. In the apogee of such a GTO, a change in perigee altitude of 10 km is obtained by a ΔV of approximately 1 m/s. The ΔV required for this mission is about 6 m/s and can thus be accomplished with simple springs. The interesting altitude region (135-250 km) to acquire data will be passed by the satellites within approximately 6 minutes of a total orbital period of 10.5 hours. In this time, a slice of atmosphere of about 500 km length can be examined.

A release strategy that maximizes the amount of vertically synchronized measurements is as follows. In the first orbit, the first satellite is ejected with the weakest springs and gets into the highest orbit. It is the first of the set to pass perigee. The time between subsequent releases is such that the interval between the passes through the atmospheric target column remain well within a typical time scale for atmospheric change. In the orbits to follow the measurement delay will at first decrease, because a lower satellite orbits faster and overtakes the higher ones. A rule of thumb for the GTO orbit is that a difference in perigee of 10 km will lead to a difference in orbital period of 12 seconds.

Assuming an acceptable delay time of hundreds of seconds, acquiring nearly-synchronized vertically spaced data will thus only be accomplished for several orbits. By applying a small ΔV in apogee of less than 3 m/s using a small cold gas system, the lowest satellite could be brought into an orbit higher (and slower) than the other ones and vice versa, in order to extend the multi-point coordination. In any case, the satellites can be designed such that they will keep operating and thus can still continue gaining single data points that, though not simultaneous, provide a useful long-term complement to the coordinated measurement data-sets collected in the first few days.

The real value of this concept, over the Dynamic Wheel, is the excess energy, which allows far more low-perigee passes (and far lower altitude perigee passes) before re-entry. The

disadvantages are the difficulty of managing the orbits to get complementary traverses and the small amount of time spent at perigee.

Comparison

Table 8 summarizes the findings. The Dynamic Wheel mission time is limited to days without reboost and up to 1 month with reboost; the individual satellites need to be rather complex. LADDERS mission time is limited to days but can feature very basic probes. Its tether operations are more complex however. The mission can be extended with the help of an electrodynamic tether and further added complexity. The GTO satellites provide coordinated traverses for only a few days and less than one hour of relevant mission data. Further data of the individual satellites can be collected for months thereafter, at the cost of additional satellite capability, to deal with the longer mission duration and higher exposure to radiation. Furthermore, since GTO orbits typically have a low inclination, the atmosphere can only be studied at equatorial latitudes. Also for other highly elliptical orbits there is a limited range of latitudes within which the relevant altitude interval of 150-250 km is visited. For a Molniya-type orbit with 150 km perigee, for example, this range remains below 30 degrees - the exact value depending on inclination and argument of perigee.

The final selection should be driven by a proper analysis of scientific user requirements. From above comparison the LADDERS concept seems most promising if the tether operations can be dealt with. The GTO and Dynamic Wheel options are more straightforward and low-risk in terms of deployment, but the satellites need to be more capable than the LADDERS probes. Compared to the GTO option, the Dynamic Wheel provides wider coverage within a shorter mission time. More generally, the Dynamic wheel concept can be used to efficiently, and based on only a single launch, distribute within an orbital plane multiple small satellites without propulsion.

Concept	**Lifetime**	**Synchronous measurements**	**Fraction of time in region of interest**	**Ground coverage**	**Probe simplicity**	**Tether simplicity**
Dynamic Wheel	weeks	+/-	>0.5	+	-	+
LADDERS	days	+	1	+/-	+	-
LADDER electrodynamic	years	+	1	++	+	--
GTO release	months	-	>0.01	-	+/-	*no tether*

Table 8. *Qualitative comparison of lower thermosphere investigation concepts with 6 probes.*

3.1.4 Artificial gravity

The need for MARS-g

Artificial gravity in orbit, through structural rotation, is the only known and most direct method that can be expected to fully prevent the known consequences of long-term exposure to weightlessness [Lansdorp 2003.I]. After residing in zero-g for half a year, the

Martian gravity may proof too much for the weakened astronaut bodies to perform effectively [Hall 1997]. Furthermore, if a crew member should fall ill during the trip to Mars, he can not always be treated properly as some common medicines like antibiotics have little or no effect without gravity [NASA 2001]. Finally, it is not yet known how the human body will respond to a reduced gravity level like that on Mars. Some negative and chronic effects to the human physique known from weightlessness experiments may persist under a martian gravity level. It may be unwise to leave humans on the surface of Mars for a sustained period of time.

Thinkable ways to mitigate the consequences of zero-g during transit could be through medicine, a man-rated centrifuge within the habitat, or a habitat which is part of a giant centrifuge. So far, medicines can only partially mitigate the symptoms and some not at all. The small man-rated centrifuge inside a spacecraft is uncomfortable and the periods spent in it are necessarily limited. Typical disorienting effects in a centrifuge are Coriolis force, gravity gradient and gyroscopic cross-coupling. A tether system however may yield a lightweight solution to rotate the whole habitat with a radius large enough to provide a comfortable environment.

It is unlikely that an interplanetary flight would be undertaken without a demonstration in Low Earth Orbit (LEO). A LEO precursor to interplanetary travel can be used to help understand effects of simulated gravity on human physiology (i.e. by having a rotating reference). The effects on human physique, psychology and performance of living and working in a reduced gravity environment such as on the surface of a planet can also be studied. Ideally a LEO research facility would provide the full range of artificial gravity levels from the benchmark case of one-g down to lunar-*g*. The optimal artificial gravity level during transit can then be selected. It is assumed that the LEO test facility should be able to spin and despin multiple times, retract the tether for crew access and perform a succession of different gravity levels. These requirements are significantly more demanding than those for an operational artificial gravity system for transit to Mars [NASA 1997].

The purpose of the analysis presented here is to evaluate whether indeed the tether system development challenge and the projected system mass is likely to be a show-stopper for manned missions to Mars. The tethered artificial gravity solution for a man-rated test facility in LEO presented here is dubbed "MARS-g" (Manned Antecedent for Reduced and Simulated Gravity).

The comfort zone

The artificial gravity level experienced in a rotating system is determined by:

$$\alpha g = r\omega^2 = \frac{v_{rim}^2}{r} = v_{rim}\omega \tag{3.2}$$

where the system's angular velocity is ω, rotational radius is r and $v_{rim} = r\omega$ is the velocity of the point around the center of rotation The gravity level as a fraction of terrestrial level is expressed by the ratio α : α_{Earth}=1.0, α_{Moon}=0.165 and α_{Mars}=0.381.

Table 9 provides a number of expressions and derivations for side effects and variations of artificial gravity that can be experienced as disorienting or otherwise uncomfortable by occupants of the MARS-g system [Clark 1960, Hill 1962, Gilruth 1969, Stone 1973, Cramer 1985, Lansdorp 2003.II]. For comparison the effects are expressed, for a given artificial gravity level, in terms of single possible design parameters, v_{rim}, r and ω. The acceptable limit levels are subject to interpretation and based on the quoted references and below discussion.

Eq.	Side effect	Description, effect on artificial gravity	Estimated acceptable level	Relationship
1	Radial gradient	Difference at $r+\Delta r$ relative to r	0.05	$\frac{\Delta r}{r} = \frac{\alpha g}{v_{rim}^2} \cdot \Delta r = \frac{\omega^2}{\alpha g} \cdot \Delta r$
2	Motion effect	Variation due to tangential velocity v_t relative to standstill	0.08	$\frac{(v_{rim}+v_t)^2 - v_{rim}^2}{v_{rim}^2} = \frac{v_t}{v_{rim}}\left(\frac{v_t}{v_{rim}}+2\right)$ $= \left(\frac{v_t}{\sqrt{\alpha g}}\right)^2 \cdot \frac{1}{r} + 2 \cdot \left(\frac{v_t}{\sqrt{\alpha g}}\right) \cdot \frac{1}{\sqrt{r}}$
3	Coriolis effect	Sideways acceleration due to radial velocity v_r relative to standstill	0.08	$\frac{2 v_r \omega}{\alpha g} = 2 \cdot \left(\frac{v_r}{\sqrt{\alpha g}}\right) \cdot \frac{1}{\sqrt{r}} = 2 \cdot \frac{v_r}{v_{rim}}$
4	Cross-coupling	In case of rotation rate $\dot{\varphi}$ perpendicular to ω there is a gyroscopic angular acceleration perpendicular to both	0.42 s^{-2}	$\dot{\varphi}\omega = \dot{\varphi}\sqrt{\alpha g} \cdot \frac{1}{\sqrt{r}} = \dot{\varphi}\frac{\alpha g}{v_{rim}}$
5	Cyclic variation	Relative variation per rotation due to Earth gravity gradient effects	0.01	$4.5\left(\frac{\Omega}{\omega}\right)^2 + O\left(\frac{\Omega}{\omega}\right)^4 \approx 4.5\left(\Omega \frac{v_{rim}}{\alpha g}\right)^2 = 4.5\frac{\Omega^2 \cdot r}{\alpha g}$
6	Crew safety	Altitude difference in case of tether scission	200 km	$4\frac{v_{rim}}{\Omega} = 4\frac{\sqrt{\alpha g}}{\Omega} \cdot \sqrt{r} = 4\frac{\alpha g}{\Omega} \cdot \frac{1}{\omega}$

Table 9. *Limitations and relationships for artificial gravity side effects*

In a rotating system a relative change will be experienced when varying the distance to the center of rotation by Δr (Table 9.1). This change should be kept within limits for scientific purpose, as subjects can spend time at different radii within the habitat, and therefore experience slightly different g-levels over time. Study results should be valid for the nominal gravity level within a certain margin. Furthermore, radial gradients within the

human body can cause internal stresses and disorientation and 'tidal effects' if the body changes orientation. Little is known about long term effects, but it seems that on the scale of the habitat or a human body, a 5% variation would be clearly noticeable and should be avoided. This puts a direct minimum on system radius, albeit not a very stringent one.

An effect not previously considered in the referenced literature is the variation in gravity experienced by an occupant moving at velocity v_t in tangential direction within the MARS-g habitat (Table 9.2). The acceptable level of variation is 8%, as adopted from elevator design parameters [Lansdorp 2003.II], considering a typical velocity of 1 m/s. Crew inside a habitat model can be considered significantly more active and prone to disturbing forces compared to passengers in an elevator, who are generally immobile and spend little time there. Limiting the motion effect means setting a lower limit to the rim velocity.

The Coriolis acceleration, well-known from centrifuge tests, will mostly cause disorientation and motion sickness, as well as disturbing tangential accelerations when moving in radial direction (Table 9.3). To account for relative disturbance compared to the gravity level, a similar limit is used as for the motion effect. Even if these levels are physically bearable, even much smaller variations (1 %) compared to the background gravity level would likely affect the motor control and manual precision that an inhabitant can achieve. One could also argue for an absolute constraint on such acceleration, as the accelerations perpendicular to the direction of motion affect directly the sense of orientation. Such an absolute constraint could be directly applied to the angular rate ω of the system.

The cross-coupling effect depends on $\dot{\varphi}$, the angular velocity of the occupant's head perpendicular to ω (Table 9.4). Also cross-coupling effects can be limited by an absolute constraint on the system angular rate. These effects cause acceleration or torque in a non-intuitive direction when for example turning one's head, or when handling a large object. Human performance studies generally put a limit for human comfort at 4 rpm [Hill 1962].

If the system rotates in LEO and in the orbital plane, there will be a variation in artificial gravity level, as a result of Earth gravity gradient effects, reaching a maximum at vertical orientation of the system (Table 9.5). Contributions are the gravity gradient effect (see Eq. 2.7) and variation in centrifugal force due to variation in the system's angular rate as a result of the action of the Earth's gravity gradient (as in Eq. 2.16). A minimum on the allowable angular rate can be derived from this, which turns out to be a not very strict requirement.

Finally, a maximum rim velocity may be introduced for safety reasons, as in case of accidental tether scission, the habitat may reach a significantly different altitude (Section 2.2.1). It should be avoided that the habitat in such a case will approach the atmosphere or altitude increase will be such that safe crew return would be made impossible (Table 9.6).

An envelope of these limits can be created (Figure 22), named the comfort zone. Even though the limits as discussed are not conservative, the envelope is tighter than those set in previous work, as summarized by Hall and revisited by Lansdorp, Kruijff & Van der Heide

[Hall 1997, Lansdorp 2003.II]. This difference is in particular due to the rim velocity limitation. It can be seen from Table 9 that for a certain level of gravity (indicated as *Moon*, *Mars*, *Earth* in Figure 22), the significant side effects (i.e. excluding the cyclic variation effect) improve with increased radius and, alternatively, with increased v_{rim}.

Note that the crew safety improves as radius and rim velocity *decrease*. In order to maintain a feasible comfort zone, crew safety considerations will drive a trade-off between launch cost and crew return capability versus minimal mission altitude. An altitude of 400-500 km seems sensible.

Limits arising from radial gradient, cross-coupling and absolute Coriolis levels approach the boundaries of the envelope near the Earth gravity design point. Although the definition of acceptable comfort levels remains subjective, its objectivity is increased near this particular design point, because at least at levels near Earth gravity data is available from ground-based research on human subjects. Therefore the comfort zone as in Figure 22 is adopted for the MARS-g design.

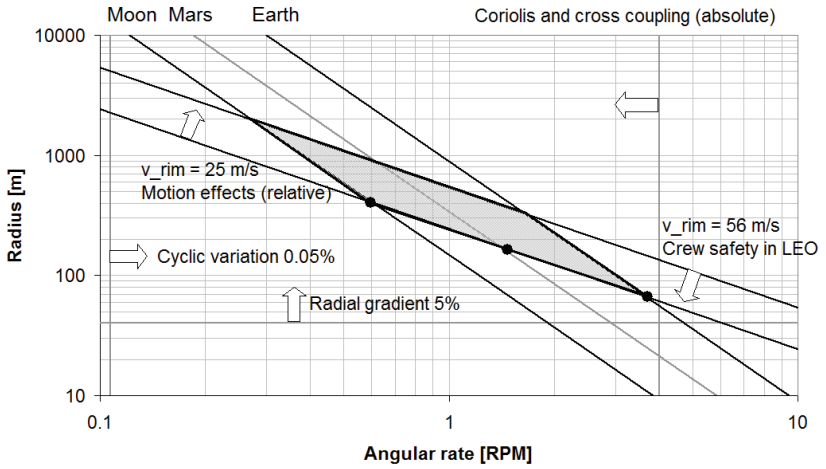

Figure 22. *Revised comfort zone for artificial gravity in Low Earth Orbit, arrows indicate the direction of improved condition; note that* $v_{rim} = r\omega$.

From analysis of Figure 22 the design points for the three gravity levels can be selected. If a single system is to be designed that can generate all three gravity levels, it would be of interest to be able to reel the tether in. When gravity level is to be increased, the ability to reel in the tether would keep the radius minimal - while remaining within the comfort zone. The minimal radius reduces the amount of tether exposed to the higher artifical gravity levels such that total tether mass can be reduced. Furthermore, propellant for spin-up and spin-down can be saved by selection of the minimal rim velocity at each gravity level, which, as can be seen in Figure 22, is equivalent to a design for minimal radius. The design points Moon, Mars and Earth are indicated with radii ranging from many tens to hundreds of meters. Perhaps counterintuitively, the preferred rotational radius increases for decreasing g-levels.

All operations will be carried out at a minimized rim velocity of $v_{rim,min}$ = 25 m/s. The MARS-g design will be driven for tether strength by the Earth level at radius $r_1 = v_{rim,min}^2/(\alpha_{earth}g)$ and for tether length by the lunar level of gravity at radius $r_2 = v_{rim,min}^2/(\alpha_{moon}g)$.

MARS-g system concept

For the MARS-g module design, Lansdorp has performed a trade-off [Lansdorp 2003.I], from which tentative system dimensions can be derived. The system is proposed to consist of a manned module and a countermass module, connected by a tether system. For the purpose of the design exercise, the manned module could be an inflatable module (e.g. Transhab-type, Bigelow Aerospace [Lansdorp 2003.I, Sorensen 2005]). Its mass, M_a, is estimated at 40 tons. The artificial gravity experienced is generated as a function of the distance from the rotating system's center of mass (radius r), which relates to the system dimension L by ratio of endmasses. A heavy countermass increases the effective radius for the manned module. To reduce cost, this unmanned countermass should however be preferably an expendable, already available in orbit, such as an ATV loaded with waste. Based on these considerations, the countermass M_c is assumed to weigh 25 tons. An advantage of the ATV as countermass is that it can be active and provide spin-up thrust (Figure 23). This system leads to a tether dimensioning as presented in Table 10.

The MARS-g system dimension of 1017 m is large compared to the largest beam structure in space. For comparison, the main truss sections of the International Space Station stretch about 100 m. However, design load levels for the MARS-g system are many orders of magnitude higher than for the ISS. A tether therefore presents itself as an enabling solution.

	g level (9.81 m/s^2)	**Rotational radius [m]**	**System dimension (*Ma/Mc = 1.6*) [m]**
Earth g	1	64 (r_1)	166
Mars g	0.38	167	434
Lunarg	0.16	391 (r_2)	1017

Table 10. *Rotational radius 25 m/s rim velocity*

The MARS-g tether deployer shall include reel-in capability. Although it will result in a more complex system, as already explained, tether mass and propellant required for a single spin-up will be reduced. Furthermore, a reeling capability will allow for conventional crew docking and access to the countermass module. A tethered endmass, even if the system is not spinning, will not be in traditional Keplerian orbit. Therefore, in between two experiments at different g-level, it is assumed that the spin is stopped and the tether is reeled in.

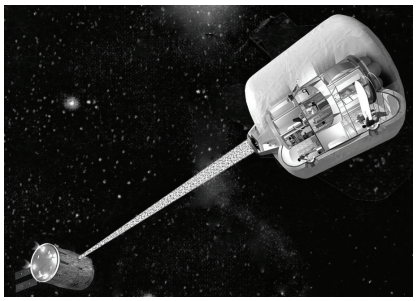

Figure 23. *MARS-g concept*

Spinning up the system, propellant and tether mass

Both propellant mass and tether mass required are dependent on the approach to deployment and spin-up.

It was investigated to spin up the tether without use of any propellant, based on conservation of angular momentum, by deploying the tether, next inducing a swing -much as in the SpaceMail application (Section 3.1.1)-, then converting this swing into rotation by rapid tether retrieval. This solution was found not feasible for the reel system design due to the required retrieval velocity, about 1 m/s at a power of 500 W [Lansdorp 2003.I].

Another method for spin-up requiring little propellant and a smaller retrieval velocity would be to increase the spin rate by phased pumping, i.e. reeling in near vertical orientation and reeling out near horizontal orientation. This method requires about 10 days to spin-up even with demanding system design parameters, namely a 0.4 m/s reel-in capability and a 3 kW power consumption.

It is therefore proposed that a conventional thruster is used that exerts a torque around the center of mass of the system. With exhaust velocity w, burn time Δt and the amount of propellant required m_p, the thrust equals $m_p/\Delta t\ w$. The torque induces an angular acceleration that can be maintained until the required rim velocity is achieved. The most efficient way of spinning up the system is obtained when the effective arm of the thrust is maximized. As $M_c < M_a$, the thruster should be placed at the countermass.

The minimum mass of the tether is determined, given a material's break strength σ and design safety factor F_S, based on the minimal allowable cross-sectional area for each section of tether and thus based on the maximum load experienced by those sections:

$$m_t = \int_0^L \rho A(L)dL = \rho\left(1+\frac{M_a}{M_c}\right)\int_0^{r_{\max}} A(r)dr = \rho\left(M_a+\frac{M_a^2}{M_c}\right)\frac{F_S}{\sigma}\int_0^{r_{\max}} g_{\max}(r)dr\,, \qquad (3.3)$$

in which the maximum distance from the center of mass to the habitat $r_{max} = M_c/(M_a+M_c)\ L$, $A(r)$ is the cross section of the tether at any point, and $g_{max}(r)$ the maximum gravity level that any point on the tether experiences. This level is dependent on the selected method of system spin-up.

Table 11 and Table 12 compare the propellant and tether mass requirements for three deployment and spin-up strategies. In this and the following calculations, the effect of the mass of the tether itself is neglected because it is found to be very small compared to the endmasses.

1. The simplest strategy, the "Single Length" method, would be to deploy the tether to achieve $r_{max} = r_2$, the radius required to satisfy the rim velocity requirement even at minimum gravity level α_{min}g, then accelerate the endmass to obtain the required artificial gravity level, following a horizontal line in the comfort zone (Figure 22), towards a greater rim velocity $v_{rim} > v_{rim,min}$ at constant radius $r = r_2$ as in Eq. 3.2. Neglecting the tether mass and reduction of manned module mass due to ejected propellant, we can derive m_p (Table 11.1). The tether mass is determined from Eq. 3.3 with $g_{max} = \alpha_{max}g$ applicable to the full tether length (Table 11.2).

2. A strategy that will be more fuel efficient is the "Minimal Rim Speed" method. In this scenario, the system is operated at minimum rim speed $v_{rim,min}$ for every target artificial gravity level. It is spun-up only after the tether length matching the required artificial gravity level and minimum rim speed has been achieved by deployment or retrieval. As in the Single Length method, an important advantage is that the required deployer would not have to carry high structural loads: the deployment loads and structural forces during rotation can be decoupled. Propellant mass is independent of the artificial gravity level per mission (Table 11.3). The mass of the tether is determined for a basic part of the tether for maximum gravity (equivalent to r_1) plus a tapered part for lower gravity levels (Table 11.4).

3. A final alternative that is considered is the "Overdeployment" method. The tether is deployed to a radius $r_3 = k\ r_2$, with the overdeployment factor k>1. An especially tuned but low angular velocity will be introduced by the thrusters. While rotating, the tether will be retracted to reach the desired end situation prescribed by the limits of the comfort zone, using the principle of conservation of angular momentum to increase the angular velocity and artificial gravity level. The final rim speed is, as in the Minimal Rim Speed method, again the minimal rim speed $v_{rim,min}$ required for comfort. The initial rim speed $v_{rim,0}$ relates to the final rim speed $v_{rim,min}$ as the final radius to r_3, from which the required propellant mass can be determined (Table 11.5). Main disadvantage of this alternative deployment strategy is the fact that a high tension tether retrieval system is required and spin-up/spin-down operations will take about 1.5 days. For the section of the tether from $r = 0$ until $r = r_2$ it can be reasoned that the optimal tether diameter will be identical to that of the Minimal Rimspeed tether. Additional tether mass results only from the additional tether length required for overdeployment and retrieval. During retrieval from r_3 to r_2 the g level increases. Integration of Eq. 3.3 from $r=r_2$ to $r=kr_2$ leads to the total tether mass (Table 11.6).

Strategy (radius)	**Eq.**	**Propellant mass**	**Eq.**	**Tether mass**
Single Length (r_2)	1	$M^* \frac{v_{rim,\min}}{w}\sqrt{\frac{\alpha}{\alpha_{\min}}}$	2	$\rho\left(M_a+\frac{M_a^2}{M_c}\right)\frac{F_S}{\sigma}v_{rim,\min}^2\frac{\alpha_{\max}}{\alpha_{\min}}$
Minimal Rim Speed (r_1 to r_2)	3	$M^* \frac{v_{rim,\min}}{w}$	4	$\rho\left(M_a+\frac{M_a^2}{M_c}\right)\frac{F_S}{\sigma}v_{rim,\min}^2\left(1+\ln\left(\frac{\alpha_{\max}}{\alpha_{\min}}\right)\right)$
Overdeployment (r_1 to r_3=kr_2)	5	$M^* \frac{v_{rim,\min}}{w}\frac{\alpha_{\min}}{k\alpha}$	6	$\rho\left(M_a+\frac{M_a^2}{M_c}\right)\frac{F_S}{\sigma}v_{rim,\min}^2\left(1+\ln\left(\frac{\alpha_{\max}}{\alpha_{\min}}\right)+\frac{1}{2}\left(1-\frac{1}{k^2}\right)\right)$

M^* depends on the location of the thruster, respectively at M_a or (baselined) M_c: $M_a^* = M_a + \frac{M_a^2}{M_c}$, $M_c^* = M_a + M_c$

Table 11. *Propellant and tether mass relationships for likely deployment methods*

Mass case (propellant for spin-up+down or tether)	**Single length [kg]**	**Minimal Rim Speed [kg]**	**Overdeployment [kg]**
Propellant α_{moon}	930	930	190
Propellant α_{mars}	1420	930	80
Propellant α_{earth}	2300	930	30
Tether mass (for range α_{moon} - α_{earth})	1140	520	610

Table 12. *Mass comparison for likely deployment methods (see text for assumptions)*

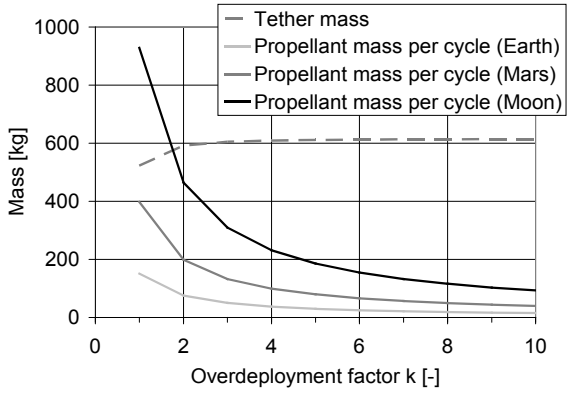

Figure 24. *Impact of Overdeployment on MARS-g propellant and tether mass*

Comparison

A comparison of the mass properties resulting from the different deployment strategies is provided in Table 12. Assumed parameters values are $w = 3500$ m/s at M_c, $\rho = 536$ kg/m^3, F_S=6, σ=1.13E9 N/m^2, $k = 5$, $v_{rim} = 25$ m/s. Note that the values in Table 12 refer to the required propellant for a spin-up plus spin-down cycle and to a tether capable to deal with the full range of α_{moon} -α_{earth}. For comparison, the total mass required for tether plus propellant to obtain only an α_{mars} g-level only once (as may be considered for a manned mission to Mars), is only 230 kg. From the dependency of mass on the overdeployment factor k (Figure 24) it is seen that the additional tether length does not add significantly to the system mass, because the additional tether experiences only little stress. The mass gain of the overdeployment method with respect to the more simple alternatives is significant, and even more so for the likely case that multiple spin-ups and spin-downs will be performed.

It should be noted that in an actual application in LEO, and in particular for the Overdeployment method, the deployment and spin-up strategy described above are somewhat oversimplified. Rim velocity will vary during the initial retraction period due to the action of the gravity gradient (Figure 1). For an in-plane spin-up from a vertically deployed tether in LEO, an initial speed $v_{rim,0} > \sqrt{3}\Omega r_3$ is required in order to end-up in a rotation rather than an oscillation (Eq. 2.10). On the other hand, much of the initial rim velocity can in principle be obtained from the swing obtained during deployment, saving some propellant. To make full use of this possibility would require selection of an optimal value for k value for each g-load case, and a more critical deployment control. The α_{earth}g-level would be obtained with $k = 2.2$ (max. 70 kg propellant rather than 30), α_{mars} with $k = 3.6$ (max. 110 kg propellant mass rather than 80 kg). Alternatively, an out-of plane rotation can be considered with free choice of k. Stability and dynamics for this case have not yet been investigated. The tether mass is heavily dependent on the minimal rimspeed selected, but for a multi-mission scenario it is not the dominant factor. The Overdeployment method is therefore baselined for the initial design of a suitable deployer.

Tether and deployer

A tether and deployer design for a LEO demonstrator has been made for Delta-Utec by Lansdorp [Lansdorp 2004] based on the Overdeployment scenario. The tether is assumed to be made of Dyneema®, a high strength fiber produced by DSM in the Netherlands. The tether is proposed to be a very flat tether of ~1 mm thickness and ~1 m width. Such a "Dyneema UD" tether can be produced using standard sheet production methods (operational at DSM). It is a safe-life design to prevent serious damage by space debris and meteoroids and is compatible with the proposed deployer, as it provides a large area of contact, thus reducing pressure loads. Dyneema® has a fiber tensile strength of 3.9 GPa and a density of only 975 kg/m^3. Because of losses in the UD design[2], it will have a tensile strength of 1.3 GPa and a density of 634 kg/m^3. A safety factor $F_S = 6$ for the tether was chosen as the product of a number of contributions [Lansdorp 2003.II], see also Section 4.3.4. Resulting total tether mass is 622 kg.

[2]C. Dirks, M. Jacobs, J. Kersjes, Personal correspondence, Meeting at DSM, Heerlen, the Netherlands, 2003.

The tether deployer has the task to reel the tether in and out, before and after each crew swap. The requirements on the deployer are quite severe. The selected deployment strategy demands that it must reel the tether while artificial gravity is being generated by the rotation of the system. The most severe conditions occur during the one-g mission: the tension in the tether, just before the reeling phase is over, equals 400 kN, comparable to the performance of a medium sized crane. An unconventional deployer design is proposed to simultaneously meet the requirements of high tension and low mass. A system has been worked out for which no tribology or transmission is required. Instead a solution with structural hinges is proposed and high force linear translators are used. The storage system is always decoupled from the tether tension. Figure 25 illustrates two separate sets of flat friction plates that automatically squeeze the tether when tension is applied, a so called self-braking structure. As one pair of plates is squeezed and moves the tether in the desired direction, the other pair moves in position to take over. The reel that collects the tether is in this way not exposed to a (significant) tether load and can be lightweight. A first design of the deployer indicates that the deployer mass will be comparable to the tether mass, i.e. some 600 kg [Lansdorp 2004].

The MARS-g system combines comfort and capability of multiple deployment and retrievals under full g-load, with a mass of only some 3% of the total system, or some 2400 kg (based on 14 cycles). Propellant to maintain stability of the endmass is not included in this analysis.

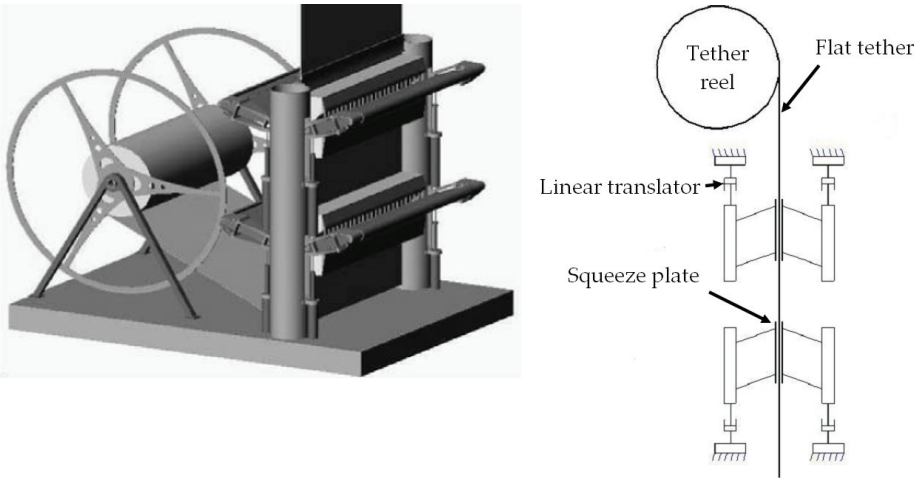

Figure 25. *Hingeless moving plate high-load tape deployer concept (see text)*

3.2 Electrodynamic deboost

Electrodynamic tethers are able to provide propulsion with little or no consumables, as they conduct electrical current and interact with a planetary magnetic field. If equipped with appropriate power supply, they can provide continuous thrust that can be modulated to change any of the orbital parameters [Cosmo 1997, Levin 2007]. These capabilities make

them attractive for demanding long term applications such as repetitive deorbiting of defunct satellites or atmospheric drag compensation of a space station.

Some uncertainties are to be resolved before such applications can be reliably implemented. Bare tether design and confirmation of electron collection performance is one aspect that will be described below. Beyond that, a crucial challenge for electrodynamic tethers is that of long-term stability, in particular with reference to light systems where electrodynamic forces may become comparable to gravity gradient forces. Simulations have been undertaken to find out how system design can help provide sufficient stability. Two example applications for relatively simple systems, without high voltage source, and thus oriented at deboost only, are studied in more detail. The effectiveness of an electrodynamic tether for mitigation of debris-related risk is critically considered. An application of an even simpler system is analyzed, a fully passive electrodynamic tether system, which may prove useful in orbit around Jupiter.

3.2.1 Assessment of OML performance in bare tether electron collection testing

No in-orbit data is available for long bare tether performance at this time. To support representativeness of the ETBSim simulations, a series of electron collection tests has been defined and performed [Kruijff 2001.I] with the following objectives:

- to test the validity of the OML theory,
- to assess orbital tether current collection capability from plasma, and
- to assess the applicability of the OML model to tethers with other than cylindrical geometry.

The approach applied exists essentially in measuring the I-V characteristics of several specimens of tethers, with various geometrical shapes and dimensions, exposed to a simulated space environment of ionospheric parameters. The specimens of various shapes and sizes are summarized in Table 13. This selection has been made to represent various design options: a simple cylindrical tether, a tape for increased mass efficiency and a dual-strand tether (for increased resistance against micrometeoroids and orbital debris). All samples are 10 cm in length, so much larger than the sample diameter. Each specimen has been placed between two guards of equal dimensions, such that the measurements are made in a cylindrical plasma geometry without significant edge effects. The experiments have been designed to investigate the impact on the current collection caused by perturbations due to both the ambient geomagnetic field and the magnetic field self-induced by the current flowing in the tether, neither of which is included in the derivation of the OML model. They are compared to those of Gilchrist e.a., who has performed electron collection tests on (unguarded) cylindrical and tape samples of 10-30 cm length, in a plasma generated by a Hall thruster, however without geomagnetic and self-induced field effects [Gilchrist 2002].

The large plasma chamber facility of IFSI-CNR has been selected as a suitable facility for the proposed tests. The tests were designed, performed and analyzed by F. de Venuto & G. Vannaroni [Kruijff 2001.I], the results are summarized here.

Type of electrode	Dimensions
Single wire	Diameter 0.8mm
Single wire	Diameter 2mm (with current carrying wire in center)
Bifilar wire	Diameter 0.8mm, center-to-center 2.8mm
Tape	Width 3.6mm, Thickness 0.05mm

Table 13. *Dimensions of tether samples used in the plasma tests*

Test chamber geometry and conditions are provided in Table 14 and Figure 26. The Debye length λ_D is a fundamental plasma scaling parameter in terms of which the OML validity can be expressed [Sanmartin 1999]. The test conditions can be considered typical for a Low Earth Orbit tether operation. Although the voltage bias applied (200 V) is lower than the typical potential of kilovolts for space applications, it is still highly suprathermal with respect to the energy of ionospheric electrons ($\cong 0.2$ eV), and therefore can be considered representative for the electron collection process in high potential regimes (see also Eq. 2.29).

The resulting I-V characteristics (Figure 27, Figure 28) show the collected current I_{exp} at the applied bias voltage V, normalized to the electron thermal current I_{th} (Eq.2.30), $I_{norm}=I_{exp}/I_{th.}$ Due to the proportionality of both currents with both plasma density n_{pl} and the electrode surface this normalization eliminates the effects associated to the plasma density variation resulting from the sample's current collection as well as the effects due to different dimensions of the various tether samples. Two curves (in solid lines) indicate the OML uncertainty (Eq. 2.29) due to the spread of the electron temperature. A first observation is that there seems to be a systematic tendency to exceed the predictions of the model. The discrepancy from theory can be approximately evaluated about 25%, the largest deviation being associated to the tape sample. The tape and multi-strand tethers have been initially oriented with minimum cross-section towards the plasma beam. When oriented perpendicular to the flow, the tape shows a 20% reduction in current, probably due to wake effects. Gilchrist e.a. observe quite a similar trend, with up to 15% increased collection efficiency with respect to OML above 50 V. They find however that the perpendicular tape collects 5-10% more than the parallel, possibly due to sample end effects, due to the lack of guards, or source drainage, which seems to particularly effect the parallel sample.

In any case, the OML does provide a good first guess estimate of electron collection performance, for all tested tether shapes, including tapes and multi-strand tethers, at least for a sample width less than or equal to $2 - 3\lambda_D$. A useful lesson from this is that multiple (n) wire tethers of diameter d can be treated (as far as electron collection is concerned) as a single wire of diameter $n*d$. Note that Gilchrist e.a. have performed tests to as much as $15\lambda_D$ tape width, and although some reduction in efficiency is observed, possibly due to source drainage, the results for these samples do not go more than 12% under the OML prediction at 300 V [Gilchrist 2002].

Facility	SIM.PL.EX at IFSI-CNR
Ambient plasma electron temperature	2000 K
Ambient plasma density	5e12 m^{-3}
Sample bias for I-V curve measurement	0 - 200 V
Ambient geomagnetic field B	0 and 0.3 e-4 T (orthogonal to both plasma flow and tether sample)
Debye length λ_D	~1.4 mm
Current for self-induced field test	0 - 10 A
Sample length	10 cm (plus 10 cm guard on either side)
Sample distance to plasma source	2.25 m
Plasma reference monitoring	Langmuir Probe for plasma density, electron temperature and plasma potential Retarding Potential Analyzer (RPA) for ion beam energy
Ion source	Synthesis A^+ accelerated to ~8 km/s
Electron source	Filament heated at thermoionic temperatures

Table 14. *Test conditions*

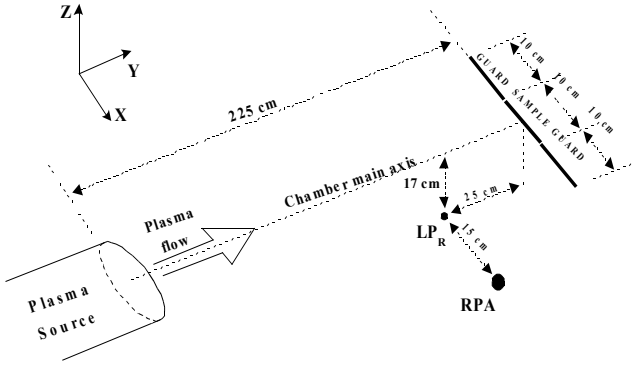

Figure 26. *Experimental set-up of plasma tests*

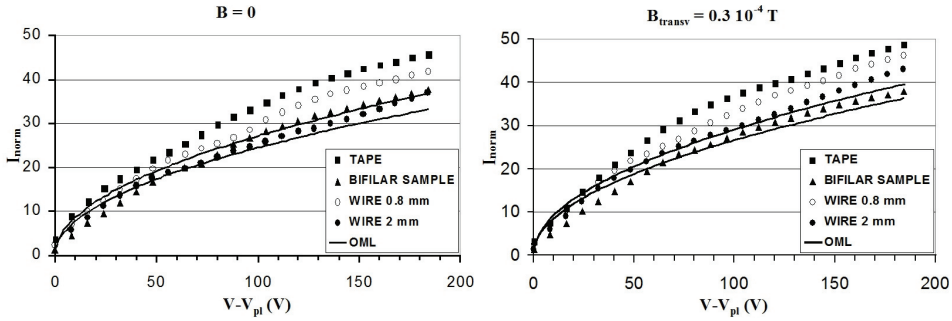

Figure 27. *I-V characteristics at B=0 (left) and B=0.3 10^{-4}T (right)*

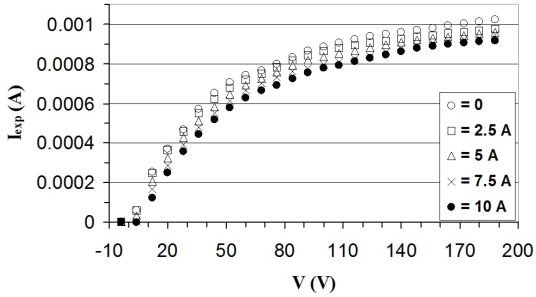

Figure 28. *I-V characteristics at various DC tether currents.*

The geomagnetic field is found to not perturb significantly the current collection from the plasma, which is plausible when considering that the electron gyroradius at LEO environmental conditions (about *5* cm) is appreciably larger than the cross-sectional dimensions of the tethers under test [Sanmartin 1999]. For large tapes (centimeter scale) additional tests are required, but in the SIM.PL.EX. facility such a large sample would lead to draining of the electron source.

As far as the self-induced field is concerned, the effect of self-inducing DC current has been tested in the 2 mm cylinder sample. A reduction proportional to the DC current is found of about 10% at its maximum level (10 A) corresponding to the maximum potential (190 V). Such a reduction is in line with expectations: the current produces a crossed system of magnetic and electric fields, causing an $\mathbf{E} \times \mathbf{B}$ electron drift along the tether that tends to reduce the collected current. For likely mission currents of 1 or 2 A this effect can be considered negligible.

3.2.2 Tethered deboost and dynamic instability

Occurrence of long term instability of electrodynamic tethers has been evidenced in numerical simulations [Estes 2000.IV], connected with the ProSEDS mission. It is found due to the longitudinal component of the magnetic field and increases with inclination. Several investigations [e.g. Levin 1987, Pelaez 2000.I,II, Dobrowolny 2002.I,II, Levin 2007] have been undertaken with the aim of clarifying the various underlying instability mechanisms for electrodynamic tethers. Energy is continually pumped into the system, which causes lateral oscillations and eventually tether slackness or uncontrolled motion. The long term instability severely limits mass-critical electrodynamic tether applications. For these cases it must be characterized and appropriately tackled, either by system design or by active control methods.

Dobrowolny developed a linearized analytical model, simplifying the environmental conditions and decoupling transverse modes from endmass librations [Dobrowolny 2002.I]. The modeled system is operating at maximum obtainable current level following OML theory. An instability is observed, as an exponential growth in transverse modes. Out-of-plane endmass librations, coupled to in-plane librations, show a wave-packet behavior. The result indicate that there is a maximum current level for stability.

For comparison, a simulation of the same system was performed by ETBSim, which is based on a more general, non-linear model (Section 2.3.2). The environment was initially set to match the Dobrowolny simulations, featuring a simplified dipole magnetic field and sinusoidal plasma density. As in Dobrowolny's findings, ETBsim produces in-plane and out-of plane endmass librations [Kruijff 2001.I]. General behaviour is similar, e.g. wave-packet modulation is recognized and the libration seems stable, although the amplitude and modulation period differ. These differences are thought to originate in several simplifications in the applied linear theory with respect to the numerical simulation, such as series truncation. In addition, cross-coupling between libration and transverse modes was found to be significant (e.g. Figure 30). At the integration timesteps used, it was found that the system becomes instable beyond numerical accuracy within about 2 weeks, although the libration mode is as yet hardly excited.

Fluctuations of electron density and magnetic field strength as they occur in orbit around Earth further worsen the situation. For a typical case (7 km, 1 mm bare tether, h=1000 km, i=50°, 700 kg and 15 kg endmasses) including also the ionospheric irregularities (IRI-95 model) and the Earth's 436 km magnetic dipole offset, ETBSim shows that within about a day's time, transverse waves severely affect tether tension, which does not occur without these effects.

These results trigger the question whether system design choices or other solutions can be identified that contribute to stability for the full duration of a typical electrodynamic tether application. Simulation results addressing a variety of design options are here described.

As a case study, a relatively simple deboost application has been selected, intended for satellites that have failed or completed their nominal mission ("defunct", Section 2.2.2). It is initially assumed that the tether endmass is deployed downward. The endmass contains not only a cathode but all active systems including the tether deployer itself. In this way the interface to the defunct satellite is minimized. The tether is assumed bare. Based on test simulations the following reference tether is defined (used for all simulations in this section unless specified otherwise):

- 6 km fail-safe mechanical part, 1.2 kg.
- 6 km fail-safe conductive part, built out of two strands bare aluminum (each 0.32 mm diameter, treated for $\alpha=\varepsilon=0.3$), two mechanical strands, total 5.3 kg.

Stability was investigated for tethered deboost of a defunct satellite of 700 kg at 700 km initial altitude and 11.5 degree inclination. A lightweight endmass of 15 kg has been assumed initially. As a practical, objective measure for instability, the (simulated) occurrence of tether slackness is proposed (i.e. zero tension), which is assumed to coincide with loss of control (Figure 33). This occurrence can be expressed in mission time, however the more pragmatic measurement used here, referring to the mission objective, is the drop in altitude achieved.

For the full range of parameter settings reported here, even at currents limited to as little as 0.2 A, the simulations showed a process of excitation of skip-rope (combination of first in-

plane and out-of-plane transverse modes). The tether eventually starts to resemble a whip with the light endmass on its tip, cyclically inducing tension shocks and further transverse waves, that finally cause the tether to become slack. Such behavior has also been noted during the simulations carried out for ProSEDS[3]. Consequently, all simulations show a nearly identical tension development, where only the onset of the instability differs in time from one simulation to another.

A typical example for the deorbit behavior is shown in Figure 29, which highlights the impact of inclination. The runs are stopped at occurrence of tether slackness. Shown is the in-plane transverse mode. It is measured in degrees as the angle from the line between endmasses to the line between defunct satellite and middle of the tether. At larger inclination the onset of instability is delayed due to the lower electrodynamic force resulting from a lower perpendicular magnetic component. Descent rate is also reduced for the same reason. Despite the fact that out-of-plane dynamics are more pronounced at higher inclination, the tether in such a highly inclined orbit achieves a somewhat greater altitude drop before instability occurs.

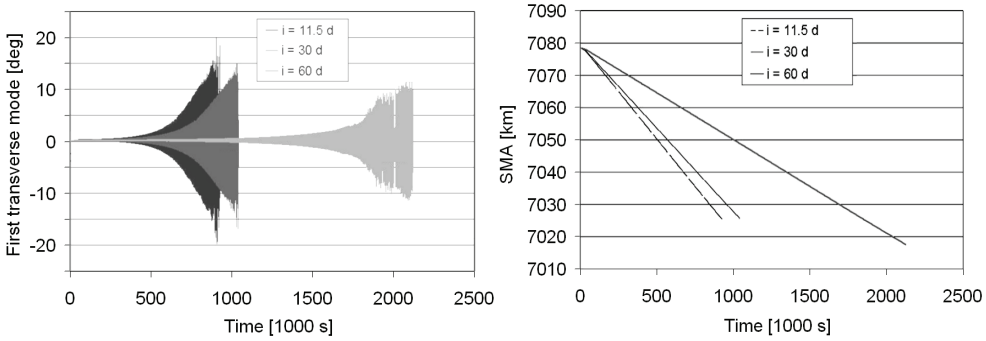

Figure 29. *Effect of inclination on stability (1st transverse mode and achieved SMA drop)*

Simple control laws do not reduce the onset of instability, due to the coupling between librations and transverse modes, as illustrated in Figure 30. A current control is applied to dampen the in-plane librations. The control is an anti-phased current modulation superimposed on a constant current (0.3 A), assuming perfect knowledge of the in-plane and out-of-plane angles (e.g. through GPS or phase reconstruction from tension measurements). Although the control is, briefly, effective in damping the in-plane libration, the first transverse mode is excited and eventually cross-excites the in-plane libration mode beyond control as well. Similarly when a current control is applied that dampens both in-plane libration and first transverse mode, the second transverse mode is excited, with similar disturbing results on the lower modes.

Note that in recent years Levin has developed a method based on tether modes and phase estimation that, although not able to fully subdue the instability appears successful at postponing it significantly [Levin 2007].

---

[3] Enicro Lorenzini, Private communications, February 2001

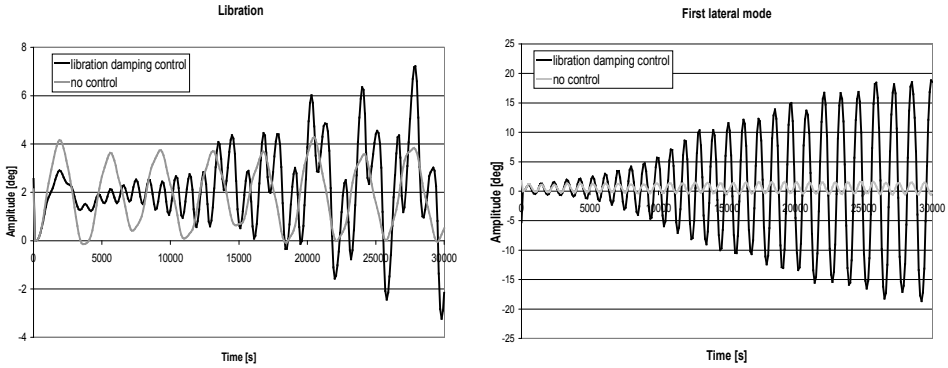

Figure 30. *Damping of in-plane libration (left) excites first transverse mode (right).*

In support of such active current control further design options were considered. Most of the system adaptations that tend to improve time to instability increase the ratio of tension (Eq. 2.16) versus Lorentz-force (Eq. 2.28), although not always the achieved altitude loss is improved as well.

Current limitation for example reduces the cyclic variation of the Lorentz force and of its distribution over the length of the tether. This is particular true if at a level sustainable by the lowest plasma density within one orbit. Most simulated cases ran at such a level, of 0.2 A. The current level can be increased as the orbit gets lower due to increasing plasma density, such that the deorbit rate improves. In the simulations, tether current is assumed limited by ohmic dissipation through a variable resistor near the cathodic end. Such a system has the advantage that, due to the ohmic voltage drop the tether will be negatively biased over a large part of its length (Figure 31). In the negatively biased section no electrons are collected, thus resulting in a nearly constant current over much of the tether length. Under such current limitation, additional bare tether length leads to simultaneous increase of both gravity gradient and Lorentz force. The fraction of tether that features constant current is also increased and simulations find stability improved.

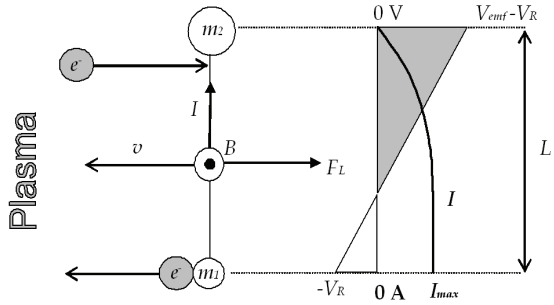

Figure 31. *Current limitation due potential drop* V_R *by resistor at cathodic end*

Increase of cathode endmass is a costly solution but contributes to stability improvement. If endmass and current are both increased by the same amount, as expected the system will still drop faster in altitude, but will also outlast the lighter, low-current reference system before instability occurs.

A mechanical tether segment has been included in addition to the conductive segment in the reference design. This has been done for two reasons. On one hand, it ensures a low deployment friction during the initial part of the deployment. Secondly, although inclusion of a mechanical tether segment represents some extra system mass, for the simulated application it increases the tension and system's passive long-term stability more effectively than an increase of endmass by the same amount would do.

An even more effective use of extra mass is achieved when the tether is deployed *upward*, with a dummy endmass -the extra mass required for this concept-, whereas the cathode, deployer and electronics remain at the defunct satellite, now the lower end of the tether system. In such a case, for a bare tether or mechanical/bare tether combination, the torque arm around the center of mass (near the defunct satellite), available to the resulting Lorentz force, is reduced. The case presented in Figure 32 is based on the reference 12-km tether with a 15-kg endmass limited at 0.2 A. This adapted system is eventually destabilized when the second transverse mode overexcites. Note that it was found that the electrodynamic tether needs not to be deployed accurately to a vertical. A non-zero in-plane angle before cathode activation has no negative impact on stability.

Finally, as an alternative way to maintain stability, a prograde rotating tether system has been proposed (see also Section 3.2.4). To achieve the desired system spin, the 15 kg endmass needs to be provided with an initial ΔV of about 30 m/s against the direction of orbital velocity. The spin-induced centrifugal force will increase with time as the spin accelerates due to the Lorentz torque and this increase helps to maintain stability. The spinning tether solution will operate on the average at a 30% of the Lorentz force of a vertical tether, due to the unfavorable angle of the tether with respect to the magnetic field lines during much of the spin. If a second cathode is added on the opposite side of the tether, this fraction is increased to about 60%. The additional complexity and loss in Lorentz force may be compensated for since current limitation is no longer required.

Apart from these measures that directly affect the balance of Lorentz force and tension, more subtle design trade-offs, such as for tether material properties, can have a significant effect as well. A low stiffness/viscosity ratio has been found to be specifically powerful for postponing instability, Figure 33. Note that a significant effect of tether internal (Coulomb) damping as evidenced by TiPS [Barnds 1998] will likely have a beneficial effect on stability also if there is no spring-mass oscillation, but is not represented by ETBSim.

Some non-trivial effects are reported in [Kruijff 2001.I]. It is for example found that tether cooling that occurs during the eclipse period of an orbit has a favorable effect on stability. A decrease in ohmic resistance due to tether cooling balances the negative effect on current collection as a result of the decreased plasma density on the eclipse side of the Earth. The equilibrium temperature of the tether depends on the ratio of optical properties α and ε (Eq.

4.30). A ratio of α/ε close to 1 with low values both for α and ε, for gradual temperature change, will further increase the system's passive long-term stability.

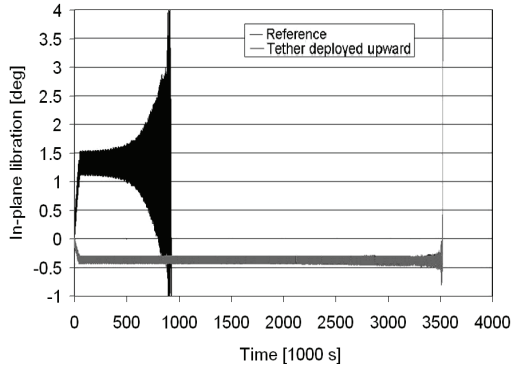

Figure 32 *Cathode location impact on stability (in-plane libration), Reference has the cathode on the endmass, deployed downward*

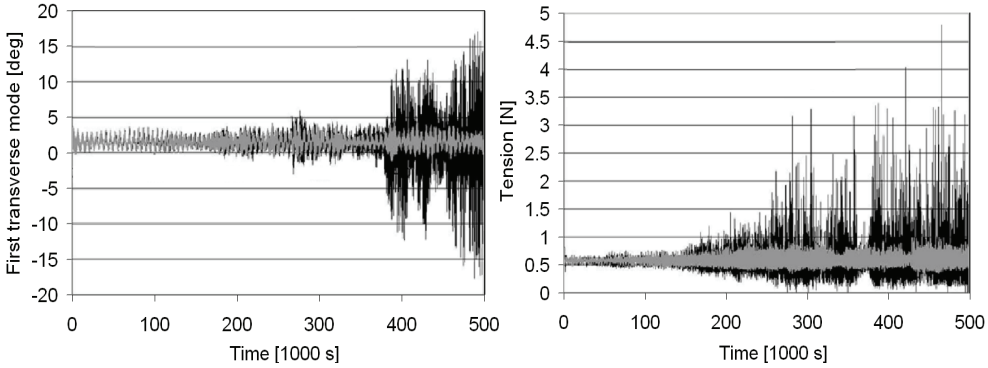

Figure 33. *Effect 16-fold decrease stiffness/viscosity ratio on transverse mode and instability (gray).*

With the toolbox of possible measures described here tether oscillatory behavior can be constrained during the duration of the deboost. Table 15 provides an overview. The most effective system design tools are system spin-up, upward deployment direction of the endmass, increase of endmass and mechanical tether length, selection of a proper current level that can be maintained over tether length and time, high viscosity and low stiffness.

Note that when the high plasma-density ranges of the ionosphere are reached, below 600 km, it is no longer recommended to use a tether for deorbit, rather disconnect the tether altogether (Section 3.2.3). A deboost with limited current takes up to a month, during which active collision avoidance may be required, e.g. by ground control of descent rate. The benefit of a release at this altitude is not only that total collision risk is reduced but also the requirement for maintaining stability. This less ambitious approach in fact makes the tethered deboost application both more safe and more practical.

Parameter	Finding
System spin (centrifugal force)	Requires spin-up of endmass. Effectiveness decreases by 70% (single cathode) or 40% (with second cathode) but no current limitation required (Section 3.2.4).
Tether release	Reduces stability duration requirement.
Tether viscosity / stiffness ratio	Dampens modes.
Current control	State estimation method [Levin 2007]. Has not been verified in this work.
Defunct satellite and endmass location	Torques are lower when endmass is up, tether is higher in orbit.
Additional mechanical tether	Increases gravity gradient force at low mass cost.
Current limitation	Limit below level of minimum within orbit to reduce fluctuations. Further reduction increases time to instability, but reduces the attained altitude drop.
Tether length	Increases gravity gradient force and Lorentz force.
Optical properties	Reduces diurnal cycle effect.
Endmass	Increases gravity gradient force but increases system mass.

Table 15. *Recommendations for maintaining stability for bare tether deboost application with light-weight non-functional endmass*

3.2.3 Tethered deboost and collision risk

Tethers can contribute to the debris mitigation effort. In Section 3.1.2, a niche has been identified for mechanical tethers, particularly for a combination of launch assist and spent stage deorbit. Electrodynamic tethers however can be employed for active and propellantless reduction of *many* types of space debris, including for example defunct constellation satellites [Forward 1998]. An electrodynamic tether system requires no deorbit burn propellant, and, especially if passive, can keep the deorbit module simple.

However, also the risk that such tethers themselves pose to other satellites in orbit must be recognized. The extended collision area of a tether sweeps through a significant volume of the orbital environment even for fairly brief operations, such as for example a two-week deorbit of a defunct satellite. Consideration of tether collision risk has already led to several cancellations of missions and experiments over the past decade (Section 1.3).

The question rises how benefits and risks compare to each other for the case of debris mitigation by electrodynamic tether. In this section electrodynamic tether applications for deorbit are considered while taking into account the added risks caused by the tethers themselves. First, the conventional alternative, deboost by retro-rocket, is briefly considered. Then, more extensively, the tethered deboost net risk is compared to that of the "Business As Usual" (BAU), which is a completely passive approach.

The conventional retro-rocket deboost system, with little doubt, is superior over electrodynamic tethers in terms of collision risk mitigation. In a worst case, the system will malfunction and the defunct satellite ends up in a BAU situation, just as the tether system could if deployment fails to initiate. A preference for an electrodynamic tether system, if found comparably reliable, will thus primarily depend on system mass and cost. Tether deorbit systems of very low complexity have been produced, albeit not demonstrated yet [Hoyt 2000]. Also from a perspective of system mass an electrodynamic tether system could be of interest.

A system mass comparison is provided by Heide & Kruijff [Heide 2001.I] based on estimates for the tether system mass from Forward & Hoyt [Forward 1998] versus a rocket mass based on Schonenborg regarding an autonomous system for typical constellation satellites [Schonenborg 2000]. It is concluded that electrodynamic tethers offer considerable mass advantage for deorbit of heavy objects, by up to an order of magnitude for multi-ton objects such as spent stages, and even for small satellites of only hundreds of kilograms if the orbital altitude is sufficient, larger than 400-600 km.

Given the choice for a tethered system over retro-rocket deorbit, the electrodynamic tether system performance shall be compared to Business as Usual. Heide & Kruijff propose a simplified methodology for such a comparison in which three major parameters need to be evaluated [Heide 2001.I]:

1. Probability of break-up collision with debris and non-guided operational satellites

A collision with debris that would lead to cutting of the tether, no matter what the secondary consequences may be, is assumed to be catastrophic by itself. Such a strict assumption is likely to be imposed for tether operations [APEX 1997][4]. Tether robustness against impacts is to be achieved by failsafe design (multi-strand tethers such as the Carroll Caduceus [Kruijff 1998] or Hoytether [Forward 1995]) or a safe-life design (tapes, Section 4.3.1). A multi-strand tether with a width of 10 cm is assumed. Catastrophic is considered impact with any debris of diameter >10 cm or any non-guided operational satellite.

For comparison to the BAU case, a collision with the defunct satellite is considered catastrophic if the impacting particle is large enough to lead to break-up of the satellite. Critical impact energy of the particle is assumed to be 40 kJ/kg, for a typical case this is a particle of about 10 cm [Anselmo 1999]. No further risk assessment is performed on the parts after break-up.

2. Active avoidance requirement

If it is operationally viable and the tether system deorbit rate is controllable (e.g. by a variable ohmic resistance, Section 3.2.2), active avoidance can be considered. Note that

[4] This is perhaps a conservative approach. It can be reasoned that a tether cut does not lead to a significantly worse situation than BAU. The impacting debris may only be superficially damaged due to the tether's low ballistic coefficient. If it is also assumed that the remains of the tether can be disconnected from the endmasses when the tether is cut, the free-floating parts will deorbit quickly and risk is thus contained [Heide 2001.II].

all objects larger than 10 cm are being tracked from the ground. If the number of actions to avoid these objects is limited, it may prove feasible to reduce tether-system collision probability to (near-)zero. For active avoidance, a safety box around operational satellites or debris shall be considered. The expected number of tether maneuvers is to be determined required to avoid passing through these safety boxes.

When considering active avoidance by tethers, the probability of loss of control, or a transition from the controlled case to the uncontrolled case, should be taken into account, e.g. in case of an unplanned endmass release. If, for a particular tether system, probability of such failures is found significant, the active avoidance should not be solely relied upon and the other two parameters presented here should be considered with more relative importance.

3. Burden on operational satellites

The expected number of avoidance maneuvers required by operational satellites is to be determined. If the tether system descent rate is uncontrolled and many operational satellites need to avoid the tether system it would be at the least a burden to be considered in the trade-off, and perhaps a cost driver. Also the BAU for defunct satellites will accumulate dangerous approaches. A sensible comparison can thus be made.

In the evaluation of these parameters, tether-tether collisions will not be considered. It seems unlikely that tethers become so abundant that tether-tether collisions will be an issue. Even if multiple constellations would be electrodynamically deorbited in overlapping periods of 5 years, 40 deorbits per year could be a reasonable maximum occurrence, equivalent to about 4 tethers in space at any time. It should be possible to coordinate the deorbits of these to avoid inter-tether collisions.

Failures of the tether system are in principle also not taken into account. A failure before deployment does not affect the comparison between the several scenarios. An alternate scenario with some likelihood is an intentional tether release from the remaining system in case of contingencies such as inadvertent deployment, partial deployment, erroneous upward deployment, excitation of large oscillations or last minute collision avoidance. In such a case the debris would fall back into the BAU situation, whereas the lifetime of the tether, depending on whether the cathode is still attached and operational, is either reduced or increased by no more than a single order of magnitude (Heide 2001.I). Since that would be a second order failure with limited probability the resulting risk will not affect the comparison.

Useful estimates can be most conveniently produced with the help of a scaled *sweeping area* A_{sweep} (rather than the tether's orbital lifetime or area-lifetime product) [NASA 1995]. The sweep area is the averaged projected area around the debris (plus tether) under investigation, through which operational satellites or other debris should not pass. This area moves at orbital velocity v_{orbit} assumed constant during the degradation time $t_{degrade}$. The product of the averaged values is the sweeping volume V_{sweep}, from which the collision or

avoidance probability p can be estimated taking into account debris or satellite density $\rho_{objects}$ for the appropriate object size range:

$$p = f\,\rho_{objects}\,V_{sweep} = f\,\rho_{objects}\,A_{sweep}\,v_{orbit}\,t_{degrade} \tag{3.4}$$

Although Eq. 3.4 would be accurate only under the hypothetical assumption of a uniform and constant spreading of objects and thus represents no more than a rough first order estimate for the actual value of p, it is considered sufficient for a quantitative comparison between the tether and BAU operational approaches. The factor f is used to take into both the effect of averaged relative velocity between object and debris as well as the projected future increase of the debris environment.

Since the latter effect is assumed of predominant influence on the relative results for the alternatives, f is dubbed the *Future* Factor, and fV_{sweep} the *scaled* sweep volume. The future development of the space environment is relevant in particular for evaluation of the Business As Usual case, where satellites are left to be deorbited mainly by atmospheric drag. BAU deorbit times can span as much as centuries. Future use of space is predicted as an almost linear increase in number of operational satellites with about a factor 3 uncertainty [Anselmo 1999, ESA 1999]. Considering the future number of spent stages and debris, a more moderate increase can be considered than the worst case (exponential) scenario. A runaway effect of debris-debris collisions is not foreseen. In line with current trends, future users are expected to take increasing responsibility to carry deorbit systems or launch stages into reduced-lifetime orbits. For this comparison a linear increase of both debris and operational satellites with a factor 3 in 100 years is assumed.

Finally, a subjective assumption of critical impact is included namely that propagation of risks over degradation time is limited to a 150 years horizon in view of huge unknowns in developments of access to space and alternative debris removal techniques. The choice of 150 years is rather arbitrary and this should be considered when evaluating the results, however it serves to create awareness of the lack of meaning of indefinite risk propagation.

A schematical representation of the methodology can be found in [Heide 2001.I].

As an example the method has been applied to a range of tethered deorbits, for a typical 700 kg constellation satellite [Forward 1998, Schonenborg 2000]. For estimations of orbit degradation, ETBSim has been used as well as rough lifetime evaluations based on Vannaroni e.a. [Vannaroni 1999]. The tether is supposed to be bare for efficiency, while its endmass librations are assumed to be maintained within 30 degrees. For typical tether lengths of 5 - 10 km and effective diameter of 0.8 mm the Lorentz-force is some decinewton at maximum plasma density altitude (300 km) to millinewton level at high altitudes (1500 km). This force will reduce the semi-major axis (and hence the mean altitude) of the tethered system orbit at rates from 2 to 50 km/day, decreasing with increasing debris mass, inclination or altitude. The tether is assumed to have a linear mass density of 2 kg/km. Stability is guaranteed by a viscous tether design and current limitation (Section 3.2.2). The tether is equipped with an additional 3 km mechanical tether (1 kg) to assist deployment. The atmospheric density profile is characterized by an average exospheric temperature

T_{exo} = 1050 K. The effect of decoupling of tether and cathode from the debris is evaluated as well. The decoupling is simulated by introduction of a momentum transfer decreasing the tether semi-major axis 5*L*, while satellite semi-major axis is increased by 0.3*L*. After decoupling, the thrust of the tether is conservatively reduced to 20% of maximum obtainable thrust to account for instability effects.

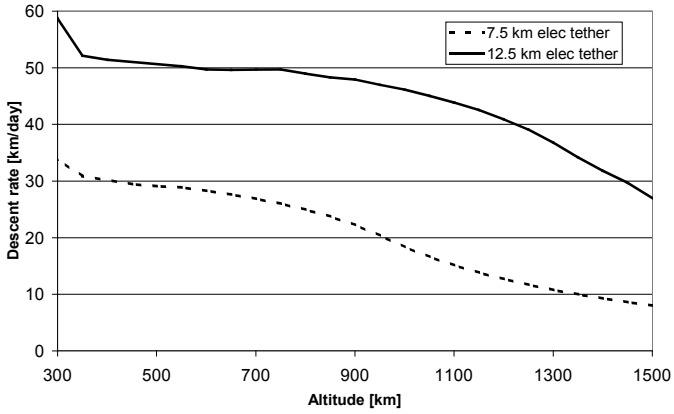

Figure 34. *Descent rate of 700 kg satellite*

For the resulting system and two electrodynamic tether lengths, Figure 34 presents the descent rate of the defunct satellite as a function of altitude, for an equatorial orbit.

Uncontrolled deorbit

The simpler tethered alternative to BAU is to have an uncontrolled deorbit. For such a tether solution to be of interest, the total number of avoidance or alert situations for guided operational spacecraft should be of equal or lesser order of magnitude than in the BAU case. Also, collision probabilities shall be compared. This can be done directly through sweep volumes in this case. A >10 cm debris object is presumed catastrophic for a defunct satellite [ESA 1999] as well as for a 10 cm wide multi-strand tether. Identical debris or operational spacecraft densities would have to be multiplied with the sweep volume to come to a risk estimate.

For the tether case lifetime is much shorter than for BAU and the Future Factor $f = 1$, but the sweep area A_{sweep} is larger. The sweep area for BAU is taken as the defunct satellite or spent stage's typical dimension squared (2.57 m for a satellite, 3.1 m for a spent stage [Anselmo 1999]), whereas for the tether it is approximated as the product of tether length and average object diameter. From data presented in Wertz & Larson the average diameter of objects >10 cm was determined to be about 1.7 m [Wertz 1993].

In Figure 35 and Figure 36 the scaled sweep volume is plotted versus the initial altitude for deboost systems with an electrodynamic tether length of respectively 7.5 and 12.5 km. In the figures is indicated the sweep volume for the electrodynamic tether deorbit system including the defunct satellite as well as for the decoupled system, i.e. the sum of individual

sweep volume of the defunct satellite and of the tether plus endmass after decoupling at the indicated altitude. For comparison, the contribution to the latter sweep volume of just the defunct satellite, after decoupling of the system and without the tether, is included. This contribution is approximately equal to the BAU case and is used here for both purposes. Finally the target sweep volume is shown, namely for a satellite with a reduced lifetime of 25 years [ESA 1999], including adjustment for Future Factor.

Both graphs show that it would be advantageous to decouple the tether and debris once a certain altitude has been reached. The figures show that a tethered system, if it remains attached to the defunct satellite till re-entry, will at no altitude be able to achieve the desired sweep volume of a piece of debris with 25 years lifetime. As expected, the longer tether has the better performance (see also Eqs. 2.32 & 2.35). Yet for both tethers the critical length for decoupling is around 700 km altitude. Unfortunately, the decoupled satellite at 700 km is still above the suggested reduced lifetime orbit of 25 years. Releasing the debris only 100 km later, at 600 km, decreases the remaining sweep volume by a factor of 2.5. This seems to be the better solution for an uncontrolled tethered debris mitigation system.

It is also suggested that maybe unnecessary risk would be taken for use of tethers at altitudes above 1100 km (for a 7.5 km tether) to 1400 km (for a 12.5 km tether). If a tether is used at such altitudes a larger length is recommended. This conclusion depends on the imposed maximum of orbital lifetime of 150 years that is recognized from the sharp bend in the curves that include a decoupled satellite. Without the assumption of a maximum temporal horizon the tethered system would be favorable even at high altitudes.

Depending on initial altitude and mass of the debris, a maximum inclination will exists where the collision risk will still be acceptable. The deorbit behavior of the above cases, as quantified in Figure 34, refers to an equatorial orbit – the most favorable inclination. Maximum obtainable descent rates scale roughly with the angle between the system's velocity and the (co-rotating) magnetic field. Time needed to deorbit satellites or spent stages increases significantly with inclination, and, with it, the sweep volume and collision risk. An increase in inclination from equatorial to 45° decreases the recommended maximum altitude for a 12.5 km tether deorbit from 1400 to 1100 km.

The comparison of tether vs. BAU presented here depends on a number of strong assumptions. In case future space will be more populated, the Future Factor should be raised, the BAU scaled sweep volume (approximated here by the decoupled debris) would be significantly higher and the effective range increases. The same would be true if particles smaller than 10 cm would be considered to lead to break-up of the debris but not to break-up of the tether.

The actual risk of a catastrophic event for a tethered deorbit is dominated by the risk of unexpected cut of the tether. There are many more pieces of large debris than there are operational satellites. With about 15000 debris objects in LEO, or a density of approximately $\rho_{objects} = 1.5\ 10^{-8}\ km^{-3}$ from Figure 35 and Eq. 3.4 it can be found that about 0.013 impact can be expected during the tethered deorbit from 1500 km. So there is about 1% chance of mission failure.

For an uncontrolled descent, probability of impact on an operational satellite - assuming about 500 active satellites in LEO - is about 0.04%. It is here assumed that those satellites are distributed equally over the LEO volume, i.e. a density of approximately $5x10^{-10}$ km^{-3}.

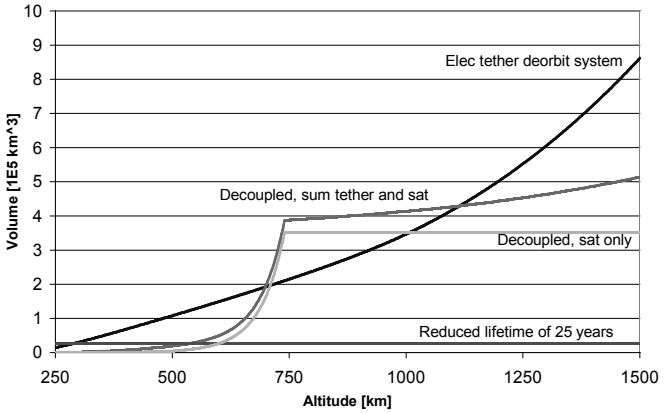

Figure 35. *Sweep volume vs. initial altitude for 0.8 mm 7.5 km electrodynamic tether (+ 3 km mechanical) without avoidance (deorbit time from 1500 km is about 70 days)*

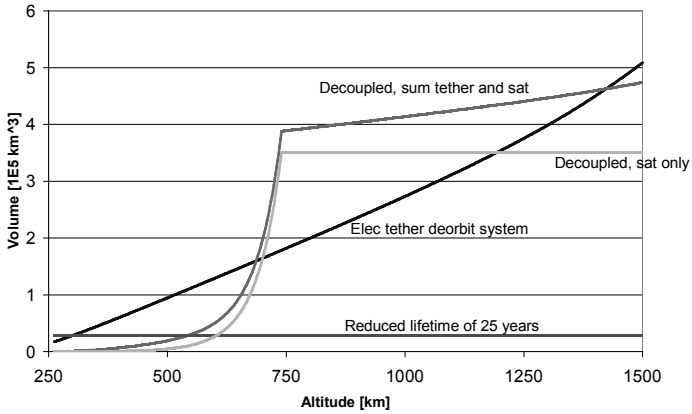

Figure 36. *Sweep volume for 0.8 mm 12.5 km electrodynamic tether (+ 3 km mechanical) without avoidance (deorbit time 1500 km ~30 days)*

Controlled deorbit

One could try to avoid the debris objects actively through current control by telecommand, but this seems an impractical approach. Due to the limited knowledge of the tether position because of librations the sweep width is then to be increased from 1.7 meters to about 5000 m, leading to 5000/1.7 x 0.013 or about 40 evasive maneuvers during the descent of approximately 70 days. Considering the descent rate of about 20 km/day and a total tether length of 10.5 km, this is barely possible. Some extra time should be taken into account since the avoidance of one piece of debris should not lead to getting too close to another. The 1%

risk of tether cut should thus be accepted. If the broken tether pieces are disconnected from their endmasses, consequences of such a cut should be minimal.

If it would however be possible for the tether system operators to at least actively avoid operational satellites, the tether option relative to BAU risk could be made rather attractive. In order to determine the feasibility of such a scheme, the number of avoidances is determined. The safety envelope around an operational satellite now becomes the relevant sizing parameter for the sweep volume. As the exact position of the full tether cannot be predicted, an avoidance maneuver has to be initiated if the tether is expected to sweep anywhere through the safety envelope. Due to orbital elements estimation limitations, such envelopes are typically several times longer (related to true anomaly estimation) than wide (inclination), and range from hundreds of meters to several kilometers. In the future the safety envelopes can be expected to go down, because of technical advances, but also higher risks may be accepted to reduce operational cost. An average width S_W of 100 m is assumed. The envelope is assumed to be a box with dimensions S_W=S_H=0.4S_L [Heide 2001.I]. The height of the sweep area is then determined by the sum of tether length L and height S_H of the safety envelop. The width of the sweep area is determined by the sum of the tether's oscillation amplitudes (half the tether length for a 15 degree libration) and the aspect-average of width S_W and length S_L of the safety envelope, or approximately $2/\pi$ (S_W+S_L) (compare Eq. 2.36). Approaches of active satellites are assumed to occur in the horizontal plane, but from a random direction. We thus find the following approximate measure:

$$A_{sweep} \approx (L+S_W)(0.5L+2S_W) \tag{3.5}$$

The maximum acceptable rate of evasive maneuvers may first be estimated. Evasive maneuvers in the most extreme form can be performed by electrically disconnecting the cathode thus stalling the tether descent. The total amount of maneuvers should not exceed that which is physically possible: one at a time. Nor should it significantly decrease the descent performance. An evasive maneuver for a 10 km tether might take several days at 800 km, and about a day at 400 km. The acceptable number of evasive maneuvers is thus likely to be once every 3-10 days, depending on the accepted delay in descent time.

In fact, for the environment and system described here, only about one avoidance can be expected per deorbit, which seems entirely feasible from an operational point of view. Heide & Kruijff find in [Heide 2001.I] that this result does not depend strongly on tether length. Again a decoupling of the tether from the debris at 600 km would reduce the need for avoidance maneuvers. Even if the tether descent is controlled, it may be more attractive from an operational point of view to release the tether from the defunct satellite at this point.

From a point of view of debris mitigation and compared to BAU, controlled tethered descent thus seems an attractive option. It should be taken into account that the number of avoidance maneuvers per descent will increase in the future, especially when more constellations will be brought in place. Around 1000 km there is a peak in satellite density, and it is not unlikely that several evasive maneuvers will be packed in a small timeframe. This possible complication remains to be assessed.

Conclusion for dedicated deorbit systems

Uncontrolled deorbit by electrodynamic tether is less effective for debris mitigation than the retro-rocket and momentum transfer (limited to upper stages) alternatives, because of the electrodynamic tether's much larger orbital exposure. With respect to Business As Usual collision probabilities and avoidance needs are within the same order of magnitude, and suitable niches exist, depending on altitude and inclination. A rough application range is found for the investigated example case of 700-1500 km and 0-65° inclination. In this altitude range there is also a significant mass advantage with respect to rocketed deboost. Longer tethers could be used to extend the application range to higher altitudes and inclination. Outside LEO (>2000 km) the plasma density and magnetic field strength should however be considered insufficient for electrodynamic tethers. Note that also applications for upper stage deorbit from GTO [e.g. Yamagiwa 1999] are not recommended, since performance of electrodynamic tethers relative to BAU will be reduced by a further order of magnitude [Heide 2001.I]. In all cases it is recommended that the tether is disconnected at around 600 km altitude. Such a release would also ease design measures to prevent dynamic instability.

Descent rate control can make the tether solution more attractive. If descent rate control is applied for avoidance of operational satellites, only about one avoidance maneuver per descent needs to be made. At the cost of several weeks of additional operations this could tip the scale and make the tether system comparable in safety to retro-rocket systems. The control of avoiding catalogued debris (>10 cm) is not feasible and here a certain risk may have to be accepted. A safety disconnect system should be implemented on the endmasses for the case of tether failure, in order to reduce the remaining collision probability to one close to that of the BAU case.

Travelling debris removal systems

Apart from dedicated deorbit systems mounted on single satellites, a powerful and essentially propellantless possibility for removal of existing debris could be provided by a hybrid form of the travelling tether systems of Section 3.1.2, which would combine electrodynamic propulsion and momentum transfer. This system would travel through space toward a selected piece of debris and use electrodynamic drag to move towards a sufficiently low orbit. It would then release the debris into the atmosphere (or into a short-lived orbit) using momentum transfer. The system's orbit itself would be raised, and with the help of electrodynamic propulsion it would maneuver itself close to the next piece of debris. It is not a major problem if such a system is very heavy, because of reusability. A long and wide tape tether would then be required to limit deorbit times with the larger system mass (Section 2.2.2). Stability issues (Section 3.2.2) would need to be solved, potential reeling (to reduce the sweep volume between deorbit activities) and the rendez-vous and docking with debris would be major challenges.

In the TERESA concept [Bade 1993] it is claimed that about 100 objects could be removed in a timespan of 7 years using a 93 km tether. So deorbit times per satellite are comparable to that of the dedicated deorbit system described in this section, but the tether is about 10 times

longer. If the tether would be continuously exposed during this period, the sweep volume would be 10 times as large and possibly not competitive with BAU. It should therefore be attempted to significantly limit the tether exposure between debris dockings, leaving a major challenge to quickly adjust orbit.

Carroll notes that about 1500 objects in LEO account for over 98% of the 1900 ton of debris in orbit [Carroll 2002]. A very significant fraction of debris mass in LEO is represented by mostly Cosmos upper stages in a 83-85° inclination at about 1000 km altitude. In his Debris Shepherd concept Carroll proposes an interesting possibility that deals with some of the TERESA problems, namely to use the tether system to collect these masses rather than deorbit them. This would create a single very large mass that could be very useful for advanced tether applications (Section 1.2).

New insights have been obtained in the EDDE study [Pearson 2010]. The main innovation here is that the tether is spinning. The spin greatly improves dynamic stability, allowing for greater currents to flow, and, with proper selection of the spin plane, unimpeded performance at high inclination can be achieved. A control has been developed by Levin [Levin 2007] that allows for highly efficient change of orbit. It is claimed EDDE can climb about 200 km/day and change inclination by 1.5°/day. A dozen 100-kg EDDE vehicles could remove about 99% of LEO orbital debris within 7 years. The system contains multiple solar panels distributed over the length of the 10 km tether in order to collect the required 7 kW of electrical power. The overall system is claimed to be only a few hundred kilograms. Rendez-vous and docking also for this system is still essentially unresolved, although some concepts have been proposed.

3.2.4 A rotating tether around Jupiter

Tethers around Jupiter have been proposed for thrust and power generation purposes [Gallagher 1998, Castronuovo 2002, Sanmartin 2003, 2005, 2008]. Jupiter is an interesting case to explore the potential of tether applications. Section 2.2.2 describes how the effectiveness of an electrodynamic tether depends on the magnetic field strength of the central body, the orbital velocity and the plasma density. A planet where these parameters are particularly pronounced, is Jupiter. At the same time, the strong gravity field demands significant ΔV for orbit change. It may not be easy to obtain the energy required for this from solar power since the solar radiation intensity is 25 times lower at Jupiter than at Earth. Furthermore, gravity gradient forces are low at typical distances from Jupiter whereas the predicted electrodynamic forces and current levels are so high that stability issues and heat dissipation will become dominant. High levels of radiation may prohibit complex control electronics.

It is investigated in this section if using a rotating tether, a simple, mostly passive, system operating around Jupiter could be a possibility, that may be launched as piggy-back on a larger "host" mission to the large moons of the planet.

The proposed mission of the system is to provide in-situ data of the Jovian plasmasphere and a (multi-)probe release into the Jovian atmosphere at relatively low entry velocity with

little impact on the host orbiter. The concept is based on a bare aluminium tether, without insulation, and does not require an active plasma contactor such as a hollow cathode. The Lorentz drag force on the system is to be used to lower the orbit from initial highly elliptical to near-circular atmospheric entry. It is proposed that stability is guaranteed by the Lorentz-torque, which is found to act such that if the system is given a modest initial rotation, this rotation will self-accelerate, keeping the tether taut through centrifugal force and stable through the gyroscopic effect. The rotation will also provide an accumulated ΔV capability at time of probe release. The assumption is introduced of a straight tether, spinning within the orbital plane.

In order to obtain a quantitative expression for the targeted performance, an equatorial orbit is assumed. Jupiter is assumed to have a non-inclined dipole magnetic axis. The orbit is thus not necessarily circular, yet perpendicular to the local magnetic field direction, see Figure 37. The Jovian plasmasphere and magnetic field characteristics are modeled according to [Divine 1983, Gallagher 1998].

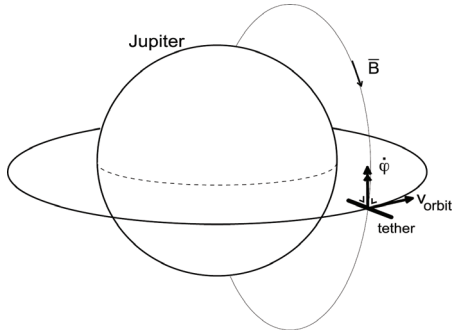

Figure 37. *Tether in simplified orbital configuration around Jupiter*

In the absence of a cathode, the circuit is closed through ion collection (Figure 38). Ion collection is much less efficient than electron collection, due to the mass ratio of electrons and ions, which is why e.g. in Figure 31 it is not considered. A stable current will flow when space charging effects create an equilibrium balance between regions of electron and ion collection[5].

To estimate ion collection according to the OML model, in Eq. 2.30, the electron mass m_e can be substituted by an equivalent ion mass $m_{i,eq}$. If several species of ions are available, the total collection is assumed to be the sum of individual contributions, so that the equivalent ion mass can be derived to be

$$m_{i,eq} = \left(\Sigma f_i \cdot \sqrt{\frac{n_{val\_i}^3}{m_i}} \right)^{-2} , \tag{3.6}$$

[5] Note, around Jupiter this proposed approach is in fact a conservative oversimplification. It is assumed here that there is no secondary emission of electrons due to impact of ions on the tether. Such an emission would increase current and Lorentz force and should not be ignored for a tether bias above 1 kV [San Martin 1993], such as is the case for a 10 km tether around Jupiter. For further evaluation, it is recommended that this effect is experimentally quantified.

with f_i the fraction of ion density (0..1) for component i, n_{val_i} the ion valence and m_i the ion mass in atomic mass units (number of protons and neutrons).

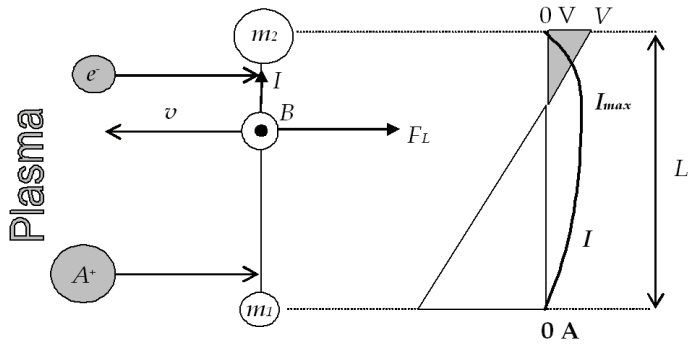

Figure 38. *Bare conductive tether electron (e^-) and ion (A^+) collection without active cathode*

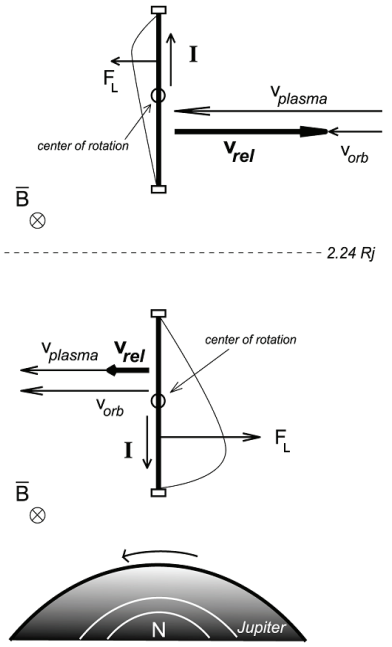

Figure 39. *Resulting Lorentz force distribution on bare tether, prograde circular orbits around Jupiter. The force acts as drag below 2.24* R_j *and as propulsion beyond 2.24* R_j. *Averaging the force over one revolution leads to a net force in the direction opposite to the relative velocity* v_{rel}. *The* v_{rel} *equals the difference between the orbital velocity and that of the co-rotating plasma* $v_{rel} = v_{orb} - v_{pl}$.

A relationship between the part of the tether that is collecting ions (l_i) and the part collecting electrons (l_e) can be found from the current balance in the point of the tether that has reached zero potential with respect to the plasma (Figure 38, Section 2.2.2, based on Eq. 2.31),

$$\frac{l_e}{l_i} = \sqrt[3]{\frac{m_e}{m_{i,eq}}} \tag{3.7}$$

Figure 39 shows a schematic of the current collection for the bare tether in a circular prograde orbit around Jupiter. Note that for r>2.24 R_j Jupiter's co-rotating plasma moves faster than the local circular velocity. Furthermore, the direction of the Jovian magnetic field is opposite to that of the Earth magnetic field. As a result, for circular prograde orbits around Jupiter, the Lorentz force acts as a drag force inside 2.24 R_j and as propulsive force outside of 2.24 R_j. For retrograde orbits, the force will always act as a drag force [Dijk 2003.I].

An overall quantification of resulting currents and forces can be deduced for the system. The prevailing ions for the Jovian inner plasmasphere ($r < 3.8\ R_j$) are S^+ ($f = 0.7$) and O^+ ($f = 0.2$). The resulting equivalent ion mass $m_{i,eq}$ of 26.5 u in this region leads to a ratio l_e/l_i of approximately 0.01. This fraction could increase to a maximum of ~0.1 at large distances from Jupiter, where cold protons become the dominant ions.

Figure 40 shows the maximum achievable bare tether current for a circular prograde orbit around Jupiter. The tether mass is 100 kg. The dip in both collected current and Lorentz force around $r = 2.24\ R_j$ occurs where the velocity of the co-rotating plasma equals the orbital velocity for a prograde circular orbit, beyond which the Lorentz force changes direction. Apart from the dip, a steady rise can be observed as we get closer to Jupiter, to milliamps and more. The magnitude of the Lorentz force itself rises from micronewtons by several orders of magnitude. The dependency on length is also plotted, for a fixed tether mass. A longer narrower tether is more effective at the same mass than a shorter wider one.

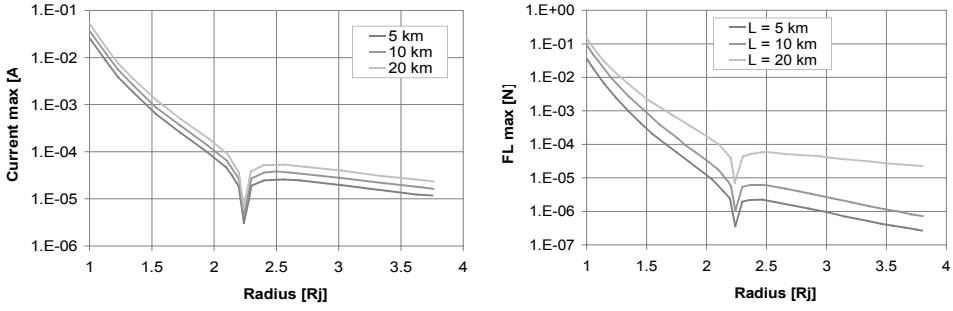

Figure 40. *Maximum achievable current (top graph), magnitude of Lorentz force (lower graph). Bare 100-kg aluminium tether in prograde circular Jovian orbit, width inversely proportional to length.*

In the case under study, the tether will rotate so the plasma potential along the tether, induced by the electric motive force, becomes a function of the rotation angle φ. Both the orientation and the magnitude of the Lorentz force is changing during a revolution of the rotating tether system, with the maximum Lorentz force (in equivalence with Eq. 2.32) acting on the tether when oriented perpendicular to v_{rel}, i.e. $\varphi = 0$. The component of the Lorentz force perpendicular to v_{rel} becomes zero when integrated over an entire revolution, leaving only a net force in the direction of $F_{L\max}$ (i.e. opposite to v_{rel}),

$$\overline{F_L} = \frac{1}{2\pi} \cdot 2 \int_{-\pi/2}^{\pi/2} F_{L_{\max}} \sqrt{\cos\varphi} \cos\varphi \cdot d\varphi = \frac{4\sqrt{2}}{3\pi} F_{L_{\max}} \approx 0.6 F_{L_{\max}} \tag{3.8}$$

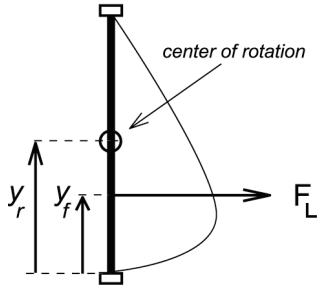

Figure 41. *Definition of the rotational arm for the calculation of the Lorentz force induced moment on the bare tether.*

Consider now Figure 41. The co-ordinates y_r - y_f are measured always from the lower end of the tether, y_r refers to the center of rotation and y_f refers to the work point of the total force. Independent of the angle φ, the work point of the resulting Lorentz force for each of the tether sections collecting electrons resp. ions can be determined to be at 5/14th of the length of these sections [Dijk 2003.I]. If we neglect the Lorentz force contribution of the collected electrons $F_{Li} << F_{Li}$, we can equal the torque Ψ to the product of the Lorentz force F_{Li} and the moment arm being either y_r - y_f (φ in [½π ..½π]) or (L - y_r) - y_f (φ in [½π ..1½π]). As changes in y_f (due to different composition of the ion population in an elliptic orbit, Eq.3.6) are very small (<3%) y_f can be assumed constant. For the increase of the energy of the tethered system per rotation ΔE_{rot} we can now write,

$$\Delta E_{rot} = \int_0^{2\pi} \Psi \cdot \mathrm{d}\varphi = \tfrac{3}{5} B d_i e n_\infty \sqrt{\frac{8eE_m}{9m_{i,eq}}} l_i^{\frac{5}{2}} \cdot 2(L - 2y_f) \cdot \int_0^{\pi/2} \sqrt{\cos\varphi} \cdot \mathrm{d}\varphi \approx \tfrac{4}{7} F_{L_{i,\max}} \cdot L \tag{3.9}$$

It follows that the increase in rotational energy per rotation is proportional to the Lorentz force and does not depend on the location of the center of rotation y_r. This can be explained because of the anti-symmetry of the resulting torques in the two halves of the tether rotation with respect to the center of rotation. The resulting moment on the tether always acts counterclockwise (as seen from the ecliptic north pole). The rotation of the system will therefore continuously accelerate once an initial rotation is provided in this direction. An averaged torque $\overline{\Psi}$ acting over a full rotation 2π adds a $\Delta E_{rot} = 2\pi\overline{\Psi} = 2\pi \cdot J \cdot \overline{\ddot{\varphi}}$, with J the moment of inertia of the tethered system and $\overline{\ddot{\varphi}}$ the average angular acceleration, an expression for the trend of increase in angular rate is found:

$$\overline{\ddot{\varphi}} = \frac{\Delta E_{rot}}{2\pi \cdot J} \approx \frac{2}{7\pi} \frac{F_{L,\max} L}{J} \tag{3.10}$$

This increase in angular rate with time is thus persistent and proportional to the maximum Lorentz force. Through Eq. 3.10, an intermittent angular rate measurement through e.g.

Doppler-shift of a simple on-board carrier signal or even a radar reflection can provide information on the local plasma conditions.

One example is worked out with the use of the tether simulator ETBsim. The different parameters for this example are described in Table 16. The 200-kg system is in a low circular orbit. A significant angular acceleration can be noticed which is virtually constant on the timescale of a single day (Figure 42). The descent rate (500 km/day and increasing) is significant as it will lead to atmospheric entry of the system within weeks.

Orbit	**Circular prograde Jovian orbit at 10.000 km altitude (1.14 R_J)**
Tether dimensions	10 km x100 mm x 0.038 mm - 0.065 m effective diameter
System mass	200 kg (100 kg tether, 2x50 kg endmass)
Initial rotational velocity at tip	0.17°/s, i.e. 30 m/s relative tip velocity

Table 16. *Simulator values for Jupiter tether example case*

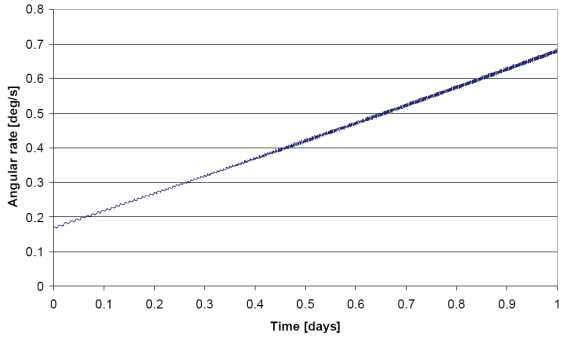

Figure 42. *Increase in angular rate over time for a rotating bare tether in Jovian orbit*

The angular acceleration can be used to prevent instability of the tether dynamics (Section 3.2.2). To maintain stability, the ratio between lateral force (Lorentz force) and centrifugal force (CF) is the decisive parameter. For the simulated configuration Van Dijk, Kruijff & Van der Heide find empirically that stability is maintained in a circular orbit as long as (approximately) $F_L < F_{CF}$ [Dijk 2003.II]. With rotational energy E_{rot} proportional to $L \cdot F_{CF}$ via $J \cdot \dot{\varphi}^2 \div L \cdot L\dot{\varphi}^2 \div L \cdot F_{CF}$ and ΔE_{rot} proportional to $L \cdot F_L$ according to Eq. 3.9, a useful measure for stability is $\Delta E_{rot}/E_{rot}$, which must be kept small to remain stable. So as long as the increase in Lorentz forces is gradual (less than a doubling) over the timescale of a rotation, and given a stable initial rotation ($E_{rot,0} >> \Delta E_{rot,0}$), stability of the system is inherently guaranteed in any orbit. The tether break strength thus becomes the physical limitation for the system. Even if the tether is reinforced with modern materials such as Dyneema®, in a low circular orbit, the tether would break under the steadily increasing centrifugal force within weeks.

A simulation of the system at 1.14 x 10 R_j provides some insight into the dynamics of the system in a more realistic initial elliptic orbit (Figure 43). The steep tension increase in perigee is obvious, the tension problem will quickly become serious also in this orbit.

An alternative concept is worked out [Dijk 2003.I] in which deorbit from an 1.14x50 R_j is performed in a timescale of months, using a gas-release system as passive cathode for improved deorbit performance [Gilchrist 1998]. The complexity of the system is increased, but the concept could allow for a basic control limiting the angular velocity. Van Dijk, Kruijff & Van der Heide provide detailed models and derivations, as well as consideration of further system and mission aspects in [Dijk 2003.II].

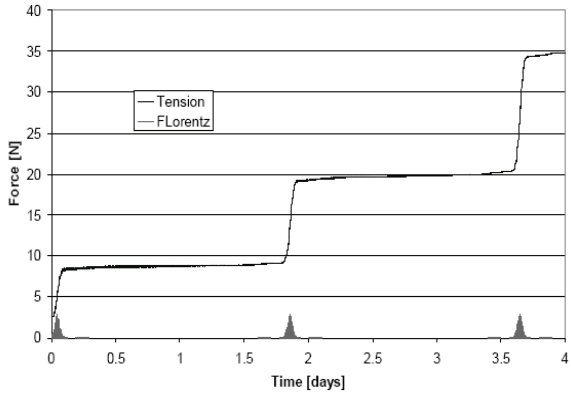

Figure 43. *Tension and Lorentz force for a rotating tether system in 1.14x10 R_j elliptic initial orbit.*

The concept investigated here is meaningful in Low Earth Orbit. A bare aluminium tether experiences a Lorentz drag and a broken piece of tether will therefore have the tendency to remove itself from orbit. This property provides a level of inherent safety to the use of bare tether that is not shared by insulated tethers. The self-accelerating effect guarantees long term stability for a tether if brought into sufficient initial spin. The angular acceleration itself provides information on the plasma and tether interaction.

3.3 Responsible orbital niches for use of tethers

Various tether applications have been discussed that are technically feasible today. Such applications, especially in LEO, will however only be considered if safety can be demonstrated in case of contingency (Section 1.3). If for some reason the tether deployment or control system malfunctions, and the tether would become a hazard, or as a last resort to avoid a collision, it should be possible to disconnect the tether completely on either side by an autonomous system or telecommand. This will decrease the tether's ballistic coefficient or alternatively, the ratio of mass to drag-area. The decoupled tether remaining in orbit is eventually re-entered primarily due to the combined mechanism of atmospheric drag, solar pressure (see also Section 6.4.1) and ion/electron currents (Section 2.2.2).

For these orbit-degradation mechanisms to be sufficiently helpful in risk mitigation approximate limits to orbit of choice have been determined, using ETBSim (Table 17). It is assumed here, based on discussion with the debris community in the context of the YES experiment [APEX 1997], that catastrophic mission failure is equivalent to tether system failure followed first by tether release and then by a collision of the free-floating tether with an operational satellite. The acceptable probability of this chain of events is assumed to be 0.0001, equivalent to a probability of collision of 0.001-0.01 in case of a seemingly reasonable tether system reliability of resp. 90-99%.

Because of the low ballistic coefficient for the mechanical tethers described here (about 0.1 - 1 kg/m^2) atmospheric drag is sufficient to get a free tether out of lower LEO (<500 km) in a matter of days [Warnock 1993]. Electrodynamic tethers are more dense, but the tape concepts offers in a mass-efficient manner not only a large collection but also a drag area (0.2-1 kg/m^2). Note that the solar cycle can affect the atmospheric density by a factor of 10 at 350 km to even 30 around 700 km altitude, equivalent to an altitude range for similar drag conditions of ±50 km at 350 km to ±200 km at 700 km.

Lunar-solar perturbations are independent of tether drag area and are relatively small disturbances for tethers. They are periodic and non-dissipative and their main effect is on the perigee altitude of GTO orbits with tens of kilometers, depending on the constellation of Sun and Moon [Cook 1962]. The density increase from a perigee reduction can however have a significant effect on orbital lifetime (factor two for a 5-10% reduction in altitude) [Bergamaschi 1987].

As atmospheric density decreases exponentially with altitude, in high orbits (above about 600 km) drag solar pressure is the dominate force affecting the perigee and apogee altitudes. Here the momentum exchange between the Sun's radiation (1370 W/m^2) and the spacecraft can become dominant. It is essentially independent of height. The induced acceleration a_{SP} can be approximated using the following relationship [Wertz 1993]:

$$a_{SP} \approx 4.57\text{E-}6\ (1+f_r)\ A/m, \tag{3.11}$$

with A/m the area to mass ratio, and f_r (0..1) depending on the type of reflection.

For (near) circular orbits, solar pressure is essentially non-dissipative when averaged over one orbit: over the course of one orbit, the solar aspect angle with the velocity vector rotates once as well. It can however still cause lifetime reduction. Solar pressure will then tend to affect eccentricity through equal and opposite effects on perigee and apogee. If the solar aspect angle with respect to the line of apsides remains consistent, a perigee point will become more pronounced and as it is lowered, atmospheric drag will increases exponentially. The solar aspect angle depends on the rotation of the Earth around the Sun, nodal and apsidal precession. For median inclinations, around 45±15°, this consistency is maintained long enough to create a beneficial effect. For tethers with ballistic coefficients typical of mechanical tethers, MTBSim simulations indicate that the safe application altitude can be extended from about 550 km to 800 km [Heide 2001.I].

The effect of solar pressure in GTO was extensively studied for the YES satellite, with multiple solar pressure models and orbit propagators. YES carried a 35-km long Dyneema® tether on-board (22.3 m^2, 5 kg, see Section 6.4.1). In GTO, if the Sun is properly positioned with respect to the line of apsides, solar pressure can be very effective in bringing down perigee, because of the large fraction of the orbital period spent in apogee. The GTO of Ariane 5, the launcher used for YES, has a perigee of 600 km, and is in principle unsafe for tethers as it is too far out for a rapid, drag-induced re-entry. The solar pressure was however found to work favorably for a range of RAAN (Right Ascension of the Ascending Node) of about 150° equivalent to a daily launch window of 10 hour duration. The free-flying tether lifetime could for these cases be reduced from decades to only 1-3 months.

For the case of bare electrodynamic tethers, there is another mechanism that helps reduce lifetime in LEO (Section 3.2.4). A free flying tether with its (light-weight) cathode still operational will re-enter quickly due to the high Lorentz drag combined with the significantly reduced ballistic coefficient resulting from decoupling of its major endmass. The tether is likely to start spinning or tether dynamics may become instable. Resulting performance losses can be compensated to some extent as current limitation will not be required. For a typical mission below 1200 km, most proposed bare tethers will deorbit within 10 days [Heide 2001.I].

If for some reason the tether is not or no longer connected to a cathode, even without a device to emit electrons, a small current will still flow due to ion collection (Section 3.2.4). In LEO the ion environment is dominated by atomic oxygen. In a conservative case, disregarding electron emission, $l_e/l_i = (m_e/m_i)^{1/3} = 0.0324$. Integrating the current, and calculating the (maximum) Lorentz drag force (equivalent to Eq. 2.32) the total maximum drag for the free tether becomes, as compared to the cathodic case with electron emission:

$$F_{free} \approx \frac{F_{cathode}}{200}, \tag{3.12}$$

typically in the range of millinewtons. This does not mean that the lifetime of a free tether will be 200 times worse than that of the nominal mission. The Lorentz drag is significantly smaller than gravity gradient tension for an aluminium tether of several kilograms and several kilometers length (Eq. 2.14). The tether will thus tend to tend to stretch at least the center part of the tether vertically. Inherent safety is provided because of the fact that the ion-driven current will flow, no matter which side of the tether happens to be at the top end or at the bottom. Due to the loss of both endmasses the ballistic coefficient will be improved by at least an order of magnitude. For a 1200 km mission, a typical deorbit time of several months can thus be expected, which may be acceptable for a contingency case.

Table 17 summarizes the results in the form of a recommended window for safe use of tether systems, under the assumption that those systems have similar design parameters and safety features as described. It is noted that the International Space Station represents a particular case of concern. To avoid approach to the International Space Station in case of failure, for experimental tether missions a lower inclination (under 51.6°) or altitude below 300 km is recommended.

	Atmospheric drag only	**Solar pressure**	**Ion/electron current**	**Lunar-solar**	**Combined**
Mechanical tether	LEO: <550 km GTO perigee: <400 km	LEO, i≈45°: <800 km GTO perigee: <800 km	-	GTO perigee: <500 km	LEO: <550 km LEO, i≈45°: <800 km GTO perigee: <800 km
Bare conductive tether	LEO: <500 km GTO perigee: <400 km	LEO, i≈45°: <700 km GTO perigee: <700 km	LEO, i<65°: <1500 km (*) LEO, i<75°: <700 km GTO: perigee <600 km	GTO perigee: <500 km	LEO, i<65°: <1500 km (*) LEO, i<75°: <700 km GTO: perigee <700 km
Free tether acceleration [m/s^2]	-0.5 [150 km] -10^{-5} [700±200 km]	$\pm10^{-5}$	-10^{-4} [400 km] -10^{-5} [1500 km]	$\pm10^{-6}$	-
Note	Depending strongly on solar activity	GTO: 60% reduced launch window	(*) Upper range for >15 km tethers only	Depending on Sun-Moon orientation	-

Table 17. *Free tether deorbit mechanisms, indicative altitude limits for safe use (see text), excluding spinning electrodynamic tethers.*

These windows allow for most of the applications discussed in this Chapter. Tether systems that aim to counteract atmospheric drag, operate in the upper atmosphere, or deliver capsule deorbit services would typically focus on a 200-1200 km altitude regime.

Momentum transfer could be considered for deorbit of a good fraction of upper stages, including future small launchers and, more questionably, since depending on a suitable RAAN, Ariane 5 in GTO. Since below 500 km lifetime of spent stages is not considered a debris issue under current guidelines, and above 800 km mechanical tethers are not safe, tether systems would be only of real interest for spent stage deorbit in a narrow region of perigee altitude, or, alternatively if also a significant service for the payload can be obtained (Section 3.1.2).

Whereas mechanical tethers have perhaps been sufficiently demonstrated to justify an application, even for the simpler electrodynamic applications there are important open development areas such as stability control, manufacturability, deployability and in-orbit testing of fail-safe multi-strand or tape tethers. Bare tethers are assumed to be used since they require no dedicated electron collector, are simpler in design and provide inherent safety. The recent successful passive deployment of the T-Rex bare aluminium tether [Fujii 2009] stems hopeful, although this 3 cm wide tape tether was only 300 m in length. Longer tethers may be required for debris mitigation purposes than proposed in the past, often based on idealized performance [e.g. Hoyt 1999.I]. Some measures to obtain dynamic stability have been proposed, of which spinning is a particularly potent option. The risks of tether deployment, complexities of the operation and likely orbital exposure should be well-weighed against the potential benefits for debris mitigation.

Electrodynamic deorbit offers a cleaning service not only to spent stages but also to satellites after their useful life is completed. It delivers a very quick deorbit with respect to BAU, but very slow compared to momentum transfer or retro-rocket deorbit. Typically electrodynamic tethers provide however a significant mass advantage. From a risk mitigation point of view, a system with descent rate control seems particularly attractive. For a simpler, uncontrolled system the resulting collision risk seems perhaps to offer only marginal improvement with respect to the BAU approach, but it should be considered that removing satellites directly after use is not only good custom, but also an important way to make the risk of debris manageable and independent of future trends. An uncontrolled electrodynamic deorbit system should only be considered between about 700 and approximately 1500 km altitude (depending on the system design and inclination). For risk minimization, at an altitude of 600 km the tether should be disconnected from the payload. A fail-safe or safe-life tether is recommended, the possibility of intentional or accidental tether cut is to be taken into account. Tether cut is not likely to significantly contribute to the debris environment if attached heavy endmass(es) are released in response.

Various simplifying and generalizing assumptions have been made in the analysis, usually conservative, that should be reviewed on a case-by-case basis, including the Future Factor, solar activity, a maximum temporal horizon, the definition of catastrophic events and current limitation related to dynamic stability.

Part II - *Development of a SpaceMail system*

The genius of a construction lies in its simplicity. Everybody can build complicated things.

— Сергій Павлович Корольов (Sergei Pavlovich Korolev)

Part II of this thesis describes the design of a safe tether and the development and testing of a tether deployer system, including spool, brake system and controller.

4 Design Aspects of a Safe Tether

My name is Riesselmann, and I don't like tethers.

— Werner Riesselmann, one of the people that helped forward the YES2 project within ESA, as he introduced himself to the YES2 team in 2001

The development of the SpaceMail system, subject of Part II of this thesis, requires design of both the tether itself and its deployment system. This Chapter will focus on the tether. The prime material of choice, Dyneema®, is described and the Dyneema® tether braid is characterized. The tether material properties and dimensions affect the risk factors introduced by the tether deployment, such as recoil and meteoroid risk. An appropriate mitigation strategy is developed.

4.1 Characterizing the tether properties

Dyneema® SK65 is selected as material of choice for most of the tether length and the material and tether properties are discussed or determined in this section. Ultra high molecular weight polyethylene, like Dyneema®, is known to display complex mechanical properties, that are also temperature dependent (generally decreasing with temperature) [Kromm 2003]. For the SpaceMail flight, room temperature tests are therefore considered worst case.

4.1.1 Material selection

Various requirements are relevant for the selection of a tether material. The material shall be suitable for winding and deployment. It is advantageous if a tether can be wound and unwound without significant bending and torsional stiffness or shape memory. That enhances deployment performance and predictability of the endmass dynamics. Materials that can be produced as thin uninterrupted fibers can be loosely braided to improve integrity and combine the individual fibers' break strength while retaining sufficient flexibility. Also, braids maintain better integrity under torsion than twisted wires. Another critical parameter is that the tether material should interact gently with guides and other structural parts or mechanisms as it rubs along them at high velocity during deployment. The material should ideally display low friction levels and little abrasion. Polymers are good candidates to display such properties.

Total system mass is a prime driver behind material selection for space systems. Low tether mass can be achieved for mechanical tether applications if the tether material has a high specific strength σ_{br}/ρ_V or, alternatively, breaking length $\sigma_{br}/g\rho_V$ and characteristic velocity $\sqrt{(\sigma_{br}/\rho_V)}$, i.e. be both strong and light to provide high ΔV without succumbing under its own

weight (Section 2.2.1). For more modest applications such as SpaceMail ($\Delta V \approx 120$ m/s) a decisive parameter can be the maximum payload size that can be deorbited for the same tether mass, and also this parameter improves if the tether is made from a high specific-strength material.

A low material density can provide benefits as well as disadvantages. A low-density material can well have high specific strength but requires a relatively large volume for storage. Fortunately, due to its cubic dependency on dimension, mass benefits will generally outweigh the additional cost of volume, such as increased encasing structure. This may not hold yet for the small systems of early applications. However, for thin tethers with modest strength requirements, the dominant design driver will often be survival probability, i.e. resistance to meteoroids and debris particles. This probability is governed primarily by the average projected width of the tether (Section 4.3.1). A low density will thus in most cases be a favorable property.

Other properties could be relevant depending on the exact application and position within the tether. This may lead to a hybrid tether design. For a certain single application different materials can be utilized at different places within the tether. A material's melting point, heat capacity and general thermal dependency are relevant properties particularly on those sections of the tether that are in contact with hot parts (such as bare aluminium structures in sunlight) or where large braking forces are applied by friction. There these properties can dominate selection of material or tether diameter (Section 4.3.3). High optical reflectivity makes it possible to observe tethers optically from the ground. Low absorption coefficient and high emissivity help keep a tether cool once deployed. For long duration missions with high strength requirements, environmental resistance to Ultra Violet radiation (UV) or atomic oxygen could play a role. Stiffness and damping affect tether dynamics. A stiff tether can be well controlled as long as it is under tension but it is more prone to slackness and resonances. Viscosity is a beneficial property to dampen longitudinal oscillations and increase dynamic stability (Sections 3.2.2, 4.1.5, 8.4.3). These properties depend also on the manufacturing procedure. Non-linear behaviors such as creep and hysteresis will limit predictability of the behavior and are therefore undesirable.

Table 18 provides some tether material properties. Some other materials are added for comparison. Newer and stronger variants of these materials are continuously appearing on the market, therefore this data is only indicative.

Polyaramid (marketed as Kevlar and Twaron), is a classic candidate for space tether materials, known from bullet-proof vests. It is high-strength and heat resistant up to 500°C. There are some disadvantages to the use of Kevlar for tether deployment [McKenna 2004]. It has a rough surface and high yarn-to-yarn friction coefficient of 0.15. It tends to crack and flake when bent repeatedly around a small radius (<10 tether radii). Under repetitive wet yarn-on-yarn abrasion or buckling abrasion Kevlar has a limited lifetime. For example, detectable strength loss occurs after 1000 bucklings, severe strength loss after 20,000.

More recent superfiber developments such as the experimental polyketon Carilon (not in production, Section 4.4) and the heat-resistant Zylon have been found sensitive to material

degradation under ultra-violet. Vectran is in many ways similar to Kevlar, it is rough and sensitive to repeated buckling. M5 strength properties are promising, but it has not been available for this project.

Dyneema® is a ultra high density polyethylene with a crystallinity of 97% or higher. A gel spinning process produces a high molecular alignment responsible for the material's high tensile strength. Its volumetric density is less than water. Very smooth to the touch and flexible, it has a yarn-to-yarn friction coefficient of only 0.06. This is one of the reasons it is a popular material for kiting. The material has a fatigue resistance about 10 times better than Kevlar and hardly gets damaged under repetitive bending and rubbing [McKenna 2004]. Tethers from the same material, though branded in the US as Spectra, have been used successfully in the SEDS and TiPS missions. Due to a high reflectivity these polyethylene tethers could be observed optically from the ground [Carroll 1995.I]. Their high emissivity $\varepsilon \approx 0.8$, and low absorption coefficient $\alpha \approx 0.2$ guarantee a low temperature in a space environment, at which its mechanical properties further improve (Section 4.3.3). The material becomes brittle only below -150°C.

On the other hand, degradation of strength and other properties starts at 70°C and its melting point is only 150°C. The mechanical properties have been found relatively sensitive to UV radiation, although this does not necessarily preclude safe use (Section 4.4). The fibers are coated with an anti-static film of about 1% mass fraction for smooth behavior on guides during the various winding and unwinding processes.

Dyneema® SK65 by DSM High Performance Fibers in the Netherlands has been selected as primary material of choice. Despite recent availability of higher grades such as SK75, for consistency the SK65 grade has been used exclusively throughout this project.

Material	Tensile strength [GPa]	Density [g/cm^3]	Characteristic velocity [km/s]	Modulus of elasticity [GPa]	Melting point [Heat resistance] [°C]
Polyethylene (Dyneema SK65)	2.8	0.97	1.70	77	150 [70]
Polyethylene (Dyneema SK75)	3.6	0.97	1.93	116	150 [70]
Polypropylene	0.6	0.91	0.81	2	160
PPT Aramid (Kevlar, Twaron)	2.8	1.44	1.39	109	[560]
PBO (Zylon)	5.8	1.56	1.93	270	[650]
PIPD (M5)	>5.8	1.7	1.85	350	[530]
Aromatic polyester (Vectran)	3.2	1.4	1.51	75	330 [220]
Aluminium	0.6	2.7	0.47	70	660
Steel	2.8	7.8	0.60	200	1500
Carbon nanotubes (experimental)	3.6 to 150	1.4	1.60 to 10.35	800	>1000

Table 18. *Fiber and wire material properties. Values are indicative only.*

4.1.2 Braiding of the tethers

Dyneema® SK65 tethers have been specifically produced for the project. A tether is typically braided from fiber bundles. Through the braiding process the strength of the thin fibers can be combined while a highly flexible cable is obtained with good integrity and resilience against torsion [McKenna 2004].

A braid will not reflect one-on-one the fibers' properties. The braid, depending on braiding angle, the level of tension and compression, will have about 10-20% lower density than the pure polyethylene density of 970 kg/m^3. The linear density on the other hand may be increased by 3-10% compared to a equal-length bundle of straight fibers, due to the angle of the braid. Due to internal rubbing, also viscosity of a braid is increased. Elastic behavior of a braid or rope is non-linear, specifically low when tension levels are low, whereas in addition recoverable and non-recoverable elongation is observed under consistent loading. The strength of the braided tether is reduced with respect to the sum of fiber strengths (Section 4.1.3). Loads are not distributed perfectly symmetrically over all fibers, the fibers are necessarily under an angle with the tether direction and they receive additional bending and stresses from the pressure of adjacent fiber bundles. As the selected Dyneema® material is very smooth and already has an antistatic coating on the fibers as delivered, no oily substances or further additives are required in the braiding process. The main effects of braiding to take into account as compared to the fiber properties are reduction in break strength and reduced stiffness at low tension.

Commercial Dyneema® braids undergo a thermal prestretch of about 20% at 140°C to remove the play due to braiding, stiffen and stabilize the behavior for high tension applications. The prestretched tether will display stronger shape memory when wound onto a spool creating a coil shape in a low tension unwinding, with its own spring behavior that displays very low stiffness (Section 4.1.4). Loading or heating can lead to some relaxation to the previous, unstretched state.

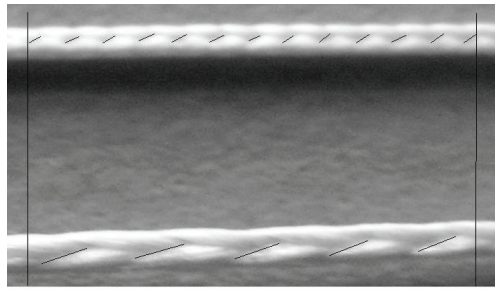

Figure 44. *Dyneema® (R) 8x200 braids, 3 mm, vs. 7.5 mm stroke, 20.1 g/100 m vs. 18.5 g/100 m*

For this project some particular treatments have been implemented. In addition to thermal prestretch, a cold prestretch of about 30N is considered. During the initial inertia-driven part of deployment, the performance at very low tensions (<0.1 N) is critical. Behavior of a

stiff thermally prestretched tether would then be governed by the shape memory effects. The selected "plaited length" or stroke of the braid (due to braiding angle) impacts tightness and suitability for splicing, bending stiffness, linear density, shape memory and general feel. For this project mostly a tubular braid of 8 bundles of 200 denier linear mass density ("8x200") has been selected with a large stroke of ~7.5 mm, for maximum handling, flexibility and easy splicing (Figure 44). To speed up the manufacturing process, the tether is sometimes produced in a number of equal pieces that are manually spliced together, typically without loss of strength.

4.1.3 Break strength

Break strength of Dyneema® tether samples has been determined by pull test in the context of the TSE, YES and YES2 projects, for various braids and treatments.

Tensile strength of the sample braid is hard to reproduce reliably and can deviate significantly from the manufacturer's value of 2.8 GPa for fibers. It is recommended to express the strength of a tether in terms of actual load, rather than as tensile strength $\sigma_{br.}$ This is because the cross-sectional area of a tether is ambiguous. The fibers are not aligned with the tether, the cross-section is not circular and it is partially void of fiber material. The fiber cross-sectional area A_{fiber} should ideally be used, which is simply computed as ratio of linear and volumetric density:

$$A_{fiber} = \rho/\rho_V . \tag{4.1}$$

However, as it is common practise to use a circular cross-sectional area A based on the unstretched diameter of the tether, a tensile strength is calculated here based on this definition.

Tensile test results are presented in Table 20. For Dyneema® SK65 braids, the resulting tensile strengths range from 44-73% of the fiber strength, with an average of 56%. Thermally prestretched tethers should show a somewhat higher strength, but the improvement was found to be not significant. When dealing with braids rather than fibers, a significant correction factor must be thus taken into account. A proper fixture involves wrapping of the ends of the tether sample various times around a shaft of ten to twenty times the tether diameter. Clamping by squeezing of the fibers or through a knot results in stress concentration and fiber damage, significantly reducing the performance further, about by a factor 2, as evidenced in Table 19.

Project	Tether braid	Fixture	Test location	#	Break Force [N]	StDev [N]	diameter [mm]	Break strength [MPa]
YES2	8x400 SK65	knot mid	Reggio Emilia	5	256	20	0.7	665
YES2	8x400 SK65	knot edge	Reggio Emilia	5	284	20	0.7	737
YES2	8x400 SK65	clamped	Reggio Emilia	5	210	20	0.7	546

Table 19. *Pull test results for YES2 projects (weakened tether)*

Project	Tether braid	Fixture	Test location	#	Break Force [N]	StDev [N]	Diameter [mm]	Tensile strength [MPa]
YES	7x100 Dyneema ® SK66	wound on rod	Tether Applications	3	165	-	0.3	2334
YES	11x215 Spectra	wound on rod	Tether Applications	3	800	-	0.6	2829
TSE	8x400 SK65	wound on 25 mm rod	EuroCord	1	692	-	0.7	1799
TSE	10% thermal prestretch	wound on 25 mm rod	EuroCord	1	782	-	0.7	2031
TSE	21% thermal prestretch	wound on 25 mm rod	EuroCord	1	708	-	0.7	1838
YES2	8x400 SK65	wound on 8 mm rod	Reggio Emilia	5	567	20	0.7	1474
YES2	8x200 SK65	wound on rod	Krefeld	2	300	-	0.5	1528
YES2	8x200 SK65 4% prestretch	wound on rod	Krefeld	2	240	-	0.5	1222
YES2	8x200 SK65 6% prestretch	wound on rod	Krefeld	3	337	-	0.5	1715

Table 20. *Pull test results for the YES, TSE and YES2 projects*

4.1.4 Stiffness and viscoelastic effects

Stiffness *EA*, with *E* the Young's modulus of elasticity, has been measured for various tethers with different prestretch and load histories, in three ways.

The first method (A) is using a pull bench on a sample of approximately 20 cm to measure the strain versus the tension, until breaking. Break strain is found to be about 3.5% of full length for a non-prestretched tether, and reduces for freshly prestretched tethers yet increases again if such tethers have become flexible following one or more winding and unwinding cycles. A disadvantage of this rather standard test is that it provides information on stiffness especially for tension levels close to the break strength, but not for the low tension levels that are typical during deployment (2-10 g for most of the deployment, 100-500 g for final braking), see Figure 45.

The second method (B) involves a hanging tether of about 3 m. A suspended mass is changed in steps, and the length change is monitored each step. Detailed effects at low tension can now be studied. The suspended mass is first increased then decreased. Stabilization effects due to the load history are apparent. Even a limited dynamic preloading (winding at 1 N, Figure 46) plus static preloading at 5 N is found to have a significant impact on low tension stiffness.

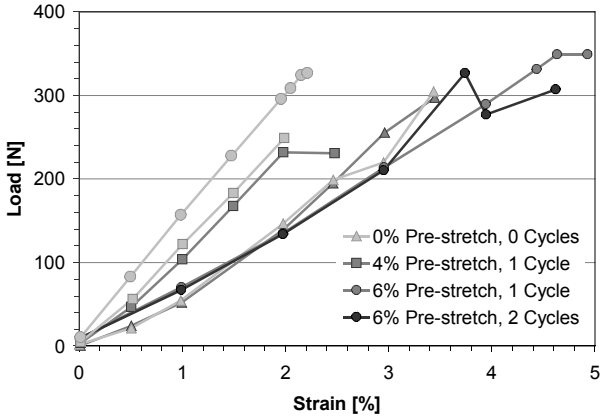

Figure 45. *Strain test performed on Dyneema® SK65 8x200 tethers with various thermal prestretch and loading history (10 N winding/0 N unwinding cycles).*

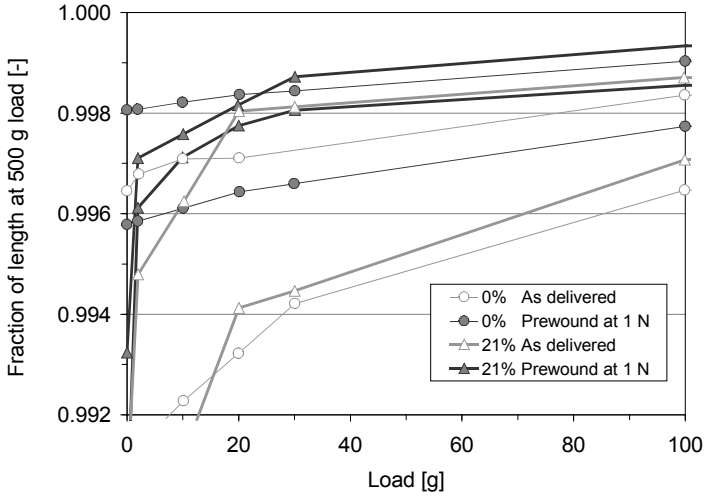

Figure 46. *Coil and strain effects for prestretched tethers*

The third method (C) is a combination of A and B, in which a pull test set-up is used at low tension levels. Repetitive testing can be performed on the same sample. This testing has been performed on the YES2 tether by University of Modena and Reggio Emilia. The load is selected to approximately match that of a final shock at the end of deployment and has been applied 20 times. Between loading 10 and loading 11, the load is completely removed and a new data sampling is started. A complex behavior is observed (Figure 47), that is typical for ropes [McKenna 2004]. Multiple loadings stiffen the tether by removing flexibility due to the braiding. At the same time a creep-like behavior is visible as the braid is compacted and

(bundles of) fibers and possibly molecules are being more aligned, increasing the sample length. Full release of the tension lets shape memory dominate and the tether returns much to its initial state. The resulting stiffness starts at EA = 1000-2000 N for the very first loading (the "awakening" of the braid) but reaches already a near-stable value during the second loading, EA = 4000-5000 N. As the flight tether is wound under 10 N pretension, the awakening can probably be assumed to have already occurred by the time of deployment.

A stretch and relaxation test was also performed (Figure 48). At various points during the stretching process, the tether sample is allowed to relax at constant length. The fractional relaxation appears rather constant. Upon continuation of the pulling the original curve is quickly followed again. A hypothesis for this behavior is that the fibers or molecules inside the fibers get slowly aligned when under static tension, causing them to lengthen a bit, and strain to drop, yet stiffness to increase, until strain is increased again to a higher level then before, where a new reservoir of fibers or molecules is "unfolded and stretched". The fibers lengthen a bit this way but from cycle to cycle the relaxation reduces because the percentage of un-stretched molecules decreases.

Note that it also has been consistently observed that, after tension is fully removed, a tether shrinks even below its original length. This is probably an additional effect related to memory from before braiding or 30 N cold prestretching during the braiding process.

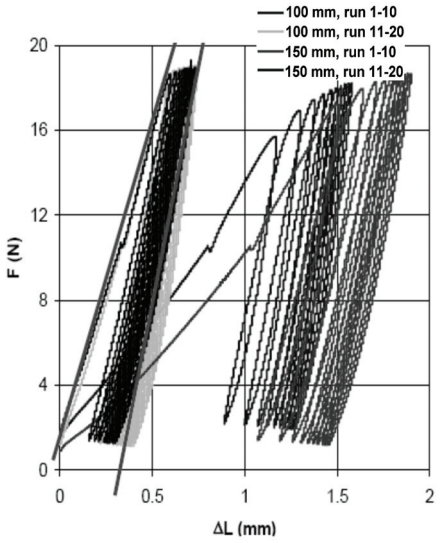

Figure 47. *Cyclic load-displacement diagram 100 mm and 150 mm Dyneema® tether*

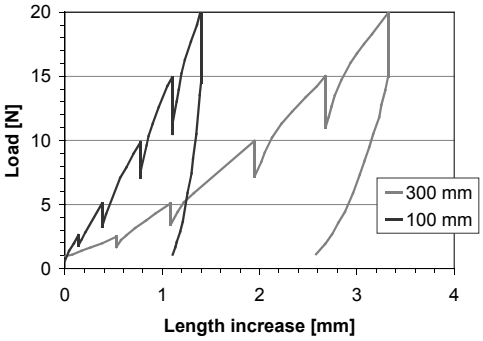

Figure 48. *Relaxation test 100 mm and 300 mm Dyneema® tether*

Table 21 summarizes the results. The case B data represented here focuses on the wound/preloaded case for low tension which is considered most relevant for flight. Data points are plotted in Figure 49, assuming a break strength of 300 N for 8x200 and 700 N for 8x400 braids. The general trend of increasing stiffness or decreasing braid contribution for increased loads is clear and can be estimated within about 30% accuracy.

It can be seen how for thermally prestretched tethers at very low tension the coil shape memory superimposes on the braid and fiber stiffnesses and the tether behaves as a very weak spring in the regime of deployment tensions. The rigidity of the prestretched tethers may also lead to irregular behavior on the brake system at low tension (Section 5.4.4). For these reasons, for flight a tether is selected with only cold prestretch, with an assumed EA ≈ 5000 N in the range of deployment tensions.

Project	Tether braid	Test location	Method	Load [N]	n	EA [N]	d [mm]	E [GPa]
YES2	8x200 SK65	Krefeld	A	300	2	8570	0.5	43.6
YES2	4% thermal prestretch	Krefeld	A	240	2	12000	0.5	61.1
YES2	6% thermal prestretch	Krefeld	A	337	3	14670	0.5	74.7
TSE (*)	8x400 SK65	Delta-Utec	B	0.1	1	616	0.7	1.60
TSE	8x400 SK65	Delta-Utec	B	5	1	4109	0.7	10.7
TSE	10% thermal prestretch	Delta-Utec	B	0.1	1	62	0.7	0.16
TSE	10% thermal prestretch	Delta-Utec	B	5	1	6214	0.7	16.1
TSE	21% thermal prestretch	Delta-Utec	B	0.1	1	174	0.7	0.45
TSE	21% thermal prestretch	Delta-Utec	B	5	1	6216	0.7	16.2
YES2	8x200 SK65	Delta-Utec	B	1.2	1	4000	0.5	20.4
YES2	8x200 SK65	Delta-Utec	B	17	1	6200	0.5	31.6
YES2	8x200 SK65	Reggio Emilia	C	20	2	4700	0.5	23.9

(*) TSE tests with method B were performed on 1 N wound, 5 N preloaded tether

Table 21. *Stiffness tests on Dyneema® tether*

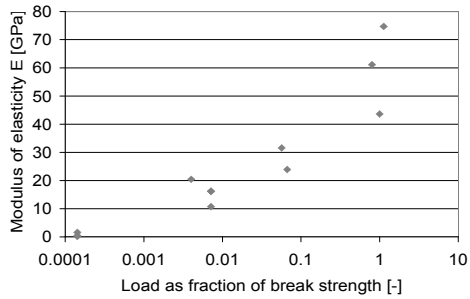

Figure 49. *Modulus of elasticity vs. load (Dyneema® tether)*

4.1.5 Damping

The amount of energy dissipation that occurs due to friction between fibers and bundles within the braid during stretching and relaxing of the tether (and to a lesser extent between molecules within the fiber) can be expressed using the damping ratio ζ. It has been estimated by a drop test, involving a variety of tethered masses (40 g to 1.7 kg) dropped from a range of heights (2.5 to 8 m).

For an underdamped system (ζ<1, leading to oscillatory response) two successive amplitudes x_1 and x_2 will have a ratio of

$$\frac{x_1}{x_2} = \frac{Ce^{-\zeta\omega_n t_1}}{Ce^{-\zeta\omega_n (t_1+\tau_d)}} = e^{-\zeta\omega_n \tau_d}, \tag{4.2}$$

with $\tau_d = \frac{2\pi}{\omega_d}$ and $\omega_d = \omega_n\sqrt{1-\zeta^2}$ (Figure 50). The logarithmic decrement δ is defined for a full oscillatory period as

$$\delta = \ln\left(\frac{x_1}{x_2}\right) = \zeta\omega_n\tau_d = 2\pi\zeta\frac{\omega_n}{\omega_d} = \frac{2\pi\zeta}{\sqrt{1-\zeta^2}}, \tag{4.3}$$

from which:

$$\zeta = \frac{\delta}{\sqrt{(2\pi)^2+\delta^2}}. \tag{4.4}$$

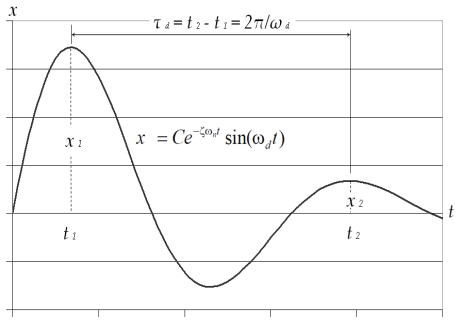

Figure 50. *Underdamped oscillation*

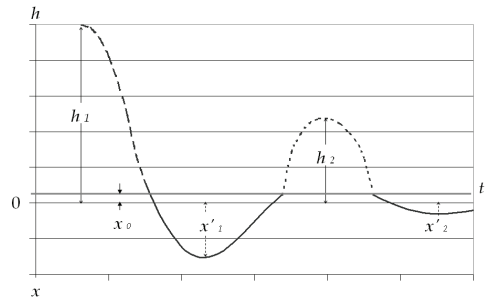

Figure 51. *Droptest damping dynamics (*h *&* x *at different scales).*

In a drop-and-bounce the tether will be tensioned only through (approximately) half of an oscillatory period (Figure 51). No damping will occur during the ballistic drop from known initial height h_1 and during the bounce up to maximum altitude h_2. Consequently the full-period logarithmic decrement for which Eq. 4.3 is defined will be twice that as would be indicated by the deepest points of successive bouncings x'_1 and x'_2. Furthermore, in the ballistic phase, the potential energy mgh takes the role of the spring energy $kx^2/2$. The logarithmic decrement may thus also, and more conveniently, be estimated from the ratio of heights:

$$\delta = \ln\left(\frac{x'_1}{x'_2}\right)^2 = 2\ln\left(\frac{x'_1}{x'_2}\right) = 2\ln\left(\sqrt{\frac{h_1}{h_2}}\right). \tag{4.5}$$

Note that in reality, due to the effect of gravity, there is some additional damping as the tether loses stretch and tension between the equilibrium point to the actual slack point. So the effective damping period is somewhat larger than half a harmonic period. The impact will, however, be small if the ratio η between equilibrium extension x_0 and maximum extension x_1' due to the bounce is small:

$$\eta = \frac{x_0}{x'_1} = \frac{g}{|\ddot{x}|}, \tag{4.6}$$

since $kx_0 = mg$ and $k(x'_1 + x_0) = mg + m|\ddot{x}|$, and, from the (damping free) energy balance, $x'_1 \approx \sqrt{(2mgh/k)}$, $\eta \approx \sqrt{(mg/2kh)} << 1$ for the tested cases. Alternatively, Eq. 4.5 can be said to hold if the peak tension is much larger than the weight of the test mass (or equilibrium tension).

All experiments are filmed by camcorder and results have been deduced from analysis of the footage. Generally, the first bounce of the end-mass is very clean and straight as the center of mass of the end-mass is then still aligned with the tether direction. At the maximum amplitude, velocity is zero, so a clear image of the maximum amplitude can easily be found within the footage. The results suggest a damping coefficient $\zeta = 0.06\text{-}0.09$ (Table 22). A value $\zeta = 0.08$ is assumed. No significant dependencies have been found within the investigated range of drop height, maximum acceleration, peak tension or tether length [Ishkov 2006].

h_1 [m]	m [kg]	l [m]	#	Approx. max tension [N]	ζ [%]
0.13	1.72	2.5	4	95	8.9
0.15	0.12	2.5	4	27	6.7
0.20	0.12	7.8	3	18	7.4
0.27	0.12	7.8	7	21	6.3
0.36	0.06	7.8	4	17	7.8
0.34	0.02	7.8	1	9	7.5
0.48	0.02	7.8	1	11	8.4

Table 22. *Damping coefficient drop tests*

4.1.6 Outgassing and extraction

Outgassing of Dyneema® SK65 samples has been performed for YES2 by ESTEC's TEC-QMC laboratory (Materials Physics and Chemistry Section) according to the ECSS Q70-02a standard (Materials Report Number: 4604). Measurements of 3 samples are averaged at 125°C, after outgassing of each sample at 125°C for 24 hours at a pressure below 10^{-5} mbar.

The material is compliant with the limits defined by the standard. Total mass loss averages 0.34% (including), 0.03% is collected as condensable volatile on a 25°C plate. The recovered mass loss of 0.29% provides the estimate of the fraction of outgassed material other than water, for which ESA's upper limit is defined as 1%.

An extraction in chloroform has also been performed, removing any soluble substances, including esters and carbohydrates to about 1.9% by mass. A significant amount of the extracted matter is thought to originate from anti-static coating that is applied on the Dyneema® during the fiber manufacturing process.

4.1.7 Friction behavior

Tether friction has been determined in combination with the planned contact material. An aluminium pole of 13-24 mm diameter is used as main contact surface for the SpaceMail tether deployment system (Section 5.4). The exact value of the coefficient depends for a large part on the surface coating and roughness of the pole. The rationale and influence of the barberpole design and surface treatment is discussed in detail in Section 5.4. Friction is estimated from fitting of tension measurements of a deploying tether against a brake performance model for various brake settings. Other, simpler, methods have been crudely explored for tests that aim to identify *a priori* whether friction may be majorly dependent on tether thermal prestretch or atmospheric density.

To determine the effect of tether heat treatments on friction, the drop time for a small sliding tethered mass has been used. A drop test is performed on the tethers over a drop of 3.08 meters. A mass m_1 of 32 g attached to one side with a countermass m_2 of 10 g causes the tether to slide over 2 horizontal aluminum 12.7 mm diameter bars at 9 cm distance (Figure 52). The masses are small, representing deployment tension levels. The radius of the bars is selected to represent the foreseen pole, whereas their separation is necessary to prevent the lines on either side from interfering. Twenty handclocked measurements have been made for each tether (Figure 53). Such crude measurement method of about 0.1 s accuracy is judged sufficient considering the qualitative test objectives as well as the actual spread in drop times.

The friction coefficient f is estimated using the following simple model that assumes exponential friction increase with the bend angle (Section 5.4.1):

$$f = \frac{\ln\left(\frac{m2}{m1}\cdot\frac{\left(1-\frac{2h}{gt^2}\right)}{\left(1+\frac{2h}{gt^2}\right)}\right)}{\theta} \tag{4.7}$$

with θ the total deflection angle in radians, π in this case. In this model the tether mass, about 0.5 g, is neglected.

The estimated friction coefficients turns out to be 0.28±0.015 for the untreated tether, 3.2% higher for the 10% prestretched tether and 6.5% higher for the 21% prestretched tether.

Possibly the observed effect of prestretch is not so much related to different surface interactions but more to increased dissipation as the more stiffened fibers are being bent around the pole. This dissipation is not represented as a separate parameter in this simple friction model.

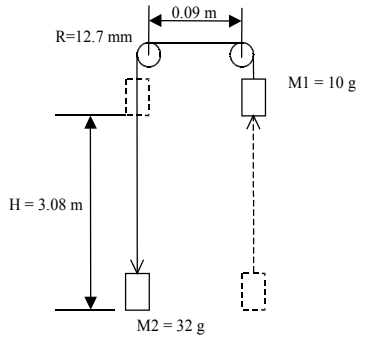

Figure 52. *Friction droptest set-up*

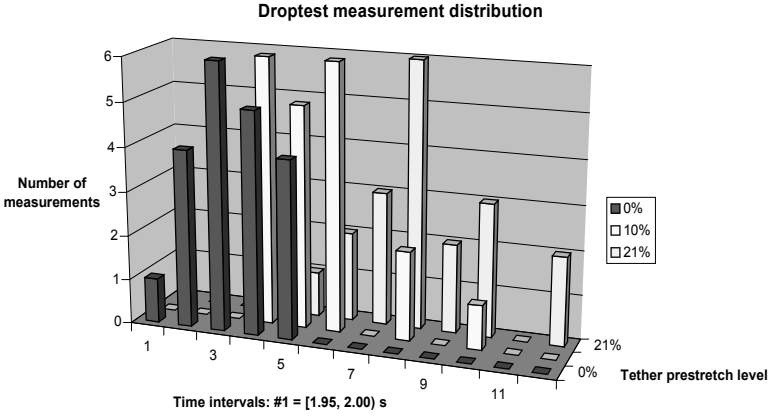

Figure 53. *Droptest histogram for various tether types to estimate friction*

To assess whether vacuum conditions significantly affect (static) friction, a drop-mass set-up including a barberpole engineering model has been built in a vacuum chamber (Samara State Aerospace University, Samara, Russia, Figure 54). The tether is draped over suspended metal rods to obtain a safe distance to the pole box, and to allow for smooth sliding, thus obtaining the possibility to test the barberpole in horizontal configuration as displayed. A known mass is attached to each side, 2 and 20 grams, the larger on the outgoing side. The tether is wrapped a number of times around the barberpole, keeping the masses from dropping. The pole can be driven (turned) by a controller set-up outside the vacuum

chamber. If the number of wraps is reduced, at a certain point, the masses will start to drop and this critical position can be converted to a friction estimate (Section 5.4.1). Vacuum level achieved is about 5.10^{-2} mm Hg. There is an observation window on either side.

The test is performed 6 times in ambient atmosphere, and 4 times in vacuum according to the procedure in Table 23. Each test in vacuum, with only minimal equipment and access requirements, can establish one measurement for friction coefficient. The results show virtually the same friction coefficient in both cases , 0.26±20% ambient vs. 0.24±33% vacuum. Either of the extremes of measured friction coefficients can be recovered by a controller correction of only 0.2 wraps (ambient) or 0.4 wraps (vacuum).

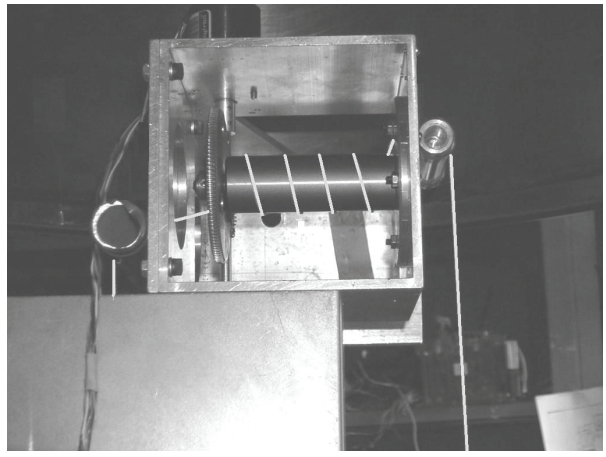

Figure 54. *Set-up in vacuum chamber test. Incoming side on left, outgoing on right. Masses are suspended from the tether on either side (not visible). The tether path is highlighted for clarity.*

1	The pole is turned to 3 turns initially
2	The set-up is put in identical and stable configuration. By manually pulling the heavy mass down some 10 cm, the tether is pulled through the barberpole and reaches a consistent equilibrium helical shape around the pole
3	Establish vacuum
4	Turn the pole back in small steps from three turns until the heavy mass slides down, but the light mass does not slide up. This indicates that the slack created by turning of the wheel on the incoming side is taken by the heavy mass on the outcoming sign, so the friction in the system has lowered close to the weight of the heavy mass. Before that level the light mass may move down but the heavy mass remains in position.
5	Turn in small steps back until not only the heavy mass drops but the small mass starts rising. The friction level now equals 50 - 2 = 48 grams. The downward motion will yet be irregular. Note the value of turns. This is the main measurement.
6	Turn the pole back 0.5 turns at once. The mass will start dropping more smoothly. The drop time and behavior (smooth or interrupted stick-slip) is noted and provides the second, qualitative measurement, which is also used to verify that indeed the pole was in a critical position earlier.

Table 23. *Friction in vacuum test procedure*

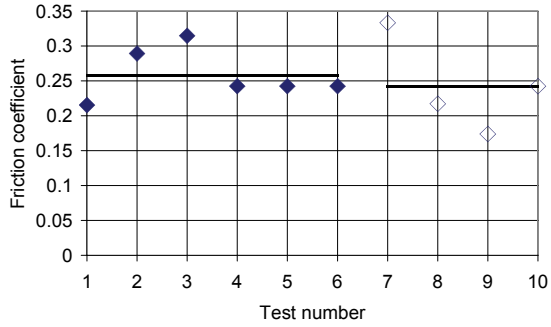

Figure 55. *Friction coefficient ambient vs. vacuum. The black lines indicate average value*

4.1.8 Twist and internal braiding torque

A tether can exert a torque as a result of twisting of the tether as a whole or due to build-up of twist in the fiber bundles during the processes surrounding the braiding. This torque affects the tether sliding behavior when it passes the brake system (Section 5.4.1), and may in extreme cases also impact the tether shape and end mass motion after deployment in weightlessness. Preliminary tests indicate a torque level in the order of about 1e-8 Nmm/° for a single meter 0.5-mm diameter tether at deployment level tensions [Kruijff 1999.I].

A log of tether twist and a twist control strategy is therefore introduced. Axial deployment from a spool leads to introduction of one full twist per deployed loop (Figure 56). Clockwise unwinding is defined to introduce *negative* twist in a tether. As the loop length is dependent on the spool diameter, the amount of introduced twist per meter varies over the full unwinding. As the tether is captured on another spool for a subsequent unwinding, a further varying twist, or one in opposite direction could be superimposed. A simple effective method to manage this potentially complex matter is to wind the tether from a reel (perpendicular from its shaft) onto a spool core installed with alternating orientation for each winding cycle (Section 5.2.1). In this manner, no twist is introduced during winding, and each unwinding the opposite twist is introduced compared to the previous, keeping the total amount of twist in check.

A tether braiding torque sometimes becomes apparent when the tether is bent or tensioned. Untwisted tethers regularly have a natural tendency to curl up when compressed, but not always. Manual twisting generally leads, as expected, to a curling tendency, which can be superimposed on the natural tendency, and can also be used to cancel out a natural tendency. The direction of the internal torque can be determined from the curling tendency (Figure 57): if two ends are brought together, the tether assumes a shape of minimum energy. The braiding torque within the tether can be quantified by twisting the tether in the proper direction until the curling tendency has disappeared. The relevance of this effort is that the (negated) number of twists applied per meter can help to predict the tether dynamic behavior when in contact with a pole friction surface (see Section 5.4.1).

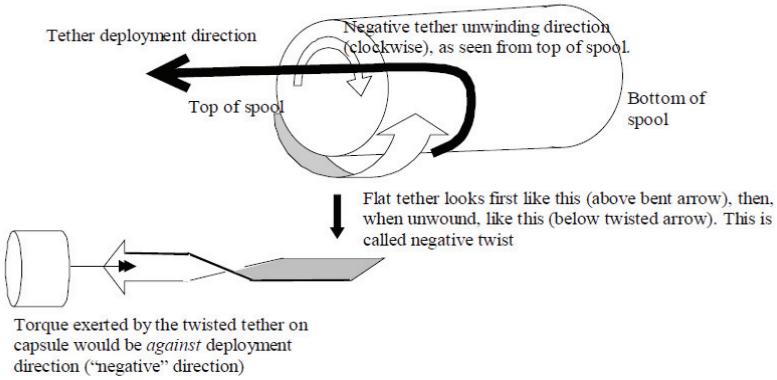

Figure 56. *Tether twisting during unwinding and definition of sign*

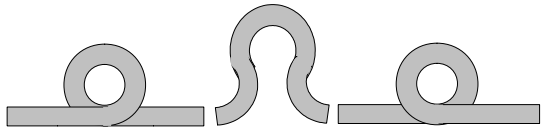

Figure 57. *Curling tendency on tether compression indicates positive (left), zero (mid) or negative internal torque (right)*

Tether torque results from a twisted tether through the combination of two effects: fiber torsion and torque from tether tension components around the tether core. Let τ be the number of tether twists per meter. Beam theory predicts torque Ψ_D for a beam of diameter D purely due to shear forces,

$$\Psi_D = 2\pi\tau G I_p = \frac{\pi^2}{16}\tau G D^4, \tag{4.8}$$

with I_p the polar moment of inertia and $G \approx 0.177$ GPA, the modulus of rigidity of polyethylene.

A circular bundle with diameter D of fibers of diameter $d = D/n$ will contain, taking into account the filling degree of tightly packed cylinders, about $\pi^2/8\sqrt{3}n^2$ fibers. Each fiber in the bundle will be torqued by the same amount, τ. If there would be no transfer of shear forces between the fibers, the shear-forces induced component of the the total torque $\Psi_{d,sh}$ for the bundle would then be,

$$\Psi_{d,sh} = \frac{\pi^2}{8\sqrt{3}}n^2 \cdot 2\pi\tau G I_p = \frac{\pi^2}{8\sqrt{3}}n^2 \cdot \frac{\pi^2}{8\sqrt{3}}\tau G\left(\frac{D}{n}\right)^4 = \frac{\Psi_D}{\frac{8\sqrt{3}}{\pi^2}n^2}. \tag{4.9}$$

For $\tau = 100$/m, $D = 0.75$ mm and $n = 50$, the resulting torque would only be about 6e-7 Nm. Measurements of torque under a 10 g load have been performed and suggest a significantly stronger torque for these conditions of about 5e-4 Nm [Kruijff 1999.I], close to the value that

would be expected for a uniform thread. This indicates that as a result of a finite bending stiffness contact pressure transfers the shear stress between adjacent fibers and lets the bundle act much as a single wire, $n \approx 1.5$.

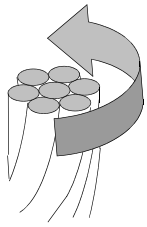

Figure 58. *Simple model of torqued tether as bundle of twisted fibers*

The tension in the tether will also contribute and this contribution will depend on tension. Assume for simplicity that all fibers in the tether are parallel (Figure 58). If such a tether is twisted, the central fiber will stay in place and only experience torsion. Fibers on the outer rim of the tether at radius r describe a helical shape with angle θ for which will hold:

$$\tan\theta = \frac{1}{2\pi r\tau}. \tag{4.10}$$

In reality the fibers are bundled and braided, so they change position within the tether. The simplified assumption of parallel fibers can be seen as an average. If the tether is carrying a load T in axial direction, one should however take account of the braid, and one can assume the axial load is distributed uniformly over the fibers spread uniformly over the (total) cross-sectional area A. Note that in contrast, in a twisted tether of parallel fibers, the highest strain would occur in the outer fibers, which have the most increased path length compared to the original length due to the helix shape (an analogous situation is presented in Section 5.4.1). In our simplified mode, a fiber at radius r will carry a load $\mathrm{d}T$ under angle θ, with a component in tangential direction $\mathrm{d}T_t$

$$\mathrm{d}T_t = 2\pi r\tau\frac{T}{A}\mathrm{d}A. \tag{4.11}$$

The stress related torque can now be calculated as follows.

$$\Psi_{d,st} = \int \mathrm{d}\Psi_{d,st} = \int r\cdot\mathrm{d}T_t = \int r\cdot 2\pi r\tau\frac{T}{A}\mathrm{d}A = \int_0^{\frac{D}{2}} r\cdot 2\pi r\tau\frac{T}{\frac{\pi}{4}D^2}\cdot 2\pi r\mathrm{d}r = \frac{D^2}{4}T\tau \tag{4.12}$$

This simple result shows strain-based torque is linear in tension and depends only on the twist and radius of the tether. For our example a torque of only 6.3e-8 Nm would result. At low tension levels this is a rather negligible contribution. The total torsion for the twisted tether thus becomes:

$$\Psi_d = \Psi_{d,sh} + \Psi_{d,st} = \tau\cdot\left(\frac{\pi^4 D^4}{n^2}\frac{G}{128\sqrt{3}} + \frac{D^2 T}{4}\right), \tag{4.13}$$

as mentioned with n ≈ 1.5 from experiment [Kruijff 1999.I].

4.1.9 Tether length effects: shape memory, viscoelastic recovery and creep

In a Dyneema® braid, shape-memory type behavior occurs at three levels. First, the braid can assume a coil shape after a winding process, especially thermally prestretched braids (Section 4.1.2). Second, fiber bundles that make up the braid can be aligned and tightened or angled and loosened up, as the braided tether is stretched, relaxed or compressed, affecting the braid density and diameter. Thirdly, the highly stretched and aligned long molecules of polyethylene may have a memory of a more natural, coiled configuration, that is for example triggered under untensioned heating. This multilevel behavior provides for complex creep and shrinkage characteristics. An attempt has been made to quantify the behavior under relevant conditions for space tether deployment.

Subjecting the tether to a number of 10-N load cycles can lead to a shortening of the Dyneema® tether with respect to initial length (Figure 59). This seems to be more true if the tether is squeezed (between rollers or plates) to obtain the tension load than if it is subject to a suspended load. The friction and possibly heating and deformation trigger a shape memory effect. The effect is stronger for thermally prestretched tethers, particularly if a temperature close to melting point has been applied without sufficient tension to stretch the molecules within the fibers significantly (as has been observed for YES2's tether "*Erik*"). At a temperature of 140°C a prestretch of at least 20% is recommended. Shrinkage is immediate but continues after the loading event for 30 minutes or so. The first loading causes generally a more significant shrinkage than the subsequent ones.

In contrast, after 20 seconds of loading of the tether by 14 N suspension only, no shrinkage is measured. Therefore it is deemed wise to control tension during winding with friction applied to the reel shaft rather than by squeezing roller guides in the winding machine (Section 5.2.1).

During continuous loading (such as in storage conditions) there is a creep effect and viscoelastic behavior can be observed. A 3-m long 8x200 tether has been kept under 15 N tension, and is observed to stretch about 0.5% in tensioned length in two hours, then remain virtually constant. After one day of relaxation, most of this creep has receded (or viscoelastically recovered) by a relatively slow shrinkage process. A further one day loading recreates similar creep in tensioned length. At removal of the load, there is some immediate shortening of about 0.3% (consistent with elastic behavior), followed by further viscoelastic recovery over the coarse of a day. This time a more permanent length increase effect of about 0.5% is observed also in the untensioned length, apparently caused by creep.

The various effects operate and interact in a complex manner. For the typical parameters of the SpaceMail mission each of these effects has a length impact of 0.1-0.5%.

To make the effects smaller and more predictable a number of measures has been taken. It is decided that the targeted flight tether only receives a cold prestretch of 30 N before winding (to remain well over the maximum tension expected in flight). The length measurement method has also been further scrutinized. One interesting finding is that the measurement wheel's diameter, around which the tether bends, is increased by 68% of the tether diameter,

rather than the expected 50%. The effect of slip on the measurement wheel has been shown to be less than 0.1%, and the effect of twist even less. Eventually, a procedure is established in which calibration segments of the tether are marked and measured both during winding and after unwinding to establish several correction factors taking into account the accumulated effects of elastic stretch on the measurement wheel, creep, viscoelastic and shape memory, as well as consistent contributions to length measurement errors such as slip.

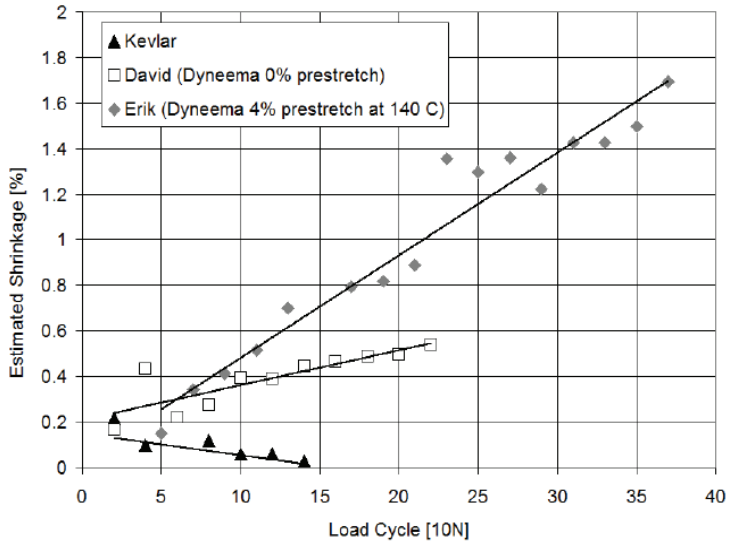

Figure 59. *Shrinkage (memory) due to load cycles. Triangle: Kevlar. Square: Tether* David *(0% prestretch). Diamond: Tether* Erik *(4% prestretch).*

4.2 Protecting the host platform

An early deployment stop may cause a threat to the deployment platform as the endmass may end-up lingering in its neighborhood and quickly or eventually collide. It is here assumed that the initial separation and deployment velocity is obtained by a spring system rather than by an extensible boom or cold gas thrusters. Mitigation approaches have been implemented. These include selection of sufficient initial velocity, addition of a shock damping system and design of the tether and its fixture to break or release in case of severe jerks.

4.2.1 Securing separation from the deployment platform

The question rises what should be the initial ejection energy E_{eject}, endmass m and ejection velocity V. As discussed in Section 2.1.4, the initial deployment is governed by inertia and has to overcome friction in the system until the built-up gravity gradient effect outweighs the friction level. A minimal ejection energy is therefore required. There are also arguments

to limit ejection energy, namely to limit system mass and improve safety during integration and, in flight, prevent high pitch-off rates that can result in tension oscillations, slackness or endmass rotation. Conditions are derived for minimum ejection energy and endmass to guarantee deployment.

First of all, the kinetic energy of ejection determines the minimum length that the tether deployment can achieve at minimal deployment friction (T_0), during the inertially-governed part of deployment. Kinetic energy should exceed energy dissipated by friction: $E_{eject} = E_{kin} = ½\, mV^2 > T_0 l$. Sufficient length should be achieved for gravity gradient (Eq. 2.7) to take over the deployment, $3ml\Omega^2 > T_0$, from which a condition for minimal ejection energy (Eq. 4.17) can be derived. From this perspective, for a given ejection system with known energy, a larger payload mass, at lower ejection velocity, is more robust.

A special consideration could be to deal with unforeseen spool friction peaks T acting over a short time interval Δt. They can in principle be considered to act to increase the effective T_0 (Section 8.5.1), but do introduce an additional risk. Ejection momentum mV determines the amount of dissipative friction shocks and jerks that that can be accepted during early deployment: $mV >> \Sigma(T\Delta t)_{shock}$. The impact of this contingency on the ejection energy requirement can thus be written as Eq. 4.18. The issue is that such brief peaks can lead to near instantaneous deceleration. If deployment is controlled by a barberpole brake aiming at a particular deceleration (Section 5.4), the spool peak level T will be amplified by the brake proportionally to the endmass m. Before the brake controller can respond and turn down the brake level, the deployment may be stopped. For this case, opposite to the earlier conclusion (Eq. 4.17), for a given ejection energy, robustness of deployment will decrease with increased mass.

Secondly, the tether (not the endmass) deploying at low velocity may often get, very briefly, stuck due to internal static friction peaks T_{stuck}. This behavior depends on uniformity of the spool unwinding and has to be experimentally determined. In fact, any friction controlled deployment with somewhat irregular tension can be seen as a continuous tug-of-war between tension peaks and endmass inertia. In a jam, the kinetic energy E_{kin} is transferred to strain energy E_{strain} and a strain tension T_{max} arises that may overcome jam tension T_{stuck}:

$$E_{kin} = \frac{1}{2} m\dot{l}^2 = E_{strain} = \frac{1}{2}\frac{EA}{l}\Delta l^2 = \frac{1}{2}\frac{l}{EA} T_{\max}{}^2 , \tag{4.14}$$

$$T_{\max} = \dot{l}\sqrt{m\frac{EA}{l}} . \tag{4.15}$$

A friction peak has the ability to stop the tether, with mass ρl (briefly), if it is larger than the jam tension T due to inertia of the tether mass:

$$T = \dot{l}\sqrt{\rho EA} . \tag{4.16}$$

If the tether gets stuck, once the shock reaches the moving payload, the tether will start to stretch further, due to inertia of the still moving payload, and tension will rise towards T_{max}. If $T_{stuck} < T_{max}$ or T_{stuck} drops in time, then deployment will continue. Usually the margins in

this process are large enough that the tether never actually comes to a standstill, but it can also undergo a 'stick-slip' process as described, especially during low velocity deployment. Therefore initially a condition must hold as expressed in Eq. 4.19 in terms of E_{kin}. At the end of nominal deployment, at large tether lengths (EA/l is low) and at low deployment velocity this mechanism can well be the prelude to deployment stop accompanied by a lightly bouncing endmass. For the purpose of initial deployment safety, a stiff tether will help, and so does the fact that the tether is still short. For a given ejection system, this requirement for ejection energy is independent of payload mass. It remains however important to design the spool properly and avoid high levels of T_{stuck}.

Eq.	Threat to continued deployment	Condition
4.17	Early deployment friction	$E_{eject} > T_0^2/(3m\Omega^2)$
4.18	Cumulative effect of friction peaks	$E_{eject} >> ½ (\Sigma(T\Delta t)_{shock})^2/m$
4.19	Instantaneous jerk	$E_{eject} >> ½ T_{stuck}^2 l/EA$

Table 24. *Causes of early deployment stop*

4.2.2 Understanding recoil

The main concern for the operator of a platform from which a tether is to be deployed is an unexpected sudden jam in early deployment. It may lead to rebound of the endmass and collision, or a wrapping of the tether around the platform and, again, eventual collision of the endmass with the platform. It must be said that, considering the faultless flight record from a deployment perspective (SEDS-1, SEDS-2, TiPS, Table 1) and 650 km of deployment tests performed in the context of YES, TSE and YES2 projects (Table 39), the probability of a jam for a spool deployment can be considered very low (the situation is different for reel deployments). Nevertheless due to a controller problem, spool integrity issue or faulty structural design a tether jam remains conceivable and must be addressed. An effort is undertaken to identify zones of deployment based on jam response, assuming a tether as yet without any mitigation means included. Next, for each zone an adequate mitigation approach is sought. In the context of the YES2 project, tether simulator tools have been developed for this purpose by Sergei Naumov (SSAU) and Dr. Chris Blanksby (RMIT).

The Naumov tool is a basic 2-DOF tether simulator with straight tether assumption, able to integrate the relevant tether and gravity forces (Section 2.1) during a typical early deployment [Ishkov 2007]. At a given time a jam can be introduced. The dynamics of the jam are calculated using the relevant differential equations. The jam effectively reverses the velocity vector at the moment of a jam and provides a tension peak following closely Eq. 4.15, yet including the effect of damping. As a result of the velocity inversion, the tether becomes slack and the endmass undergoes unconstrained motion until distance between the

host platform and endmass becomes equal to the "jammed" tether length, at which time a second impulse is applied. And so on.

Simulations are performed for a 12-kg endmass ejected at 2.4 m/s with a 0.5-mm Dyneema® tether with properties as in Section 4.1.1. The results suggest to divide the deployment in three zones (Table 25). At very short lengths, there may be a direct impact of the host. The critical phase extends to a few hundred meters, within which the tethered endmass will erratically orbit the host. A damping factor of 0.075 (equivalent to an approximate reduction in velocity of around 30% per bounce) leads to a limiting deployed length for this phase of 350 m. Without damping this phase could extend to as much as 800 m. For jams later into the deployment there is no risk to the host.

Zone	Length	Description	Note	Countermeasure
1	0-10 to 100 m	Collision on rebound	The endmass contacts the host directly upon rebound. The exact limit depends on the host shape and size. For larger lengths the Coriolis effect causes a drift that leads the endmass past the host upon first passage.	Dissipate jam energy (Section 4.2.3), passive tether release (Section 4.2.5) or cut (active)
2	10-100 to 350 m	Orbiting of host	The endmass orbits the host erratically, the tether is likely to attach to the host at some point, shorten the free tether length and alter the trajectory until eventually impact is imminent. Impact energy gets lost with increased initial length and increasing number of snags before impact.	Active tether cut
3	>350 m	Safe bounce	The gravity gradient is large enough to recover the bounce before the endmass reaches the host, or even to prevent significant slackness altogether.	No measure required

Table 25. *Safety domains in case of tether jam*

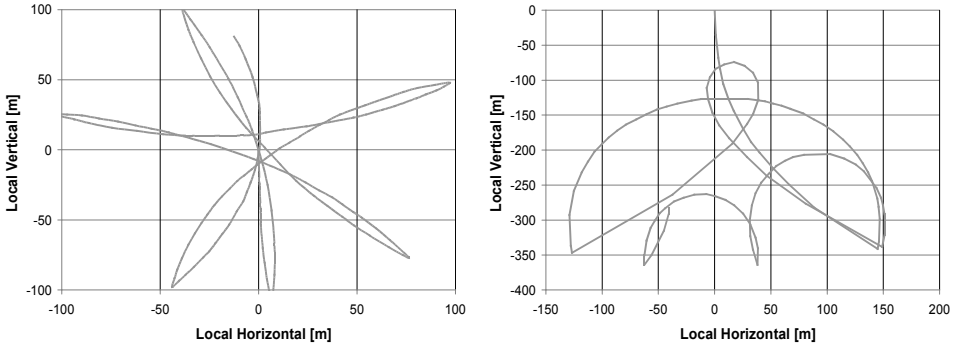

Figure 60. *Jam simulation using simple velocity reversal, length = 110, 360 m*

A qualitative assessment of the wrapping event has been made for YES2 by Dr. Chris Blanksby (Royal Melbourne Institute of Technology). His flexible tether model uses a lumped mass representation of the tether, includes full tether flexibility and 3-dimensional motion, similar to MTBSim (Section 2.3.1). The model is also capable of simulating tether – structure contact, including identification of contact events and post-contact dynamics. Multiple contacts can be studied within a given simulation. An important limitation is that the model contains no damping. In Blanksby's simulation the tether passes the platform twice without contact. After the third bounce, a skip-rope motion causes the tether to slide along the platform body and at some point it gets caught. This event effectively shortens the length of the free tether, further exciting the skip-rope mode and thus the number of subsequent contacts quickly increases.

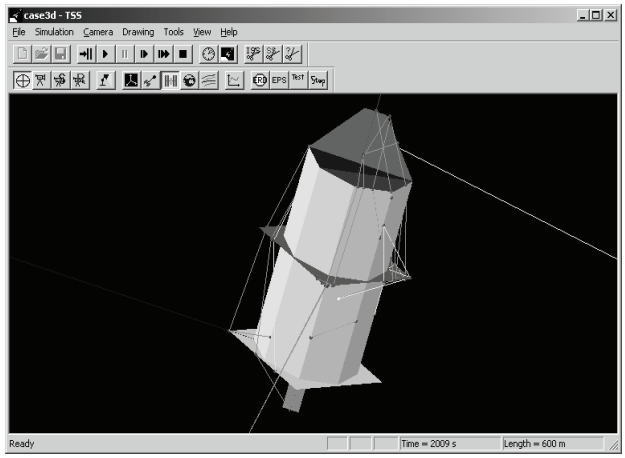

Figure 61. *3D Contact modeling of 600 m jammed non-viscous tether on Foton vehicle*

4.2.3 Ripstitching

Damping decreases the critical deployment zone in which an anomalous jam leads to wrapping of the endmass around the host platform. Inclusion within the tether an additional passive damping system that triggers in case of anomalous shocks can further decrease this zone. At the same time the approach velocity of the endmass towards the host platform is reduced, buying time for a software-controlled autonomous tether cut, before the tether can wrap around the host. Also the likelihood of a direct impact can be decreased.

The concept of the "ripstitch" damper system is sketched in Figure 62, showing a single "rip", or tether section folded in S-shape and stitched together with a thin cotton thread with as little as 1-N break strength. Multiple rips can be sewn inside the tether adjacently. If a shock leads to significantly increased tension a number of rips are expected to break and the freed tether can stretch, pulling the cotton threads through the tether braid, dissipating energy in the process. In the design of the ripstitch it is assumed that a discrete number of rips will break at any given event.

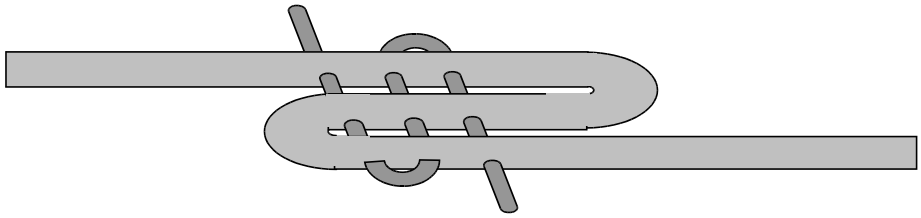

Figure 62. *Diagram of ripstitch principle (three tether layers joined with thread)*

The trigger tension should be lower than the peak tension that can be expected for a jam at the critical length of deployment. Minimum jam tension is to be expected at maximum length, Eq. 4.15. For the YES2 case critical length is 350 m and jam tension is 7 N (Section 4.2.2), Figure 63. Trigger tension should however be higher than the maximum tension that is expected in a nominal deployment, to avoid inadvertent triggering. This value is for YES2 is about 3 N. The selected target trigger level is therefore set to about 6 N.

Through Eq. 4.15, the trigger tension also determines the velocity at which no further rips will break, which in turn determines the recoil velocity. For example, in case of 10 N trigger tension, 12 kg endmass and a tether stiffness $EA = 5200$ N the velocity at which the last rip will break is approximately $v = 0.04\ \mathrm{m^{½}/s} \cdot \sqrt{L}$. At a critical length of 400 m this means that velocity can be reduced to 0.8 m/s until the ripstitching stops. Of the remaining energy, 40% will be dampened in the bounce due to the damping (assumed $\zeta = 0.08$), so a 0.6 m/s initial recoil velocity can be expected. On the approach to the host, gravity gradient acceleration will further reduce the relative velocity. In this manner, the time to reach the host platform is stretched and the maximum velocity near it can be calculated, with and without ripstitch. For the above case, velocity near the host platform can be reduced, by the ripstitch, to very low values (order of maximum 0.15 m/s, Section 7.4.1). The approach time is increased to minimally several minutes, providing ample time for on-board software to reliably recognize the anomalous event and cut the tether autonomously. The endmass will then pass ahead of the host mass due to Coriolis effects. Wrapping and collision are both avoided. Note that for a jam very close to the host platform a collision cannot be avoided. A passive release system is necessary for this case, subject to the next section.

The energy dissipation per unit length determines the total length of the ripstitching section, which should be as short as possible for practical reasons and to reduce deployment energy losses due to friction peaks (see Sections 4.2.1 & 8.3.3). Increasing the number of stitches per rip increases energy density, but unfortunately, also the trigger tension (Figure 64). The number of stitches per rip is thus empirically fixed to nine.

Two important design parameters are thus the trigger tension and the energy dissipation potential. A rip of 1 cm with 9 stitches is used as design reference. It has to be established whether the trigger tension and energy dissipation are consistently reproducible.

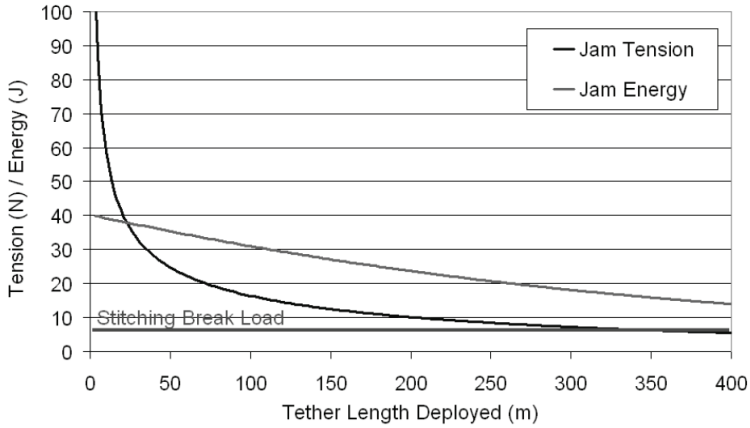

Figure 63. *Ripstitch applicable range in deployment*

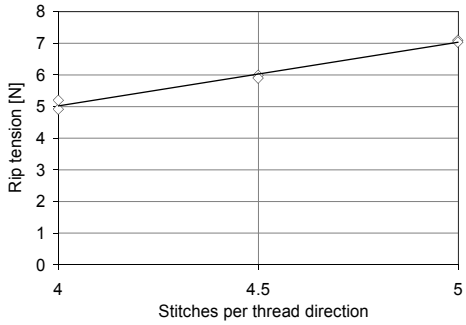

Figure 64. *Ripstitch break tension vs. number of stitches*

The spread in trigger tension is determined by means of a series of consecutive pull tests on the same sample with gradually increasing tension. Results on a sample of 1 meter (86 rips stitched) are provided in Figure 65. Nine successive tests cover all rips. The results show consistent break tension of about 4-5 N. Most of the rips are broken in the first seven tests. Only the last two rips show increased break tension of 6 N and 6.5 N. A second 50 cm sample has been prepared with 36 rips for which the number of stitches per rip is increased to 12. The length of the rip is increased to 12 mm. Six tests break all rips. Figure 66 show the satisfactory test results with a consistent trigger level between 5.5 and 7.2 N.

To determine the energy dissipation per rip, drop tests are performed both in a gravity environment and in zero-g. The limitation of a gravity environment is that a chain effect can take place that is indicative but not fully representative of the orbital condition. When a rip breaks, the tether is several centimeters longer, such that the mass will drop further, causing a new jerk and new rips to break.

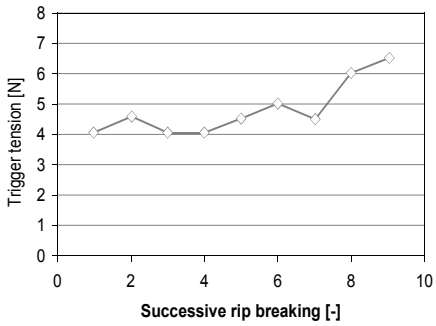

Figure 65. *Ripstitch break tension (successive tests) 9 stitches per 10 mm "rip"*

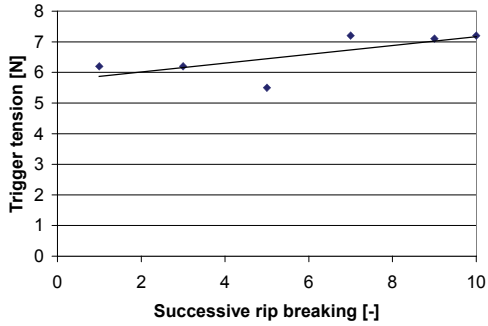

Figure 66. *Ripstitch break tension (successive tests) 12 stitches per 12 mm "rip"*

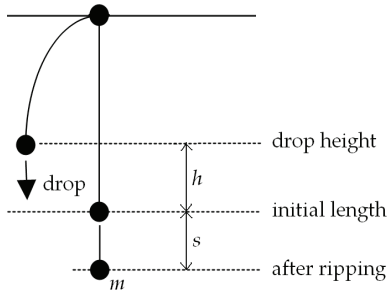

Figure 67. *Ripstitch drop test dimensions*

A drop test is performed with a sample with $N = 28$ rips, a length $L = 87$ cm and mass $m = 118$ g attached. Figure 67 sketches the drop from height h above the position of what would be the endpoint of the unripped sample as suspended from the attachment point ("initial length"). Ripping stops and velocity is dissipated at a distance of s below that position. Due to the unfolding of the S-shaped rips, $s = 2\, N_{broken}\, l_{rip}$. It is assumed all potential energy E becomes kinetic and is then (largely) dissipated, so,

$$E = mg \cdot (h+2\, N_{broken}\, l_{rip}) - \Delta E \cdot N_{broken} = mg \cdot (h+s) - \Delta E/l_{rip} \cdot s/2 = 0. \qquad (4.20)$$

With h the required drop height, ΔE the estimated dissipated energy per rip, m the drop mass, $g = 9.8$ kg·m/s^2, $l_{rip} = 11$ mm the length of a single rip. The required drop height h can be selected to break a significant amount, but not all of the rips, using the above equation rewritten as:

$$h = [\Delta E/(mg) - 2l_{rip}\,]\, N_{broken}. \qquad (4.21)$$

Assuming an expected 6 J/m dissipation capacity and a target of breaking of 11 rips of the 28, a drop height of 0.4 m is selected. It can be verified whether indeed the selected mass will cause the rips to break, based on an estimated tether stiffness of EA = 5000 N. Equivalent to Eq. 4.15, from conversion of potential to spring energy the maximum force can

be estimated that will occur when the original tether of 0.87 m is stretched due to the dropping mass:

$$F_{\max} = \sqrt{2\frac{EA}{L}mgh} \ . \tag{4.22}$$

It is 73 N, more than sufficient to break the first rip. The actual drop results in 10 broken rips and $s = 22$ cm. The ripstitch energy dissipation is then characterized from 4.20: $\Delta E = 0.072$ J/rip or 0.065 J/cm.

The breaking of rips stops when the velocity of the endmass has reduced such that the shock tension drops below the trigger level $F_{rip} = 6$ N. At the final length of 109 cm to reach this tension a maximum of 4 mJ residual energy may be present, as solved from Eq. 4.15. It is less than the energy potential of one rip ($\Delta E = 0.072$ J), so the maximum amount of energy could be dissipated by this system. This is generally true if

$$F_{rip} < \sqrt{2\frac{EA}{L}\Delta E} \ . \tag{4.23}$$

In order to evaluate whether the performance will be maintained without the the staggered type of ripping in a gravity environment, five tests are performed in a zero-g environment using the ESTEC drop-tower facility. Two of these tests concern reference tethers (no ripstitch) three tests are performed on the lighter ripstitch version (9 stitches per rip). For comparison, three more ground tests are performed using the same method as described above.

The ESTEC drop tower set-up provides about 1.5 s zero-g environment inside a small capsule equipped with video camera. The tests are performed at flight representative peak tensions. Inside the drop capsule, one end of a ~36-cm tether with ripstitching is fixed to the capsule's bottom plate, whereas the other end is attached to an endmass (122 g). The endmass is connected by a rubber band to the top of the capsule (Figure 68, Left).

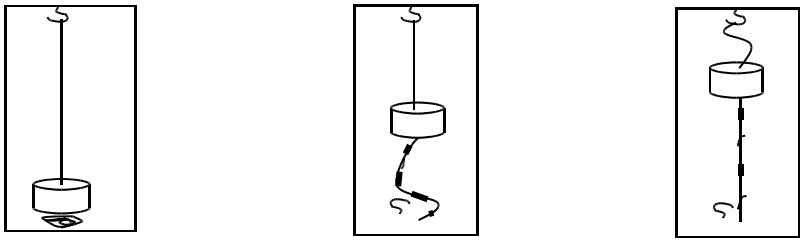

Figure 68. *Drop tower set-up for ripstitch test*

Before the drop the mass is suspended from the rubber band with spring coefficient k, such that $mg = kh$, with the initial strain h. The tether is slack. During the drop, in weightlessness, the rubber band contracts, initially accelerating the mass with exactly 1 g, until the rubber band in turn becomes slack. The endmass motion will continue (Figure 68, Middle) in free flight for about 3 cm with kinetic energy equal to initial spring energy $kh^2/2 = mgh/2$. When the distance between weight and bottom of the capsule reaches that of the sample length,

the weight is stopped abruptly, causing a tension shock, causing in turn the ripstitching to take place (Figure 68, Right). The mass should then lose most of its energy. These steps take place within 0.5 s. The remaining ~1.2 s until impact of the capsule can be used to quantify the remaining energy in the system. The capsule box is 50 cm in height, the rubber band is about 13 cm, stretched under 122g to about 44 cm. The stitched tether is 36 cm. Note that with this set-up to achieve the correct energy level it is not required to know the properties of the rubber band, as long as the initial stretch h can be tuned properly. The energy at moment of jam equals $mgh/2 = 0.19$ J. The peak tension due to the jam is evaluated to be 75 N, so sufficient for ripstitching. Six stitches of 6-7 mm are included in the tether, so about 3 will break, and after the test the tether will be ~44 cm.

By video inspection (Figure 69) the kinetic energy after jam, in the form of rotation and velocity, is determined, as to estimate the dissipated fraction as well as the tension to which the last broken stitch has been subjected.

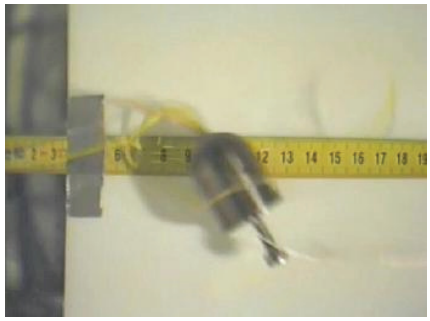

Figure 69. *After ripstitches break, the mass floats rather than jumping back*

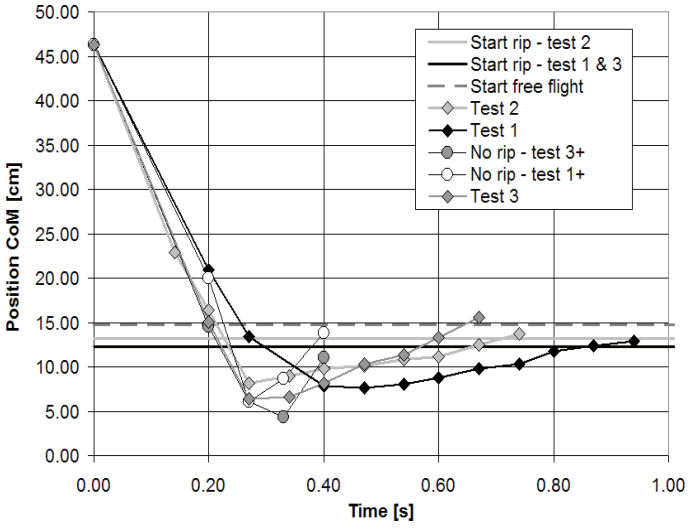

Figure 70. *ESTEC droptower ripstitch test results*

Test	Rip-stitch	Energy [J]	Length tether [cm]	Free flight [cm]	Broken rips [-]	Broken rips [mm]	Jam tension [N]	Energy remaining [%]	Fraction rotation [%]	Energy per stitch [J/m]
1	Y	0.19	35.70	2.50	4.00	27.00	6.4	0.5	5	7.0
1+	N	0.19	43.70	10.50	0.00	0.00	32.8	18.3	5	-
2	Y	0.19	34.80	1.60	5.00	33.00	6.3	0.5	3	5.7
3	Y	0.19	35.60	2.40	4.50	30.00	13.7	2.9	14	6.1
3+	N	0.19	43.80	10.6	0.00	0.00	44.0	33.6	12	-

Table 26. *ESTEC droptower ripstitch test results*

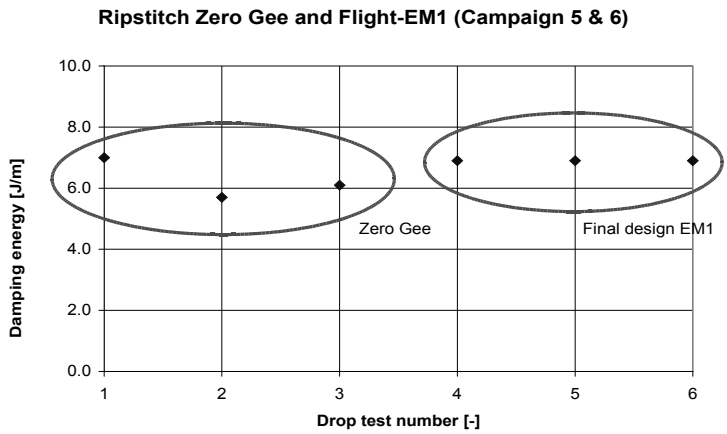

Figure 71. *Comparison of zero-gee ripstitch test results vs. ground tests*

Results of the five drop tests are presented in Figure 70 and Table 26. They show that considerable damping is taking place, also in the reference test without ripstitching. Possibly the damping coefficient exceeds the value $\zeta = 0.08$ determined earlier. The energy remaining after ripstitch is consistent with expectations, 1-6 mJ. The effectiveness of the concept could be confirmed and the energy dissipation per unit length is found to be sufficiently reproducible at about 7 J/m leading to about 6 m ripstitch section for a 40 J ejection. The results are in line with three further ground tests (Figure 71).

Some further checks have been performed. Two samples are exposed to vacuum for half a day, no impact on performance was noticed. A ripstitch section is also deployed several times at 2.5 m/s through the foreseen deployment system without noticeable issues.

4.2.4 Dissipative clamping

As an alternative to ripstitching, a section of "pull-through" tether can also be pulled through a tight hole, the diameter tuned such that only a shock tension of 6 N or higher would pull tether through the bottleneck, and in doing so, dissipate energy through high friction. There are several advantages to this approach over the ripstitching. It is to be done

on the end of the tether on the endmass side and can thus also perform the functions of pretensioner and tether fixture. No ripstitch section has to be led through the deployment system. The system is simple to manufacture and easy to tune. An issue is that the system will not work if the endmass is entangled in the end of the tether. An additional small storage device will be necessary to contain the necessary amount of pull-through tether.

In an exploratory test, an 80-g mass attached to an 8-strand 0.6x1.1-mm Kevlar tether, threaded through a narrow gap tuned for 6.7 N pull-through tension, is dropped from 2 m height. In three tests performed, the mass came to rest rather consistently at 240, 237 and 243 cm. Therefore the total potential energy dissipated is 1.9 J per drop, over 40 cm, or 0.048 J/cm, roughly the same as for the ripstitch. A margin-tether section of 8.5 m length is thus necessary for a total damping of 40 J ejection energy. This can be stored with about 90 wraps inside a 3 cm cylinder to be placed outside the bottleneck.

A fundamental reason why this system has not been further developed is that it is not compatible with the tie-down concept (Section 5.3.4). These tie-downs are cotton knots that hold the tether in place during launch. They need to be broken with 40-N 20-ms jerks following the ejection impulse. Such jerks act directly also on the endmass and will activate a damping system connected there. The ripstitch, in contrast, can be located within the tether safely behind the tie-down region.

4.2.5 Passive tether release solution

In case of a sudden jam in the very first meters of the deployment, even before or during the deployment of the ripstitch section, jam tension will be tens to hundreds of Newton, as the ripstitch cannot or only partially be activated. A strong recoil of the endmass to the host platform is to be expected leading to near-certain impact. In this case it is best if the tether is designed to release completely somehow. It should either break under the estimated peak tension, or, if this is not possible, a passive system is to be implemented that leads to immediate release of the tether.

It is found that the dissipative clamping concept is in fact suitable here. A bottleneck at the endmass, for the tether to be threaded through, can be implemented. The end of the tether is not fixed to the endmass in any way. It can slip through the bottleneck, albeit only at relatively high tension levels.

This bottleneck/tether fixture shall fulfill some requirements. It shall provide a safe release of the endmass in case of a jam, during the earliest section of the tether deployment before the ripstitch is fully deployed. The design point shall be the point of this section where the hypothetical jam shock load would be lowest and is the least likely to release the tether from the bottleneck, i.e. at the maximum tether length in the zone of interest. For our example case, with a 6-m ripstitch section and about 7 m of tether included to absorb the tie-down shock (Section 5.3.4) plus 2 m margin, about 15 m is chosen as a reasonable worst case length. The tether shall however not release in case of a nominal deployment. As the tie-downs are broken during ejection, with about 40 N peaks, the system shall not yet be activated. The bottleneck must thus be tight enough to generate a slip friction significantly larger

than 40 N. The tether must also be stiff enough or ejection energy high enough. In case of a jam at the design point of 15 m, a peak shock tension significantly larger than the slip tension shall occur (i.e. another instance of condition Eq. 4.19). The "pull-through" segment of tether to be stored outside the bottleneck shall be sufficiently long to avoid inadvertent release e.g. due to brief anomalous shocks during the deployment (as discussed in Section 4.2.1), but short enough to guarantee that an actual jam will actually pull it through the bottleneck in its entirety.

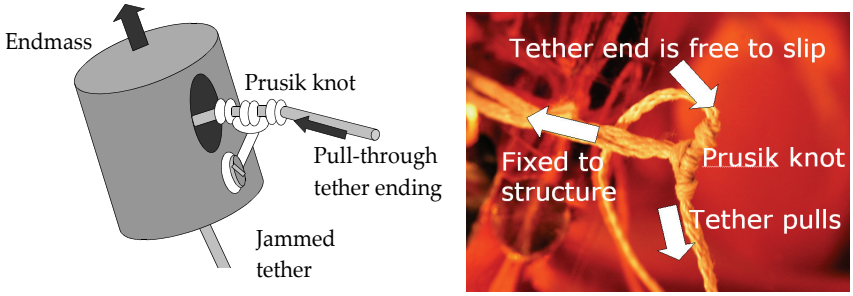

Figure 72. *Prusik knot fixture (concept and YES2 implementation)*

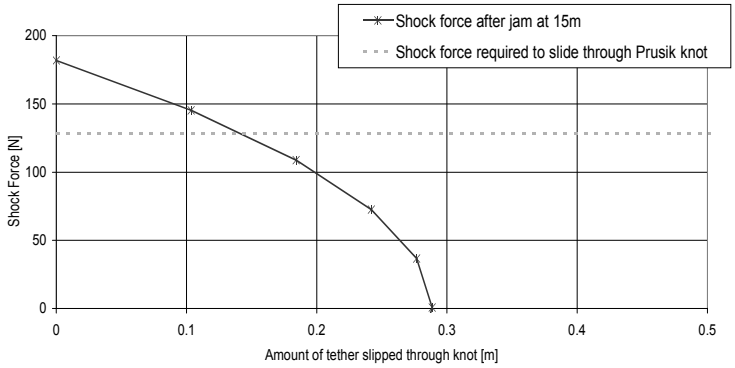

Figure 73. *Determination of optimal "pull-through" length,* EA=*6700 N*

The selected bottleneck design is based on a Prusik knot (Figure 72), which has the practical advantage that the tether can slip through conveniently in one direction, during installation and pretensioning, but will resist slip when the tether is pulled in opposite direction during a jam-type event. A large number of pull tests is performed to build up statistics for different configurations of Prusik knots. It is found that a 4-wrap knot has about 2-3 times higher slip friction level than a 3-wrap knot. Standard deviation of the measurements is found to be 20% of the slip tension value. A 3-wrap knot with 55 N slip tension is selected, providing reasonable probability that the tie-downs will not initiate the slipping.

The length of the pull-through tether segment has been selected according to Figure 73. As the tether is squeezed through the bottleneck, it will dissipate energy and the endmass velocity will consequently be reduced. As more tether slips through the bottleneck, the remain-

ing inertia of the endmass can generate less 'jam tension'. At the length of tether where this reducing jam tension level drops below the bottleneck's slip friction, the slipping will stop and the endmass will recoil. This assessment provides the maximum length of the free tether end. For YES2, it is selected to be 14 cm.

4.3 Avoiding threats to tether integrity

A tether's diameter can usually not be simply determined from the nominal, operational tension level and the manufacturer's fiber strength data. The tether may need to resist tension jerks during anomalous deployment. The space environment threatens a tether's integrity during its useful lifetime through meteoroids, debris, UV radiation and atomic oxygen. If the tether is decelerated by friction, the thermal loading should be taken into account, in particular for Dyneema®, which melts already at 150°C. In this section a number of considerations to be taken into account is highlighted.

4.3.1 Debris and meteoroid risk

Single-line tethers are prone to debris and meteoroid impact. Tether survivability depends on abundance and impact energy of the debris and the (more energetic) meteoroid particles [Klinkrad 2006], as well as on tether design.

Although the distribution of both debris and meteoroids in Low Earth orbit is complex, the combined flux can be considered exponential within the range of applicability and is suitable for relatively simple survival probability models [Klinkrad 2006]. Figure 74, taken from [Penson 2003] shows the predicted cumulative flux at 1000 km altitude, computed with ORDEM2000, a semi-empirical engineering model developed by the NASA Johnson Space Center that includes short term predictions for LEO, based upon remote and in-situ observations. According to this model, at 300 km, a 30-km long 0.5-mm diameter tether can expect an impact of approximately 0.001 particle of its own diameter inside the duration of one orbit (90 minutes).

A variety of results is available from ground testing from which a critical impactor diameter can be estimated. Extrapolations by Sabath from measurements up to 15 km/s indicate that a meteoroid of 53% of the tether diameter can suffice to sever an untensioned or lightly loaded tether (5% of tensile strength) [Sabath 1996.I,II]. Sabath estimated, in contrast, that a *debris* particle needs to be on the average 81% of the tether diameter to be >90% destructive. Penson & Burchell have found that a glass ball with 254-μm diameter and a velocity of 5 km/s is capable of severing a sample of the 0.5-mm Dyneema® YES2 tether [Penson 2003].

Calculation of tether survivability from this type of experimental data is not a trivial exercise. The impact risk is to be integrated over the range of aspect angles. For each angle, from an orbital environment perspective, a different flux and energy distribution of debris and meteoroids may occur. For each impactor at a given aspect angle, the effective impact surface also differs. Grazing impacts will generally only do partial damage. The radial distance to the tether's central line, within which an impacting particle can cut the tether,

depends not only on the aspect angle and tether projected width, but also on the impactor diameter and energy. The effective width for critical impact is thus not trivially defined. It ranges from zero (for a particle of critical diameter and energy that requires central and perpendicular impact) to, possibly, the sum of radii of tether and particle (for a large highly energetic particle that cuts the tether even when barely grazing the tether). The total probability of tether severing is calculated by integration of the impact and severing probability of all particles larger than the critical diameter [McBride 1997, Anz-Meador 2001].

In an approximating approach, an "*effective critical impactor diameter*" can be defined that yields the same probability, when related solely to the coinciding impactor flux estimate (as in Figure 74), the mission duration and the total exposed tether surface area, as projected perpendicular to its center line. Typical estimates of an effective critical impactor diameter range from 0.2-0.5 *d*, with *d* the tether diameter [Hoyt 1995, Cosmo 1997].

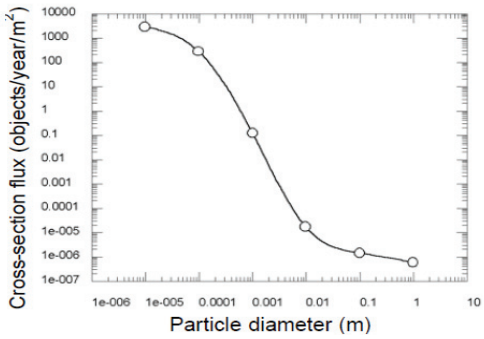

Figure 74. *Cumulative particle flux at 1000 km, computed by ORDEM, from [Penson 2003]*

For both the comprehensive and simplified approaches it remains challenging to combine flux estimates and impact data to generate reliable models for meteoroid and debris survivability (see Table 27), partly due to the limited flight data (Section 1.3). The SEDS-2 tether broke after 4 days, the remaining 7 km section remained intact for a further 54 days until re-entry. The TiPS tether was not cut until after 10 years. Both tethers were under low strain.

Hoyt & Forward [Forward 1995] suggest the following model for the Mean Time Before Failure t_{MBF}:

$$t_{MBF}\,[\text{years}] = \frac{1}{\pi\sigma L\,[\text{km}]}\, d\,[\text{mm}]^{f-1} = \frac{1.05}{L[km]}\, d\,[\text{mm}]^{2.46} \qquad (4.24)$$

where $\sigma = 9.58\ 10^{-9}$ craters/s·m^2, based on LDEF measurements [NASA 1991] and $f = 3.46$ is an empirical parameter. Note the irregular units. A simple alternate formula, adjusted based on SEDS-2, is that of Carroll [Carroll 1995.I]:

$$t_{MBF}\,[\text{years}] = \frac{f}{L\,[\text{km}]}\,(d\,[\text{mm}] + 0.3)^3 \qquad (4.25)$$

Carroll sets $f = 1$. Forward[6] suggests $f = 2.85$ in order to take into account flight data until 1997.

Survival probability can then be calculated from t_{MBF} and mission duration $t_{mission}$ through:

$$p = e^{-\frac{t_{mission}}{t_{MBF}}} \tag{4.26}$$

McBride's comprehensive model yields a rather conservative estimate of the survivability, consistent with SEDS-2, but not with TiPS. Penson, using also samples of the selected YES2 tether, concludes even more conservatively. According to Sabath, Carroll and Hoyt/Forward, the cut of the SEDS-2 tether should be regarded as an anomalous cut, probably due to debris originating from the launch of the experiment.

	SEDS-2 (20 km,0.75 mm)	**TiPS (4 km, 2 mm)**	**Model**	**Reference**
Sabath	486	~8600 (extrapolated)	Debris & meteoroids LEO, untensioned tether, 'cut' when 90% damaged, based on impact tests	Sabath 1996
McBride/Taylor	11 (-8,+16)	295 (-230,+440)	Debris & meteoroids, comprehensive model incl. velocity distribution and penetration.	McBride 1997
Penson	0.6	23	Debris & meteoroids LEO, ORDEM flux. Assuming cut when hit by particle with 0.25 d_{tether} from 5 km/s impact tests on Dyneema.	Penson 2003
Carroll, $f = 1$	21	1110	Debris & meteoroids LEO, empirical fit.	Carroll 1995.I
Carroll, $f = 2.85$	60	3166	Debris & meteoroids LEO, empirical fit.	See text
Hoyt/Forward	10	520	Debris & meteoroids LEO simplified model.	Eq. 4.24
Flight	**4**	**3700**	**Actual environment.**	

Table 27: *Tether mean lifetime model estimates (days) versus actual experiments*

The Carroll model with $f = 2.85$ is used for debris impact estimates for the projects in this thesis as the most representative, providing the best match to flight data. The risk of tether cut during the 30 km 0.5 mm YES2 deployment (1 km·day of exposure, Section 7.3) is then estimated at 0.2%. The particle flux at 300 km that provides this same value of impact probability, as predicted by ORDEM2000, is equivalent to an effective critical impactor diameter of 0.6 d.

Long term tether break-up

A floating tether in a long-lived orbit, due to subsequent random impacts will eventually break up in smaller pieces that need each to be individually tracked. Figure 75 demonstrates this process, as produced by the CutSim simulator (see also Section 4.4.2). Since larger fragments have a greater chance of being cut, the number of large fragments decreases rapidly. Within little over 2 years a 50 km 0.7 mm tether is be severed into fragments under 2 km length.

[6] Private communications 1997

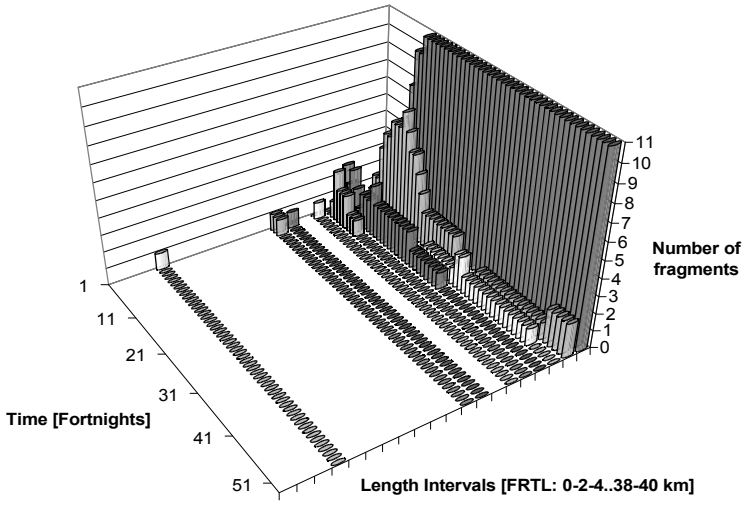

Figure 75. *CutSim simulation of a 50 km, 0.7 mm tether break-up due to meteoroids and debris in LEO (scale cut off at 11 fragments per length interval. FRTL=From Right To Left).*

Flat and multi-strand tethers

Proper tether design can increase tether lifetime and delay tether break-up into smaller, hard-to-track pieces.

A flat braided tether for example has a longer lifetime than a tubular (round) braid. This is because of the integration of several effects. Larger (thus rarer) particles are necessary to cut the tether impacting on the front side. At the same time, small particles impacting on the flat side have to impact at very low incidence, so the view factor of the vulnerable tether part to the random small particle background is small. However there are relatively more small particles. Integration of the combined effect around the tether cross section can be done, e.g. using Eq. 4.25. An additional positive effect is gained from the fact that the small particles in order to cut through the tether have to pass through the whole width of the tether, whereas tests have shown that small particles often get stopped within the tether itself [Sabath 1996.I]. Tether tapes manufactured from film material can be much thinner still, and thus have better lifetime performance from a perspective of particle survivability.

Multi-strand tethers provide further improved performance. The simplest type is the double-strand tether or Carroll Caduceus, which has however the splice location as a single point failure. One step more complex is the triple-strand tether, Figure 76. The strands are connected to one another in multiple places (nodal points), hundreds of meters apart. When one of the lines is cut, another takes over. The probability of *all* lines being cut between two nodal points is very slim. More elaborate net-like structures such as the Hoytether have

been proposed and prototyped by Forward & Hoyt and have the potential of increasing lifetime by many orders of magnitude [Forward 1995].

Multistrand tethers come with some challenges. It is not yet clear whether the multiple lines can be kept apart effectively in space. Build up of static charge in case of mechanical tethers will provide for a separating force, however, a twist in the tether may make the tether locally vulnerable. In case of conducting tethers, there will be an attraction force in two current carrying strands. Active separators may be required. Construction, winding and deployment is not trivial and rather costly but has been successfully demonstrated for e.g. YES (Section 5.3.7).

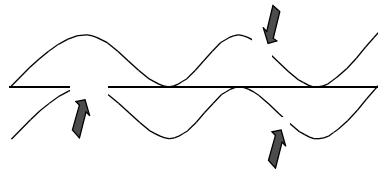

Figure 76: *Principle of triple-strand tether. It is shown to survive three cuts.*

Survival probability of multistrand tethers is approximated. Consider a total tether length L, with n nodes, each node providing a length of s of ineffectively separated tether. Under the conservative assumption that, at s, an impact that cuts a single tether line also cuts the combined bundle, Eq. 4.27 is derived to estimate survival probability for the double and triple-strand tether design [Delta-Utec 2001]:

$$
\begin{aligned}
p' &= 1 - e^{-\frac{t_{mission}}{L \cdot t_{MBF}}} \\
l' &= \frac{L}{n} - s \\
p_{dualstrand} &\approx 1 - n(p's + p'^2 l'^2) \\
p_{triplestrand} &\approx 1 - n\left(p'^3 l'(2l' + s)^2 + p'^2(2l' + s)s\right)
\end{aligned}
\qquad (4.27)
$$

As an example, for a 6000 m tether in orbit for 1 month, the survival probability for four different designs with identical mass is compared in Table 28:

1. single round tether d = 0.43 and 0.8 mm,
2. flat tether (tape) a x b = 0.05 x 0.75 and 0.1x 1.4 mm,
3. Carroll Caduceus double strand, d = 0.3 and 0.56 mm, n = 50, s = 2 m,
4. triple strand tether, d = 0.245 and 0.46 mm, n = 120, s = 2 m.

Table 28 also indicates the average projected width that affects atmospheric drag (and lifetime), thermal balance and solar pressure effects on the tether. The double round tether performs an order of magnitude better than a single strand, whereas the triple tether has already very minor cut risk. A single strand tether provides sufficient survivability for short missions and allows for an extensive test campaign.

Equal mass tether types	Dimension	Risk of cut estimate (% over 1 month)	
	Average projected width [%]	0.83 kg (6 km)	2.9 kg (6 km)
Single round	100	38	13
Tape	227	17	4.7
Double round	<141	3.7	1.2
Triple round	<173	0.11	0.012

Table 28. *Tether design comparison (cut risk)*

4.3.2 Other degradation mechanisms

In the 1990s, an ESA Alert was released related to strength losses reported due to long term UV exposure in a space representative environment [Matcham 1998]. Indeed a loss of strength of 43% in 83 equivalent solar days was reported, accompanied by a reduction of the material's break strain. For very short missions or missions driven by meteoroid/debris survivability this decrease in performance may not be relevant.

UV/VUV testing performed in the context of this thesis confirms degradation chemistry through significant coloration (yellowing) but, due to cross-linking, little mass loss occurs such that low-tension integrity seems secured (Section 4.4).

The effect of the LEO space environment and particular atomic oxygen degradation on polymers was studied on the LDEF platform. This unmanned free flying spacecraft on which several polymers were mounted, was exposed for 69 months to a LEO space environment and found similar degradation results for the various relevant polymers. A material of 1 mm thickness would erode in about 3 years at 333 km (LDEF End of Life) vs. 30 years at 467 km (LDEF Beginning of Life) [NASA 1991].

4.3.3 Thermal loading during friction braking

Another possible threat to tether deployment is overheating of the tether. If a tether deployment is controlled by friction, this means kinetic energy of the deployed equipment is being dissipated and will be converted into heat Q, concentrated at the friction surface between brake and tether. Assuming initially equal temperatures for brake and tether, as the brake heats up, and fresh tether keeps being fed over the friction surface, a fraction $0.5 < \eta < 1$ of this heat will flow into the tether, as was indeed observed in vacuum tests [Carroll 1995.I]. At high deployment velocities, η can be expected to approach 0.5 (equal distribution of heat at contact surface). The rise in temperature ΔT for a tether with heat capacity c_p can then be estimated as follows:

$$\begin{aligned} \Delta T &= \frac{\Delta Q}{m \cdot c_p} \\ \Delta Q &= \eta \cdot F \cdot \Delta L \\ m &= \rho \cdot \Delta L \\ \Rightarrow \Delta T &= \frac{\eta \cdot F}{\rho \cdot c_p} \end{aligned} \tag{4.28}$$

Assuming the tether cross section A is designed to deal with the maximum tension occurring during the deployment by a Factor of Safety F_S with respect to the material break strength, and a material volumetric density of ρ_V, this rise in temperature can be expressed in terms of material properties, *independent* of the tether cross-section, deployment profile or endmass:

$$\begin{aligned} F &= \frac{\sigma_{br}}{FS} A \\ \rho &= \rho_V \cdot A \\ \Rightarrow \Delta T &= \frac{\eta}{F_S} \cdot \frac{\sigma_{br}}{\rho_V \cdot c_p} \end{aligned} \tag{4.29}$$

This means that for example for Dyneema® (Table 18, c_p = 1850 J/kg·K), and a $F_S = 10$, the tether temperature can be expected to rise between 75 and 150 degrees due to deployment friction, which can be an issue considering the melting point of 150 °C.

In reality, the heat will not distribute throughout the tether equally in the short time of brake passage, and locally it will get even more hot, especially at high deployment velocities. For Dyneema®, axial thermal conductivity exceeds transverse conductivity by a factor 100. At standstill the tether will locally approach the brake surface temperature, so it is important to keep the brake cool. Tether design safety factors may have to be adjusted to deal with the friction heating. Alternatively, the section of tether that is subject to the heaviest braking can be manufactured from Kevlar or Zylon. Note that deployment from a reel avoids these thermal issues for the tether altogether, as the heat dissipation takes place within the reeling mechanism.

Note also that after deployment, the tether generally cools down quickly due to thermal radiation into open space. A cylindrical tether irradiated on one side (projected area A_{proj}) maximally by the Sun with Q_{Sun}, and faced to open space on the opposite side, will find itself under the following heat balance:

$$\begin{aligned} A \varepsilon \sigma_B T^4 &= A_{proj} \alpha Q_{Sun} \\ \Rightarrow T &= \sqrt[4]{\frac{\alpha}{\varepsilon} \frac{Q_{Sun}}{\pi \cdot \sigma_B}} \end{aligned} \tag{4.30}$$

With the Boltzman constant σ_B = 5.67 10^{-8} $Wm^{-2}K^{-4}$ and a Q_{Sun} = 1400 W and tether properties as in Section 4.1.1, a Dyneema® tether's equilibrium temperature is 208 K or -55°C.

4.3.4 Design safety factors

There is no simple generally valid safety factor for selection of tether diameter [Lansdorp 2006]. It has been shown that it is not sufficient to take the fiber strength with a common engineering safety factor based on tension due to nominal deployment and centrifugal forces. Stress concentrations from braiding and clamping have significant impact on the strength. Friction braking exerts local heat loads (Section 4.3.3). A sudden stop of deployment leads to a tension peak (Eq. 4.15), which will be high at short tether lengths. Tether failure may need to be accepted and can even be beneficial in such a case. For long duration missions, material degradation may have to be taken into account. In some cases, the diameter has to be designed based on impact survivability. Strength of multiple strands in combined tethers cannot just be added, as they will not be equally loaded. Table 29 provides an overview of the considerations.

Factor	Impact on safety factor	Applicability	Reference
Temperature	Eq. 4.29	Section of tether subjected to high friction brake load.	Section 4.3.3
Survivability	Minimal diameter from Eq. 4.25.	Thin tethers/long duration missions.	Carroll 1995.I
Braid/Effective tether diameter	Factor 1.4-2.3	All braids. Splices should be tested.	Section 4.1.3
Clamping/knots/small bending radius	Factor 2	Avoid if possible.	Section 4.1.3
Atomic Oxygen	0.33 mm per year of mission duration at 333 km.	Multi-year duration, low altitude (<500 km), thin tether mission (particularly multistrand).	NASA 1991
Ultraviolet degradation	Factor 1.4 for 1 month, factor 2 for long duration mission.	Thin tethers.	Matcham 1998
Shock due to deployment snag	Eq. 4.15, margin depends on knowledge of tether properties.	Part of deployment where tether integrity must be maintained.	Section 4.2.2
Deployment control overshoot, irregularities in friction/deployment mechanism	Suggested engineering design factor 1.25-1.5 on maximum deployment tension depending on tests and simulations.	If deployment tension is driving factor.	-

Table 29. *Summary of tether design factors*

4.4 Reducing collision risk by environmental disintegration

An important limitation to tether mission design remains that a safe altitude must be selected and that, in case of some failure, the tether should be cut loose from both endmasses to reduce lifetime and collision risk with operational satellites (Section 3.3).

Tether missions have indeed been cancelled because of perceived or calculated risk to in particular the International Space Station (Section 1.3).

A tether material that fully degrades after its useful lifetime would render void such risks and would open the way for inherently safe and much less limited use of tethered momentum transfer. SpaceMail could be performed from higher altitudes within LEO. Applications in highly elliptical orbits [e.g. Ockels 1996] would become feasible, as well as demonstration missions for more ambitious applications (Section 1.2). In this section, the search effort for such a material is reported.

A selection of candidate tether material samples has been tested in vacuum chambers under UV and VUV exposure. The samples have been chemically characterized to describe the processes that have occurred and the mass loss has been quantified. Based on the result, adjustments to the materials have been made and new, conclusive tests are performed.

4.4.1 Requirements

The material would have to be a fiber or thin line material, practical for handling during production and testing, light, stiff and strong during the hours to days of operation, yet it would fully evaporate in a predictable way when exposed to the space environment for a significantly extended time. Three possible degradation mechanisms for a tether come to mind.

Firstly, the tether could be designed to break into large loose pieces, hundreds of meters in length, that each have a favorable area over mass ratio. A common tether material could be interspersed with small parts of degradable material. The strength and stiffness requirements for that material can be relatively low in this concept. It is however probably preferable to only release the endmasses from the tether. Tracking of the rogue object will thus be simpler and the tether end will dip deeper towards the atmosphere by gravity gradient, accelerating deorbit.

An alternative approach would use common material fibers bound by a binder that would evaporate or degrade, leaving behind a cloud of relatively harmless micro-filaments. Small dust particles however can still impart significant damage to satellites. Discussions with the space debris committee indicate that nevertheless this degradation mechanism could be acceptable[7].

The final and most definite solution would be a full break-down of the tether into molecules. This method requires a flexible, degradable material and should likely be based on existing fiber materials. Based on promising indications from existing degradable materials and considering the added potential of an aggressive space environment, this first search has limited itself to such a complete degradation mechanism.

The degradation time for the searched material must be short enough to sufficiently limit the collision risk with other satellites (Section 3.2.3), and longer than the mission duration considering a suitable safety factor (Section 4.3.4). A 6 month degradation period is targeted

[7] Private communications W. Flury (ESOC) 1999

as an acceptable maximum, equivalent to $O(10^{-2})$ collision risk following an already unlikely event of mission contingency.

Degradation processes currently in use on Earth, i.e. photo-oxidation and biodegradation, are not directly applicable in absence of oxygen and bio-activity, but it is initially assumed that the aggressive space environment can provide an alternative mechanism. As indicated in Section 4.3, erosion by atomic oxygen and degradation by both Ultra Violet (UV) and Vacuum UV (VUV) are the destructive processes that are most effective in space. Up to now, most space application research has focused on the effects of and protection against atomic oxygen. However for the material to be effective outside the lower regions of LEO, it must be degradable by UV & VUV only. Ideally the reactions should take place at passive equilibrium temperatures of the tether, which can be controlled by some extent by addition of IR-absorbers to the material.

4.4.2 Mechanics of degradation

In advance of test planning, it is considered useful to gain some insight into the mechanics of degradation for long molecules due to random scissions, and in particular the presence of incubation before the onset of evaporation. Based on discussions with Gijsman [Kruijff 1999.II] a simple model is developed, CutSim, to perform scission simulations for a qualitative understanding. Molecule parts that have become shorter than a given fraction of the molecule length are assumed to evaporate. CutSim assumes the molecules to be neatly aligned and shielding the ones behind from incoming photons (Figure 77), i.e. a penetration depth of a single molecule. The model is optimistic in the sense that cross-linking between affected molecules does not occur. Cross-linking (or gel-forming) creates intricate, web-like molecular structures that affect the material's mechanical properties and counteract the scission effect. It makes evaporation highly unlikely. Based on typical values for the considered polymers, evaporation is assumed to occur at 1/3000th of molecule length. Figure 78 and Figure 79 display the typical mass degradation function for a single molecule.

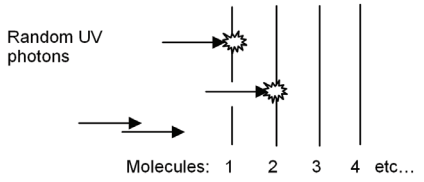

Figure 77. *Scission schematic of performed simulations. Molecule 1, receiving yet another scission, is now cut up into 4 pieces of which one has evaporated.*

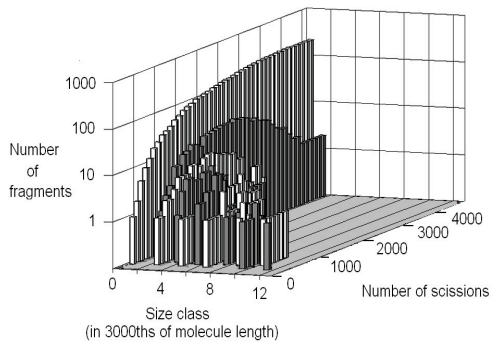

Figure 78. *Example of distribution of particle size for a molecule in a layer under UV radiation, as a function of time.*

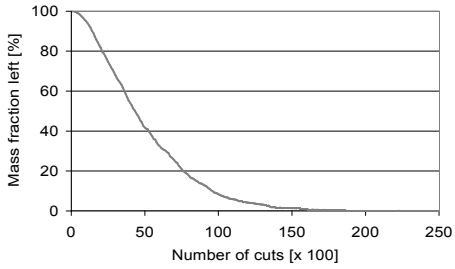

Figure 79. *Mass loss vs. time of a single long molecule being cut at random by UV (qualitative shape only)*

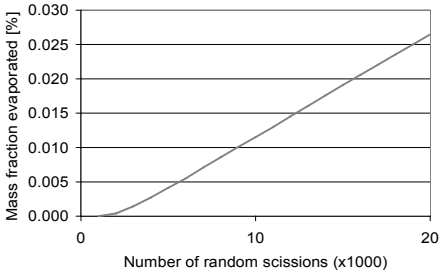

Figure 80. *Mass loss vs. time of a layer of 10000 long molecules under UV*

For a multi-layered flat surface (here 10,000 molecules thick), the general trend is that apart from a very brief incubation time relative to the time required for total mass loss, as expected, mass degradation will be virtually linear with time, Figure 79. Such a trend was for example found by Brinza [Brinza 1991], who recorded an onset for Teflon linear degradation under VUV (acceleration factor 4) after 60 days. Note that for a more realistic, larger penetration depth the incubation time will be significantly longer, whereas total degradation time will be hardly affected. For a material to degrade fully within months it is therefore likely to, for all purposes, remain intact during the tether mission time of order days.

4.4.3 Degradation chemistry

In the Earth environment all polymers show UV-degradation due to the combined effects of photolysis and oxidative reactions, the latter generally being the dominant process. Photo-oxidative degradation is due to a radical-based auto-oxidative process [Kruijff 1999.II]. The lifetime of polymers can be controlled by additives or changing the molecular structure of the polymer. In most cases an enlargement of the lifetime is required, which is achieved by adding stabilisers. However, additives can also be used to decrease the polymer lifetime, mostly based on enhancing the oxidative reactions.

Besides photo-oxidation direct photolysis can lead to (accelerate) the degradation of polymers. So-called chromophores within the polymer materials absorb wavelengths of the sunlight spectrum, of which only wavelengths above 290 nm have sufficient energy to cause a dissociative (cleavage) process resulting in degradation. Chromophores can take a multitude of forms. They can be internal in-chain impurities such as hydroperoxides or carbonyls formed during storage, processing or weathering or external impurities as polymerisation catalyst residues, additives (e.g. pigments, dyes or antioxidants), pollutants from the atmosphere or metal traces from processing equipment. They can also be present as parts of the molecular structure of the polymer or as charge transfer complexes between oxygen and the polymer chain.

In space different conditions apply from those in an ambient atmosphere that affect degradation processes. Because of the very low concentration of molecular oxygen the photo-oxidative degradation will hardly take place. Furthermore, high vacuum causes outgassing of

any gaseous additives to the tether material. On the other hand, highly energetic wavelengths below 290 nm, until about 200 nm, are present in sunlight in space as they are not absorbed by the ozone layer. Photolysis can only occur when light is absorbed and the energy of the absorbed wavelength is higher than the bond dissociation energy. The majority of polymers show only limited absorption above 290 nm, but it is increasing for shorter wavelengths. The energy of these wavelengths is in general higher than a lot of bond dissociation energies such as those of C-C and C-H. Even shorter wavelengths around 160 nm contain sufficient energy to break C=C and C=O bonds [Kruijff 1999.II]. Thus in space photolysis will be of much greater importance than on Earth.

Hydrocarbons like polyethylene (PE) and polypropylene (PP) only show UV-absorption below 250 nm, radiation which is absorbed by Earth's atmosphere. Thus these materials will not show photolysis in an Earth environment, but can undergo photolysis in space. This photolysis is a process that includes various scission, transfer and cross-linking mechanisms (Figure 81).

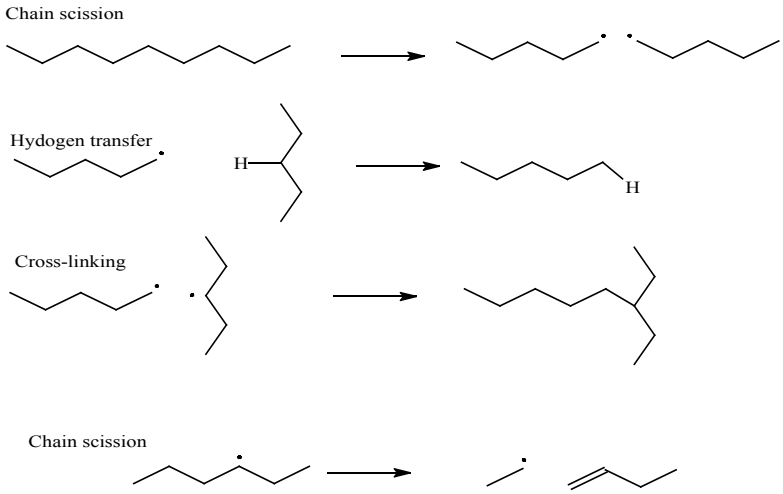

Figure 81. *Photolysis mechanisms for polyethylene.*

For ketones, esters and amides the most important photolysis reactions are the Norrish I and II reactions [Kruijff 1999.II]. The Norrish I reaction lead to chain cleavage and radicals. In the presence of oxygen these radicals will start the oxidation and can thus accelerate degradation significantly. However, cross-linking is often very likely. The Norrish II reaction lead to chain cleavage and an unsaturation in the chain without the formation of radicals. In an oxygen-poor environment, Norrish II will be the dominant cleavage reaction.

Note that the energy to activate photochemical reactions comes from the absorbed light, which means that the rate of photolytic reactions should not depend on temperature. However for the Norrish I and II reaction in polymers it is found that their rate depends on temperate, which is explained by the influence of temperature on the mobility of chains in the polymer. The influence of temperature on the quantum yield (amount of reactions/absorbed photons) of the Norrish II reaction is especially noticeable at low temperatures. For example the quantum yield for a

polyethylene CO copolymer containing 1% of CO decreases from its high temperature value above -25°C to zero at -150°C [Hartley 1968]. Temperatures in this range could be expected in space for untainted polymers (Section 4.3.3).

4.4.4 Polymer degradation research

Only limited tests have so far been performed in space or on-ground on isolated UV/VUV effects on polymers.

In space, most material degradation information is based on the Long Duration Exposure Facility [NASA 1991]. On the trailing side of LDEF that was shielded from AO, and exposed to UV for about a year, samples were present of PE, Hostaphan & Mylar polyester, PET & PA6/6. Unfortunately no mass loss results have been published and the samples are no longer available.

One of the more relevant LDEF experiments, S1006, was located on the side receiving 6500 Equivalent Sun Hours (ESH), with a temperature between –21 and +51 °C. On the sides it received about 1/200th of the ram AO flux, found insignificant. This experiment contained samples of films of polyethylene, polyester, nylon as well as Kevlar fibers. Branching and cross linking was found for polyethylene while crystallinity decreased by 40%-65%. Thermal cycling and UV heat dissipation caused micro-gravity surface melt showing up as microscopic spheres [Letton 1991].

The experiment FRECOPA was on the LDEF trailing edge, and thus shielded from AO, so it is possible to see the influences of UV alone. No erosions were reported (or measured), although material samples of Kapton, FEP, FEP/Ag and PSB were exposed for 11110 ESH [Durin 1991].

Tests have also been performed at ESA/ESTEC on Kevlar and Dyneema® under UV, because of the degrading effects on the strength of both materials. Also here, no mass measurements were made [Matcham 1998]. Grossman performed a test of VUV (115-300 nm) and its interaction with 50-100 eV AO, for 20 Equivalent Sun Hours (ESH) [Grossman 1997]. He concluded that PE degrades little by VUV, but VUV causes crosslinking that negatively affects the AO-induced mass loss. For FEP Teflon however, a degradation rate several orders of magnitude higher was noted, as well as a synergistic degrading effect of VUV with AO.

Considerable information is available from ground tests for FEP Teflon [George 1991, Cross 1994], a material known as UV resistant. Mass loss measurement have been done on FEP Teflon [Brinza 1991], a 0.1 gram film of 2 mil thickness exposed for 92 days at an acceleration factor of 4. FEP is most sensitive for the 121 nm peak in VUV (hydrogen Lyman-alpha emission) of the Solar spectrum. In a similar process as produced in Figure 80 the results show a 60 day induction before a linear mass loss, of up to 5%. Scission is mostly present in C-C (chain scission) and Carbon-Fluorine bonds. Embrittlement of the surface layer suggest a high cross-linking.

4.4.5 Material selection

A selection of polymers for testing is therefore made based on the characteristics for both UV-absorption and photolysis, and low expected levels of cross-linking. As development of new materials lies outside the scope of the effort, availability is another selection criterion.

Since FEP Teflon is considered a material resistant to the space environment, it has been concluded no clearly suitable materials can be identified from literature.

For hydrocarbon photolysis, the ratio between chain scission and cross-linking will depend on the radical formation rate, the higher the concentration of radicals (indicated as dots in Figure 81) the more probable cross-linking becomes. Tertiary radicals as will be formed in PP (referring to the tertiary carbon atom in the repeat unit, outside the main chain) are less likely to cross-link than main chain (secondary and primary) radicals, which are formed in PE [Kruijff 1999.II].

For the more complex polymers, the expected behavior regarding the Norrish reactions has been considered.

- Polyesters and polyamides could be promising, as they show a larger UV-absorption than hydrocarbons, especially the (partly) aromatic polymers.
- For polybutylene terephthalate, Norrish II and I reactions lead to 'methyllactone' [Rivaton 1993], which might evaporate and prevent cross-linking.
- E/CO (ethylene-carbonmonoxide), polyketone, is prone to photolysis at the the CO group. The ethylene-carbonmonoxide part can however only undergo the Norrish I reaction. Because of the high concentration of ketone groups cross-linking is very likely. If propylene-carbonmonoxide is also present, as e.g. in Carilon, that will undergo both Norrish I and II reactions, so here less cross-linking and more scission at the CO groups is expected [Andreopoulos 1994]. E/CO materials with higher propylene fraction than Carilon (less than 7%) are unfortunately not available.
- Polyacrylates are polymers that contain hetero atoms (e.g. O or N) in the side chain. Under UV, the esters groups undergo mostly Norrish I but also Norrish II reactions followed by different consecutive reactions. The photolysis of polyacrylates leads to cross-linking to a large extent, however the photolysis of polymetacrylates mainly leads to chain-scission, which is also true for e.g. poly-butyl metacrylates, PBMA.

Due to lack of availability, limited suitability for manufacturing of tethers or toxicity, some promising materials were not considered as tether material option.

- PBMA, poly-butyl methacrylate, has been used for deploying spherical netlike antenna structures in the 1960s [Stimler 1968], but no fibers can be made form this cellophane-like material. It has been the only material that was found during the literature search of which large scale and rapid degradation can be confirmed, about 1 mm in a month at 138 C. Perhaps a further development of this material with different groups replacing the butyl-group, could be promising[8].

[8] John Oldson for NASA, private communications 2000

- Polysilanes have very high quantum degradation yields and can be made into a fiber. However, the UV-absorption of this polymer is low so additives would be required. The material is very hard to produce and consequently high-priced.
- Formula C (Polyisopropene) is an ESA sponsored development (Ref. 260, ESA T.E.S.T. program), but is too rubbery to make fibers from. It has nevertheless been included in the below reported tests, yet only samples exposed to open air conditions were found to degrade.
- Poly(p-phenylene-2,6-benzobisoxazole) (PBO, Zylon) is a rigid-rod isotropic crystal polymer. Also M5 is a rigid rod polymer (AKZO Nobel). It has not been possible to obtain samples. These materials look like polymeric UV-stabilisers, although PBO strength is known to degrade significantly with UV exposure on Earth, possibly due to involvement of oxidative reactions.

From these considerations, a selection was made of materials suitable for fiber manufacturing, as listed in Table 30.

Polymers	UV absorp.	Mechanism	Exp. rate	Cross-linking	Description
PE	Low	Hydrocarbon	Low	Possible	Polyethylene (e.g. Dyneema)
PP	Low	Hydrocarbon	Low	Not expected	Polypropylene
Aramide	High	Norrish 1	?	Likely	E.g. Kevlar, Twaron
PA6	Med	Norrish 1&2	Med	< PE	Polyamide (e.g. Nylon)
PET	High	Norrish 1&2	High	Probable	Polyethylene terephthalate.
PBT	High	Norrish 1&2	High	< PE, PA6, PET	Polybutylene terephthalate
Polyketon A	-	Norrish 1&2	Med	Likely	Carilon. Ethylene & 7% polypropylene alternating with CO in 50% mol fraction. Sample contains UV stabilizers
Polyketon B	Med	Norrish 1&2	Med	Possible	E/CO, polyethylene in which ~1% of CO is polymerised.

Table 30. *Selected UV-degradable tether polymer materials*

4.4.6 Explorative testing of selected pure materials

The selected pure materials have been subjected to a simulated space environment [Kruijff 1999.II], in a thermal vacuum without (atomic) oxygen exposed to UV lamp light. VUV and UV tests have been performed in separate chambers at ESTEC QMC. Mass loss is the primary measurement but also humidity, temperature and visual changes are noted at every stage and chemical analysis is performed on the samples e.g. to understand the amount of cross-linking.

For each of the two tests a batch of samples has been prepared. The samples consist of mostly films, but also some fibers and tethers for comparison. Thickness of the films ranges from 30-200 μm. They are sized about 40-150 mg at 5-15 cm^3 (UV) and 10-50 mg at 3 cm^2 (VUV). For every material within each batch, three samples are prepared: the front sample (exposed to UV or VUV); the back sample (not exposed to light, but in thermal vacuum); the reference sample (kept in conditioned ambient environment without light).

The spectra of the UV and VUV lamps are displayed in Figure 82. Because the UV lamp spectrum is quite wide-band, acceleration factors have been determined based on measurements in four bands using a MicroPulse Intellirad MP-300 (Table 31). The spectrum of the lamp used should be comparable to that of the solar spectrum in space (including VUV).

Because of the high light-intensity, in the UV test good thermal contact is necessary to control temperature and avoid melt. Therefore the samples have been mounted to a curved copper sample holder using pieces of (acrylic) second surface tape. The temperature of two Dyneema® reference samples (front/back) and that of the sample holder are monitored during the tests with a PT100 thermistor. The difference in temperature with the other samples is estimated through a thermal model to be ten to twenty degrees, mainly due to the difference in contact pressure. In the VUV chamber, hardly any heat is produced, and the samples have been clamped using small aluminum bars. Temperature is measured using a PT100 in a sample of Polyketon B. Temperatures are selected in somewhat above the average of the expected tether application range (-100°C to +50°C), as more chemistry is expected at higher temperatures.

The UV-only test has been performed in ESTEC's Bake-out facility at an acceleration factor of 1-1.5, for a duration of 5 days. The VUV testing is performed in the smaller SoRaSi facility, with an acceleration factor of 20-30, for a duration of 7 days.

	Wavelength band [nm]	**Sun [W/m^2]**	**Acceler. factor**
UV-A	320-390	40.7	0.66
UV-B	270-360	37.9	0.77
UV-B1	260-340	15.5	1.09
UV-C	220-290	2.6	1.62

Table 31. *Calculated solar acceleration factor UV test-setup*

Both the total and recovered mass loss are determined. Just after the test when the samples are still dry from the vacuum, the weight of both the front and back sample is measured and compared with their weights before the exposure. Subtraction of the relative weight loss of the back sample from that of the front sample should make up for the effects of humidity and outgassing (assumed identical for both samples) and provide a measure for degradation only. After several days in a contained and controlled environment, the samples will have absorbed water and a weight measurement of the exposed samples can be compared with

the weight of that sample before test in the same environment, annulling the humidity effect and providing a total measure for outgassing plus degradation. For each material the mass dependency on humidity between 54% and 65% is characterized and used to correct for any difference in ambient humidity of the 'before' and 'after' measurements (ranging from 54 to 58%).

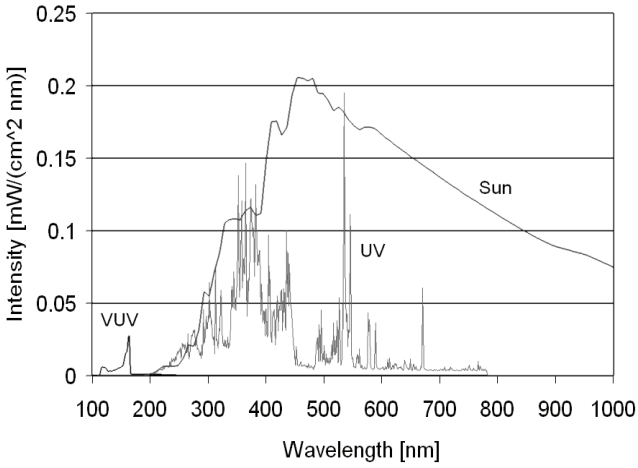

Figure 82. *Sun and measured lamp spectra*

To determine the degradation mechanism two types of analysis have been performed on the UV test samples at DSM Research. Fourier Transform Infrared (FT-IR) and Gel Permeation Chromatography (GPC). The first one gives information about the photo-chemistry, the second one about the consequence (chain scission or cross-linking). The GPC measurement is destructive as the sample needs to be dissolved. It can only be performed for a few of the materials (PET, PBT & PA), as the polyolefins require different equipment. The ECO and Dyneema samples cross link during the test, the part that is not soluble shows a decrease in the molecular weight. PP does not cross link and show some chain cleavage.

The results of the test are reported in Table 32, Figure 84 and Figure 85.

The optical effects of the UV test show no surprises: PP is expected to change color only if stabilizers are present, which is probably not the case. The other colorings are due to chemical changes in the material itself. For VUV the white powderish substance on the PP suggests degradation, at which particles are created of a size in the range of visible light wavelength. It is therefore quite possible that these particles are transparent to VUV and the underlying material will continue to degrade.

As to compare the different samples, the mass measurements have been translated into degradation time per millimeter of material. It is seen that degradation is not sufficient if the measurements of this test are representative for long term exposure. At least 1-2 orders of magnitude improvement is required. The VUV degradation rates are very low, because of the low intensity of the radiation in the Sun's spectrum. Under VUV PP degrades the most

of the samples studied. PE degrades very little under VUV (as was already noticed by Grossman), but reasonably under UV. PBT shows hardly any degradation. As expected Polyketon B (E/CO) degrades reasonably well under UV, but not under VUV. Its quantum yield for scission, according to Toronto University, is higher than that for cross linking, so full degradation is eventually expected. Polyketon A, despite the still present stabilizers shows promising degradation.

The UV-degradation of the majority of the samples has not led to new IR bands . Only for Polyketon B new bands at 1641 and 908 cm^{-1} are found. These bands can be ascribed to unsaturation, which are formed according to the Norrish II reaction (without cross-linking).

Table 33 shows the GPC results for some non-polyolefins. The molecules get smaller for PET, but PA and PBT show no real improvement in molecule mass. This is also clearly displayed by the increase of insoluble material, suggesting (heavy) crosslinking. Even PET cross-links considerably. Note that the corrected fractions of insoluble materials can be compared, but it has to be considered that PA is very transparent to UV and much of the radiation must have just passed through. PET, PA and PBT can be considered not suitable as a DUtether material.

Polymers	**Degradation rate UV [years/mm]**	**Degradation rate VUV [years/mm]**	**FT-IR**	**GPC**	**Optical (UV)**	**Optical (VUV)**
PE	40	78000	Very slight difference	Table 33	Light yellow	Slightly colored
PP	110	1200	No difference	Table 33	Unchanged	White powderish substance
Aramide	Not tested	1400	No difference	-	-	No visible coloring
Polyamide 6	70	10000	No difference	Figure 85 Table 33	Light yellow	Slightly colored
PET	40	11000	No difference	Figure 85 Table 33	Brown yellow	Light brown yellow
PBT	Degrades at rate below measurement accuracy	7500	No difference	Figure 85 Table 33	Yellow	Slightly colored
Polyketon A	19	1100	-	-	Yellow	Yellow
Polyketon B	10	20000	Figure 84	Table 33	Slightly yellow	Slightly colored

Table 32. *Degradation test results for polymers under UV/VUV exposure*

Figure 83. *Sample holder in Bake-Out facility*

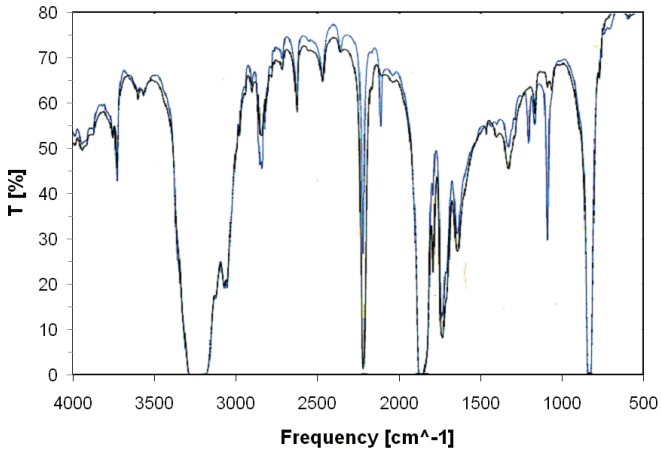

Figure 84. *IR spectrum change for Polyketon B (ECO).*

	PET	PA	PBT	Dyneema***	ECO***	PP
Mn_{ref} [kg/mole]	32	19	21	660	26	135
Mn_{sample}	22	14	16	87	5.4	65
Mw_{ref} [kg/mole]	54	43	34	22000	185	270
Mw_{sample}	36	81	46	205	26	185
Not dissolved ref [%weight]	0	0	0	0	0	0
Not dissolved sample*	3	24	7	11	45	0
Not dissolved sample [%thick]**	9	24	12	22	45***	0

Mn: mole weight averaged by number, Mw: mole weight averaged by weight, * As measured, ** Corrected for sample thicknesses relative to that of PA

Table 33. *Molecular properties for exposed polymers studied, from GPC test*

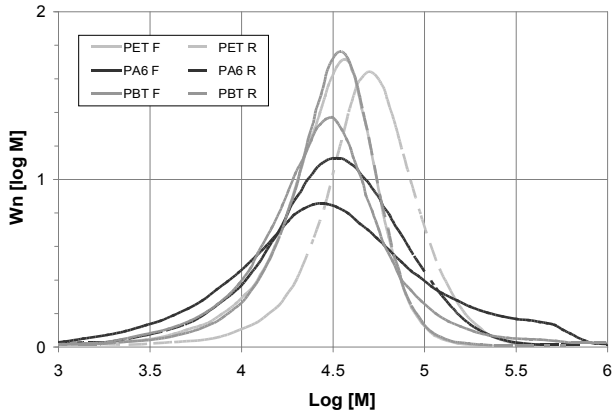

Figure 85. *Gel Permeation Chromatography results (From bottom to top: PA6, $PA6_{ref}$, PBT, PET_{ref}, PET, PBT_{ref}).*

The best candidates left overall are PP and the polyketones. Their behavior might be improved by adding UV photoinitiators to PP, by increasing the propylene fraction of Polyketone A and, possibly, by increasing the CO fraction in Polyketone B. Pretests in an ambient environment have also indicated that the Polyketone B degradation strongly improves at higher temperatures (particularly above the glass temperature of -80°C). IR-absorbers may be added to keep this material 'warm' in space.

As mentioned in Section 4.4.2, there might be an incubation effect in the degradation process that lasts sufficiently long to affect the results in a negative way, i.e., a degradation is measured after a week of exposure that is lower than the actual final equilibrium rate. This incubation effect can only be relevant for the UV test and not for the VUV test, because the VUV test has had an equivalent exposure equal to the total required degradation time. Furthermore in VUV the penetration depth is very small, so the incubation time will be small as well.

The incubation time for VUV degradation can be roughly estimated from the CutSim results with a correction for the UV penetration depth. CutSim assumes a penetration depth of a single molecule. An estimate for the incubation time can be deduced from the value as given by CutSim multiplied by the true and maximum number of molecules passed by during penetration of a UV photon. It will always be an overestimate, because penetration will not take place at random through the penetration layer, but will decrease (strongly) with depth. Therefore the upper part of the layer will receive most scissions and the material will degrade as something between a material with a 'single molecule' penetration layer (short incubation) and one with randomly distributed impacts throughout its non-zero penetration layer (long incubation).

Assuming a density of 1e15 molecules per mm^3 and a penetration layer of 20-30 μm (valid for PET/PBT. PA, PP, PE will have a much higher penetration and therefore higher

incubation time), the one-dimensional penetration layer is about 2000 molecules deep[9]. Assuming an evaporation at the scission of a 1/3000th of the original molecule, the incubation time will be ~5000 cuts, so an upper estimate of the incubation time may be 1e7 scissions duration. CutSim (Section 4.4.2) predicts that 7000 cuts are necessary per molecule when evaporating linearly. At a typical measured degradation rate of 10-100 years/mm there will be about 1e7 scissions per year into the one-dimensional layer. This means that the incubation time upper estimate may be as long as 1 year.

However, consistency between the data on which the incubation time estimate is based and the incubation time itself precludes such extreme values. It can be reasoned that the incubation time is rather in the order of weeks, and the results obtained are likely an underestimate of the true (linear) degradation that would occur over half a year of exposure [Kruijff 1999.II].

4.4.7 UV/VUV exposure test on enhanced selection

Based on the results , a longer test has been performed on the Polyketone B and PP, this time in UV combined with VUV to understand also cross-influences. Considering the very mild degradation rates achieved so far, the focus of this second test has been on trying to obtain a maximally degrading material to obtain sufficient basis to continue with an optimization process. Unfortunately the more promising material, Polyketone A, has at this time been withdrawn by the supplier.

Various changes have been introduced to increase the chances of success along these lines Table 34. It is decided to test only with films, no longer with tether samples, as they are harder to produce and more difficult to control thermally. PP is used with different types of photoinitiators, in order to move the degradation into the more abundant UV range. The CO fraction of the other candidate, the Polyketon B (ECOLyte with molecular mass of about 20,000 Daltons by University of Toronto), is increased from 1% to 9%. This increase leads to significant degradation of the mechanical properties (the films break easily when handled), however as stated before, the primary goal of the second campaign is to find an extreme datapoint. An additional material, 2% Ethylene-MVK (methyl vinyl ketone) has been provided by Prof. Guillet from the University of Toronto for the second campaign, a material expected to break down faster than ECOLyte and thus considered a potential candidate after the somewhat sobering results of the first test campaign.

As the original sample holder has been designed for tethers and long thin films, it cannot provide sufficient contact for the small thick samples used in the final test. A new all-aluminum sample holder is therefore designed (Figure 83). The initiators used are given in Table 35. The samples used are shown in Table 36. The total UV exposure is comparable to that of the target duration of 6 months in space. Since 33% of the samples is exposed and the sample thickness is only 0.5 mm, the exposed area is intended to fully evaporate and ideally a mass loss of 33% should be obtained.

[9] Private communications P. Gijsman, 2000

The Bake-Out Facility has been adapted by ESTEC/QMC to include both UV and VUV lamps and achieve a considerably higher maximum UV acceleration factor ~5-6 (UV-B1/C). Only a single VUV-lamp out of the two possible ones is used, such that the acceleration factor approximately matches that of the UV (i.e. 3-4).

Action	**Effect**
Window changed from SiO2 to CaF2	Transparent to UV, but now also to VUV
Mirrors polished and aluminum tube inserted between lamp and samples, sample holder position moved away from lamps with respect to trial runs	Increase of acceleration factor UV-C from 1 - 1.5(test 1) to 3 - 4
Test duration increased	6-9 weeks*
Sample thickness increased	0.5 mm
Sample holder redesigned, use of thermocouples and PT100s, i.s.o. only PT100s	Improved thermal control (sample temperatures in front and back are equal)
Sample chemistry	PP with added photoinitiators, Polyketon B with 9% CO i.s.o. 1%
Samples and placement	Front and back (no reference samples), 9x9x0.5 mm, 6 mm radius circular area exposed.
Temperature	8 C, after 5 weeks raised to 30°C, due to failure after 6 weeks at 140°C for 16 hrs.

* After 6 weeks, a failure in the LN2-supply caused a 16 hour rise in temperature, invalidating the results for some samples. ** Corrected fraction: (%F-%B)*Total area/area exposed

Table 34. *Test set-up adaptations*

Initiator	**Melting point (C)**	**Vapor pressure at high T**	**g/mole**	**Class**	**UV Absorption peaks (nm) – *all absorb VUV* (below 200)**
Irgacure 184	44-49	High	204	α-Hydroxy-ketone, monomers	240-250 & 320-335
Irgacure 369	110-114	Low	367	α-Amino-ketone	325-335
Irgacure 500	liquid @ room temperature	High	193	α-Hydroxy-ketone, mixture	240-260 & 375-390
Irgacure 819	131-135	Low	418	BAPO, phosphor based	360-365 & 405
Esacure Kip 150	110 (flash point)	Low	205	Polymeric hydroxy-ketone, oligomer	208-212 & 240-250
Benzophenon	Low (boiling point at 1 m Hg = 108 C)	high	low	Benzophenon, monomers	230-260 & 330-360

Table 35: *Photoinitiators used with PP during final UV degradation testing*

Material	Chemistry	% mass loss front	% mass loss back	% (front - back)
PP 184 .01	V	0.34	0.27	0.07
PP 184 .1	V	0.34	0.38	-0.04
PP 184 1	V	0.63	0.8	-0.18
PP 184 5	V	2.32	3.2	-0.88
PP BEN .01	V	0.29	0.31	-0.03
PP BEN .1	V	0.32	0.27	0.05
PP BEN 1	V	0.42	0.64	-0.23
PP BEN 5	V	1.57	2.79	-1.22
PP ESA .01	C	0.32	0.26	0.06
PP ESA .1	C	0.33	0.35	-0.02
PP ESA 1	C	0.54	0.73	-0.19
PP ESA 5	C	1.51	1.57	-0.06
PP 369 .01	C	0.3	0.2	0.09
PP 369 .1	C	0.36	0.38	-0.02
PP 369 1	C	0.65	0.77	-0.12
PP 369 5	CC	2.85	3.17	-0.33
PP 819 .01	CC	0.28	0.22	0.06
PP 819 .1	C	0.8	0.77	0.03
PP 500 .01	V	0.34	0.31	0.03
PP 500 1	V	0.56	0.82	-0.26
MVK	-	0.33	0.13	0.21
ECO 9%	-	0.53	-0.07	0.61

Table 36. *Results test second phase (MVK & ECO molten after 66% of exposure time), the ESA=Esacure, BEN = benzophenon, other = Irgacure. The fractions (.01, .1, 1, 5) are in weight %. Mass loss is indicated as positive. The sample mass is approx. 40 mg, the UV exposed fraction is about 33%. V = high vapor pressure initiator, C = front colorization, CC = colorization both front and back.*

As can be seen from the results in Table 36, despite the measures taken to enhance degradation, the observed mass loss is poor, much lower than the 33% target, and follows a distinct pattern. It must be taken into account that the brief temperature control failure after 6 weeks has in some cases led to evaporation of the photoinitiator additives (see below). The general difference with the earlier results may be explained by the lower temperature (8°C) and lower intensity of VUV. For PP without initiators, VUV is the only effective light source. Note also that a smaller surface is exposed for evaporation compared to thickness and surface of the sample. Because of the clamping of the samples, evaporation is diffusion-limited.

At very low initiator fraction, there is a small relative mass loss of *Front* samples with respect to *Back.* However, the back samples, not exposed to UV, have lost significantly more mass than can be explained by the fraction of photoinitiator itself. This mass loss of about 0.25% can be seen as an offset mass loss due to outgassing of unknown nature.

Cases with relatively high mass loss, show a loss in the order of, yet less than, the fraction of photoinitiator additive, so evaporation may be involved. Particularly on the Back samples the losses are approaching the total initiator content. The non-UV-exposed samples on the back, in most cases, have lost even more mass than the equivalents on the front. This discrepancy becomes larger for samples with higher fractions of photoinitiator as well as for samples with initiators that have been identified as evaporation-sensitive (i.e. high vapor pressure initiators Irgacure 184, Irgacure 500 and Benzophenon).

A hypothesis related to the sensitivity of the reaction to light intensity can explain degradation on the back samples occurring and sometimes even greater than that on the front. The light intensity or acceleration factor may have been supra-optimal for the Front samples, causing them to cross-link rather than degrade, whereas the Back samples degrade because of the low intensity of scattered light. Other than in earlier tests the holder has been placed quite backward in the chamber, allowing a much larger fraction of stray light to pass beyond the sample holder. This hypothesis leaves room for optimism to find a UV degradable material.

In order to explain the paradoxical results, a representative selection of the exposed samples has been further analyzed by Gijsman (front and back samples of Irgacure 184, 0.01% and 5%). The investigations show that at least some light has reached the Back samples and caused chemistry. The Back samples seem to show at least some light-related degradation, since some of them show circular (light) colorizations, other than the expected thermal colorization that would cover the full square of the sample. Spectral measurement indicates absorption of UV in the Front samples after test, providing evidence that some level of initiator is still present. GPC tests show 27% of cross-linking for the exposed part of the 5% Irgacure 184 Front sample, compared 12% for 0.01% Irgacure 184. The initiator has therefore contributed to increased chemistry, and significant cross-linking, which may have impaired mass loss on the front.

The hypothesis however does not explain how the mass losses on front and back of the sample holder for most samples are very close to eachother. It also does not explain by itself why the samples with lower initiator mole mass (high vapor pressure) show the largest difference between Front and Back samples.

The observations in fact suggest that evaporation of the initiator and the polymer material has dominated the measurements. This explains why the mass loss on the Back samples seems so close to the concentration of photoinitiators, aside from the 0.25% offset. The Front samples may have become plugged by UV reaction products, blocking further evaporation of initiator.

To verify this hypothesis, three different outgassing reference tests have been devised, without exposure to UV. They are performed by ESTEC/QMC [Guyt 2001].

Firstly, a continuous mass-loss measurement in vacuum is performed of unexposed, 5%, Irgacure 369 (low vapor pressure) and Benzophenon (high vapor pressure) for a series of temperatures: -10, 9, 30, 125°C (each 24 hrs at 10^{-6} mbar). The purpose is to find out whether and at which point during the earlier tests evaporation of initiator has taken place. The results indicated that outgassing only causes significant weight loss when sample temperature is increased from 30° to 125°C. As expected, the high vapor pressure Benzophenon shows a little greater tendency to evaporate already at 30°C. It can be concluded that the initiators were still fully present in the samples and active during the first 6 weeks of the UV/VUV test.

Secondly, a bake-out of unexposed 0.01%-samples is performed (Irgacure 369 and Benzophenon) in order to understand the consistent observed offset weight loss of 0.25%. All 4 non-UV-exposed samples show an initial weight loss of 0.254 - 0.339%. Note that the contribution of humidity has been measured as well and is about one order of magnitude smaller. This amount is indeed compatible with the consistent weight loss observed for the 0.01% samples. It can thus be suggested that this is an offset weight loss caused by the transition to vacuum conditions rather than by UV exposure and it is not caused specifically by high temperature. Subsequent spectral measurements of the condensate suggest that what evaporates is actually PP material. In order to obtain the UV effect, at least this 0.25-0.3% offset should be subtracted from the total measured weight loss of all tested samples. As a consequence we may conclude that the 0.01% samples have been shown to have (relatively) poor UV degradation performance.

Finally a full bake-out of the already exposed 5%-samples is performed, for both Front & Back, at 125°C for 24 hrs (Irgacure 369 and Benzophenon), Table 37. Condensate spectra are then also taken. Now that the samples are not clamped-in tightly for 66% of their surface, the (remaining) photoinitiator is free to evaporate without much need for diffusion. The objective is to understand how much initiator was still present in the samples at the end of the UV exposure test, how much had evaporated, and how it is linked to the initiator vapor pressure and UV exposure. The results are clarifying.

Apparently, Benzophenon, as example of a high vapor pressure initiator, already lost all its evaporable initiator during the UV/VUV test, when still clamped-in tightly. Benzophenon is not only eager to evaporate, but the PP/Benzophenon combination also has good diffusion properties. The small weight loss measured (0.08/0.02%), if judged from the spectral test on the condensate, is due to PP evaporation. It is likely that ~2% already evaporated during the production baking of the sample and the rest evaporated (with good diffusion) during the UV/VUV test, leaving virtually nothing to evaporate during the extra bake-out test. For Irgacure 369, the significant loss in both Front and Back cases during this extra bake-out is in fact due to evaporating initiator, as clearly shown from the condensate spectra. In both cases, the total mass loss for the Back sample (in UV/VUV test and bake-out combined) approaches closely the mass loss measured during the unexposed sample's outgassing test.

In other words, after the combined exposures, all initiator was able to come out from the Back samples.

The results also suggest that the evaporation of initiator from the Front samples has been limited by chemistry initiated by the UV exposure. The Front samples do not release as much initiator mass. As said, the UV absorption analysis shows that these front samples still contained initiator after the exposure even for the case of the high vapor pressure initiators. The UV radiation during the first 6 weeks of exposure have somehow encapsulated the initiators, probably by cross-linking and gel forming, keeping them from evaporating even at high temperatures. Apparently this encapsulation effect has been stronger for the high vapor pressure initiators.

In conclusion, weight loss measured in the second test campaign is partly due to initial evaporation of PP due to vacuum conditions only and partly due to initiator loss as a result of a high temperature phase near the end of the test. Significant chemistry has nevertheless occurred in the UV exposed areas, i.e. discoloring, cross linking and encapsulation of the initiators, none leading to significant PP mass reduction. The 9%-CO ECOLyte and MVK materials do not significantly degrade in mass.

Sample	**Weight Loss* [%]**			
	UV/VUV Test	**Extra Bake-out**	**Total**	**Unexposed Ref**
Benzophenon 5% F	1.57	0.08	1.65	2.89
Benzophenon 5% B	2.79	0.02	2.81	
Irgacure 369 5% F	2.85	0.44	3.29	4.35
Irgacure 369 5% B	3.17	0.82	3.99	

* Contributions: initial vacuum loss ~0.3%, initiator evaporation, degradation.

Table 37. *Mass loss results samples with photo-initiators*

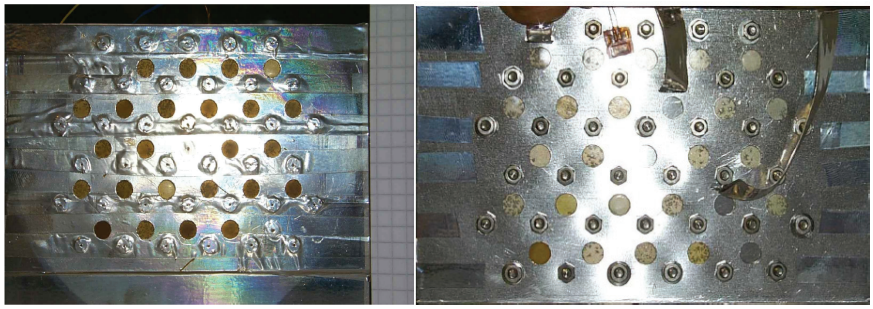

Figure 86. *Samples after UV and VUV exposure, front and back*

4.4.8 Conclusions and outlook

The concept of a tether material degrading in the space environment allows for extended tether applications. UV/VUV exposure has been identified to be the principle mechanism for such a material and a degradation time of ~6 months/mm has been set as a target. Based on the expected chemistry, possible tether materials have been selected. Testing of these materials for a week in both UV and VUV has led to exclusion of most of them due to cross-linking, but also to the identification of a few materials of interest, in particular polyketones (showing favorable reactions) and PP (for which the absorption frequency has to be shifted). Possibilities have been identified for improvement of the performance by chemical additives. It has been attempted to move the sensitivity of the non-crosslinking PP towards the UV range using various kinds of photoinitiators.

Unfortunately, no significant degradation is observed, also not in materials for which such behavior has been claimed or suggested by external parties (Formulation C, ECOLyte, MVK). The most promising candidate Polyketon A, an alternating copolymer of pol(alpha-olefin) katalysts and the reactive carbon monoxide, shows significant degradation despite the presence of (for this application unwanted) UV stabilizers, but the material has been withdrawn by the manufacturer. Other promising materials, such as PBMA (not suitable for tether braiding) and polysilanes could not be obtained for tests. For most of the materials studied the absence of oxygen and/or the presence of cross-linking is the most important inhibitor to fast mass loss.

It remains a possibility that the set-up and photo-initiator selection have had a negative impact on the results. The high acceleration factor may have caused the cross-linking in the PP sample. Although most photo-initiators classes have been included, the Benzildimetyl-ketal and Metallocene (esp. Zirconium based) classes and the monomer IPPBP have not been investigated. Stabilizers may be necessary additives as well. Increased (ineffective) UV absorption may have taken place by initial degradation or colorization of the samples. Free-radical generators such as the commercially available Michler's ketone as well as oxidizers (e.g. the poisonous peroxide or sodium nitrate) could be included within the tether material to enhance degradation processes and make them more similar to processes on Earth. The temperature of the tether may have to be raised through colorants. To avoid evaporation of the additives, the photoinitiators should be locked inside the chain.

5 Deployer System Development

Right on your tie!

— Erik Jan van der Heide proclaims success of the first closed loop tether deployment test, Summer 2000.

5.1 Introduction

The concept worked out for flight demonstration in this work is based primarily on the Small Expendable Deployer System (SEDS), for its simplicity and flight record. It is based on deployment from the outside of a fixed spool rather than from a rotating drum or reel. Deployment velocity of such a system can be measured with optical detectors and is controlled by tension. Of the various means available to control the tension, SEDS concept or "barberpole brake" has been revisited and worked out into a breadboard and flight model. The brake's performance has been analyzed in detail. This Chapter considers the full tether deployer development based on spool and barberpole brake, including the control system and the tether deployment tests that have been performed to validate and characterize it.

5.1.1 Technology heritage

The SEDS missions in 1993 and 1994 demonstrated respectively a mostly passive uncontrolled single-stage deployment to a large angle, and a controlled deployment to the vertical (Table 74). Both missions successfully deployed a 0.78 mm Spectra tether of 20 km length shortly after launch from a Delta-II spent stage [Carroll 1995.I]. Both missions deployed the tether from a passive, fixed spool and involved friction braking using a so-called barberpole brake. The barberpole concept is taken from textile industry and allows to apply tension over a large range, by guiding the deploying tether a number of times along a helical path around a cylindrical pole. Whereas this friction brake was used in open-loop on SEDS-1, the SEDS-2 mission used it to actively control the deployment in closed-loop based on deployed length estimation. In order to determine the tether length during deployment, two diode-transistor pairs were placed across the gap between spool core and canister wall (Optical Loop Detectors). In this design, each loop deploying from the spool subsequently passes between each of the pairs and interrupts beams of infrared light transmitted from diode to transistor. The interruptions are counted and the number of loops deployed can be determined.

The SEDS system concept has already been considered for a SpaceMail demonstration, [Carroll 1995.II]. Unfortunately, the SEDS SpaceMail demonstration mission never flew.

In Europe, the first tether activities were initially more inspired by the reel-based TSS missions [Dobrowolny 1994]. First, reel and reel-spool hybrid systems were breadboarded

and an open-loop deployment test rig was developed in the FIESTA[10] and TATS projects [Alenia 1995], see also Section 3.1.1. A reel can directly control unwinding speed, although this does not necessarily mean that the endmass trajectory is controlled as well. Slackness of the tether may be an issue if the unwinding rate of the tether is too high (Section 2.1.4). Compared to passive spools, reel systems are characterized by more complex and more bulky hardware, that have a poor flight record (Section 1.3). In practice, they so far have mostly led to failure (with the exception of TSS1R). In contrast, spool-based deployments have so far all been successful (Table 1).

Attention in Europe next shifted to the spool concept, with as primary perceived challenge to overcome the lack of direct control of deployment velocity. Early spool deployer development in Europe focused therefore on precise control of deployment tension. In the RAPUNZEL deployer concept [Sabath 1997], tension in the tether is controlled through an electromagnetic hysteresis brake. As the tether exits the spool it is guided around a co-rotating pulley that can be constrained by electromagnetic torque and thus applies a tension. The tether next is guided through a swivel. The tether tension affects that swivel's amplitude. The amplitude is used as feedback mechanism to help apply the tension more precisely according to a target profile.

In a co-operation with TU Munich and the Munich-based company Kayser-Threde, a deployer breadboard has been tested successfully in zero-g up to a tension of about 2 N (Figure 87). In this test it is demonstrated that tension control of deployment is feasible. In addition, the unwinding dynamics of the tether from a spool in low gravity environment is recorded and it is shown that the tether can be guided successfully through the system without getting stuck [Sabath 1997].

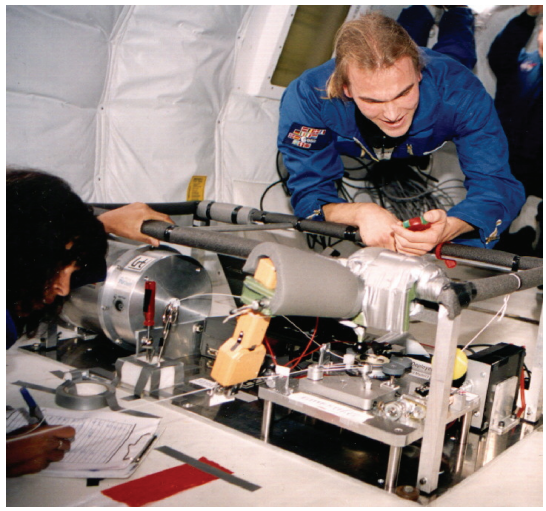

Figure 87. *The author operating RAPUNZEL canister and brake system in parabolic flight*

[10] A 1994 study by a DASA/RST-led consortium for DARA

When comparing the RAPUNZEL deployer with the SEDS system, the RAPUNZEL is able to establish tension levels more accurately but is rather more complex. Its attainable tension range with the as-built system is a limiting factor. The SEDS system's flight record, its relatively small number of components and guides, its scalability and large tension range are all factors that make the SEDS barberpole concept suitable for a low-cost demonstration development.

With particular focus on the SEDS system, Ockels, Heide & Kruijff have developed noise models and a simple deployment controller. Their two-stage deployment approach [Ockels 1995] satisfies the SpaceMail requirements of accuracy and robustness (Section 3.1.1).

5.1.2 SpaceMail system concept for momentum transfer

The SEDS hardware concept is selected also as a starting point for the remainder of this work. This chapter focuses mainly on the deployment system, or rather, the tether-related hardware: tether spool, the canister protecting it, the optical loop detection system (OLD), control software and the barberpole friction brake with stepper motor. The SpaceMail system or momentum-transfer system includes in addition the ejection system, the on-board computer, the stepper driver, the tether cutter assembly with relays box, the re-entry capsule and the activation system for capsule release.

Figure 88 sketches, for simplicity, only the key components of the suggested tether momentum transfer system. Before flight, the tether has been wound onto a spool and characterized under controlled conditions. An ejection system initiates the separation between platform and endmass. The tether is then deployed from the spool that is fixed inside a canister mounted to the platform. The endmass include the re-entry capsule. Such a configuration with the tether on the platform allows the endmass to be very lightweight and guarantees also proper orientation of the tether exit point. The tether is unwound as it is pulled over the head of the spool towards a central, small exit guide and, for each loop, crosses sequentially each of the Optical Loop Detection (OLD) infrared-beams. This allows the OLD electronics to register the passage and forward signals from each of the “encoder” channels to the control system. The control system processes the signals to generate the length and velocity of deployment. The results are compared to a reference deployment table stored on-board (length and velocity versus time). Using predetermined feedback gains and a mathematical model of the spool and brake system, the required setting of the barberpole brake is computed. This setting is then commanded to the barberpole brake mechanism in order to control the deployment by friction. At every control interval of several seconds the number of wraps of tether around the pole is adjusted. Even if the tension is significantly different from nominal, only small position adjustments are required.

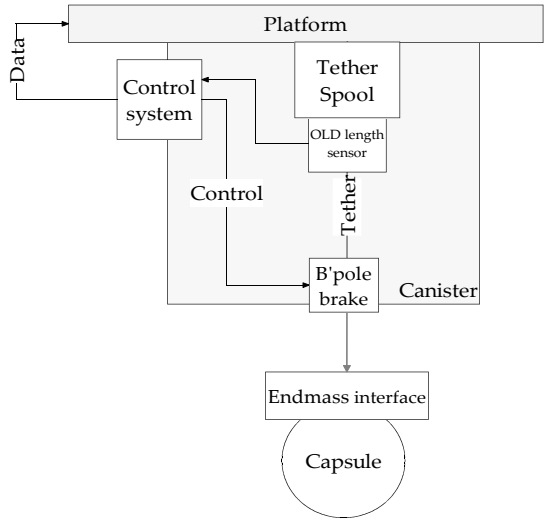

Figure 88. *Simplified overview of the proposed tether momentum transfer system.*

5.1.3 Overview of development and challenges

Experience with the SEDS-derived deployment system towards the eventual SpaceMail system development has been achieved over the course of various projects, as reported in the remainder of this thesis. In 1997, the YES satellite design includes the SEDS deployer hardware itself. YES also carries an innovative fail-safe double strand tether (Sections 4.3.1 & 6.3.1). A deployment test using SEDS hardware and a double-strand tether, similar to that used in YES is performed. Around 2000 follow the development of a European deployer and the first closed-loop deployment tests in support of the TSE project (Tether System Experiment). TSE is a feasibility study with breadboard development. As YES2 starts in 2001, SEDS hardware is no longer available due to International Trade in Arms Regulations (ITAR). A new flight system is therefore independently developed and qualified.

The physical simplicity of this hardware comes at the price of behavioral complexity. The work reported here intends to improve the understanding of the deployer behavior. Friction is fundamental to tether dynamics and the control of the endmass trajectory. The friction behavior of tether, spool and brake are therefore described through a mathematical/empirical model and its parameters. The model is used as a guide to dimension the hardware. It is also included as part of the controller software. The hardware and controller performance is determined through simulation and test, as well as the acceptable range of the model parameters. The suitability of the deployer for its intended purpose -accurate momentum transfer- can eventually be assessed by quantifying the model parameters as they materialize during in-orbit demonstration, and by comparison to this allowable range.

However, first a significant investment is done in the development of proper facilities, to make tether windings and to test tether deployment as realistically as possible.

5.2 Support facilities for development and test

5.2.1 Winding machine

To produce spools from the tether for both testing and flight, a high precision winding machine has been developed, mainly for thin-line mechanical tethers (Figure 89). The main challenge for the device is to make stable, reproducible windings. The machine makes a record of tether length versus number of wound loops, such that later the deployed length can be determined using a unwound loop counter system. Winding tension and the gap width between adjacent tether loops is also recorded for traceability purposes. Through a sequential pretensioning system, the motion of the unwinding reel is stabilized and winding tension is controlled from about 10 N down to 8 N near the end of the tether. Although the system is designed for low slip on the measurement wheels, a calibration is necessary, to correct for winding strain and for the effective diameter of the tether itself when bent around the measurement wheel.

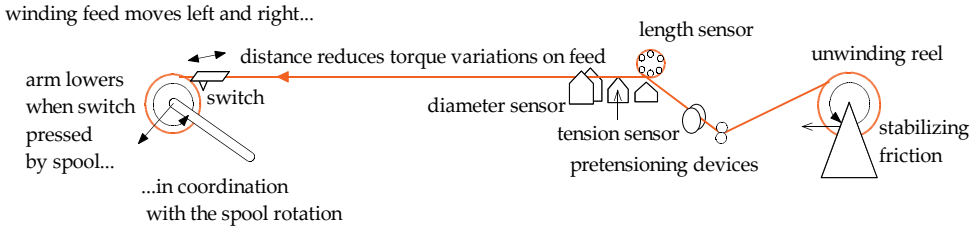

Figure 89. *Schematic representation of winding machine and actual device*

As the tether is being wound it is taken from a reel at several meters from the winding head, minimizing bending angles at the winding feed, keeping tension constant and torques on the winding feed low and minimize variations. The winding feed moves back and forth over a rail along the axis of the rotating spool, controlled by software and actuated by a stepper motor for high precision and compact winding. The spool itself is driven by a more powerful DC motor with encoder. In order to help keep the two motions synchronized, a

calibration is performed with the help of an optical sensor every time the feed passes the middle of the rail. Geometry of the machine is designed such that the tether has a constant and low bending angle from winding head onto the spool, reducing torque effects while still allowing for a feed of tether close to the winding (Figure 90).

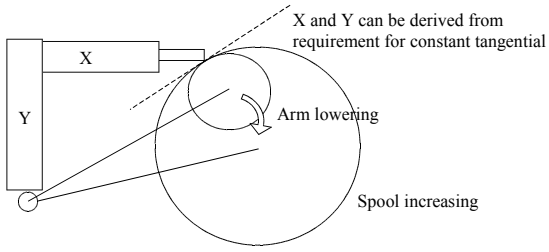

Figure 90. *Geometry of spool arm location for constant, slightly inclined tangential at winding head considering increasing spool diameter during winding*

5.2.2 Unwinding machine

The performance of a tether system in space depends not only on the well-predictable gravity-gradient force, but also for a large part on particular and variable hardware factors, that may cause irregularities in applied friction levels and deployment rate and may adversely affect controllability. In order to characterize such effects as well as to study controller robustness in a real-life and real-time deployment situation, two generations of tether unwinding machines have been developed. A first concept is implemented as part of the European Space Agency's project Tether System Experiment [Gavira 2000], based on the pre-existing TATS facility. The second generation is developed completely anew for the YES2 project, taking into account the lessons learned from the TSE study. Apart from being a research tool, the facility is indispensable as it provides a possibility for a full ground validation of flight hardware.

First generation (TSE test rig)

The TMM&M (Tether Mechanisms Materials and Manufacture) open-loop deployment test stand [Alenia Spazio 1994] has been upgraded by the TSE team to accommodate a real-time tether dynamics simulator and the possibility for testing closed-loop deployment control [Kruijff 2001.II].

The test rig (Figure 91) contains an element consisting of the space experiment's hardware and software (Satellite Part), as well as an element simulating the space orbital environment (Space Part). The tether, through its tension and deployment velocity, provides the only connection between the two elements.

The basic element of the Space Part is a real-time tether simulator that commands the deployment velocity based on tether tension as determined from measurements by a weigh-beam sensor (0 to 3 N, 1 mN resolution). This tether tension results from the hardware performance of the satellite part. It is combined with simulated gravity, aerodynamic and other forces in the real-time tether simulator and the resulting effect on deployment velocity

is applied by pulling the tether through a motor-controlled roller system. The instantaneous character of the start of deployment, i.e. an endmass ejection by springs, can be realistically simulated as the roller system in rest can be coupled to a rotating flywheel through a clutch and brought up to initial speed in a fraction of a second. Because the applied deployment velocity, due to inevitable system imperfections, will be slightly off from the simulator's predicted velocity, the rollers are PI-controlled, securing that also the total deployed length is close to the simulated length. With the machine, a deployment velocity of at least 14 m/s can be obtained. The rollers expel the tether into a collection bin and it cannot be reused.

The Satellite Part contains the tether deployer system and its deployment control software. The Satellite attempts to control the deployment according to its on-board algorithms by control of the tether tension. For an effective control, some measurement of the deployed length or deployment velocity is necessary. The sensor system available to the deployment controller is the Satellite's own system, as the one that would be available in space. The controller receives no other information on the deployment from the Space Part. This set-up allows for a testing of the autonomous control of the deployment by the Satellite, and an off-line comparison between the Satellite's measurements and the Space Part's imposed deployment.

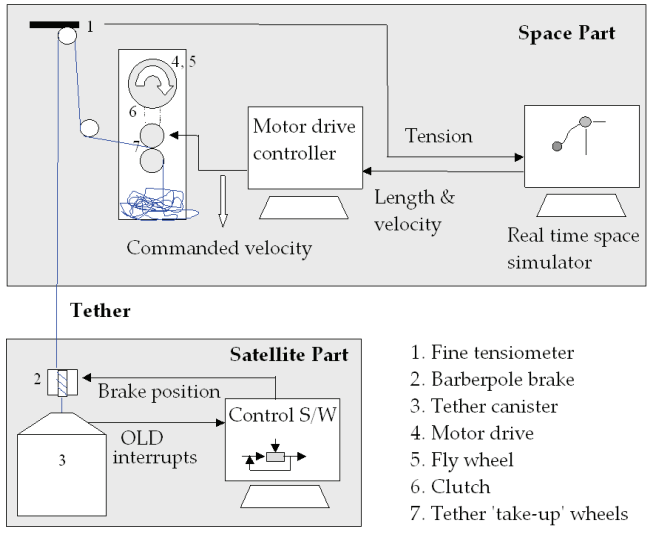

Figure 91: *Simplified Schematic of TSE Test Set-Up*

For the purpose of deployer hardware characterization, the facility can run in a simpler, open-loop mode, in which the deployment velocity is simply commanded and tether tension is recorded. The spool friction can be determined over a range of velocities and as a function of length, and the Satellite's tension control system can be set into different positions as to calibrate its performance before flight.

The facility has been successfully used in open loop to study the effect of different braids of tether, and to characterize the spool itself as well as a tortuous path ("barberpole") friction

brake. Performance at high velocity and tension has been separately demonstrated. In the lower velocity range, closed-loop deployments have been successfully performed [Kruijff 2001.II], Section 5.6.1. A problem that is here observed, however, is a resonance between the tether control and the dynamics of the motor drive that is limited by the inertia of the flywheel. For this reason, and in order to implement a number of other improvements, a second, fully new facility is developed.

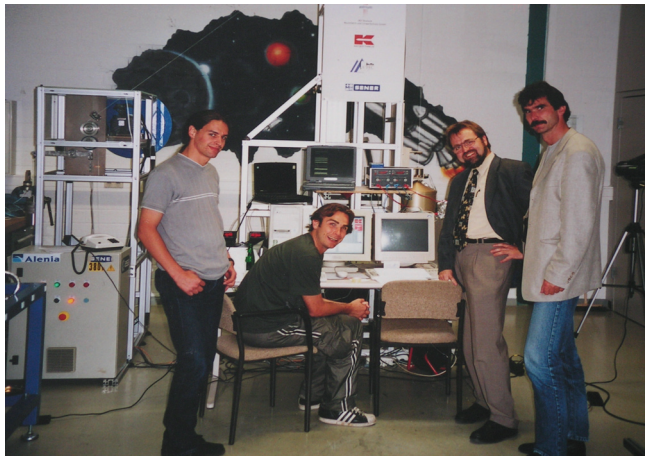

Figure 92. *TSE unwinding test rig at RST Rostock and part of the crew*

Second generation (YES2 test rig)

In the context of the YES2 project a second test rig has been developed according to the same concept as the TSE facility but with implementation of a number of lessons learned using technology from textile industry (Table 38). It is a compact, modular and mobile test facility that has featured in various conferences and universities, and flew twice on parabolic flights, Figure 94 [Heide 2003.II, Hyslop 2005]. The rig is improved in the following aspects:

- recovery and reuse of the tether,
- improved performance in terms of precision,
- higher attainable deployment velocity,
- avoidance of resonance issues,
- compact and mobile design,
- highly automated test set-up and data logging.

The roller system with flywheel is abandoned in favor of a godet, one of the spin-ins from textile industry. The godet is a very smooth steel cylinder of 10 cm diameter, that can be rotated by a DC motor, around which the unwinding tether is wrapped a number of times before it comes off again. As long as the tether leaving the godet is kept under a non-zero level of tension (e.g. applied by a flow of air) the wraps guarantee virtually zero-slip and the smooth cylinder causes virtually no damage or deformation of the tether. Godets are

generally used in textile industry in the production line of fibers. Hot, relatively weak fibers are extruded and need to be moved away with a precise velocity from the extruder without slip, under low tension, and within a specified temperature range.

With the godet in the tether test rig, a deployed length precision and accuracy of 0.1% can be obtained with Dyneema®, compared to a precision of about 0.5% and accuracy of about 2.5% that has been obtained with the TSE facility. High tether forces can be applied (>25 N) and very high deployment velocities can be obtained (>25 m/s). The system has low inertia, so no resonance issues, and can simulate ejection without need for a fly-wheel.

The facility uses compact high range and low range tensiometers that measure tension by compensating the tether pressure through an electromagnetic force.

To allow for more extensive testing and to be able to characterize even a flight tether itself (before flight), a third part has been added, the Recovery Part. The Recovery Part contains a heavy duty high speed reel to collect the unwinding tether, the Back-Up Winder. This reel must ideally be commanded to wind at exactly the deployment velocity, so up to 25 m/s. Since the relation between angular rate of the Back-Up Winder and godet speed varies as the Back-Up Winder's spool diameter increases, and because the recovered spool builds up a considerable inertia, it is not possible to match the reeling speed to the deployment velocity precisely at any time. To deal with the mismatch, a buffer is placed between godet and Back-Up Winder that can hold tens of meters of tether.

A standard textile industry fournisseur from IRO GmbH is equipped with adapted control electronics in order to perform this function. The fournisseurs' tether collection mechanism has a very low inertia and, with the proper sensors, can be accurately controlled to match exactly the godet speed. Fournisseurs are typically used in the weaving and knitting industry. For the weaving process the yarns in fill and warp direction are accelerated from zero to high speed at every stroke, which could be a jerky process. In order to have low and constant incoming yarn for the weaving process, the yarns are delivered from a spool by an air jet, with constant speed to the fournisseur, which actively places the loops nicely onto a buffer (Figure 93). The buffer can now meet the pulse-wise demand of the weaving ship and will release the yarns under low constant tension, but high acceleration as required.

For the tether test facility, the incoming speed (godet speed) is not constant, but determined by space tether dynamics. For this reason, a highly accurate sensor is placed between the godet and fournisseur to determine the differential speed for both devices - the Vacuum Buffer. This Vacuum Buffer also secures the non-zero tension level required by the godet. Simply put, the Vacuum Buffer is a 20 cm tube, attached to a source of underpressure, that sucks in a loop of the deploying tether between godet and fournisseur. The depth of the loop is measured at high frequency (1 kHz) by a large number of optical sensors placed along the tube. As a difference in speed between the godet and fournisseur builds up, the length of the loop changes, and a controller acts to correct the fournisseur speed.

Figure 93. *Fournisseur with yarn. Tether enters on left.*

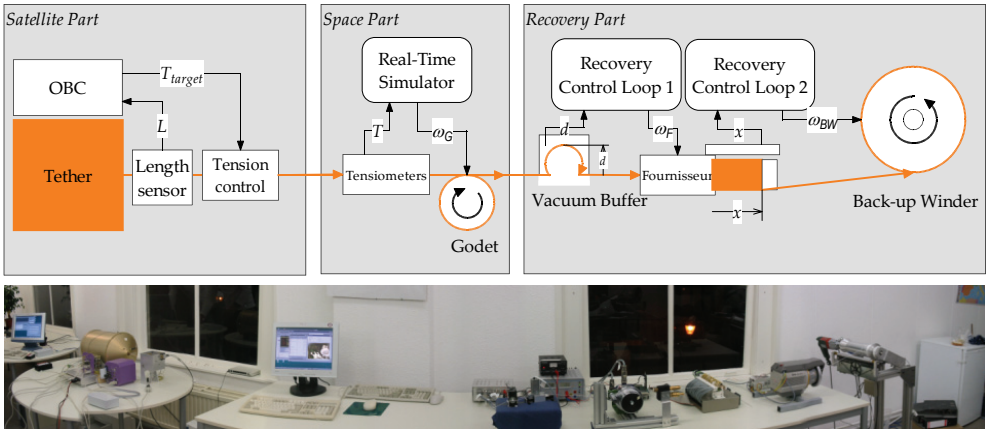

Figure 94: *Schematics of Rig v2: Space Part (yellow), Satellite part and Recovery part; actual set-up.*

Parameter	Unwinding rig v1	Unwinding rig v2
Project context	TSE	YES2
Real-time tether simulator	BeadSim	RTBSim
Logging of settings for each test	Manual	Semi-automated
Drive system	Squeeze rollers, clutch and flywheel	Godet (low inertia)
Maximum unwinding velocity [m/s]	14	25
Maximum tension	>40 N	>25 N
Tether recovery	No	Yes
Option to control ambient temperature and atmospheric density	No	Yes
Test rig mobility	Not suitable for transport	Desktop system, modular & easily transported

Table 38. *Specs and evolution of the unwinding rig*

On the software side, test initiation software has been developed in Delphi Pascal that secures control and proper initialization and traceability of all variables. Partially automated

test procedures avoid unnecessary anomalies during testing. Data storage and filing is automated. A 3D visualization of the tether deployment in space helps create a sense of dimensions and timescale and mentally prepare for a space experiment.

Most of the test rig control is developed in Matlab-Simulink/Real Time Workshop and runs as embedded system on the so-called Target PC, whereas the real-time tether simulator is an executable based on MTBSim (Section 2.3), communicating through serial port. For modularity and risk reduction, the 3D visualization is a separate program receiving only inputs from the simulator via the Windows clipboard function.

Test rig limitations

A number of minor limitations of the unwinding rig (v2) have been identified that may be considered during tests, as well as for the development of upgrades. They are mostly related to limitations inherent to the real-time tether simulator, high frequency and tether flexibility effects, and are currently not considered critical:

- A freely deploying tether in space has a variable bending around the deployer's exit guide. The tether deployment angle in combination with the attitude of the deployment platform, as well as possible transverse waves determine the outgoing tether angle. It has an impact on (generally slow) friction variation of about 10-20%. It can be implemented through a (manually or automatically) rotating guide. This added complexity for the test rig is considered not critical and has not been implemented.
- Neither simulator nor test rig currently takes into account the limited propagation speed of tension within the tether (Section 2.3.2). Indeed, the period required for tension distribution is significantly shorter than that for other typical cyclic motions, such as e.g. the spring-mass motion. For a Dyneema® tether the assumption of infinite speed of sound is also unlikely to interfere with the control delay. For a short tether sound waves traverse the tether much faster than the control delay, for a longer tether a sound wave dampens out over a few periods (Section 8.4.3) and significant additional damping is expected to occur if the tension-wave energy is reflected at the various wraps of the tether around the barberpole.

  An undesired control resonance can however occur during the final deceleration. A steep change in the barberpole brake may then has an immediate and disproportionate impact on the tether deployment rate but not, as directly, on the endmass motion (see also Section 8.4.3). The pole control could then overreact during the subsequent control cycles, which, in combination with the effect of the arrival of the first reflection of the transmitted wave, could lead to repetitive triggering of new and increasingly stronger waves. This as yet unconfirmed possibility may require a relatively slow final deceleration and temporarily a slower, less aggressive feedback as to average out velocity measurements over several wave periods.
- There is a subtle limitation of the test rig related to the representation of tether strain. In the current set-up, the commanded velocity for the test rig is a filtered version of the simulated deployment velocity, i.e. the speed at which the tether is pulled from the

spool. Another component to the total rate of tether length increase is the strain rate due to changing tension in the tether. Deployment velocity and strain rate redistribute almost instantaneously or within seconds in response to changing friction, whereas the endmass velocity (or better, the total length rate) changes only slowly due to endmass inertia.

The difference in response of a deployment in the test rig vs. a deployment in space is as follows. For both environments it is true that any increase in friction inside the deployer leads to an increased stretching of the tether, be it due to endmass inertia (in space) or the continued torque of the unwinder (in the test rig). The relationship between the friction and the tether strain depends on tether stiffness.

The stiffness of the tether in the test rig is very high compared to that in space. In a space deployment, the tether stiffness decreases with deployed length, according to $k=EA/l$. This decrease is significant as the length passes through orders of magnitude from its initial value of about 50 cm to a final length of tens of thousands of meters. In contrast, the stiffness of the deploying tether segment in the test rig can be considered constant and very high, as the distance between deployer and the unwinding device is constant and short (about one meter). As a result, in the test rig, tether stretching due to increase in friction occurs almost instantaneously.

The godet-imposed velocity should thus be considered to be identical to the tether velocity inside the deployer, and this is how it is treated. Determining the resulting strain and impact back on the deployment is exclusively the domain of the simulator. Strain rate effects due to cycles much slower than the simulator's control cycle of 1 s duration, such as those introduced by barberpole brake action, are well represented through this solution.

In the test rig, in case of a fast peak of tension within the deployer, the deployment, as driven by the godet, does not respond to this peak directly. It will at first continue undisturbed, no matter the amplitude of the peak, and the peak will pass quickly. Only the average tension over the current control cycle is communicated to the simulator, smoothing the effect of the tension peak. The simulator responds only in retrospect and will thus command only a somewhat decreased deployment velocity for the next control cycle.

In an actual deployment in space it may, in some cases, take several seconds before the strain tension overcomes the increased friction, and a stick-slip process could result (Section 4.2.1). If the physical response to such fast tension changes is to be reproduced more reliably, the control frequency of the test rig has to be sped up. As tension peaks at constant deployment velocity take generally in the order of 10 ms to occur, a fast control-simulation cycle at about 1 kHz is necessary to correctly represent this behavior, compared to the 1 s currently in use. It is not obvious whether the godet can respond at such frequencies. The response requirement may be delayed, at some loss of representativeness, by including a variable slack between deployer and godet, e.g. a movable guide attached to a spring-damper system.

- Oscillations of the tether attachment point on the endmass may have an impact on early deployment through a backcoupling with the deployment strain and tension (Section 8.3.3). This feature is planned, but not yet included into the simulator and may thus eventually also be represented by the test rig.
- Other limitations to be taken into account are the gravity effect on both vertical spools (resulting in a difference between loops unwinding upward vs. downward) and horizontal spools (where the bottom half of each loop deploys more easily than the top) with respect to the zero-g environment. The unwinding rig v2 is compact however and has been taken into a zero-g plane for dedicated testing. The thermal vacuum environment of space is also not present. Atmospheric drag can have an effect at high deployment velocities. To account for the latter, the unwinding rig v2 is equipped with a container for the full deployer within which temperature and atmospheric density can be controlled (e.g. by helium).

5.2.3 Hardware emulator

A much simpler system has been built as a development support tool, the "hardware emulator", allowing to test control algorithms and software in real-time using the flight software and flight On-Board Computer, or engineering model (Figure 95), without actual tether deployment. In this tool, the space part is a separate PC with a real-time tether dynamics simulator, which again provides the initial conditions of deployment. It however also contains models of some of the Satellite Part hardware (tether spool and brake system). Through these models, it translates the deployment velocity directly into OLD pulses, such that no actual tether unwinding is necessary for these tests. Initial parameters and hardware model parameters can easily be, and usually are, disturbed to test for robustness.

The On-Board Computer receives those pulses as it would receive true OLD signals, and filters them to determine length and velocity as well as the required control activity. Its electrical output intended for the stepper driver electronics of the barberpole brake system is intercepted by the space part PC and converted to tension, using the brake hardware model. The real-time simulator uses the calculated tension level to simulate the deployment and predict OLD pulses over the next time step.

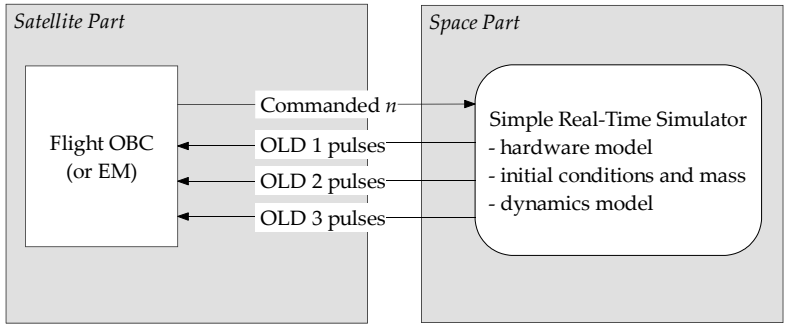

Figure 95: *Deployment emulation concept.* n *is the desired brake position.*

5.2.4 Deployer system testing overview

In total over 650 km of tether have been deployed in the course of this work, of which for over 500 km detailed test data has been collected. Table 39 provides a high-level overview of all deployer system characterization and verification tests. Apart from their usage for closed-loop deployment tests, the unwinding rigs have also been used in open-loop mode, in order to characterize hardware performance under various environmental conditions. In some case, only parts of the test rigs are activated or third party facilities have been used. The hardware characterization and environmental effects tests 1-3 and 5-7 are discussed in Sections 5.3.6-5.3.8, 5.4.4 & 5.4.5. The closed-loop deployment tests 4, 8 and 9 are described in Sections 5.6.1 & 5.6.2. For completeness the table includes also the YES2 mission itself and a number of preflight verification and post-flight investigative tests. These mission-related tests 10-20, are described in Chapter 8.

5.3 Spool development

The design of the spool, made up of a core with the tether wound around it and including the OLD length detection system, is described in this section.

5.3.1 Core and canister

The spool is a tether wound onto the outside of a metal core. This core is designed to support and enhance mechanical stability of the wound spool, and contribute to a relatively smooth and uniform deployment tension. Its design should not increase the risk of tether jam unlikely. The core is conical narrowing towards the top in the tether deployment direction to ease the tether coming off the spool and to reduce cyclic effects on tension (Section 5.3.6). The bottom of the spool is fixed lightly sank into to a closed plate, reducing any exposed edges that could interfere with the deploying tether.

Although most of the tether will be wound in criss-cross manner, the most central part of the winding will be parallel wound. Parallel winding ideally reduces unwinding tension and somewhat counteracts the steep increase in deployment tension that is found close to the metal core surface, although it is sensitive to cyclic patterns in unwinding tension (Section 5.3.6). For volumetric and mass efficiency and in order to reduce the amount of tether for which deployment tension is very high (close to the core), the diameter of the core is rather narrow. The narrow section of wound tether requires support from flanges for stability under the launch environment. Inside the flanges, only a parallel winding is possible. Outside the flanges, a parallel winding is unstable, so the more stable criss-cross winding pattern is used. It provides in itself sufficient stability for the launch environment. The bottom side of the core has a steep flange for improved winding quality, whereas the top flange is tapered and rounded to help smoothen unwinding and reduce stick/slip behavior (Figure 96).

#	Purpose	Deployer system	OBC	Control SW	OLD	Deployment
1	1995 Zero-g deployment, RAPUNZEL verification	RAPUNZEL Breadboard	N/A	N/A	N/A	Open loop using reel in zero-g
2	Double-strand tether, atmospheric drag and hardware characterization	Mini-SEDS	N/A	N/A	Mini-SEDS	Open loop using SEDS rig
3	Multiple tests: hardware characterization	TSE Breadboard	N/A	N/A	Breadboard	Open loop TSE rig (V1) 0.1-14 m/s
4	Multiple tests: First stage controllability	TSE Breadboard	PC	PC	Breadboard	Closed-loop TSE rig (V1)
5	Multiple tests: hardware characterization and environmental effects	YES2 Breadboard	N/A	N/A	Breadboard	Open-loop YES2 rig (V2)
6	2003 Zero-g deployment and brake	YES2 Breadboard	N/A	N/A	N/A	Open-loop YES2 rig (V2, partial)
7	2006 Zero-g hold-phase control in zero g	YES2 Breadboard	Breadboard	Breadboard	Breadboard	Open-loop YES2 rig (V2, partial)
8	Multiple tests: first stage controllability	YES2 Breadboard	Breadboard	Breadboard	Breadboard	Closed-loop YES2 rig (V2)
9	Multiple tests: second stage controllability	YES2 Breadboard	Breadboard	Breadboard	Breadboard	Closed-loop YES2 rig (V2)
10	S/W verification, signal robustness	None	EM (full)	EM	None	Simulated
11	OLD system qualification & deployer characterization	FM	None	None	FM	Open loop full deployment, full velocity range
12	System test	FM	FM	EM	FM	Open loop <4 m/s
13	Flight tether and friction characterization	EM	EM (partial)	Near-FM	-	Full open loop deployment, full velocity range
14	Closed loop deployment test	EM	EM (partial)	Near-FM	EM	Full closed loop
15	Critical functionality, contingencies, interfaces	FM+Foton	FM	FM	FM	None
16	FM S/W performance	Emulated (PC)	EM (partial)	FM	Emulated (PC)	Full closed loop
17	MISSION	FM	FM	FM	FM	Full closed-loop
18	Software testing	EM	EM (full)	FM	EM	High speed
19	Software testing	Emulated (PC)	EM (full)	FM	Emulated (PC)	High speed
20	OLD failure test	EM + DC/DC converter	EM (full)	FM	EM	High speed deployment

Table 39. *Overview of deployer system testing performed*

For protection and to avoid tether jam, the tether spool is contained within a canister. During testing, the canister shape was found to have a rather minor influence on tether tension [Hyslop 2005], see also Section 5.3.7. Some sort of container is necessary though to help contain the tether that is thrown outward by the centrifugal force during high speed unwinding. Although the wall friction increases the tension in the unwinding tether, the containment of the outward flying tether also acts to stabilize its path such that only a small part of the tether is in contact with the walls. It is designed to minimize stray light into the tether canister. The tether passes through the center of the canister top into the base of the barberpole brake box.

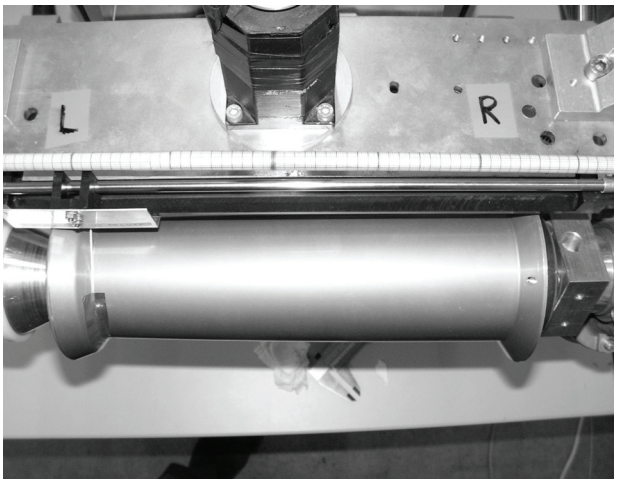

Figure 96. *Tether core in winding machine. Top is left.*

5.3.2 The length detection system

As the tether unwinds from the spool and exits through the center of the top of the canister, it passes sequentially and cyclically through the infrared beams between the OLD transmitters and receivers (Figure 97). The OLD receivers in the top of the core sense those passages, and the OLD signal conditioning electronics provide clean interrupts to the On-Board Computer (OBC), where they are further processed to yield a deployed length estimate. The most recent core design is hollow to include most of the system for length detection based on infrared transmitter receiver pairs - the Optical Loop Detection system (OLD) - in particular the infrared receivers and the associated electronics box. By combining these elements within the core itself the paths of the sensitive receiver signals to the signal conditioning unit are short and Electromagnetic Interference (EMI) issues are mitigated. The receivers are buried in the top of the core, effectively shielded from stray light. The OLD infrared transmitter counterparts are placed in the top of the canister, around the canister's tether exit.

Based on performance and voltage response tests, the distance between transmitter and receiver has been optimized as to guarantee a strong signal and passage of the tether through the most sensitive section of the beam, about 2-5 cm from the emitter, for variety of

tether velocities - and therefore ball angles (Section 5.3.6). The emitters are angled with respect to the core, as to increase the distance from the canister exit and thus reduce the time of passage of the tether through the beam. A faster passage increases the signal gradients and helps to recognize also a very slowly deploying tether.

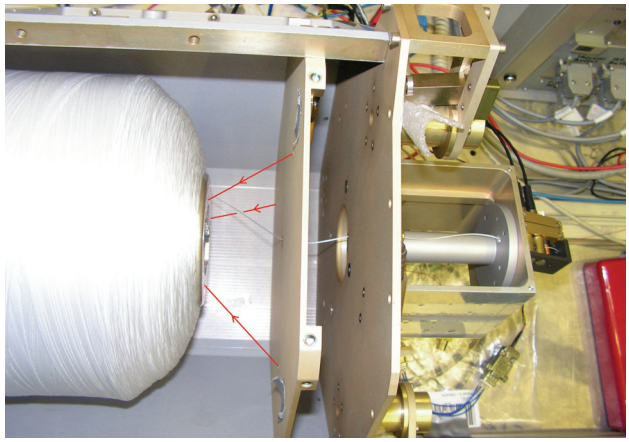

Figure 97. *Top of spool showing infra-red OLD beams*

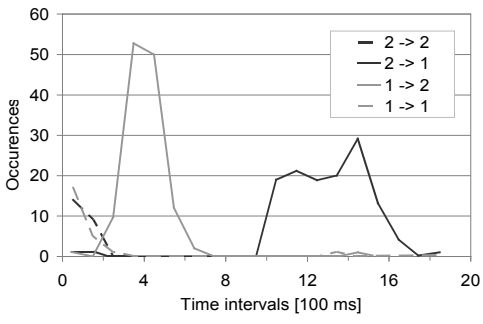

Figure 98. *OLD transition time histogram*

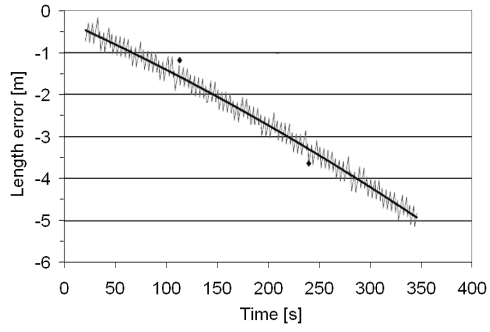

Figure 99. *OLD length estimation error during a TSE deployment*

The performance of the OLDs is critical to the deployment control. A failing OLD pair or missed passage has to be identified and corrected for and distinguished from jitter or a vibrating tether. Nominally, the various channels would be triggered cyclically, for example 1-2-1-2-1-2. During deployment tests it is not always immediately clear if a measured sequence is complete, has a jitter or if part of a cycle or (more than) a full one is missing. Various methods are available to analyze the data. Figure 98 Is a representation of TSE deployment data for a canister in which two OLD pairs are placed at 90° from each other. A passage from channel 1 to channel 2 therefore takes only a quarter of the time as the passage from channel 2 to channel 1. For a constant deployment velocity test, the histogram of time delays between channel transitions distinguishes clearly between the nominal transitions, jitter and missed signals. Figure 99 shows the development of the difference between the

unwinding rig's measured length and the length estimation based on deployed loops. The error follows closely a quadratic curve, as the dependency of length on turns is itself quadratic (Section 5.3.3). Despite some major steps in the development of the difference, the curve's continuity indicates that there are no errors. Another useful tool to investigate the source of observed irregularities is to compare the number of observed transitions to the results expected for random or nominal sequences (Section 8.3.2).

5.3.3 Tether winding

As described above, the inner, approximately 4-km length of the winding are wound in parallel style. The remainder is wound at a significant angle, or in other words, in criss-cross manner, for increased stability. This means that the tether is wound under an angle α, chosen to result in an integer number of spool turns per winding feed cycle, such that a new cycle is placed tightly against the previous cycle and a compact spool is obtained, Figure 100 [Rothwell 2001]. A larger angle (less turns per cycle) would provide more stability, but decreases quality due to tether torque effects at the winding head and spool edges. An angle of about 7-10° is therefore selected as compromise.

It has been found that control of the winding process, to obtain a reproducible spool, is often a combination of proper consideration of geometrical issues and an empirical approach. The winding machine design, e.g. to reduce undesired torques during the process, is key to the quality obtained (Section 5.2.1). A true optimization is hard due to the non-linear behavior of the tether, but a large number of incremental improvements has been made.

For example, due to the increase in diameter as the winding progresses, the winding angle of the tether on the spool decreases, reducing stability of the spool. Therefore, at certain intervals, the number of turns per cycle needs to be decreased (Figure 101). The transition points are chosen such that as much as possible, a gentle smooth decrease is established, which is acceptable as the outside of the spool will experience less launch loads. The selection of proper transition points requires an accurate *a priori*, and regularly updated estimation of the geometry of the spool, i.e., diameter and width of the spool vs. wound length.

A sudden increase in winding angle will lead to a reduction of the spool width (~250 mm) by as much as 5 mm, dependent on the distance d of the tether feed, and this has to be corrected for. If d is finite and the feed moves at constant speed, the effective spool diameter is decreased with respect to the range of the feed along the winding by 2δ, where $\delta \approx d \tan\alpha$ (see Figure 102). If this effect is not taken into account, a new, less wide layer cannot reach the edge of the previous layer and be secured against it, so it will collapse even further. To avoid this sudden step in the spool shape, the range of the tether feed motion along the width of the spool should be increased by typically several millimeters at the time of transition in turns per cycle.

Another issue illustrated in Figure 102 is the tendency of the spool to build up its edges, due to the concentration of tether overlap resulting from the change in feed direction. Over a range $s \approx 2d$ considerable overlap can occur, which can cause a build-up of tether on the

edges and significant decrease in spool quality. In an ideal case ($d = 0$, and a flexible tether), there is no additional overlap at the edge of the spool when the tether feed changes direction (left in the Figure). An edge build-up (flanging) forces a larger distance of the feed from the bulk of the spool, and a steeper surface for the tether to follow the feed's change in direction. Both these issues contribute to lesser winding precision and more overlap, hence a run-away effect is imminent when edge build-up occurs. By selecting a minimal exit hole diameter for the winding feed and by keeping it close to the surface of the spool (small value of d) overlap at the edges will be minimized and in general positioning of the tether is more precise. In this way the winding can stay sufficiently flat without further manipulations such as active compression of the edges.

The spool geometry itself is a dynamic one. As the layers accumulate, pressure in the internal of the spool builds up, the inner tether is compressed, loses (some of) its tension and is pushed outward. This is one of the reasons that the imposed tension is reduced toward the end of the winding. The spool is tapered (it has a ramped edge) amongst others to avoid excessive compression of the inner parts, to smoothen out edge build-up and to provide a clear path for the tether during unwinding. Too much tapering would lead to a low winding angle, and reduced stability of the outer layers, so also here a compromise is sought.

As the spool grows in diameter and closer to the feed, a switch on the bottom of the feed is pressed and the spool's core is automatically lowered to keep the winding feed at constant distance (about 1-2 mm) from the spool, Figure 90.

The winding can be performed largely autonomously in about 24 hours (32 km). If necessary, it can be stopped and restarted or even reversed. When the winding is stopped for some reason, geometric measurements are made of the spool dimensions to verify and update the geometry model of length vs. radius and winding angle and record the location of any visible anomaly or irregularity. After winding, the spool is removed, installed in the deployer hardware and placed in the unwinding machine (Section 5.2.2). Certainly a test tether, but even a tether intended for flight will generally be unwound and rewound more than once.

Various parameters are under control or being observed over these repeated windings and unwindings, such as tether shrinkage, tether twist, tether friction behavior and spool unwinding tension (e.g. Section 8.1.1). The record of winding angle, but in principle also other critical parameters such as winding tension or speed, can be used to segment the winding and determine a linear fit of loop length vs. number of wound loops (Figure 103) or, in other words, a quadratic fit of length vs. number of wound loops (Figure 104). The error of such a fit is generally below 0.1% (Figure 105), although effects such as creep and shrinkage will have to be taken into account separately (Section 5.3.5).

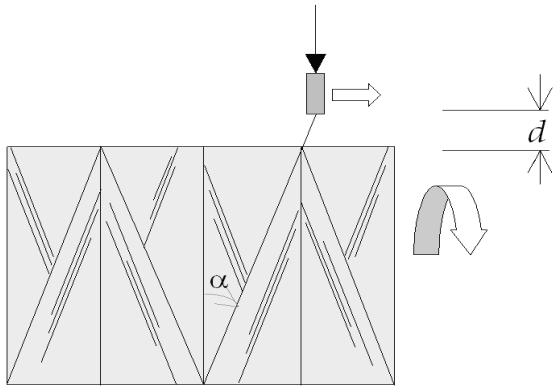

Figure 100. *Definition of winding angle α (4 TPC spool).*

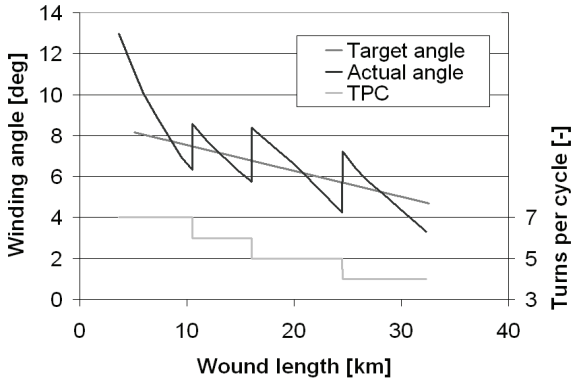

Figure 101. *Example of development of criss-cross winding angle α over tether length and selection of Turns Per Cycle (TPC).*

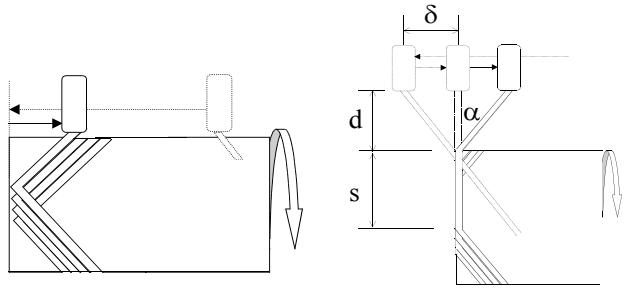

Figure 102. *Overlap at the edges due to distance d of tether feed from winding (highly simplified).*

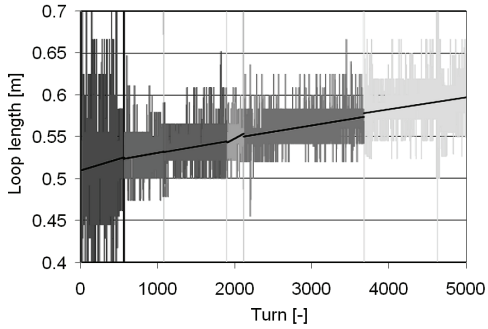

Figure 103. *Winding loop length vs. number of loops*

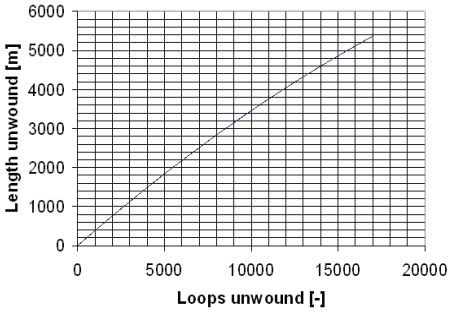

Figure 104. *Length vs. Loops (example)*

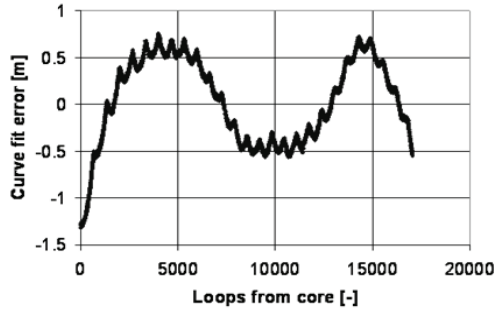

Figure 105. *Typical model vs. measured length error*

5.3.4 Tie-downs

The tie-downs are little knots of cotton applied to the tether on the outer layers after each winding, used to keep the tether in place and maintain the applied pretension, thus providing an exceptionally simple but effective means to keep the spool stable during launch vibrations. They are carefully threaded with a needle at the site of a layer crossing or top or bottom of the spool through the outer piece of tether and at least one piece of tether, a layer below and still restricted to move freely. Three strategically placed knots are sufficient to maintain stability during launch vibrations. Even if only a bit of pretension is kept by the knot, within a few loops of tether around the spool tension will rise exponentially until pretension is restored (an analogous mechanism is explained in Section 5.4.1). The subsequent knots help to keep the low-tension part of the outer tether in place.

The breaking of the knots at deployment will cause a tension pulse and remove some significant amount of energy from the system. It is therefore characterized (Figure 106). Depending on the spool geometry, breaking of a tie-down at 2.5 m/s creates a spike of about 20-40 N in the tether for some 10-30 ms, and produces an energy dissipation of ~1.0 J (±0.55 J at 1 σ). The cotton break strength itself is about 10-15 N. Note that the maximum load on the already deployed tether at breaking of the knots may be higher, as it will be amplified on the bending angle around guides following the exit from the canister.

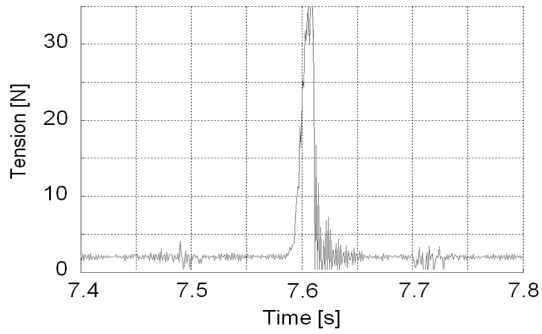

Figure 106. *Typical tension peak measured during breaking of tie-down*

In the flight winding, the location of the tie-downs is carefully selected. Upon ejection, the tie-downs must be placed before the ripstitch section deploys, as otherwise the ripstitch would break and deployment would halt (Section 4.2.3). The peaks also have a positive contribution to the ejection dynamics. Any spring-based ejection, due to asymmetry and misalignment within the system will lead to some pitch-off rate of the endmass, typically several degrees per second. The tether attachment point on the endmass will thus turn away from the line of motion between endmass center of mass and the deployer's tether exit point. The tie-down tension peak in the tether will apply a restoring torque that dissipates a significant fraction of this unwanted rotation energy. Conveniently, the corrective torque is proportional to the amplitude of the undesired pitch-off rate. After several seconds, the larger the pitch-off rate, the larger the arm of torque of any peak in tether tension will be and the more energy will be dissipated from the unwanted rotary motion.

5.3.5 Flight spool characterization procedure

The completed tether spool will be unwound and rewound at least once before flight, mainly for characterization purpose. Test tethers can be wound and unwound more than 10 times before the tether is optically and mechanically degraded. Additional benefits of unwinding and rewinding are a further mechanical settling of the tether and in case of thermal prestretch, reduction of the bending stiffness (Section 4.1). Finally, the unwinding twist in the tether can be reduced through a single unwinding. To these purposes, after each winding, the spool is removed and installed within the canister placed inside the specially developed unwinding machine (Section 5.2.2).

After a first full winding a full unwinding is done. The first meters of the unwinding are to further improve the tether length estimate: the unwound pieces of tether will have somewhat shortened due to shrinkage (Section 4.1.9). The measurements made of true unwound length of several ~3 m calibration sections are compared to the recorded winding lengths for these sections. A predictive correction factor is introduced. In this manner a length prediction accuracy for the whole tether is obtained of around 0.3%.

Next T_{in} is determined, the function of spool friction that will feed into the barberpole to be further amplified (Eq. 5.1). Modeling of such a function will be necessary in order to control the deployment more effectively.

$$T_{in} = T_0 + f(l, \dot{l}) \tag{5.1}$$

It contains the '*minimal deployment tension*' T_0 and a velocity dependent component. T_0 is the force required to pull the tether from between lower layers off the spool. It is dominant at low velocities (<1 m/s), generally about 1 cN (equivalent to about 1 gram force). T_0 is of critical importance in the early deployment when both gravity gradient and velocity are small (Section 2.1.4), but becomes less relevant when velocity increases. T_0 is a function of the winding and environmental conditions. For the criss-cross winding at the start of deployment, it oscillates with each loop deployed. It can be measured in a dedicated test set-up (Section 8.5.1). In the parallel winding, there are various cyclic dependencies (Section 5.3.6). For most purposes it can be considered a constant. Because it is important to understand its value in the context of the full dynamic behavior it is also derived indirectly from tests performed with the barberpole brake (see Section 5.4.3) after the second winding.

The spool friction dependency $f(l, \dot{l})$ is separately characterized. Experience from the SEDS projects suggests the following model [Bortolami 1993]:

$$f(l, \dot{l}) = I \frac{\rho \dot{l}^2}{\left(1 - A_{sol} \frac{l}{l_{tot}}\right)^E}, \qquad A_{sol} = \frac{\pi d_{spool}{}^2 - \pi d_{core}{}^2}{\pi d_{spool}{}^2} = 1 - \left(\frac{d_{core}}{d_{spool}}\right)^2 \tag{5.2}$$

with I a dimensionless inertia multiplier, A_{sol} the annulus solidity depending on diameters d of spool and core, and E a dimensionless area exponent. Note that ρ is again the linear tether density expressed in kg/m.

As can be seen in Eq. 5.2 the deployment tension is rather strongly dependent on deployment velocity. It is roughly proportional to the kinetic energy instantaneously conferred to the tether as it comes off the spool (Section 2.1.5), amplified by any contact with guides, the canister wall (high speed) or spool core (low speed). At higher speeds with increased centrifugal force (typically >3 m/s) the tether leaves the spool at steeper angles and hits the canister wall, where friction presumably causes a multiplication of the inertial term.

The value of I can be determined, in conjunction again with T_0 for confirmation, by running a variable-speed unwinding test, up to high velocities (10-25 m/s), at the beginning of a spool. The remainder of the test is particularly telling for the parameter I. A trend fit gives the required parameters. The assumption of a constant value of T_0 is checked by returning the rig to low speed at the end of the test, to make a comparative measurement.

Eq. 5.2 also indicates that tension increases with length during the last few kilometers (Figure 124), dependent on the area exponent E. E acts on a measure of the cross-sectional

area as is enclosed by the last deployed tether loop. The effect could be related to the small radius, increased bending and increased amount of loops to be unwound per second. From tests, it appears however to be originating more consistently from the fact that, unlike the tether, the core is not compressible [Hyslop 2005]. There is an effect of depth within the spool, where embedding of the tether takes place within layers deeper inside the spool, under pressure of the pretensioned outer layers of the spool (Section 5.3.6), and depending on the (lack of) compressibility of the enclosed core and deeper tether layers. Other cyclic fluctuations, particularly for the case of parallel winding at low velocities, are amplified with the average tension level (Section 5.3.6). Fortunately, this increase in average and fluctuation of tension as described by the area exponent is confined to the last few kilometers of the spool. Typically deployment velocity will be high here and cyclic effects are reduced. Furthermore, the final part of the tether can be used as margin with an inherent tendency to slow down any excess deployment. *E* can be found by running a variable velocity test at later stages in the spool.

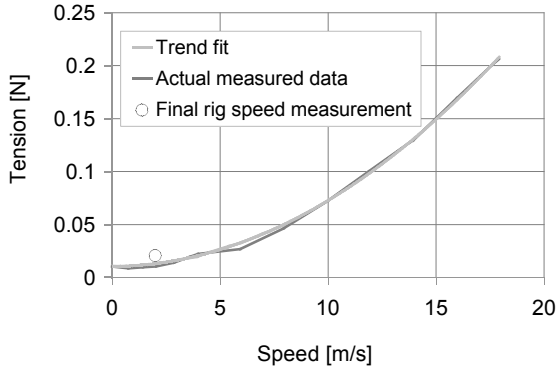

Figure 107. *Spool parameter calibration, here* T_0*=0.01 N,* I = *3.1,* E = *1.4*

Second winding and partial unwinding

As the tether is unwound axially, during its first unwinding, a twist will be introduced in the tether (Section 4.1.8). Such twist can lead to tether coiling and low tension spring effects during the mission, as well as irregular behavior on the brake system (Section 5.4.1) but can quite easily be canceled out (at time of the next unwinding) if an inverted orientation of the core is used during the second winding, i.e. swapping core top and bottom (Figure 96).

For a flight tether, in the second winding, at the point where the flight target length is reached, the tether is locked to the spool with three temporary cotton knots, while still on the winding machine and under winding tension. An additional 1.5 km margin is then wound on top of the flight spool. This margin contains several more marked pieces of which the wound length is registered precisely. As the margin is unwound, the unwound length of the marked pieces is measured to quantify the tether shrinkage one last time (Section 4.1.9).

Most of the margin is however used to perform a characterization of minimal deployment tension T_0 and the barberpole brake friction (Section 5.4.3).

The tether is then cut at the tie-downs, the additional pieces (ripstitch and Kevlar, see Section 7.4.1) are spliced and put in place, flight tie-downs are tied (Section 5.3.4) and the temporary ones removed (Figure 108). The tether is now ready for transport and flight.

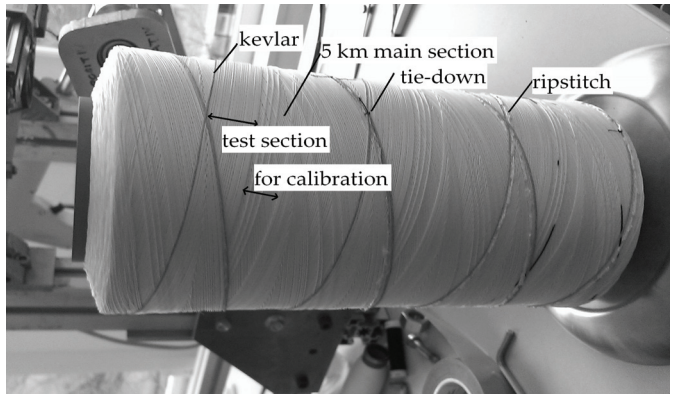

Figure 108. *Criss-cross 5 km test spool right after winding*

5.3.6 Drivers of patterns in unwinding tension

The use of T_0 as a constant suggests a smoothly developing tension, and this model is quite acceptable on the time scales of deployment dynamics, typically nominal deployment velocity or tension varies over a period of minutes. However it is useful to understand what kind of patterns can be recognized in unwinding tension at shorter timescales, namely the deployment of a single loop (20-75 cm), a criss-cross cycle (4-7 loops) or a layer of tether (100-400 m).

Generally, it matters whether a deployment occurs at low velocity, in which case the tether rubs over all the downstream part of the core, or the centrifugal force is strong enough with respect to T_0 to release the tether from the core ("ball effect"). Another important parameter is whether the winding is parallel or criss-cross. Parallel windings show generally low deployment friction, but long layer related cycles, strong directional dependency, and the possibility of strong flange-related amplification at low velocity. Criss-cross windings instead have a cycle at the loop unwinding frequency.

Tension cycle for a single deployed criss-cross loop

Zooming in on the low velocity deployment tension variations for a single criss-cross cycle, depending on the winding and environmental conditions we may encounter a fairly uniform tension level, or one much more pronounced. The pronounced pattern contains a dependency on current unwinding direction, the regular crossing of other layers, and the nearly unrestrained release of tether near top and bottom of the spool. Components to the pattern are discussed in Section 8.5.1.

Ball effect

At high velocity (>1 m/s) the tether (both from parallel and criss-cross spools) unwinds in a ball shape, such that the outgoing tether never touches the spool or core flange. Generally smaller tension amplifications and cyclic effects are created. However, the ball shape will vary with the distance between the outgoing loop and the canister exit. At large distances the ball is shallow, and hence the angle between the spool and the outgoing tether is small (high tension). At small distances the ball has a much sharper curve and the angle of the outgoing tether is large (low tension). The amplitude of the effect is about 10% (Figure 109). No dependency on core slope has been identified. As it is a layer effect, the effect has a low frequency. For the parallel winding each layer contains 100-200 m of tether, for the criss-cross winding at larger radius this is about 150-400 m.

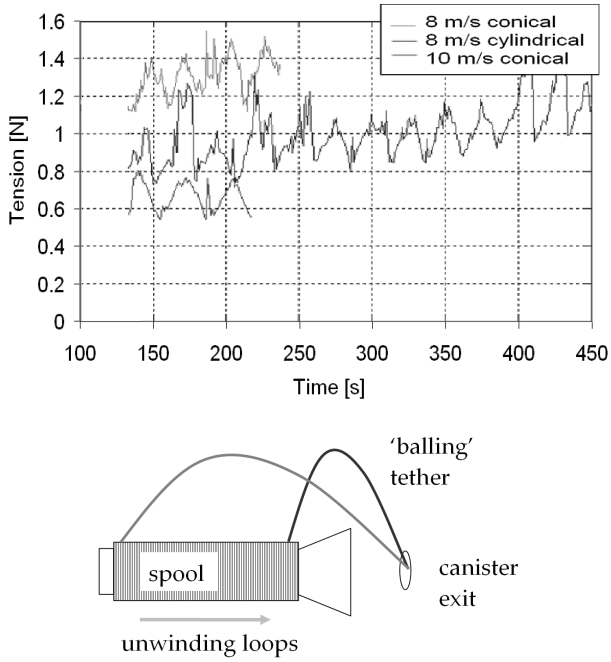

Figure 109. *Ball Effect (n=1); visual time tagging of layer changes shows correlation with tension troughs and peaks*

Core shape

When a parallel-wound tether unwinds from a cylindrical core, it cycles through respectively "hard and easy" layers. As the tether unwinds from the end closest to the canister exit (top) toward the end farthest from the exit (bottom), the tether just slides right off. As the tether unwinds in the opposite direction, the tether has to scale first its neighboring loop: a hooking effect that increases the tension (Figure 110). A conical core makes it easier to overcome this problem and reduces the effect.

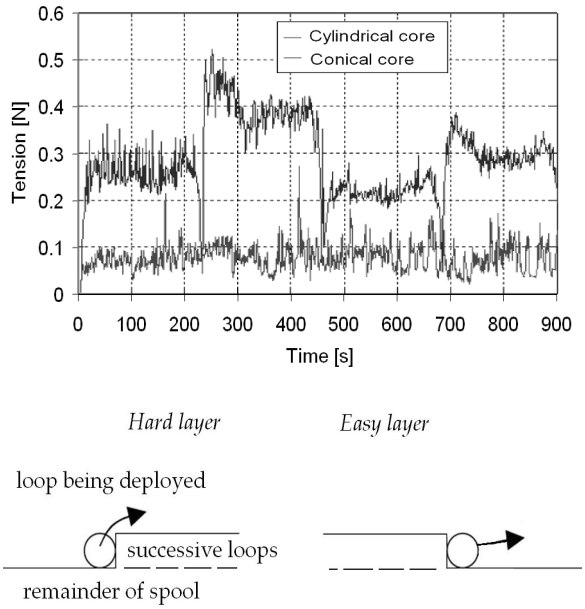

Figure 110. *Cylindrical vs. conical core with parallel winding at low deployment velocity; hard-layer/easy-layer concept.*

Core flange

At low velocity (<1 m/s), when T_0 dominates the tension, the tether takes practically the shortest path towards the canister exit. In the parallel section this means that the tether bends and rubs over the flange edge. Similarly to the ball effect, the angle between the spool and the outgoing tether changes with a period of two layers and will thus show a similarly shaped zigzag profile (Figure 111). This issue is relatively insignificant for the SpaceMail mission as it only has relevance in the very last meters of deployment, when the rapidly deploying tether is being brought to a standstill.

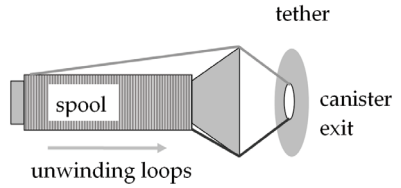

Figure 111. *Flange effect on tether tension (parallel winding)*

The effects have been observed to combine to complex, but often recognizable shapes (Figure 112). An overview of the relevance of the various effects within the different phases of deployment is provided in Table 40.

Low velocity		
Hard-layer/easy-layer	Parallel winding, affected by layer compression and core slope.	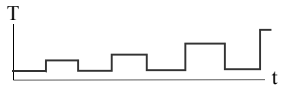
Flange effect	Parallel winding, angle of tether coming from spool, affected by layer compression.	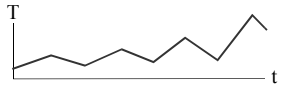
Compressibility of inner layers	Close to core.	
Total	By superposition.	
High velocity		
Ball effect + compressibility effect	Angle of tether coming from spool.	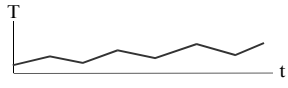

Figure 112. S*pool unwinding tension patterns.*

Location in spool	**High velocity**	**Low velocity**
Near core (parallel)	Area Exponent tension rise	Area Exponent tension rise
Parallel	Ball (small effect)	Flange (large effect) Hard layer/Easy layer
Criss-cross	Generally smooth	Loop cycles, winding cycles

Table 40: *Summary of spool unwinding tension patterns*

5.3.7 Other system design impacts on unwinding tension

In the early days of the winding development a number of qualitative tests has been performed to understand whether design parameters such as tether braiding, cross-section shape or winding angle have some significant influence on the unwinding tension.

Various facilities have been used. One test is performed with a fail-safe double strand tether at Tether Applications' open-loop tether unwinding facility, as part of the 1997 YES project. This test included also a helium-filled canister to study the impact of atmospheric drag on the unwinding of the tether by varying the air density. The others are performed on the two in-house developed rigs (Section 5.2). In particular those tests performed with the

Unwinding Rig v1 has allowed only to make rough qualitative conclusions, as the winding quality and reproducibility, developing over the years, is not yet achieved. Also in this rig the rather costly tether cannot be reused, which severely limits the total number of tests that can be performed. Some tests are therefore repeated on the Unwinding Rig v2.

Parameter	Value	Test set-up	Result
Double-strand tether	34.6 Km double strand of 2 x 130 Spectra.	Unwinding Rig (at Tether Applications, San Diego)	T0=0.0085, I=3.8, E=-0.8 Comparable to single strand spools.
Tether prestretch	Thermal prestretch 8x400 vs. untreated.	Unwinding Rig (v1)	Effect smaller than spool differences.
Tether flatness	Mechanically flattened 8x200 vs. round.	Unwinding Rig (v1)	Effect smaller than spool differences.
Tether braiding	8x200 vs. 4x400	Unwinding Rig (v1)	Not analyzed (expected to be not noticeable compared to spool differences).
Tether diameter / linear density	8x400 vs. 8x200	Unwinding Rig (v1)	Lower and smoother tension for thinner tether (Figure 114).
Spool winding angle	0-15°	Unwinding Rig (v1)	Effect smaller than spool differences.
	idem	Unwinding Rig (v2) & Flight	Impact on frequency is noticeable (Section 8.3.2).
Spool quality, density/compactness	Gaps between adjacent loops from negative (overlap) up to 90% of tether diameter.	Unwinding Rig (v2)	Loop overlaps cause lasting tension disturbance (Figure 123).
Winding pretension	5-7 N	Unwinding Rig (v1)	Effect smaller than spool differences.
	2.5-11 N	Unwinding Rig (v2)	At low tension, patterns are more pronounced (Figure 121).
Canister shape (e.g. effect of open canister during test)	Various cardboard canister shapes.	Unwinding Rig (v2)	Effect smaller than spool differences (Figure 119).
Core shape and dimension	Various core cone angle, diameter and flange size.	Unwinding Rig (v2)	Significant effects (Figure 116-Figure 118).

Table 41. *Unwinding tests: overview of system design impact on tension.*

Impact of tether design

In the context of the European Space Agency's YES project (1997, Chapter 6), over 31 km of a Carroll Caduceus double-strand tether has been unwound from a mini-SEDS canister, a small version of the SEDS deployer, by Tether Applications in San Diego. The tether is made of 2x130 twisted braid (0.32 mm per strand) Spectra (similar to Dyneema®) with a linear density of only 4.8e-5 kg/m. The two strands are spliced together every ~500 m. The tether has been stored

on a spool for about 1 year. The spool parameters T_0, I and E are determined and found to provide a good fit of the model to the measured tension (Figure 113). Despite the significantly different tether design, the spool parameters are still found to be within the range of values given by the spools of the single strand, 0.8 mm SEDS tether [Bortolami 1993] and the spools developed for this work. The model of Eqs. 5.1 & 5.2 can therefore be considered rather widely applicable.

The model of Eqs. 5.1 & 5.2 predicts at higher velocities an almost linear scaling with tether's linear density, which is put to the test within a single spool on the Unwinding Rig v1 with the help of a splice from an 8x400 to an 8x200 tether with half the linear density. The results show that not only the absolute value of the tension, but also the spread decreased at the moment of transition (Figure 114).

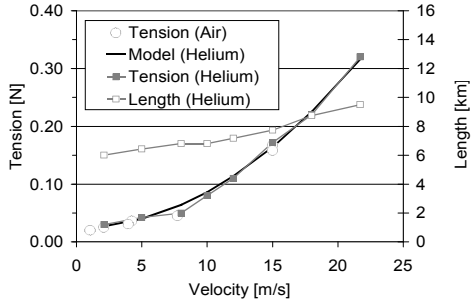

Figure 113. *Effect of atmospheric density on deployment tension vs. velocity (double-strand tether)*

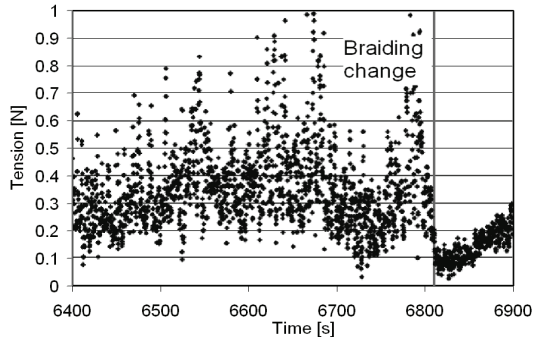

Figure 114. *Tether linear density effect on tension (TSE test)*

Core and initial spool diameters

Apart from core flange and cone angle that lead to cyclic effects, the diameter of the core may also impact the final tension and possibly also the initial amount of tether on the winding. Both these parameters impact the annulus solidity, and physically, the compression level of the inner windings of the spool. Although the model of Eqs. 5.1 & 5.2 has proven its usefulness to provide a fit for tension data for a given spool, it is of interest to

understand if the model also is able to *predict* effects based on winding and design differences, as can be expressed through the annulus solidity.

Consider the four spools A,B,C & D indicated in Figure 115. The tether on all three spools A, B & C have been deployed until the same diameter d_1 (indicated by a fat circle). The tether on the B and C spool however has (nearly) fully deployed until the core, whereas the spool A still has a significant amount of tether remaining: the core diameter is smaller for the spool A (shaded area). The difference between the spools B and C is that the original diameter before unwinding is smaller for the spool on the right (dotted line). Spool C and D have deployed the same amount of tether (L_2), but the core of spool D is smaller. All other parameters remaining equal and deployment velocity being equal and non-zero, the model would predict that the current deployment tension $T_A=T_B$, $T_B>T_C$ and $T_D>T_C$.

Test data indicates however that reality is more complex. $T_B \approx T_C$ and even $T_B<T_C$ if $d_1>d_{core}$ as in A, see Figure 116, Figure 117. Indeed $T_D>T_C$ (Figure 118), but the effect is more pronounced than the model would predict. Note that most tests are performed at rather low velocity (1 m/s) and a tension amplification of about a factor 3 [Hyslop 2005], still the observed tension levels are high enough to assume dynamic effects are playing a significant role (i.e. much larger than a few centinewton). Many of the tension profiles show the typical zig-zag behavior of flange or ball effect (e.g. in Figure 112).

An exception holds for the deployment of the inner layers of a 4 km tether, directly from the core where they experienced more compression than the 450 m equivalent (Figure 116) and for which tension is fully dominated by the easy-layer hard-layer effect. This is no longer obvious if these tests are repeated on top of a 2 km tether layer (Figure 117). At the now increased radius, tension levels for the final meters are decreased for both the 4 km and the 450 m tether, but in different ways, and the effects are more strong on the tether that has been precompressed.

A smaller radius thus amplifies tension on its own account. It is also suggested that a larger pre-deployment compression (L_1 larger in case A, i.e. deployment at the same radius, of an initially larger spool) yields a stronger dependence on remaining distance to the incompressible core.

In short, there seem to be three behavioral regions. The uncompressed outside of the spool, the compressible inside of the spool and the zone near the uncompressible core. The boundaries depend on the initial spool and core dimensions. In the tests performed, the inside region has typically been much less presented than is the case for flight spools and therefore further conclusions are hard to draw.

An explanation for the suggested zonal behaviors can be hypothesized based on observations made during the winding process. Spool dimensional measurements and observations, made during winding, show that as more pretensioned tether is wound about a spool, the inner layers are being progressively pushed outward. Whereas the outer layers are still under tension from the winding process, it is suggested that the inner layers have lost tension due to compression, which reduces the circumference of each loop there. As the

slackened inner layers are pushed outward, they create more space and allow for deeper embedding of the tether, between lower layers or with respect to the adjacent loop or layer crossings.

This would be less so near the incompressible core, where the tether keeps its tension and compactness, although any gaps from winding imperfections will still be exploited for embedding, supported by the increased pressure. As the tether unwinds, the compressed layers are gradually allowed to bounce back into their original shape. This process can in fact be observed, as during unwinding the width of the spool decreases by several millimeters. The expansion increases again the pretension on the loops, however, the embedding cannot be reversed and cyclic effects may be amplified. Within the parallel part of the winding, the flanges reduce to some extent the outward push. Compactness of the spool, so close placement of adjacent loops, therefore is important here to reduce the embedding and make the unwinding tension more smooth.

These results indicate that reality is too complex to separate effects by single parameters and many more well-controlled tests would be necessary to do so. Although it has been shown that the model of Eqs. 5.1 & 5.2 can be used to obtain a good tension prediction for a given spool design (e.g. Figure 107, Figure 113), it holds for now no predictive value for other spool designs: the parameters *I* and *E* are an as yet unknown function of the initial annulus solidity. Spools with different core diameter or different initial diameters, and probably also those with different tether length, require a separate characterization of parameters *I* and *E*.

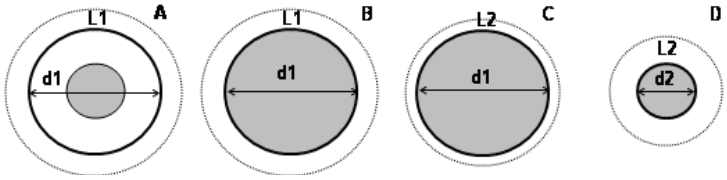

Figure 115. *Four spools, initial size indicated by dotted line, deployed until the thick black line, d1>d2, L1>L2. The core is indicated in gray.*

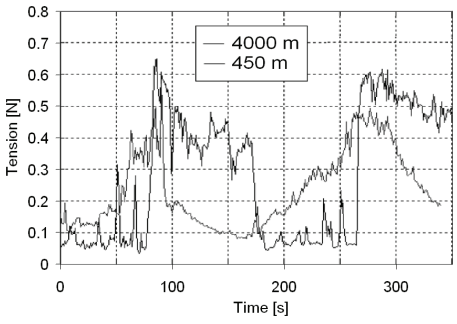

Figure 116. *Unwinding tension close to core vs. initial spool dimensions, as Spool B (L_1=4 km), Spool C (L_2=450 m).*

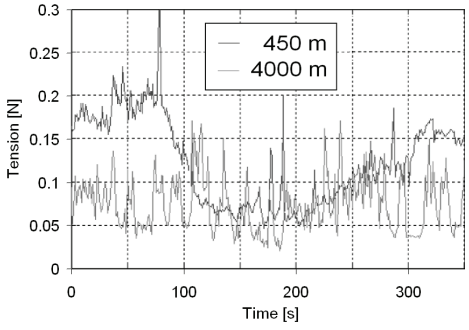

Figure 117. *Unwinding tension inside spool vs. initial spool dimension, as spool A, L_1=450 m or L_1=4 km.*

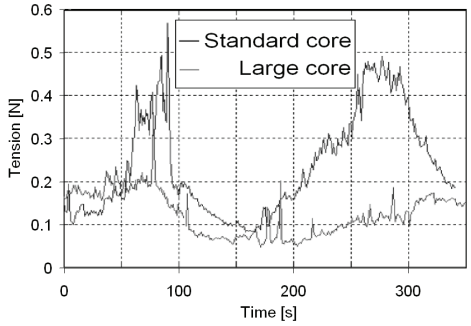

Figure 118. *Unwinding tension vs. core dimensions, as spool C and D (L_2 = 450 m)*

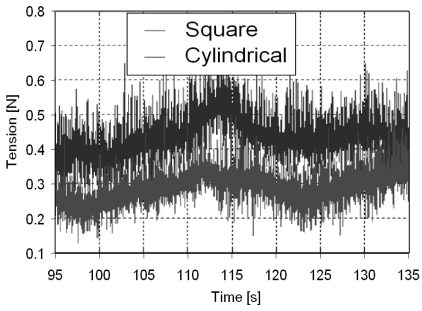

Figure 119. *Tension comparison of flat panel and curved panel canister breadboards during 8m/s deployment*

Canister shape

Experiments have been performed on a variety of spool shapes. The SEDS canister is a seamless cylinder with conical top. It is optimized for low mass and low friction. The TSE canister is similar, but has a seam at the interface between cylinder and cone. It can be considered a non mass-optimized breadboard version of the SEDS canister. The RAPUNZEL canister is a simple cylinder with a flat top (Figure 87). Finally, the YES2 canister is a hexagon shape with flat top, with rounded internal edges, mass-optimized and designed for simplicity and more particularly, structural strength. The YES2 canister carries the ejection system and thus fulfills an important structural function within the YES2 system. It has been checked if a panel structure would have a detrimental effect to the deployment due to some possible whipping effect. A worst case situation, represented by a deployment from a square box mock-up canister, is compared to one from the TSE canister, the cylinder plus cone. 1000 Hz measurements are performed for high velocity deployment at 8 m/s, sufficient to resolve the ~100 Hz whipping that would be expected within the square box.

Figure 119 shows that the tension profiles are qualitatively comparable. Close inspection of the tension data reveals no peaks that could be correlated with cyclic wall contact. Note that the raised tension level with the square canister is most likely due to the tests occurring at slightly different locations within the spools. The hexagonal canister has therefore been approved for the YES2 design.

It is advantageous to place the canister exit at a distance from the top of the core. For example, it reduces cyclic ball effects. The conical top of the SEDS and TSE deployers provide a mass optimized manner to achieve this result. At extremely high velocity and centrifugal forces it may also help to reduce the amount of bending of the tether around the canister exit guide, as compared to a flat lid at the same distance from the core. Such a situation has not been observed in the YES2 tests however. A flat top plate for the canister is thus also approved.

Winding parameters

Pretension and winding angle are some of the primary controls during the winding process. An unwinding test performed on the Unwinding Rig v1 in order to obtain a first impression on the effect of changes in winding angle (5,6,7 turns per cycle) and winding tension (4-7 N) revealed no clear influence [Kruijff 2001.III]. Further tests covering ranges of 6.5 N-9 N winding tension levels have led to the same conclusion, Figure 120. The significantly lower tension for the first criss-cross pattern layer is due to the outer zone effect. On the other side of the curves near the core, the clear rise in tension is the one described by area exponent *E*.

Although at pretensions above ~5 N little effect is seen, below a certain threshold, the *E* effect becomes suddenly much stronger. It is hypothesized that if a spool is wound below this threshold tension, the lower layers may get slack or otherwise more likely to be compressed. As explained earlier some additional tension will then be required at unwinding to pull the tether loose from its deeper layers, and *E* will appear larger (Figure 121). The zigzag seen in this figure is due to the flange, not the ball effect as velocity is rather low.

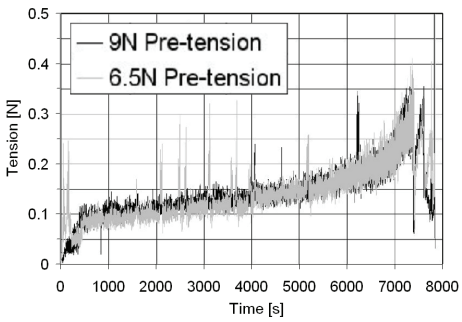

Figure 120. *Impact of winding pattern change on tension*

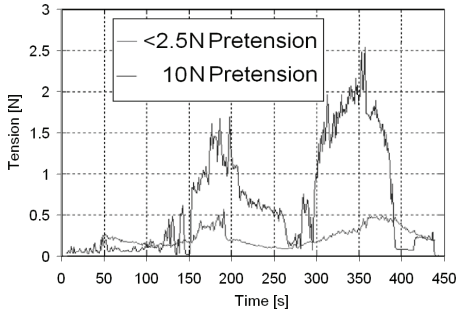

Figure 121. *Comparing different pretensions for 450m spools during 1m/s deployment*

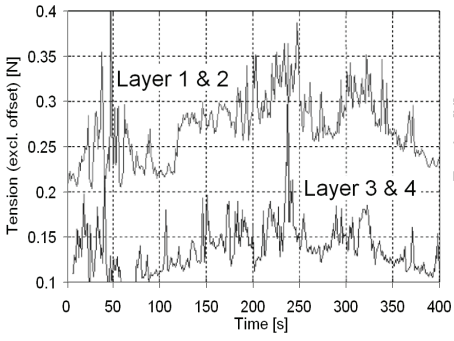

Figure 122. *Repeating spool imprint, 0.5m/s deployment. Average tension level has been offset for comparison.*

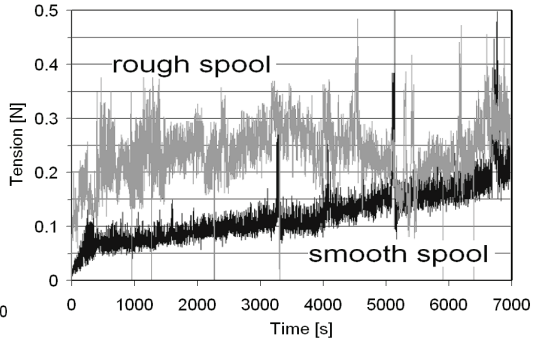

Figure 123. *Relationship between unwinding tension and winding mistakes (0.5m/s)*

Winding quality

Consistency in the unwinding tension profile requires a very smooth spool with few mistakes. Winding errors (gaps, overlaps) made in one layer have a clear signature in unwinding tension, and the errors propagate into the next layer. Particularly in the parallel winding flaws in the spool propagate into the next layer throughout the spool and usually do not fully disappear. Figure 122 shows how the tension history from subsequent layers is consistent. Figure 123 compares a spool with several winding errors to a flawless spool that has a clear gradual tension increase.

5.3.8 Reproducibility of unwinding tension

A number of unwindings have been repeated in different conditions to analyze at least qualitatively the influence of important environmental parameters. The aim is to obtain an understanding of the predictive value of a deployment test in ambient laboratory conditions for flight situation. Table 42 summarizes these tests, which are detailed mostly in [Hyslop 2005]. Some of the prepared tests have not been performed or the results have been ignored. Some of the delivered tethers (namely *Erik* and *Ferdi*) have been preheated at too high temperature and show evidence of melt, exposed fiber ends and generally present a T_0 about ten times higher than nominal. A number of these tests have instead been performed in a simplified test set-up (for T_0 measurement only, see Section 8.5.1).

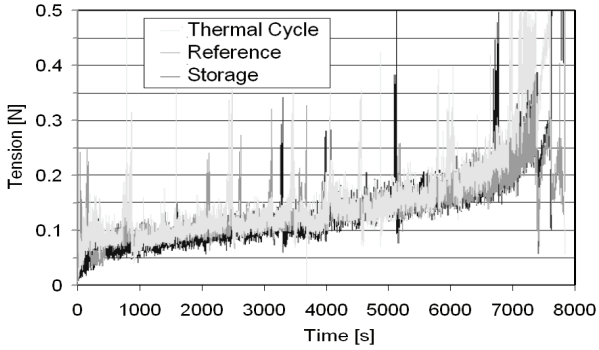

Figure 124. *Tension effects of different spool treatments (0.5m/s)*

Spool treatments

A spool has been put through different treatments then re-wound in an identical fashion for comparison. One treatment is a simple storage at room temperature for 1 month. Another treatment involves placing the spool in a 50°C thermal chamber for 6 cycles of 8 hours each. The storage appears to have no effect but the thermal cycles may have increased the tension near the core (Figure 124). Whereas these tests focus on the dynamic and diameter effects, various environmental effects tests performed at a later stage are targeted at investigation of T_0. From these tests it is concluded that thermal cycling can significantly increase the averaged value T_0, particularly due to increased settling of the spool. Storage seems to have an effect of tension reduction on the outer layer, thermal vacuum exposure seems to have

led to some reduction of T_0 in the outer 15 m, whereas no impact of humidity or temperature as such could be identified (Section 8.5.1).

Parameter	Value	Test set-up	Result
Temperature	Elevated temperature during unwinding (40°C)	Unwinding Rig (v2)	No significant effect
	Low temperature during unwinding (0°C)	T_0 measurement	Section 8.5.1
Thermal vacuum exposure	Post thermal vacuum exposure (-20 to 50°C, $1.2 \cdot 10^{-3}$ Pa)	Unwinding Rig (v2)	Test not representative due to out-of-spec tether (*Ferdi)*
	Post thermal vacuum exposure (16 to 40°C, $2 \cdot 10^{-4}$ Pa)	T_0 measurement	Section 8.5.1
Atmospheric drag	Helium filled canister	Unwinding Rig (at Tether Applications, San Diego)	Effect smaller than 3%
	Helium environment for canister and brake	Unwinding Rig (v2)	Test set-up but not performed due to time constraints
Humidity	0-48%	T_0 measurement	Section 8.5.1
Gravity	Vertical vs. horizontal position of canister	Unwinding Rig (v2) Rapunzel	[Sabath 1997]
	Unwinding in zero-g, 2nd ESA Student Parabolic Flight Campaign	Rapunzel	[Sabath 1997]
	Zero-g vs. 1 and 2 g, 5th ESA Student Parabolic Flight Campaign	Unwinding Rig (v2)	Impact on tension pattern, no effect on average distinguished
Exposure to launch vibration	Random (10-12 grms, x,y,z) and low level sine sweep	Unwinding Rig (v2)	Tether intact but test not representative due to out-of-spec tether (*Ferdi)*
Storage	1 month	Unwinding Rig (v2)	No significant effect
	3 days	T_0 measurement	Section 8.5.1
Rewinding	1-20 times	Unwinding Rig (v2)	Tether degrades and softens with time. Tension pattern can be reproduced.

Table 42. *Overview of tests to study unwinding tension*

Space environment

Tether unwinding in space occurs in vacuum and at weightlessness. No budget has been available for a deployment test in vacuum. Vacuum can be thought to have an effect on friction and the inertia multiplier, through an effect on atmospheric drag. The problem is therefore split in two. A test of static friction in vacuum is performed for the barberpole in

particular as primary friction element (Section 4.1.7). To study the impact of atmospheric drag, data analyzed of a dynamic deployment test that has been performed partially in a helium and partially in an air environment. Helium has approximately seven times lower density than air and thus only about 14% its drag. During the test, the canister is being purged with helium, the actually achieved density is not measured. A dynamic test at velocities from 1 to 15 m/s has been performed under both conditions and reveals a minimal effect, and no more than 3% increase in tension due to atmospheric drag (Figure 113).

In order to verify correct deployment performance of the spool in weightlessness (unwinding of tether, entry of barberpole), two parabolic flight experiments have been performed. A third test focuses on barberpole behavior. In ESA's 2nd Student Parabolic Flight Campaign several kilometer of tether has been deployed from the RAPUNZEL canister [Sabath 1997]. The deployment shows to be smoother than on ground, in particular as compared to a horizontal canister configuration. ESA's 5th Student Parabolic Flight Campaign features the Unwinding Rig v2 (without the tether recovery equipment). Two series of about 30 parabolic manoeuvres are performed, where each parabola is characterized by three main phases. 20 Seconds of 1.8 g ("Pull up") is followed by the microgravity phase, also roughly 20 seconds, with an acceleration of ± 0.05 g for the vertical axis (z-axis) and ±0.01 g along the x- and y-directions. After the microgravity phase, a 20 second vertical acceleration is reached once more, 1.8 g ("Pull down"). The rig is run at 1 m/s for the duration of each parabola, as shown in Figure 125. The transitions from 1.8 to zero g are not discernible, neither for criss-cross nor for parallel windings. Cyclic tension patterns are due to the flange effect, as seen on ground tests. It is concluded that gravity has no detrimental effect on deployment tension.

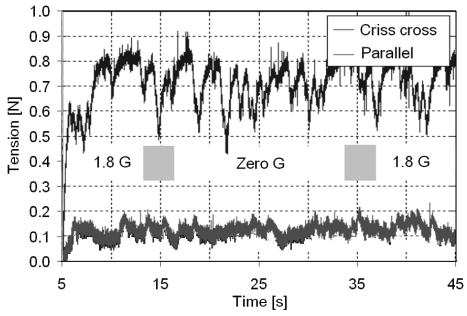

Figure 125. *Unwinding tension at various g-levels*

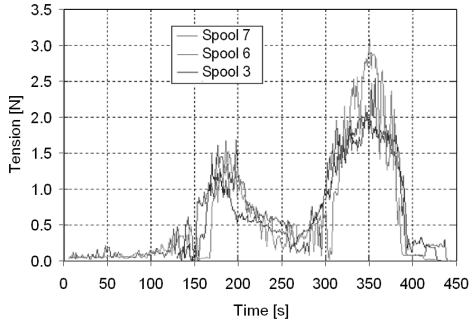

Figure 126. *Reproducibility of tension history with the same tether, 1 m/s (n=1) deployment*

Reproducibility

Reproducibility of spool tension by subsequent windings has been demonstrated already in an early stage of development in a variety of tests, such as Figure 124 for a large spool and Figure 126 for the final phase near the core, where variations are maximal (spools #3,6,7). The typical variation of ±15% seen here at a timescale of tens of seconds requires only minor adjustments of the barberpole (Section 5.4). Note that spool quality and presumably

reproducibility has since increased with further development of the winding machine. Overlaps causing particular noise levels (Figure 123) are virtually absent in the latest spools, compactness has increased, layers and winding angle transitions are planned and the spool geometry is monitored and controlled. Due to the winding machine evolution, edge build-up - a primary source of gaps and irregularities (Section 5.3.8) - is practically absent in the most recent spools (Figure 97), #50 and up.

5.3.9 Conclusions and recommendations

Trends, patterns and dependencies in the winding tension on environmental and design parameters have been qualitatively investigated to identify major factors that are to be taken into account for tether spool design and mission preparation. Although only a subset of the available data has as yet been analyzed and further testing is required if results are to be quantified, a preliminary understanding has been achieved. A number of conclusions and recommendations can be made.

Increasing the understanding of the hypothesized three zones of behavior within a spool is recommended by further tests and further analysis of tests already performed. Furthermore, a modeling of the evolution of pressure and tension within the spool as a result of winding pretension is recommended.

Particular detrimental to spool quality are overlaps, and improper combinations of spool compressibility and pretension development over the spool. From many perspectives, for the parallel winding it is more challenging and more critical to obtain a good quality and smooth tension profile. Particularly the flange and easy-layer hard-layer effects can lead to large variations, but this is limited to the final hundreds of meters on the spool, which can generally be held in reserve.

In the more recent windings performed for this project, pretension is being slightly decreased with increasing spool radius to reduce the amount of compression and slackness within the spool. The spool winding process has also been given a constant tapering to this purpose, yielding (in combination with compression effects) a rounded spool geometry (Figure 97). In iteration with the investigation, improvements have been introduced into the winding machine, in particular aimed to reduce torques on the winding head, gaps and overlaps (Section 5.2.1). A procedure is implemented to prevent tether twist and to correct length measurements for tether shrinkage and other effects. Compact and uniform spools with few gaps and more controlled outer dimensions are created, therefore they are expected to further increase predictability and reduce cyclic effects. A characterization procedure has been defined, to determine the parameters for the SEDS model of spool tension.

5.4 Barberpole development

This section describes the modeling, development and testing of a tortuous path (or "barberpole") friction brake system for deploying tethers, based on the capstan principle used in textile industry.

5.4.1 Performance modeling

Consider a tether with diameter d without bending stiffness following an inclined path around a cylindrical pole with radius r ($R = r + 0.5\,d$) and length l_{pole}. Tether entry and exit point are fixed and located on the extremities of the pole, such that the tether is in direct contact with the surface. The friction coefficient between tether and pole is f. Let the tension at the entry of the pole be T_{in}.

Capstan relationship, effect of tether mass and pole geometry

For a simplified case of a massless tether and $l_{pole} = 0$, the capstan relationship [e.g. McKenna 2004] provides the relationship between T_{in} and the tension at the exit from the pole, T_{out}.

$$T_{out} = T_{in} e^{2\pi f n}, \tag{5.3}$$

with n being the number of wraps of the tether around the pole and $\varphi = 2\pi n$. The exponential response allows for a large range of control with minimal actuation effort, i.e., changing the number of wraps by only little.

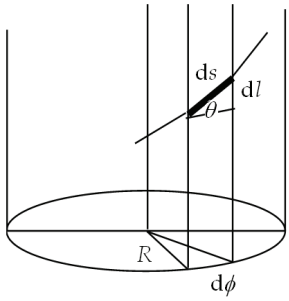

Figure 127. *Coordinates on a cylinder*

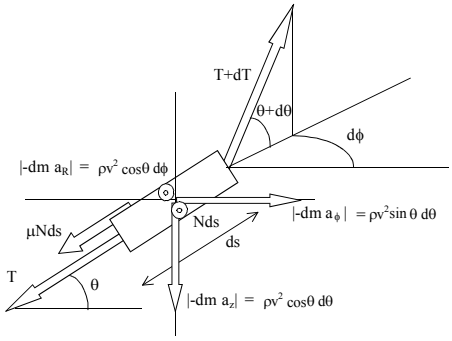

Figure 128. *Force balance on a tether segment around a cylindrical surface*

If $l_{pole} > 0$ the tether may be assumed to follow the shortest path around the pole, and it will describe a helix, ascending the pole with constant angle θ. The length of tether in contact with the pole s can now be expressed as (Figure 127):

$$\begin{aligned} s &= \frac{l_{pole}}{\sin\theta} \\ \tan\theta &= \frac{l_{pole}}{2\pi n R} \end{aligned} \tag{5.4}$$

Now consider a tether with linear mass density ρ ($\mathrm{d}m = \rho\,\mathrm{d}s$), and no restriction on the angle θ and the friction coefficient f. Incoming and outcoming angles of the pole are free to develop. Friction coefficient f can be function of tension or local condition. Let the tether be moving along the pole surface at constant velocity $v = \mathrm{d}s/\mathrm{d}t$. Suppose that the tether path has reached a steady shape on the pole.

$$\begin{aligned} \mathrm{d}s &= \frac{R}{\cos\theta}\mathrm{d}\varphi \\ \mathrm{d}z &= \sin\theta\cdot\mathrm{d}s = R\tan\theta\cdot\mathrm{d}\varphi \end{aligned} \tag{5.5}$$

In cylindrical coordinates, the accelerations of the segment $\mathrm{d}s$ can be easily expressed as (assuming a cylindrical pole, $\mathrm{d}R/\mathrm{d}t = \mathrm{d}^2R/\mathrm{d}t^2 = 0$):

$$\begin{aligned} a_R &= -R\dot{\varphi}^2 \\ a_\varphi &= R\ddot{\varphi} \\ a_z &= \ddot{z} \end{aligned} \tag{5.6}$$

With the assumption $\mathrm{d}v/\mathrm{d}t=0$ and $v=\mathrm{d}s/\mathrm{d}t$, this can be rewritten as:

$$\begin{aligned} \mathrm{d}m\cdot a_R &= -\rho v^2\cos\theta\cdot\mathrm{d}\varphi \\ \mathrm{d}m\cdot a_\varphi &= -\rho v^2\sin\theta\cdot\mathrm{d}\theta \\ \mathrm{d}m\cdot a_z &= \rho v^2\cos\theta\cdot\mathrm{d}\theta \end{aligned} \tag{5.7}$$

The force balance in respectively radial, tangential balance and pole-axis direction becomes (Figure 128):

$$\begin{aligned} N\cdot\mathrm{d}s &= (T-\rho v^2)\cos\theta\cdot d\varphi \\ \frac{\mathrm{d}(T-\rho v^2)}{T-\rho v^2} &= f\cos\theta\cdot\mathrm{d}\varphi + \mathrm{d}\theta\cdot\tan\theta \\ \frac{\mathrm{d}(T-\rho v^2)}{T-\rho v^2} &= f\cos\theta\cdot\mathrm{d}\varphi - \mathrm{d}\theta/\tan\theta \end{aligned} \tag{5.8}$$

Equating Eqs. 5.8b & c leads to the necessity of a constant θ, given the force field sketched:

$$\mathrm{d}\theta\tan\theta - \mathrm{d}\theta/\tan\theta = 0, \forall\theta \Rightarrow \mathrm{d}\theta \equiv 0 \tag{5.9}$$

Therefore, the simplified geometric relations apply (Eq. 5.4a & b). The force balance in tangential direction can be integrated to yield an expression for tension. The deployment velocity $\mathrm{d}l/\mathrm{d}t$ can be introduced, being equal to $v = \mathrm{d}s/\mathrm{d}t$. The tension in the tether as it leaves the barberpole is nearly proportional to incoming tension according to:

$$T_{out} = \left(T_{in} - \rho\dot{l}^2\right)\cdot e^{\cos\theta\int f\cdot\mathrm{d}\varphi} + \rho\dot{l}^2 \tag{5.10}$$

This is a result with interesting implications for the system physics. Notice that this formula contains the term previously introduces as "rocket term" (Eq. 2.15). It predicts that the rocket term passes the brake unamplified. For constant friction coefficient f, the formula simplifies and tension depends nearly exponentially on the turn angle φ:

$$T_{out} = \left(T_{in} - \rho \dot{l}^2\right) \cdot e^{2\pi f n \cos\theta} + \rho \dot{l}^2 \tag{5.11}$$

Or, expressed in geometrical design parameters:

$$T_{out} = \left(T_{in} - \rho \dot{l}^2\right) \cdot e^{2\pi f n \left(1 + \left(\frac{l_{pole}}{2\pi n (r + 0.5 d_t)}\right)^2\right)^{-0.5}} + \rho \dot{l}^2 \tag{5.12}$$

In conclusion, the tether should assume the shape of a helix with angle θ which can be calculated from the number of turns and geometry of the pole. Furthermore, a tether deploying from a spool has a minimum tension of the rocket term $\rho \dot{l}^2$. For such a T_{in} Eq. 5.11 guarantees that the normal force will remain positive and thus contact with the pole is guaranteed. A non-stiff tether deployed from a spool at constant velocity will thus be in contact with the barberpole brake regardless of density or deployment velocity. This conclusion does not necessarily hold for stiff tethers (required bending moments will set a tougher condition to meet), nor for decelerating deployment (inertia effects of tether at low friction end). Probably deceleration will not give any problems for the tether-to-pole contact: strongly decelerating deployment is typically initiated by the barberpole friction itself.

Figure 129 plots the predicted performance for poles with various ratios R/l_{pole}, according to Eq. 5.11, relative to the idealized exponential barberpole (Eq. 5.3). Plots are provided for two different friction coefficients: $f = 0.1$ and 0.3. On the vertical axis is plotted the relative performance (1 = idealized exponential), with steps of 5%. Horizontal (*back-to-front*) is the number of brake turns from 0 to 5, with steps of 0.25 turn. Horizontal (*left-to-right*) is plotted the ratio R/l_{pole} from 0 to 0.25, with steps of 2.5%. A relatively thicker pole performs better, and so does a pole with a lower friction coefficient. A dip in performance is recognized around 1 turn. For higher friction coefficients, this loss is more pronounced. For poles with R>0.125 l_{pole}, performance is generally better than 80%, so a simple exponential fit will suffice. Thinner poles however have heavily degraded performance.

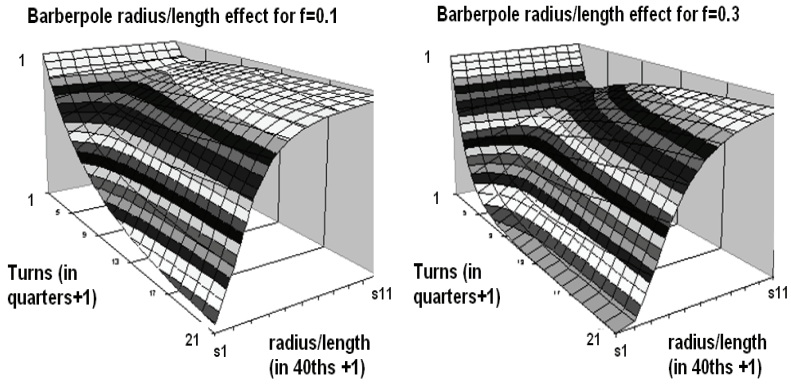

Figure 129. *Predicted performance relative to idealized exponential barberpole for two friction coefficients*

Entry guide effect

For an actual barberpole system, the entry and exit guides need to have a smooth curvature r_g to protect the tether integrity. Therefore a certain distance from the pole d_g is to be traversed by the tether (Figure 130). As the tether travels from the guide to the tangential to the pole, it does not contribute to the targeted increase the tension. Both the effective number of wraps n_{eff} and the effective height h_{eff} of the pole will thus be affected. Consider the following simplified symmetric configuration.

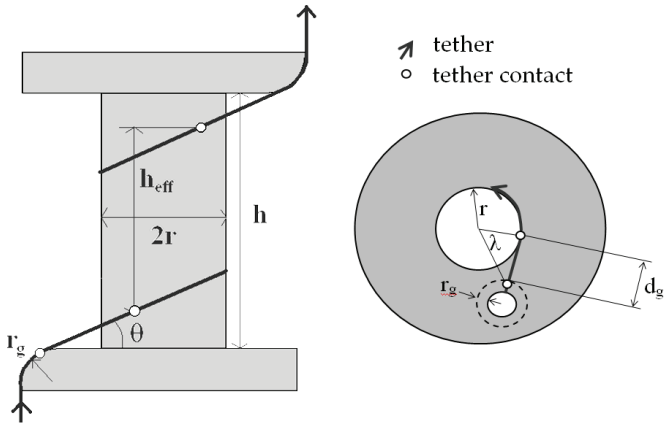

Figure 130. *Barberpole model geometry*

If the azimuth angle between the guides is defined as $2\pi n$, the following implicit geometric relations hold, from which θ, h_{eff} and n_{eff} can be derived. h_{eff} can be used as l_{pole}, and n_{eff} as n in e.g. Eq. 5.12.

$$\begin{aligned}
&\tan\lambda = \frac{d_g + r_g \sin\theta}{r} \\
&n_{eff} = n - \lambda/\pi \\
&\tan\theta = \frac{h + 2r(1-\cos\theta)}{2\pi n_{eff} r + 2d_g + 2r\sin\theta} \\
&\Delta h = \tan\theta \cdot (d_g + r\sin\theta) \\
&h_{eff} = h - 2\Delta h
\end{aligned} \tag{5.13}$$

The friction experienced on the inner sides of the guides depends also on θ. The barberpole tension can be rewritten for a realistic configuration including inner-side guide friction f_g as follows:

$$T_{out} = \left(T_{in} - \rho i^2\right) \cdot e^{2\pi f \cdot n_{eff} \cos\theta + f_g(\pi - 2\theta)} + \rho i^2 \tag{5.14}$$

The friction effect of the outer side of the guides depends on the geometry of canister exit relative to the barberpole entrance, as well as on the tether exit angle, for example as it leaves into space. This will provide additional but straightforward multiplication factors.

The above approach can be adjusted rather easily to handle (numerically) more complex configurations, and will not be further discussed here.

Observations and stiction hypothesis

Preliminary tests have been performed with various pole materials (Vespel, steel, aluminium) and geometries, tether types and braids. It is observed that not in all cases the angle θ remains constant over the pole, even if stable in time, see for example Figure 132. Rather, the angle can increase or decrease with distance travelled on the pole. The behavior seems to depend on many factors such as tether design, tether twist history, pole design and wrapping direction of the tether around the pole. To understand the deviation from the prediction and to assess possible effects on pole performance, a preliminary hypothesis for this behavior has been developed.

In order to change the angle θ, a force component is required that is perpendicular to the tether direction and tangential to the pole surface. Friction seems to be the only mechanism available to exert tangential force, even though friction, as commonly defined, acts exclusively against the direction of motion. It is proposed that this unknown perpendicular component may be proportional to normal force by a factor ν, in equivalence to the friction coefficient, acting tangential to the pole surface yet perpendicular to the friction, in a direction in which there is no apparent motion of the tether. The parameter ν was hence tentatively dubbed *stiction coefficient*.

Now let $T^* = T - \rho v^2$ and let us assume $\nu << 1$. Then Eq. 5.8 can be adapted to:

$$\begin{aligned} N &= \frac{T^*}{R}\cos^2\theta \\ \mathrm{d}(T^*\cos\theta) &= (f\cos\theta - \nu\sin\theta)\cdot(T^*\cos\theta)\mathrm{d}\varphi \\ \mathrm{d}(T^*\sin\theta) &= (f\sin\theta + \nu\cos\theta)\cdot(T^*\cos\theta)\mathrm{d}\varphi \end{aligned} \tag{5.15}$$

Eq. 5.15b & c can be combined, with the help of Eq. 5.5a and Eq. 5.15 to yield:

$$\begin{aligned} \mathrm{d}T^* &= f\frac{T^*}{R}\cos^2\theta\cdot\mathrm{d}s \\ \mathrm{d}\theta &= \nu\frac{\cos^2\theta}{R}\cdot\mathrm{d}s \Rightarrow \\ \tan\theta &= \tan\theta_0 + \frac{\nu}{R}s \end{aligned} \tag{5.16}$$

in which Eq. 5.16c, obtained from integration of $\mathrm{d}\theta$, provides the helix shape on the pole. For any s, θ is determined, whereas z and φ follow from Eq. 5.5. The equation shows that the tangent of the angle θ is proportional to the distance travelled on the pole. Eq. 5.5a can also be directly integrated using Eq. 5.16c, yielding direct dependencies of θ and z on φ (with substitution of Eq. 5.16c and Eq. 5.5b):

$$
\begin{aligned}
s &= \frac{R\varphi}{\cos\theta_0}\left(\frac{\sinh(\nu\varphi)}{\nu\varphi} + \sin\theta_0 \frac{\cosh(\nu\varphi)-1}{\nu\varphi}\right) \Rightarrow \\
\theta &= \arctan\left(\frac{\sinh(\nu\varphi)}{\cos\theta_0} + \tan\theta_0 \cosh(\nu\varphi)\right) \\
z &= \frac{R}{\nu}\left(\frac{\cosh(\nu\varphi)-1}{\cos\theta_0} + \tan\theta_0 \sinh(\nu\varphi)\right)
\end{aligned}
\tag{5.17}
$$

Eq. 5.17 shows no dependency of tether shape on the incoming tension. The relationship for θ shows to be independent from the pole dimensions except for the remaining unknown, the constant offset θ_0. This θ_0 follows implicitly from introduction of a constraint (obtained from the appropriate geometrical consideration such as in Eq. 5.13) from the pole dimensions into Eq. 5.17c,

$$h_{eff} = z(\frac{n_{eff}}{2\pi}) \equiv z(\varphi_{exit}) . \tag{5.18}$$

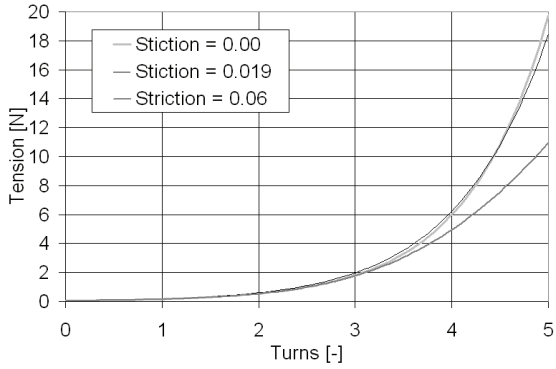

Figure 131. *Tension level at turns out of total of 5 turns*

The tension in the tether is now obtained from Eq. 5.16a & b:

$$T^* = T_0^* e^{\mu\frac{\theta-\theta_0}{\nu}} , \tag{5.19}$$

with θ from Eq. 5.17b to provide the dependency on φ.

Figure 131 provides a comparison for three stiction coefficients ν = 0, 0.019 and 0.06, for friction coefficient f = 0.2, where $\nu = 0$ is the ideal case (Eq. 5.19). T_0^* is taken at the contact point of the pole and the effective pole length is 0.067 m in all cases. What is of interest to note is that due to the stiction and deviation from the helix, the exponential behavior flattens out to linear behavior at large number of turns, as indeed seen in the TSE experiments [Kruijff 2001.III]. Note that for a real pole design, T_0^* should take into account the entrance guide bending angle in an iterative manner (analogous to Figure 130 and Eq. 5.13). For a large stiction coefficient, this bend is large (Figure 133), and this provides a multiplier that helps to compensate somewhat for the loss in tension.

When compared to an experimental set-up, the model based on the stiction hypothesis appears to be able to describe adequately the geometry of the tether path on a pole (Figure 132) and indeed also allows for a solution with negative θ_0 that has been observed in experiments (Figure 133). Such a negative solution or "collection of loops on the brake entrance" is of concern, as the tether could get caught in the gap between toothwheel and pole. This gap should therefore be designed significantly more narrow than the tether diameter.

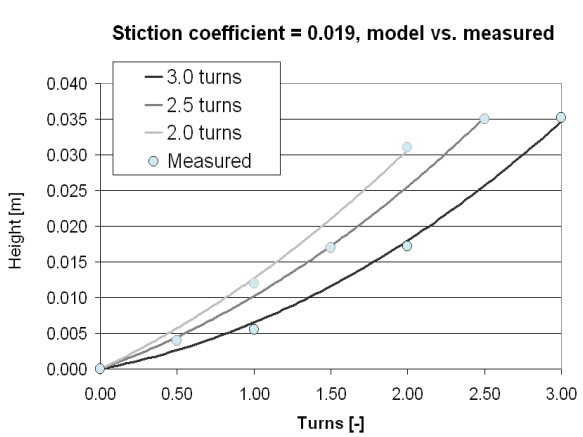

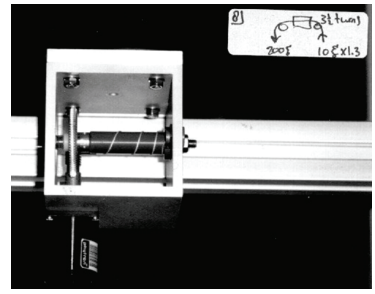

Figure 132. *Measured helix deviation vs. fit by stiction*

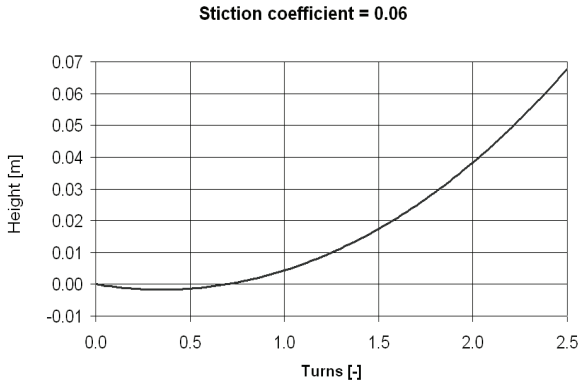

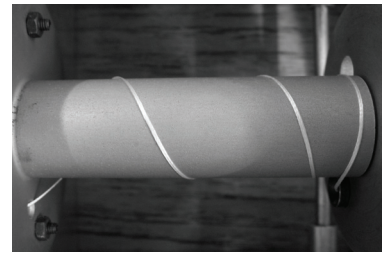

Figure 133. *High stiction (left) shows negative entry angle, as observed for rough pole (right)*

Possible origins of stiction behavior

The physical origins of the stiction coefficient are herewith however not yet explained. To this extent, qualitative tests have been performed with various tethers with different diameters and braidings, as well as some types of chains. Tests are performed on poles of different dimensions, both cylindrical and curved poles for a variety of materials, coatings and roughnesses. Manual twist, wrapping direction on the pole and direction of motion are systematically varied, although so far only qualitatively.

Analysis of the results points in the direction of tether twist/torsion and tether diameter as two main drivers. In a qualitative manner, the tendency of loops to collect at the entrance or exit of the pole (positive or negative stiction coefficient) seems to be described as follows (expressed as "LT"):

$$LT = (TW + MT) * WF + PT \tag{5.20}$$

All factors in this model have direction and magnitude. In practise it is shown that each effect is of the same order of magnitude so it is possible to cancel out one with another.

- *LT*, Loop Tendency, expresses the tendency of loops to collect on one side of the pole or the other. Movement to the incoming side is defined positive.
- *PT*, Pole Tendency, expresses that the tether on the pole has a fixed additive tendency to move the loops to one side or the other independent of the other factors.

One contribution is an actual perpendicular friction component that is caused by the introduction of twist into the tether as it travels around the pole and each cross-section maintains its orientation with respect to the pole, causing a small perpendicular velocity component on the contact area. This effect is therefore a result of the non-zero tether diameter and will be quantified below.

A related contribution is due to the torsion within the tether resulting from the same twist and wrapping around the pole. The tether has a small torsional stiffness (Section 4.1.8) and will respond to some extent as a helical spring being stretched, which tends to contract, and will succeed more where tension is low, or at the incoming side. The twist per meter of tether τ can be estimated from spring theory:

$$\tau = \frac{1}{2\pi R^2}\frac{dz}{d\varphi} = \frac{1}{2\pi R}\tan\theta \tag{5.21}$$

The local twist can be converted to torsion (Section 4.1.8) and all torsion effects together, as will be described below, can be translated into a contraction of the helix towards the entrance (or vice versa).

Note that the *PT* related twist level τ is only present on the pole itself. Imagine a tether that is pulled through a black box by a non-spinning pulling device. If it is untwisted as it enters a black box it can only be turned but not obtain twist as it leaves: the number of twists over the entire tether length cannot exceed the amount of turns applied within the black box.

A cone angle (and possibly squashing of the tether at higher tension) or curved pole (Section 5.4.2) will lead to a negative Pole Tendency. Empirically it is determined that a larger pole roughness decreases the tendency of the tether to collect near the entrance. This supposed relationship is not yet understood.

- *TW*, Twist Torque, is the effect because of torque resulting directly from pre-existing (generally uniform) tether twist. Twist can be identified visually as

described in Section 4.1.8. Clockwise (positive) twist is linked with positive torque (*TW*). The twist adds to the total tether torque (Section 4.1.8).

- *MT*, Manufacturing Torque, is the torque in the tether that is not related to twist applied during winding and unwinding. It can be quantified by manually twisting the tether in the proper direction until the curling tendency is negated (Section 4.1.8). Presumably, manufacturing torque can be added to a tether during the braiding of the tether from various fiber bundles (Section 4.1.2). For example, if the unwinding of the different bundles for the braiding process occurs at somewhat different tension, they will be braided at different lengths, causing any external load to concentrate in only one or a few of the bundles, leading to asymmetic stresses and torque. It is also possible that the fiber bundles are being twisted in slightly different amounts as they come axially off the spools provided by the material manufacturer, leaving a net torque as the bundles are braided together. Possibly, non-uniform heat treatment could also change the mechanical properties of some of the bundles. Finally, a braid from an uneven number of bundles would show Manufacturing Torque. Shape memory and bending stiffness can lead to torques on the pole at the entrance. Most of the described possible contribution would be tension dependent. Pre-stretch appears to reduce the magnitude of *MT*.

The intensity of the combination *TW+MT* can be readily observed by verifying the curling tendency. The *TW+MT* torques will contribute to the tether coil's spring behavior described above. As a result, positive torsion in a tether wrapped in anticlockwise (positive) direction around the pole will tend to exert a force on the pole surface that forces it towards the entrance, collecting there ("positive loop tendency"), and will succeed to do more so if the tension is low (close to the entrance), the twisting is strong or if the tether diameter or torsional stiffness is large. The effect is reversed for an opposite (clockwise) wrapping.

- *WF*, Wrapping direction Factor, is either 1 or –1. The direction that the tether is wrapped around the pole determines the direction of the Loop Tendency effect of the torque related to the combination *TW+MT.* Clockwise wrapping corresponds with *WF* = -1. Anti-clockwise wrapping gives *WF*=1.

Figure 134 demonstrates clearly that wrapping direction indeed has a significant effect. A Dyneema® 7x100 tether has been twisted at 50 twists/meter and led through the barberpole system from right to left, wrapping 3 times in clockwise direction, and in the opposite direction. The effect is not symmetric, suggesting that an additive effect independent of the torsion must exist: the Pole Tendency. The Pole Tendency also appears for a (supposedly) torque-free string of beads which shows indeed no impact from wrapping direction yet still a noticeable stiction-type effect is observed on many pole types. The wrapping direction has been found to be an important tool to adjust the tether behavior on the pole and obtain the required performance, as exemplified in Figure 134: the positive wrapping case provides good performance.

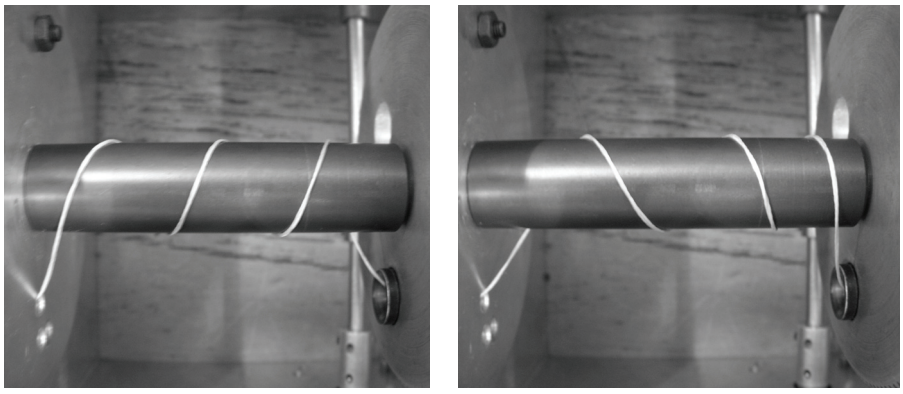

Figure 134.*Effect of positive (left) vs. negative wrapping (right) on the helix shape: Wrapping Factor. The tether has positive internal torsion and moves from right to left.*

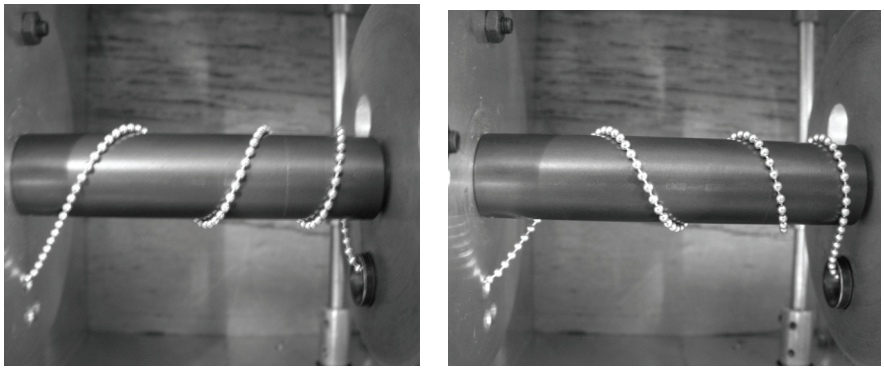

Figure 135. *On a beaded tether without torsion, wrapping direction has no effect, yet still the helix is disturbed: Pole Tendency. The tether moves from right to left.*

With the insights obtained, two tether characteristics have appeared that can explain the introduction of forces perpendicular to the tether.

1. For a tether with non-zero diameter, the torquing of the tether that is introduced as the coiled tether is extended along the pole length creates a small perpendicular velocity, and thus friction will not be exactly against the tether direction.
2. A tether with non-zero stiffness and torsional rigidity will tend to behave as a coiled spring, especially where tension is low. A first step has been made to work out these effects, as they can serve to quantify the stiction coefficient and describe the actual tether path. However, no extensive analysis has yet been done.

Ad 1. Tether diameter effect in absence of torsional stiffness

The fact that the tether diameter has a non-zero value means that the tether core follows a different trajectory than the part of the cross-section that is in touch with the pole. Note that the tether can be observed not to twist as it turns over the pole, the same side of the tether

remains in contact with the pole along the full length of its helical path, whereas a point on the tether on the outside of the helix will remain on the outside. Daniel Poelaert[11] describes this observation: "the tortuosity curvature of the irregular helix (by analogy with Bernouilli's Beam Theory) is compensated by a twist or torsion in the tether". This triggers the question whether it is possible that the point that touches the pole may have a velocity component perpendicular to that of the tether core, and in this manner a friction force can indeed occur perpendicular to the tether motion, giving the appearance of the hypothesized stiction. A model has been made assuming a tether without torsional stiffness, as can be imagined to be a series of beads or coins on a thin line (Figure 135). Poelaert has provided the required mathematics. For completeness, a summary of his derivation is hereby reproduced. Poelaert expresses the velocity of the contact point of the cross-section in helical frame. As compared to the velocity v of the cross-sectional center point purely in tether direction, he finds a somewhat smaller absolute velocity at the contact surface, however with a small perpendicular component.

$$\mathbf{v}_{surface} = v\left[(1-\frac{r}{R}\cos^2\theta)\cdot\mathbf{e}_t + \frac{r}{R}\sin\theta\cos\theta\cdot\mathbf{e}_\theta\right] \tag{5.22}$$

from which the friction force (per unit length) follows (assuming $r/R<<1$):

$$\mathbf{F}_f = -\left[fN\cdot\mathbf{e}_t + fN\cdot\frac{r}{R}\sin\theta\cos\theta\cdot\mathbf{e}_\theta\right] \tag{5.23}$$

From the second component one can derive the friction torque on the tether :

$$\Psi_f = fN\cdot\frac{r^2}{R}\sin\theta\cos\theta \tag{5.24}$$

This second term defines the friction-related part of the stiction coefficient v_f:

$$v_f = f\frac{r}{R}\sin\theta\cos\theta \tag{5.25}$$

Therefore, the larger the pole roughness, the stronger positive will be the loop tendency *LT*. Still this value of v_f is generally very small (<0.02) but can change significantly over the pole. The equations of motion in $\mathbf{e}_r$, $\mathbf{e}_t$, $\mathbf{e}_\theta$ directions now become respectively:

$$\begin{aligned} N &= \frac{T^*}{R}\cos^2\theta \\ \frac{\mathrm{d}}{\mathrm{d}s}T^* &= f\frac{T^*}{R}\cos^2\theta \\ R\frac{\mathrm{d}}{\mathrm{d}s}\theta &= f\frac{r}{R}\sin\theta\cos^3\theta \end{aligned} \tag{5.26}$$

Thus, θ will have the tendency to augment with s. The derivatives can be integrated (with substitution of Eq. 5.5) to yield an expression for the tether path and the resulting tension:

[11] Private communications Daniel Poelaert, 2001

$$\sqrt{1+\tan^2\theta}-\sqrt{1+\tan^2\theta_0}+\ln\frac{\tan(\theta/2)}{\tan(\theta_0/2)}=f\frac{r}{R}\varphi$$
$$T^*=T_0^*e^{\frac{R}{r}\ln\frac{\tan\theta}{\tan\theta_0}} \tag{5.27}$$

Ad 2. The effect of torsional stiffness

In addition to the friction torque effect, for a tether with torsional rigidity, the various components described so far that contribute to tether torque, create a coil with a spring-like behavior: the twisting due to tether wrapping, the pre-existing twist and the manufacturing torque. The tether will orient itself such that the spring force at a cross-section of the tether is balanced by the *z*-component in tension T_z. The torque in a spring relates to this component as:

$$\Psi_{spring}=T_zR\cos\theta \tag{5.28}$$

Equating this to the tether torque from Eq. 4.13

$$\Psi_{spring}=\Psi_d\Rightarrow T_z=\tau\cdot\frac{4d^2}{R\cos\theta}\cdot\left(\frac{\pi^4}{32\sqrt{3}}d_{fiber}^2G+T\right), \tag{5.29}$$

with τ representing the various components of twist such as the pre-existing twist and coil twist from Eq. 5.21. This force and its increment with dT can be introduced into the balance of forces of Figure 128, Eq. 5.8c. Substituting also Eq. 5.8b, a relationship between dθ and dφ can be determined. The helix angle θ thus follows from dθ as the tether goes around the pole by dφ. Tension follows from Eq. 5.8b and the *z*-position on the pole follows from Eq. 5.5b.

Discussion

Various simplifying assumptions have been made. Most of all, bending stiffness and shape memory have been ignored. A stiff viscoelastic tether traversing from entry guide to pole under low tension will not be straight. The coil effects described above will be strengthened. Furthermore, the friction coefficient and velocity have been assumed as constant and the helix shape as static. Finally, a non-straight pole, as well as squashing of the tether at increasing tension will lead to a non-zero value for dR/dt. No complete model has yet been produced or validated.

Nevertheless, the basic elements for a model for the path of a moving tether around the barberpole have been presented. The insights and tools obtained are adequate to understand basic barberpole functionality, monitor and take into account parameters of potential importance, recognize aberrant behavior and if that may occur, suggest relevant countermeasures.

The barberpole tension performance and its deviation from a pure exponential has been made plausible. The impact of tether mass has been assessed and it is shown, under the assumption of a flexible tether, that for a spool deployment contact between tether and pole can be guaranteed. Tools have been provided to model the effect of entry and exit guide

geometry. The tether path shape on the pole and the tether tension as it exits the pole can be estimated.

The hypothetical stiction coefficient has been proposed to account for the deviation from the helix shape. A path description has been derived for constant stiction coefficient. Experimentation and analysis reveals that the stiction coefficient has several components that act together as to determine the final path shape. The finite tether diameter causes a friction component perpendicular to the tether velocity. Another contribution originates from the wrapping and stretching of a tether with torsional rigidity around a pole, and from pre-existing twist and torque in that tether.

The results have lead to an effective redesign of the barberpole geometry as well as of its gear to avoid the tether getting tangled near the pole entrance (Section 5.4.2). The tether is wound in such a way that unwinding leads to zero twist. Remaining twist found in the tether can usually be adequately dealt with by choosing the wrapping direction of the tether around the pole.

5.4.2 Development

Although the concept of a capstan is selected for friction control, with the SEDS barberpole as a successful example, there are multiple thinkable implementations to integrate the pole into a structure that controls the tether's tortuous path. Following some simple breadboarding in the TSE project (Figure 132) a choice is made to go through a full development from scratch, rather than a reverse engineering of the SEDS brake, in order to increase understanding and optimization of the performance by modeling, design trade-offs, analysis and tests.

Requirements for the brake design are derived starting from the target application of a safe and precise capsule re-entry using a 0.5 mm Dyneema® tether, with the possibility in mind to expand functionality to more demanding applications. A low cost system is targeted that should be compact, light-weight, simple to manufacture and reliable. Performance should be sufficiently predictable such that feedback can compensate. A faster turning pole is better, but more demanding for gear and stepper driver selection. Based on simulations a maximum interval of 10 s is defined for a single wrap. For reliability and safety the system shall have little moving parts and few tether guides. The design should effectively conduct heat away from the friction surface (Section 4.3.3).

The required tension range can be derived from the dynamics of the space mission. The demonstration mission is likely to end up with a minimal payload size to reduce cost, about 10-15 kg (see also Section 4.2.1), requiring a tether tension to range from 10 mN to 3 N, covering already a factor 300. Some sort of exponential performance is therefore preferred. The capstan concept enables this range with only 5 wraps around the pole. The design takes into account the need for significantly higher brake loads than required for the demonstration alone. A maximum number of 10 turns is taken as a design target.

Several configurations have been considered in order to obtain a high-performance barberpole [Menon 2007].

Figure 136 shows some compact early configurations with minimal gear.

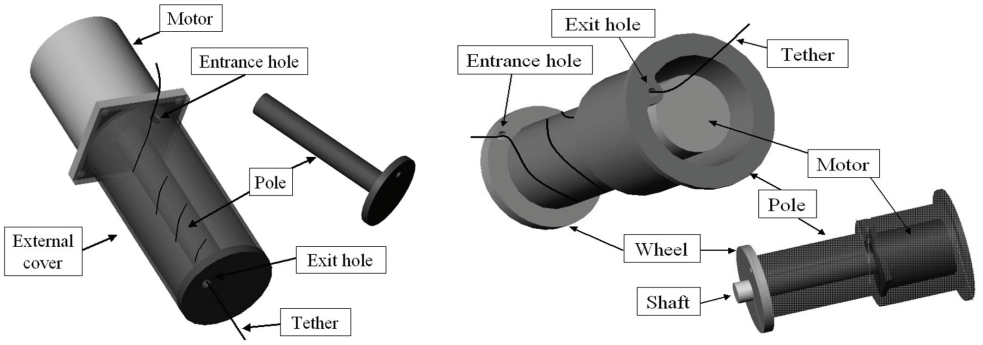

Figure 136. *Early barberpole configurations without gear*

In the configuration on the left the motor turns the pole around its axis and winds the wire. One problem of this configuration is to raise the number of turns above a certain level, due to the increasing torque on the pole shaft. The designs faces the complication that a bearing system must be employed to increase the mechanism stiffness. The designs is not suitable for good thermal conduction, away from the pole. The possibility of melting the tether thus exists.

The configuration on the right is an example with a non-rotating pole. The tether tension at the entrance is small, so the entrance itself can easily be rotated. The position of the tether entrance hole is controlled by a motor through a shaft inside the pole surface. To keep the shaft short, the pole can be widened further. Friction heat can be easily dissipated in this concept. It is not worked out further because of the pole diameter that is required to fit the motor, as well as the necessarily large diameter of the path of the tether entrance. It would require a larger distance between canister and pole to obtain the small bending angles necessary to maintain a low minimal deployment tension.

A further design, used as breadboard model, is shown in Figure 137. This design is most similar to the SEDS brake system and is made up of a pole fixed to an external casing, that also acts as heat sink and benefits thermal dissipation. The entrance hole is located on a tooth-wheel, which is controlled by a motor through a shaft and a worm-gear. The worm gear mechanism uses no lubrication and is low friction. The large gear ratio makes it possible to use a low power motor. A stepper motor is chosen for its deterministic nature which enables open-loop software control. The tooth-wheel is kept still during the launch phase by the irreversible transmission-mating mechanism. No current needs to be provided to the mechanism during the launch. A second, passive worm to support the tooth-wheel during launch has been considered, but rejected as over-design.

There are a number of obvious differences with respect to the SEDS system. Unfortunately, the number of available European vacuum stepper motors is limited. These vacuum

steppers are mostly precision devices, as is in fact not required for this application. The Phytron ZSS 24.200.0.6, a bi-polar motor, is selected for the breadboard, despite the large number of steps required for a single shaft rotation; it requires 200 control steps to make one shaft revolution, versus the 4 steps of the SEDS motor. The gear ratio is increased from the SEDS' 80:1 to a 120:1 ratio. This reduces the required motor torque and further improves stability at launch. The toothed wheel has a rather large diameter, again to reduce the required motor torque, but also, for research purpose, to be able to house entrance guides at various radii from the pole center.

The pole's base design is adjusted for increased thermal conductivity and heat capacity. The pole, ground plate and guide are a single integrated piece. Vespel, a low friction polyimide, is used for the entrance guide. The exit guide is milled directly into the aluminium frame, to provide optimal heat transfer in the place where tension is high. Bronze sliding bushes are employed at the rotating interfaces in order to reduce friction.

The pole itself is larger and fatter than the SEDS pole. This trade-off is based on the model results and test recommendations (Section 5.4.1). It provides behavior closer to the exponential (Eq. 5.12, Figure 129) and reduces the ratio of tether-to-pole diameter on which the Loop Tendency depends (e.g. Eq. 5.25), while it provides a good separation between tether loops also at a large number of wraps. The larger dimensions also serves to reduce the (not-yet-modeled) impact of tether bending stiffness.

The pole has a slight curvature to guide loops away from the entrance, where otherwise the tether may collect (Section 5.4.1). It has a 24.2 mm diameter at the entrance hole and a 23 mm diameter near the exit hole. The section of the pole follows an arc profile with a 4 m radius as sketched in exaggerated form in Figure 138. The resulting semi-cone angle at entrance is 1°. This angle is based on rough preliminary tests that show that the axial force component induced by this angle is sufficient to drive the loops towards the more narrow end of a pole. The exit side of the pole is cylindrical (0 degree) as to avoid collection of loops on this side. In this way, the Pole Tendency is well-established. The wrapping direction of the tether around the pole can be used as a final means to adapt to the tether unwinding twist to reduce any remaining Loop Tendency.

A breadboard of this design has been built for experimental tests. In Figure 137, the tether goes through the entrance hole of the tooth-wheel, turns six times around the pole and goes through the tether-cutter subsystem. The tether can be seen to wind with a regular helical path around the barberpole as intended. The breadboard system is subjected to deployment tests for characterization and performance demonstration (Sections 5.4.3, 5.6), as well as thermal and thermal vacuum tests.

The required dynamic torque that the stepper motor should deliver to the gear is estimated based on the friction level of 2 Nmm measured on the breadboard mechanism at room temperature. A preliminary design target of 10 Nmm is chosen for the flight model because thermal, misalignment and resonance issues can heavily increase friction. Reduction of torque performance due to mechanical resonance has been assessed. It is found to be worst at low temperatures (–40°C). For reduced mechanical resonance, a half-stepping mode is

selected [Graczyk 2008]. A high stepping frequency of 8 kHz is then required in order to reach a control speed of 6 s/wrap. At such high frequencies motor torque decreases significantly due to self-induction effects.

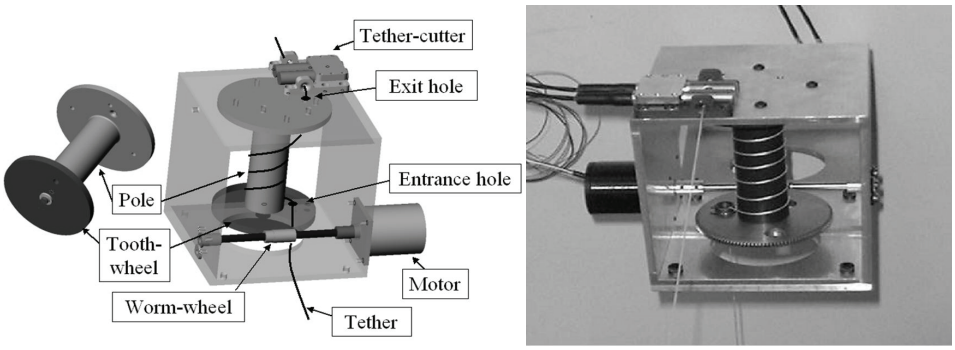

Figure 137. *Breadboard barberpole configuration*

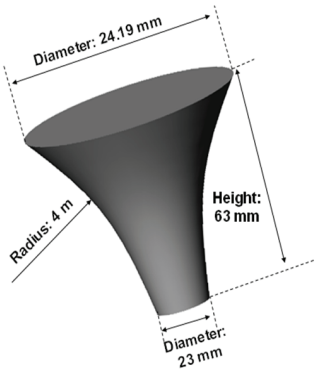

Figure 138. *Sketch of curved pole (exaggerated curvature)*

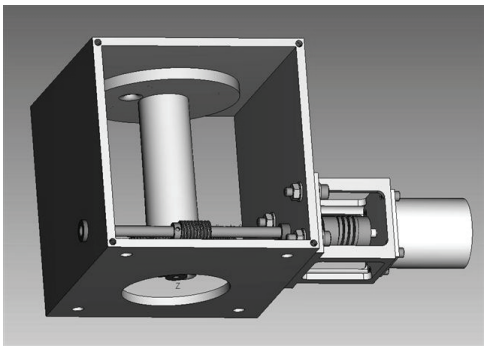

Figure 139. *Final configuration for YES2 barberpole*

The final flight design is developed based on the breadboard model test results (Figure 139). In this design, the gap between pole and gear is minimized below 0.1 mm to avoid tether catching. Worm shaft alignment issues and temperature dependencies that have led to failure of the breadboard at low temperatures have been resolved by addition of a flexible coupling between motor and shaft. Furthermore, analysis of the wheel gear behavior, based on thermal cycle and thermal vacuum testing, has led to a redesign and robust concept of the critical gear shaft fixture ("shoulder screw").

Based on the barberpole model and breadboard test results, the tether exit hole is placed near to the pole axis, although at the same time the bending radius of this guide is increased to 3 mm to reduce wear on the tether. With this configuration of entrance and exit holes the pole has a loss of effective turns of about $n - n_{eff} = 0.25$ (Section 5.4.1). A procedure has been developed to apply hard anodization coating and to fine-tune the surface roughness to achieve the target friction coefficient $f = 0.2$. Surface roughness is adjusted with respect to the breadboard, to about 1 micron (Section 5.4.4). Main driver here is to achieve extended performance also at a high number of turns.

The motor is scaled up to a Phytron VSS 32.200.1.2, which delivers larger torque and can handle larger coil currents of up to 1.2 A. The worm gear is equipped with a worm that forwards the wheel by two teeth each shaft rotation, such that a rotation time of 6 s/wrap can be achieved at 4 kHz half-stepping frequency.

The torque and thermal characteristics of the motor depend largely on the electrical driving of the motor coils. The effective torque is proportional to the time-averaged coil current. At high step frequencies, self-induction within the coils slows down the build-up of current and reduces the resulting torque of the motor. A high voltage of 24 V is therefore selected to speed up the current build-up. The coils are low-impedance (~1 Ohm) and cannot sustain maximum averaged currents larger than 0.6 A due to vacuum derating requirements.

In order to avoid that the current through the coils exceed that maximum, a chopper circuit is included, which switches off briefly the supply when current exceeds a set threshold. As soon as the supply is removed, the coils run dry of current at the same speed at which they were charging before. A fast chopping is therefore necessary to maintain approximately a constant current oscillating closely around the 0.6 A target. The chopper control circuit is clocked at 40 kHz, as higher levels are found to cause interference issues.

An additional feature is included to raise the torque level. In the half-step mode, the two motor coils are powered in alternating manner. During 25% of the period, only a single coil is active and the other coil rests. When one coil rests it is possible to lead a $\sqrt{2}$ higher current through the other active coil without exceeding the allowable continuous (averaged) coil loading. This adjustment is called "shaping" and leads to an estimated 14% higher torque.

The torque level is determined by static and dynamic torque measurements in ambient conditions. For one static torque test a set-up is used in which a horizontal arm is mounted to the stepper motor shaft. The torque is determined by sliding a weight along the arm, until it cannot be held in place anymore. Another test yielding similar results, sets in motion the

maximally loaded arm at various low initial drive frequencies, true static being obviously 0 Hz (Figure 140). The static torque can be converted to dynamic torque following the stepper motor specs: at the maximum recommended half-stepping frequency of 4kHz, about 40% of the torque level will be lost.

Dynamic torque is measured by Spiliotopoulos' method [Spiliotopoulos 2008], Figure 141. The motor shaft twists a rubber band until the motor stops due to the increasing counter-torque. A blocking mechanism then keeps the twist in the string. The maximum dynamic torque can now be measured with a weight scale. A dynamic torque of 13 Nmm is provided by the final system (average coil current I = 0.58 A, 4 kHz), in line with the predictions made from the static tests.

A stepper driver subsystem with control software has been developed implementing these specifications [Graczyk 2008], (Section 7.4.2). Total power supplied at 24 V is about 14 W, of which most is dissipated in the switching electronics. Only about 1 W is dissipated in the motor's coils, and will heat up the barberpole housing.

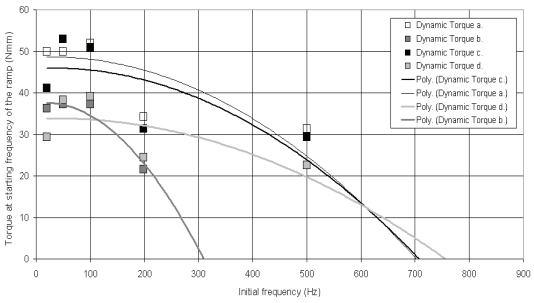

Figure 140. *Available torque (before slipping) at initial frequency at start of a ramp to operating frequency (4 kHz), up to 1 A average coil current.*

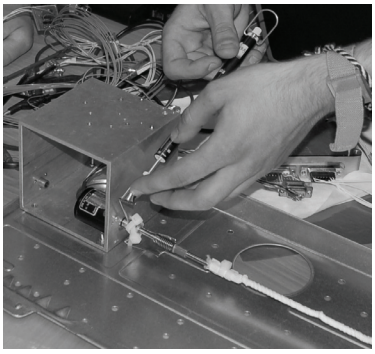

Figure 141. *Stepper motor dynamic torque measurement*

A thermal analysis is performed [Menon 2007]. Under conservative assumptions of conduction, no heat sink for the subsystem and a 50% heat transfer into the pole, the pole is simulated to increase in temperature by about 50 K during an extreme final braking event at 5 N from 18 m/s. This increase is acceptable and will not lead to tether melt. Nevertheless, thermal paste is applied to further improve thermal conduction away from the pole.

The complete barberpole system has now been readied for verification. The flight unit has been subjected to wear tests, and mechanical performance is demonstrated in a thermal subsystem test between –40° and +80°C. Finally, as part of the YES2 system it has been subjected to tether deployment, thermal vacuum and vibration tests (Section 5.2.4).

5.4.3 Spool-barberpole characterization procedure

With the dynamic dependency known (Eq. 5.2, Section 5.3.5) the deployer friction model can be completed if T_0 and f are determined next (e.g. Eq. 5.3). At low velocity tests, T_{in}

approaches T_0 (Eq. 5.2), so a fit of low velocity test data to Eq. 5.3 (or one of the more complex versions derived in Section 5.4.1) is suitable to determine both T_0 and f. At a constant deployment velocity of 0.5 m/s, the barberpole is turned up in steps from zero to the maximum and back, various times. Tension is measured and averaged out per barberpole position. An exponential fit is added from which T_0 and f are derived.

The traditional SEDS exponential model for the barberpole, Eq. 5.30, is based on combination of T_{in} from Eqs. 5.1 & 5.2 with Eq. 5.3, and taking into account the bending around guides due to system design (θ_g), deployer orientation with respect to the local vertical (θ_{ref}) and tether in-plane angle θ. It has been evaluated against the more complex model of Eq. 5.12. The more simple model is found to give sufficient match to test data (Figure 142) thus Eq. 5.30 has been retained for further analysis.

$$T = \left(T_0 + I \frac{\rho i^2}{\left(1 - A_{sol}\frac{l}{l_{tot}}\right)^E} \right) e^{2\pi f(i)n + f_g\left(\theta_g + \left|\theta - \theta_{ref}\right|\right)} \tag{5.30}$$

Similar characterizations have been done for each tether-pole combination. For the Vespel pole with a 8x400 tether (TSE project), a friction coefficient f = 0.174 is found (Figure 143), [Kruijff 2001.II]. For all the tests performed, the standard deviation for the tension data is about 15-30% of the measured average above 3 turns, and up to twice this amount at zero turns (Figure 144, Kruijff 2001.III). The engineering model pole shows a deviation from the exponential for a large number of turns (n>5), above which the performance becomes more linear (Figure 145). This behavior is reminiscent of the effect of high stiction coefficient (Section 5.4.1) although this has not yet been confirmed.

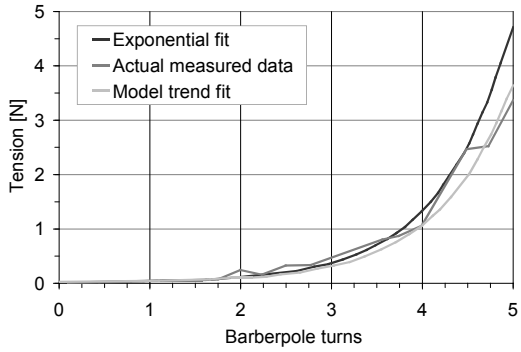

Figure 142. *Barberpole performance vs. simple and extended model*

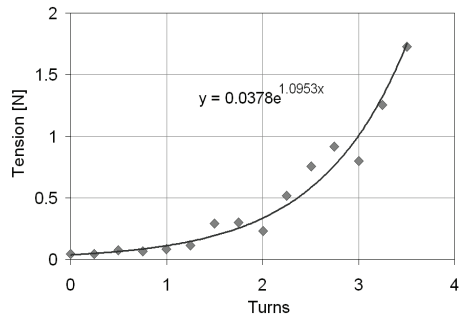

Figure 143. *Average tension vs. turns for non-centered pole configuration*

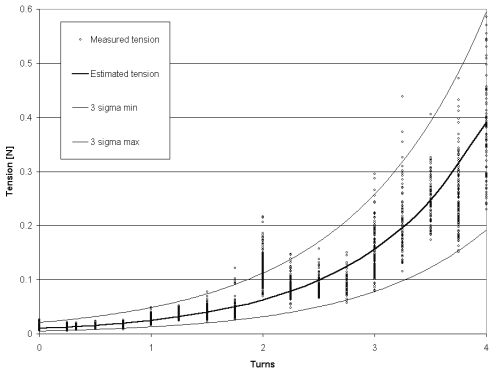

Figure 144. *SEDS barberpole performance for double-strand tether (note the pronounced anomaly at n=2)*

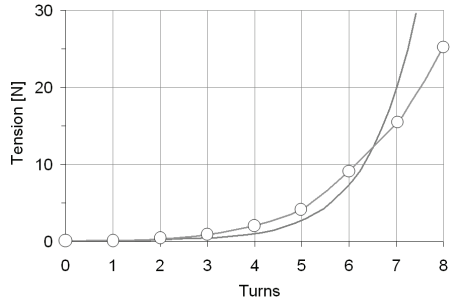

Figure 145. *Breakdown of exponential fit at large number of turns*

5.4.4 Effect of design parameters

Table 43 summarizes the tests that have been performed in order to understand the possible impact of a number of design parameters on friction and barberpole performance.

It has been suggested to align the tether canister exit hole with the zero-turn position of the barberpole entrance guide. This alignment allows for a very low friction passage without any bending in the zero turn position, and therefore for a minimal friction deployment. If a non-zero number of wraps is applied however, the variation in bending angle of the tether towards the entrance guide has a noticeable oscillatory impact on the tension with turns (Figure 146). It is therefore recommended to center the pole shaft over the exit hole instead.

A number of tests has been performed to identify any interaction between tether, winding and pole, and its influence on friction coefficient. The criss-cross winding angle (4 vs. 5 tpc) has no noticeable impact on tension (Figure 147). Also a flattened tether displays similar friction behavior as a round tether (Figure 148). Results do suggest that a stiffer, thermally prestretched tether leads to a steeper tension response with turns, so a higher friction coefficient.

In order to better understand the winding dynamics of the tether around the pole, and identify the best diameter or surface treatment to match the models, several poles with different shapes and roughness have been manufactured and tested. The characteristics of the poles are summarized in Table 44. One curved pole is included in the tests, as described in Section 5.4.1. A polished aluminium surface leads to a perceived too-low friction coefficient, so the curved pole is tested with 2 different surface treatments. Surface roughness for the poles has been determined by ESA/ESTEC using a Mitutoyo Surftest SV-3000. The measured peak-to-valley height is found to correlate to the roughness itself and ranges from 5-20 micron compared to a roughness range of 0.5-2.5 micron, so one order of magnitude larger. The sandblasted poles wear down during deployment tests, so a hard or anodized coating is advised.

Design Parameter	Value	Test set-up	Result
Entrance guide centering	Entrance guide centered over canister exit vs. pole shaft.	Unwinding Rig (v1)	Pole shaft centering recommended.
Spool winding angle	4 tpc vs 5 tpc.	Unwinding Rig (v1)	Effect smaller than spool differences.
Tether prestretch	Thermal prestretch 8x400 vs. untreated.	Unwinding Rig (v1)	Pole friction seems increased.
Tether flatness	Mechanically flattened 8x200 vs. round.	Unwinding Rig (v1)	Effect smaller than spool differences.
Double-strand tether	34.6 km 2 x130 Spectra twisted braid, stored 1 year, spliced every ~500 m.	Unwinding Rig (at Tether Applications, San Diego)	$f = 0.146$ (similar to single strand tether), Figure 144.
Tether twist	Approx. -20 to 20 twists/m.	Unwinding Rig (v2)	Strong influence on helix shape and stability on pole.
Inlet position	5-15 mm	Unwinding Rig (v2)	Improved when closer.
Pole coating	Hard coated, anodized, roughened, polished.	Unwinding Rig (v2)	Some impact on stability of loops.
Pole roughness	0.5-3 micron	Unwinding Rig (v2)	Friction coefficient vs. roughness.
Pole curvature	Cylindrical vs. curved.	Unwinding Rig (v2)	Curved pole is more helical and shows better exponential fit at large turns.
Pole diameter	13-24 mm	Unwinding Rig (v2)	Larger diameter provides steeper tension increase.

Table 43. Barberpole parameter test summary

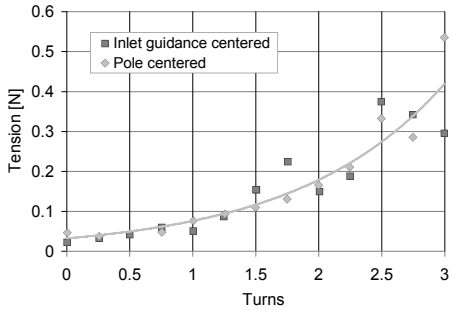

Figure 146: *Average tension vs. turns for centered and non-centered pole configuration*

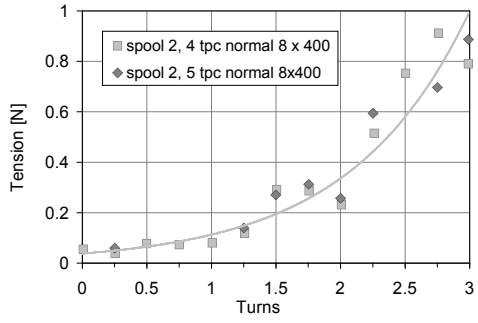

Figure 147. *Effect of winding angle on pole performance*

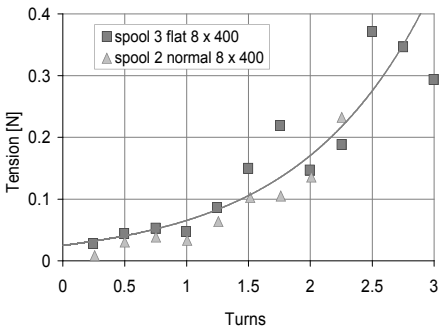

Figure 148. *Tether cross-section impact on pole performance*

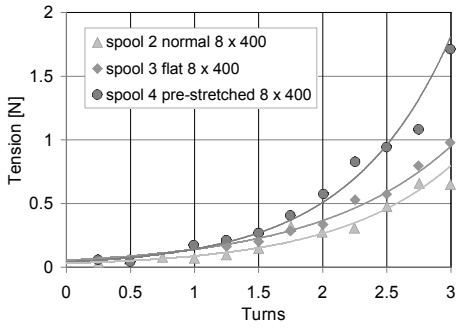

Figure 149. *Tether pre-stretch and pole performance*

Pole	Friction	Roughness [μm]	Diameter [mm]	Coating
1	0.25	0.57	24	3
2	0.24	0.76	17	3
3	0.18	0.64	13	3
4	0.18	0.59	17	1
5	-	0.75	13	1
6	-	0.7	24	4
7	0.34	1.74	24	5
8	0.28	1.92	17	5
9	0.3	2.26	13	5
Curved 1	0.21	-	24	2
Curved 2	0.25	2.7	24	4

Table 44 P*ole characteristics. Coating index: 1=polished aluminium, 2=hard anodized, 3=hard coated, 4=sandblasted-hard anodised-polished, 5=sandblasted.*

During tests, the poles of Table 44 are mounted, successively, in the engineering model barberpole casing. For each test, the number of tether wraps around the pole is increased in stepwise manner from 0 to 3.5, with 20-s duration steps of 0.25 wrap, at a constant velocity of 1m/s. 1 km tether - wound on a 70 mm diameter spool core - is deployed. Tether tension data is recorded with a frequency of 1 kHz. The one-sigma noise around the tension at each number of turns amounts to ~30-40%. As explained in Section 5.4.3, the friction coefficient is estimated from an exponential fit.

Figure 150 shows the results of the average tension of the tether for the three sandblasted poles. Especially for the sandblasted pole (high friction coefficient) there seems to be a clear trend of increasing friction performance with pole diameter. According to the mathematical

model this would not so much be a true friction effect, rather it is improved tension amplification (Figure 129). Figure 151 shows experimental results concerning the two coated big poles, which differ mostly in shape (cylindrical vs curved). The curved pole seems to maintain longer its purely exponential behavior, which is probably related to the fact that the cylindrical pole has an early onset of instability of the helix pattern. A vibration of coils is observed for this pole from about 2.5 turns. Brief overlap of loops or a deviation from the helix shape may lead to loss of friction. Figure 152 compares the exponential fits for different surface treatments, from which the sandblasted pole clearly stands out. In general, the exponential shape is well followed until about n=3 or 3.5. After that level, generally some relative losses in tension can be observed (except perhaps for the curved pole).

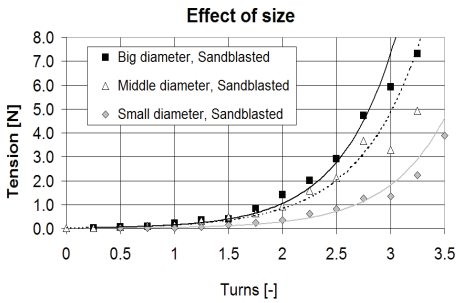

Figure 150. *Pole diameter vs. performance*

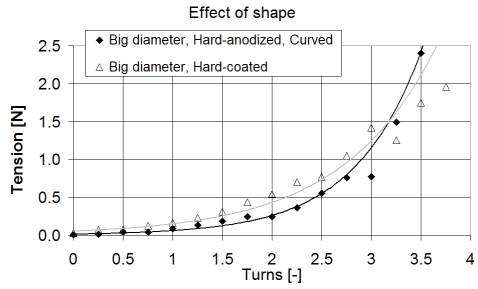

Figure 151. *Average tension of the tether for the coated big poles (cylindrical vs curved)*

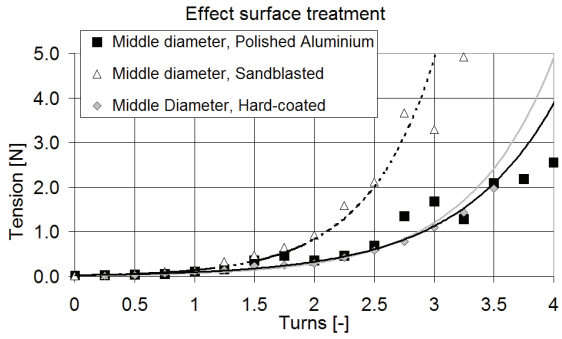

Figure 152. *Surface treatment vs. pole performance*

In Figure 153, a trend between roughness and friction coefficient can be observed. As this graph combines a wide variety of poles, there is a considerable spread. It is partly caused by the diameter and geometry effects described above, but for smooth poles, the cause of variation is less understood. It may be related to the difference in surface treatment, which have a rather distinctly different feel to the human hand, despite nearly equal roughness. Figure 154 provides an overview of the measurement distribution with respect to surface treatment. The various tests indicate a predictability of friction coefficient from measurements of about +/- 20%, which is taken into account in mission simulations.

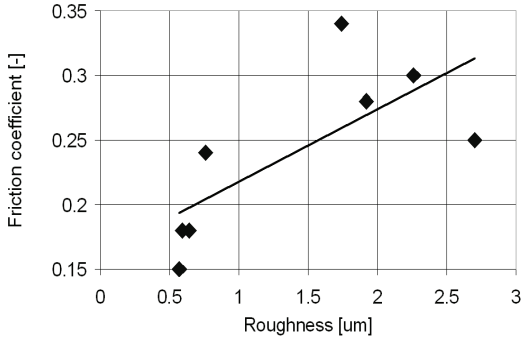

Figure 153. *Surface roughness vs. friction coefficient*

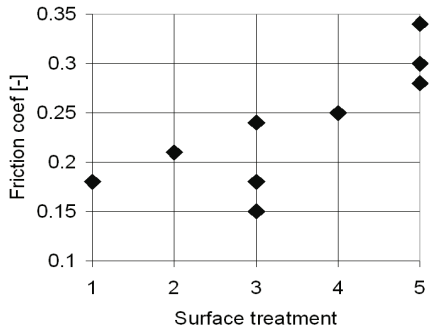

Figure 154. *Friction coefficient vs. various surface treatments. See Table 44 for surface treatment index*

Visual observations

Figure 155a and b. show respectively the path of the tether around the sand-blasted and smooth-surface wide diameter poles. Whereas in a. the tether winds around the pole with a quasi-perfect helix, in b. the tether is mainly gathered near the tooth-wheel. This is not consistent with the prediction of , indicating that the cause of the deviation here is not the tether diameter (Eq. 5.25), rather to the tether's torsional rigidity and/or the Pole Tendency (Section 5.4.1).

Visual observations consistently indicate that the homogeneity and regularity of tether winding around the pole can be maintained for very large numbers of turns (>>5) by selecting the appropriate friction coefficient (>0.25), and/or by applying a mild curvature. Having a too high friction coefficient or too high curvature can even lead to collection of loops on the exit side of the pole. With the present roughness the curved pole with the entrance cone angle of 1° overcompensates the Loop Tendency (just) slightly too much. A bit lower friction coefficient is acceptable.

It can be concluded from comparison of the visual observations against the exponential fits that the Loop Tendency, or deviation from the helix shape, in itself does not (yet) lead to decreased performance, at least for the limited amount of turns tested here. If the helical shape deviation gets extreme, tether loops can overlap. In that case friction output is reduced significantly with respect to the exponential model. The situation will be much worse if some entanglement with tether or gear would occur.

A second issue that has shown up in the visual observations is instability of the loop position. In some cases, the wraps are shifting back and forth over the pole, even at times overlapping. Onset of instability is found to be directly associated with loss of performance. Its causes are as yet unclear. Apart from a shared cause with the Loop Tendency, tether irregularities from shape memory, tether stiffness and twist, noise in incoming tension due to layer crossings are some directions for further study. Overlapping seems to occur mostly at high turns (>2.5), on narrow poles with low surface roughness, at low irregular incoming

tension and for thick tethers. Simple tests indicate that velocity and temperature seem not involved in the cause of this undesired effect. The fluctuation is far less when the incoming tether is delivered consistently slack into the barberpole, or when the incoming tension is stable and high (~10 cN). An unexplained trend-breaker is the thin hard-coated pole, which seems to postpone the onset of instability.

a. 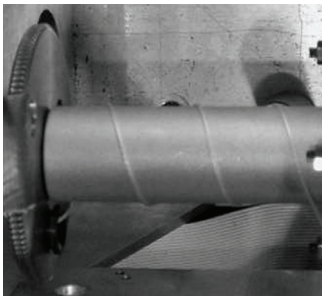 b. 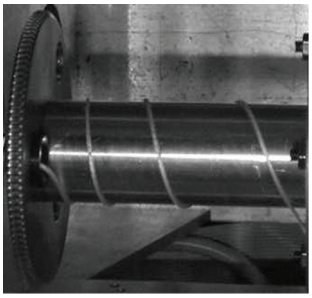

Figure 155. *Path of tether around sand-blasted (a) and smooth-surface (b) wide diameter poles*

Design recommendations

It is concluded that a surface roughness of 1-2.5 micron is required, because a polished surface has low friction coefficient, associated poor helix shape and early onset of instability. A coating, preferably hard anodization, is required to avoid wear of the surface. A large pole length relative to tether diameter can be expected to reduce the risk of tether overlap. A larger pole diameter both experimentally and mathematically predicts better tension amplification performance. Thermally, a large pole heats up less. Some curvature can be introduced to avoid collection of the tether on the incoming side (reducing also risk of overlaps), delaying also a bit the onset of instability. Too much curvature causes collection on the exit side as well as, possibly, instability. The best performance is thus expected from the curved, hard anodized, large pole.

5.4.5 Reproducibility

The influence of some environmental parameters of primary importance is studied to provide confidence in reproducibility of the findings (Table 45). Unfortunately, no deployment could be performed in vacuum, so only a brief static test is performed (Section 4.1.7). Gravity seems to have no significant effect on tension behavior. During a parabolic flight experiment, gravity level has been varied from zero to 1.8 g, for approximately 20 seconds each. Results are presented in Figure 156 for 0, 0.5 and 1 turn. Apart from the (winding related) cyclic peaks in tension, the figure shows no step change in tension at the g-level transition ($t \approx 15$ s). Section 5.6.2 reports on the results of another critical zero-g test, namely the turns reduction at zero velocity during the hold phase. A clear dependency of friction coefficient on velocity exists, particularly in the lower velocity regime, and leveling out above 2 m/s (see also Section 8.1.1).

Environmental parameters	Value	Test set-up	Result
Velocity	0.5 vs. 13 m/s, up to 4.5 turns	Unwinding Rig (v1)	16% higher friction at high velocity, possibly due to differences in pole temperature or tether twist [Kruijff 2001.III]
	0.25 to 2 m/s	Unwinding Rig (v2)	25-30% increase from 0.5 to 2 m/s,
Temperature	Elevated temperature during unwinding (40°C)	Unwinding Rig (v2)	No effect recorded.
Vacuum	Friction in vacuum	Static, Section 4.1.7	No significant effect, data more noisy in vacuum.
Gravity	At 0-0.5-1 turn Zero-g vs. 1 and 2 g 5th ESA Student Parabolic Flight Campaign	Unwinding Rig (v2)	No significant effect.
	0-10 turns, zero velocity, zero-g 43rd ESA Parabolic Flight Campaign	Unwinding Rig (v2)	Starting dynamics of second stage confirmed.

Table 45. *Environmental parameters influence on barberpole performance*

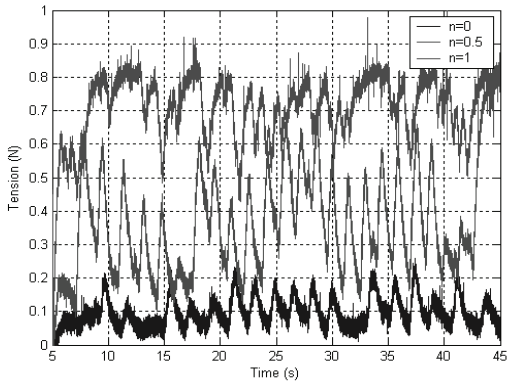

Figure 156. *Effectiveness of barberpole in zero-g (from ~15-35 s). Criss-cross spool pattern (n=0 is bottom curve)*

5.5 Controller development

In this section, the development of the reference deployment trajectory and feedback control is reported. The feedback controls the barberpole and uses OLD-based length and velocity estimation algorithms. The final control parameter is the selection of release time. The attainable landing accuracy based on the control design is verified by the MTBSim simulator.

The controller is implemented into the breadboard deployer system with a two-second control interval and based on (only) two OLD's. A flow diagram of this breadboard control

software is provided in Figure 167. The implementation into the flight system is discussed in Section 7.4.3. Both breadboard and flight system (Engineering Model) have been used for closed-loop deployment tests (Sections 5.2.4, 5.6).

5.5.1 Deployment trajectory

Literature provides a wide range of schemes in order to develop deployment trajectories and control [Fujii 1996, Sabath 1996.I, Ohtsuka 1997, Glaessel 2004, Zimmermann 2005]. As the barberpole brake is not accurate enough for open-loop control alone, yet allows for significant corrections with only little control effort, a combined approach of a reference deployment with feedback has been selected for the SpaceMail application. A pragmatic approach for the SEDS-2 mission has been followed in this direction by Bortolami e.a. [Bortolami 1993]. They divide the deployment time in a number of intervals, with a certain barberpole brake setting for each interval. For each combination of brake settings over time, the deployment trajectory is integrated using a trajectory propagator, assuming a circular drag-free orbit and a massless, straight and inelastic tether. The cost function is defined by the deviation of the final state from a stable position with a constant and correct length at the vertical. An optimum is found by iteration.

Real tether and deployer effects have to be taken into account as well (see Section 2.1.5). A demonstration flight at low altitude will encounter significant atmospheric drag. With a low endmass, as is likely to be selected for launch cost reduction, the tether mass is not negligible. At low tension levels and high deployment velocities, the tether can develop significant bulging due to Coriolis force acting along its length. Such bulging can in turn lead to transverse waves in the tether. Abrupt final braking can lead to longitudinal oscillations and slackness, endmass rotation and wrapping of the tether around the endmass. This can endanger proper endmass release. The deployer hardware as developed is limited in the minimum tension level it can apply (Eq. 5.30). Furthermore, in order to allow margin for control and improve robustness, a minimum number of brake turns shall be assumed for the nominal deployment trajectory.

It is straightforward to take such complexities into account if the MTBSim simulator is used as the vehicle for a multiple-shooting type optimization of the trajectory (Section 2.3). A parametrization of the deployment trajectory is then necessary, as well as a cost function and an optimization method. Two distinct methods have been implemented for the first and second stage of deployment.

A first-stage deployment reference trajectory can be generated by applying, in MTBSim, a tension law devised for this purpose, based on the known deviation of the state from the final target. Various such simple feedback algorithms have been evaluated, but usually involve tether retrieval, which is not feasible for the spool system [Heide 1996.I]. A particularly fast deployment-only trajectory can however be achieved by the method described by Levin in [Beletski 1993] (reproduced in Eq. 5.31), with the value of the parameters determined as represented in Table 46. A fast deployment indicates a larger average velocity and therefore is likely to be more robust. For a small endmass a relatively high ejection velocity and large first stage length is required. For a 12-kg endmass, values of

$\dot{l}_0$ = 2.4 m/s at L_0 = 3 m, and a target length of L_1 = 3400 m is selected, providing sufficient gravity gradient for a secure second stage start, yet enabling a sufficient swing angle for efficient re-entry (Section 2.1.4, [Ockels 1995]). The tether density equals ρ = 0.185 kg/km.

The parameters are optimized by a genetic algorithm that is integrated within MTBSim [Biesbroek 1996]. The cost function includes deviation from the final length, final velocity and pendulum oscillation energy (based on Eq. 2.11), with additive penalties for breaching minimal velocity, tension levels and other boundary constraints.

A typical resulting set of parameters is provided in Table 46 with a deployment trajectory plotted in Figure 157. Typical for this type of deployment is an inertia-driven deployment with a steep drop in initial velocity, towards a minimum (point A), where gravity gradient forces take over and accelerate deployment. Deployment is then decelerated smoothly in such a way that the endmass moves back to the vertical and no residual angular rate is left at the point that the vertical is reached and deployment has stopped (point B). Levin's method is characterized by a specific transition in tension (here at t=2000 s) that initiates a steeper acceleration at fraction f of the total tether length. This jump can be removed by proper selection of parameters or by manual (local) smoothening of the tension profile, generally without large penalty to the fitness and the final conditions.

	$l \le f L_1$		$l > L_0$
	$t \le t_1$	$t > t_1$	
a	a_1	a_1	a_2
b	b_1	b_1	b_2
v_r	$v_1\left(1-q+q\cos\left(2\pi\frac{t}{t_1}\right)\right)$	v_1	v_2

a_1	4.236	-
a_2	5.770	-
b_1	5.691	-
b_2	4.718	-
f	0.515	-
t_1	1166	s
v_1	0.427	m/s
v_2	0.077	m/s
q	0.0312	-

Table 46. *Levin first stage deployment method parameters*

$$T = \frac{M(m+0.5m_t)}{M+m+m_t}\Omega^2\left(al+(3-a)L_1+\frac{b}{\Omega}(\dot{l}-v_r)\right) \qquad (5.31)$$

Given the simulated solution, it can next be treated as a reference trajectory, to which feedback can be applied based on length and velocity estimates alone.

The reference trajectory for a second stage of deployment to a large angle is rather simple to obtain, even by hand. A semi-manual optimization to determine a second stage trajectory has been implemented as a first method. It is essentially composed of three sections. Initially the brake is turned down to a minimum value that leaves room for feedback, about 0.5 turns. This allows a reasonable in-plane angle to be achieved despite the relatively long

first stage length [Ockels 1995]. The deployment velocity increases essentially exponentially. The deployment can end with a slow smooth braking or a fast end-brake algorithm aimed at preventing longitudinal oscillations, which uses the currently achieved state and target end-state of zero deployment velocity as parameters [Kruijff 1996]. The mid-section is segmented further down into about three intervals. For each interval a suitable initial brake position is determined iteratively, by hand, by interaction with the simulator output. The brake position is interpolated between these points over the intervals. The objectives of this iteration are twofold. First of all the tension level should be kept high enough to avoid tether bulge and transverse waves from building up. Secondly, if necessary, the deployment velocity can be smoothened further, before the final braking, by limiting the maximum deployment velocity below about 13 m/s. A typical resulting trajectory is provided in Figure 158 and Figure 159.

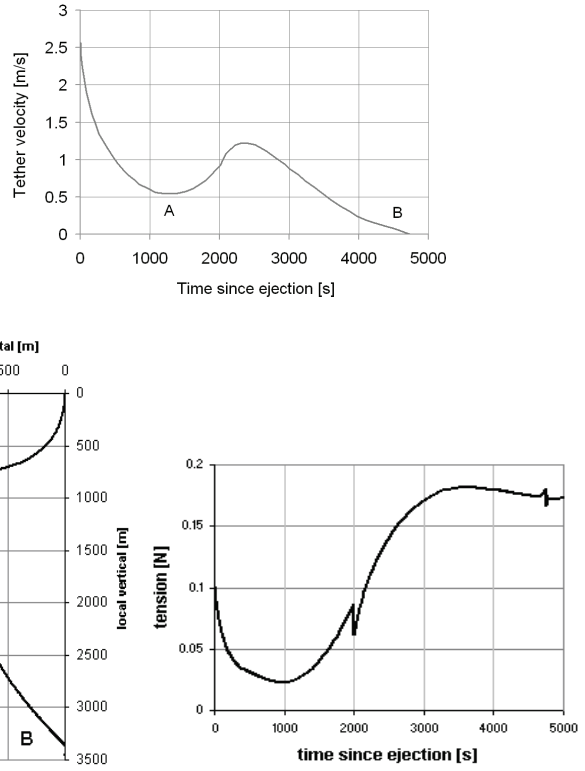

Figure 157. *First stage deployment profiles*

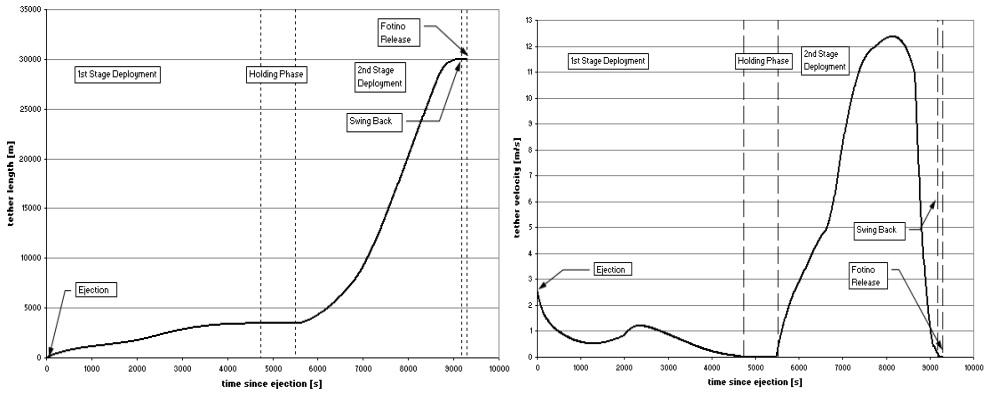

Figure 158. *Full deployment profile using Levin's first stage method and manually iterated second stage – length and velocity*

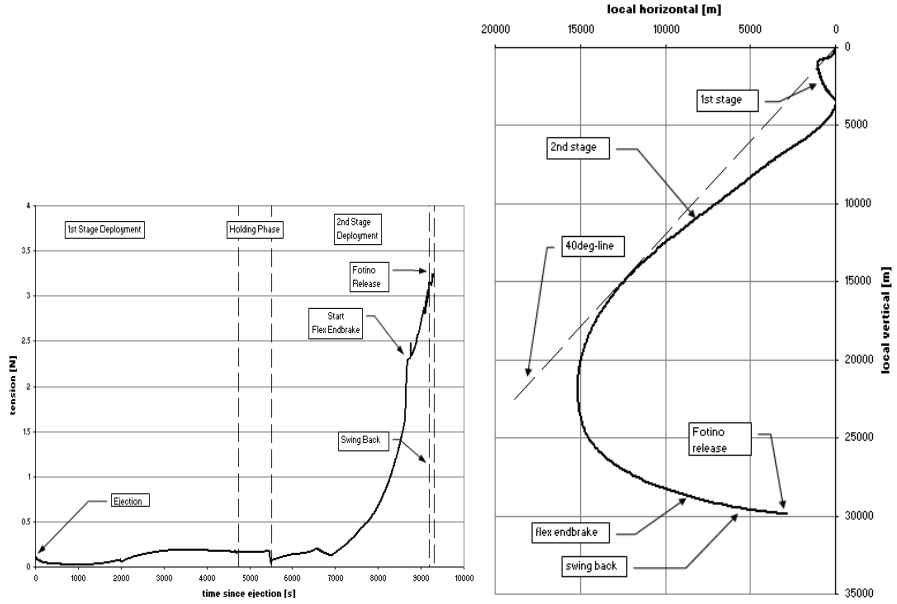

Figure 159. *Full deployment using Levin's first stage method and manually iterated second stage – tension and LHLV plot.*

Because a manual optimization is not fully reproducible and to an extent subjective, a more formal method has been sought for deployment trajectory determination, taking into account the flexible tether boundary conditions. Paul Williams has worked out a solution in three developmental steps that are summarized here [Williams 2006,2007,2009]. In his first step, Williams considers a rigid massive tether in circular orbit. The problem definition includes the barberpole tension performance model.

A number of boundary constraints are applied: a nominal ejection velocity $\dot{l}_0$ = 2.2 m/s; a first stage length of 3400 m and a second stage length of 30.0 km; a minimum velocity during the critical part of the first stage of 0.5 m/s; a maximum deployment velocity in the second stage of 13-15 m/s; yet obtain an effective swing angle of at least 30 degrees. The latter is a rather limiting requirement but necessary to provide the required ΔV to the capsule. The barberpole brake position shall have a minimum n>0.5. Finally there should be a gentle final deceleration to avoid spring-mass oscillation of the endmass.

The reference deployment is determined by defining and solving the single-phase optimal control problem. Hence, as a cost function, minimum deployment acceleration and minimum tension rate throughout the deployment are used. The deployment is discretized and optimized using direct transcription. Terminal swing angle of the second stage and deployment time are chosen manually. These values as well as the ratio between the terms in the cost function have to be iterated to generate a feasible solution. Figure 160 shows the result for the first stage. The deployment is in essence similar to the one developed using genetic algorithm optimization (Figure 158), although more smooth and somewhat faster. The figure also shows the result of a successful actual deployment test (Section 5.6.2) using feedback (Section 5.5.4).

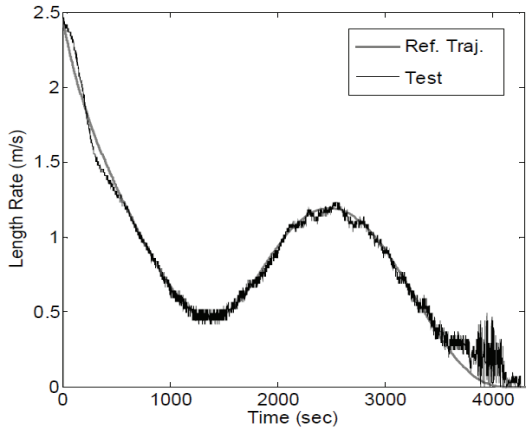

Figure 160. *Deployment velocity in first stage - simulated control*

The resulting profile is then run in a lumped mass model simulator developed by Williams as well as in the MTBSim simulator for verification. The tether shall for example not bend beyond 1-2° due to Coriolis effects, as not to create a standing transverse wave after deceleration. The endmass shall not bounce and cause tether slackness. It is also observed whether the simulated barberpole controller is indeed able to follow the reference trajectory. Several such iterations are typically necessary to obtain a suitable trajectory.

In a second developmental step, Williams has refined his model to include aerodynamic drag, found of significant influence on optimal trajectory determination at low altitude (below 300 km), particularly with respect to the in-plane angle achieved. For its influence on

aerodynamic drag changes over each orbit, orbit eccentricity is also taken into account. Furthermore, because hardware tests have indicated that tether-pole friction significantly reduces at very low velocities (Section 5.4.5), this dependency is also taken into account. Typical optimization results for various cost functions are shown in Figure 161a. The deployment angle and influence of atmospheric drag is shown in Figure 161b. A maximum velocity of about 12 m/s is reached, whereas the maximum deployment angle in the second stage reaches 40°, with deployment completion at 20° and an effective final swing angle of 30° (see Section 2.2.1). This is a significantly smaller swing angle than proposed in [Ockels 1995]. The difference is a combined result of the low endmass, large first stage length, relatively short second stage length (30 km) and the margins maintained on the brake and the deployment velocity. Due to the low orbital altitude, under 300 km, no larger angle is required.

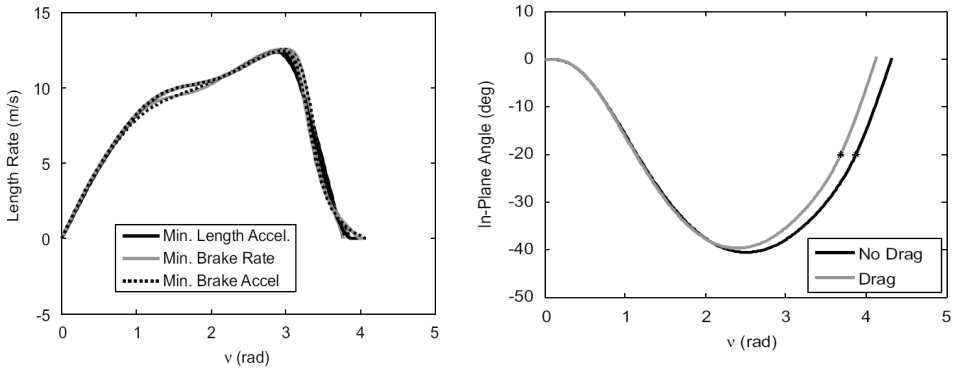

Figure 161. *Second stage deployment optimization [Williams 2007]*

In a third developmental step, only briefly summarized here, Williams approaches the optimization from a different angle. Taking the resulting profile of the second step as a starting point, Williams assumes the worst case high friction level as nominal with the intention to achieve a more robust reference profile. The reason is that in the presence of feedback (Section 5.5.4) the sensitivity of a tether deployment to errors in the friction estimate is asymmetrical. Lower friction can be easily controlled by adding barberpole wraps. A significantly higher tension however cannot be controlled beyond the zero barberpole position. Williams employs a lumped mass model of a flexible inextensible tether such that transverse oscillations can be kept minimal through inclusion in the cost function. The number of parameters can now be kept small if for optimization a multiple shooting method is used, with explicit propagation of the state trajectory by means of an integrator. Simulated annealing is chosen as optimization method. The work concludes in a successful definition of reference trajectories [Williams 2009].

5.5.2 Release time control

A final control opportunity in the momentum transfer mission is related to the release of the endmass, which is critical for orbit insertion accuracy. Various release options can be considered (Figure 163). Release of the endmass from the tether before tether disposal provides optimal momentum transfer and accuracy (method A). Release of the endmass only after tether release from the host platform may be preferred by the host, but the recoil on the endmass leads to a large dispersion of its trajectory (method B). It would then be better to keep the tether attached to the endmass into re-entry as a "drag tail", providing the simplest technical solution, as well as a means of passive attitude control for the endmass at time of re-entry (method C). Method C is illustrated as simulated by MTBSim in Figure 164 [Kruijff 2003.I, Stelzer 2006].

Method A is recommended to avoid tether recoil towards the endmass for maximum endmass trajectory precision and maximum momentum transfer efficiency. The timing for such a release should ideally be done in real-time based on a state-propagation, based on GNSS positioning on the endmass, such that maximal landing accuracy can be obtained [Heide 1996.I]. For simplicity however, a release system with a pre-fixed timer starting at ejection can be put on the endmass. Landing position can still be influenced by controlling the exact moment of the start of the second stage. A later start shortens the duration until release of the swing to the vertical; release will take place at a larger in-plane angle.

Landing accuracy also depends on swing phase at release (Figure 162). The endmass can best be released shortly before the vertical in the swing is achieved. In the StarTrack and TSE studies, different optimal angles of release (5-10° before vertical) have been found, depending on the error models and system parameters used [Ockels 1995, Heide 1999]. At this time, the momentum transfer effect is increasing with time and nearing its maximum. Any error in release time is largely compensated by the change in this effect. A later release will be compensated by the faster swing motion at the time of release, leading to steeper re-entry, as simulated by MTBSim [Ockels 1995, Heide 1999]. The impact is significant. An error of 10 s in swing phase at time of release therefore leads only to a landing point shift of about 10 km. This contrasts against a shift of 80 km that would, for comparison, result from a retro-rocket firing for deorbit mis-timed by the same 10 s (at 8 km/s orbital velocity).

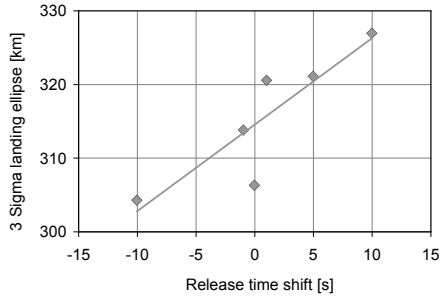

Figure 162. *Impact of capsule release time on landing error*

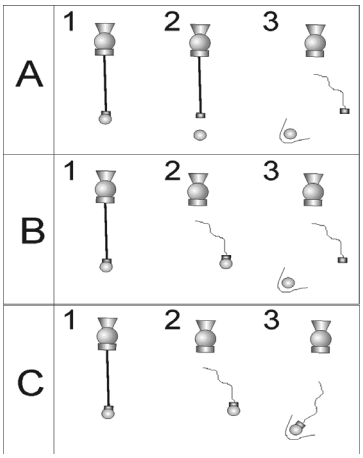

Figure 163. *Options for tether and capsule release*

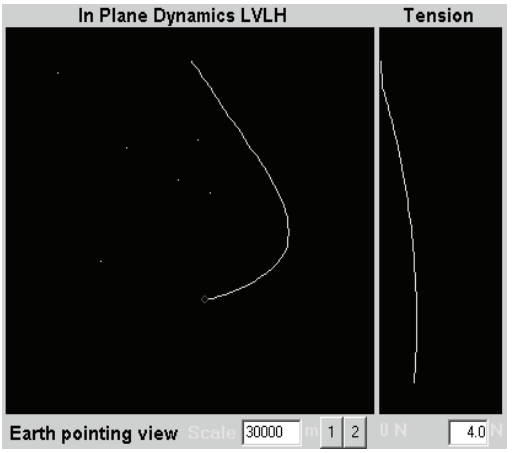

Figure 164. *Simulation of tether capsule at re-entry*

5.5.3 Length and velocity determination

Control of the deployment by feedback towards the reference profile is done based on length and length rate data only, in absence of a reliable method to observe the in-plane deployment angle or endmass position. To this purpose, a number of simple algorithms has been developed.

The deployed tether length is the measure of choice for tether length, rather than the stretched length or the distance between endmass and deployer. This deployed tether length is derived from the number of deployed loops, which in turn is based on the registered order and number of OLD pulses (Section 5.3.2). As the tether is unwinding from the spool, the diameter of the spool decreases. For each spool part, a quadratic fit is therefore used, expressing the unwound number of loops vs. the deployed tether length, with a typical precision better than 0.1% and accuracy better than 0.3%. The most recent deployment tests have achieved also an accuracy of 0.1% (Table 39).

The loop count algorithm itself is based on transitions rather than passages alone. In this way it deals inherently with the most common noise source: vibrations of the tether in front of a single OLD. If more than two OLD channels are in use, this approach also inherently deals with the next common source of error without any loss of quality: a single OLD malfunction.

Whenever an OLD signal arrives from a particular channel, the transition algorithm simply adds a fractional number of loops to the total deployed, based on the current OLD channel number and the previous. Assume for example that three OLD channels are in use. Consider Table 48. As the tether unwinds axially from the spool, it passes the three OLD channels, simply tagged "1", "2" & "3", necessarily subsequently and repetitively in a fixed order: 1-2-3-1-2-3-1...etc. (Row A). If an off-nominal order of pulses occurs (e.g. **1-3**-1-2-3), the algorithm assumes an intermediate pulse has been missed, in this case Channel 2 (Row B),

and the software fills in the gap by counting 2/3rd of a loop (Table 47). In case two subsequent pulses arrive from the same channel (e.g. **1-1**-2-3) tests show that it is most likely that the tether vibrates briefly in front of a single channel, Row C. The transition table contains a zero and the noise is ignored (Table 47).

A simple filter can be implemented, in addition, to deal with a *double* OLD failure. Suppose that at one point in the deployment two OLD channels are failing, e.g. Channels 2 and 3 (Row D*)*. If the pulse interval between the subsequent Channel 1 signals lasts much longer than a tether vibration in front of a single channel (Row C), and approximately as long as an integer number of full loop deployments, this situation may be identified as a double OLD failure. A decision may be made by the filter to count a full loop (*italics* in Table 47). The identification of a reliable and critical interval duration is of fundamental importance for this filter.

This critical interval duration has been defined as a function of filtered velocity, and includes a software programmable parameter. Ground tests have revealed a particular weakness. Suppose there are indeed two failing channels and only one OLD is operating. If a slow noise occurs now as well and the filter is falsely applied, as a result, the velocity estimate will increase above the actual value, whereas the critical interval duration will be *decreased*. The brake may now be unnecessarily applied, leading to a deceleration of deployment and thus an increase of the *actual* interval duration for the only functional OLD. A subsequent false identification thus becomes even more likely. This can lead to a runaway effect. To prevent this (rather extreme) failure case, the ground tests have been used to determine a safe filter parameter value. The filter nevertheless still carries a certain risk of confusion with a slow tether vibration, for example in case the deployment is of an irregular nature.

	Previous channel		
Current channel	**OLD1**	**OLD2**	**OLD3**
OLD1	0 *(or 1)*	2 / 3	1 / 3
OLD2	1 / 3	0 *(or 1)*	2/3
OLD3	2 / 3	1 / 3	0 *(or 1)*

Table 47. *Logic for loop count based on OLD transitions*

A	Normal	1	2	3	1	2	3
B	One channel failure	1	-	3	1	-	3
C	Isolated tether vibration	1-1	2	3	1	2	3
D	Double channel failure	1	-	-	1	-	-

Table 48. *Typical OLD channel activation sequences*

Now that the tether length is known, the velocity can be computed. The velocity estimate shall be both smooth to avoid overshoot, as well as responsive to sudden changes in deployment, for increased accuracy. A low pass-filtering is applied by averaging of the most recent rates of length increase, where the latest measurement is given more weight than the others. The rational behind this filter is illustrated by Table 49. The logical steps presented in this table are mathematically equivalent to a weighted average. The starting point is the estimation of a raw deployment velocity from the ratio of increase in deployed length and time over the selected control interval of two seconds [Step 1-2 in Table 49]. This raw velocity typically has a significant noise with respect to the deployment velocity, Figure 165 (shown for first stage). To allow for a smoother feedback algorithm, this velocity is filtered to obtain the estimated velocity. The filter shall be applied such that a length error is accepted once built up, but the length error should not build up further [Steps 4-6]. Furthermore, large changes in velocity from one time step to the next are dampened in this manner [Step 7].

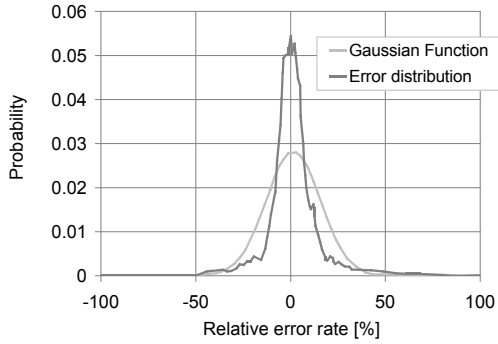

Figure 165. *Error in raw velocity compared to filtered velocity (TSE)*

0	**During an initial phase right after ejection, filtered velocity $VF = V_{ref}$ (reference velocity)**
1	At a constant interval of 2 s, the length estimate L[n] at time t and interval n is updated
2	At the nth interval, raw velocity $V_{raw}[n] = (\Delta L/\Delta t)n$
3	$VF\,[n] = Average(V_{raw}[n\text{-}N]..V_{raw}[n])$, N being the filtersize
4	Testlength $L_{test} = Sum(VF[1]..VF[n]) * \Delta t$
5	Length inconsistency because of current VF is $Error[n] = L[n] - L_{test}$
6	Improved estimate is $VF\,[n] = VF\,[n] + 0.25 * (Error[n] – Error[n\text{-}1]) / \Delta t$
7	Dampen large changes $VF\,[n] = VF\,[n\text{-}1] + 0.25 * (VF\,[n] - VF\,[n\text{-}1])$

Table 49. *Rationale of weighed average velocity filter*

The weighed-average filter is shown to be simple yet robust and smooth yet fast responding, with a delay on steep velocity changes of about 8-10 s. For comparison, the SEDS mission included a low pas filter of 0.02 Hz [Lorenzini 1996]. More complex filtering methods have been explored, based on (dynamic) error models such as the Gaussian shown

in Figure 165, but have not yielded significantly better results [Kruijff 2003.IV]. Simulated performance is found to provide a good qualitative indication of actual test performance, Figure 166. Simulations have therefore been used to determine the parameter values that best fit a typical deployment profile.

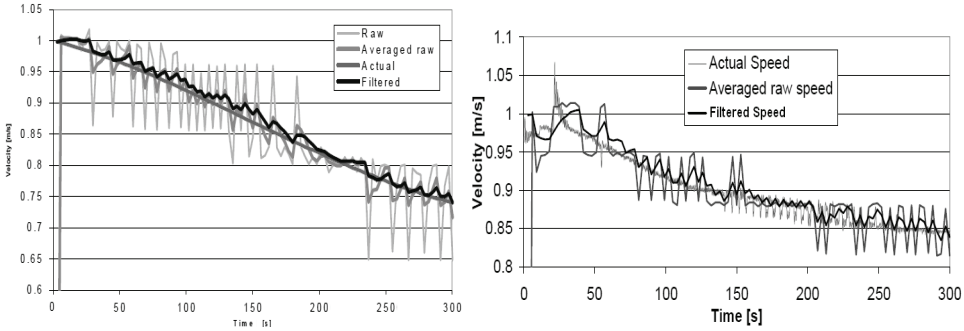

Figure 166. *Velocity filter performance (TSE test), simulated left, test right*

5.5.4 Feedback control algorithms

At a regular interval the measured state is compared to a reference deployment table stored on-board containing length and velocity versus time. Based on the error and the nominal control a new brake position is then determined. The nominal or 'reference' control is preferably expressed as reference tension T_{ref} rather than as reference number of turns n_{ref}, because a tension profile can be used as reference for any system with given mass properties independent of the exact deployer parameters. The corrected brake position n to be applied can then be expressed as a function of T_{ref}. There can be various approaches towards determining a correction for position n. Consider the following generic expression for a correction α to be applied:

$$\alpha = k_l(t)\Delta l + k_{\dot{l}}(t)\Delta\dot{l} + k_1(t)\int_0^t \Delta l dt \tag{5.32}$$

Consider for the sake of discussion the simplified relationship between tension and turns:

$$\begin{aligned} T &= T_{in} e^{2\pi f \cdot n} \\ n &= \frac{1}{2\pi f} \ln \frac{T}{T_{in}} \end{aligned} \tag{5.33}$$

Bortolami e.a. have studied a number of feedback methods in the context of SEDS-2, based on the number of turns, with constant gains and $k_l = 0$. The authors report that for constant k, it is required to apply the feedback with respect to the reference brake profile in order to take the nonlinearity of the system into account [Bortolami 1993]. Therefore, a control of the form $n = \alpha$ leads to poor nominal performance and no robustness. Also a purely additive approach with respect to the nominal brake profile still is found to show insufficient robustness:

$$n = n_{ref} + \alpha = \frac{1}{2\pi f}\ln\frac{T_{ref}}{T_{in}} + \alpha \tag{5.34}$$

Instead, they suggest the following approach, which has been implemented for SEDS-2:

$$n = n_{ref}(1+\alpha) = \frac{1+\alpha}{2\pi f}\ln\frac{T_{ref}}{T_{in}} = \frac{1}{2\pi f}\ln\left(\frac{T_{ref}}{T_{in}}\right)^{1+\alpha} \tag{5.35}$$

The same length and velocity error at a larger number of brake turns results in a larger adjustment in turns, and, due to the exponential tension response, an even stronger adjustment of tension. A small error could thus lead to a large tension fluctuation during the braking phase which could in turn trigger tether oscillations.

An approach to obtain a milder, perhaps more intuitive control would be to determine the required change in tension in order to return to the reference profile:

$$\begin{aligned} &\Delta T = \alpha_T \\ &n = \frac{1}{2\pi f}\ln\left(\frac{T_{ref} + \alpha_T}{T_{in}}\right) \end{aligned} \tag{5.36}$$

This response in principle is weaker than the one given by Eq. 5.34. In order to deal with lack of robustness reported by Bortolami e.a., a non-linear approach based on physical considerations was proposed in [Ockels 1995, Heide 1996.I], the Energy Feedback. The energy of the system is calculated using a straight non-flexible tether model in free orbital motion (Section 2.1.2). The energy is determined for the reference case, as well as for the measured state. The expression for energy contains also the in-plane deployment angle. In absence of angular position information, the reference angle is used. Based on the difference in system energy and the available tether length, the required feedback can be determined.

$$\alpha_T = k \cdot \frac{E - E_{ref}}{L_{end} - l} \tag{5.37}$$

L_{end} being the final deployment length of the stage including a suitable margin, k suitably chosen, and different for first and second stage. The method has been applied successfully in e.g. [Kruijff 2001.II], as well as in [Sabath 1996], however, it leads to control overshoot early in the first stage deployment (Section 5.6.1).

Another approach has therefore been implemented, based on proportionality of the correction α (from Eq. 5.32) with T_{ref}, still with constant gains and k_I=0.

$$\begin{aligned} &\Delta T = \alpha T_{ref} \\ &n = \frac{1}{2\pi f}\ln\left(\frac{T_{ref}}{T_{in}}\right) + \frac{\ln(1+\alpha)}{2\pi f} \end{aligned} \tag{5.38}$$

Despite the similarity to Eq. 5.34, good results are obtained (Section 5.6.2).

Paul Williams has proceeded to develop the simple feedback structure of Eq. 5.34, dealing with the non-linearity, by assuming feedback gains variable with time, obtained through

receding-horizon optimization using a Gauss-Lobatto Quadrature discretisation [Williams 2006,2007]. Later William e.a. employ a similar feedback, this time including non-zero k_I, for additional robustness [Williams 2009].

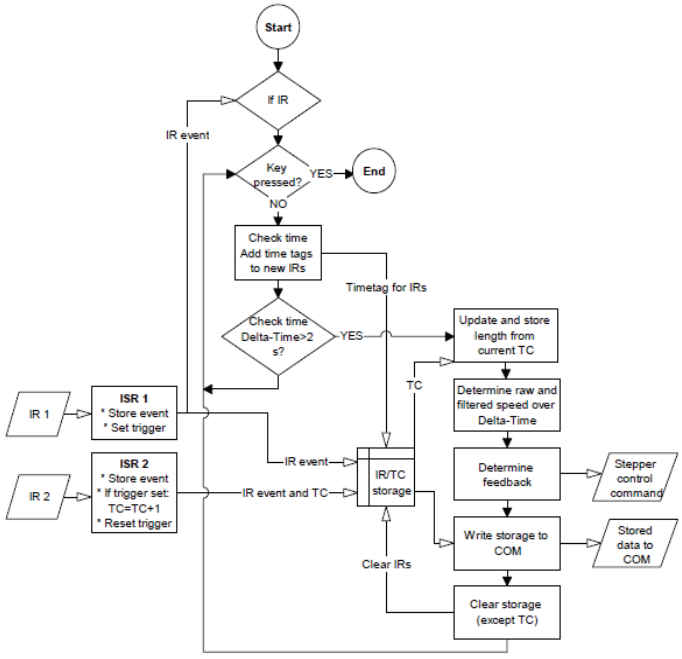

Figure 167. *Flow diagram breadboard control software, TC = loop count, IR = OLD interrupt request*

5.5.5 Performance and robustness testing

The controller has been implemented into MTBSim for simulation of its behavior. The trajectory and feedback robustness is tested through Monte Carlo simulations. The MTBSim includes a sophisticated re-entry simulator module and is suitable for an end-to-end analysis from ejection until capsule landing, with which the optimal release time can also be determined (Section 3.1.1) [Ockels 1995]. Based on the hardware characterization tests (Sections 5.3.5, 5.4), and the unknowns in both launch parameters and atmospheric density, error models have been defined (Table 50).

An example of the spread in deployments as a result of a Monte Carlo run is provided in Figure 168. A view of the deployment trajectory is shown here in local vertical/local horizontal system with respect to the deployer platform. Flight direction is to the left. The endmass location is plotted as one dot at 150-s interval for each of over 600 Monte Carlo runs. The nominal ΔV vector of norm 113 m/s is represented in the bottom of the graph. For each run, the vectorial errors in ΔV is also plotted to scale, at the location of capsule release.

A typical resulting landing area is also provided in Figure 168. This area is for a 12-kg endmass and a lightweight 40-cm diameter, 5-kg spherical re-entry capsule (see also Section 7.4.5). The landing area of 384 km is comparable to what could be achieved using a retro-rocket system for such a capsule [Schonenborg 2000]. A good part of this area is the result of the ballistic, atmospheric entry phase, due to the low ballistic coefficient of the capsule. Sensitivities of the landing error to various capsule designs, orbital parameters, atmospheric models and conditions are provided by Calzada in [Calzada 2004].

Atmospheric entry angle is an important design parameter for the re-entry capsule. Figure 169 provides an insight into the range of entry angles that the capsule may be subjected to as a result of several design parameters. The target location within the landing zone is fixed only after launch, based on the launcher's achieved orbital parameters. This selection may have an impact on entry angle as indicated. The range in entry angle, for the nominal mission design, that may be obtained as a result of the tether deployment errors is determined from the Monte Carlo simulation (indicated as "nominal"). The potential impact of a change in nominal mission design has also been computed: a target tether length between 28 and 32 km and the possible range in release angle within the swing are the parameters plotted in the figure.

The influence of all these parameters is small compared to the acceptable range for the capsule and trajectory design. Therefore, the parameters mentioned can be freely selected, without regard for the impact on entry angle. There is also no need for inclusion of the error in entry angle in the cost function for optimization of release time. For this reason, only landing accuracy considerations have been used for release time selection.

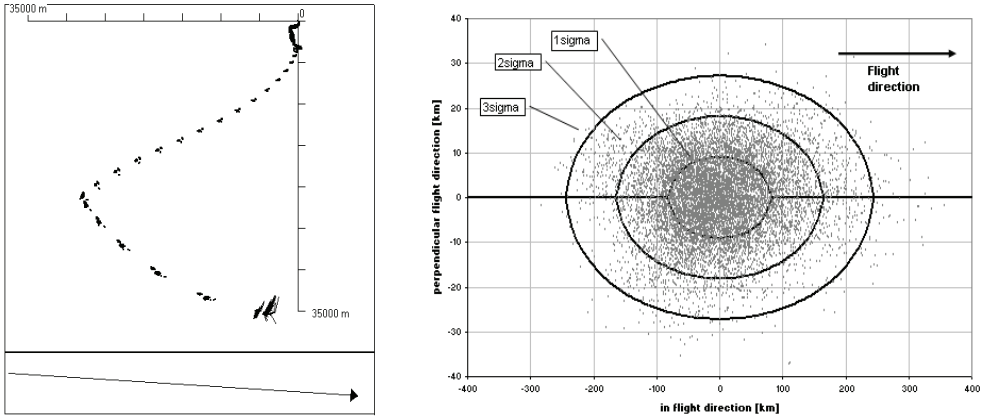

Figure 168. *Overview of 603 Monte Carlo simulations before tests.*

Disturbance	Sigma	Magnitude (3.09 σ = 99.8%,1 σ = 68.3%)
Tension modeling (tether deployment)		
T_0	3.09	±60%
I	3.09	±30%
f_g / f	3.09	±30%
Tether Properties		
EA	3.09	-50% to +100%
ρ	3.09	±5
Environmental uncertainties		
F10.7 solar flux	3.09	±24 (absolute value) around solar minimum of 70
AP geomagnetic index	3.09	±10 (absolute value) around average of 15
atmospheric model		GOST 4401 (1981)
$\rho_{atmosphere}$	3.00	25%
wind = f(altitude)	1.00	>90 km z: 22.7 m/s m: 20 m/s
z – zonal		90-60 km z: 12.8 m/s m: 9.3 m/s
m – meridinal		60-0 km z+m: 20 m/s ; angle 15°
Ejection Mechanism		
ejection velocity	3.09	-10% to 5%
IP/OP-angle at ejection	3.09	±5°
Measurement inaccuracies (measurement & filter noise)		
barberpole turns n	3.09	±0.1%
tether length/velocity	3.09	±2%
S/W & H/W limitations		
-		no disturbance
Orbital parameters (Foton nominal orbit insertion and measurement errors)		
perigee/apogee altitude	3.09	±500 m
inclination	3.09	±0.01° (±900 m)
true anomaly	3.09	±0.18° (±15 km)
Deployer platform mass		
m_{Foton}	3.09	±50 kg
Telecommand-time inaccuracy		
$t_{ejection}$	3.09	disturbed via true anomaly
$t_{2ndstage}$	3.09	±1 s
Re-entry capsule properties		
drag coefficient	1.00	±0.05
lift over drag	1	±0.01

Table 50. *Disturbances applied for MC-simulation*

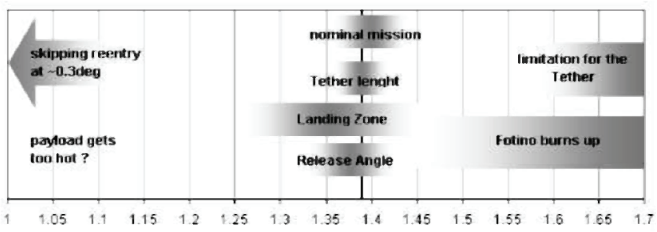

Figure 169. *Ranges for re-entry angle in degrees of Fotino capsule (by M. Stelzer)*

5.6 Closed-loop deployment testing

A series of flight-representative system validation tests has been performed on the various iterations of deployer hardware design and software (Table 39), using the deployment test rigs described in Section 5.2.2. These validations have three distinct objectives. Firstly the system functionality is to be demonstrated through a representative range of deployment conditions, including sensors, interfaces and dynamic interactions between the subsystems. Secondly, the control performance and robustness, rather than being determined from simulation only, is to be verified in actual deployment. Thirdly, any unexpected differences between deployment test and simulation will have to be studied to eventually make both as realistic to flight conditions as possible. A better understanding of the representativeness of both simulation and test rig shall allow to define a more effective test program, reducing the need for actual deployment testing and relying on less costly simulations and emulator tests where possible.

The second and third objectives in particular require a real-time test rig, with the deployment velocity responding (in closed-loop) to the friction as generated by the deployer hardware, in a manner similar to that in space. To this purpose, the test rig is coupled to a real-time tether simulator, see Section 5.2.2 for details. Tests using this facility are referred to as “closed-loop deployment tests”.

The focus of most of the tests is on the first stage, the low-tension low-velocity deployment to the vertical, since this is the part most sensitive to system friction deviations and therefore the most challenging from a control point of view. Some second stage deployment tests have also been performed. They have their own particular challenges, such as high deployment velocity, higher brake pole temperatures due to higher friction levels, and, as a practical consideration, the need for a near full-length tether.

5.6.1 First stage deployment tests using the TSE unwinding rig

These early closed-loop deployment tests have been performed on breadboard deployer equipment in the context of ESA's Tether System Experiment project (TSE) [Kruijff 2001.II, Kruijff 2001.III]. The TSE reference mission is based on a 45 kg re-entry capsule that is ejected by springs in downward-backward direction from a Progress-M vehicle at about 1 m/s. It is subsequently deployed from a 7-kg, 35-km long Dyneema® tether. The barberpole function is performed by a simple breadboard system, Figure 170. The canister in use is cylindrical with conical top, similar in dimensions to the SEDS canister as featured also on the YES (Chapter 6). The hardware has been placed into the TSE unwinding rig (Section 5.2.2). The two-stage tether deployment is based on the StarTrack approach [Ockels 1995, Heide 1996.I]. It includes Levin's first stage, set to 3.3 km and with its parameters optimized by genetic algorithms. The first stage is followed by a 60 degree forward second stage deployment, smooth end-brake and swing-back to the vertical, near which the tether would then (in an actual flight) be cut. The closed-loop control is based on the Energy Feedback (Section 5.5.4). An intentional worst-case ejection velocity error is

applied of 3% (0.97 m/s in stead of 1 m/s). During the first tens of seconds, as the velocity filter is collecting information, no feedback is applied.

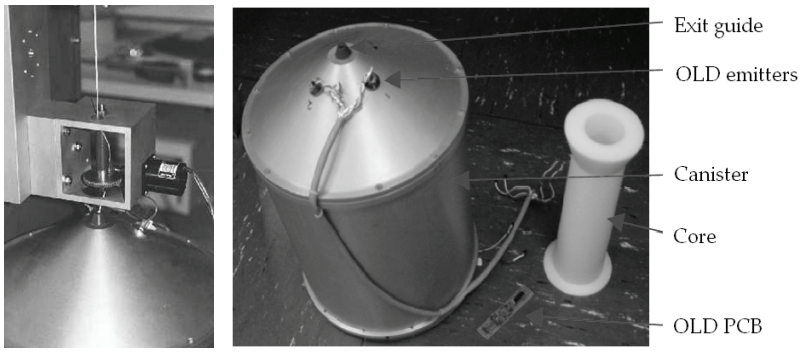

Figure 170. *TSE breadboard hardware*

In Figure 171-Figure 176 a set of first-stage test results ("RTS") is plotted against the data from the reference file ("Ref"). In Figure 171 and Figure 173 the length and the in-plane angle are depicted respectively. The in-plane angle is the result of the real-time numerical simulation of the tether deployment based on the measured tension. Both graphs indicate an adequate performance of the deployment system and the controller, especially taking into account the data displayed in Figure 175 and Figure 176. In Figure 175 the tension is plotted against the reference tension. The noise in the barberpole-induced friction can be noted, although the average tracks the nominal profile. Figure 176 shows the required barberpole turn corrections, or the commanded number of turns versus the reference profile. Since the reference length profile is generally followed rather nicely, Figure 176 provides a good measure for the barberpole brake model errors as from 1500 s. As the velocity starts to decrease in the final 1000 s of deployment, the barberpole effectiveness seems to have decreased, and a corrective additional 1.5 turns is required to maintain the nominal deployment profile. This relatively sudden decrease in effective friction may well be related to the oscillations in actuated deployment velocity observed in this period.

During the first 1500 s the velocity of the deployment reveals a relatively large oscillation. The feedback then overcomes this start-up problem (Figure 173). The same behavior shows up in pretest simulations (compare Figure 173 and Figure 174). The overshoot is therefore considered to be a result from the initial errors combined with a local lack of feedback effectiveness. Apparently the inertia driven part of deployment requires a feedback different from the remainder of the first stage. This type of initial overshoot has prompted the development of a feedback with varying feedback parameters (Section 5.5.4).

Despite the initial overshoot, and just as in the simulations that have been run in the pretest investigation, the velocity error can be kept under control and the final length error remains in the order of meters. The congruence between simulation and test suggest that the Monte Carlo disturbance modeling gives a good indication of the performance of the actual hardware.

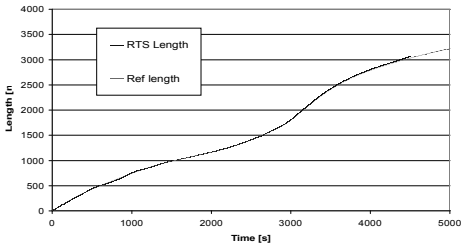

Figure 171. *Deployed first stage length vs. reference (TSE)*

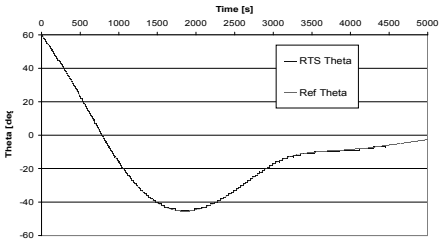

Figure 172. *Deployed first stage in-plane angle vs. reference (TSE)*

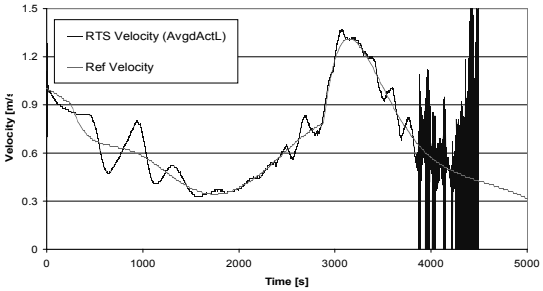

Figure 173. *Deployed first stage velocity vs. reference (TSE)*

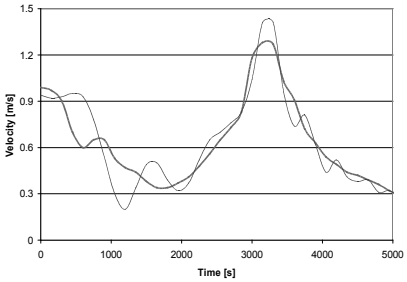

Figure 174. *Deployed first stage velocity vs. reference (MC simulation)*

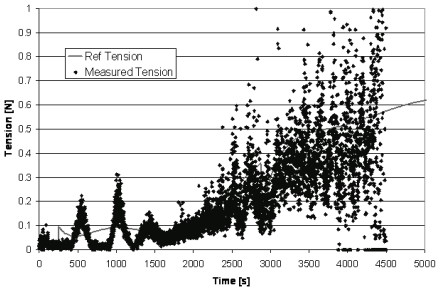

Figure 175. *Measured tension (TSE)*

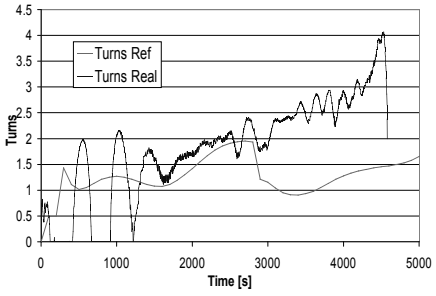

Figure 176. *Barberpole turns actual vs. reference (TSE).*

At the end of the deployment after 3880 s, again oscillations start sweeping up in the simulated deployment velocity, this time with a much shorter period of about 6 s. Although the deployment accuracy is not noticeably affected, it has led to a manual abort of the test as the oscillations cause the deployment to alternately halt (or even drive backward) and increase strongly, several hundreds of meters before the nominal end of deployment.

At first the resonance is thought to be one between the simulated tether spring-mass motion (due to the simulated tether stiffness *EA*) and the control of the unwinding wheels in the test set-up during the braking phase. The identification of this problem leads to a reevaluation of

an important simplification of the tether test rig software. The deployment velocity as commanded by the simulator to the TSE version of the test rig includes -not realistically- also the strain rate of the tether. A more realistic test set-up actuates only the velocity at which the tether is deploying from the canister, and not include the strain rate. The strain rate is nevertheless included to make the commanded velocity more smooth. At low velocities or at steep deceleration this decision can have an impact. For example, if the deployment has stopped, any residual oscillation of the endmass on the tether will unrealistically be translated into a commanded deployment with alternatingly positive and negative velocity. Now in this first test, the period of the deployment velocity oscillation of 6 seconds happens to be comparable to the longitudinal oscillation period of a 3 km tether with an EA = 5000 N and 46-kg endmass. It is therefore expected that simply an EA increase by a large factor, to e.g. 100,000 N, will solve the problem in a next test. However this is found not to be the case. Another mechanism for the resonance has therefore to be identified.

Closer inspection of the test rig controller data reveals that a control system resonance starts already earlier, right after the deployment peak at 3200 s into deployment, affecting the actuated deployment velocity, minutes before the simulated deployment velocity itself starts to oscillate.

It is necessary here to explain a bit more the unwinding rig's philosophy for deployment velocity actuation. The real-time tether simulator calculates the deployed length and deployment velocity based on the tension input. The control software of the unwinding motor drive has as its task to command the speed of the rig's flywheel to match as accurately as possible this simulator deployment velocity output. The flywheel inertia makes it impossible to follow any commanded velocity precisely (Section 5.2.2). It is therefore commanded with the help of a feedback loop. The drive's encoder returns to the control software the velocity as actuated and the number of rotations of the take-up rollers, such that the actually deployed length can be determined. In order to minimize the accumulation of deviations between actually deployed length and deployed length in the real-time tether simulator, a correction is applied to the commanded velocity.

Figure 177 shows the actuated velocity, the simulated velocity and the commanded or requested velocity that includes the length correction. The implementation of the length correction appears to cause a peak in the control to appear in a cyclic manner. The flywheel's large inertia combined with these corrections makes the system's velocity oscillation sweep up, even though the simulated velocity is still smooth.

It can be imagined that at first the actuated deployment oscillation has little effect on deployment tension and therewith little effect on simulated deployment. However it seems that under rapid velocity oscillations, the barberpole became less effective, leading to larger number of turns and larger noise in tension, eventually around 3880 s impacting the simulated deployment velocity and strain rate in resonance, possibly with each other, but in any case with the actuation system.

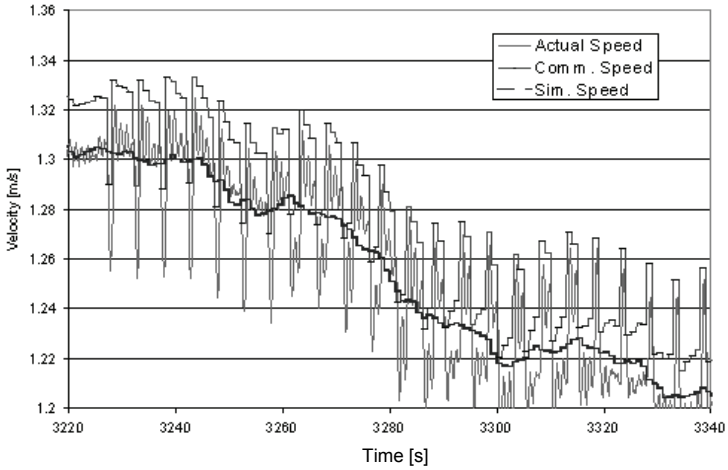

Figure 177. *Different Hardware Control Speeds Leading to Resonant Oscillations in the Test Rig. The smoother curve is simulated, the top curve commanded.*

Although the test has been aborted at 93% of the target deployed length due to aforementioned test-rig related resonance, the data shows that the deployer hardware and feedback, despite being pestered by the eventually highly irregular deployment, is still able to control the deployment and keep errors within 20 m or 0.65% of length, and a fraction of a degree (in-plane angle).

5.6.2 First and second stage tests on YES2 unwinding rig

Test rig improvements

Based on the lessons learned with the TSE unwinding rig, as well as the added requirements of mobility and tether recoverability a completely new, more compact and lighter unwinding rig has been developed. The flywheel, with its inertia issues is replaced by a godet (Section 5.2.2). Although the TSE experience has shown that the vertical canister set-up (Figure 92) provides a tension profile over the course of a single unwinding of a loop that is hardly affected by gravity [Kruijff 2001.III], for compactness the new test rig uses a horizontal spool configuration. It has been verified to work sufficiently well. The initial feedback overshoot is tackled by implementation of a new, simpler feedback with variable gains (Section 5.5.4, Eq. 5.38). The simulator algorithms (Section 2.3) are adapted to allow for a decoupling between deployment velocity (applied by the test rig) and strain rate (calculated by the simulator).

The deployments described in this section have been performed with breadboard versions of the YES2 barberpole, On-Board Computer (OBC), OBC software and OLD electronics, and with the TSE canister. They are performed in an early stage of spool development (see also Section 5.3.3). Due to, at this time, still unresolved limitations in the winding machine measurement system, length estimation of the windings is about 1% accurate. For the

improved generations of winding machine and spools, an accuracy of 0.1% has since been achieved. Closed loop deployment tests on these improved spools have been performed using the flight hardware Engineering Model (Table 39, Section 8.1.4), but are not reported here.

First stage deployment, undisturbed

Seven undisturbed closed-loop deployment tests are performed assuming an endmass of 12 kg and with a 32-km tether length. The outer 4.8 km are wound at 4 turns per cycle. A typical result (Test 015) is presented here. For the initial test no intentional disturbances are introduced. This means that the initial velocity is nominal, spool and pole parameters in Eq. 5.30 are selected to match the characterization tests and (simulated) tether properties in the test are identical to those used during determination of the deployment profile and feedback parameters.

A deployment to a (simulated) vertical orientation has been achieved (Figure 178, Figure 179). As a result of the modifications in the feedback, no longer an overshoot in the early deployment is created. Deviations from the reference profile remain very small. The tether deployment is initially stopped at the exact target length (better than 0.1%) at $t = 5900$ s. However, as the test rig's unwinding machine is stopped, the tension becomes slack on the tensiometer and provides no more signal to the real-time simulator. As a result the test rig is commanded to deploy further. This continues for some tens of meters, Figure 181b. At the conclusion of deployment, the (simulated) in-plane angle is librating by just 0.2°, and clearly less than the 3° target. The same value of 0.2° is also found as average final libration angle for all further undisturbed tests. Also the velocity follows the reference profile very closely. The velocity oscillation around $t = 3600$ s can be attributed to an irregularity in the spool. During the final gradual deceleration at the end of deployment, velocity is very low, and the velocity error therefore is also very small (<0.04 m/s). In fact it is not enough to trigger sufficient feedback (Figure 181b). Also, at this very low deployment velocity of only centimeters per second, the OLD's have been sometimes observed to fail to register a tether passage.

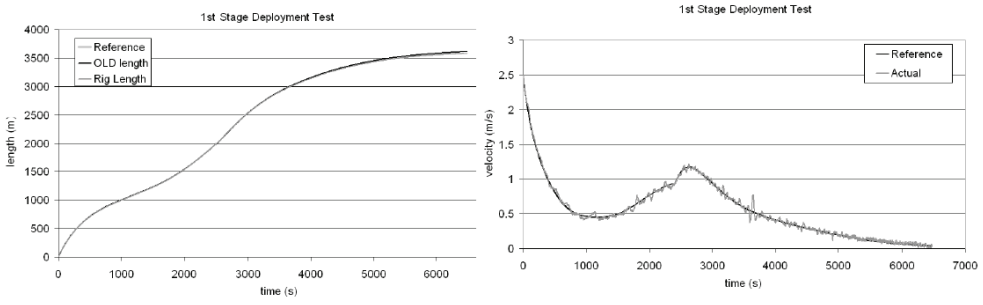

Figure 178. *First stage deployment test (closed loop control) length and velocity vs. reference*

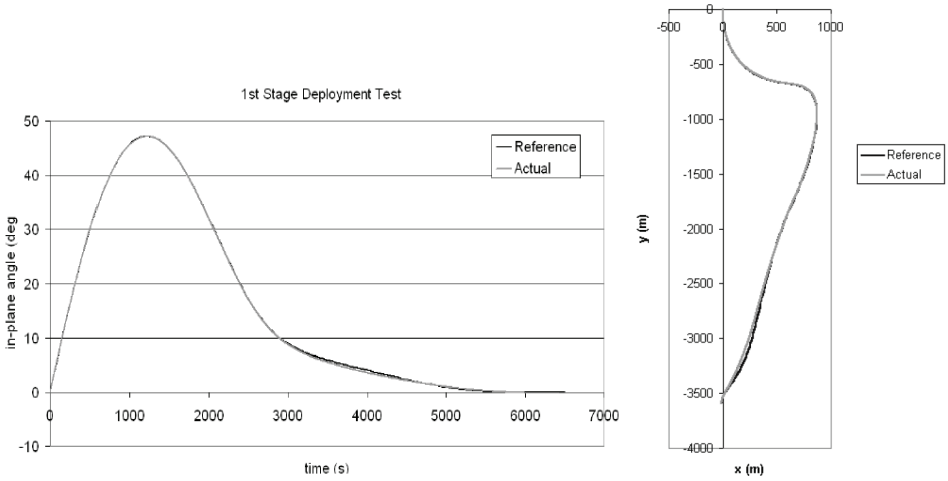

Figure 179. *First stage deployment test (closed loop control) simulated in-plane angle and LHLV trajectory*

The tension noise can be seen to increase with tension and at lower velocities, Figure 180. The barberpole position required to follow the nominal profile deviates generally less than 0.5 turns from the nominal profile based on hardware characterization. At velocities from 0.5 m/s down to 0 m/s up to a full additional turn is required, suggesting that the friction coefficient reduces at low velocities.

The (simulated) transverse tether motion can be observed from Figure 181a, where the in-plane angle of various points on the tether are compared. The transverse wave have an amplitude of no more than 0.3° and a period of about 250 s, as predicted by Eq. 2.19.

Near the end of deployment (5700-5900 s), tension oscillates in about 27 s periods, equivalent with a winding cycle of 4 loops of about 75 cm each. As the velocity reduces, the period for unwinding of one winding cycle becomes longer. The velocity oscillates 90° ahead of the tension. In this case both deployment velocity and strain rate contribute in harmony and about equally to this oscillation. What is shown in the figure is only the deployment velocity. The barberpole develops smoothly at this time, and does not resonate with the deployment oscillation.

Both the strain and endmass deceleration are a direct result of the friction. Any new friction level is introduced within seconds over the (relatively short) length of the tether, being translated into an increased strain with help of the endmass inertia, or a reduced strain through additional extraction of some centimeters of tether from the canister. The resulting tension then controls the deceleration of the endmass. At very low endmass velocities it is possible that it takes a while before enough strain is built up to overcome the friction and a partial or full spring-mass motion follows. (Note for comparison that a pure spring-mass oscillation at zero deployment velocity would have a period of about 20 s with maximum 4 cm/s strain rate amplitude, Eq. 2.17). Deployment velocity and strain rate can thus alternate as components of the motion of the endmass.

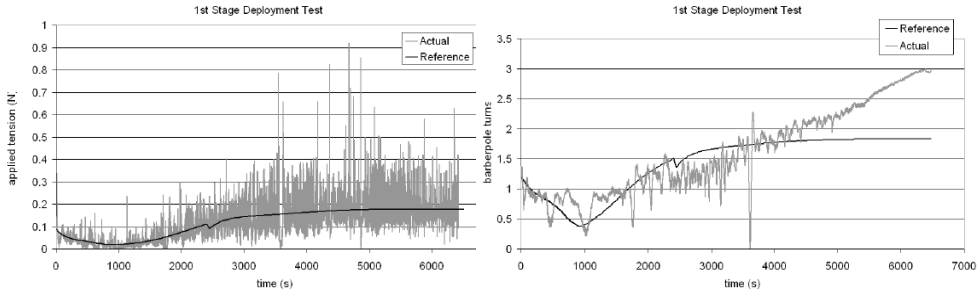

Figure 180. *First stage deployment test (closed loop control) tension and barberpole position*

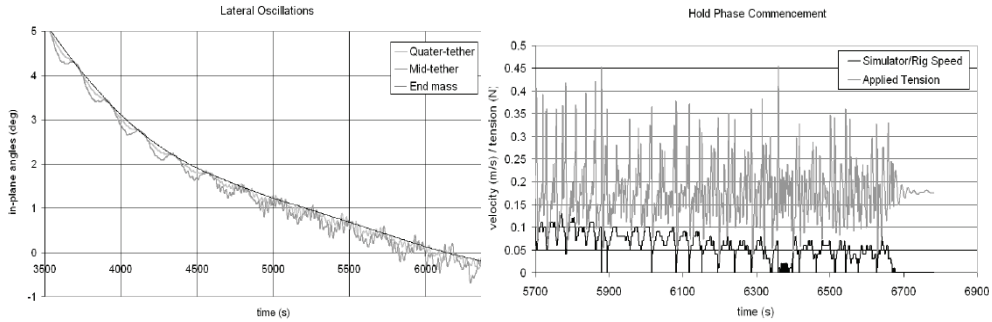

Figure 181.*First stage deployment test (closed loop control) simulated tether oscillation (a.) and behavior during final deceleration (b.)*

Based on the results of the undisturbed closed-loop first stage tests, a number of system improvements have been introduced.

- The observed velocity irregularity has prompted further development of the winding machine's precision (Section 5.2.1).
- The unrepresentative, *staccato* continuation of deployment by some tens of meters after first stage completion, caused by a slack tether on the tensiometer, has triggered a revision of the test rig software. It improves the rig's functioning as it keeps the tether under tension during the hold phase, by applying a very low (and for all purposes negligible) velocity of 2 mm/s. In this way the tensiometer can determine the friction level and the simulator can reproduce the deployment stop (and restart) more realistically.
- Because of the lack of feedback at very low velocities at the end of the first stage, it is recommended to raise the feedback parameters near the end of deployment. To make sure the flight OLDs can deal with very slowly moving tether, specific tests have been performed and OLD placement with respect to the passing tether has been improved (Section 5.3.2).
- Following the observation of low barberpole effectiveness at low velocities, an adjusted friction model has been developed (Section 8.1.1).

First stage, disturbed

To evaluate the robustness of the deployer, some tests have also been performed with several parameters in the space simulator and controller altered, with respect to the values as used to prepare control parameters and reference trajectory. A heavily disturbed case, Test 011, is here discussed, based on the following disturbances:

	Controller/reference file	**Actual (test rig simulator/deployer hardware)**
Orbit altitude [km]	300	290x280 km
Exospheric temperature [°C]	1000	600
Ejection angle	0°	10°forward from local vertical
Friction coefficient	0.3	0.25
T_0	0.03 (from t=500-1000 s)	0.01

Table 51. *Environmental disturbances purposefully introduced for Deployment Test 011.*

The resulting deployment is satisfactory and matching simulations with similar disturbances. Final libration is approximately 5°, well within the approx. 10° libration required for sufficiently accurate landing (Section 5.5.5) and primarily caused by the initial ejection angle error. There is no feedback to in-plane angle as such, and any initial error will thus not be actively controlled away, although the error is nevertheless dampened, particularly for backward ejections. Length overshoot is just 0.3%, well within the allowable 3%.

The large error in minimal deployment tension (a factor 3), introduced at a critical time, causes the deployment to come to a complete halt, despite the barberpole turning down to zero. The deployment however recommences and reacquires the reference profile smoothly. Some oscillatory behavior is visible, related to imperfections in the velocity filter of the controller. Further tests show this matter resolved, e.g. Test 032, Figure 183b. For Test 032, T_0 = 0.02 instead of 0.01, measured friction is increased by 3σ, a 5° forward ejection error has been introduced and initial velocity is 2 m/s rather than 2.5 m/s.

Hold phase

After the first stage, when the deployment has been stopped by the controller with the minimal amount of turns possible, the hold phase algorithm is activated. This algorithm is designed to trigger a small increase in barberpole turns whenever the OLDs register the unwinding of a new (and undesired) tether loop. This algorithm may lead to accumulation of wraps of the tether around the barberpole brake. Before the start of the second stage, these accumulated wraps need to be unwound. The pole will turn back and the present gravity gradient (about 0.18 N) should now extract the freed length of tether around the pole, without the unwinding wraps untangling.

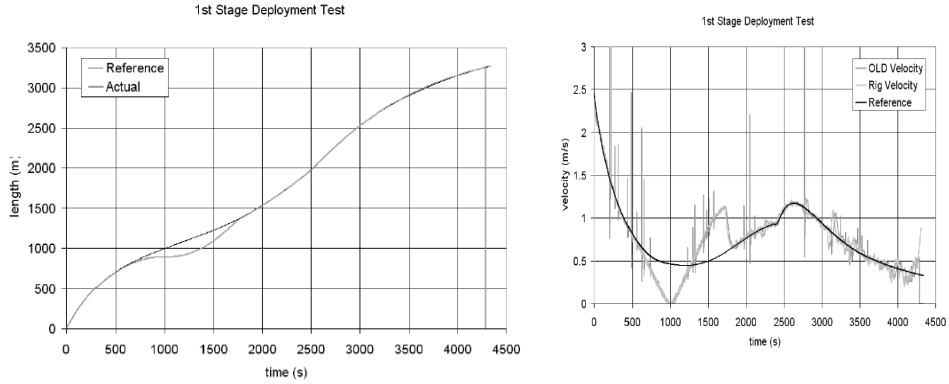

Figure 182. *First stage deployment test (disturbed, closed loop control) length and deployment velocity vs. reference*

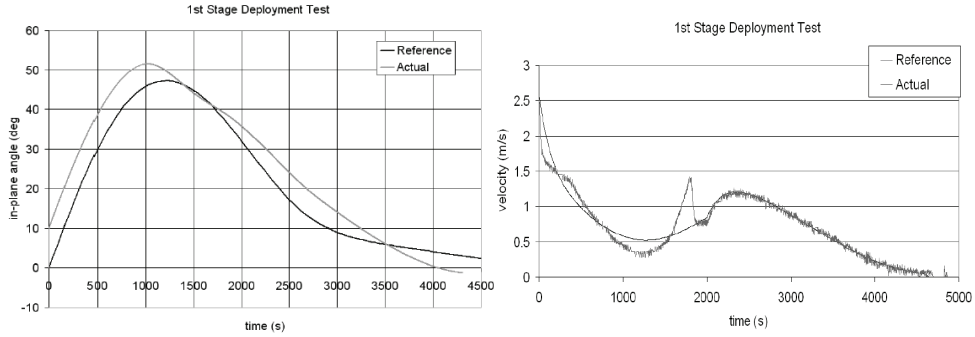

Figure 183. *First stage deployment test (disturbed, closed loop control) simulated in-plane angle and Test 015 deployment velocity*

The behavior of the tether inside the canister during the hold phase, as well as the unwrapping of accumulated loops on the barberpole have both been tested in a parabolic flight campaign. The tether inside the canister is observed to remain calm and does not oscillate in front of the OLDs nor does it spontaneously deploy. Slowly unwinding loops are correctly registered by the (now improved) OLD system. Up to eight wraps of tether around the barberpole can be consistently unwound without entangling. As additional margin the maximum allowable number of accumulated loops during the hold phase is recommended to be set to six.

The end of first stage, hold phase and start of second stage have also been tested in closed loop on the test rig, using the YES2 flight design's Engineering Model. The deployment is smoothly stopped at the end of the first stage, keeps still and is restarted quickly into the second stage (Figure 184).

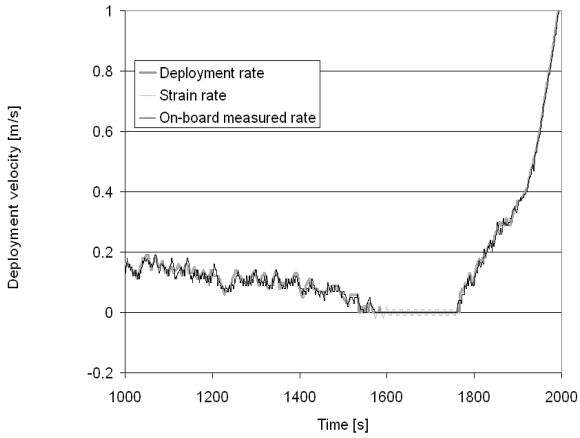

Figure 184. *Deployment velocity and strain rate near hold phase*

Second Stage test

During the second stage of deployment, the gravity gradient is already large enough to provide ample margin for control. Still, this stage has its own challenges. Some closed-loop second-stage deployment test have been performed, some partial and one full, both undisturbed and disturbed, in order to confirm the behavior of the system and the control ability at high velocities. Also the barberpole's ability to decelerate the endmass effectively is put to the test. It should not cause strong oscillations nor show any overheating that may cause a melting of the tether.

The results of the full deployment test are presented in Figure 185-Figure 187. Generally speaking, the deployment is smoothly controlled. There is a small error in actually deployed length of 0.3% (caused by OLD failure) vs. the target of under 3%. The tracking of the in-plane trajectory is better than 0.5° (vs. the target of under 5°). The on-board measured length deviates less than 0.1% from the nominal length. The required barberpole braking deviates generally less than 0.5 turn from the nominal, Figure 185b. The plots show some features of interest however.

Most importantly, the test has actually been performed in two parts due to a test rig software memory overflow at 1600 s (the failure has since been solved). The recommencement of the test has required a new initiation of the both the test rig's simulator and the deployer's on-board computer. Both need to continue from a state that matches, as well as possible, the final state of the previous test. Unavoidably, the restart includes some distorted initial conditions. The test rig needs to ramp up from zero to 8 m/s, due to which an inaccuracy of initial length of 150 m is introduced (unintentionally). The latter explains the controller's action towards velocity undershoot from 1600-1700 s. These significant disturbances are however controlled away.

For most of the deployment the tension is smooth and follows the barberpole turns nicely. After t=3200 however, an oscillation is seen, even though the barberpole turns develop

smoothly. The oscillation is not a control resonance, but a direct result of transition from criss-cross to parallel winding. The tension effects discussed in Section 5.3.6 come into play. At high velocity the ball effect dominates, but as the deployment slows below 1 m/s, the tether starts rubbing the spool, and the hard-layer/easy-layer effect takes over. Note that the core flange is hardly exposed so has little impact. These irregularities demonstrate the value of a closed-loop test with real hardware.

Despite these real-world oscillations, the strain rate remains at the level of centimeters per second with a maximum near 3470 s of about 40 cm/s (not shown here). It will thus have little effect on the deployment and control, and based on such a deployment the swing can be expected to show few tether oscillations. During most of the deployment, the feedback does not respond heavily to the natural oscillations in tension such that the reference profile is well maintained. Near 3500 s the velocity drops too much and the feedback kicks in. A recommendation could be to avoid the parallel section for the nominal deployment, to reduce the cyclic trends in tension by e.g. a larger core cone angle (Section 5.3.6) or to take them into account in the reference turns definition, the latter being a more risky option.

The OLD velocity filter generally performs well but reveals an issue too. The rig's applied velocity significantly exceeds the deployer's measured velocity between 2500 and 3000s. This deviation could either be because of slip of the tether on the test rig drive or because of a failure of the breadboard OLD sensors. Data analysis suggests that the cause is misalignment of (primarily) one of the two OLD's, and malperformance in about 2% of the passages. The missed loops cause an irregular measured velocity which the controller attempts to maintain around the nominal profile. As a result, temporarily, the actual deployment deviates significantly from the reference. Note that, during the steep deceleration, the OLD filter estimate, which is essentially a weighted average, runs behind on the actual velocity, but no control resonance is caused by it, Figure 188.

An earlier high velocity test using the TSE breadboard barberpole brake has led to melt of the tether, indicating a pole temperature of around or above 150°C (Kruijff 2001.III). This is one of the reasons that the brake has since been redesigned (Section 5.4.2). The temperature of the YES2 breadboard barberpole is verified in this test. It does not go above 30°C during the braking (ambient temperature 21°C) thus there is little worry of tether melting during the deployment, Figure 187b.

Finally, a disturbed second stage deployment is performed, see for disturbances as applied, Table 52, and for the results, Figure 189.

	Controller/reference file	Actual (test rig simulator/deployer hardware)
Orbit altitude [km]	240 x 280	234 x 286
Exospheric temperature [°C]	800	920
Ejection angle [°]	0	10 (forward from local vertical)
Friction coefficient f [-]	0.35	0.25
Minimal deployment tension T_0 [N]	0.01	0.01
Stiffness EA [N]	6000	4440
Inertia multiplier I [-]	3.7	3.1

Table 52. *Environmental disturbances purposefully introduced for second stage deployment test.*

The acceleration at start of the second stage is significantly faster than nominally planned because of the very low barberpole position in the nominal file. The error is however slowly corrected. Again, around the same point in the deployment, the OLD seems to miss loops erratically or possibly slip occurs on the unwinding wheel, leading to control noise. The test is eventually stopped due to a technical malfunction in the test rig's tether recovery part.

Improved outlining of the OLD's and subsequent testing at 18 m/s appears to have solved the OLD sensitivity issue. Furthermore it is recommended to have a set-up with three OLD's rather than two (Section 5.3.2). An algorithm to deal with just a single OLD (and thus a double OLD failure) is also recommended and included.

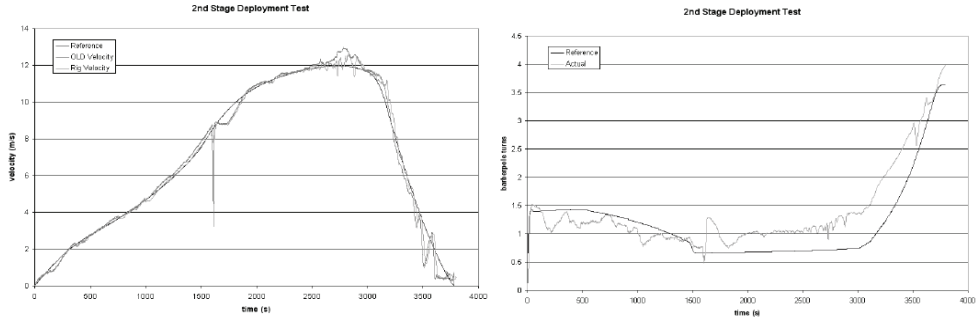

Figure 185. *Second stage deployment test. Left deployment velocity vs. reference. Right brake control, reference versus actual. The spike at* t*=1600 s test results from a test stop and restart.*

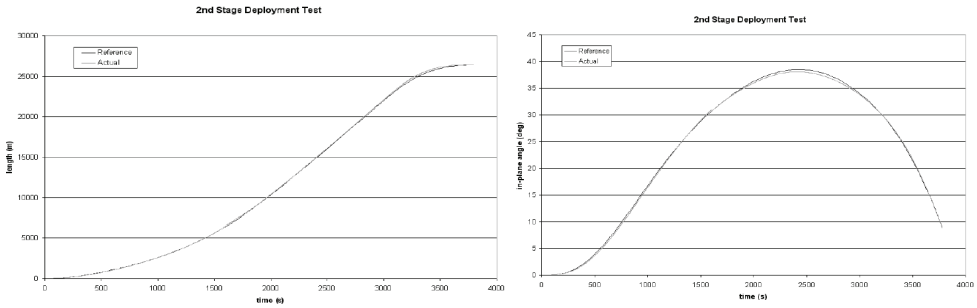

Figure 186. Second stage deployment test. *Left deployment length vs. reference versus achieved. Right simulated in-plane angle vs. reference.*

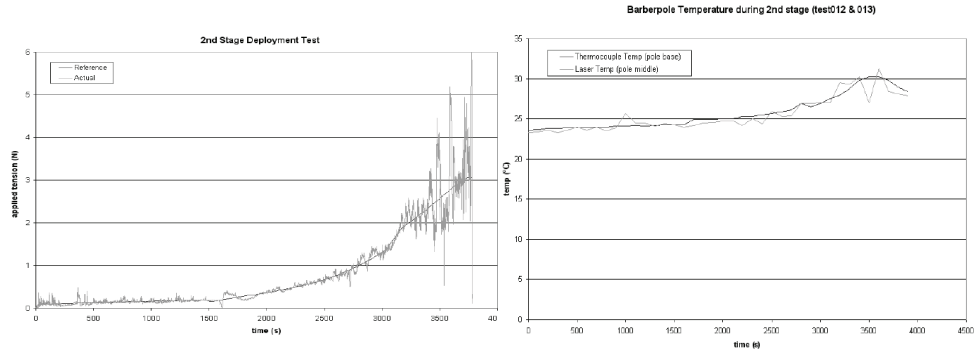

Figure 187. *Second stage deployment test. Left deployment tension vs. reference. Right barberpole temperature measurements.*

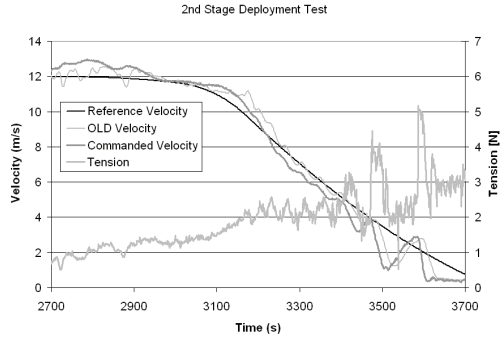

Figure 188. S*econd stage deployment test. Zoom on deceleration, controller velocities and tension.*

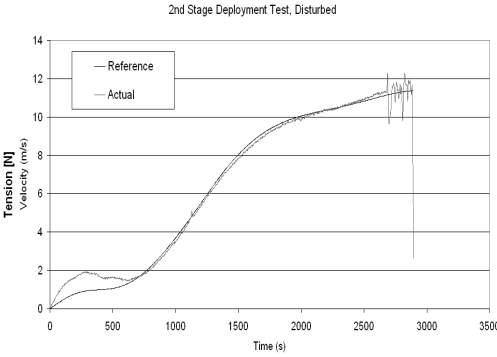

Figure 189. *Second stage deployment test disturbed. Deployment velocity vs. reference.*

5.6.3 Discussion and Recommendations

The real-time closed-loop deployment tests have involved the actual deployment hardware and control software, and a new level of realism has been achieved for tether deployment ground tests. This is considered to be of significance, as tether deployments cannot easily be evaluated on ground, and flight experiments for the sake of technology development have been found to be forbiddingly costly (Section 1.3).

The tests have been technically successful for various reasons. Controllability of the two stages of deployment as well as of the hold phase are confirmed. Disturbances have been artificially introduced to the system, e.g. by changing the simulated environment with respect to the environment that has been used to develop the control. System response remains within the 3σ-performance range as defined by simulation only (Section 5.5.5), and in general response was akin to simulated performance. Other disturbances have been unintentionally introduced by the hardware, particularly tension irregularities of the winding (since removed) and cyclic behavior for the parallel winding (now mostly avoided for nominal deployment). No deployer system resonances have been encountered, and (simulated) strain rates remain low even in case of steep deceleration at the end of the second stage, so the risk of such resonance is judged to be small.

A number of deployer system improvements has been implemented as a result of the observations. In particular, the OLD performance is found to be critical, which in the TSE breadboard has not been all that stable. The YES2 deployer design shows no such problems. Feedback gains have been tailored to deal with the recognized issues and the barberpole friction model has been adjusted. The winding machine has also been improved based on unwinding results, e.g. the length measurement precision has been improved by an order of magnitude.

The test rig itself has evolved through two major developments, and now allows mobility, recovery of the tether for re-use and a prompt low-inertia response to velocity changes. With the unwinding rig v2, for example, parabolic flight tests could be performed, and a second stage deployment test, interrupted due to technical issues at a deployment velocity as high as 8 m/s, could nevertheless be successfully restarted and completed. The unwinding rig has undergone a multitude of incremental improvements, such as more proper commanding of deployment velocity to the motor drive. One of the latest adjustments allows the facility to deal better with static conditions, such as the hold phase and transition to the second stage.

Part III – *The Young Engineers' Satellites*

Поехали! (Poyekhali!)

— Yuri Gagarin's plain words on the launch pad, 'off we go!'

Experimental data show that the cable successfully deployed to its full length of 31.7 km (19.7 miles), the longest manmade structure ever deployed in space.

— Guinness Book of Records, YES2 entry, 2009 edition

Part III of this thesis describes the YES (1996-1997) and YES2 projects (2002-2007). It discusses the lessons learned that are relevant for future tether and innovative experiments, and concludes with the analysis of the YES2 flight data.

6 The First YES Satellite

The engineer of tomorrow should excel in only three things: creativity, initiative and responsibility.

— First Dutch astronaut Prof. Dr. W.J. Ockels to his students, 1994

In October 1997, the second Ariane 5 qualification flight A502 launches the Young Engineers' Satellite (YES) as one element of TEAMSAT (Technology, science and Education experiments Added to MaqsatH). The other element is called TEAM and contains four further experiments (FIPEX, AVS, VTS & ODD). TEAMSAT is a 350-kg experiment box mounted to Ariane 502's upper dummy satellite MaqsatH. TEAMSAT has been conceived and built within only 8 months.

In orbit, good data is obtained from most experiments. However, the tether deployment cannot be performed and other failures occur as well. These problems are partially due to factors beyond control of the development team or the result of engineering issues but can also be attributed to lacking communication and cooperation within the team.

YES experiment	Objective	Main components
Tether	Rotating tether in GTO for controlled momentum transfer	Double strand tether, SEDS canister (incl. 2 optical loop detectors), barberpole brake and Airtec tether cutters, Tether Orbit Insertable (TORI) with autonomous tether cutter, ejection system, absorptive tether, Joris! (OBC), ranging S-band transponder (Olympus engineering model).
Commercial Technology	Evaluate use of commercial technology in GTO. Take images of tether and barberpole brake	Powerdwarf PC104 (back-up OBC), two adapted QuickCam CCD cameras.
Accelerometers	In-orbit demonstration of MEMS technologies (maiden flight)	Triad 442T (2x) (LIGA and Si sensors), connected to Joris!
GPS	First reception of GPS signals from below local horizontal	Adapted Trimble Tans II, connected to PC104 and Joris!
Sunsensors	Student-built attitude determination system	2 Units connected to OBDH (ESTEC developed On-Board Data Handling System)
Radiation experiment	Technology demonstration	Scintillating Fibre (maiden flight) & RadFET (for reference), connected to OBDH

Table 53. Overview of YES experiments and related components

6.1 YES and its objectives

YES has been proposed by Van der Heide & Kruijff at the International Astronautical Congress (IAC) in Beijing in October 1996, adding functionality to the Ariane 502's dummy payload and featuring a tether experiment in Geostationary Transfer Orbit (GTO). The experiment consists of 2 autonomous satellites: the Young Engineers' Satellite (180 kg) and the 12-kg Tethered ORbit Insertable (TORI), Figure 190. YES has been delivered to ESA/ESTEC by Delta-Utec in May 1997, under joint sponsoring of ESA and the Dutch aerospace development agency NIVR. It contains 7 experiments, most of which have stand-alone value but together support scientifically or technically a 35-km tether deployment between YES and TORI.

The YES satellite contains the tether and has as its primary objective to investigate tether dynamics in GTO, and specifically the particularities of deployment and dumb-bell dynamics in an elliptic orbit. The GTO orbit has an ellipiticity of 0.72. The tendency of tethers to go into rotation above an ellipticity of 0.44 can be used for various purposes (see Sections 1.2, 2.2.1, 3). In case of YES the demonstration goal is a re-entry of the TORI endmass at near-interplanetary velocity. Further primary objectives are the study of endmass attitude behavior and demonstration of momentum transfer and endmass release technology.

Secondary objectives are to be achieved by further technology demonstration experiments. A GPS receiver has been included to study performance at higher velocity and higher altitude than the GPS system is intended for. Two types of radiation sensors are also added: a RADFET sensor, to measure ionizing dose in GTO behind thin shielding, and a Scintillating Fibre Detector to measure particle fluxes in GTO. A compact PC104 486 computer and two QuickCam web-cameras are integrated to demonstrate the use of commercial technology for short space missions. Finally, to demonstrate the applicability of MEMS technology for use in space, the newly developed LIGA/Si sensor technology is to be tested in the form of 3-axis accelerometers [O'Rourke 1997].

6.2 Mission design

YES, the Young Engineers' Satellite is contained inside the TEAMSAT box together with the Tethered ORbit Insertable, which is a 12-kg torus-shaped endmass (TORI), and TEAM, which contains the remaining experiments of TEAMSAT. The TEAMSAT box as a whole is mounted to MaqsatH, a 2100 kg cylindrical dummy satellite. Whereas YES carries the tether deployer, TORI is essentially a metal dish with only two subsystems: an autonomous tether cutter system added for mission safety, and an absorptive tether - a sort of deployable rod that serves to bring it outside the TEAM box.

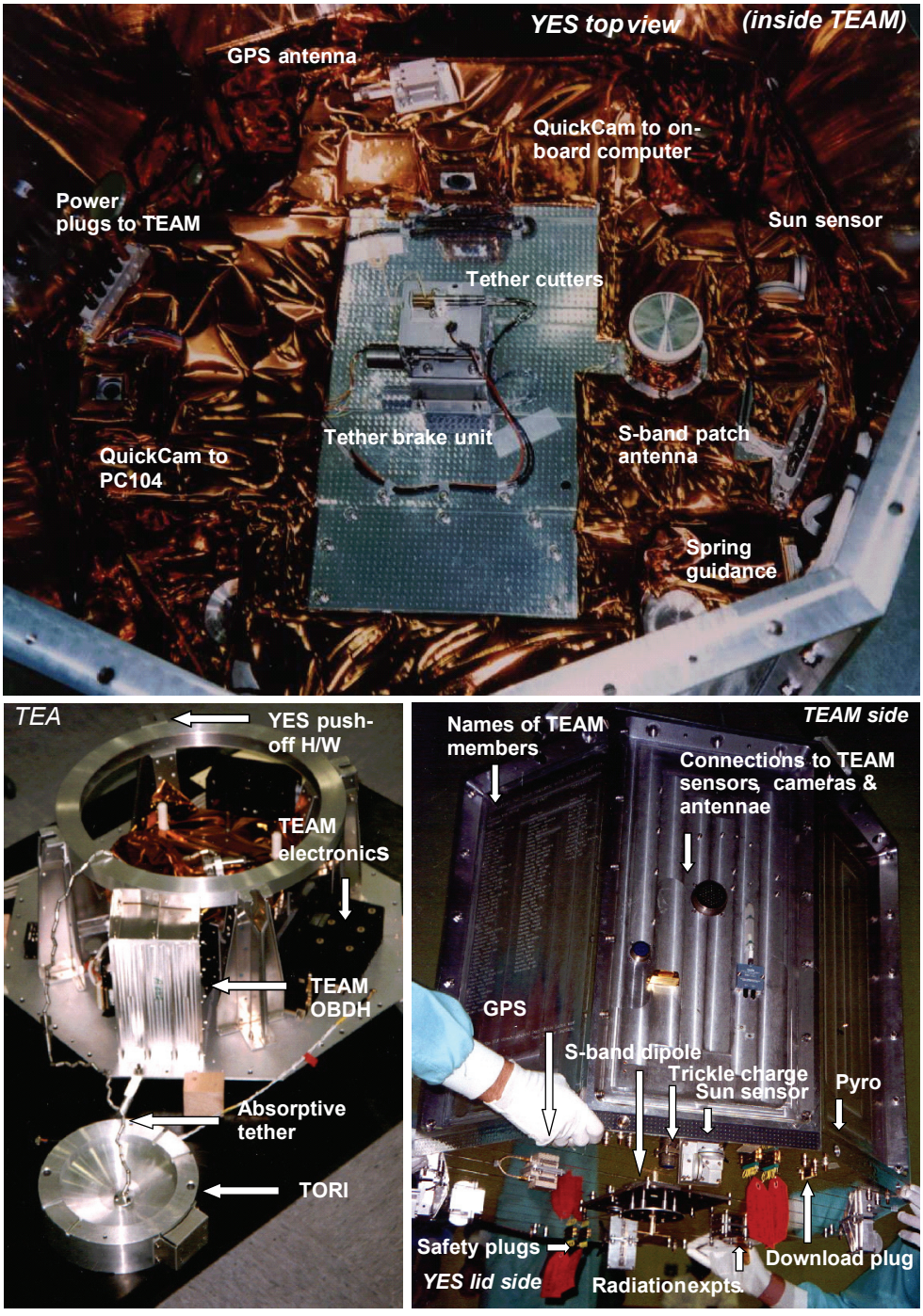

Figure 190. *YES and TEAM*

The tether mission is planned to start at a true anomaly of 90° with a backward downward ejection of the YES satellite out of the TEAMSAT box at 1.7 m/s, see Figure 191. Shortly after YES ejection also TORI is pushed out of the box by small springs and will be restrained by the absorptive tether. A deployment of the tether from YES will follow, aided by the gravity gradient forces, at a velocity fluctuating about an average of 2.5 m/s. In the first apogee after ejection, 15450 s after ejection, the deployment will be smoothly stopped as the tension drops due to the release of TORI from the box, by a cut of the absorptive tether attachment. This manner of smooth deployment stop minimizes the occurrence of tether slackness. The newly created tethered system, consisting of YES tied to TORI, will have an apogee and perigee altitude smaller than those of MaqsatH. The system will pick up an in-plane rotation during its pass through perigee as gravity gradient increases strongly. These rotations are prograde, i.e. in the direction of the orbit. Each rotation requires 50 minutes to be completed. Close to the apogee, a moment is selected when TORI is swinging backward with respect to the orbital motion. At this time the tether will be cut at the YES side.

The timing of the cut will be based on ranging measurements of the YES satellite. YES has a coherent transponder [Kruijff 1998]. Its ranging capability is used to determine the motion of the YES satellite, from which also the tethered system's center of orbit can be derived. If the tether is fully deployed, the distance between YES and the center of orbit is 2.9 km. The orbit of the tether system's center of mass can be assumed to coincide, approximately, with the orbit of a point mass. It is possible to reconstitute this orbit from integration and averaging of the YES motion. The range accuracy of the transponder is around 20 m. This suffices to determine the motion of YES with respect to the center of mass. The tether is cut when three requirements are fulfilled. First, YES must be within a 75 minutes from apogee. Second, TORI should be at lesser altitude than YES. Third, the angle between TORI, YES and the local Earth direction must be less than 45 degrees. The latter two requirements are met if the transponder is at least 2.1 km higher than the system's center of mass. Three windows of each 12 minutes duration are available for each passage through apogee.

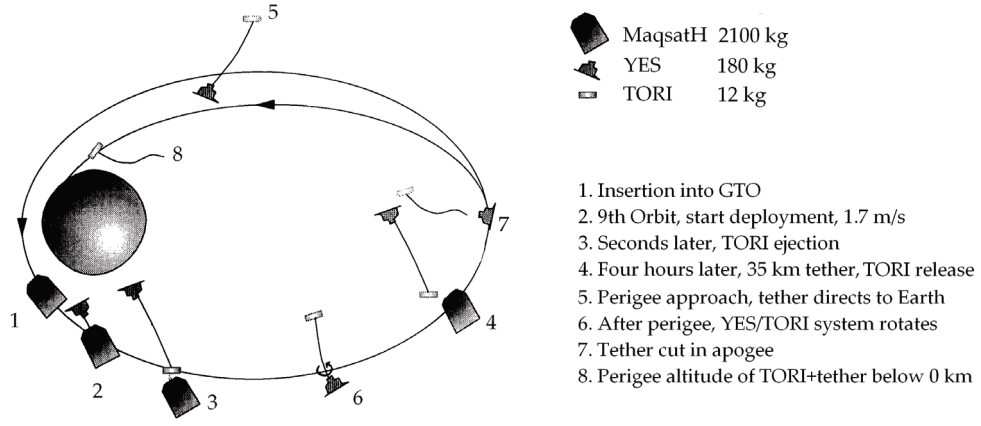

Figure 191. *The YES mission profile design*

6.3 Subsystems design

6.3.1 Tether and deployer subsystem

For the YES project, a SEDS deployer system could be made available on short term and has been selected for this reason. It includes a barberpole with tether cutters and a canister with two Optical Loop Detector (OLD) tether passage sensors integrated (infrared emitters/receiver pairs).

The 35 km tether itself is housed inside the canister and is detailed in Figure 192. The tether connects to TORI on the TEAM side through a 260-m long, 0.7-mm diameter Kevlar section, such that contact with a sunlit and hot TORI will not lead to tether melting. Due to the low foreseen tension loads of only a few Newton, most of the tether can be very thin. For micrometeoroid survivability and low mass, it has been manufactured as a double strand, Carroll Caduceus design, with stitches every 180 m, and a 1% excess length for the second strand (Section 4.3.1). Each strand is a 7x100 Dyneema® braid, with a rectangular cross-section. The last 10 meters to be deployed are again a more rugged single strand tether.

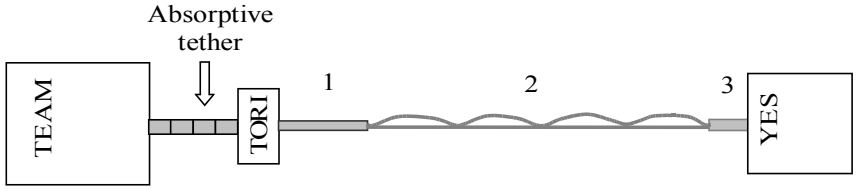

Figure 192. Y*ES tether design (see also Table)*

Segment	Tether segment design	Length [m]	Break load [N]	Melting point [°C]
1	1 strand 8x400, 0.7 mm Kevlar	260	450	425
2	2 strands 7x100 Dyneema® SK66	34750/35100	275/165	150
3	1 strand 11x215 Spectra	10	800	150

Table 54. *YES tether properties*

Table 54 provides an overview of the tether properties. Note that the longer strand within the double strand section is slack under normal conditions. Electrostatic forces are supposed to secure adequate separation between the strands. The industrial specification for the strand break strength is 240 N. Testing by J. Carroll provided a lower result of 165 N per strand. The shorter tether will under normal circumstances, carry the tension by itself. For loads above 45 N or a strain larger than 1%, the second strand will join in carrying the tension. Under break load (3.6% strain), the shorter tether will carry 60% of the tension, which results in a 275 N break load if both strands are intact.

The tether is wound tightly in criss-cross pattern around a hollow core, in total about 86000 loops. It is finally tied down by 3 knots located on the outside of the winding with about

2 m spacing, which need a 20-30 N tension jerk and 0.5-1.0 J to break. The winding is performed with pretwist such that at unwinding this twist is canceled out. The two strands have been positioned tightly together on the spool and, every 180 m, have been manually stitched together. The excess 1% length was inserted at this point, folded as a 90 cm loop and positioned next to the already wound part.

An open-loop deployment test of a 35-km long double-strand tether has been performed on an engineering model. No particular issues were observed. The OLD transition algorithm has been successful in identifying actual loops deploying and friction behavior of the spool and pole has been assessed (Section 5.2.4).

The Tethered ORbit Insertable, TORI, attached to the opposite end of the tether, is fixed between TEAM and YES by two pretensioned pyrotechnic bolts. Upon cut of the first bolt, a weak spring will eject TORI with 0.2 m/s out of the TEAMSAT box. A hollow on the TEAM-facing surface of TORI houses the so-called 'absorptive tether', that is tuned to absorb TORI's ejection energy as it extends to its full length of 1.4 m. TORI is then linked to the MaqsatH by this 0.8-cm link [Ockels 1987] that in effect becomes a rod and oscillation damper. The absorptive tether is a steel cable encased in alternating cylindrical and spherical beads. If the cable is tensioned, the beads are pressed together and when bent, a friction force is induced between them, thus dissipating energy.

When deployment is finished, the absorptive tether is cut by the second pyro at the TEAM end and TORI is released to create the free flying system TORI-tether-YES. TORI contains two payloads, a "personal item container" and on the opposite side, an AUtonomous TEther Cutter circuitry (AUTEC). The AUTEC is triggered by a microswitch upon ejections and will cut the tether 3 days after ejection, to cover for contingency cases. The cutters used in YES are a military-grade AirTech tether cutter, designed for parachute applications.

6.3.2 Stabilization of the satellite by tether torque

YES has no active attitude control system and this imposes a challenge to successful deployment. If the initial tip-off rate is higher than a few degrees per second, the nominally low tether tension will not be able to prevent YES rotation. The YES may wrap itself inside the tether, halting deployment.

Analysis has in fact shown that tip-off rates as high as 10°/s can be expected with the crude ejection mechanism of the YES. Four heavy springs are preloaded by 2 kN each to press YES out of the TEAMSAT box. One group of six copper beryllium pyrotechnic bolts and a second group of two more bolts on the YES lid restrain the YES to the TEAMSAT box (Figure 190). In two independent steps the pyros are cut. The first step cuts the group of 6 bolts leaving 2 opposite bolts around the axis of the lid with the highest moment of inertia (9 kg·m^2). Once the last two pyros are fired, the tether mission starts The stored energy of the springs will provide a velocity increment $\Delta V = 1.7$ m/s to the 180 kg YES satellite. Guiding are provided only by the conical spring contact plates, and by the edges of the YES structure. The main contribution to the tumbling is due to the delay between firing of the last two pyro's: about 1 ms at 1 σ.

The initial tip-off rate must therefore be limited by other means. The Ariane 5 launcher can for example provide an initial spin rate as a means of passive stabilization. A rate of only 0.5 rpm has however been requested by the YES team, as a compromise between two conflicting requirements. Firstly, there should be sufficient spin to prevent a transition into flat spin (tumbling) of MaqsatH or YES during the deployment phase. A flat spin is unwanted as it leads to unknown ejection attitude and wrapping of the tether around YES during deployment. Secondly, the spin stabilization should be weak enough such that the torque exerted by the tether on the YES during tether system rotation will orient YES mostly along the tether, again to avoid wrapping.

As an alternative solution, application of an additional braking profile has been studied to increase the tension in the initial seconds of deployment, to dissipate rotational energy [Kruijff 1998]. The stepper motor would start turning directly after ejection close to maximum velocity, hold for a few seconds and turn back again. The short but open loop brake pulse must be tuned to reduce to an oscillation any initial tumbling of YES within the expected range.

6.3.3 Supporting systems

Most of the remaining subsystems of the YES satellite are designed in support of the tether experiment. They are positioned around the tether canister, which is centrally located within YES (Table 53, Figure 190, Figure 195).

The YES is not a typical satellite, rather is shaped by some particular requirements and opportunities. It is designed for a mission maximal 7 days, a limit imposed due to limited availability of the S-band communication window. The design is driven by development time and low-cost rather than mass. YES therefore carries, where-ever possible, engineering models and flight spares, or re-flies components of earlier ESA missions. As a result it is using for example ESA flight-spare rechargeable batteries as a primary power source. There is no need for solar panels. The batteries are the major design and mass drivers of the system. They are placed around the centrally located tether canister. Another majorly simplifying condition is that YES, as explained has no active attitude control system, except the tether. Some instruments and payloads involving new technologies were delivered at low or no cost by their developers to have their maiden flight on YES. Commercially available parts are used for selected functions, with adjustments and testing for sufficient shock, vacuum and outgassing properties. Where possible, multiple solutions and margins were implemented in parallel to create flexibility and redundancy.

The YES structural design is a rigid cross-shape placed on top of an octagonal plate that serves as lid for the TEAMSAT box and as base plane for the satellite's sensors and antenna (Figure 190). The lid plate also houses wiring and the pyrotechnic bolts that connect the plate to the TEAMSAT box. An intermediate platform level houses further electronics including the GPS system, computers and a space qualified transponder. The canister protrudes through this level. The top of the satellite is a plate that covers the tether canister. Mounted on this plate are patch antenna’s (designed to avoid tether catching) and more

sensors, as well as the barberpole brake system. Before ejection, because this top panel then resides inside the TEAMSAT box, the S-band antenna there is switched off.

Three computers are wired up to control the YES satellite, as detailed in the electrical overview diagram (Figure 195). The On-Board Data Handling system provides a direct telecommand and telemetry link to the other two computers and the GPS system on-board. It is an innovative system using asynchronous virtual channel multiplexing and was delivered to TEAMSAT by ESTEC [Habinc 1998] for its maiden flight. Its latching circuitry is also used to fire the pyro's. Furthermore it provides analog data interfaces to some of the sensors.

The custom-designed YES on-board computer 'Joris!' is able to control nearly all experiments autonomously or based on telecommands and takes care of data storage and preparation of telemetry. The design is based on two cold-redundant SH7032 RISC controllers from Hitachi operating at 32 MHz with alternating host selector and optional external host (the PC104, see below). The host controllers share access to a Field Programmable Gate Array (FPGA) and 32 MB of Flash storage.

The FPGA controls the various interfaces. It offers a more flexible interface to the GPS, in addition to the OBDH link to the GPS. Also it controls and switches the power for the stepper motor of the barberpole brake and connects to the interface electronics for the OLD circuitry that are integrated on Joris!. It interfaces with the barberpole camera through a parallel port. The FPGA is one of the few single-point failure component, as a redundant version would be electronically too complex. However, the interfacing is highly simplified, which is the reason that this solution has been accepted.

Several features have been included to increase robustness for the Joris! as a whole, including watchdog circuitry that controls the host selection, latch-up detection and redundant software loading both for controller and FPGA.

Joris! runs the Joris On-Board Software (JOBS), which is based on a simple multitasking operating system μCOS written in C and C++ (Figure 193). JOBS features use of direct memory access, multitasking and semaphores to control the data traffic between different tasks. JOBS supports a full range of features for telecommands and telemetry of real-time and historical data. The software is patchable by telecommand.

A third On-Board Computer is included, a commercially available PowerDwarf PC104 486, added as a demonstrator for future use on the YES2 satellite. It is also intended as a back-up host in case the Joris or JOBS would not be operational. The flexibility of the interconnection between the computers has been used when the optical link between TEAM and YES proved to be unreliable. The PC104 has successfully served as a relay to provide telecommands via TEAM to Joris!. The PC104 is connected to a commercial QuickCam camera that is pointed at the deploying tether. The PC104 has been only slightly modified for space flight. The board has been coated and components glued to withstand launch vibration. The processor has been given a thermally conductive link to the metallic housing.

Two newly developed Triad 442T Micro-Electro-Mechanical Systems (MEMS) accelerometers built by Forschungszentrum Karlsruhe are installed symmetrically with respect to the YES

center of mass and approximately 30 cm away. Their primary sensing elements are manufactured with X-ray lithography and are based on the principle that a small seismic mass suspended by springs can be balanced under accelerations by electrostatic force. Obtainable accuracy and resolution are respectively 1μg and 1μg/√Hz. For lack of calibration, due to thermal hysteris and thermal drift the guaranteed accuracy during YES is below 0.4 mg. When compared to the order of magnitude of the expected accelerations during the mission it can be seen, that during the larger part of deployment no accurate tether tension level can be determined (Table 55). The main use of the accelerometers is however to witness major mission events qualitatively such as ejection and final deceleration, tether spinning, release of TORI and the tether cut. Contingencies may also be observed, such as periods of slackness and potential tether jamming.

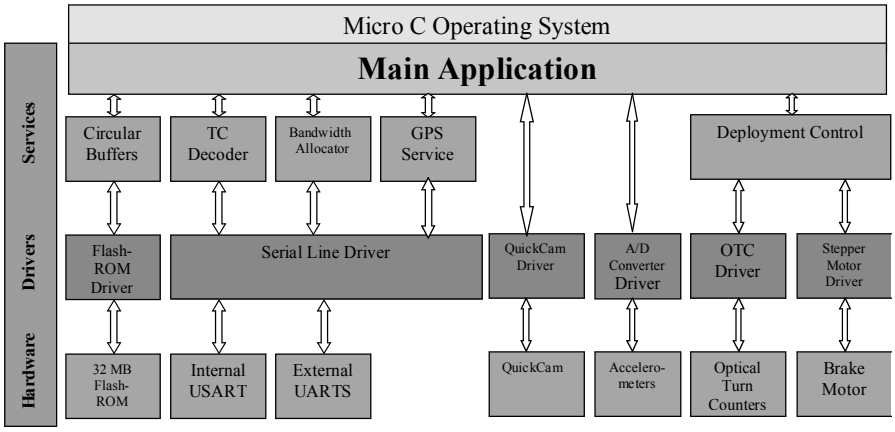

Figure 193. *YES OBC and Software layout*

Measurement objective	**Scale**
Ejection	4 g
First minute of deployment	peaks of 20 mg
Larger part of deployment	10-60 μg
End of deployment	5 mg
TORI ejection	drop to 0.1 mg
Spinning YES-TORI system	0.6 mg
Tether cut	drop to 0 g
Spin/tumbling	25-200 μg

Table 55. *YES potential accelerometer measurement objectives*

The two QuickCams on-board are intended to witness the ejections and the deployment of the tether. These black-and-white CCD cameras have a resolution of 320x240 pixels, and a field of view of 30x23°. Both are mounted on the top cover plate of the YES satellite, inside the TEAM box until YES ejection. One unit observes the brake system and the way the double strand tether

passes around the barberpole, Figure 194. The tether cut can be witnessed as well. The second unit is oriented to witness the ejection of YES and TORI and the deploying tether (Figure 190).

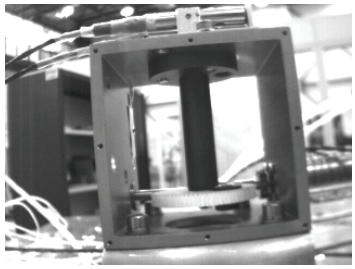

Figure 194. *YES barberpole photographed by QuickCam*

A Trimble TANS II GPS receiver LEO configuration **[**Pol 1997**]** is added to assess whether a commercial GPS receiver could be used for future short space missions, providing relative GPS positioning of tethered systems. The selection of the unit has been for reasons of price and availability. It is the first time that a GPS receiver is used at an altitude above the GPS constellation, where only Earth-skimming signals can be received, arriving to YES below the local horizontal plane. In GTO perigee, the receiver experiences a high orbital velocity of nearly 10 km/s. The GPS is planned to collect signals from the side lobs of the GPS satellites when YES is at 20.000 km altitude as well as raw data from the weak signals of the satellites "*behind*" the Earth when YES is in apogee. Ideally, about 1-4 satellites are expected to be in view in this range of the orbit. Two antennas are connected to the single receiver. One is on the outside of the TEAMSAT box and is operational both before and after ejection. The other is mounted on the top plate of YES and can be used only after ejection. The GPS is connected both to Joris! and directly to the OBDH. The Joris! GPS application propagates the YES orbit to support the performance of the GPS.

There are 7 student-developed solar aspect sensors on the TEAM/YES satellites that can be used to determine the direction of the sun vector with an accuracy of 2.5 degrees **[**Noteborn 1997**],** and therefore will give information about the spacecraft attitude and rotation rates.

6.4 Mission Summary

6.4.1 Tether experiment cancellation

The risk posed by the tether to the operational satellite environment has been assessed. It is negligible for the nominal YES mission. The tether would reenter within a day and would spend only a fraction of this time in the LEO region where most operational satellites are concentrated. However in an off-nominal mission scenario, the tether with its 35 m^2 projected surface area could stay in orbit for much longer.

In this case, the tether orbital lifetime would be mainly dependent on the effect of solar pressure. The effect is of one order higher than that of the gravitational effect of the Sun and

Moon and the effect of atmospheric drag at 600 km (Section 3.3). The line of apsides of the orbit may be oriented such that the solar pressure decelerates the tethered system at apogee causing the perigee altitude to drop. The effect is strongest when the solar vector is perpendicular to the line of apsides. The angle between the lines of apsides and the solar vector is not constant. The initial angle is a function of launch time and is shown in Figure 197. Due to the nodal regression of 0.373°/day, the apsidal precession 0.738°/day and the rotation of the Earth around the Sun by 0.986°/day, the angle between the line of apsides and solar vector, as depicted, recedes with 0.621°/day. Taking into account the precession of the orbit, the integrated effect of solar pressure on the re-entry time of the tether is calculated as shown in Figure 196.

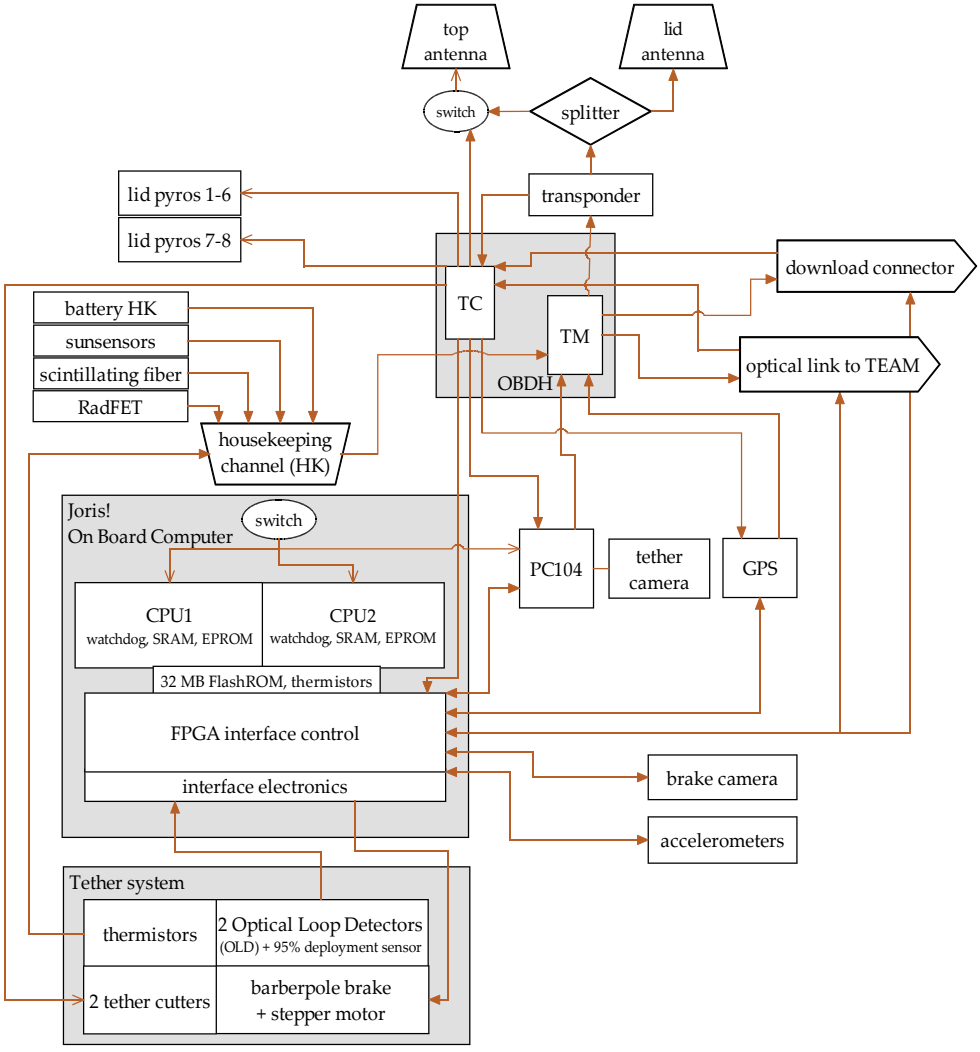

Figure 195. *YES Electrical diagram*

For these calculations, the reflection coefficient is 0.8, absorption coefficient is 0.2. The effective drag surface is based on a rotating tether (22.3 m^2). The tether is assumed disconnected from both its endmasses by the primary release system on YES and the Autonomous Tether Cutter (AUTEC) on TORI. No atmospheric drag is assumed above 150 km. When the tether dips below the critical perigee height of 150 km, the atmospheric drag will quickly circularize the orbit and re-entry will take place. The calculations were verified by independent efforts [APEX 1997].

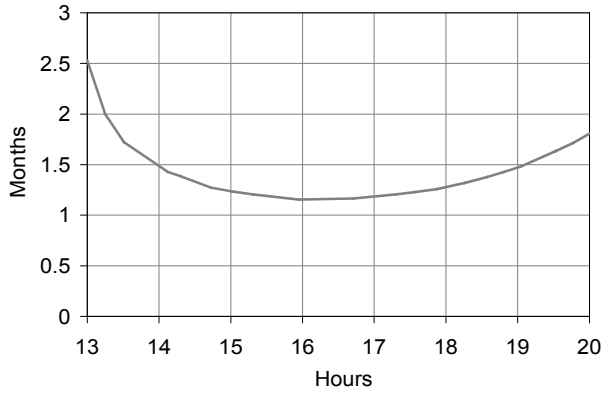

Figure 196. *Deorbit time YES tether from GTO in months as a function of launch time in Kourou Local Time (KLT)*

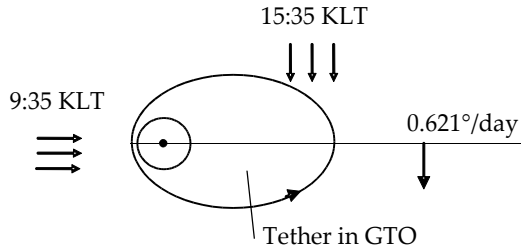

Figure 197. *Relative nodal recession of GTO orbit with respect to solar pressure direction. The Sun position with respect to the line of apsides depends on the Kourou Local Time of launch (KLT).*

The graph shows the time needed for the perigee to drop to 150 km, against the hour of launch. Launches before 13.00 KLT will not lead to a quick burn-up and lifetimes in the order of (tens of) years can be expected, with an associated collision risk with operational satellites of order 0.1% [APEX 1997]. This risk figure is generally considered not acceptable. Launches after 13.00 KLT will leave the tether in orbit for some few months and would lead to a reduction of the risk by two orders of magnitude.

The launch window of Ariane 5 was finally selected in May 1997, unfortunately between 9:00 and 12:00 KLT. This time is not compatible with the proposed risk mitigation approach

and it has been decided not to deploy the tether on YES. In fact, the tether has been physically disconnected from TORI before launch (Figure 190).

6.4.2 Experiment Control Center

In the six weeks before launch the then crude Electrical Ground Support Equipment (EGSE) is developed into a sophisticated Experiment Control Center (ECC), with graphical user interfaces for the Prime Investigators (PI), prepared telecommand sets and detailed final mission planning [Jones 1998]. The European Space Operations Center (ESOC) is in charge of the control of the satellite and takes care of the transfer of the data to the ECC.

Although YES is to be launched with the tether experiment's computer Joris! disabled, an engineering model is built up in the ECC and connected to the TM/TC loop. In this way it cannot be distinguished from a system operating on the YES satellite. The Joris! Engineering Model thus supports the YES experiment by processing in real-time GPS data and by preparing automated GPS telecommands. The Joris! Engineering Model is also set-up to perform, with support of ESOC, and through the communication link with the YES satellite, a mock tether experiment according to the original mission timeline, in order to gain tether mission control experience.

6.4.3 Mission operations

On the 30th of October 1997 the Ariane 502 is launched. It reaches an orbit significantly deviating from the nominal GTO orbit, with a period of 7.8 hours instead of the target of 10.7 hours, calling for an improvised mission scenario. Moreover TEAMSAT is inserted without spin stabilization, and ends up in a nearly flat spin, see Table 56 and Figure 198. With some difficulty, communication is finally established. Images from Ariane's Speltra separation taken by the TEAM's VTS camera are received soon thereafter. They are used by the author to determine the off-nominal attitude, flat spin direction and rate using an improvised cloud pattern identification from comparison with Meteosat images. The results are later confirmed and enhanced by both the sun sensor data from YES as well as the star sensor data from TEAM's AVS [Betto 2000].

Insertion parameter	**Nominal**	**Achieved**
Perigee altitude [km]	580.942	531.337
Apogee altitude [km]	35926.000	26746.241
Spin rate [°/s]	3	0.08
Nutation angle [°]	0	74
Nutation rate [°/s]	0	0.3

Table 56. *YES (A502) nominal vs. achieved orbit insertion*

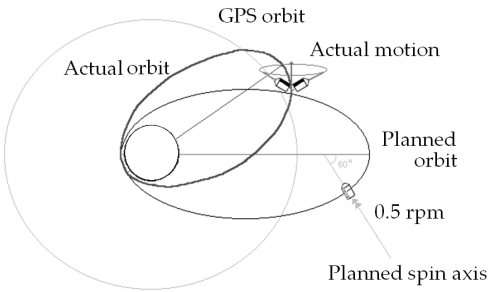

Figure 198. *YES (A502) nominal vs. achieved orbit insertion ([Pol 1998] & CNES)*

The first part of the mission, before YES ejection, has been reserved mostly for the TEAM experiments, such that TEAM can benefit from the large batteries inside YES via a set of banana plugs. TEAM collects images, tests a star sensor and measures the atomic oxygen flux in perigee.

During this period, contact with YES is reserved for health checkouts and preliminary measurements. The communication link is limited to one satellite at a time, so switching is required between YES and TEAM. Also, until ejection, YES has only hemispherical coverage, and because it is tilted strongly from the nominal orientation (Figure 198), communication with YES has become a matter of opportunity. Periodic telemetry black-outs due to the tumbling last about 5-10 minutes. Nevertheless, during the first five orbits, contact with YES has been successful and good quality data had been received multiple times from the operational experiments (Figure 199): the radiation experiments, the self-developed sun sensors, technology demonstrations (PC104, camera) and the GPS.

On the third days of the mission, at the 6th orbit, ejection of YES is planned, with two TEAM cameras set to witness the event (Figure 201). The ejection will expose a second antenna for telemetry and also for the GPS, thus enhancing their coverage to omni-directional and improving YES performance. Furthermore, ejection will expose the two cameras on YES and an additional sun sensor. In advance of the ejection, the 'rehearsal' tether mission is being prepared. Based on the available power, a further one or two days of operation are foreseen.

The operators are however unable to switch on the YES telemetry, despite numerous trials. The passive thermal design of YES has been based on a Sun-pointing lid, with a nominal inclination of +48°. With the satellite in a flat spin, the Sun inclination actually varies periodically between approximately -68° (effectively shadowing the lid) and +36°, as a result of which YES is cooling down slowly. It is now believed that the transponder at this time is cooling down below operational range, and it stops operating. Hoping that the failure would be somewhere in the direct command reception, it is finally decided to try to switch on YES telemetry via the back-up routing for telecommands, that leads via an optical link from TEAM to YES. The optical link is known to be unreliable. Command signals through it have therefore been isolated from the rest of the commands and are only considered as a last resort. As soon as the command is sent, a number of times the 'YES eject' flag in the

housekeeping is raised and a drop in the battery temperature of TEAM is noticed. Garbled data is received through the optical link. Somehow, despite carefully implemented safety features, such as a digital verification of the telecommand code and the multiple inhibits in the pyro arming circuits, both sets of pyros must have fired and YES has been ejected. One orbit later, both VTS and AVS make images of a bright object closing in on TEAM. It is highly likely that this is YES (Figure 200).

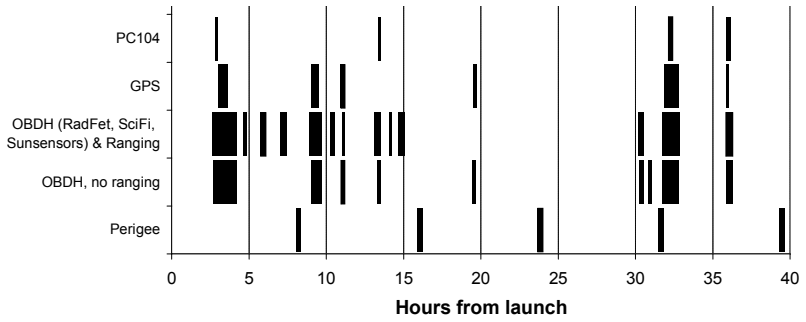

Figure 199. *Operations of YES mission*

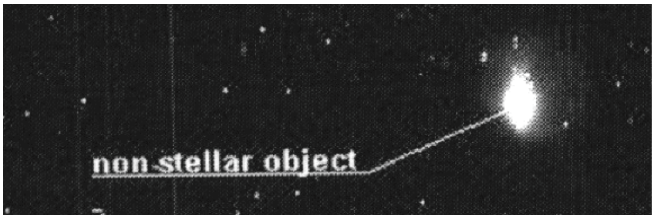

Figure 200.*Object observed by AVS (TEAM) one orbit after ejection. From apparent size and low relative velocity to TEAM, it was determined to be YES*

Simulations show that YES cannot possibly be any further away than two kilometers, depending on the orientation at ejection. Figure 200 suggest a distance of only tens of meters. Communication with YES can however not be re-established, suggesting continued failure of the transponder. The search is stopped when even the most optimistic power estimates predict battery depletion, about 96 hours after launch (Figure 201). The new orbit of YES is later confirmed by radar tracking and optical images taken from the ground.

6.4.4 YES mission data

Contact with YES has been for 5 orbits, about 40 hours, about half the planned duration, during which all instruments performed nominally but with limited visibility for camera and GPS antennas. Distributed over 15 communication sessions for health checks, YES has provided 6 hours worth of real-time data (Figure 199). The body nutation rate is established from the sun sensor data with 0.1 °/s accuracy, and the inertial spin rate has been estimated with 0.02 °/s accuracy. Analysis of the GPS signals received provides evidence that for the first time, GPS data has been received below the local horizontal plane from Earth-skimming signals (Figure 202). Both radiation experiments have performed well and

provide the first Scintillating Fibre radiation data from space as well as RadFET data inside the Van Allen belts. The PC104 demonstrated excellent health and the QuickCam CCD images showed no evidence of radiation damage. [Noteborn 1997, Pol 1998, Kruijff 1999.III] report the results in more detail.

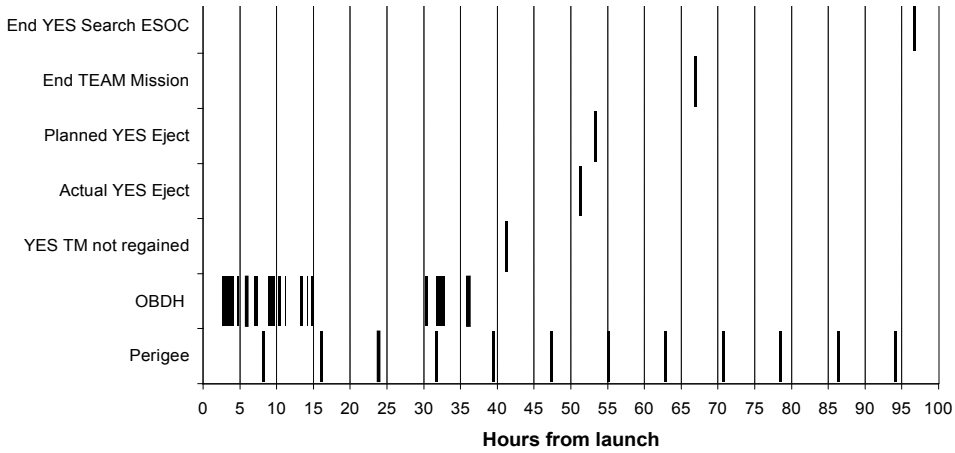

Figure 201. *Events timeline of YES mission*

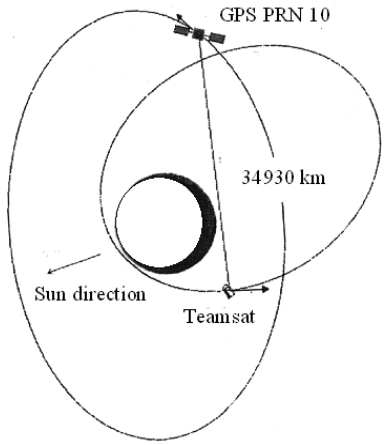

Figure 202. *Reception by YES of GPS signal (PRN 10) as seen from the North Pole [Pol 1998]*

6.5 Aspects of the YES project approach

6.5.1 Challenge and opportunity

The history of YES and TEAM satellites' development is reminiscent of the early days of spaceflight, in terms of schedule and level of pragmatism during the development. The project gets a go-ahead in November 1996, about one month from the initial idea. At the

official kick-off of the development, the satellites are to be launched within 5 months, and to be delivered within 10 weeks. In that short timeframe also a challenging tether mission has to be prepared. Most of the planned team members at this time have little or no experience and the budget is severely limited, initially about 700kEuro for the 350-kg TEAMSAT as a whole.

A number of simplifying conditions and conceptual decisions help the project to get started effectively and get the preliminary TEAMSAT design accepted for launch on Ariane 502. It has been decided to include both TEAM and YES in a common strong box, to minimize safety issues with respect to the launcher. For instance, there is no mass constraint for the initial design, due to the dedicated character of the launch opportunity. A target mass is estimated, based on an inventory of likely components and a straightforward non-optimized design. This target mass will then however be adhered to. From a communication point of view, the S-band communication frequency reserved for launch operations will be used. This frequency is reserved for one week after launch, setting a limit to allowable TEAMSAT lifetime. This lifetime is more than sufficient for all the experiments. It will keep the operational costs low, and makes it possible to work with non-space-qualified components. The power system can be simplified significantly, as batteries can be used as sole power source. Furthermore, spin stabilization is planned, a passive attitude control to further simplify design.

The unique work location has proven to be especially helpful for turning the concept into reality. The team is collocated at ESTEC, most within a single large room (now the Erasmus User Center). ESTEC test facilities and experts are made available by ESA. In the first weeks of the project a successful search is performed at ESTEC for reusable retrieved flight components or engineering models. Carefully maintained batteries from ECS-2 are donated, as well as 12 left-over space qualified pyrotechnic devices and transponders from the EUREKA platform and the Olympus project. These represent some of the most critical components and form the basis for the TEAMSAT conceptual design.

6.5.2 Conceiving a satellite in 8 months

It is first attempted to deliver in time at least the physical satellite as an integrated piece of hardware. It is already considered likely that there will eventually be a launch delay that might buy the team more time for software development and tests later. Guideline for both the design and hardware search is that overdesign, if a simplification, is to be preferred over optimization.

The initial focus of the project is on identification of components and configuration. This is necessary also because a mass-representative dummy of TEAMSAT is to be constructed with priority. This dummy will be used in case the actual TEAMSAT is not available for the scheduled vibration tests. A full-scale wooden/foam mock-up is being fabricated, following closely component selections in order to do develop the configuration and do the first practical fit-tests. Foam representatives of the ESA-donated components as well as of the already selected SEDS tether deployer help to establish the initial configuration within weeks.

The remaining TEAMSAT components and subsystems are obtained and collected in various ways. Some components, such as the real-time, asynchronous and multiplexing OBDH, as well as the RADFET/Scintillating Fibre radiation experiments happen to be under development at ESA. The YES and TEAM project will provide a focus and maiden flight opportunity. Also industry has offered instruments, such as accelerometers and GPS at low cost, as an act of sponsoring or for a maiden flight. Hardware to be purchased is selected based on price and most of all a delivery time of less than 8 weeks. Often commercially available components are selected, such as the tether cutters or cameras, then slightly adapted and tested at ESTEC as a part of the YES qualification. Remaining parts are to be developed by the team, including the on-board computer, the power distribution system and the autonomous tether circuit. In certain cases, multiple options are developed in parallel, and spare input and output signals are included for robustness against later design changes. An example of this approach is the link between the two on-board computers Joris! and the PC104. Electronics are integrated in an ESTEC clean room. The ESTEC workshop manufactures the structure for both TEAM and YES in parallel with the design and also still during integration. Most hardware is delivered or built within about the first four months of the project (Figure 203).

System engineering is performed pragmatically. As a result of this approach, the final product is capable but in no way optimised, and very close to the original concept with nearly all planned performance plus some guest payloads.

The system design is tracked under responsibility of the lead system engineer and shared with the team on a continuous basis. A product tree is maintained from which mass and power budgets are updated about once every two weeks. Electrical interfaces are graphically displayed in a few block diagrams and distributed on paper and through public display. A dedicated harness team collects, checks and maintains exact pin-outs in a single large document. The critical item list is updated in a daily meeting, the timeline in a weekly meeting per item in the product tree.

Most requirements are not gathered in a single document but communicated orally or by email and included in subsystem design update descriptions that are distributed regularly. System and subsystem requirements are generated ad hoc, starting from the initial conceptual design, mission and experiment objectives and accounting for spares and margins. Particularly closely followed are the interface requirements of the OBDH and Joris! Computers. A noticeable exception is made for the development of the JOBS software, for which an extensive User Requirement Document and Architectural Design Document are produced. For this case, such a level of documentation is deemed necessary, due to the complexity of JOBS and the relative isolation of the software team.

Two internal reviews have been held in January 1997, during the transition from design to integration: a Critical Design Review and a Mid Term Review (Table 57). Despite the announced launch delay, at the CDR a large number of open issues is identified, as well as a manpower shortage. At the MTR, solutions for both problems were delivered, in the form of additional ESA staff support, the integration manager. Integration, subsystem verification

and system testing is to be performed within the next four months. In parallel, only now that all electrical connections are well-defined, software development is initiated.

The integration effort is organized per physical level within the satellite. Every individual component is assigned to a responsible person and to one out of four priority levels. Progress per component is henceforth tracked on a weekly basis. The satellite parts are assembled in the ESTEC Highbay, which is not a clean room but the team's restricted and well-ventilated working room.

Verification before and during system integration is mostly performed informally, and formally thereafter. Before integration, the typical procedure at subsystem level consists of the lead engineer's review of design, the designer's performance tests and oral or written briefings thereof. Electrical subsystem tests are performed in parallel with the integration, with intermediate software versions. Once the system is integrated, the shaker test is performed with most of the harnessing not yet connected. This is judged as acceptable, due to TEAMSAT's safe box approach. Following the shaker test, the TEAMSAT is reassembled, this time with harness connected. Detailed test procedures and test reports are now also produced for electrical subsystem and system tests. Three comprehensive functional test campaigns, of about two weeks each are planned: one campaign before shipment to the launch premises in Kourou, and two campaigns on location in Kourou where also final adjustments are made and the final version of software and time tagged telecommands are uploaded, as well as the most recent GPS almanac and ephemeris.

During the Kourou test campaigns, mistakes have been made that have degraded the YES performance further. Because of the cancellation of the tether experiment, a decision has been made to lower the priority of the YES experiment and no dedicated manpower is available during the second campaign.

To save time, it is decided not to cover the YES lid with multi-layer insulation (MLI), as recommended by the thermal design engineer. This MLI was suggested to provide better protection in case of an off-nominal solar orientation due to a possible shift in launch time. During the YES mission, this decision can be directly related to the suspected cause of failure of the YES transponder shortly before ejection. The off-nominal orbit insertion combined with limited thermal robustness unfortunately causes the transponder to cool down below its operational limits.

The lack of manpower has also lead to a breach of procedure leading to an unrecoverable failure of the Joris! on-board computer. The Joris! computer failed when a software update was installed on the flight model -after a seemingly-minor change of a parameter- *without* a-priori verification on the engineering model, as the procedure prescribed. The procedure was breached since the available engineer was not only under severe pressure, distributing his attention over various subsystems, but also not sufficiently knowledgeable about the Joris! hardware design. The changed parameter happened to concern the watchdog reset interval, which was selected longer than the actual reboot trigger time. This led to a continuous and unstoppable cycle of Joris! rebooting. As the tether experiment had already been cancelled, the impact is limited to the loss of the accelerometer experiment and of one

of the two cameras. All other experiments have primary or back-up connections to the remaining two on-board computers.

6.5.3 Milestones and manpower

All-in-all the YES design approach has been ad-hoc and opportunistic, with a linear "first things first" approach as illustrated in Figure 203. During the project, two major launch delays have been announced: the first after ~1.5 months at a time that the TEAMSAT design had reached significant maturity, the second occurred during integration. The first delay basically has allowed to fly the YES itself instead of the dummy, the second has allowed to do detailed testing and develop the flight software. The timeline shows a relatively long testing period, but also in hindsight, this could not have been much more compressed. The detailed milestones of the YES project are summarized in Table 57.

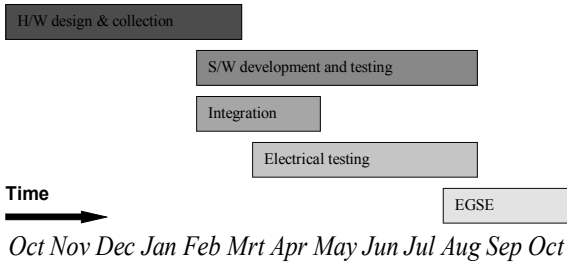

Figure 203. *YES development timeline*

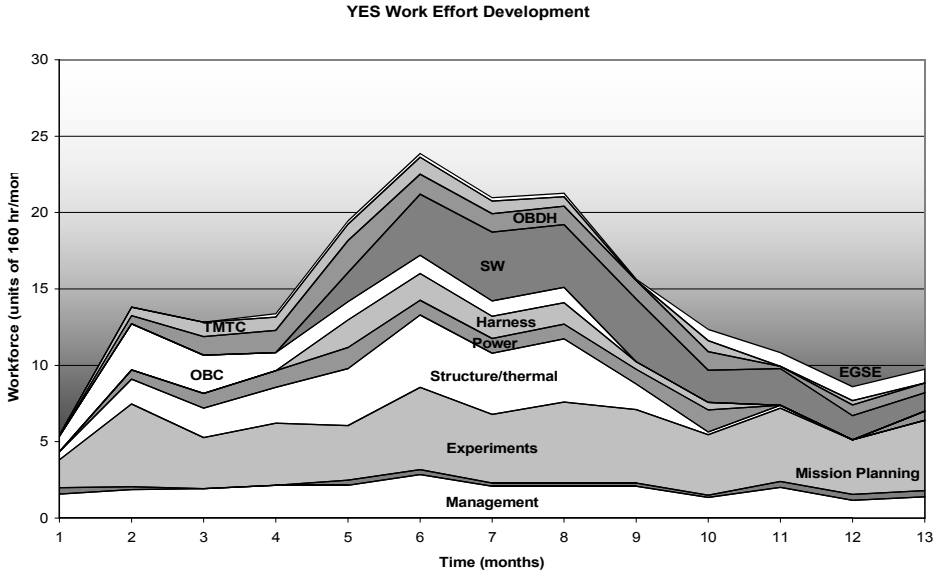

Figure 204. *YES work effort development*

Date	Event	Projected launch date
9 October 1996	YES proposed at Dutch stand at IAC Beijing.	21 April 1997
24 October 1996	YES proposal to ESA Headquarters.	-
15 November 1996	TEAMSAT funding secured, official kick-off.	-
1 December 1996	First design decisions made	-
20 December 1996	Launch delay announced.	15 July 1997
7 January 1997	Mock-up completed.	-
l6 January 1997	CDR	-
24 January 1997	MTR, ESA integration engineer assigned.	-
31 January 1997	TEAMSAT dummy passes structural testing.	-
February 1997	Launch delay announced.	30 October 1997
Begin May 97	First full TEAMSAT integration.	-
30 May 1997	TEAMSAT structural test passed [Bradford 1997].	-
7 June 1997	FRR	-
11 June 1997	Tether experiment cancelled [APEX 1997]	-
20 June 1997	YES full functional test, test version of software (S/W)	-
End July 1997	YES Kourou, test period I, fixes, flight S/W v1.0	-
9-14 September 1997	Test period II, flight S/W v2.0, system initialization, Joris fails	-
15 September 1997	Last data access to YES	-
30 October 1997	Launch & first data YES	As planned
1 November 1997	YES transponder dies, YES ejected	-
3 November 1997	End of TEAMSAT fligth T0+80 hr	-

Table 57. *YES project timeline*

About 69 people have contributed to the YES development: 17 students, 23 young engineers (less than 4 years working experience) and 29 senior engineers. Many of them have worked part-time or spent considerable time on the TEAM satellite as well. The Full Time Equivalent (FTE) for the work on YES contribution varied from 5 people (initially) to about 20 people (integration and S/W), on the average about 15 (Figure 204). The on-board software is rather complex and therefore has claimed a significant part of the total effort.

6.6 Lessons Learned

6.6.1 Failure analysis

As hinted already in the previous sections, various problems have led to degradation of the YES mission. These problems include first of all the cancellation of the tether experiment, but also the pre-launch failure of the YES on-board computer Joris!, and finally the loss of

YES telemetry during the mission. They have been critically analysed in detail in [Kruijff 1999.III], a schematic overview of the results is provided in Figure 205. A summary of the primary failures, causes and effects is provided in Table 58. Some other problems could be resolved thanks to the various redundancies within the system. The failures that persisted are caused by a combination of exceptional factors.

External causes beyond control of the team have played a role here, most notably the decision to launch at an hour incompatible with the YES request as well as the strongly off-nominal attitude of YES.

An important internal contributor has been the increasing friction within the team. A degrading team atmosphere has led to exclusion of sufficient and sufficiently knowledgeable manpower from the second test campaign in Kourou and thus contributed to the loss of Joris! and YES telemetry during the mission. A negative atmosphere within the team has been created due to time pressure, conflict between responsibility and authority, stress, personal factors and a competition for resources between YES and TEAM.

Other internal causes, at the same time, are more related to the YES engineering approach under time pressure. The Joris! failure is an example of insufficient communication and traceability of documented information. Overall, the Joris! development has proven to be too complex, and probably has been a poor design choice given the time pressure. Similarly, the tether experiment was perhaps too demanding. Virtually no ground-testing for the experiment has been performed. The mission's nominal success probability was therefore judged low and this affected negatively the risk analysis.

Date (1997)	Failure	Primary external cause	Primary team mistake	Impact on YES mission
May	APEX Steering Committee cancels tether experiment.	Launch hour changed from YES request, increases collision probability.	Insufficient testing, probability of nominal mission success too low.	Primary objectives cannot be achieved.
September	Shortly before launch Joris! is disabled.	Delays cause financial limitations.	Internal friction (key experts not present), time pressure, under-management (miscommunication), procedure not followed.	GPS degraded, accelerometers, brake control, imaging of brake lost.
November	Shortly before planned ejection, communication with YES is lost.	Off-nominal insertion by A502, unfavorable orbital attitude.	Internal friction, time pressure (thermal insulation not applied).	No post-ejection mission (omni-directional coverage for GPS, imaging of ejection/Earth).

Table 58. *Main problem summary YES mission*

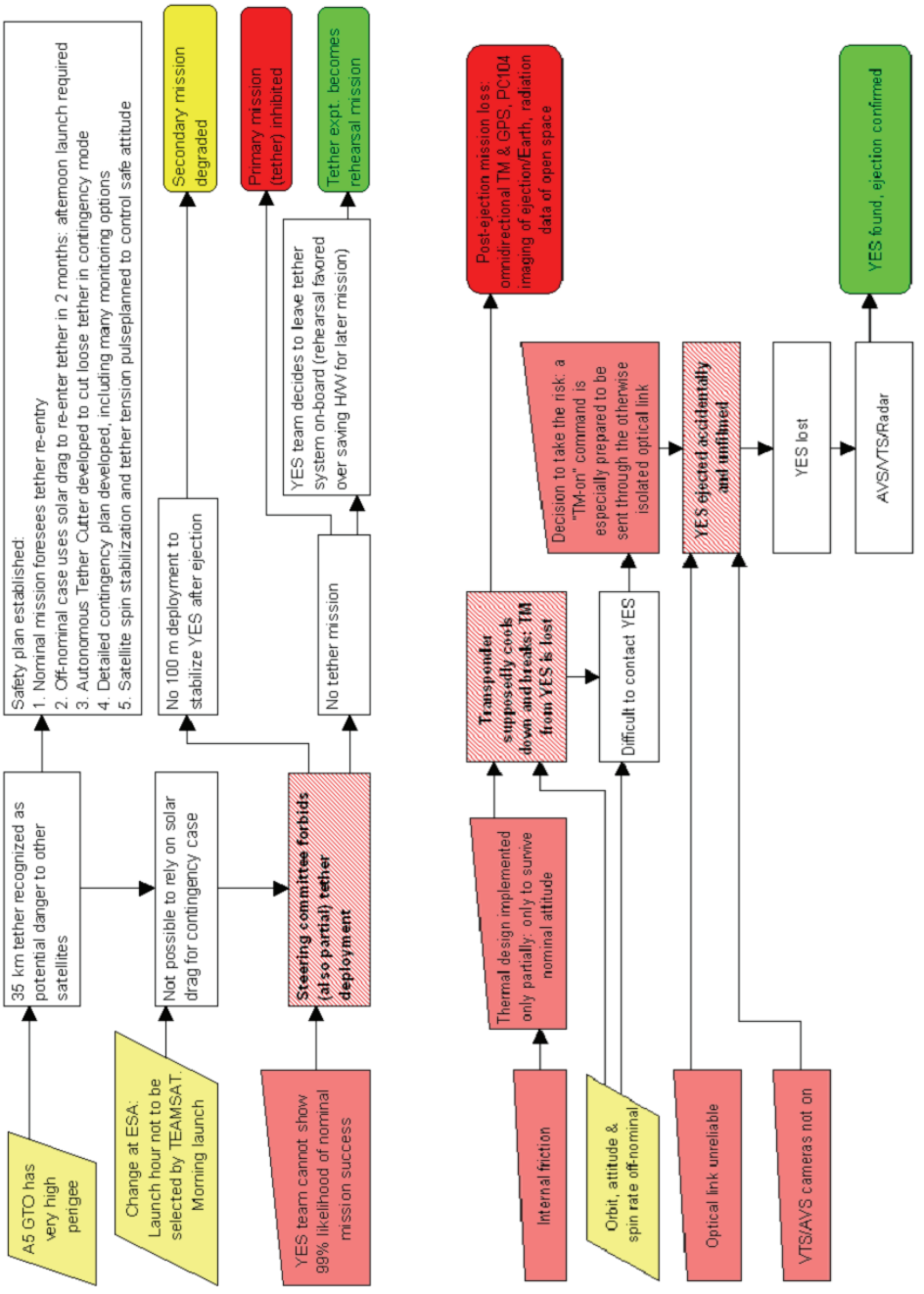

Figure 205. *Failures in the YES project, relationship between external and internal causes, incl. partial recovery. From left to right - pre-launch cancellation of tether experiment; Loss of communication & premature ejection of YES; PC104 harddisk failure in shaker test (recovered) & legend; command problem due to interference (recovered); failure of Joris OBC (impact limited).*

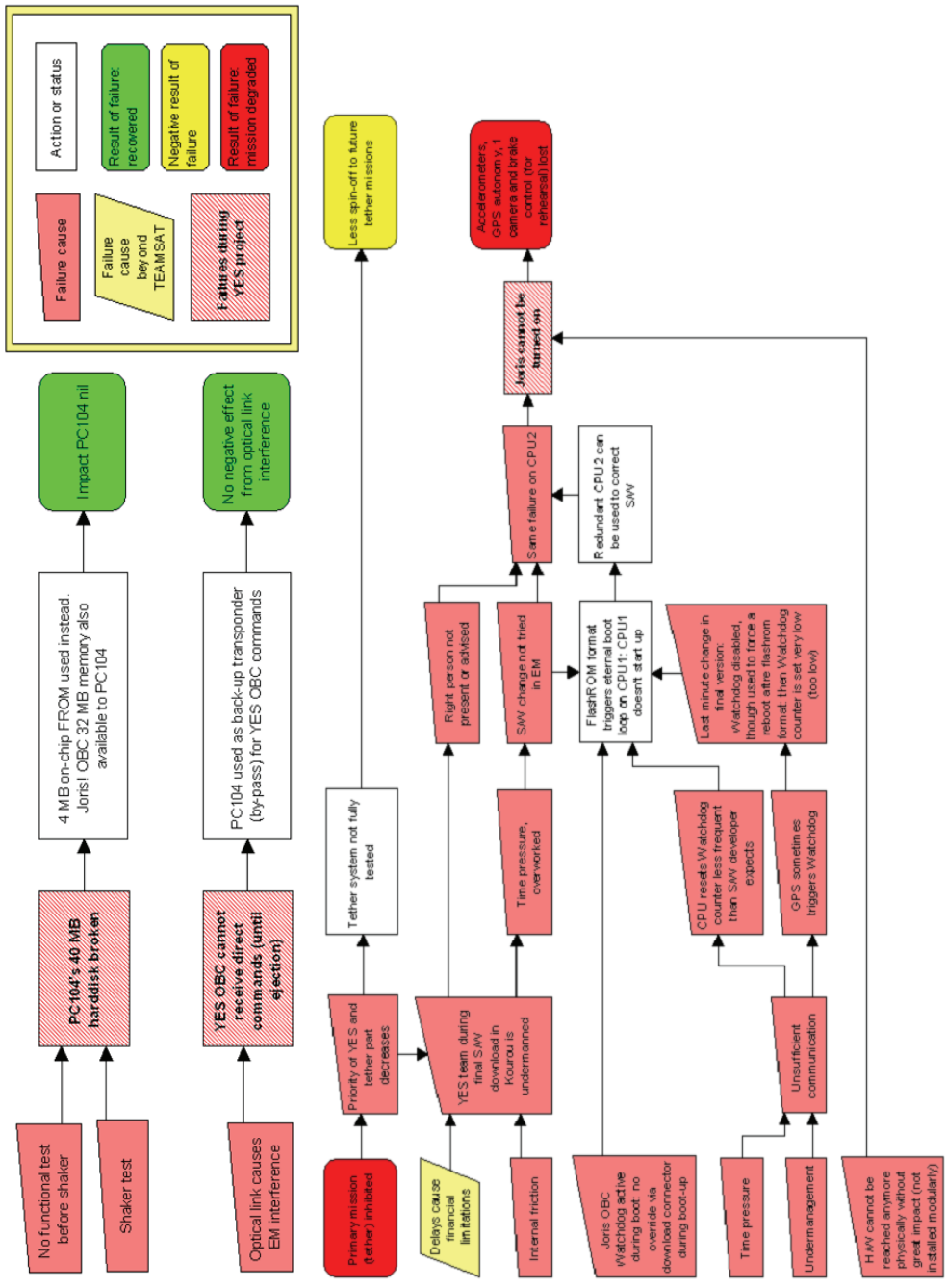
Action or status
Result of failure: recovered
Negative result of failure
Result of failure: mission degraded
Failure cause
Failure cause beyond TEAMSAT
Failures during YES project
No functional test before shaker
Shaker test
PC104's 40 MB harddisk broken
4 MB on-chip FROM used instead. Joris! OBC 32 MB memory also available to PC104
Impact PC104 nil
Optical link causes EM interference
YES OBC cannot receive direct commands (until ejection)
PC104 used as back-up transponder (by-pass) for YES OBC commands
No negative effect from optical link interference
Primary mission (tether) inhibited
Priority of YES and tether part decreases
Tether system not fully tested
Less spin-off to future tether missions
Delays cause financial limitations
YES team during final SW/ download in Kourou is undermanned
Right person not present or advised
Time pressure, overworked
SW change not tried in EM
Same failure on CPU2
Joris cannot be turned on
Accelerometers, GPS autonomy, 1 camera and brake control (for rehearsal) lost
Internal friction
Joris OBC Watchdog active during boot: no override via download connector during boot-up
FlashROM format triggers eternal boot loop on CPU1; CPU1 doesn't start up
Redundant CPU2 can be used to correct SW
Last minute change in final version: Watchdog disabled, though used to force a reboot after flashrom format: then Watchdog counter is set very low (too low)
CPU resets Watchdog counter less frequent than SW developer expects
GPS sometimes triggers Watchdog
Time pressure
Undermanagement
Unsufficient communication
H/W cannot be reached anymore physically without great impact (not installed modularly)

6.6.2 Recommendations for a follow-up project

Even if YES is an atypical project and not without problems, it has been shown that the model of involving young inexperienced people in an intense project, if sufficiently inspiring, can lead to exceptional results. Of course it will not be possible to built satellites in the manner of YES routinely. A free launch without mass constraint is a rare luxury. The YES platform was essentially based on spare parts and engineering models from previous ESA missions and a one-time generous and intense support of ESA staff. These resources cannot be reproduced at will. However, the YES experience and the failure analysis provide a reference case for a follow-up development, both from a point of view of tether experiment definition and for more programmatic lessons learned (Table 59).

The many new sides to the tether experiment and the apparent simplicity of such a highly visible technology have contributed both to its attractiveness and its risk. It has to be appreciated that the enthusiasm for a tether experiment has been the basic driver behind the proposal of YES. However, the success probability of the nominal tether experiment in GTO was considered very low, due to the many uncertainties, complex stagings and insufficient testing. In addition lifetime of a mechanical tether in the Ariane 5 GTO orbit, with its 600 km perigee altitude, can be tens of years and is heavily dependent on launch time. For a successor mission, a safe orbit is preferable below the Space Station (350 km) and a complete testing of all aspects of deployment and staging is necessary.

The same dichotomy holds true for the very fast, and low-cost approach towards the YES development. Management of a successor educational mission should be more mindful of time pressure and team motivation and communication aspects. The same aspects that allow for the project to happen, can lead to risks and to malfunctions.

For example, as the YES project horizon was short and the scope rather unique, it has been relatively easy to motivate people to dedicate themselves to it. The intensity of the project, right from the start, has added a sense of urgency and has brought the team to focus on priorities and achieve a high level of productivity and effectiveness. A lot of time has been saved with the confidence that problems can be solved as they came along. In this way an efficient planning can be done. The collocation pioneered by the YES team has been a key factor of success, and has found follow-up not only during YES2, but also has been a model for the set-up of ESA's EuroMoon project (1998-2000) and the Concurrent Design Facility (CDF) in ESTEC.

On the other hand, the continuous strain and proactiveness as required from the YES and TEAM groups have led to irritations and sometimes a sense of competition, conflicts of (too much) responsibility and (too little) authority, as well as conflicts between effort and recognition. These factors have affected the trade-offs and therewith the quality and robustness of the final product. Motivation and involvement are powerful enablers but can be turned around into frustration if not handled properly.

1	Lessons learned lists seem trivial until you experience them yourself.
2	High and relevant productivity can be obtained in an educational project if technical needs are taking preference over educational value.
3	In some way, YES has been a one time shot, e.g. free launch opportunity without mass limit, free use of available space-qualified hardware components and free involvement of ESA experts. A follow-up experiment has to account for this.
4	Regular short team meetings with strict time limit are effective (about 1-2 minutes per person per day.)
5	Making a decision is often better than making the optimal decision. It helps here to quantify where possible; build in margins to deal with future changes; take responsibility; and have the confidence that with creativity later problems will be solved.
6	Motivation is an emotion - negative team interactions have been the prime reason for crucial failures.
7	What seem the fixed rules of the institute can be bent if necessary (the consequences will have to be accepted).
8	Getting to hardware early on pays off - get off the paper ASAP.
9	Find a balance between communication and documentation. One does not replace the other.
10	Test test test!

Table 59. *Programmatic lessons learned summary from YES project*

6.6.3 Heritage of the YES tether system development

The YES project has made some contributions to the tether community, even if it has not featured a tether deployment.

Some relevant tether system developments have been made. A first tether experiment in a highly elliptic orbit has been designed and implemented. With the double-strand fail-safe Carroll Caduceus tether a new type of tether has been developed, wound and qualified for launch. A similar tether has later been deployed in a test set-up (Section 5.3.8). The degradable tether concept and investigation (Section 4.4) also is a spin-off from the YES tether experiment.

YES has triggered a high level investigation in Europe into the danger of creating space debris with tethers, involving industry, universities and the European Space Agency [APEX 1997]. This lead to independent verification of solar pressure and solar-lunar gravity effects on tethers in GTO, followed by the definition of safe orbital regimes (Section 3.3). It has also triggered the development of an approach to estimate tether mission risk (Section 3.2.3).

The implementation has revealed a number of further criticalities that have been given particular attention in YES2 (Section 7), such as safe orbit selection and ejection system design for low pitch-off rate. The contingency and mission decision tree method developed for YES has been used as a basis for the YES2 contingency analysis. The development and

test of on-board and ground segment software has revealed problem areas that were tackled well from the beginning of the YES2 development, such as the importance of a user interface that guides the user through the mission and parameter settings, and automated logging of the selected parameter settings for each test.

Finally, the YES electronics developments have benefited later projects. The success of the PC104 has lead directly to the selection of a PC104 as YES2 flight computer. The integrated on-board computer design with tether control features has been the basis for new developments, such as the SID computer (Tether Applications, USA) and the YES2 OLD electronics (Section 7).

7 YES2

Simplicity, Commonality, Gradual Change, Perseverance.

— The key principles of the Russian space program that have served as inspiration for the YES2 development, as quoted from Marc Toussaint (ESA, 1994)

7.1 Introduction

The idea for a second Young Engineers' Satellite (YES2), early 2001, followed completion of the deployment tests for the TSE project [Kruijff 2001.II, Kruijff 2001.III] and the identification of the Russian Foton microgravity platform as a very suitable and safe platform for a SpaceMail demonstration mission [ESA 2005]. The YES2 is primarily funded by the ESA Education Office and the Human Spaceflight directorate (HME). It is developed, designed, built and tested by prime contractor Delta-Utec with the help of some hundreds of students, according to the applicable ESA design standards in the Foton project.

The initial focus for the YES2 has been the development of a lightweight re-entry capsule, that would be deorbited by tether and would be able to land without parachute, providing in this way an inherent degree of safety [Kruijff 2002, 2003.II]. An Inflatable Re-entry capsule (AIR) has been under designed, planned to be re-entered accurately over Swedish territory [Kruijff 2003.I, Morel 2003]. Flexible heatshield materials have been tested and selected [Heide 2003.I]. In 2004 a partial prototype of the inflatable capsule has been constructed [Benetti 2004]. Following an assessment of cost and ESA interest, the AIR has however been abandoned in favor of an innovative, ultra-light spherical capsule, Fotino [De Pascale 2006, De Pascale 2008, Asma 2008]. The Swedish territory has been replaced by the landing zone in Kazakhstan that is intended for manned Russian spacecraft, and that is also in use for Foton itself.

The YES2 SpaceMail project uses a 30-km long swinging tether to accurately deliver Fotino to the ground. The project's three high level objectives are:

1. to provide space education,
2. to demonstrate controllability of a two-stage tether deployment, and finally,
3. to demonstrate SpaceMail by determination of the capsule landing point.

From a point of view of tether system and mission objectives, the project is a logical successor to the SEDS missions. SEDS-1 demonstrated a single stage open loop deployment to a large angle. SEDS-2 included a closed loop deployment to the vertical, using a barberpole brake system. YES2's two-stage deployment combines a first deployment stage controlled to a vertical, under low gravity gradient levels, with a second stage to a large forward angle. It is followed by a swing back to the vertical and a targeted capsule release

(see Section 3.1.1). YES2 builds on the SEDS deployer concept, but relies on European-developed technology only (Chapter 5).

This chapter covers the relevant design aspects of the YES2 experiment, the mission and the lessons learned for development of small tether experiments. The mission data analysis is covered in Chapter 8.

7.2 System design

7.2.1 YES2 and Foton

YES2 is designed to operate from a Russian platform, Foton-M3, which carries ESA microgravity experiments, under the flag of ESA's HME department (Figure 208). This platform provides several advantages. Foton's orbital altitude of 300 km is well below that of the ISS, therefore the probability of collision of the tether with the ISS is extremely low. On top of that, Foton provides power, some basic telemetry and telecommand capabilities that simplify the YES2 design. It features attitude control to provide an initial orientation for endmass ejection. Due to its large mass (7 tons) it can serve as a stable platform. Foton itself carries a 2500-kg re-entry vehicle, which is pressurized and temperature controlled. Although for lack of space YES2 subsystems cannot be housed here, the vehicle contains an ESA equipment, the Telescience Support Unit (TSU), that provides a back-up data storage function to YES2 via a serial cable. Groundstations on Russian territory are available for basic Foton telemetry and telecommand during the YES2 mission, whereas the TSU data is downloaded directly to ground stations in Canada (Saskatoon) and Sweden (Kiruna).

Foton is primarily a microgravity mission. In order to minimally disturb the other payloads, YES2 is switched on for its tether mission only on the 11th day of the 12-day Foton mission.

7.2.2 Key elements

As depicted in Figure 207, YES2 has three elements:

1. **Fotino**, the 6 kg re-entry capsule containis recovery beacon, science payload, transmission to ground and parachute.
2. **MASS**, the 8 kg tethered subsatellite Mechanical and data Acquisition Support System, retains and decouples the Fotino capsule. MASS also contains a science package and transmitter to FLOYD.
3. **FLOYD** (Foton LOcated YES2 Deployer). This 22 kg system containing the tether deployer is bolted onto Foton-M3, and will eject the MASS/Fotino endmass towards Earth. It also provides the mechanical strength and serves as the sole interface to Foton.

An overview of the YES2 main elements and connection to Foton is provided in Figure 206 and Table 60.

FLOYD is the most critical element. The main components of tether deployer are a barberpole brake driven by stepper motor and three tether passage sensors (Optical Loop

Detectors or OLD). The OLDs are critical for deployment control and are the most direct source of deployment data. At least one of them must be operational. FLOYD contains also the deployment control On-Board Computer (OBC), the ejection system and three independent tether cutters. Last but not least, it houses the tether spool with 31.7 km of 0.5-mm thick Dyneema® tether.

Other critical elements for mission success are the MASS on-board timer and capsule release system (MASS-Fotino Decoupling or MFD), as well as the beacon inside Fotino, which is required for confirmation of the capsule landing point.

System	Subsystem	Description
Foton	Battery Pack	Mounting location of YES2.
	TSU	Telescience Support Unit, storage and S-band transponder external to YES2.
	SSAU GPS	Experiment by YES2 Center of Expertise (Samara State Aerospace University) mounted on battery pack(GPS+Glonass and magnetometers).
	TM	Foton telemetry system.
	TK	Foton real-time and time-tag based pulse command system.
	Power	27 V power supply.
FLOYD (Foton Located YES2 Deployer)	Canister	Contains tether and core, as well as various electronics, incl. a UHF receiver.
	Barberpole	Brake system with tether cutter assembly.
	Stepper Driver	Controls for barberpole position based on OBC signals.
	OLD	Optical Loop Detection (length sensor).
	OBC	On-Board Computer, interfaces with Stepper Driver, PDU, OLD, UHF receiver, Foton TM and TSU.
	PDU	Power Distribution Unit, also controls ejection and tether cut via Relays Box.
MASS (Mechanical and data Acquisition Support System) subsatellite	MBox	Contains microcontroller, one gyroscope and two magnetometers, MFD timer and power conditioning.
	GPS	GPS+Glonass system.
	UHF	Transmitter.
	MFD	MASS-Fotino Decoupling system, releases Fotino capsule.
Fotino re-entry capsule	DAS	Data Acquisition System (incl. sensor board, thermocouples, pressure sensors, gyroscopes, accelerometers, magnetometers, UHF transmitter.)
	PRS	Primary Recovery System, including ARGOS beacon, parachute system and Beacon & Parachute Activation System (BAS/PAS).

Table 60. *Overview of YES2 relevant systems and subsystems*

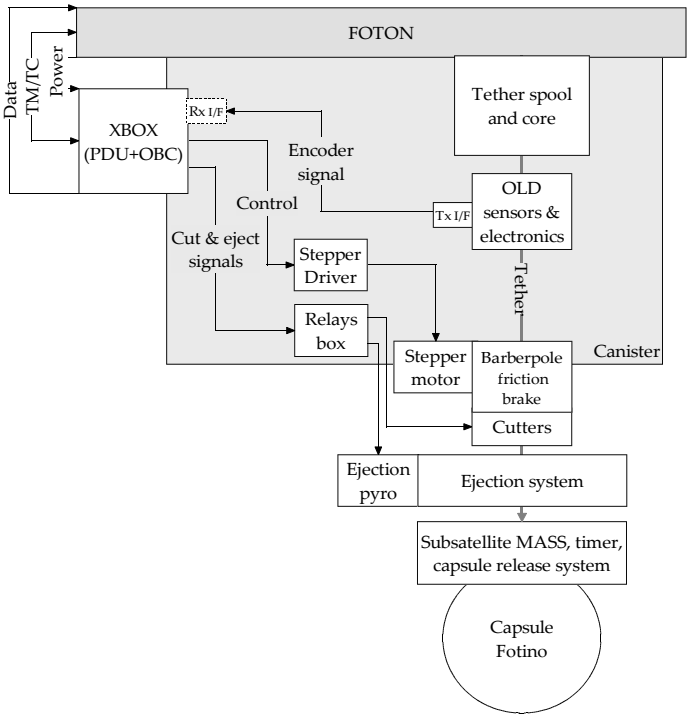

Figure 206. *Simplified overview of the YES2 relevant to the tether momentum transfer system.*

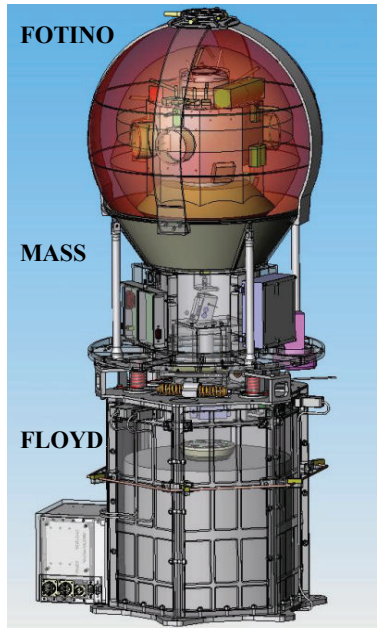

Figure 207. YES2 contains FLOYD (Foton LOcated YES2 Deployer), MASS (Mechanical and data Acquisition Support System) and Fotino, the spherical re-entry capsule.

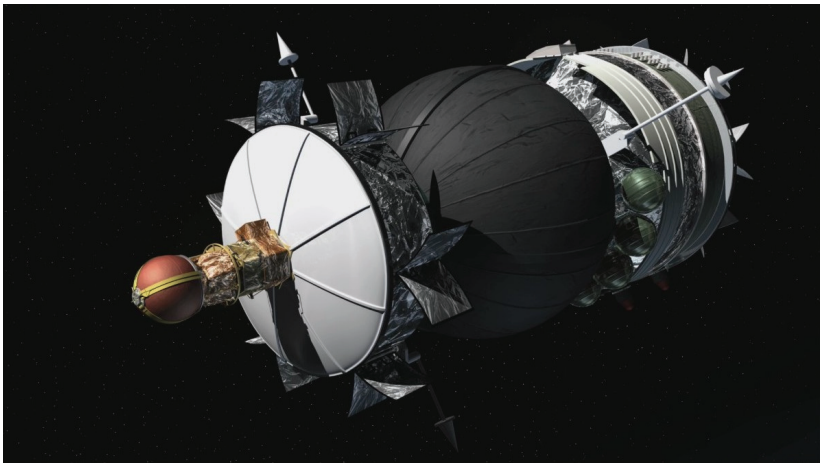

Figure 208. YES2 on Foton during the first 11 days

7.2.3 Interfaces to Foton

The six-bolt mechanical connection between FLOYD and Foton's battery pack is designed such that the thermal link is very poor, about 20 K/W. In the days before the YES2 mission starts Foton is maintained in uncontrolled, random orientation. In a worst case the Foton outer surface around the interface could therefore cool down to temperatures as low as –120 °C.

FLOYD and Foton are electrically interfacing through 4 connectors (YK1 through YK4), These include Power, Telemetry and Data. Detailed specifications are provided in Table 61. The fourth connector delivers the Telecommands from Foton to the YES2 (referred to as TC or YTK). The telecommands are six time-tagged pulse commands that control the YES2 mission (Table 62).

Each physically separated system (Foton, FLOYD, MASS, Fotino PRS and Fotino DAS) has its own zero potential level with a single ground point. Each system is electrically isolated from the others via DC/DC converters, mechanical relays, opto-couplers and RS422 drivers.

In support of YES2, a GPS/GLONASS system has been installed on the Foton battery pack, by Samara State Aerospace University, the YES2 Center of Expertise in Russia. It is planned to work in conjunction with the MASS GPS system, to resolve for the tether position with respect to Foton. It has two diametrically positioned antennas (Figure 209) and is furthermore equipped with a set of magnetometers.

7.2.4 System characteristics

Table 61 summarizes some of the system's main characteristics.

Dimensions	1020 x 410 x 475 mm
Mass YES2	35.7 kg (FLOYD 21.8 kg, MASS 7.9 kg, Fotino 6.0 kg)
Mission Duration	7 hours
Ground Support	TsUP Russian Mission Control in Moscow (Telemetry, Telecommand) Payload Operation Centre in Kiruna (Sweden) and Saskatoon (Canada): science data
Attitude Control	Foton platform (with FLOYD) is actively controlled, MASS/Fotino stabilized by tether tension
Telemetry	Telemetry system via Foton. YES2 status summary is stored on FLOYD every 30 s. A maximum of 90 min worth of status summaries can be transmitted from YES2 to ground via Foton TM at one time (unidirectional, 16 bit parallel at 10 Hz), inside a window of 2-4 minutes per orbit, following a trigger by the TKTM telecommand. Telemetry system via TSU: detailed YES2 data report is transmitted to TSU every second (bidirectional RS422, 19200 bps) and stored there, forwarded to ground by TSU over Kiruna or Saskatoon. Also provides data storage recovered after Foton landing
Datalink MASS-FLOYD	Unidirectional UHF (ISM-band, 437 MHz), 1200 bps, 0.5 W, hemispherical, vertical polarization patch TM antenna, large loop hexagonical circular receiver antenna [Rolo 2007].
Datalink Fotino-Ground	0.5 W omnidirectional, transmits last 300 s of data every 30 s. 437 MHz, Manchester coding, 12.5 kbps.
Power	FLOYD: 27 V unregulated via Foton S/C, nominal operation 100 Wh, peak 56 W, average 24 W during tether deployment. One of the three redundant tether cutters is powered by a YES2 battery for redundancy. MASS and Fotino have autonomous primary batteries.
Thermal	Passive thermal insulation, thermostat with heater for OBC.
Propulsion	No propulsion system; tethered momentum transfer.
Tether	Dyneema® SK65 8x200 braid 31700 m x 0.5 mm (polyethylene), 30 km to be deployed.

Table 61. YES2 characteristics overview

YES2 TC number	Name	Function
YTK2	Eject	PDU fires ejection pyro, OBC starts deployment
YTK3	Cut Tether	PDU fires tether cutter pyro's to release tether from Foton
YTK4	Start Second Stage	OBC will put in motion second stage of deployment (from 3.4 to 30 km)
YTK8	MASS ON	PDU switches on MASS and UHF receiver
TKTM	TM data	OBC will send all remaining stored mission data to TSU/DHU
YTK10	Arm pyros	PDU sets pyro arming latch, OBC prepares for deployment or tether cut
YTK12	Disarm pyros	PDU disarms all pyros (test only)

Table 62. *Overview of YES2 telecommands*

Figure 209. YES2 integrated with Foton battery pack (Samara)

7.3 Mission design

The YES2 mission consists of three phases. In the first phase, Foton executes a microgravity mission (11 days). In this period, the deployment timeline is adjusted to take into account the actual and most recent Foton orbital parameters. YES2 is switched on at the end of the first phase. In the second phase, the tether is deployed in two stages according to the adjusted timeline (2:40 hours). In the third and final phase, the Fotino makes its re-entry (40 minutes). The YES2 experiment operates for 7 hours in total. The mission events are summarized in Figure 213 and Table 63. For typical deployment profiles see Section 5.5.1. Note that the final reference profiles for deployment, determined shortly before flight, are show in Figure 250, Figure 251, Figure 253 and Figure 256.

7.3.1 Preparing for deployment

In order to be able to achieve accurate re-entry of Fotino, shortly before the YES2 system switch-on, the exact YES2 mission timeline has to be determined and uploaded to Foton. The YES2 mission is performed one day before Foton's own re-entry, Figure 208. About one day before MASS/Fotino ejection, Foton orbital parameters are determined precisely from radar measurements on-ground. Then the YES2 ground control team performs a simulation of tether deployment and re-entry based on those parameters, combined with the reference

deployment file already stored in FLOYD (essentially a table of target length, velocity and tether tension versus time). From this simulation the critical mission times are determined within a few second accuracy such as to achieve a projected landing site near the nominally assigned landing point (66.2E, 50.6N in Kazakhstan). These event time tags are next sent to Foton (Table 62). During the YES2 mission, the Foton system makes sure that at the proper time, these telecommands are then forwarded as current pulses to the YES2 unit.

Note that the time of release of Fotino from the tether (the actual re-entry orbit insertion) is hardwired before launch using a special plug on MASS. This preprogrammed time is measured relative to ejection, and cannot be altered after launch. Control of the landing site is therefore done by adjusting the ejection time and start time of the second stage of deployment (Section 5.5.2).

YES2 is eventually oriented towards the Earth. The FLOYD is then switched on by telecommand, and its health status is checked via Foton TM, in particular YES2's OBC temperature and OLD length sensor health. As Foton has spent the 11 days prior to this moment in a random orientation and with YES2 thermally isolated from Foton, there is a small risk the OBC is too cold to reliably perform the mission. Tests have indicated that the OBC is not reliable below –10 °C. Telemetry is requested from YES2 by the Foton TKTM command, which is sent once per orbit during a 2-4 minute interval, when Foton is in view of a Russian ground station. At such a time, the OBC transmits over a 20 Bytes/s link the most critical mission information on YES2 health, deployed tether length, velocity and brake position. The data is evaluated in ground control in TsUP, Moscow, against a table of nominal ranges. MASS is powered up by FLOYD shortly before ejection, in response to YTK8, and reports its status to FLOYD with a two bit code through a Releasable Connector (ReCon).

MASS and the Fotino capsule are jointly ejected when FLOYD receives the sequence of time-tagged arm-and-fire telecommands (YTK10 and YTK2). The spring-based ejection system provides 40 J ejection energy or 2.4 m/s initial velocity to MASS/Fotino (Figure 210). The MASS/Fotino pitch-off rate resulting from ejection system asymmetries is expected to be about 5°/s. MTBSim attitude simulations indicate that during deployment, tether tension is sufficient to maintain the MASS/Fotino endmass into a mere oscillation. Upon ejection, the loss of signal from FLOYD will initiate on MASS the activation timer for the MASS-Fotino Decoupling system (MFD) that is to release Fotino 2.5 hours later. At a distance of some 7 meters from Foton the MASS UHF transmitter is switched on for data transmission to FLOYD. FLOYD forwards this data to the TSU data storage unit inside the Foton capsule. Fotino is fully isolated from MASS and FLOYD and remains powered off during tether deployment. There is no data flow or telecommand capability to or from the Fotino capsule.

7.3.2 Deployment of the tether

Deployment of the first stage of 3.4 km is performed at low tension with levels of centinewtons typically. The first 500 m are the most critical. Deployment here is driven by inertia alone, and friction slows down the MASS/Fotino to about 0.5 m/s. Too high friction could stop the deployment. It is expected there will be the opportunity to monitor through

telemetry the deployed length data from this critical phase. As tether length increases, also the gravity gravity gradient between the endmasses increases, which creates a pulling force that will eventually accelerate the deployment again. All this time a controller is active on FLOYD that adjusts the tether tension as necessary. The required braking level is determined by comparison of deployed length measurements with the reference profile (Section 5.5). The first stage deployment lasts about one orbit. At the end of the first stage, when the tether is 3.4 km long and oriented vertically and stably below Foton, the controller stops the deployment smoothly (Figure 211).

Over Russian territory, a short hold phase will now start. In Siberia there may be an optical viewing opportunity of the deployed tether from the ground, if weather and time of day permits. If necessary, an update of the delayed continuation command (second stage start, YTK4) can be sent to the OBC, or any of the abort or contingency commands. During the hold phase, if any increase of length is observed, the controller will apply some gentle increase of friction.

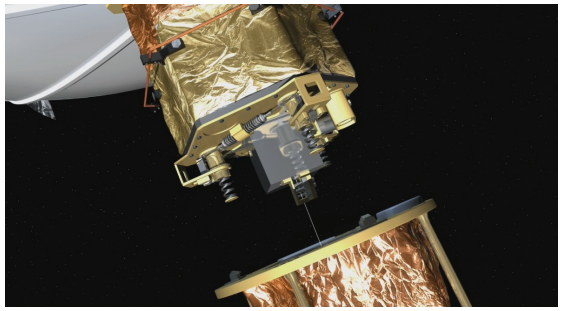

Figure 210. *Ejection of MASS/Fotino from FLOYD*

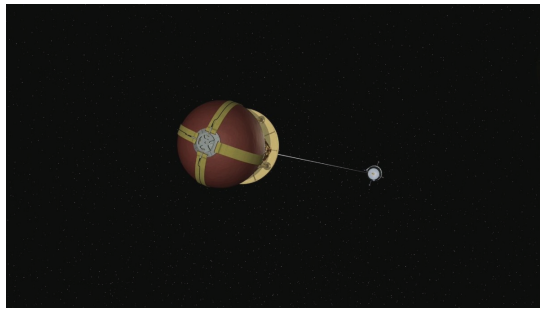

Figure 211. *MASS/Fotino 3.5 km below Foton during the hold phase.*

Upon reception of the YTK4 continuation command, the OBC will release the brake to continue the second stage's full deployment. Velocity goes up quickly due to the large gravity gradient and reaches 13 m/s within 30 minutes. Due to the Coriolis force, the MASS/Fotino runs significantly ahead of Foton at this point, at an angle of about 45 degrees. After about 35 minutes, deployment is near to completion and the tether is slowed down rapidly yet gently by the controller. A margin of 1.7 km on top of the 30 km tether length is available to deal with any controller errors.

The last phase of the tether experiment stretches from deployment completion to the release of Fotino, from MASS, and the release of MASS and the tether, from Foton. First, the fully deployed tether behaves as a gravity-gradient-controlled pendulum and MASS/Fotino swings back underneath Foton. It is at that moment, exactly 9344 seconds after ejection, that the MASS timer triggers the MASS Fotino Decoupling system (MFD) to fire and release the Fotino. This event occurs about one hour into the second stage (the exact timing of YTK4 is not known in advance of the flight). Twenty seconds later the tether will be cut on the Foton side (YTK3), releasing the MASS plus tether into its own re-entry trajectory and leaving Foton free (Figure 212). The tether remains attached to MASS and will burn at around 110 km altitude. Line of sight with FLOYD is maintained until this point, but no data from MASS is expected at this time, due to the poor link between MASS and Fotino (see also Section 7.4.2).

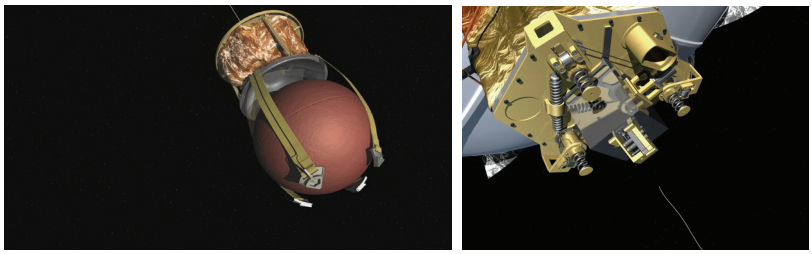

Figure 212. *Fotino is released by MFD, tether is cut, Fotino and MASS+tether coast towards the atmosphere.*

Around this time, the FLOYD, still forwarding its data to the TSU, is switched off. Foton reorients itself for its own re-entry. About 3 hours later, the TSU transmits the remaining YES2 data to Kiruna, completing the YES2 mission.

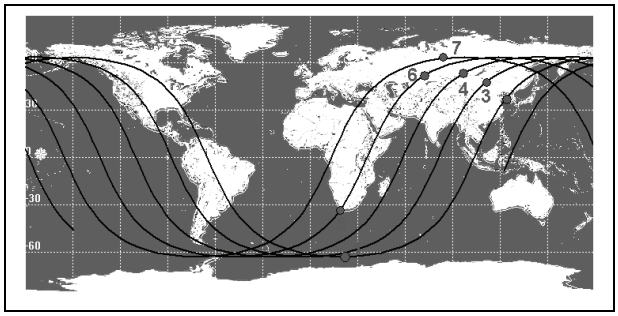

Figure 213. *YES2 ground plot with major events, reference mission*

7.3.3 Fotino re-entry

The Fotino re-entry timeline is presented in Figure 214. The timeline and trigger sequences have been designed to be robust with respect to the identified contingencies such as tether deployment and orbit insertion failures. The release of Fotino, through a break wire, starts

up the science payload contained inside, as well as a timer for the science data transmission to ground. About 1200 s later Fotino will enter the atmosphere at 100 km altitude. At this point, a wire on the nose of Fotino will melt and start the timer of the Beacon and Parachute Activation System, BAS/PAS. In the mean time, the science payload will register, store and transmit towards ground dynamic and aerothermodynamic characteristics of the re-entry. The Argos beacon is switched on when the timer reaches 5 minutes, or, alternatively, by a pressure sensor indicating that 5 km altitude has been reached. If the timer has passed beyond 5 minutes and the 5 km altitude has also been reached, the parachute will be ejected and deployed.

	Mission time [s]	Event	Orbit #	Reference
1	0	YES2 switch ON, start Foton attitude maneuver to establish NADIR-orientation.	171	Figure 208
2	1800	YES2 health and Foton attitude check.	172	-
3	7400	MASS/Fotino ejection, start of 1st stage of tether deployment.	173	Figure 210
4	13150	Start of 2nd stage of deployment.	174	Figure 211
5	16744	Fotino release, tether cut on Foton side.	174	Figure 212
6	19100	Landing Fotino.	175	-
7	24000	Switch off YES2.	176	-

Table 63. *Planned YES2 mission major events, times are indicative.*

Fotino is planned to land in Kazakhstan on September 25th 2007 at about 15 m/s touchdown velocity. The beacon and Flash memory are designed to survive the case of parachute failure and impact. The beacon signal is expected to be received within 3 hours after landing by a satellite carrying Argos equipment [Castillejo 2008]. The Argos system will triangulate the beacon position from Doppler-shift with about 350 m accuracy and report the position on the internet. Reception of this position is considered full mission success. Monte Carlo simulations using MTBSim have determined the +/-3σ landing area to be around 380x60 km, Section 5.5.5 [Stelzer 2006].

Recovery of Fotino or its data is not supported by ESA and can therefore only be an informal low-budget initiative of the YES2 students themselves. The YES2 students have built a portable tracking groundstation to be positioned along the Fotino ground track. It will be attempted to capture real-time and historical data during the Fotino descent. To aid possible recovery the Fotino's UHF transmitter switches to a homing mode and will continue to operate for at least 3 days.

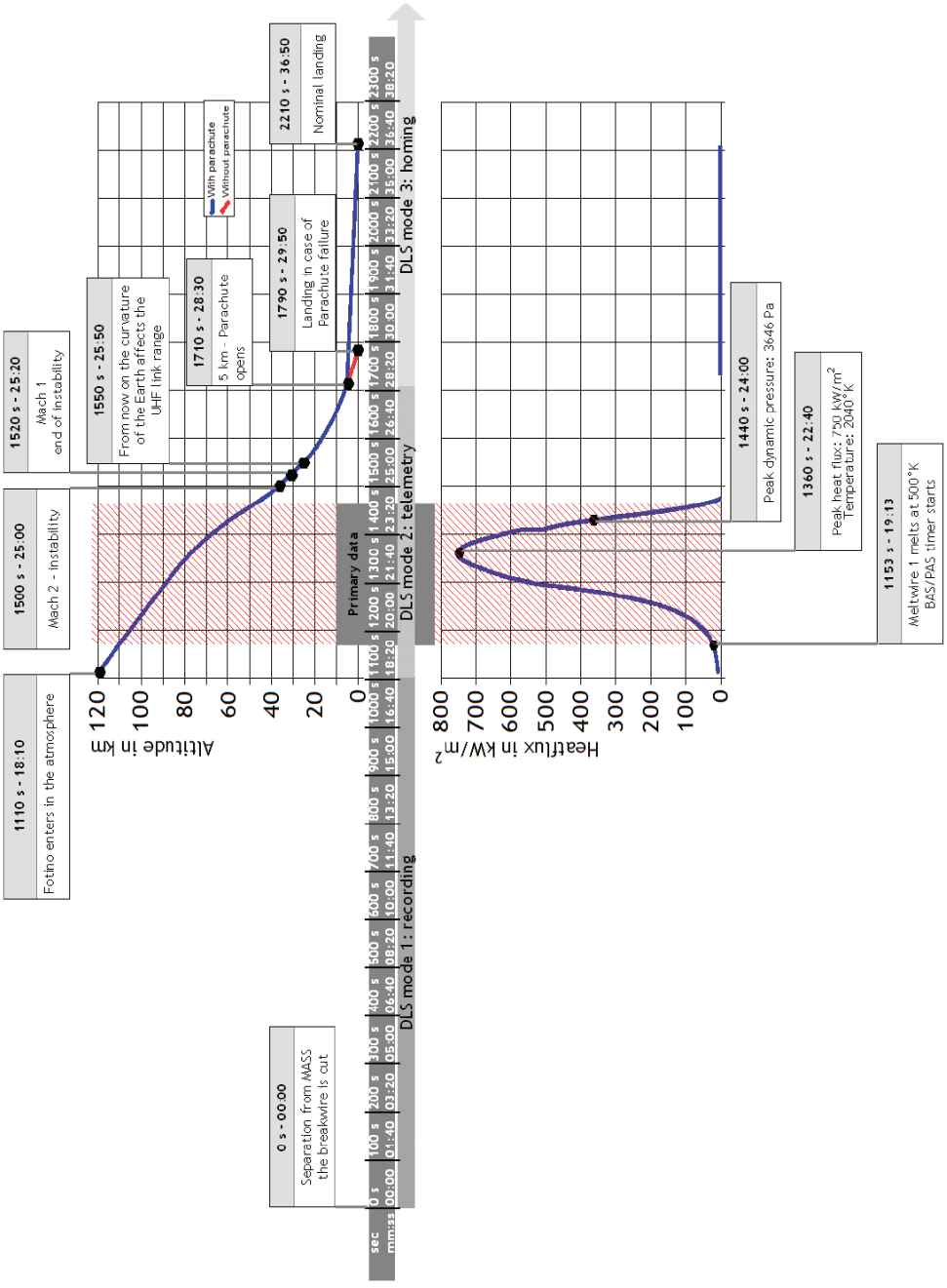

Figure 214. *Fotino re-entry timeline*

7.4 Subsystems design

In this section, the design of tether, FLOYD, MASS and Fotino are detailed to provide further insight into the subsystems relevant for this SpaceMail demonstration.

7.4.1 Tether design

The YES2 tether meets a number of basic safety needs. Its 0.5-mm diameter has been selected for high probability meteoroid survival (estimated at 99.8%, Section 4.3.1). Its low ballistic coefficient of 0.34 kg/m^2 combined with the orbital altitude below 300 km guarantees a very brief orbital exposure or days rather than weeks even in case of some failure (Section 3.3). Similar to the YES tether (Section 6.3.1) the end of the tether on MASS side is made of Kevlar, to prevent melting on contact with a hot aluminium surface. YES2 tether stiffness and damping coefficient were determined as $EA = 5000$ N and $\zeta = 0.08$ respectively based on hanging and bouncing tests (Section 4.1).

In order to deal with the risk of jamming and bounce-back during deployment, with the potential to collide with the Foton platform or wrap around it (Section 4.2), the tether deployment was separated in various failure-mode regions. For each region a suitable safety measure was implemented. In general it must be considered that, the longer the tether, the lower the shock that it will experience in case of jam, ranging from hundreds to a few Newton over the full range of deployment. The exact dependency depends on the tether properties (Section 4.2.1).

For the first 15 m tension will be hundreds of Newtons and a jam can lead to a bounce and collision of the MASS/Fotino endmass with Foton. A Prusik knot fixation (Section 4.2.4) is therefore used to connect the tether to the endmass, such that in case of such a shock the endmass can slip free. Obviously this increases risk of mission failure, but provides safety to Foton. A 3-wrap knot with 55 N slip tension has been selected, providing reasonable probability that the tie-downs will not initiate the slipping. Based on the expected shock load for a jam at 15 m, the free end behind the Prusik knot has been cut to 14 cm to provide sufficient margin (Figure 73).

A jam during the next 350 meters would cause a slow wrapping of the tether around Foton. A simple damping system in the tether (ripstitch), tuned to the minimum shock tension for this region (15-20 N) and able to dampen nearly the full kinetic energy in such a case (40 J), has been produced and tested (Section 4.2.3). Note that in case of a jam after 350 m (57 s) into deployment, the endmass would not reach Foton anymore.

Even with this system implemented from 15 to 130 m (6-57 s) into deployment a jam would lead to recoil of the endmass around Foton and additional measure needs to be taken. After a jam the endmass would float slowly towards Foton with the energy left over from the dampened shock (Figure 217). It would take at least 6 minutes before a second jam and actual wrapping would occur (Figure 216). A collision on the first pass of Foton is not a concern. The sideways drift due to the Coriolis force would prevent a direct collision. Even if there were to be a collision with the host, it will be after 3 minutes and at a very low

energy level below 0.1 J. To prevent a second bounce, which may indeed lead to a collision, an additional safety level is introduced. In the early deployment, the YES2 On-Board Computer continuously evaluates the velocity of the deployment. If a jam is noticed during the first 500 m, the tether is autonomously cut. The on-board computer needs about 30 s to recognize a jam, well within the 6 minutes available.

The resulting tether and fixure design is illustrated in Figure 215. The impact of the safety measures on the tether deployment phases and the associated risk is summarized in Table 64. Probability, severity and criticality of the contingencies have been significantly reduced (see also Section 4.2).

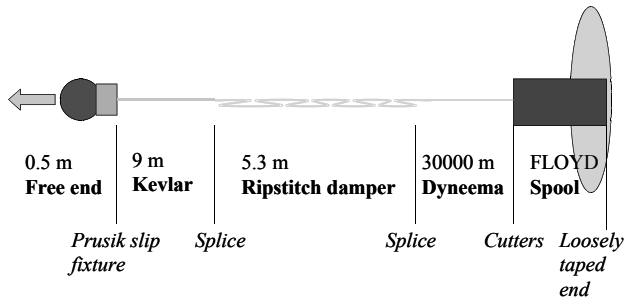

Figure 215. *Tether design and safety.*

L [m]	t [s]	Event	Risk
0 - 15	0 - 6	MASS slips free.	Safe.
15 - 130	6 - 57	MASS kinetic energy dissipated by ripstitch.	Drifting endmass. MASS/Fotino can be near Foton after 3-15 minutes, at 0.1 m/s, under 0.1 J residual energy.
130 - 400	57 - 200	Tether slackens intermittently (about every 10 minutes), eventually becomes pendulum.	Safe.
400 - 15000	200 - 7300	Pendulum.	Safe. Random re-entry.
15000 - 31700	7300 - 8900	Pendulum.	Safe. Nominal or downrange re-entry.
>31700	?	Tether comes loose if shock too large.	Safe. Downrange re-entry.

Table 64. *Risk regions and safety approach during YES2 deployment*

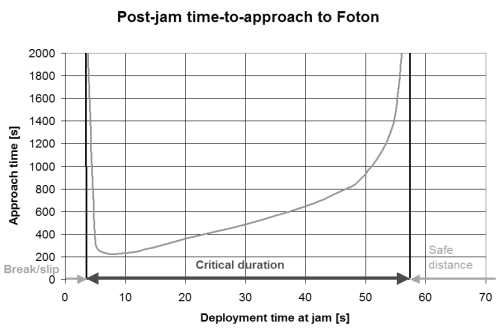

Figure 216. *Approach time to deployer platform after jam*

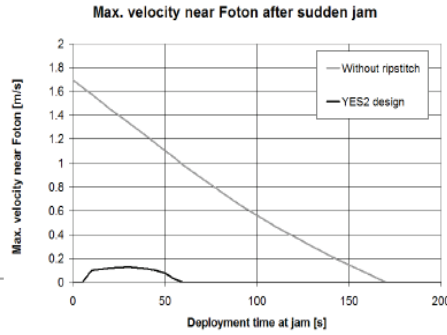

Figure 217. *Velocity near deployer platform after jam and bounce*

7.4.2 FLOYD

FLOYD functions not only as the Foton interface, but also as the base of the YES2 tower structure, and contains the tether deployer and MASS telemetry receiver (Figure 218). Its electrical subsystems and connections to Foton and MASS are schematically represented in Figure 219.

The tether spool is wound onto an aluminium core (Figure 96, Figure 220). This core is hollowed out to include the three Optical Loop Detection (OLD) receivers and the OLD signal conditioning electronics box. The infrared transmitters are placed in a compartment of the canister called the "attic". Deployment of the tether goes over the "head" of the core through a small central hole into the attic plate that covers the FLOYD tether container (Figure 97). The tether unwinds passing through the three infrared beams. The OLD signals are converted into interrupt requests that are fed to the On-Board Computer through the Power Distribution Unit (PDU) interface circuitry.

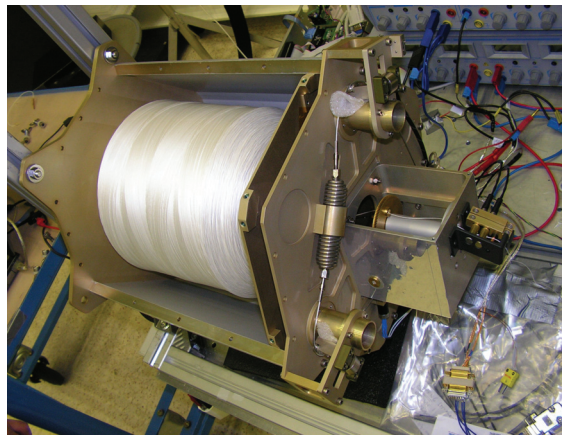

Figure 218. *FLOYD under functional test in unwinding testrig at ESA/ESTEC.*

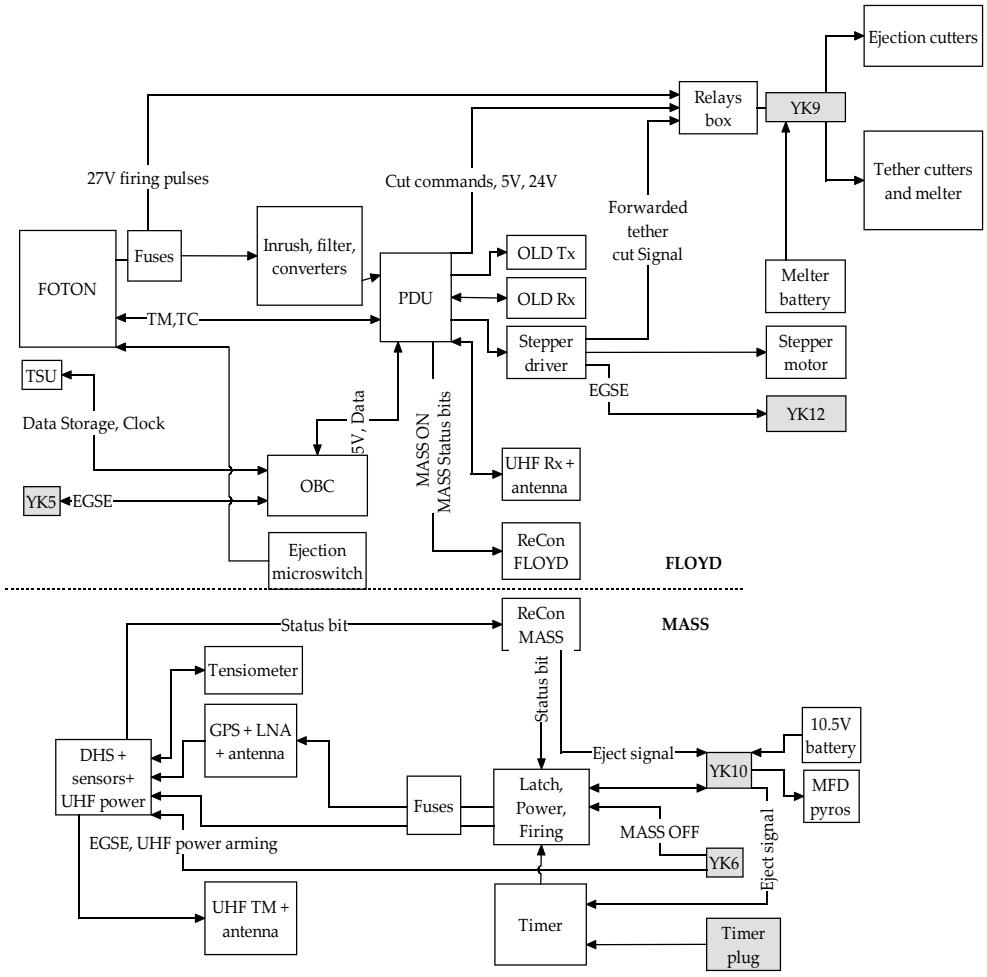

Figure 219. *FLOYD-MASS electrical overview (see text for details). The numbered YK's are EGSE connectors.*

The winding is divided into five parts, the parallel winding at the core, covered by four criss-cross parts with a winding angle setting going from seven to four turns per cycle. For each of these parts a quadratic fit of length versus unwound loops has been determined, which is used by the OBC to determine the unwound length from the incoming OLD interrupt signals (Section 5.3.3). The deployed tether length can be determined with about 0.3% accuracy (Section 5.3.5). Three tie-downs keep the tether in place during launch (Section 5.3.4). Each knot, when breaking at time of ejection, dissipates about 1 J, and lasts for about 10 ms, peaking at 40 N. This leads to loss of velocity of about 0.1 m/s but also has an intended positive side-effect. The tie downs are placed on the spool about a second's worth of deployment apart, such that as they break, the torque exerted by the tether will reduce the MASS/Fotino pitch-off rate.

The spool is contained in the canister, which is made from six panels that also provide structural strength and stiffness to YES2. The panels are hard anodized. They are mounted onto a solid structural interface plate which is mounted to the Foton battery pack with six bolts. The attic is the shallow compartment in the top of the canister. It contains not only the the OLD transmitters but also driver electronics for the barberpole stepper motor, as well as a pyro arming and firing relays box, and a UHF receiver. All boxes have their connectors on the outside of the FLOYD canister panels. The tether passes through the center of the attic into the base of the barberpole brake box.

Figure 220. *YES2 tether spool* "Florian"

The barberpole (Figure 221) is hard-anodized and about 2.4 cm diameter (Section 5.4.2). The surface roughness of about 1 micron is matched to obtain the proper friction coefficient (Section 5.4.4). The worm gear contains a Reli-a-flex flexible coupling and a Phytron VSS-32.200.1.2 vacuum stepper motor. As the tether exits from the barberpole it passes through the cutter assembly, that contains two Airtec parachute cutters (Figure 218), powered by the Foton 27 V supply, and one thermal element that is designed to melt the Dyneema® tether in about 30 seconds as a back-up, using a 3.6 V battery. The cutters are activated one by one with a 0.4 s delay, to allow for maximum functionality in case of any type of failure of either of the pyro's. The first cutter signal is received directly from the YES2 PDU, the second cutter, is controlled by the OBC's internal logic, and allows, as an added feature, for an autonomous cutting capability.

Several custom designed units of electronics control the tether deployer hardware. Outside the canister is mounted a cube-shaped box, the ElectroniX Box or XBOX for short, that contains the On-Board Computer and the Power Distribution Unit interface electronics. Inside the attic are located the Stepper Driver and the Relays Box.

The PDU, inside the XBOX, contains three Interpoint power converters in a shielded compartment, a small, 1.5 W converter for primary 5 V PDU functions, a 30 W unit to provide power to all 5 V FLOYD electronics, and a dedicated 24 V supply for the Stepper

Motor. The 27 V Foton power supply is fused and inrush limited. The Power Distribution Unit is developed not only to provide a power supply function but also for signal processing and interfacing. It validates and executes in hardware the incoming telecommand pulses from Foton. Each such pulse is represented by about 1 A current lasting for about 0.4 s. The PDU also takes the 17 bit parallel and digital telemetry output from the OBC and offers it to the Foton telemetry multiplexer system. Both functions use optocouplers. Finally, the PDU converts incoming and outgoing internal YES2 signals, mostly using RS422.

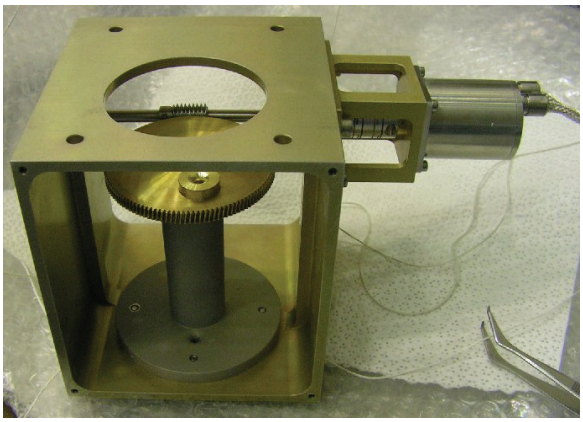

Figure 221. *YES2 Flight barberpole brake*

The XBOX contains also the On-Board Computer, a 133 MHz PC104 (SECO M543) and a Diamond Systems IO-board (MM-AT). Due to thermal limitations that became obvious in the subsystem testing, a 3 W heater has been added to the XBOX, as well as a thermostat board that switches another 6 W when the temperature drops below 20 °C. The SECO board runs the on-board software based on a QNX operating system featuring multiple software processes guarded by a High Availability Manager (HAM).

The Stepper Driver (Figure 222) has been developed as a highly compact internally redundant subsystem, based on Atmel microcontrollers, with watchdog and several other safety features [Graczyk 2008]. It is commanded by the On-Board Computer through RS422. The driver keeps track of the actual stepper motor position independent of the OBC to allow for robust control. Every control interval, if the brake has to be moved to a different position, the stepper motor is ramped up from the selected low initial frequency of coil current switching (Section 5.4.2) to its operational frequency of 4000 Hz halfstep until the new position has been achieved. A current shaping is used to maximize torque [Graczyk 2008]. The Stepper Driver is able to provide telemetry back to the OBC including temperatures and brake position, however, this communication line has eventually been rerouted to the cutter system via the Relays Box. This awkward signal routing is the result of a late change in requirements, by which an autonomous tether cut capability is added for safety. The Stepper Driver is thus being used as a relay station for the OBC's tether cut signal.

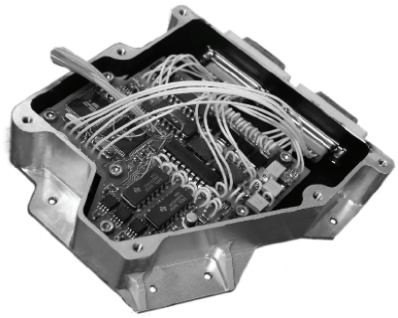

Figure 222. *YES2 Stepper Driver*

The Relays Box contains redundant latches, that arm, disarm and fire FLOYD's pyro circuitry, which activates the ejection system and the tether cutters. Latch control commands are sent to the Relays Box as RS422 pulse signals. Pyro's are double-locked: both electrical poles are latched simultaneously. A pyro "fire" pulse signal will lead to switching a relay on-and-off for the duration of the input pulse, i.e. about 150 ms. Each pyro function is redundantly performed, firstly by a mechanical and secondly by a solid state latch. Pulse power comes from the 27 V Foton supply directly and each firing pulse is individually inrush limited for current and slope.

The first pyro to be fired is that of the ejection system (Figure 223). The YES2 ejection system is a scaled-up version of a design originating from the Swedish Space Corporation that uses three springs pushing against the MASS plate. MASS is held tightly against FLOYD by three levers. The levers themselves are held by a single pretensioned cable that can be cut by a redundant Holex 2801 pyro cutter. The cut releases the levers such that the springs can freely push both MASS and the levers away. Three springs combined contain 40 J energy, to provide 2.4 m/s initial velocity to MASS/Fotino.

A misalignment between springs or center of mass and the geometrical center of the ejection system will lead to unwanted angular rates of the endmass. Such a pitch-off rate may adversely affect deployment and communication between MASS and FLOYD or may cause the tether to wrap the Fotino capsule, impairing its release. The requirement is a pitch-off rate better than 10 °/s, based on MTBSim simulations. Also a difference in length between two of the three springs of as little as 0.2 mm can cause such a rate. In order to meet the requirement, the center of mass of MASS/Fotino has been balanced within 2 mm from the ejection system center line. The springs are selected from a batch of about 20 based on uniformity in dimensions, spring constant and energy.

The ejection system plate contains also a microswitch that is read out continuously by Foton's telemetry system to confirm successful ejection. The ejection plate as a structural element supports also the barberpole brake and the FLOYD-MASS Releasable Connector interface or ReCon.

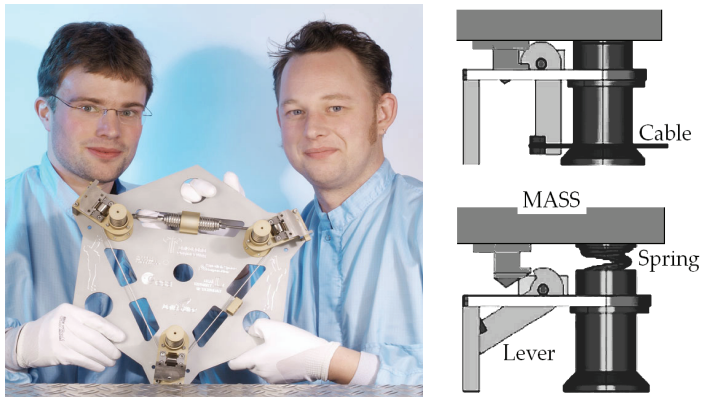

Figure 223. *YES2 students holding the ejection system engineering model, operating principle.*

7.4.3 OBC software

The OBC software, written in C++, controls the tether deployment control but also data handling, storage and telemetry (TM, TSU) as well as confirmation and execution of telecommands (TC). The eleven cooperating processes making the OBC software are shown in Figure 224. The processes are controlled and restarted if necessary by the QNX operating system's High Availability Manager (HAM). The MASTER process acts as a data serialiser and decision maker, while the actual work is performed by other processes. A full description can be found in [Spiliotopoulos 2008]. The most relevant processes for planning and controlling the tether deployment are EGSE and STEPPER.

The EGSE process is only functional in test configuration. It interfaces to the Electrical Ground Support Equipment hardware (EGSE) for upload of system software and data files, as well as to send telecommands for testing purposes. The OBC software and all its parameters are fixed before flight and uploaded through EGSE connectors. The OBC allows for late upload of a mission parameter file. Only a limited software test is therefore required in case of late changes (Section 8.1.5).

The STEPPER process is the process in charge of controlling the deployment. It calculates the current deployment velocity and deployed length based on interrupt requests (IRQs) from the OLD sensors, and commands the required barberpole brake position via the Stepper Driver according to the current mission phase, deployment profile and control parameters (Section 5.5). Robustness is included against accidental or forced reboot of the OBC during deployment.

Whenever an interrupt request from an OLD channel arrives, the OBC software marks the time and identifies the OLD channel transition to determine the increase in length and change in velocity of the tether. The transition algorithm inherently deals with a single broken OLD channel (Section 5.5.3). A filter is included to suppress high frequency noise above 125 Hz in front of a single OLD, as might appear due to tether vibrations or electromagnetic interference. Finally an algorithm is added to take care of the case where two OLD channels would be broken (Section 5.5.3).

Via the Stepper Driver, the OBC software also controls a tether cut capability. It is triggered if a tether cut command (YTK3) is received, but also can be activated autonomously if, within the first 500 m after ejection, the deployment velocity drops below 1 cm/s.

The mission is split into various phases during which the STEPPER process is expected to display a specific behaviour regarding tether deployment control. The mission phases in their nominal order are listed in Table 65. Phase transitions are made in the following cases:

- Time out (end of reference profile, nominal condition).
- Critical stage length is achieved during deployment (back-up condition).
- Cut command YTK3 is received (triggering transition to Wait Phase).
- Autonomous tether cut executed (triggering transition to Wait Phase).

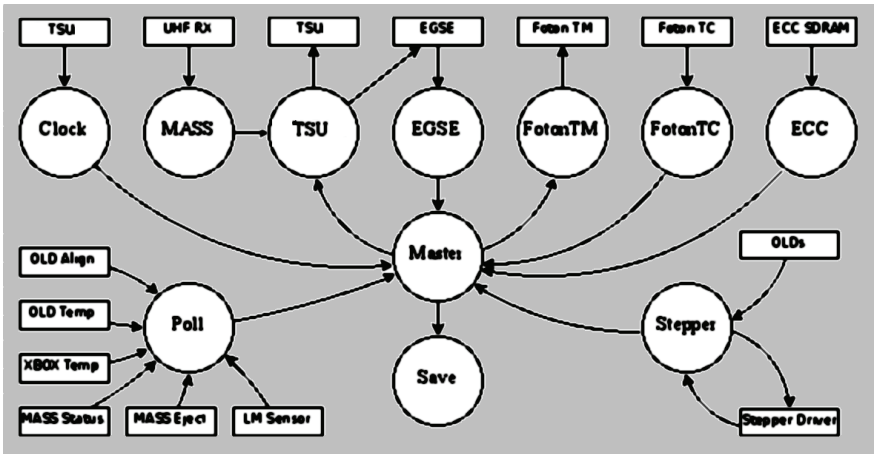

Figure 224. *YES2 control software high level flow diagram*

Phase	Description
Disabled	Initial phase, no deployment control.
Enabled	Armed for deployment, no deployment control.
1st Stage	First stage of deployment. Deployment control according to first stage deployment profile.
Hold	Tether deployment stopped with minimal brake.
Transition	Prepare to continue deployment.
2nd Stage	Second stage of deployment. Deployment control according to second stage deployment profile.
Swing	Tether brake set to maximum.
Wait	Send cut tether command (for redundancy), end of mission

Table 65. *YES2 software control phases*

7.4.4 MASS

MASS is a piece of support hardware with as primary function restraint and accurately timed release of Fotino into its re-entry trajectory. Furthermore, it provides inertia to the deployment of the tether. Finally, MASS has a science subsystem with transmitter to contribute to the tether deployment data collection. Figure 219 provides a schematic overview of the electrical subsystems involved in these functions.

MASS has a very basic signal connection with FLOYD. MASS is powered on through mechanical latches by a power pulse from the FLOYD PDU (following YTK8), that arrives to MASS via a Releasable Connector (ReCon). MASS can only be powered off through an EGSE connector (YK6). Before ejection status bits are exchanged via the ReCon. Some seconds after ejection, MASS transmits data to FLOYD via a one-directional UHF link. The FLOYD OBC directly forwards the data from MASS to the TSU for storage and post-flight recovery.

The MASS structure provides an interface to the FLOYD ejection system, the MASS Plate, on which also the ReCon and patch antenna's for UHF and GPS are mounted, as well as a centrally mounted cylinder of 20 cm diameter. The cylinder supports a cone in which Fotino is placed (Figure 207). The circular MASS Plate, opens into the cylinder, providing a cavity. In launch configuration this cavity contains the FLOYD barberpole brake system as it protrudes from the ejection system.

The tether is routed from FLOYD to the MASS structure. As the tether exits the FLOYD cutter bracket it loops around a pulley mounted inside the MASS cylinder and connected to the MASS tensiometer. From there the tether exits sideways to the outside of the cylinder. Here the tether is finally connected to the outer structure of MASS via the Prusik slipping knot.

Three brackets are mounted on the outer surface of the cylinder, holding the UHF transmitter, a Russian-built GPS/GLONASS receiver, the Battery Box as well as the MBOX. The MBOX houses electronics for the science function, provided by the Data Logging System (DLS), as well as for the primary function of MASS, which is to provide reliable and timely release of Fotino.

The MASS DLS measures the dynamic behavior of the sub-satellite and the tether. A 0.5 N tensiometer, three magnetometers, and a gyroscope are connected to the MASS DLS. The MASS DLS also collects data from the GPS/GLONASS receiver. It forwards all data in real time to the UHF transmitter at 1200 bps. The power to the DLS is fused such that the critical MASS electronics, that control the release of Fotino, are protected.

The Timer Board initiates the firing signals for the MASS-Fotino Decoupling pyro's. It contains a triple hardware timer of which the median time is used. The firing time is programmed by a hardwired plug. The plug allows for a 4 bit coding of release time, anywhere between 8192 and 10112 s, in 128 s resolution and at better than 1 s precision.

A Latch, Power and Firing board (LPF) receives the firing signals from the Timer Board and makes sure three pyro's are fired in the MASS-Fotino Decoupling system (MFD). It also provides 5 V power to the Timer Board and 10.5 V to the Data Logging System. After ejection, 10.5 V is also sent to the GPS/GLONASS unit.

The MFD is a crossed-belt system with the purpose to restrain Fotino during launch and deployment. The belts are held together with a Kevlar cable on top of Fotino. Three cable cutters secure its release, until they are fired by the LPF. One of the cutters also cuts an electrical "break wire", attached to Fotino, which starts up the Fotino science system.

7.4.5 Fotino

Fotino is a small re-entry vehicle of 40 cm diameter and 6 kg mass. It has been developed as a minimally sized spherical capsule that could bring a meaningful payload from space to Earth. The spherical shape has been selected for simplicity of design analysis and of construction. Fotino includes a parachute, and is to be retrieved by means of a beacon [De Pascale 2006].

Fotino is a technology demonstrator that carries also a scientific experiment. The technology to be demonstrated concerns low-cost and light-weight structural and flexible heat shield materials. The core of the capsule is made of polyurethane (PU) foam, whereas the heatshield is made of low density Alumina flexible felt protected by vacuum-formed alumina-based material, impregnated with red silicon ablator. The spherical PU core contains an aluminium octagonal lightweight box, that is positioned around the central parachute cylinder and houses the electronics and scientific payload (Figure 226) [De Pascale 2006, De Pascale 2008]. Fotino probes a yet untried regime of re-entry where useful lessons about the atmosphere can be learned. With its relatively low ballistic coefficient it will decelerate primarily during the rarefied and slip flow regimes [Asma 2008]. From a scientific point of view the spherical shape is also considered interesting as flight data can be straightforwardly fitted to the models.

A model of the capsule was tested in the Plasmatron facility at VKI, Brussels, under a representative enthalpy profile based on simulations using the MTBSim's re-entry physics model that merges results from CFD (Computational Fluid Dynamics, continuum regime) and DMCS (Direct Monte Carlo Simulation, rarefied regime), Figure 225.

Despite its small size, Fotino contains two separate electronics systems, the Primary Recovery System (PRS) and the Data Acquisition System (DAS), schematically represented in Figure 228 and Figure 229.

The Primary Recovery System's main component is an Argos beacon (see Section 7.3.3). The Argos beacon is designed to survive an impact without parachute, and for this purpose it has its own battery and a system that keeps the power running once it has been switched on, even if the wiring to Argos breaks. The beacon uses two diametrically oriented DDRR loop antenna's intended to achieve near-omnidirectional transmission. These antenna's are the more sensitive part of the PRS system.

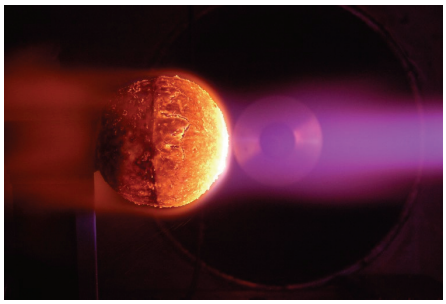

Figure 225. *Fotino model in Plasmatron*

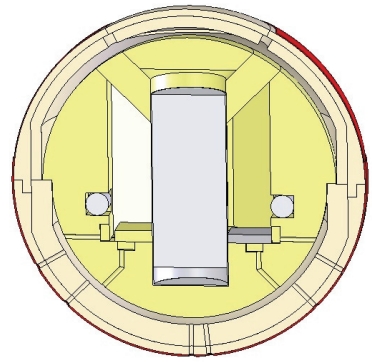

Figure 226. *Cross section of Fotino structure*

To reduce the probability of failure and risk at impact, a parachute system is included. The single parachute is about 1 m diameter and decelerates Fotino from 60 m/s to 15 m/s. The parachute is folded and kept between two halves of a foam container, the "sabot". The ejection system for the parachute is compact and uses two concentric springs (Figure 227). The smaller, central spring opens the heatshield at the back of the capsule by pushing on the sabot. The outer spring accelerates the sabot with chute out of Fotino at 10 m/s, sufficient to overcome the worst case atmospheric drag force and extend the parachute cord. Once outside of the capsule, the two sabot parts split up and the parachute is released. Various safety features are included to avoid inadvertent firing of the pyro.

Both Argos power and parachute ejection are triggered by the Beacon and Parachute Activation System (BAS/PAS), a logic device in hardware. A timer starts to count down from 300 s after a wire on the capsule nose has molten early in re-entry. A pressure switch, triggering at 5 km altitude, is used in combination with the timer. It switches on the beacon using "OR"-logic for reliabilty, and initiates ejection of the parachute using "AND"-logic for safety.

Fotino's Data Logger System (DLS) is similar to that of MASS, and is switched on when Fotino is released from MASS, as a break wire is cut by a MFD pyro. The DLS transmits science data to the ground in UHF, using two DDRR antennas, but stores the data on Flash as well. The transmission starts based on a timer, at about 1000 seconds after release, i.e. shortly before atmospheric entry, and transmits the most recent 300 s of data in bins of 30 s. Shortly after landing, about 40 minutes after release, the DLS switches to homing beacon mode to assist recovery.

The DLS is connected to a large number of atmospheric sensors and dynamic sensors. The atmospheric sensors are 8 absolute pressure sensors, 4 high precision relative pressure sensors, functioning as absolute sensors in vacuum, and 15 thermocouples, distributed over

the front heatshield of the capsule for maximum science return. Dynamic sensors include on-chip gyroscopes, magnetometers and accelerometers. Fotino also contains some passive experimental radiation sensors.

Figure 227. *Fotino parachute ejection system*

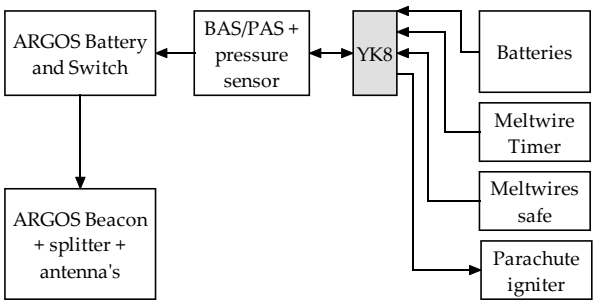

Figure 228. *Fotino PRS electronics diagram. YK8 is an EGSE connector for arming and monitoring.*

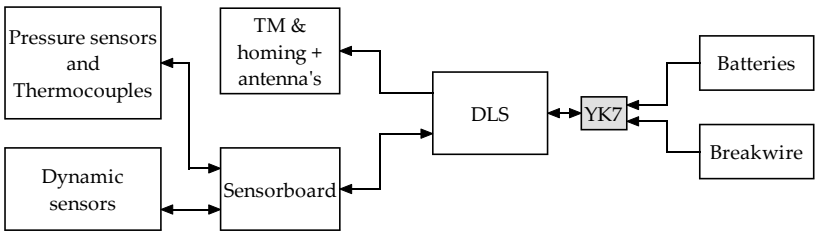

Figure 229. *Fotino DAS electronics diagram. YK8 is an EGSE connector for arming, monitoring and programming.*

7.5 Management of the YES2 project

7.5.1 Systems engineering tools and approach

YES2 has been developed to the relevant design standards within ESA, taken and tailored from the European Cooperation for Space Standardization (ECSS) and the documentation standard in use by the ESA/MSM-G department (GPQ-MAN-01, 1998). Documentation deliverables have been inherited from the QPQ standard, as well as the requirements for traceability of configuration items, interface requirements and verifications. In addition, particular attention has been paid to traceability of trade-offs and design decisions, inventory management, safety, definition of manufacturing processes and operational procedures as well as streamlining of interface documentation.

Two web-based interactive system engineering tools have been developed. These tools, STEFI and ALBATROS, have made it possible to achieve traceability and efficiency, even with a large, disperse and volatile group of team members.

The first tool, STEFI (Support Tool for Eternally Filing Issues) serves to document, organize and formalize the rationale of design trade-offs, and make those discussions transparent and easily accessible to all team members. STEFI is a simple tool that has saved a lot of time as decisions can be traced back and reiteration of similar discussions is prevented.

The second tool, ALBATROS (Automated Listing, Budgeting and Traceability RepOSitory), is a flexible configuration item management tool [Hambloch 2007]. The ALBATROS tool contains all -about 15000- configuration items of YES2 and their interrelationships. Configuration items in YES2 are defined very broadly as all entities that are considered valuable to keep track of, including contact information, requirements, project documentation, subsystems, hardware parts and their storage locations as well as signals and their connections. It is based on a product tree that starts from a subsystem tree whereto all new items are logically attached. Interrelations between the items can be easily defined. Specific queries and processing functions can then be defined that search and process the tree via those relationships.

Because the tool is accessible for all team members and from anywhere on-line, a single status of the system is available at all times. Inconsistencies are thus effectively prevented. An advantage of ALBATROS is that the often monotonous and repetitive task of configuration control can be easily distributed between team members. This allows the system engineer to focus on primary tasks, such as system design and verification of documents, rather than on data-entry and consistency checks.

ALBATROS can produce semi-automatically much of the required and often-used product assurance documentation. Examples are the requirement flow down and traceability matrix, the validation matrix, harnessing manufacturing procedures and electrical interface documentation. The tool provides all sorts of overview listings and budgets such as for the inventory, assembly logs and system mass budget.

Electronic files are managed separately from Albatros. Documents, even if only intended, are registered on ALBATROS, and when written, kept in a single "pool" on an FTP server. Version control and naming of documents is performed manually according to a predescribed standard. Software versions are maintained through an automated CVS system.

7.5.2 Innovation from education

Under the lead of Delta-Utec, the YES2 subsystems have been designed and built with the help of hundreds of students and young engineers. Around 180 students from 25 countries and 50 universities contributed with design reports and hands-on work to the YES2 effort. The work has resulted in about 100 internships, 90 conference papers and 50 Bachelor and Master Theses. Over 200 more students participated in early brainstorm sessions or project work. An overview of educational results of YES2 is provided in [Kruijff 2003.III, Kruijff 2007].

In working effectively with this many students, a personal relationship between management and the students has been found fundamental, such that mutual interests are appreciated and respected. Task assignments and trade-offs, for example, have taken into account the need for student motivation. It has helped therefore that, as with YES, the innovative and challenging character of the tether and also of the re-entry system has clearly contributed to the motivational value of the project. The objective has been for the students to lose fear of creating and to have confidence in the scientific principles they have been taught. Furthermore, the students have been maximally challenged and provided with as much responsibility as they are comfortable with. Some particularly involved students have been given the possibility to grow and for example manage newly arrived team members. Personal issues have been addressed with care, and in most cases, housing and other primary needs could also be arranged. The students' satisfaction level with their participation has remained high both during and after the involvement.

A side effect of this approach has been that the design has been partially shaped by the educational objective. This has worked out in two directions. Not all the innovative work ended up in the final design. For example, in the early stages of the project, considerable effort has been invested in the development of an inflatable re-entry capsule prototype that was eventually not completed but replaced by the simpler Fotino. On the other hand, students and universities yet without experienced in space technology have introduced novel solutions from other domains such as textile, material and information technology.

Similarly as for YES, YES2 has been performed under considerable financial constraints, yet has been helped forward by its sympathetic character. In contrast, more industrial SpaceMail initiatives have proven to be not financially viable [Sabath 1996.I, Alenia 1995, Gavira 2000].

All in all, the YES2 project is a product of an interaction between education, innovation and motivation, as schematically represented in Figure 230. It has led to an output beyond

education or a satellite design. In addition, meaningful technology development and innovation has been achieved.

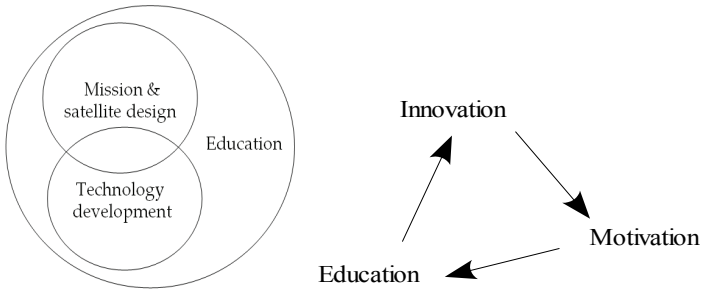

Figure 230. *The productive interactions of a sufficiently challenging educational project lead to more than just design*

These results have not been trivially achieved however. Students often need intense management and require several months to get accustomed. It happens regularly that they are required to leave before they can complete their task. Information transfer between the generations and provision of consistency throughout the project are thus key needs. It has proven critical for success that a dedicated core of involved professional provides this continuity. In case of YES2, Delta-Utec has carried the project responsibilities. It has provided a clear and continuous interface, guarded the project focus and has made the final design decisions. It is recommended for challenging projects with extensive student involvement that such a dedicated core of professionals performs at least the planning and management, finds necessary sponsors, defines the system requirements and leads the critical tasks of systems engineering, knowledge management and system verification. If there are knowledge gaps within this core team, there is a responsibility to involve external experts.

7.5.3 Project phasing

The YES2 project, in retrospect, has gone through three phases. In each phase, a different path has been followed. Table 67 provides insight into the timeline and events that define the YES2 project. The three identified phases have been framed for clarity:

1. a brainstorm phase,
2. a detailed design phase, and the
3. integration phase.

The *brainstorm phase* involved about 250 students and 25 universities, and focused on requirements set-up, conceptual ideas and trade-offs, parallel conceptual design works, dynamics analysis and preliminary testing. The brainstorm inputs have been many yet dispersed and not necessarily consistent. It has been necessary for Delta-Utec management to actively integrate them into a consistent Preliminary Design [Kruijff 2002, Kruijff 2003.I-IV].

The *detailed design phase* that followed can be characterized by two major subphases. Firstly, the design, analysis and test and secondly, the production of formal Critical Design Review (CDR) documentation, targeted to meet the required quality standards. At any time about 60 students have been involved, located at Delta-Utec and ESA/ESTEC (mission & system engineering) as well as at four Centers of Expertise: University of Patras (mechanical design), Samara State Aerospace University (mission analysis), University of Reggio Emilia (capsule design) and Hochschule Remagen/Krefeld (tether deployment and winding). The design effort has proven to be very well suited for student involvement. The CDR documentation effort has been a time-consuming challenge covering multiple generations of students.

The *integration phase* has been performed with about 25 students, all as interns in Delta-Utec and at ESA/ESTEC. This phase resembles the YES construction in the sense that it has been intense and productive and has required only a single generation of collocated students. Such a team configuration seems to be a prerequisite for successful completion of a volunteer satellite project. During this phase it has been discovered that the YES2 project has lacked continuity in certain knowledge domains. For YES2 this lack concerned particularly the field of electronics. As a result, a number of trouble-shooting exercises have become necessary. External experts have been hired to resolve some critical issues, whereas for other systems emergency solutions have been implemented or degraded performance has been accepted.

As is clear from the project timeline, YES2 has not been immune to fundamental design change, often driven by budget or other non-technical incentives. It has been descoped or expanded several times, thus renewing again and again the challenge and need for motivation. It is probably not possible in future projects to avoid such changes a priori. Rather it is important to clarify to the team members that these dynamics are part of a living project and belong to the reality of space engineering.

7.5.4 Lessons learned from YES and YES2

Most of the success factors of YES have been successfully re-applied. The team has been maintained through a flexibility in the way of student involvement. The assignment of priority levels has helped to bring focus into the development. Collocation has been critical during integration. The final year of YES2 resembled the YES development in terms of intensity, time pressure and sense of achievement.

For YES2, most of the YES pitfalls have been avoided. Broken team spirit and excessive complexity could be prevented by persistently maintaining a single, clear direction. Testing has been made a primary part of the system development (see e.g. Section 5.2.4). The first four years of development, testing and documentation have clearly paid off. A much higher quality product has been built, that is reproducible, and this has been achieved in good team spirit.

YES2 featured also some new challenges and problems. The focus on testing and the increased documentation requirement has made the horizon too long for a single generation

of students and the sense of urgency has often been absent. Whereas the YES design has remained consistent and flexible throughout the project, YES2 design requirements were changed throughout the project, often outside team control. The mass constraint became tighter with time and new features and requirements were added along the way, often for non-technical reasons. The design went through many stages of change and (re-)optimisation. Safety concerns and financial uncertainty caused more delays. This amounted to time pressure and exhaustion and would cause a failure that could, in retrospect, have been rather easily prevented (Section 8.5.1). The often-made attempt by the YES2 team to optimize the system, sometimes but not always by necessity, has limited the flexibility and contrasts against the YES approach to include margins where possible. More than for YES, education has been a primary objective this time, so work packages have been defined sometimes largely by academic rather than direct project interest. This has led to reduced focus and a stretched project duration. Considering the experiences of YES (manufacturing oriented) and YES2 (education and curriculum oriented), it can be concluded that a good compromise is to limit the educational element to closely guided internships and thesis works.

The most important lessons learned are summarized in Table 66.

1	Persistence is a key element of creativity.
2	Be open & responsive to critics.
3	It is hard to MISS : it is hard to make it simple & smart.
4	It pays off to design with margins and back-up options, to plan for extensive testing & to invest in quality management (traceability of design, configuration items, trade-offs).
5	Motivation, education and innovation can reinforce eachother. Responsibility is a key element of motivation.
6	Working with students can be enabling but is not trivial. Close guidance and continuity is required. System engineering, the requirements and verification is best left to experienced engineers. Educational considerations should not overrule technical ones – thesis works and internships are therefore the best suited mechanisms. Due to the ad-hoc nature of funding and organization, regular compromise and re-scoping is hard to avoid.
7	To be productive, collocation is key.
8	Get in external know-how when necessary despite cost.

Table 66. Summary lessons learned from YES and YES2

2000 – December	Project preparation starts.
2002 – April	Kick-Off.
2002 – Summer	Promo tour to 30 universities. Capsule concept brainstorm starts [Kruijff 2002, 2003.II].
2002 – October	Tether test rig presented at IAF Houston , built by Center of Expertise Remagen/Krefeld.
2003 – April	Inflatable capsule from Cranfield selected [Morel 2003]. YESSim re-entry simulator development starts [Calzada 2004].
2003 – July	1st Russian-European Samara Space Summer School, including 30 students from Russia and Europe. Focus on capsule stability and tether safety issues. [Belokonov 2003]
2003 – July	Parabolic flight tether deployment tests.
2003 – August	Heatshield sample testing in ARCS, Vienna [Heide 2003.I].
2003 – August	YESSim tether simulator development gains momentum.
2003 – October	IAF Bremen, YES2 contributes with no less than 10 papers. Patras Center of Expertise joins (mechanical, dynamic, thermal).
2003 – December	PDR (Preliminary Design Review) [Kruijff 2003.IV].
2004 – February	SSAU, Samara opens Center of Expertise.
2004 – March	Inflatable capsule prototype by Center of Expertise Reggio Emilia [Benetti 2004]. FLOYD breadboard operational.
2004 – July	ESA drops inflatable capsule due to cost. Fotino is proposed as replacement. Its hands-on design and development kicks-off immediately with drop test from plane during 2nd Russian-European Samara Space Summer School.
2004 – July	YES2 final configuration and mission profile fixed (vertical tower; XBOX no longer inside Foton but mounted on canister panel). YES2 aims for CDR in 2005.
2004 – Autumn	Tether deployment test campaign for flight spools starts. Winding machine for flight spools operational [Camps 2005]. YESSim completed [Stelzer 2005].
2004 – October	ESTEC Workshop. STEFI trade-off tool introduced.
2005 – January	First closed loop deployment tests result in success.
2005 – April	CDR fails. Fotino needs major redesign. Request from ESA to upgrade YES2 to meet ESA's ECSS quality standards. Major redocumentation required. No extra funding available. Therefore, a student design core team of 4, the "Tiger Team", supports Delta-Utec.
2005 – May	Foton-M2 mission. Planned demonstration of a Fotino precursor on Foton-M2 is cancelled due to lack of funding.
2005 – October	ESA requires science instrumentation and parachute system to be added to Fotino in exchange for additional funding.
2005 – November	ALBATRoS system engineering tool on-line. Place of YES2 on Foton-M3 highly uncertain due to unspecified reduction of mass availability, mass reduction effort starts.
2006 – February	Pre-CDR workshop. Emxys company joins to support the YES2 electronics design.
2006 – March	TsSKB performs feasibility study for inclusion of YES2 on Foton-M3. Interface requirements for YES2 updated. [TsSKB 2006]
2006 – Spring /Summer	Fotino heatshield passes Plasmatron tests at VKI, Brussels [Asma 2008]. Capsule drop tests to verify parachute system. They fail three times due to human errors.
2006 – April	CDR passed [YES2 2006]. Start of implementation of Review Item Dispositions.

2006 – July	Go-ahead to purchase flight hardware and construct the satellite. Team of 25 students starts internship at Delta-Utec.
2006 – August	Foton-M3 team announces interface requirements updates for YES2, including poor thermal connection to Battery Pack.
2006 - Summer	RF equipment testing [Castillejo 2008]. High-altitude balloon test of Fotino electronics postponed.
2006 – July to 2007 – January	PCB manufacturing and test.
2006 – September to 2007 January	Mechanical parts manufacturing at Bradford Engineering. Final mass reduction effort.
2006 – November	Safety review. Decision to switch from gas generator to spring based parachute system for Fotino [Hausmann 2008].
2006 – December	Tether winding starts in ESTEC clean room
2007 – January	YES2 Mass Dummy Unit completed. Team moves to ESTEC for integration and subsystem tests. The intended flight tether, "*Ferdi*", found too sticky due to manufacturing flaw. Cold vacuum subsystem tests indicate problems for barberpole gear and OBC. Gear is redesigned. XBOX equipped with heater and external MLI. YES2 EGSE development starts.
2007 – April	YES2 system tests completed: EMC, thermal cycle, shaker, mission test.
2007 – May	YES2 shipped to Samara, Russia. New tether, "*Florian*", produced to replace "*Ferdi*".
2007 – June	*Florian* tested and integrated in Samara. System tests with Foton-M3.
2007 – July	Final software testing (on engineering model) with closed loop deployment in test rig. Shipment YES2 to Baikonur.
2007 – August	Safety review requires addition of autonomous tether cut feature. It is implemented in Baikonur. Final mission parameters determined and uploaded.
2007 – September 14	Launch.
2007 – September 25	Mission.

Table 67. *YES2 Main events timeline*

8 YES2 Mission and Results

One test result is worth one thousand expert opinions.

— Wernher von Braun

This Chapter presents the various steps from final flight preparation to flight, data analysis and flight data matching by simulation.

8.1 Flight preparation

The flight preparation phase of YES2 is described in this section. Before the flight, the tether deployer friction model parameters need to be estimated. Using those parameters, the control gains and reference trajectory can be determined and uploaded. Tests are performed in order to verify the performance.

8.1.1 Deployer characterization

The first step in the preparation of the in-orbit tether deployment is a final estimation of the deployer parameters of Eq. 5.30. Tension behavior is measured with the unwinding test rig for two sets of parameters, using two types of deployment tests: a full deployment to characterize the spool, and partial deployment to characterize the brake. The results are summarized in Table 68.

The first subset of parameters, related to the dynamic tension effects, is determined based on a full test unwinding of the pre-final spool, without making use of the brake system. A predetermined deployment profile is followed, approximately representative of the nominal flight profile, but according to discrete velocity steps.

Figure 231 shows the test results for the YES2 flight winding. It can be seen that the simplified tension model fit overestimates the tension at low velocity when there is not yet a centrifugal tether ball created that interacts with the canister. As a consequence, the best fit underestimates the tension at high velocity. At low velocity, when the deployment control is more critical, it will be relatively easy to increase friction, so even though a better fit could be achieved by using separate models for low and high velocity, the fit has been accepted as a conservative approximation guaranteeing deployment. After completion of this test, the spool needs obviously to be rewound in a similar manner.

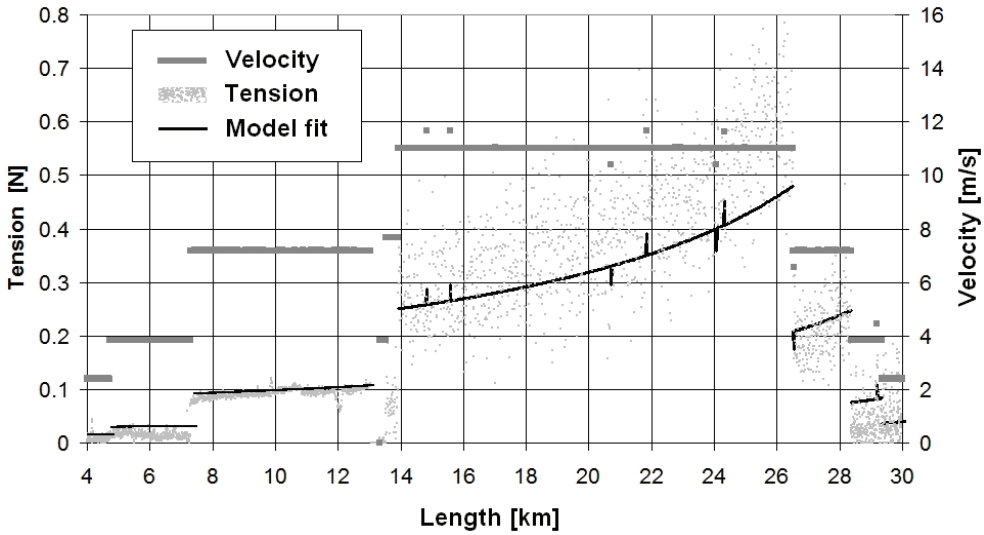

Figure 231. *Test results for determination of deployer hardware model parameters, unwinding tension as a function of length at various constant velocity levels.*

The remaining parameters, related to the brake performance can be determined from just a partial unwinding. It is important that the tether unwinds with the same twist characteristics as in flight, as this affects the behavior on the brake (Section 5.4.1). For this reason an excess amount of tether is wound on the spool, and this extra kilometer is used for a brake performance test. Deployment is performed according to a tight schedule, at three velocities (0.5 m/s, 1 m/s, 2 m/s). For each velocity setting, the brake is positioned step-wise through its range of settings (from low braking activity to high, and back), and at each setting, the average tension is measured. The velocity settings are revisited twice to obtain better statistics. The data is used to determine the friction coefficient and the spool's minimal deployment tension (tether stickiness) as a function of velocity.

The same procedure is followed for the engineering model and for the flight model tether. In case of the flight model, the excess tether is cut off after unwinding and stored for future reference as a tether section with the same manufacturing history and a winding/unwinding history as close as possible to the flight tether.

Figure 232 shows the result for final flight pole. The data points are tension averages over a 15 s interval. The standard deviation of the tension data typically ranges from 20-30%. The curve fit is obtained using a least squares fit. The logarithmic representation underlines the exponential behavior to at least 6 wraps (effectively 5.75, see Section 5.4.1). T_0 can be estimated from the multiplier of the fit, 0.0085 N, and taking into account effect of various guides in the flight system it will be about 0.01 N. The friction coefficient is determined from the exponent 1.082 and is approximately $1.082/2\pi \approx 0.17$. At low turns the pole can be seen to be less effective, probably due to poor contact pressure at the low incoming tension present during the test.

Further research has shown that the friction coefficient *f* depends on velocity and varies most at low velocity, under 2 m/s - a situation occurring during much of the first stage. Unwinding tests have therefore been performed at various velocities.

The analysis has been performed for the various combinations of tethers and poles in use (engineering and flight models, Figure 233). *Florian* is the flight tether, *Ferdi* is the engineering model tether. Due to circumstances (Section 7.5.3), the tether *Florian* was never tested on the flight model of the pole, the likely performance is therefore extrapolated from the available data.

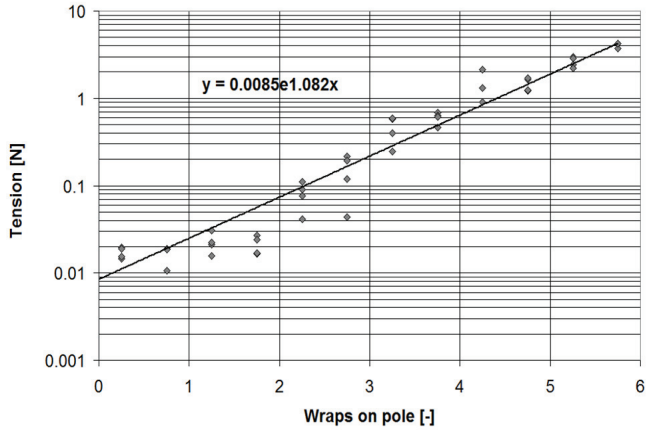

Figure 232. *Exponential relationship between barberpole brake turns and tension*

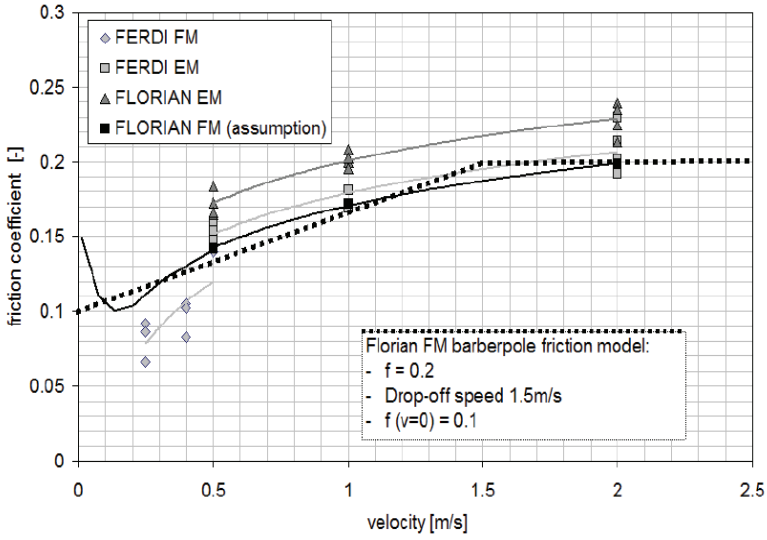

Figure 233. *Tether-barberpole friction coefficient estimate for flight based on ground tests*

Parameter	Symbol	Pre-flight value
Tension [N]	T_0	0.0085
Inertia multiplier [-]	I	8
Density [kg/m]	r	0.000182
Annulus solidity [-]	A_{sol}	0.9
Area exponent [-]	E	0.73
Friction coefficient [-]	f	= 0.2 above 1.5 m/s deployment velocity, decreasing linearly to 0.1 at zero deployment velocity
Friction coefficient on guides [-]	f_{guides}	0.184
Bending angle over guides [rad]	θ_{guides}	0.64
In-plane orientation of Foton [rad]	θ_{Foton}	0, assumed

Table 68. *Pre-flight deployer model parameters*

8.1.2 Developing and testing of the deployment algorithms

The reference deployment is determined by defining and solving the single-phase optimal control problem where variable feedback gain parameters are obtained through receding-horizon optimization using a Gauss-Lobatto Quadrature discretisation, Section 5.5. The problem definition includes the barberpole tension performance model and the following boundary constraints that are imposed for reasons of deployment robustness and to improve effectiveness and accuracy of the momentum transfer (Sections 3.1.1, 4.2.1):

- a nominal ejection velocity v_0 = 2.2 m/s, based on ejection energy and the estimated effect of the tie-downs braking
- a first stage length of about 3400 m and
- a second stage length of about 30 km,
- a minimum velocity during the critical part of the first stage of 0.5 m/s,
- a maximum deployment velocity in the second stage of 13 m/s, yet
- obtain an effective swing angle of at least 30 degrees (Section 2.2.1). The latter is a rather limiting requirement but necessary to provide the required ΔV to the capsule.
- a gentle final deceleration to avoid spring-mass oscillation of the endmass.

Each of about ten deployment trajectories suggested in iterative steps by the optimization process (length and velocity vs. time, hereafter referred to as "profile") [Williams 2007, Williams 2009] has been verified in the MTBSim simulator. This check is performed in order to verify the settings are compatible with the (simulated) software controller, to confirm that the tether does not bend due to Coriolis effects, which may cause a standing transverse wave after deceleration, and finally, to make sure the endmass does not bounce after

deployment is stopped. A preliminary selection has been made based on the minimum velocity early in the deployment, a higher value of the minimum velocity is considered to provide a more robust profile. Various remaining profiles have been compared using five sets of extreme parameter disturbances. The most robust one has been selected. The most extreme cases used are presented in Table 69. They cover a large dispersion compared to the nominal values of Table 68:

Worst case	v_0 **[m/s]**	**f**	T_0 **[N]**	I
High friction	1.7	0.3	0.03	20
Low friction	2.4	0.12	0.0055	2

Table 69. *Extreme cases for deployment pre-flight robustness simulation*

As acceptable output for these cases is defined a length error of under 3%, and a first stage oscillation angle under 10˚, as well as limited transverse and longitudinal wave excitation (i.e. avoiding occurrence of tether slackness at any time during the mission). The controller output of the advanced simulator for the most robust and smooth solution is used as the final nominal profile.

A number of other parameters are set in the flight software initialization file. Some of these parameters impact details and trade-offs of the deployment control. Velocity filter parameters are one example. The filter size, i.e. the number of historical velocity estimates taken into account by the velocity filter impacts the trade-off between smoothness of control versus delay of the controller response (Section 5.5.3). The parameter is set to four values, equivalent to eight seconds of historical data. Another example is the duration of initially uncontrolled deployment. For a number of seconds after ejection, the filter will be filled with the reference velocity rather than with the measured velocity, in order to provide an opportunity for the filter to establish an accurate estimate. The brake feedback will be started after 16 seconds. With these values, YES2 aims at a more alert control than SEDS-2, where the filter has a cut-off frequency of 0.02 Hz (50 s period) and feedback is not activated until 750 s into deployment [Lorenzini 1996].

The initial position of the barberpole has been subject to a trade-off as well. Having no turns on the pole would ease initial deployment and would more likely lead to full deployment in case of gear or stepper mechanism failure. A single turn on the pole would increase the shock of the breaking of the tie-downs and therefore increase the stabilizing effect on ejection dynamics. However, in case of gear or stepper failure, this option could lead to a close-to-nominal, yet single stage, passive deployment. A zero turn position is selected.

Another barberpole setting is the maximum allowable brake position during the hold phase, such that the brake can be successfully released at the start of the second stage, without the tether jamming in the brake mechanism or gear. In a parabolic flight test, it has been

established that a maximum number of seven wraps of the tether around the barberpole can be unwound in a zero-gravity environment without tether jam.

Some contingencies are covered by software and controlled with programmable parameters. For example, if the second stage start command (YTK4) for some reason does not arrive, the holdphase timeout parameter (set to 2200 s) makes sure the second stage will still be executed – late, but better than never (see also Section 7.4.3). The value for this timeout value has been selected to still have sufficient flexibility for ground control to adjust the second stage start time during the mission, whereas, in case of YTK4 failure, a close-to nominal performance can be achieved.

A similar autonomy has been included for a contingency tether cut. In case of cut command malfunction (YTK3), the YES2 OBC has been programmed to cut the tether one hour after the end of the second stage. An autonomous tether cut has also been included in case the deployment velocity drops below 1 cm/s during the first 500 m of tether deployment (Section 7.4).

With all parameters decided upon, ideally MTBSim is used to perform a Monte Carlo run to verify robustness (Section 5.5.5). The ±3σ landing area obtained for this case has a dimension of about 384x60 km, typical for ballistic re-entry capsules. The relatively large cross-range is due to the large susceptibility of the light-weight Fotino capsule to wind.

8.1.3 Testing the flight software

In a next step, the deployer hardware emulator (Section 5.2.3) is used to test the On-Board Computer (OBC) and its software without actually deploying a tether (Section 7.4.3, using an engineering or flight model depending on availability). It is intended to verify, in a real-time environment, successful parameter upload, electrical signal interaction with the surrounding equipment and, finally, controller performance.

In absence of the physical tether deployer, not only the tether deployment, but also the performance and electrical interface signals of that tether deployer, are simulated in real-time by the emulator, which runs on a standard PC. The emulator mimics signals from the tether length sensors (the Optical Loop Detectors or OLD) and feeds them to the OBC. The emulator receives the stepper driver control commands from the OBC, and uses this information to calculate what would be, in a real situation, the new barberpole position, the resulting friction, and the impact on the tether deployment velocity and thus on the OLD signal output. And so on. Telecommands can also be sent and telemetry monitored.

This approach allows to realistically test the OBC, software and controller performance. The initial conditions (such as Foton-M3 semi-major axis, ejection velocity) and hardware parameters (e.g. barberpole brake friction coefficient) in the emulator can be disturbed with respect to those used in the OBC to test controller robustness. Hardware failures can also be straightforwardly simulated e.g. by disconnecting one or two of the OLD input signals or by performing a reboot of the OBC during deployment. Because the PC104 requires as much as 38 s to start-up, the OBC controller software extrapolates the deployment over the time of reboot to estimate length deployed in the mean time. For this reason, the OBC saves critical

deployment status parameters once a second into Flash memory. The emulator is also used to tune parameters of the software's OLD pulse filter (Section 5.5.3).

The emulator test can replace a full system test in the project's development phase when design is being tuned or changes rapidly, but also after system completion. At that time, when electrical system performance has already been demonstrated, the emulator can be used to quickly verify the impact of late changes in software parameter settings.

8.1.4 Testing the system

The tether deployer and controller performance can be tested realistically in the closed-loop deployment test rig (Section 5.2.2), and in case of YES2, this has been done 3 months before launch using an engineering model of the deployer system. Such tests are much more laborious than an emulator test. The winding required for a single full unwinding test takes minimally two days to produce. Although an experienced engineer can then do several tests in one day, it is recommended two more days are reserved for preparation and execution of a test. The closed-loop deployment test adds features that the emulator does not provide:

1. the full flight system can be used, so electrical signals are more realistic,
2. loop unwinding irregularities as a result of the spool winding are represented (stick-slip process),
3. tension peaks resulting from winding pattern and irregularities appear realistically,
4. actual, rather than simulated hardware performance is featured (with respect to unwinding tension, brake friction etc.),
5. impact of environmental features can also be assessed (zero-g, vacuum, off-nominal temperature, impact of thermal cycling, vibrations etc.).

The YES2 test rig in particular has proven to be suitable even to test subtle features, such as maintaining zero deployment velocity during the hold phase (by increasing the brake slightly if a loop deploys) and the restart of deployment at the beginning of the second stage (Section 5.6.2). In such situations, stick-slip processes occur on the deployer, and the tether may be alternatingly deploying and halting depending on the balance between gravity gradient tension and the friction in the deployer. The test rig's godet (or deployment actuator) is however designed for applying velocity to the tether, not tension. To realistically simulate a hold phase and the stick-slip processes that may occur, the godet probes the deployer friction level by deploying at a minute velocity of about 2 mm/s. The measured tension is a measure of the deployer friction and is compared to the simulated tension for a non-deploying tether, in order to determine whether at any time the tether would start to slip.

The unwinding test rig (version 2) can reproduce the effect of tether oscillations on deployment velocity to a good extent. The RTBSim simulator includes tether flexibility, while the test rig godet has a low inertia and can quickly respond. An earlier test rig (for ESA's TSE project) was found to uncontrollably resonate in such cases due to the large inertia of the drive system, see Section 5.6.1. Also the case of a bouncing endmass on the

tether, in combination with intermittent deployment is realistically reproduced. Some limitations of the YES2 unwinding rig are described in Section 5.2.2.

8.1.5 Making late changes

It is convenient to have the possibility to make late changes. For example it may be necessary to adapt controller parameters to deal with late changes in the launcher's orbital elements or the tether's endmass. All parameters in YES2 as well as the reference deployment profile are contained in an init-file that is uploaded into the YES2 OBC one week before launch. Until that time, new init-files can be revised and updated.

The init-file generator developed for this purpose is a separate piece of software with a user-friendly graphical user interface. It provides warnings of potential anomalous data entry and logs copies of all input inputs and files used for traceability. This set-up makes it possible for example that the deployment profile and feedback gain optimization can be based on the latest insights and system parameters and can be reliably updated without impacting the flight software.

It may also happen that the actual flight software requires an update. This has in fact happened with the YES2 software after interface communication tests with the Foton-M3 vehicle, two months before launch. Impact of any change in software, even if not directly related to the tether deployment control must be verified.

For this reason the emulator system (Section 8.1.3) has been brought along to the launch site, together with an engineering model of the OBC. The final emulated real-time deployment tests were successful and the new software and parameters were uploaded.

Note that the YES2 mission design does allow for introduction of small changes during the actual flight, to respond to a safety critical situation or to updated orbital parameters. Although neither the software parameter values can at this time be changed nor the Fotino release time from MASS, a number of events *can* still be controlled by time-tag (ejection, start second stage, cut tether: see Table 62), and this is sufficient for finetuning of the mission. The final telecommand timeline is uploaded one day before the start of deployment.

8.2 Mission summary

Launch of Foton-M3 and YES2 on a Soyuz rocket from Baikonur is as planned on 14 September 11:00:00 UTC. The orbit achieved is so close to nominal that the planned tether mission timeline can remain virtually unchanged. On the 24th of September, 10 days into the Foton-M3 mission, the tether mission timeline is uploaded to Foton by telecommand based on the most recent Foton orbital parameter estimates. The mission timeline is summarized in Table 70 and Figure 234.

At this time, there is significant worry about the YES2 system temperature at switch-on. Qualification tests have demonstrated that the YES2 on-board computer may not start-up

properly if the ambient temperature is below –10˚C. Once started, the installed heaters will improve the thermal condition. YES2 is largely isolated from the thermally controlled Foton-M3 spacecraft and shielded from the Sun on one side by the 1.8 m-diameter battery pack. On the other hand, reflections from the thermal blanket on the Foton-M3 battery pack help increase the amount of received solar radiation. YES2 is powered on, on September 25th.

Fortunately, initial data from YES2, received through the Canadian ground station, shows a benign temperature of –2˚C, see also Figure 234. In this figure the shaded zones indicate periods of eclipse. The approximate temperature of the tether on the spool (OLD) and OBC (XBOX) are also indicated. These temperatures seem hardly affected by the day-night cycle that Foton is going through, only a weak change in rate may be observed. The heater works properly and is switched off as planned when the temperature breaches 20˚C. Confirmation of arming of the pyrotechnics is received next, and health data from all systems are nominal. It is then decided to proceed with the ejection and deployment as in the nominal timeline.

In the ground contacts following ejection, the OBC reports to the Russian ground station status summaries that include the processed length and velocity results as estimated by the software based on the received OLD pulse time-tags. The much more bulky data of the OLD time tags are stored on the TSU unit, and are part of the telemetry. In successive ground contacts, the following events are confirmed:

- proper ejection and safe initial separation of endmass achieved,
- first stage achieved within 10 meters of nominal length, hold phase and start of second stage also nominal.

The OBC-estimated length as collected during the final groundstation passage however, indicates only a partial deployment of 8.5 km at completion of the second stage. Telemetry further indicates that the OLD sensors' health is good, while the velocity appears to have decelerated to zero over an extended period of nearly 40 minutes, whereas all this time, the brake is set to zero. The implied very low level of deceleration is considered suspicious, as it means that friction must have somehow consistently and closely tracked the gravity gradient as it changed with tether length and in-plane angle. No physical mechanism can be offered that explains this behavior. If correct however, the Fotino and tether have been released into a low Earth orbit with a lifetime of several days and essentially a random landing location. A student team that has deployed a mobile ground station, downstream of the nominal landing site in Kazakhstan [Castillejo 2008], has not received any signal of Fotino, nor is any Fotino or MASS signal received by the ground stations in Kiruna or Canada. YES2 team members and colleagues around the world are chartered to watch for the sun-lit tether visually as it would be passing the night sky overhead, but to no avail - despite some good observation conditions. USSTRATCOM however dispatches a message that it believes Fotino has been released around the nominal time and has in all likelihood re-entered rather nominally.

Some days later, when the OLD data has been made available, post-flight analysis reveals a problem in the length and velocity registration during the second stage deployment. It

becomes clear that, towards the final part of deployment, near t_{eject} + 6260 s, an intermittent but increasingly failing registration of the received OLD pulses has led the OBC to wrongly conclude that the tether deployment is slowing down, and it has therefore released the brake [Spiliotopoulos 2008] (Section 8.5.1).

The actual events of the final part of deployment can now be reconstructed. In fact, much of the uncontrolled deployment that follows the said failure resembles the nominal deployment profile, as also in the nominal profile the second stage deployment involves very little brake effort. The lack of a controlled final deceleration towards the target length of 30 km results in an unchecked over-deployment by 1.7 km and a significant shock as the end of the tether on the spool is finally reached at t_{eject} + 8626 s, at a length of 31.7 km and a velocity of 15 m/s. Nominal deployment should have reached the target length of 30 km only at t_{eject} + 9189 s. The post-flight analysis shows that the intended swing to the vertical has nevertheless occurred and release of the tether from Foton-M3 can be confirmed as planned t_{eject} + 9364 s, very close in fact to the nominal in-plane angle for release. The high velocity deployment has led to a larger deployment angle as well as an earlier deployment stop and thus a longer swing time than foreseen, two effects that to some extent have canceled each other out. The increased tether length however has not been canceled by any other effect, such that the Fotino is estimated to have re-entered towards a projected landing point as much as 1250 km upstream from the nominal one.

The YES2 deployment's major parameters can be quantified as follows. Deployment tension has been close to nominal and varied between 0.03 N in the first stage to 0.16 N during the hold phase, while increasing to about 1.8 N in the second stage. The nominal maximum tension for the swing is 3.7 N, but in the mission, due to the over-deployment a shock of a much higher tension of 40 N was introduced as the end of the tether was reached. The passive release system on MASS, designed to trigger at a tension of about 55 N, did not activate, allowing the tether to then make the swing to the vertical. In-plane angles during deployment ranged from 0 to 50° (forward direction), with a final downward-backward swing returning from about 40° back towards the vertical. The deployment velocity ranged from 2.2 m/s initially to a 16 m/s maximum.

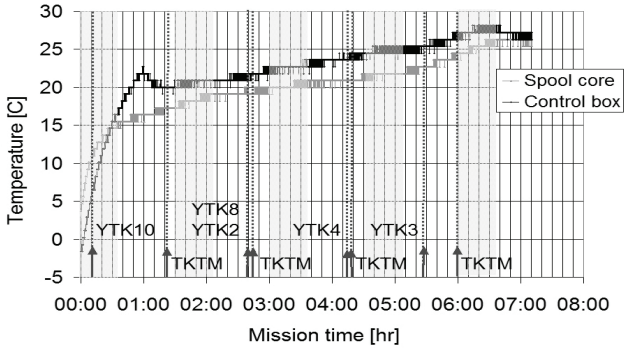

Figure 234. *Temperature development of critical systems vs. the major mission milestones during YES2 mission. See also Table 70.*

Event	Date	UTC	Orbit#	t-t_{eject} [s]	Description
Launch Foton	14 September 2007	11:00:00	1	-	-
Upload telecommands	24 September 2007	14:00:00	163	-	Representing the mission timeline.
Switch YES2 on	25 September 2007	2:03:00	171	-9813	-
First relayed raw data		2:07:00		-9573	Through TSU (data storage and forwarding): temperature OK.
YTK10		2:13:00		-9213	Arm pyro's.
TKTM		3:17:00	172	-5375	Receive telemetry (confirm arming).
YTK8		4:45:33	173	-60	Switch on MASS.
YTK2 (t=t_{eject})		4:46:33		0	Ejection.
TKTM		4:50:00		207	Receive telemetry (confirm ejection, reaching 300 m safe length).
Start hold phase		5:55:13		4120	-
YTK4		6:19:32	174	5580	Prepare for second stage deployment.
Start second stage		6:21:12		5680	-
TKTM		6:23:00		5786	Receive telemetry (confirm first stage and start second stage deployment).
Release Fotino		7:22:17		9344	-
YTK3		7:22:37		9364	Cut tether on Foton side.
Projected Fotino landing		7:57:00	175	11420	Nominal landing site 66.2E 50.6N. Ground recovery team situated downstream at 67.5E 51.6N. No beacon signal is received.
TKTM		7:53:00		11186	Receive telemetry (confirm second stage deployment).
Switch YES2 off		9:16:00	176	16166	-
Last relayed raw data downlink		12:15:00	178	-	Through TSU (data storage and forwarding) inside Foton (full download raw data).
Landing Foton	26 September 2007	~7:58:00	189	-	-

Table 70. *YES2 mission timeline, major milestones in bold.*

8.3 Data analysis

8.3.1 Analysis objectives

An important driver of both the design phase and the mission analysis is to demonstrate safety and predictability of the tether deployment and control. The achieved deployment trajectory and projected or actual landing spot is thus to be determined and compared to the nominal values.

The hardware performance is assessed based on recorded tension data and compared to results from ground tests and simulations. The predictability of deployer hardware friction and the possibility to adjust those friction levels in a predictable manner determines the hardware's potential to control the deployment. Apart from the friction and brake performance, tether properties such as stiffness, speed of sound and damping are derived from the flight data and compared to pre-flight test results. The closed-loop control software performance in the actual flight situation is to be evaluated by study of the data from the deployment sensors and the software controller and by correlating the control to the dynamic response of the deployment.

It is then attempted to match the flight data by simulation. A simulator match can help to reveal lacks in the simulator and to study hypotheses or remedies to observed deployment problems. The amount of parameter adjustment necessary in order to achieve a match is helpful input to define the applicability of the simulator or the uncertainty in the parameter value. Furthermore, the match is based only on a subset of measurements -length and velocity- yet it provides a window on all aspects of a tether deployment, including in-plane angle, tension, control activity and the occurrence of waves. It can thus generate additional information that can be compared against other available data for these remaining aspects. The simulator or its settings are ideally to be updated to account for any discrepancies found. The validity and limits of simulations and ground tests are assessed and recommendations are to be defined for the preparation procedures of future tether missions. If sufficient confidence exists, the simulator can then be conveniently used to extrapolate behavior beyond the actually occurring deployment and generate betters estimates for the landing point of Fotino in particular and more generally, for the SpaceMail landing accuracy obtainable with a certain tether deployer system.

8.3.2 Data sources and editing

Sensors and available data

A variety of sensor data is available to track the deployment (Table 71). Housekeeping information such as voltages, temperatures, commanded brake position, error flags etc. is used to correlate and verify the measurements. The primary sensors of YES2 are however the Optical Loop Detectors (OLD). A very helpful addition proves to be acceleration data from the DIMAC payload, not a part of the YES2 system. MASS has provided useful data for study of the ejection and estimation of endmass dynamics.

The Optical Loop Detectors provide the only sensory input for closed-loop control of the deployment. They are used to determine length and rate and help to reconstruct (post-flight) deployment angle and tension by means of the approximate description of tether dynamics, Eq. 2.16, or alternatively, via simulator matching.

Inside Foton, sensitive three-axis accelerometers and magnetometers, operating at 1000 Hz and belonging to the DIMAC payload (DIrect Measurement of Acceleration) [Beuselinck 2008], have registered the full deployment, as well as the subsequent swing. They have first be used for an independent derivation of tether tension. The direction of the tether near Foton can be obtained from the perpendicular components of the disturbing acceleration in Foton's body frame, if combined with magnetometer data on Foton's attitude in space. A spectrograph of the DIMAC data is used to determine the deployment rate versus time. Also the time of deployment of a number of milestone points along the length of the tether can be recognized as the major changes in the tether's winding pattern, as detailed in the winding log, leave their marks on the frequency of the tension signal.

On MASS, magnetometers, a tensiometer and a gyroscope have made it possible to determine the endmass dynamics and the disturbances created by the ejection. The behavior of the safety and securing features, included in the first 15 m of the tether, can also be monitored. The simple MASS sensor package has provided information for a range of 150 m. This is considered a positive result [Castillejo 2008], since the receiving antenna on FLOYD was heavily handicapped. The performance of this innovative hexagonical loop antenna [Rolo 2005], had been compromised by necessity when additional MLI was placed underneath it to compensate for the low conductivity between YES2 and Foton-M3.

The navigation receiver on MASS , not yet locked at 150 m distance, has thus provided no data. Navigation data (GPS/GLONASS) of the FLOYD position in space during the tether deployment has been collected by the YES2 SSAU experiment, but not yet been made available [Belokonov 2008] . In the absence of navigation data from MASS, it is not expected that this data can improve already achieved estimates for in-plane angles or tether length.

Clock alignment

The data from the various sources have been edited to align their time tags. For external sources of information (Foton & USSTRATCOM), UTC has been used. For the YES2 data analysis, the main time reference has been the TSU clock. This clock has run 42 seconds slow with respect to UTC over the 11-day Foton mission until ejection. During the YES2 deployment the error is just 0.2 s.

The DIMAC clock-source is based on the TSU and has been used to align the start of deployment based on the measurement of the acceleration resulting from the ejection event. Also the MASS clock starts at the moment of ejection. This moment is determined from the timetag of the eject telecommand as well as from extrapolation to zero of the OLD loopcount data, and is known within about 0.2 s.

For FLOYD data, both the TSU clock sources and the YES2 OBC internal clock have been used. The TSU clock signal is fed to the OBC over a long serial cable passing through the

wall of the Foton-M3 re-entry capsule and over the outside of the Foton-M3 spacecraft. In order to provide robustness, the YES2 software has been designed to be able to work with its own clock whenever the TSU signal would be absent.

Due to a software problem, the OLD interrupts carry time tags alternatingly from TSU and on-board clock sources. From study of the data it has become apparent that the OBC clock has been diverging from the TSU clock rapidly. The YES2 OBC clock has run slow 3356 μs/s or about 28.95 s over the full deployment, as compared to the corrected TSU clock. This rather large error has not been previously recognized and is thought to originate from an impact on the OBC's crystal during a cold period in the mission or even the pre-mission thermal tests.

The half of the OLD interrupt time tags that is based on the OBC clock therefore has been corrected. Representing a total interval of 8622 s, they could be corrected assuming a divergence developing linearly with time. The correction as implemented maintains the exact order of all 30547 registered interrupts. A shift in the correction function, in either offset or gain, of as little as 0.01 s over 8622 s leads to disruption of the order. Since the best linear fit prevents such a disruption completely, the maximum error in timing is 0.01 s.

OLD performance and first stage length measurement

Because of the awkward length estimates produced by the OBC during the second stage of deployment (Section 8.2), the OLD data has been carefully studied. In order to understand whether any tether passages might not have been registered, the record of OLD channel transitions (see Section 5.5.3) has been subjected to a randomness analysis. In Figure 235 an ad-hoc measure of randomness R is plotted against the "gap", i.e. the time between two successive OLD interrupts. R is defined as:

$$R = (1 - f_N) / (1 - f_{rand}) \tag{8.1}$$

where f_N is the fraction of the transition where a pair of successive OLD channels matches the nominal transition for a proper deployment (i.e. 1-2, 2-3 or 3-1), and f_{rand} is the fraction that would be expected in case of random interrupt events, e.g. due to temporary OLD malfunctioning. Perfectly random interrupts would display all possible 9 transitions in equal amounts. This analysis is particularly of interest for data gaps much longer than the average loop period. If $R \approx 1$, the OLD data seems completely random. If $R \approx 0$, the data seems systematic, matching nominal OLD performance[12]. A change in randomness appears to occur at t_{eject}+6400 s.

This analysis has revealed that in the first 6400 s of deployment, nearly all channel transitions are consistent with proper deployment, albeit sometimes irregular. Channel 1, a

[12] The graph has to be interpreted with care. Jitter or a situation with only one OLD channel operational would appear as $R>1$. For simplicity of the analysis, f_{rand} has been assumed constant over time within each interval. In reality, this is not the case, in fact, it is increasing due to the increasing domination with time of channels OLD2 and OLD3 over the most affected channel, OLD 1 (see Section 8.5.1). Because larger gaps occur later, when OLD1 is nearly non-functional, an equally random signal will receive a lower randomness. This is what is visible in the time interval between 6400 s and 8200 s, which is in fact (near) fully random.

malperforming interrupt request line on the OBC's SECO board, has been patched before the flight. It has performed a bit less in flight than Channels 2 and 3, and sometimes has missed a tether passage. Other than that all exceptions plus 30 doubtful channel transition cases have been inspected individually. It is concluded that the single gap correction feature of the OLD algorithm (Table 47B) has performed without problems during the flight, and so has the noise rejection feature (Table 47C). Virtually all instances of such noise could be verified by inspection to be handled properly. Analysis of the raw flight data shows that the third potential anomaly that was taken into account, a double-channel failure (Table 47D), hardly ever occurs and this additional failure recovery function has been found to be more damaging than helpful. A handful of obvious errors has been corrected by hand. In some cases, about once every 1000 s, no clear conclusion could be drawn. The maximum error for the first stage deployment is estimated as 20 m, based on the likelihood of the various transitions in case of OLD failure, combined with the observed number of such transitions.

After 6400 s into deployment (later refined to 6260 s) most OLD transitions related to gaps have instead been identified as random, indicating missing data.

Source	Data type	Application	Comment
FLOYD	OLD interrupt times; Barberpole position; Temperature XBOX; Command reception, timeline, ejection and tether cut status; TSU time.	Ejection velocity; Deployment length and velocity reconstruction; Timeline reconstruction and clock calibration; OLD problem analysis; Tether deployment irregularities.	Length until 6400 s; Rate until 8400 s.
MASS	Gyroscopes (angular rate); Magnetometers (angle); Temperature; Tensiometer.	Pitch-off rate capsule after ejection; Initial conditions for attitude simulation; Deployment tension calibration, pole friction.	First 70 s after separation.
Foton	DIMAC accelerations in Foton body frame; DIMAC spectrograph; Foton attitude from DIMAC magnetometer and TsSKB-provided data.	Deployment tension estimate; Foton attitude control activity; Tether exit angle, in-plane angle reconstruction, tether bending; Spool tension parameters; Confirmation final snag; Tether stiffness, viscosity, speed of sound in tether; Tether swing reconstruction, Fotino release investigation; Confirmation of tether cut; Deployment rate confirmation.	DIMAC data complete.
Foton orbital parameters	USSTRATCOM observations; USSTRATCOM estimate tether release time; TsSKB updates.	Initial conditions for matching simulations; Tether release confirmation.	-

Table 71. *Use of data sources for YES2 data analysis*

Deployment rate from OLD

With the total deployed loop count impaired during the second stage of deployment, still estimates for the deployment *rate* can be obtained from the rate at which OLD interrupts have been arriving between the data gaps. A simple way to estimate the looprate is to take the inverse of the inter-interrupt duration. A regular sequence of interrupts will result in a good local estimate of looprate. In some cases, within a brief sequence of interrupts, a small number of intermediate interrupts is missing. When applying the estimation to all interrupts these cases will yield various "secondary arms" - shadows of the actual looprate curve, as in Figure 236. The falsely represented looprates in these arms can be multiplied by the arm number to yield a better estimate. For example, the second arm, i.e. the one below the main arm, represents sequences of interrupts with a single missing interrupt. The time interval here relates to two loops unwound.

By combination of the best segments of these multiple arms, the best subset of data can be obtained (Figure 238). Due to the averaging effect, at higher looprates, the higher order arms provide more precise data. At low looprates, sufficient nominal sequences of interrupts are available such that the time intervals between subsequent interrupts can be averaged in order to obtain higher precision data. The most precise segments of the arms thus produced happen to be those segments representing gap intervals of about 0.2 s.

Despite the incompleteness of the OLD data from 6260 to 8626 s, still sufficient data is available to determine the loop rate to better than 1 Hz (about 0.3 m/s) until t_{eject} + 8250 s. The time of deployment completion is also known within one second, as a tension pulse then occurs that has been registered by DIMAC. With the help of this additional data point, the remainder of the deployment can in principle be interpolated with an accuracy of 1 m/s.

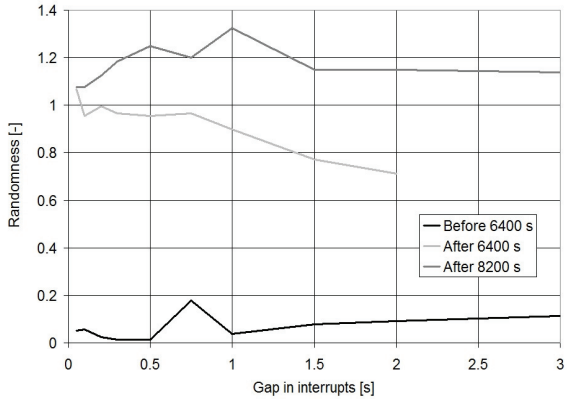

Figure 235. *Statistical analysis of OLD channel transitions intended to distinguish between normal OLD performance (randomness≈0) and OLD malfunctioning (randomness≈1).*

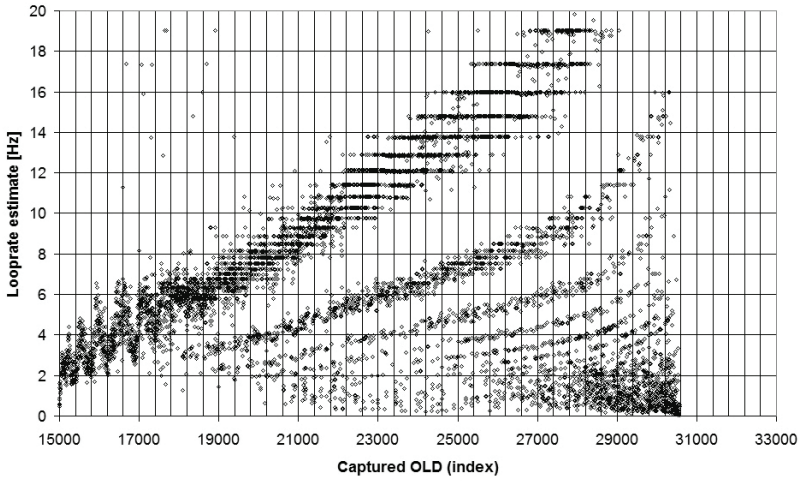

Figure 236. *Rough loop rate estimate (based on time between recurrences of successive OLD channel passage) shows multiple curves, indicative of unregistered intermediate OLD passages*

Deployment rate from DIMAC

The resulting loop rate development and interpolation has been independently confirmed with the help of a spectrograph of Foton-M3 accelerations as measured by DIMAC. This spectrograph displays the intensity of disturbances to the 6535 kg spacecraft as a function of frequency and time, based on a sequence of Fourier analyses on 32 s intervals. Remarkably, the rattling of the unwinding tether (weighing only 0.2 g/m) is clearly distinguished by the DIMAC experiment (Figure 237). It appears above about 3 m/s deployment velocity, and is resolved with a resolution of about 0.3 Hz. The spectrograph representation of Figure 237 is a manual composite of measurements in the various axes, in order to maximally highlight the YES2 looprate curve against the background levels. The spectrograph contains information that can be used to further improve the accuracy of the fit.

Details of the winding pattern can be observed, such as the cyclic frequency of the winding head (Section 5.2.1). Transitions to smaller winding angle lead to shorter loops, and an instantaneously increased looprate, as recognizable in the graph at points 1 and 2. Point 3 shows the transition from criss-cross (7 turns per cycle) to parallel winding. Finally, point 4 represents t=8626 s, coincident with the completion of deployment. It is therefore possible to extract from the spectrograph four absolute length measurements (Table 72).

At point 3, the clean looprate curve is replaced with a broad swath of looprates. This swath is not caused by increased noise as one might thinkg, but by a known particularity of the unwinding process. During unwinding of the 33 parallel-wound layers, each taking about 10 seconds to complete, the point of tether release travels from base to head of the core in one layer and vice versa in the next (see Section 5.3.6). This core is conical: the base is wider than the head of the core, by 10% in the first layer and up to 13% in the last layer (Section 5.3.1). This length per loop cyclically decreases and increases, causing a zigzag development

of loop rate for a smoothly unwinding tether. If this known zigzag is computed and superimposed on the median as recognized in the spectrograph (black line in Figure 238) a good match is found to the swath outline as registered by DIMAC (red lines). A small deviation is observed only for the last four layers of deployment, which can be explained if the looprate development is not linear but first accelerates and then flattens out (purple lines).

With the geometric knowledge, the loop rate can be reconstructed better than 1 Hz even in the parallel region, equivalent to a velocity accuracy of about 0.2-0.3 m/s. Figure 239 shows an overlay of the unwinding rates resulting from the two independent sources: the OLD rate and the DIMAC spectrograph.

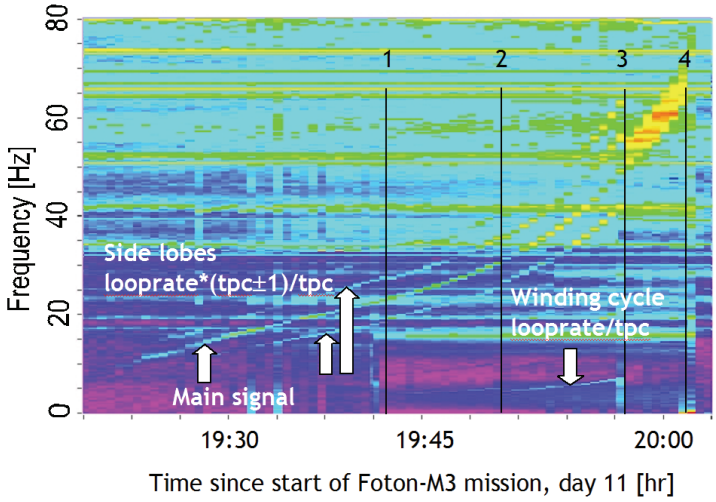

Figure 237. *DIMAC spectrograph with indication of four absolute length markers.*

	Winding event	t [s]	Length [m]	Loops [-]
1	5 to 6 turns per cycle	7512	15421	24135
2	6 to 7 turns per cycle	7937	21168	35754
3	criss-cross to parallel	8397	27979	53306
4	end of tether	8626	31705	66776

Table 72. *Winding events recognized during deployment by DIMAC instrument*

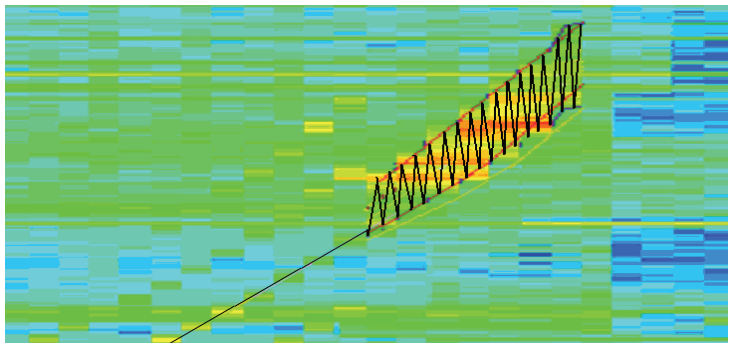

Figure 238. *Zoom of transition from 7 tpc to parallel, including sketch of zigzag looprate (black line) as would be expected based on core cone dimensions (purple dots).*

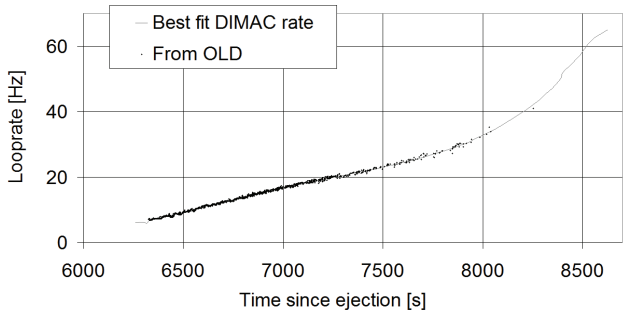

Figure 239. *Looprate development during uncontrolled deployment in Stage 2.*

Full length reconstruction

With the looprate known a length profile can be determined. The profile has been adapted with a multiplier close to unity as to obtain the correct final total wound length at the correct time. The integrated-rate based length profile thus computed matches the four known length milestones (each known from the spectrograph to within ±16 s), providing further independent confirmation. The maximum length reconstruction error during the second stage is estimated to be 0.3% or 100 m - the result of errors in winding length measurement (44 m), tether stiffness estimate (10 m), quadratic fits for loops vs. length used (20 m) and spectrograph resolution (90 m). With improved spectrograph resolution (not yet made available), about 50 meters accuracy may eventually be achieved.

Characterization of OLD malfunctioning

With the looprate known as a function of time, also the extent of OLD malfunctioning can be better characterized. The number of OLD channel passages that has been registered can be compared to the number of tether passages that has actually occurred. Figure 240 indicates how the performance of the channels breaks down increasingly with time, with OLD1 clearly performing worse than the other channels. Near the end of deployment, only about one in thousand OLD passages is registered.

The cause of this breakdown is sought in electromagnetic interference, possibly increasing with system temperature (Section 8.2). An S-shaped slow-down can be observed in the rate of worsening of the OLD performance between 7300 and 7900 s. It may be hypothesized to be related to a weak but similarly shaped slow-down in temperature increase between YTK4 and YTK3 in Figure 234, with a flattening due to entering of eclipse. This hypothesis has not been further investigated yet.

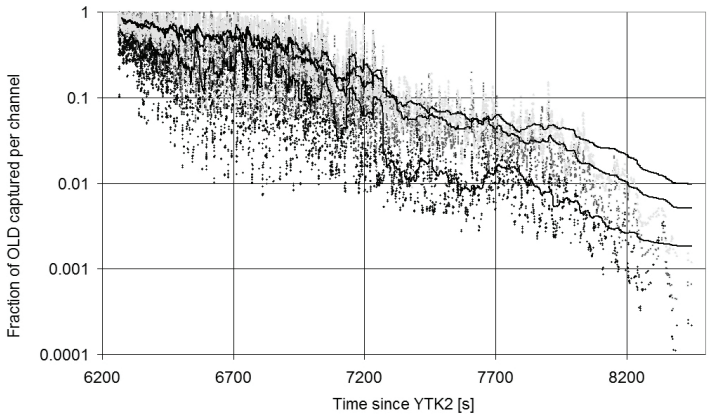

Figure 240. *Estimated fraction of registered passages over total number of passages, per OLD channel. Moving averages are indicated from top to bottom: channels 3, 2, and 1.*

Tether tension

Tether tension is primarily reconstructed from DIMAC accelerometer measurements. MASS tensiometer data has also been used.

DIMAC accelerometer data has been converted to tension assuming a mass for Foton-M3 of 6535 kg, as provided by TsSKB. This information can be expected to be accurate within 1%. A correction has been applied to account for the rocket term (Eq. 2.15) that affects tether tension, but not the acceleration as measured on Foton. Ringing of the ejection springs polluted the DIMAC data after ejection beyond usability for about ten seconds.

Initial DIMAC-based tension bias is well below 5 mN, as has been established using pre-ejection data in the microgravity environment. Various sources of drift for the DIMAC accelerometer have been removed by the RedShift team [Beuselinck 2008], related e.g. to the magnetic field and spacecraft attitude. The remaining error is less than 1 μg, or 6 cN per 1000 s. The known tension during the hold phase has been used to establish that the error is in fact below 2 cN at t_{eject}+5000 s, although during the second stage deployment, under larger disturbances, more significant drift may have occurred.

The MASS tensiometer bias has been determined to be about 15±5 mN, from fit to the DIMAC data. The MASS data is particularly useful to fill in the DIMAC data gap following ejection, e.g. for estimation of post-ejection deceleration and pitch angle reconstruction.

Impact of Foton attitude control activity

The direction of the body axis of Foton is defined as X. Perpendicular to that, in the orbital plane and initially in direction of orbital motion, lies Y. Z is oriented according to the right-hand rule. Z accelerations are indeed found insignificant throughout the deployment, so out-of-plane dynamics are ignored.

The Foton-M3 spacecraft applies attitude control using a cold gas thruster system acting in ±Y direction only (Figure 241). The control law has not been specified but seems apparent from the DIMAC data is (see also Figure 242). It appears attitude control aims at following the tether (minimizing torque) to an angle of 30˚. Above that angle, it attempts to keep the Foton angle constant.

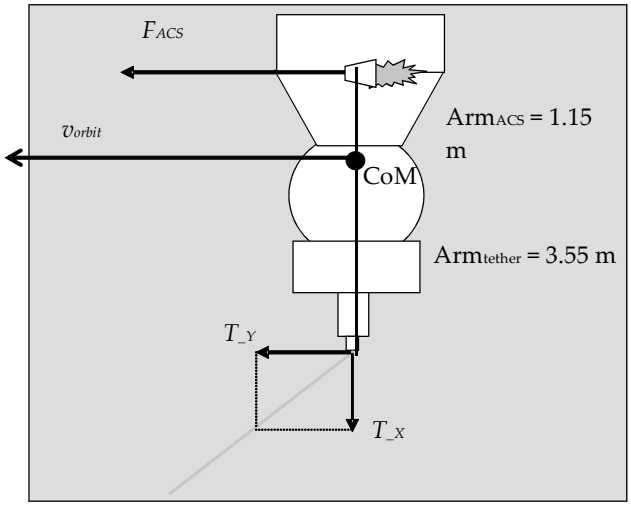

Figure 241. *Geometry of Foton attitude control to balance tether torque*

The raw Y-axis acceleration data contains clearly identifiable peaks of constant amplitude that coincide with fixed-duration bursts of thruster activity. These peaks are superimposed on the tether tension effects and can be filtered out largely simply by subtraction of the constant value. Nevertheless, the Y value, even when cleaned from Foton attitude thruster activity, remains slightly less reliable for tether tension estimation than the X value. For the initial 1000 s of deployment the Y value is small compared to the X value – as Foton tracks the tether direction. In this time interval, while tension is small, only the X value has been used for tension analysis, to reduce the noise contribution from the near-zero Y component.

The DIMAC magnetometer data has been used to determine the attitude of Foton with a claimed accuracy of some degrees. The DIMAC data accuracy for attitude reconstruction may be further reduced during Foton thruster activity (Figure 242). During the latter part of the second stage of deployment, when Foton's X-axis is inclined with the vertical by more than 30°, tether and Foton thruster torques are especially significant, as in this situation a different attitude control mode is active. A divergence of DIMAC and OLD based tension calculations is observed here (Section 8.4.1), as well as a discrepancy between the Foton's

maximum deviation from the vertical as provided by TsSKB (30.1˚) and by RedShift: Foton attitude according to DIMAC rises over 30˚ by several degrees. The magnetometer results were therefore edited by limiting the maximum Foton angle to 30˚. This simple action provides indeed a much better fit to the OLD data derived trajectory, Figure 242.

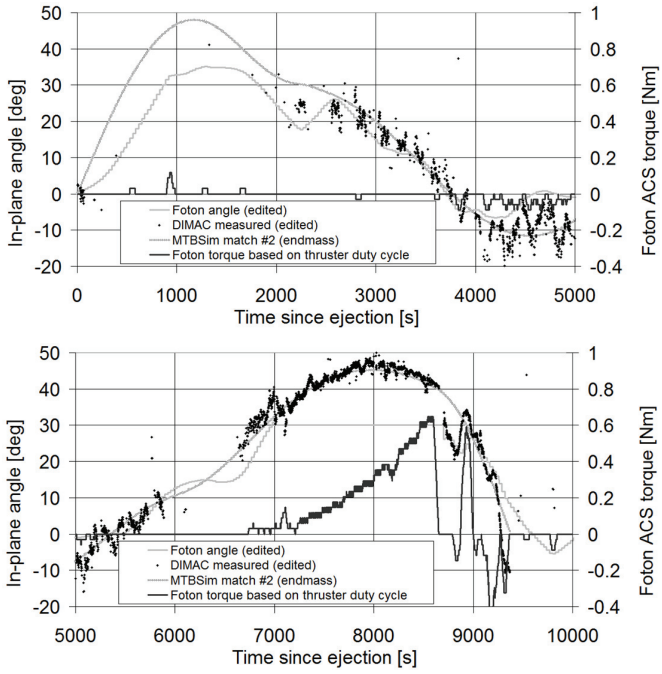

Figure 242. *Foton attitude, reconstrcuted thruster activity and tether in-plane angle*

In-plane angle

Estimates of the tether in-plane angle, at least as it appears on Foton side, are obtained by combination of the two sources of DIMAC data: the magnetometer data, providing the Foton angle with respect to nadir, and the three-axis accelerometers, providing the angle between the Foton X-axis and the tether as it exits the tether cutter bracket. Note that since the tether is not straight, it will not necessarily provide direct information on the in-plane angle of the endmass. The tether in-plane deployment angle can be determined to about 2-5° accuracy depending on the signal-to-noise ratio and the magnetometer accuracy.

The in-plane angle can also be determined from deployment reconstruction based on the length and rate profiles in combination with the simplified equations of motion or matching by YESSim simulation. In-plane estimate results of the various methods are in agreement within the 2-5° accuracy estimate, e.g. for the hold phase pendulum libration amplitude or for the maximum achieved angle as the swing starts towards the vertical (Figure 254).

MASS data

MASS tension data is obtained from the FUTEK tensiometer, which has been operating at room temperature during the mission, at which it had been accurately calibrated. Errors in tension measurements from this device are caused from friction on the pulley that is used in the measurement and is assumed frictionless. These errors are estimated to be below 10%.

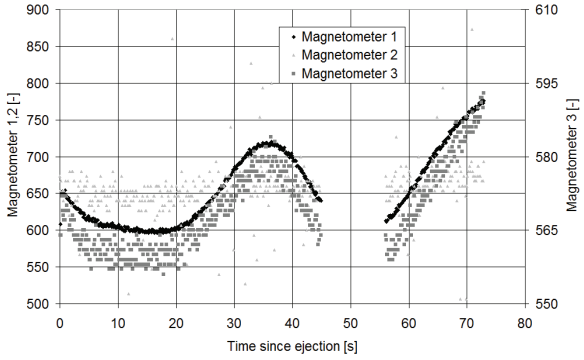

Figure 243. *MASS orthogonal magnetometers raw data*

The MASS (single) gyro data has been used to scale the magnetometer data and learn about the endmass pitch angle (Section 8.3.3). From the ratio of the three perpendicular MASS magnetometer signals it can be derived that the initial attitude dynamics have been mild and (coincidentally) inclined by only about 8.5 degrees from the gyroscope sensing direction (Figure 243), allowing direct interpretation of the data from the (single) gyro.

Magnetometer and gyro biases from MASS during the mission seem to have shifted with respect to ground tests in ambient temperature. The bias estimate in the gyroscope measurement has been refined by a fitting process. The dynamic data from magnetometer and gyroscope have been matched to results of attitude simulations that are in turn based on torques as derived from MASS tensiometer and DIMAC accelerometer data (Figure 248).

Foton orbit

The data on Foton-M3 orbital parameters provide indirect information on tether deployment and momentum transfer. Foton-M3 has been tracked before and after the YES2 mission by USSTRATCOM. A "precision in altitude of +61/-75 m could be achieved with 99.3% probability using their Special Perturbations model (SP), rather than SGP4"[13]. The data match the calculations from the Russian counterpart mostly within 200 m, see Figure 244. Several estimations of two-line elements have been made each day, but over the course of the YES2 deployment only a single observation has been made. After the release of Fotino over Asia, USSTRATCOM has not been able to track it, their first measurement station being Hawaii, suggesting that it has re-entered over Asia.

[13] Private communications with Taft Devere, USSTRATCOM, 23 October 2007.

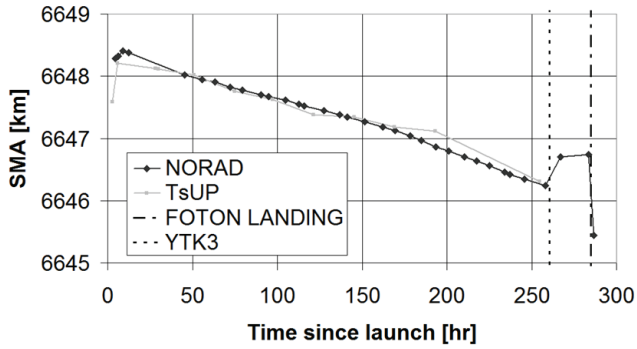

Figure 244. *SMA Foton from TLE USSTRATCOM and TsUP*

8.3.3 Deployment reconstruction and interpretation

The deployment starts with ejection of the MASS/Fotino endmass. The first minute after ejection has been studied in detail, as a number of disturbances are expected to be introduced as a result of the ejection that can affect the remainder of the deployment:

- Error in ejection velocity (nominal 2.4 m/s).
- Endmass pitch rate due to ejection springs mismatch or center of mass offset from the body center line.
- Unknowns in dissipation of tie-downs at 0, 0.75 and 3.75 m length, little cotton knots holding the tether in place during launch. Each tie-down is expected to dissipate some 2 J of energy, resulting in a total 0.2 m/s velocity loss, or an effective ejection velocity of 2.2 m/s. The third tiedowns is placed such as to have a beneficial effect and decreases the capsule pitch-off rate.
- Unforeseen behavior and dissipaton during passage of the ripstitch segment through the system, a relatively thick (~1 mm) 5.3 m long piece of tether, starting from a length of 9 m. It shall be verified that the ejection event does not cause the ripstitch to activate. The tension should stay below 6 N.

Analysis of the OLD data indicate an effective ejection velocity of 2.2 m/s (circle in Figure 245), matching the nominal value, taking into account the braking of the tie downs. A fit, applied over the first 70 seconds, between the velocity derived from integrated acceleration on one hand and the OLD derived velocity profile on the other confirms this ejection velocity. The acceleration levels are derived from measurements from DIMAC and MASS tension measurements. The fit is made by adjustment of the initial velocity offset, for the curve based on integrated acceleration, such that this curve predicts the same total length as the OLDs have also registered, within the interval of 70 s after ejection.

The breaking of the tie-downs may be recognized from the slight irregularity in the OLD pattern directly after the time of their expected occurrence, t_{eject}+0.3 s and t_{eject}+1.7 s (vertical arrows in Figure 249), as well as in brief and sharp tension peaks registered by MASS

[Kruijff 2009.II]. The more steady peak in tension visible shortly after ejection in Figure 246 can be related to the deployment of the ripstitch section, and remains within limits. For the reason of such disturbances, the on-board velocity filter is programmed to use only reference file information during the first 8 seconds.

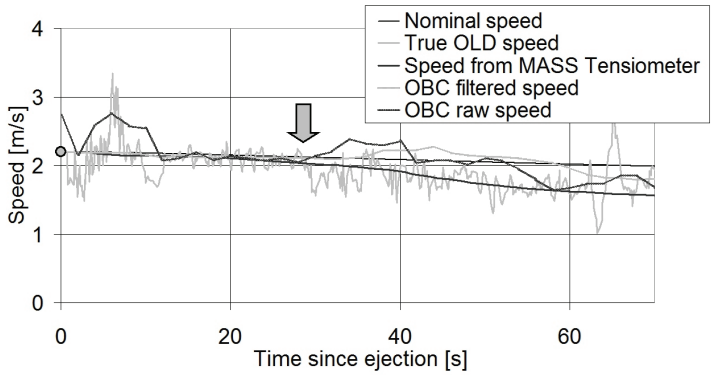

Figure 245. *Velocity information directly after ejection*

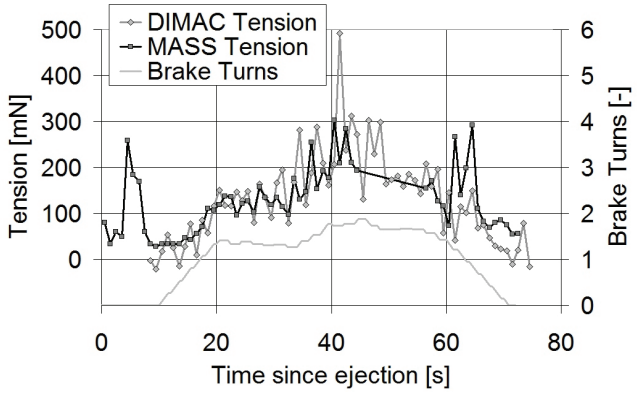

Figure 246. *Tension, averaged per second, and braking activity directly after ejection.*

The pitch-off rate of the capsule has been determined from MASS gyroscope and magnetometer data (Figure 247) to be only 1.55±0.3°/s (Figure 248). As compared to the design requirement to remain below 10°/s, this demonstrates successful alignment of the MASS/Fotino system's center of mass and nominal performance of the 40 J ejection system. The breaking of the last tie-down appears to have caused a favorable reduction of the pitch-off rate by about 20-25%, matching the foreseen effect (Section 5.3.4) [Stelzer 2006].

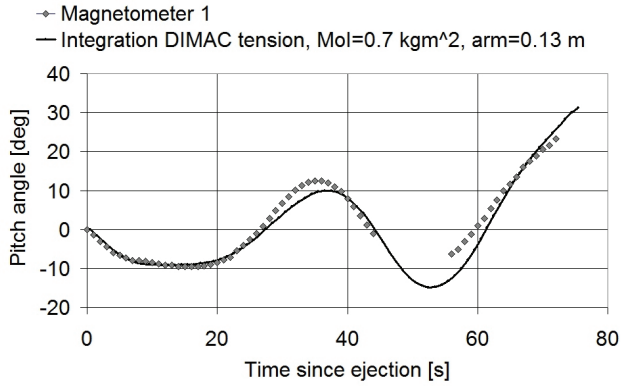

Figure 247. *Pitch angle based on Magnetometer 1 data and DIMAC-based simulation*

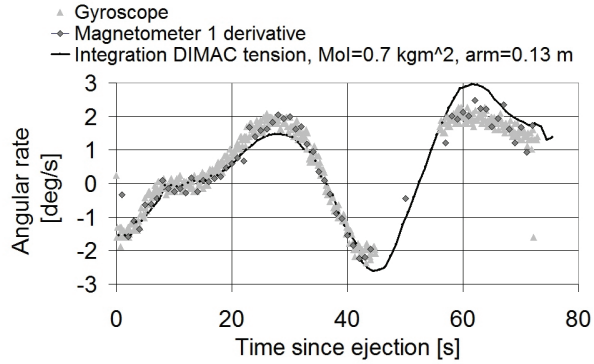

Figure 248. *MASS magnetometer and gyro data directly after ejection, including simulator matching*

OLD data show that during the first few minutes the deployment is quite irregular. Deployment appears to take place through a stick-slip process. In addition, two types of anomalies are observed in this brief interval. Firstly, some OLD pulses are missing from a single channel. The filter correctly filters in for them (squares in Figure 249). Secondly, sometimes there are two subsequent pulses from the same channel with a relatively long interval between them (light diamonds).

The latter is a more ambiguous sequence that has been investigated in more detail and is found to have caused a control problem. These successive signals from a single channel may be caused either by jitter of the tether during the stick-slip process (Table 47C), or, by a subsequent two-channel OLD failure (Table 47D). A double OLD failure would mean a full loop has deployed in between the two same-channel pulses. The OBC filter is programmed to assume this explanation and the software adds a loop, increasing the length and raw velocity for that moment in time.

It is however concluded that the same-channel transitions are due to jitter, rather than a double OLD failure, for several reasons. Firstly, throughout the remainder of the first stage, events as indicated are quite rare, only about 25 in total for about 4700 loops. Instead they generally are associated with recognizable stick-slip patterns in the surrounding time interval (as determined by visual inspection of the data). These stick-slip patters occur only during two distinct phases, at the start and at the end of the first stage deployment. Secondly, statistical analysis of occurrence and OLD channel signature of long duration gaps shows that such gaps are about 20 times more likely to maintain proper order of the pattern than random OLD malfunctioning would predict (Section 8.3.2). Most such occurrences are therefore related to tether jitter. Finally, the deployment velocity profile that the OBC filter extracts, by assuming the noisy events are missed loops, shows an anomalous deviation from the trend around $t = 35$ s (Filtered Velocity in Figure 245). This breaking of the trend does however not occur when the gaps are attributed to stick-slip jitter (see the curve for the unfiltered True OLD Velocity).

The OBC's double-channel failure algorithm has therefore been applied unnecessarily, several times in a row shortly after ejection, and has counted multiple false loops of tether. As a result of the false triggerings, the deployment velocity has been overestimated by about 10% for some tens of seconds. The response of the controller to this event has been to turn up the level of braking, as can be seen in Figure 246. The increased brake activity after $t = 30$-35 s decelerates the endmass significantly, some 40 cm/s under the nominal velocity. By itself this is not a problem as the brake can be released to recover this loss in velocity. But because also the tether minimal deployment tension (stickiness to the spool) just exceeds the acceptable range (Section 8.3.4), there is no possibility to recover immediately.

As regards to the cause of jitter during this stick-slip process and a similar one at $t = 5$ s (horizontal arrows in Figure 249) it is plausible that it is the result of tension disturbances due to endmass oscillations in combination with the (still) short tether length. Note also that the irregularities coincide in time with the onset of maximum pitch amplitude (Figure 247).

This initial irregular stick-slip behavior smoothed out as distance to the Foton-M3 increases and disappears at about 470 m. Around the 1-km point, the minimum deployment velocity of 0.3 m/s is reached. The tether stickiness on the spool is the dominant source of tether tension here. At low deployment velocities, tension reconstruction from both DIMAC and OLD data indicates a $T_0 = 0.023$ N, about 2.7 times higher than nominal, but below the acceptable maximum of 0.03 N for which the deployment profile is designed (Figure 257). At velocities above 1 m/s, the various data sources imply an out-of-spec $T_0 = 0.04$ N.

After the 1-km point, gravity gradient forces take over and accelerate the deployment such that the lost distance due to the sub-nominal velocity is eventually compensated for. During this period, OLD data shows a rather smooth unwinding behavior. At the time the length meets the nominal value again, the deployment velocity is significantly higher than nominal (Figure 251). At t = 2220 s, a length of 2 km and a velocity of little over 2 m/s, the controller kicks in and decelerates the deployment steeply. This abrupt braking leads to transverse waves with a period of about 250 s, that in turn result in irregular deployment velocity. The

brake controller, does not dampen out the shock and resonates with deployment velocity changes (Figure 252). Significant transverse waves in the tether and signature tension peaks are the result (Figure 254). Nevertheless the controller manages to oscillate around the nominal trajectory and brings the system safely to a standstill at a nominal length and with an acceptable pendulum oscillation of about 10 degrees below Foton (Figure 250, Figure 260). In this last phase of the deployment, the transverse waves have induced a second period of stick-slip deployment (after the initial phase at ejection). In a few instances here, the newly introduced irregularity in the deployment leads again to faulty triggering of the double-channel failure algorithm. Despite the additional loopcounts the first stage length that has been accurately obtained. Inspection of the OLDs by statistic and visual means reveals that the length determination by the OBC has been accurate by about 10 m and the total first stage length achieved is 3378 m (±20 m) compared to a target length of 3390 m, providing a good basis for a nominal second stage deployment (Figure 250).

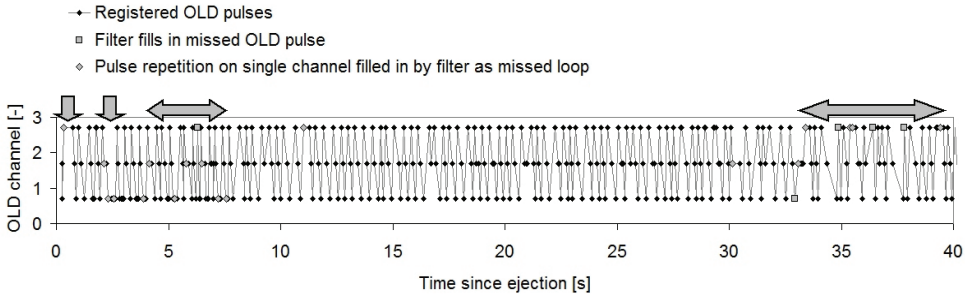

Figure 249. *OLD channel activation directly after ejection. See text.*

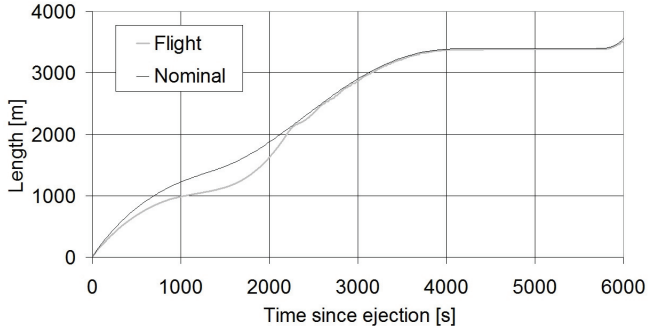

Figure 250. *YES2 deployed length, first stage*

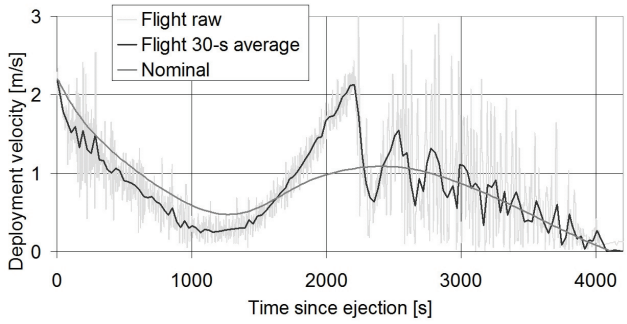

Figure 251. *Deployment velocity of YES2 mission flight data vs. nominal in first stage.*

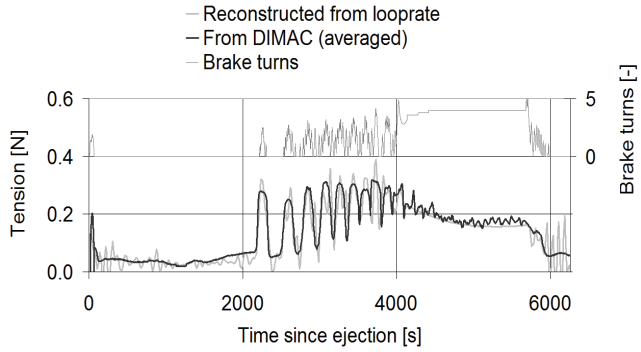

Figure 252. *YES2 flight tension and brake activity from ejection to start of second stage*

The hold phase is nominal, the length being held nearly constant by the subtle increments of 0.2 turns applied by the controller whenever a loop deploys. The transverse oscillations dampens out somewhat in this stage. Also the continuation into the second stage deployment occurs much as planned (Figure 252, Figure 253).

Some 500 s into the second stage however, the OLD data as recorded by the On-Board Computer (OBC) starts to show intermittent and increasingly large gaps on all channels. A larger and larger fraction of arriving interrupts is not recorded. The failure is due to a faulty electronics patch (Section 8.5.1). In response, the controller turns the brake to zero and the deployment continued in a free, uncontrolled manner. The velocity profile has been determined from a combination of the loop rate and the loop length as a function of loop count, information known from the winding process. The deployment has accelerated smoothly. At about 3 m/s significant rattling inside the tether canister is observed by DIMAC (Figure 237) indicating that from this moment onward the centrifugal force has lifted the tether from the spool and the "ball" starts scrubbing the edges of the canister and increasing tension significantly. A similar behavior has been seen in ground tests (Figure 231). With the brake set to zero, deployment has become somewhat faster than nominal (to 16 m/s rather than 13 m/s) and overdeploys to the full length of 31.7 km rather than the

target length of 30.0 km. There is no gentle deceleration near the end, the deployment stops abruptly at about 15 m/s, an event that leaves a distinct tension signature at t_{eject}+8626 s (Figure 265).

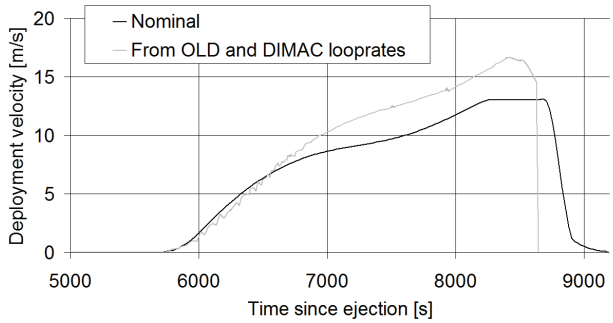

Figure 253. *Deployment velocity of YES2 mission flight data vs. nominal in second stage.*

The development of in-plane angle with time must be determined precisely if the trajectory and projected landing site of the Fotino capsule is to be determined. The DIMAC data provides information only on the angle at which the tether leaves Foton. The angle towards the endmass is reconstructed independently from the OLD data, through integration of the tether length and velocity profile according to Eq. 2.16. The same equation is used to reconstruct deployment tension throughout the deployment. These equations ignore tether flexibility aspects and assume circular orbit as well as infinite mass for Foton-M3. For this reason, a verification simulation has been made using MTBsim , also matching the loop rate profile (Section 8.4.1).

The results are combined in Figure 254. When compared to the DIMAC angle data, a good general match is found and one can clearly identify in the DIMAC data a superimposed oscillation that is related to transverse waves. The endshock at deployment completion occurs near $\theta = 40°$. The release of Fotino ($t = 9344$ s) and tether cut ($t = 9364$ s) is near $\theta = 0°$. Release of the tether near the vertical is confirmed by a sudden disappearance of tether tension at $t = 9364$ s (Figure 255).

Release at this time has been computed as well by USSTRATCOM. USSTRATCOM has identified a sudden change in Foton orbital elements (Figure 244), and calculates the moment of divergence with the original set at $t = 9365(!)\pm900$ s with an altitude impact on Foton perigee of 1050 m [Kruijff 2007.II]. This raise in altitude compares well with the momentum transfer that can be expected for a swing angle of 40° and a fully deployed tether released at the vertical if combined with an estimate of the Foton-M3 attitude control thruster effect (Figure 241). This Foton-M3 attitude control algorithm (Section 8.3.2) has been simulated by MTBSim as well. The tether effect of Foton perigee altitude can be determined to be 950 m ±3% plus 150 m ±25% for the Foton thruster contribution, or about 1100 m ± 50 m total.

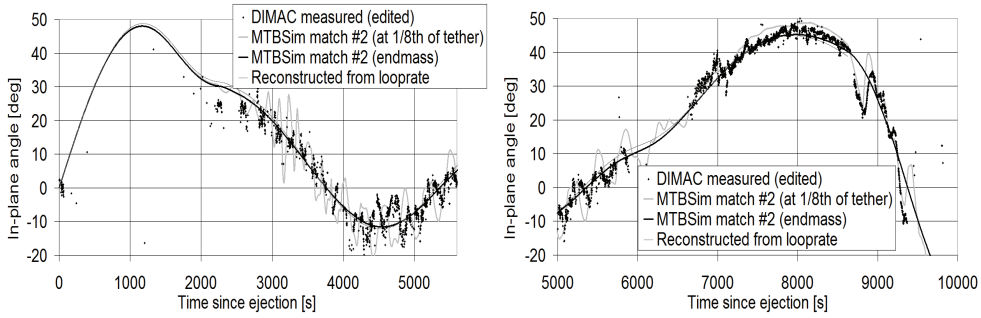

Figure 254. *The measurements and simulation of the tether exit angle with respect to Foton evidence presence of transverse waves starting from 2200 s.*

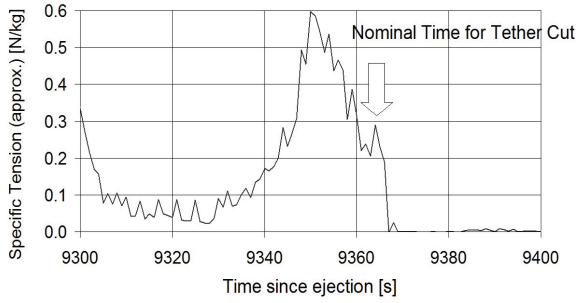

Figure 255. *Confirmation of nominal tether cut from semi-processed DIMAC data*

Length and in-plane angle profiles can be combined to provide a convenient Local-Horizontal Local-Vertical view of the tether deployment (Figure 261). The pendulum motion during the hold phase can be easily recognized. With the brake set to zero in most of the second stage a higher velocity than nominal has been obtained, leading to a higher in-plane angle than foreseen. The pronounced swing of the flight deployment contrasts against the very smooth and slow deceleration of the nominal mission, in which considerable effective swing angle (Eq. 2.11) is lost. Although the release of the endmass can be considered nominal in terms of in-plane angle, the increased swing velocity and tether length impart a greater ΔV on the endmass and a steeper entry, towards a landing point 1250 km from the nominal landing point, Section 8.5.4.

Tension has been determined indirectly from Eq. 2.16b for comparison with the more direct DIMAC data (Figure 259). The fit between these two independently determined tension reconstructions is quite good until $t = 7500$ s. From that moment some divergence can be observed. The difference in tension builds up to almost 30% at the end of deployment. The difference is thought to arise due to a variety of factors: large sensitivity of tension level to even small changes in velocity, imperfection of the model of Eq. 2.16 or the determined velocity profile, and pollution of the DIMAC measurements after $t = 7000$ s due to increasing Foton attitude control thruster activity (Figure 242). Indications for such pollution exist as DIMAC data is not consistent with Foton measurements after this time. The contribution of

model imperfection is assessed in Section 8.4.1. A more representative dynamics model (YESSim version of MTBSim) provides a tension profile closer to the DIMAC value.

In order to quantify the potential impact of the inaccuracy of the deployment velocity profile, the consequence of an adjusted loop rate has been determined. To this end, the maximum deviation from the best-fit loop rate as allowable by the limited measurement precision is applied in a direction to approach better the DIMAC tension. The impact is found small [Kruijff 2008] and negligible on the in-plane trajectory (Figure 256). The best fit is therefore maintained as the more likely dynamic estimate.

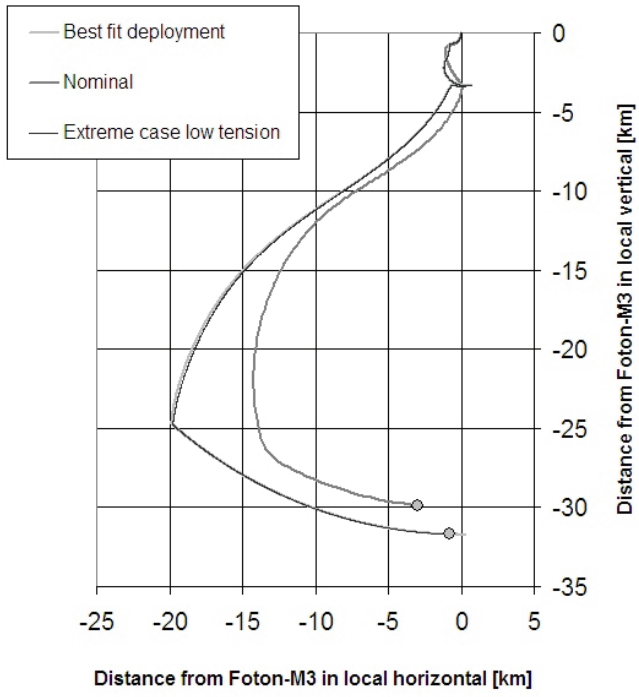

Figure 256. *LHLV plot of nominal deployment and release point vs. reconstructed*

8.3.4 Deployer performance

Three main parameters have been assessed for in-flight qualification of the deployer hardware. In other words, it has been verified whether the tether spool and barberpole brake can be sufficiently characterized on the ground to allow reliable control of deployment in space. These parameters are taken from Eq. 5.30 and some samples are plotted in Figure 257 :

1. the minimal deployment tension T_0,
2. barberpole brake friction coefficient f and
3. I, the inertia multiplier.

The minimal deployment tension T_0 (tether stickiness to the spool) is important in the early part of the first stage when gravity gradient is low and the endmass dynamics are determined by endmass inertia and the deceleration caused by this minimal friction level. Its nominal value is 0.0085 N, the acceptable level for robust control of deployment is 0.005 to 0.3 N. During the first stage of the YES2 mission, the zero-brake deployment tension is higher and ranges from 0.027 to 0.045 N, equivalent to a T_0 = 0.023-0.038 N when corrected for the dynamic term.

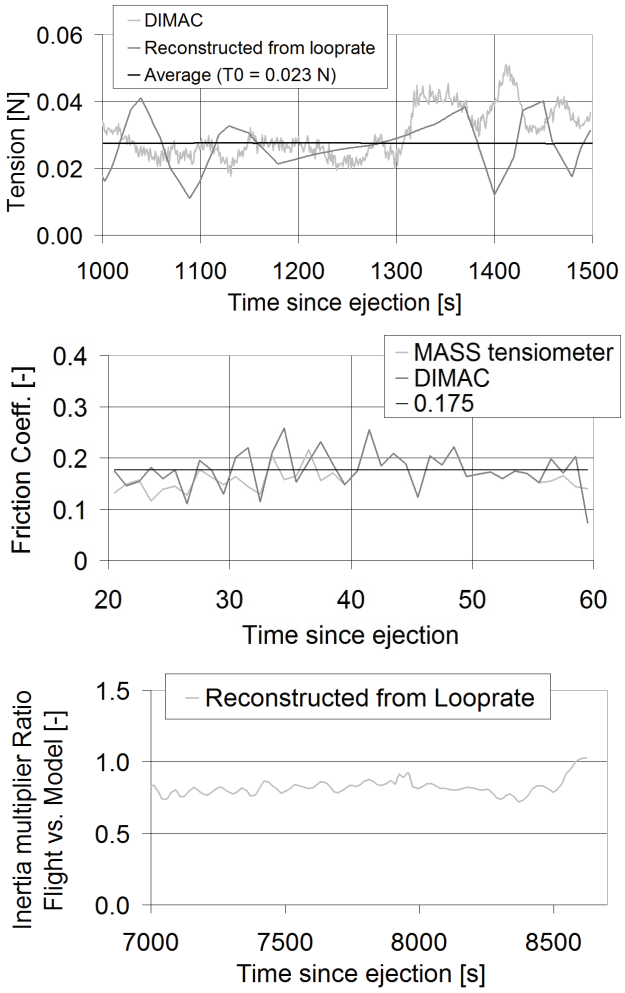

Figure 257. *Quantitative evidence of suitability of tether deployer performance for the SpaceMail application, for the three main hardware parameters.*

The barberpole brake friction coefficient *f* becomes important when the deployment needs to be controlled (for better precision) or actively decelerated. Nominal value is $f = 0.2$. A friction level below 0.12 would require time-consuming amount of activation of the barberpole and

would lead to a large number of wraps, decreasing brake effectiveness. A level above 0.3 can lead to controller resonance. A clean flight measurement is available for the initial braking phase (Figure 246) and results in a value of 0.175, well within acceptable limits. Based on DIMAC data alone, further estimates of f can be made during the braking oscillations after t=2200 s and start-up of the second stage. This work remains to be done.

The inertia multiplier I represents (in simplified manner) the dynamic dependency of spool unwinding tension on deployed length and deployment velocity, including effects such as tether inertia, shock energy and compressibility of the spool. The criticality of this parameter is not very high, as it is dominant in the high velocity deployment part of the second stage, where gravity gradient is high and deployment is rather easy to control with the barberpole brake. The acceptable range for the value of I is 2-20, with 8 as nominal. The zero-brake setting during the final part of the second stage setting allows for a thorough assessment of this dynamic effect in the deployer tension model. The result shows that the dynamic effect on tension in flight matches the preflight model within 20%. This is significantly better than the maximum acceptable deviation (-75% to +150%). The rise of the value of I at the end of deployment can alternatively be absorbed by a larger area exponent E, but this has not been investigated further.

8.4 Tether deployment data matching by simulation

8.4.1 Simulated deployment with matching velocity profile

The advanced tether simulator MTBSim (YESSim version, see Section 2.3.2) has been used to reconstruct the deployment in a more representative manner than can be done based on the simple dynamic model (Eq. 2.16). Rather than by enforcing the deployment looprate profile, such as done for the reconstruction based on the simple dynamic model, a match to the deployment rate profile is obtained indirectly from finetuning of only a few simulator parameter settings. MTBSim uses a hardware friction model and a controller software model as input. The deployment velocity is an output. As the velocity profile in flight has been well-characterized, it has been selected as the basis for deployment reconstruction. The deployer parameters T_0, f and I have been tuned manually until the MTBSim velocity output matches the flight data.

In fact, the matching exercise is a (non-automated) means to translate deployment rate data via the MTBSim tether dynamics model, into estimates of in-plane angle and oscillatory dynamics, independent from DIMAC measurements. Since each of the three deployer hardware parameters is dominant in clearly separated phases of deployment, one parameter at a time can be adjusted, such that a systematic insight is obtained in the magnitude of these values during the flight, as well as into the sensitivity of the deployment to these values. The MTBSim deployment reconstruction by matching is used for a number of other purposes. Better insight can be gained into tether properties. Once confidence has been gained into the representativeness of the simulation, extrapolations can be performed in

order to develop hypotheses. Impact of parameter settings on controller performance can be studied, and the capsule dynamics and trajectory can be propagated.

The velocity has been matched mostly within 1-3%. To achieve this precision, T_0 and I need to be tuned within 5%. They are thought to provide a realistic indication of the actual hardware performance. Some particularities have been introduced, as it is believed these may be physically meaningful. The controller malperformance shortly after ejection (Figure 249) is simulated by artificially introducing an overestimate of the velocity of 0.3 m/s over a period of 14 seconds. A setting is used for $T_0 = 0.027$ N for zero velocity (deviating by 17% from the value found in Section 8.4.3), linearly rising to 0.04 N at 1 m/s and higher. This velocity dependency of T_0 is creates a highly precise match of the low velocity deployment early in the first stage, at 0.3 m/s. Friction itself is chosen to be $f = 0.2$ for zero velocity, linearly rising to about 0.25 at 1 m/s and higher. The electrical power failure on the OLD interface is simulated by artificially introducing a condition of free deployment ($n = 0$) at $t = 6300$ s. The exact timing is not critical. The parameter I is important for the second stage deployment. A good fit can be obtained with $I = 8.2$, close to the nominal value. This fit can be improved further by splitting the deployment in 3-5 segments each with its own value for I, deviating by less than 10% from the average. Note that these values are generally closer to the nominal values than the values found in Section 8.4.3 - the reason for this has not yet been investigated. Compared to the allowable deviations (Section 5.5.5) the deviations are small.

Marked flight features are recognized, such as control activity, resonance and occurrence and characteristics of longitudinal and transverse waves. Some deviation is found in the last few hundreds of seconds of deployment, where the velocity is only known with 0.5 m/s accuracy and the effect of the area exponent E becomes noticeable.

In order to cover the extreme cases, various profiles have been developed by different tuning of I and the tether properties stiffness and damping coefficient. Two matches are reported here in particular. The first Match #1 maintains the ground estimates of stiffness but adjusts damping coefficient to match the oscillation performance after the endshock better (Section 8.4.3). A single value for I is assumed. No controller resonance and little transverse waves are produced (as described in Section 8.3.3). Match #2 uses the tether properties as resulting from the investigation (Section 8.4.3) and a closer fit to the velocity profile is targeted by segmenting the value for I into five intervals, where the value changes from segment to segment by about 10% around the average. Transversal oscillations, similar but probably heavier than those in flight, are produced. The resulting in-plane deployment trajectory matches the simple model well, to within 1-2°. The mission data is matched within its accuracy of about 2-5°. Figure 254, Figure 258-Figure 261 show the matching results vs. flight measured/derived curves. The coincidence of simulated vs. measured parameters not used for the matching exercise (tension and in-plane angle) provide confidence in the applicability of deployer hardware and tether dynamics simulations within the required level of accuracy (see also Section 8.1.1).

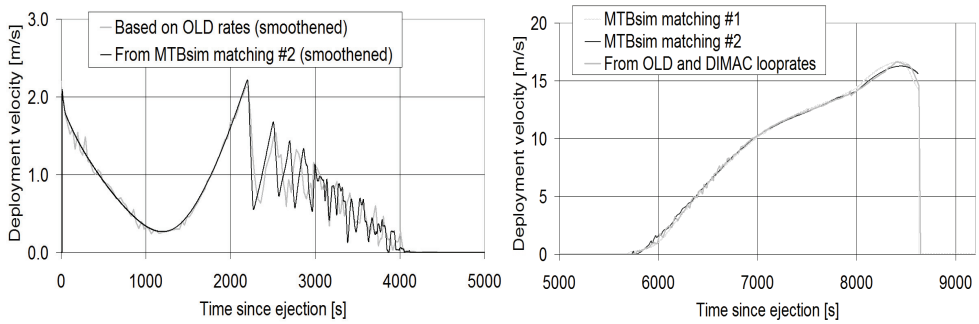

Figure 258. *Matching of deployment velocity (first and second stage) by simulation including controller oscillations*

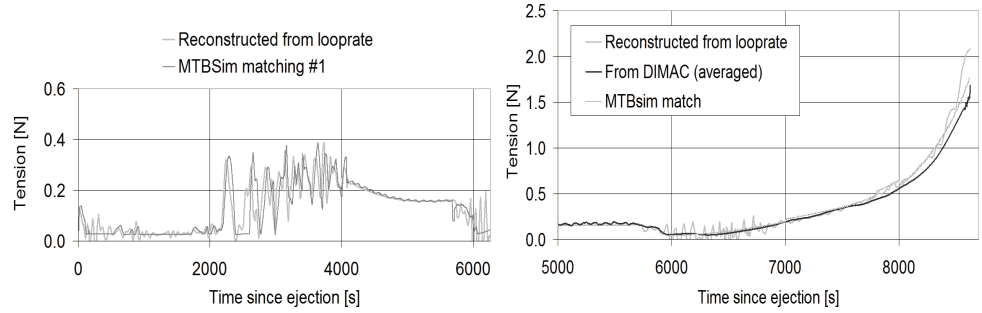

Figure 259. *Matching of mission tension by simulation*

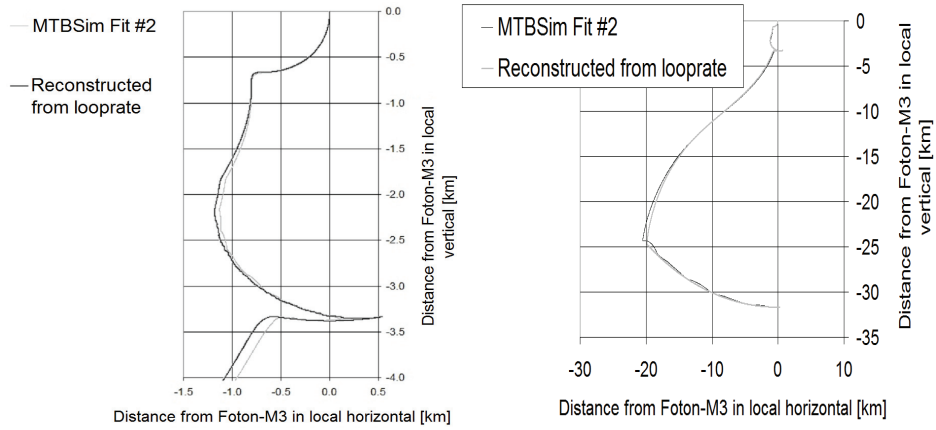

Figure 260. *Matching of deployment trajectory, first (left) and second stage (right).*

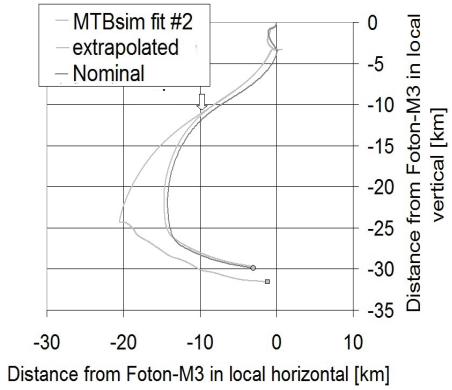

Figure 261. Nominal deployment and flight data match. The location from which OLD's were no longer registered is indicated by an arrow. Flight data match is then continued including a (simulated) OLD failure (left branch, close to actual YES2 flight), as well as without this failure (right branch, hypothetical extrapolation)

8.4.2 Controller performance

The importance of accurate simulation of deployer hardware and control software has been demonstrated in the matching exercise. Given sufficient sensitivity analysis, the insights gained can then be used to improve deployer and controller design.

In the matching simulations controller-deployment resonance with resulting transverse waves is eventually reproduced, reminiscent of the mission data as shown in Figure 262. Early matching attempts however, with a simplified on-board controller model, that assumes immediate and accurate knowledge of the velocity, did reproduce the strong deceleration at $t = 2200$ s, but deployment velocity then recovered smoothly and no heavy and enduring velocity oscillations were observed (such as in Figure 258) nor were there any tension peaks associated to transverse waves (such as in Figure 263). Adjustment of the simulator has been necessary to sufficiently improve its level of realism and make it possible to reproduce this more complex behavior observed in flight.

First, the observed macro-scale (order 100 s) pulse-wise control after $t = 2200$ s leading to repeated, large, but still relatively smooth variations in velocity (albeit no full standstills) has been obtained by properly setting the high value of T_0 as observed, combined with a slight adjustment in value for the friction coefficient f as compared to nominal. Note that the occurrence of this behavior proves to be dependent on the brake response speed, expressed in applied wraps per second. This brake response speed is programmed in software and is based on the maximum recommended operating frequency for the stepper motor. A higher response speed than the setting used during YES2 is recommended.

The higher friction alone does however not cause the heavy and fast velocity and control oscillations (order 20 s) that are superimposed on the macro-scale profile in the flight data, and that can also be distinguished in Figure 262. As a potential candidate cause, classic

stick-slip for a spring-mass system has been simulated by introduction of a static friction coefficient higher than the dynamic friction. But no significant effect has been observed.

Instead, the cause of the noisy response lies in the limitation with which the on-board velocity estimate can be obtained. The velocity is approximated from the length estimate using a low-pass filter, and its estimate is in fact smoothened and running about 8 seconds behind reality. If velocity changes only slowly, this delay leads to a small, quite harmless zig-zag brake behavior with a period of about 20 s. Under certain conditions (such as the high friction levels) this zig-zag response can resonate with the velocity. When a high velocity is measured, the velocity may in reality be already low, as the brake is turned up, it lowers even more. Then the brake is released and the pattern repeats and amplifies. Transverse oscillations can provide the momentum that create peaks in tension when the brake is applied and accelerate the tether strongly as soon as the brake is released, causing further excitation of the resonance. As a result, the higher frequency control noise is superimposed on the lower frequency pulses related to the transverse waves.

The above-mentioned simulated effects account for most of the irregularities observed in the velocity and OLD pattern seen in flight. This indicates that the endmass velocity due to macro-dynamics and controller activity govern the rate of deployment of the tether from the spool, more than capsule angular dynamics or complex physics such as stick-slip processes or sound waves in the tether. Some of the irregularities in the OLD pattern seen in the flight did however not occur during the testing or pre-flight simulations, specifically in the first minute of deployment. Here it is assumed that endmass dynamics were still influential. This is yet to be confirmed by further simulations with MTBSim upgraded to include the endmass dynamics effect on tension.

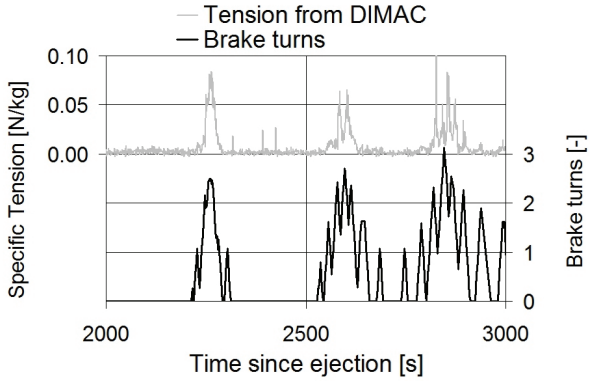

Figure 262. *Brake controller causes tension pulses in conjunction with the transverse wave that arose from the first pulse.*

8.4.3 Tether oscillations

The three main types of tether oscillations as observed during the YES2 mission are compared to simulation data. Mechanical tether wave dynamics in space are well represented by the simulator or can be otherwise understood. Note that this analysis is for a

short duration mission, and does not include Coulomb damping effects as observed in the 1996 TiPS tether mission that survived 10 years in space [Barnds 1998].

Transverse waves

Tether bending during deployment can not be fully avoided. It occurs due to Coriolis forces acting along the deploying tether. This is specifically true in early deployment when tension is low (about 3 cN in case of YES2), while at the same time deployment velocity is high (YES2 maximum velocity is 16 m/s) or if tether mass is significant with respect to the endmass (YES2 endmass is 14 kg vs. 6 kg tether). Transverse waves are introduced if low tension deployment is followed by abrupt braking, as occurred in YES2 at $t = 2200$ s. Amplification of the waves after this shock was observed as a result of the controller resonance with the deployment. In the hold phase and then the second stage, the waves become less dominant, until finally the endshock introduces new and heavy transverse waves that remained present throughout the swing and superimposed on the spring-mass oscillation.

Transverse waves are recorded by the DIMAC instrument through their signature tension shocks (especially in the first stage), but also more directly by measurements of the angle under which the tether leaves Foton, Figure 254, Figure 263. The deployment matching simulation realistically portrays both shock waves.

Spring mass oscillations and damping

In the endshock the tether is brought to an abrupt stop from a velocity of about 15.4 m/s and stretches more than 100 meters. As the tether relaxes, MASS/Fotino bounces back into a free orbital trajectory towards the local vertical below Foton. A combined orbital bouncing/spring-mass oscillation is created (including also transverse and sound waves) causing repeated tension peaks of about 10 N.

MTBSim reconstruction of the mission deployment matches this complex behavior qualitatively with proper selection of damping and stiffness, Figure 264. In this figure, the time reference is the time of completion of deployment and start of the swing back. The tether cut occurs at 740 s.

Manipulation of these tether property values, damping coefficient ζ and stiffness EA, show that general shape and frequency depend on the ratio EA/ζ^2. Higher stiffness or lower damping leads to a faster succession of pulses. The absolute numbers determine the amplitude. Good fits are obtained for a $\zeta = 0.14$-0.16 and a stiffness of EA = 5-10 kN. The somewhat higher value for stiffness is no surprise as the tension levels are higher than those expected in the nominal mission and the stiffness for Dyneema® tethers is known to rise with the loading. The damping appears to have been significantly higher than tested ($\zeta = 0.08$), which is for now attributed to a limited applicability of the test method (Section 4.1.5), although an impact of limitations of the simulator cannot be excluded.

Longitudinal waves

One event recorded during YES2 shows clear impact of a sound wave echoing back and forth through the tether several times: the end shock. The speed of sound in a tether is not related to the braiding stiffness but to the fiber stiffness and for Dyneema® is as high as a = 10 km/s. This means a sound wave should travel back and forth through the tether in about 6.5 seconds. This is close to what was observed. Figure 265 is the tension profile of the endshock recorded at Foton, the tether deployer end. The curious shape of the shock (rather than the typical sine pulse that MTBSim produces) is explained in a number of steps.

As the deploying tether is brought instantaneously to a standstill, at the site of the deployer in Foton, from about v_0 = 15 m/s, the remainder of the tether is still unaware of this event and traveling further. The information of the deployment stop travels down the full 31.7 km of tether with the speed of sound. As the deployment stop reaches any point in the tether at distance x from Foton in $\Delta t = x/a$ seconds, this point has moved $v_0 \Delta t$ and therefore the tether has built up an additional stretch by $\Delta l = x v_0/a$. Tension is assumed to remain constant and follow Hooke's law, $\Delta T = EA\ \Delta l/l$, therefore also $T = EA\ x v_0/a/x = EA\ v_0/a$.

After $P/2$ seconds, with P the observed time between shocks, the standstill reaches the other end of the tether. Fotino has significant inertia and pulls on the tether. The 15 m long ripstitch damping device mounted near Fotino activates and reduces the tension for about a second to ~6 N. Then Fotino inertia restores and increases the tension such that the shock in the tether is reflected back to Foton where it is being measured ½ P s later as a further sudden rise. As Fotino slows down, the shock level drops, until the reflection returns again, and 7 s later a third and final time. Then Fotino has rebounced and the tether is slack.

The observed pulse can be used to accurately determine some tether properties. The speed of sound a can be obtained through $a = 2\ l/P \approx 8.8$ km/s. The estimate for a inside the fiber should be corrected somewhat taking into account that the braided tether fiber is approximately 3% longer than the tether itself, yielding a final estimate of a_{fiber} = 1.03 * 8.8 = 9.1 km/s. An expression for the tether stiffness can now also be obtained from the tension measurement: $EA = 2\Delta Tl/(Pv_0) \approx 10$ kN. The maximum amplitude of ΔT of about 37 N is somewhat larger while the shock duration ½ P_{shock} = 14 s is significantly shorter than would be obtained simulating a spring-mass system with infinite speed of sound for which $T = v_0 \sqrt{(EAm'/L)} = 33$ N and ½ $P_{shock} = \pi/\sqrt{(EA/m'L)} = 24$ s, using $m' = m_{Fotino} + 0.34\ m_{tether}$ according to Yost [Yost 2002].

The measured pulse can be compared to predictions of mathematical tether model. Note that MTBSim does not simulate the speed of sound as it has an explicit assumption that the speed of sound is infinite (Section 2.3.2). Is has shown to be a more than sufficient approximation for most practical applications. Prof. Smirnov and Ass. Prof. Alexey Malashin from Moscow M.V. Lomonosov State University have kindly provided below simulation that illustrate the qualitative behavior The simulation is without damping, includes no ripstitch and has a lower EA = 5000 N, v_0 = 14 m/s and a = 10 km/s (Figure 265). The difference with the YES2 measurement is primarily due to the stiffness difference and partly also due to lack of damping in their model. Their derivation shows how Fotino is

decelerated in a sequence of asymptotic exponentials, every time the echoing shock reaches the body [Smirnov 2010]. Foton experiences a longer tension increase than at Fotino. On macro scale (so from a point of view of MTBSim comparison) the shock is delayed from Foton perspective by 7 s (albeit preceded by a 7 s lower level shock) and from Fotino perspective by 3.5 s.

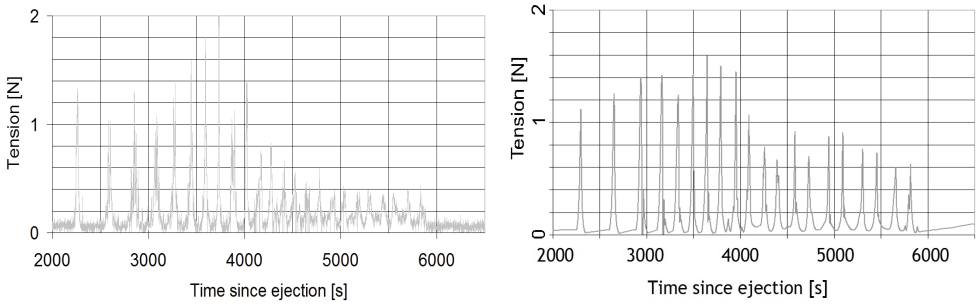

Figure 263. *Tension pulses from transverse waves during first stage and hold phase. Left: flight data, right: deployment matching simulation.*

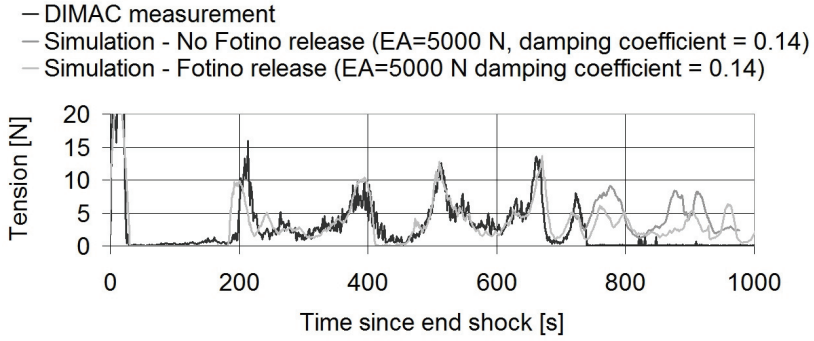

Figure 264. *Matching of complex tension signature of complex wave form (mostly spring-mass) during swing-back to vertical.*

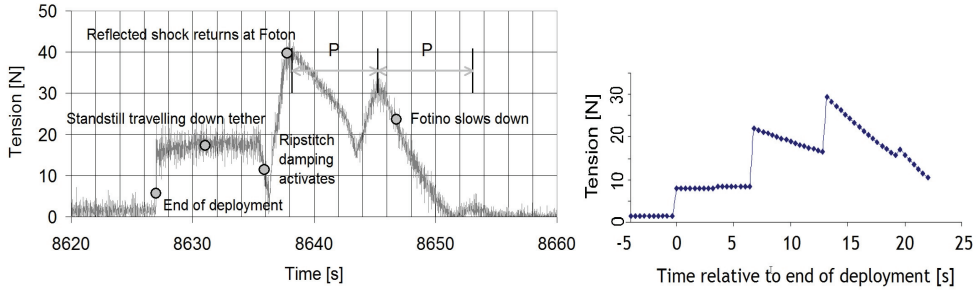

Figure 265. *Measured and simulated endshock showing echo in the tether*

8.5 Failure analysis and extrapolation of the YES2 mission results

In this section the implications of the YES2 mission analysis results are studied in a broader context. How do the results compare to those of the earlier, similar SEDS experiments? What conclusions can be drawn from the combined flight results today on predictability of tether dynamics? What can we then say about the fate of the re-entry capsule Fotino? And what are the implications for the suitability of the system for SpaceMail and other future missions? Before these questions can be answered, the anomalies observed during the YES2 mission are analyzed. They need to be viewed in the proper perspective before further projections are made.

8.5.1 Failure investigation

The YES2 mission has deviated from the nominal in various ways. In this section these problems are further investigated and possible approaches towards solutions are proposed:

- In the initial meters, the deployment has been irregular. The OLD filter's third error recovery feature (Table 48, row D) has not dealt well with this irregularity and estimates velocity too high, leading to over-braking.
- Recovery from the over-braking is then impeded due to unexpectedly high stickiness of the tether. This stickiness causes the deployment to continue below the nominal length profile for 2200 s. This leads to heavy control activity, which succeeds in getting the length development back in check. However, a controller resonance causes an excitation of transverse waves that may have been avoided given a better selection of controller parameters. Although not confirmed, tether slackness may have occurred for intervals long enough to cause large oscillatory amplitudes in the endmass which in turn may have contributed to adverse entry conditions for Fotino and increased risk of burn-up in re-entry.
- Finally, after a successful start of the second stage, the computer's registration of OLD loopcount pulses fails and leads to an overdeployment, shock and slackness in the tether as well as a too steep re-entry for Fotino. Fotino re-enters out of range of the student-deployed mobile ground station.

Initial deployment irregularity

Simulation of the impact of endmass dynamics on tension and deployment velocity in early deployment should be performed to study the cause of the irregularity. Possibly the mechanism behind the irregularity is stick-slip but simulations with stick-slip features alone without the effect of endmass oscillations have not reproduced the behavior. Dealing with this problem in practice however promises to be rather simple. Miscalculation of deployed length can be avoided simply by removing the double-failure feature (Section 5.5.3) from the software. This algorithm has proven unnecessary, as double failure has been extremely rare

during the first stage of deployment. Sufficient redundancy is already provided by the remaining OLD features. The single-failure feature worked very well in flight.

Stickiness

There have been various hypotheses for the observed unexpectedly high level of stickiness:

1. outgassing and subsequent deposit of sticky components in the polyethylene and antistatic fiber finish in the outer kilometers of the tether and/or tether guides,
2. lack of humidity as present in the ground tests that could provide a molecular low-friction film,
3. outgassing of the antistatic finish leading to fiber ends to stand out and interact, or the deploying and charging tether to stick to surfaces,
4. low temperature effects making the antistatic fiber finish stiffer,
5. chemical change in the antistatic fiber finish due to preflight thermomechanical loads and thermal vacuum environment that cause molecular bonds between surfaces,
6. purely thermomechanical effects due to expansion and contraction of the spool during thermal cycles affecting tension.

In order to study these hypotheses, the environment has to be understood that the YES2 tether has been exposed to. The YES2 tether has spent 11 days in space mounted in the center of the Foton-M3 battery pack, with YES2 unpowered and wrapped in a thermal blanket. Thermal analysis shows that the range of temperatures that YES2 has gone through before power-on may have slowly fluctuated between –20°C and +40°C as Foton's uncontrolled motion and attitude with respect to the Sun developed. When finally YES2 is switched on temperatures are relatively moderate. Presumably rather homogeneous as YES2 is wrapped fully in thermal blankets, the temperature of YES2 at the time is –2.5°C (Figure 234). At start of deployment, the tether core has already warmed up to room temperature, due to received Earth radiation and conduction from the structure heated up by YES2 electronics.

Measurements made in vacuum provide some insight into thermal conductance through a tether spool (Figure 266). It takes 4 hours for the temperature to propagate through 1.12 kg of tether mass. This test shows that temperature of the outer layer of the 6 kg of flight tether will hardly be affected by the 4-5 hours of heating during the second stage deployment, therefore tether temperature there must have remained close to 0°C.

A small test campaign has been held post-flight to test the main hypotheses' individual or combined effects. In preparation of the test plan, outgassing effects are seen as the likely main culprit. A segment of 1350 m of tether, cut from the flight tether *Florian* before launch, is wound on top of a 4700 m spool of tether *Gianluca* originating from the same fiber batch (but with tighter braid). The spool has a cylindrical aluminium core and including tether has a diameter of 130 mm, smaller than the flight spool's 250 mm. In order to obtain

approximately the same winding angle of 9°, the tether is wound at 7 turns per cycle as compared to 4 turns per cycle for the flight tether.

The tether has been deployed using a simple reel system at a typical first stage deployment velocity of 0.55 m/s (some for reference at 0.85 m/s), Figure 267.

In between deployments, the environmental conditions have been changed to study the impact of various effects (Figure 269). Starting in ambient atmosphere, the pre-flight ground test results is indeed reproduced. The tether is then cooled down and dehydrated in a dry nitrogen environment in order to provide a reference case at suspected flight temperature and without humidity. A deployment test is performed. Next, the tether is exposed to vacuum, including some rise in temperature to simulate some thermomechanical effect and to stimulate the outgassing (Figure 266). As the tether under test is significantly less massive than the flight tether, the vacuum exposure duration is restrained to 3 days. Exposure to cold in vacuum is suspected to have little effect on outgassing and is omitted. After exposure to vacuum the tether is brought into dry cold again and tested to study the vacuum effect. The nitrogen is then warmed up slowly for a dry test at room temperature to isolate the temperature effect.

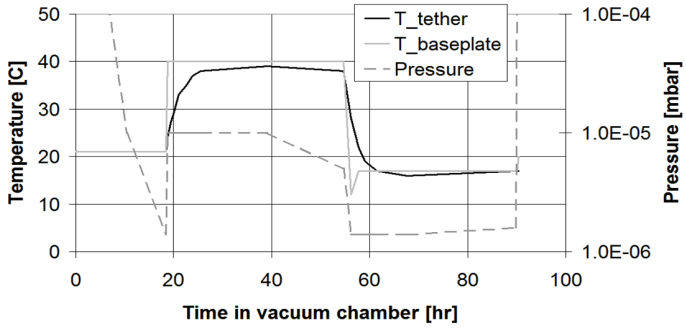

Figure 266. *Vacuum exposure characterization*

Although efforts are undertaken to isolate the various effects, some effects are obviously not reversible and are maintained following their first occurrence, even if conditions are reversed. Another challenge is to separate local effects. For example, the outer layer of the spool loses winding tension in storage conditions. Possibly the winding tension also varies through the spool. The tests performed attempt to identify also these effects.

A typical deployment tension profile is provided in Figure 268. A cyclic behavior is observed that can be correlated to the recurring location of the unwinding part of the tether on the spool. Video has been used to correlate the behavior to tension measurements to understand the link with winding geometry. Particular telling step levels of tension are labelled *Bottom/Up/Top/Bottom* and these levels are therefore used to characterize and compare the various deployment tests. These effects take place on the timescale of loops rather than layers (see Section 5.3.6), but similarly directional effects of mechanical impediments can be discerned that hamper deployment of loops over the spool or its edges.

The test results are summarized in Figure 269, where individual test conditions are represented and tests are identified by sequential numbering (Test ID #1 - #15). For each test condition the typically observed step levels are graphically represented. The occurrence of the vacuum test and transition to the *Gianluca* tether are also indicated (arrows). Moving to higher Test ID, we arrive deeper into the original spool, in total about 1400 m, 10 layers or 5 mm of depth. After a period of pause (duration is indicated), deviating behavior is seen for about 15 m (#3,#6,#11). Following that short length, behavior "normalized" to the behaviors seen in test #4 resp. #7. Most other tests are 50 m. Between test #13 and #14 a significant amount of 3 layers (350 m) has been removed.

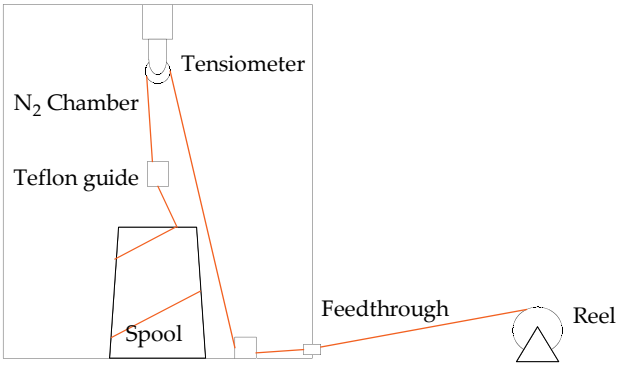

Figure 267. *Tether stickiness environmental test set-up*

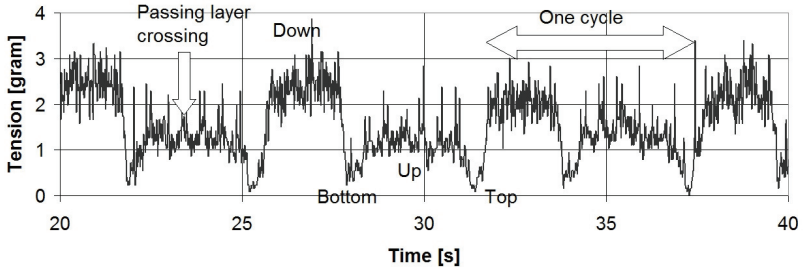

Figure 268.*Typical tension pattern for vertical unwinding*

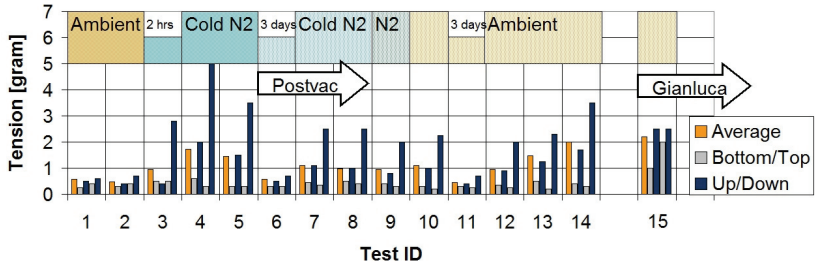

Figure 269. *Summary of tests performed and tension pattern results*

The ambient reference tests #1 and #2, as to be expected, provides results similar to pre-flight testing and shows a gentle wave of tension with two maxima per cycle, one for each unwinding direction within the cycle.

The cold nitrogen environment (#3 and further) radically changes the image (Figure 269). The minima remain in place, but the maxima are amplified and diversify into two types, one for axial deployment direction from base to top, and, about thrice as pronounced, one for the deployment direction from top back to base. Brief tension peaks can be seen to occur when the tether passes a crossing between two layers, which is where the tether has the smallest bending radius. In other words, the stickiness seems not so much increased, rather the tether interaction with the winding has, due to increased stiffness or memory or a settling of the tether onto the spool.

The return to ambient conditions (test #10) does not lead to a return to the original ambient results (tests #1 and #2). This points stronger to a settling of the tether, perhaps also at fiber level, due to the thermal change in the spool and possible other effects that could not be isolated with the test sequence as it was performed based on an initial hypothesis of outgassing effects.

This interpretation is reinforced by the fact that vacuum or hydration, which may be expected to cause changes in microscopic surface interactions, have little effect. The vacuum seems even to reduce a bit the peaks, at least in the outer 5 layers until test #13, possibly by evaporation of the surface finish in these layers.

A release of tension in the outer 15 m and return to the initial conditions is observed after the vacuum and outgassing exposure (test #6). The impacted segment of tether covers much less than the full outer layer that stretches 130 m. Any outgassing effect would affect the full layer. The tension release can thus be attributed to progressive loss of tension traveling through the tether, starting from its free end. In Figure 269 this type of behavior can indeed be observed in all three tests performed directly after a significant pause, as indicated by white blocks in the test condition bar (tests #3, #6, #11). Subsequent tests can be seen to return to the original situation.

It may be observed that the outgassing has reduced a bit the settling impact compared to the pre-vacuum cold test (#4), whereas the levels of that pre-vacuum cold test do return, deeper in the spool (#14). If this is indeed an effect of the environment change it may be explained by the hypothesis that outgassing of the surface finish reduces the settling memory somewhat, but did not reach very deep, only a partial outgassing of the outer layers may have occurred in the vacuum chamber.

To test this hypothesis, a volatiles extraction has been performed on samples of about 2 mg taken from different depths in the spool (both before and after vacuum exposure), using ether as solvent. The accuracy of the balance used is reported as 1 μg, and reproducibility is 3 μg. The reference measurement is done for a sample from the top of the spool, removed before vacuum exposure. The extraction yields a reference of 1.9% of mass loss.

Samples taken from post-vacuum exposure show less mass loss, consistent with volatiles having evaporated in vacuum. The difference of mass loss after extraction compared to the reference is therefore a measure of outgassing. From this and further samples from deeper in the spool, Figure 270 is produced. The Recovered Mass Loss for Dyneema (a standard measure for outgassing in vacuum) is also indicated, and comparison with the measurements seems to indicate that the outer layers of the spool have fully outgassed, however not so the deeper samples. The result seems thus to confirm the hypothesis that the deeper laying tether samples have outgassed less, so more antistatic coating is still present, which can explain the trend of unwinding tension rising somewhat when deeper in the spool.

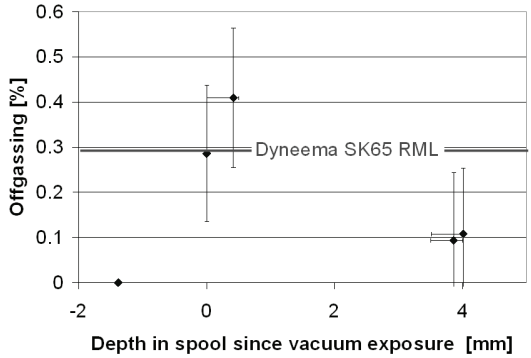

Figure 270. *Evidence that level outgassing in vacuum reduces for tether deeper inside the spool*

Alternative hypotheses, such as a slow humidification penetrating the spool over a time-span of days, or sheer randomness of the results, have been evaluated. They could not be decisively rejected but require additional non-trivial assumptions to achieve consistency with the test results (Kruijff 2009.II).

Deeper in the spool is placed a different tether, braided from the same fibers as the flight tether Florian, but much more tightly, and therefore more stiff. This "Gianluca" tether is therefore presumably less sensitive to settling effects. Unwinding tension however is found to be similarly high, although a bit more smooth. This type of braiding does therefore not provide a clear solution against high unwinding tension.

More detailed analysis is necessary to understand and prevent the increased friction from occurring, such as testing of tether bending stiffness and memory at low temperature, the effect of pre-flight removal of the surface finish, the effect of long term storage and reversibility of the effect before and after vacuum exposure. If settling rather than chemical change is the cause of the tension increase, a rewinding of the tether exposed during this campaign would provide original low tensions again. Untested conditions such as static charges or deployment in vacuum may still have further influence.

A summary of the findings with respect to the original hypotheses is provided in Table 73. The observed amplification of minimal deployment tension from YES2 flight results has

been made plausible and appears to be simply the result of mechanical settling due to cold cycling. Although it is recommended to confirm the result by a more extensive test campaign, if this is indeed the cause of the observed stickiness increase, simple pre-flight tests such as performed here will suffice to predict in-flight behavior.

	Hypothesis	Finding	Influence
1	Deposit of sticky components in outer layers.	Inner layers do not outgas much, outer layers have rather lower friction.	None
2	Humidity required for low friction.	Ambient vs. N_2 test reveals no influence.	None
3a	Outgassing of antistatic finish, tether hairy.	Outgassed tethers show no such evidence.	None
3b	Outgassing of antistatic finish, tether charged.	Outgassed layers show lower T_0 - not higher.	None
4	Antistatic fiber finish stiffens tether when cold.	Temperature of test by itself has no influence.	None
5	Flight environment causes chemical bonding between tether surfaces.	No influence found from vacuum/thermal cycling.	Unlikely
6	Thermomechanical effects.	Settling is identified as the likely cause of apparent stickiness. The opposite effect, reduced unwinding tension due to relaxation, was also observed. Retest of the same tether could confirm.	Likely

Table 73. *Overview of findings with respect to initial hypotheses regarding cause of stickiness*

Controller resonance

The simulator tool can be used as a diagnostic tool to study the impact of controller or tether properties on tether dynamics. The occurrence of persistent transverse waves and a resonance of controller and deployment velocity could for example be recreated by modeling the flight hardware and controller in detail, see Section 8.4.1. In a reverse process, by changing simulation parameters, various ways have been found to avoid or be more robust against occurrence of the unwelcome transverse waves and resonance (Table 78). It is recommended to:

- Use a faster stepper motor, able to achieve one wrap reliably in about 4 seconds rather than the 8 seconds used in YES2. This is the simplest means of preventing the problem.
- Make sure the friction level of the tether is not higher than $T_0 = 2$ cN and that of the brake is not higher than $f = 0.2$ (precise values dependent on mission parameters).
- Tune the velocity filter cut-off frequency to avoid resonance in a high friction case.
- Adjust the control gains to avoid resonance in a high friction case.

The threshold values mentioned here are particularly determined for the YES2 system and must be separately established for other designs. In addition to take into account the limited applicability of ground measurements and simulator, a sensitivity analysis should be performed, including a 20% margin on friction parameters as measured on the ground.

Missing OLD interrupts

The cause of the loss of OLD interrupt data in the second stage has also been investigated. From its onset, the performance loss has been gradually increasing, Figure 240. Examples of parameters that can be related to such a manner of signal degradation are time (e.g. component degradation or overload), deployment rate (monotonously increasing in most of the second stage) or temperature (mildly increasing by about 2 degrees per hour, Figure 234).

Some possible causes can be rendered unlikely based on flight data and pre-flight ground tests. Alignment and health signals from the three OLD channels show no degradation during the mission, even not during periods of signal outage. This is strong evidence that the sensors themselves have been properly powered and operational. Pre-flight deployment testing with integrated flight hardware has shown that the OLD electronics have no problem with providing clean pulses for the full range of looprates. Tests on the YES2 engineering model, including a robustness test and a representative deployment test have shown that both software and hardware are able to cope with the signal rate associated with very high looprates.

An indication of the cause of the failure comes from the fact that at times of signal outage, signals are mostly absent on all three channels at the same time, and would then jointly reappear. This points to a failure of a shared system, such as software (which has already been largely cleared of suspicion), the PIC controller (translation chip for the interrupt signals on the CPU board) or the joint power supply to the RS422 receivers of the OLD signal (Figure 272).

The OLD receivers get their power from the 1.5 W auxiliary DC/DC converter meant for low-power safety-critical signals in the PDU such as telecommands and telemetry, whereas the less critical OBC and OLD boards receive their power from the 30 W main converter. Within this circuitry there is an easily identifiable suspect. It is an electronic patch that deals with a known, faulty interrupt request channel (IRQ) on the OBC[14].

The OBC board selected for flight originally had only two interrupt lines available for the OLD board interface. It was then found that the third interrupt line could be activated as well, as long as sufficient power was supplied. The RS422 receiver chip interfacing between OLD and OBC could however not supply sufficient power. Therefore, an additional transistor was added to boost the output signal from the RS422 chip. It was decided to

[14]A general problem with the selected OBC board (SECO M543) has been that in the incoming unit tests, both for the flight model and several engineering models, some of the digital I/O and IRQs (not always the same) have been found non-functional. Whether this problem has been caused at the manufacturer, at the supplier or during the incoming inspection is not clear. A critical review of all boards and procedures involved has identified flaws originating at each of the three locations [Kruijff 2009.II].

connect the transistor to the same 1.5 W power supply as the RS422 chip itself rather than the main 30 W converter. This was a mistake.

A review of preflight power and voltage measurements has been done, which reveals that the patch-transistor has been overloading the small 1.5 W DC/DC converter to the edge of its range. At this loading, even a small increase of power demand leads to a steep drop in DC/DC supply voltage (Figure 271).

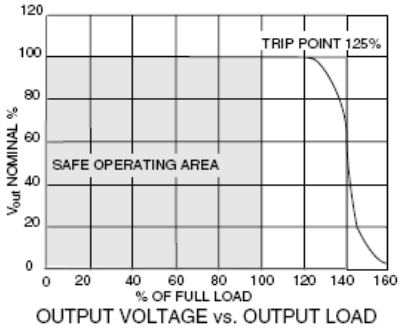

Figure 271: *From MCH2805S datasheet (5V_PDU). Maximum is 1.5W.*

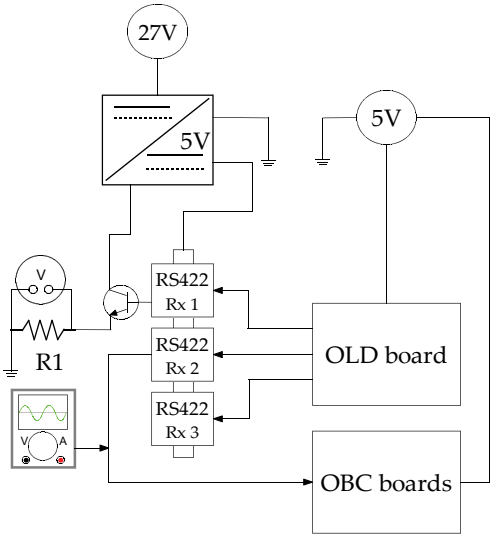

Figure 272. *Test set-up for recreation of flight condition*

Tests indicate however it is unlikely that a large enough voltage drop has occurred to disable the relevant equipment. The RS422 chips remain functional down to as low as 1.3 V, although their output drops with the input. If those output levels drop below a critical voltage level of approximately 2.5 V, no more interrupt signals are registered by the OBC. In the tests, no increased power consumption is observed for high loop rate, long duration or

excessive heating of the transistor. Also intermittent thermal shut-off of the PIC controller on the OBC has been found an unlikely failure mechanism.

Interestingly, close scrutiny of pre-flight deployment tests, after the installation of the patch show evidence that the gap problem already occurred several times, again on all three channels simultaneously, albeit briefly and for a small fraction of time (3%).

Interestingly, when an engineering model of the DC/DC converter unit is included in the rebuilt circuitry, and the power dissipation is tuned to match the pre-flight consumption level, similar signal voltage levels are obtained as measured for the flight model after patch installation (4.7 V for channels 2 and 3, and 4.0 V for channel 1). Rather than requiring a voltage drop down to 2.5 V before loss of interrupts, a remarkable effect is noticed when the voltage is dropped by as little as 0.1 V. By this minute increase in power dissipation, or even a small decrease in sensitivity of the PIC, as is commonly seen with temperature increase, noise on the overloaded DC/DC converter suddenly triggers the interrupt signals on the OBC, on all channels and at a very high frequency of about 10 kHz.

The software responds promptly to this noise. The OLD noise filter (Section 5.5.3, Table 48) is triggered on all channels. Not only the noise, but also proper interrupts indicating tether passage are then filtered out, more and more as sensitivity of the PIC or power consumption increases due to the increase in temperature. This observation seems to provide an adequate and consistent explanation of what has occurred during the YES2 flight, leading to underestimation of the deployment velocity and its consequences on the control.

8.5.2 Comparison YES2 to SEDS mission data and analysis

The SEDS-1 and SEDS-2 missions in respectively 1993 and 1994 have inspired the conceptual design choices for YES2. Furthermore, YES2 mission objectives have been defined as an incremental development of the SEDS missions. The main mission features are compared in Table 74.

The SEDS missions both featured a full tether deployment targeting to unwind all loops to reach a total length of 20 km. Whereas the SEDS-1 mission was an open loop deployment to a large angle, the SEDS-2 tether featured a closed loop deployment to the vertical at full length. To avoid control risks in the critical early phase of deployment, SEDS-2 had no braking in the first 750 s altogether. Stabilization was obtained to within 5 degees.

YES2 targeted a combination of two closed loop deployments, first to a vertical at only 3.4 km, and a subsequent large-angle deployment. YES2 has aimed to reach a smooth deployment stop at 30 km, with 1.7 km additionally wound on the spool as control margin. Considering the small endmass (albeit with virtually identical ejection energy, see Section 4.2.1) and first stage length, the YES2 first-stage libration amplitude of 10 degrees can be considered a control success. In the mission YES2 features velocities higher than SEDS-1, mainly because the final part of YES2 deployment is uncontrolled, leading to the 31.7 km full tether length.

The main length and velocity data is obtained in both missions through Optical Loop Detectors. The SEDS tensiometer was positioned at the tether exit, resulting in rather noisy

measurements. For this reason, the YES2 tensiometer is positioned at the MASS endmass, resulting in clean measurements. However, data has only been collected from the MASS shortly after ejection. High quality data on the tension has nevertheless been derived from the DIMAC three-axis accelerometer positioned close to the YES2 deployer. These measurements allow also for an observation of the tether exit angle from the deployer. In-plane angle data has been determined by combination with magnetometer data. This concept has proven to be an excellent principle for deployment observation.

The SEDS subsatellite provided endmass dynamics data throughout the mission which has been extensively analyzed [Stadler 1995]. Understanding of endmass dynamics is important also for YES2, in order to avoid tether wrapping around the Fotino release mechanism and to understand initial conditions of Fotino's re-entry. Irregularities in the first tens of seconds of YES2 deployment may be attributed to endmass dynamics. In this range the arm from tether attachment point to the MASS/Fotino center of mass is still significant with respect to the tether length. Because these endmass modes are not dampened naturally, on SEDS a heatshrink tube was added around the tether fixture. In order to limit endmass oscillations, it is important to avoid tether slackness during deployment, and include a damping mechanism as was done on SEDS.

During the SEDS missions, deployment velocity was noisy from time of ejection until it rose above about 5 m/s, with an amplitude of about 30% at 10 s averaged data [Bortolami 1993]. Explanations offered are stick-slip due to the tether surface finish and scrubbing of the tether on the core flange due to low centrifugal forces at low velocity [Carroll 1995.I]. Glaese relates stick-slip effects to sound waves [Glaese 1993]. Particularly when the brake is active and tension is high, this stick-slip is thought by the SEDS team to excite endmass and transverse tether modes.

To some extent similar behavior was observed in YES2. However, YES2 deployment velocity has been rather smooth from a minute into deployment until the large braking caused oscillations at 2200 s. These oscillations seem to be related to the controller resonance with the velocity in conjunction with transverse waves, rather than to stick-slip or sound waves. MTBSim has instantaneous tension distribution, it does not simulate the speed of sound, but the oscillations as seen in YES2 after 2200 s can be made visible, even when no endmass dynamics are simulated.

For SEDS no such resonance has occurred until the final stages of deployment. The SEDS control interval was purposefully selected much longer than that of YES2 and a low-pass filter was applied as low as 0.02 Hz, as noisy OLD output was expected in advance [Bortolami 1993]. Bortolami attributes the noisy behavior similar to stick-slip, near the end of the SEDS deployment, to spring-mass dynamics arising under increase of tension at low velocity due to scrubbing.

As far as matching of the deployment is concerned, the match achieved for YES2 appears to be rather exact and no particular problems have arisen to achieve this match. For YES2 a very precise match is obtained with a simple model, with the minimum deployment tension lightly dependent on velocity. Also the complex bounce is reproduced to such an extent that

tether properties could be well derived. The bounce tension development is similar to that seen in SEDS-1. In 1993, model and processing power limitations precluded a proper match of SEDS flight to simulator results [Glaese 1993]. Glaese explains that in SEDS-1, a nearly constant deceleration was observed that could not be well explained and a complex tension dependency was expected. Bortolami e.a. state further that, although an impressive qualitive comparison can be made if noise models are used, the tension model is too simple for a good fit [Bortolami 1993].

The minimal deployment tension according to Carroll results from stickiness and stiffness [Carroll 1995.I]. It has been displaying surprising values in both SEDS and YES2 missions. Similar to YES2, tether stickiness or minimal deployment tension for SEDS-1 was significantly higher than expected. In contrast, the SEDS-2 mission showed a significantly lower level than nominal [Bortolami 1993]. The SEDS team related the difference to manufacturer [Lorenzini 1995] and suggests a relationship between low temperature and high stickiness due to (about 1% water soluble) surface finish on the fibers (in equivalence with the known effect of braiding oils) [Wallace 1995, Carroll 1995.I]. Early SEDS tests [Carroll 1987] suggest that vacuum deployment testing produces large qualitative differences in deployment. Deployment testing at MSFC in representative thermal vacuum in fact produced estimates of the stickiness level matching SEDS-2 flight results [Lorenzini 1995, Wallace 1995].

Indeed, preflight testing in YES2 (Section 5.2.4) has identified great differences between tethers undergoing different heat treatments, and for this reason several tethers have been rejected (*Erik*, *Ferdi*). Post-flight research on the YES2 tether material shows that the anti-static surface finish applied by the Dyneema® fiber manufacturer is likely affected by thermal prestretch (in the braiding process), thermal history and vacuum exposure and could be to blame for the differences between individual tethers (e.g. tethers *Erik* and *Florian*) and flight versus ground testing [Kruijff 2009.III]. Such finish is necessary to avoid excessive spreading of the fibers during the braiding process.

For the case of the YES2 flight tether the surface finish or vacuum condition only seems to have played a secondary role. Atmospheric drag effects may contribute to a difference in deployment behavior, although helium tests performed in the context of YES have shown no significant impact of air density (Section 5.3.8). At low velocity, where stickiness is dominant, such influence should also be small. Instead, post-flight testing points mostly to a settling of the tether due to thermal cycling, amplifying the cyclic tension peaks inherent to the criss-cross winding (Section 8.5.1). As described in Section 8.5.1, simple ground tests may provide sufficient pre-flight information at least for the YES2 case. Due to budget constraints, deployment tests in a representative thermal vacuum could not be performed for YES2, but considering the rather large effects observed for relatively small environmental changes (such as a temperature reduction from 20°C to 0°C) it is nevertheless advised for future missions.

	SEDS-1	SEDS-2	YES2 stage 1	YES2 stage 2
Year	1993	1994	2007	
Tether diameter [mm]	0.75	0.75	0.5	
Tether linear density [kg/m]	0.33	0.33	0.18	
Endmass [kg]	26	26	14	
Ejection velocity [m/s]	1.64	1.6	2.2	
Control	Open loop	Closed loop	Closed loop	Closed(/open) loop
Control input	-	Optical count of unwound loops, 2 sensors	Optical count of unwound loops, 3 sensors	
Control output	Tether wraps around capstan	Tether wraps around capstan	Tether wraps around capstan	
Control interval [s]	-	8	2	
Length target/obtained [km]	20/20	19.75/19.78	3.38/3.39	30.1/31.7
Final velocity target/obtained [m/s]	0/7	0/0.02	0/0.00	0/15
Angle target/obtained [°]	-/53	0/4	0/10	40/45
Minimum tension expected/observed [N]	0.01/0.035	0.03/0.015	0.008/0.03	
Maximum tension [N]	7	2.5	1	40
Maximum velocity [m/s]	10.6/12.8	5.6/5.9	2.2/2.2	13/16
Length/velocity data	YES	YES	YES	YES
In-plane angle data	NO	Ground radar data points	YES	YES
Tension data	At tether exit and endmass	At tether exit and endmass	At endmass, deployer acceleration	Deployer acceleration
Endmass dynamics	YES	YES	Partial	NO

Table 74. *Comparison SEDS missions vs. the two YES2 deployment stages*

8.5.3 Simulator applicability and representation of flight performance by tests

Simulation vs. flight

It has been demonstrated so far that YES2 flight tether dynamics can be matched by MTBSim simulation qualitatively and, with limited additional tuning effort, also quantitatively to a high degree of similarity. Various complex behaviors such as oscillations, waves and control resonances have been reproduced by the simulator. The predictive value of the simulations with regards to these behaviors should be regarded as qualitative. It can

be considered adequate for mission planning purposes and selection of parameter values if a 20% margin is included and a sensitivity analysis is performed within the appropriate range of the various parameters.

Little can be said about the simulation of tether viscosity, since the value determined from flight data matching does not coincide with the value determined from simple ground tests. Note also that internal (Coulomb) damping has been found to be pronounced in flight [Barnds 1998], but is not included in MTBSim.

For the 31.7 km YES2 tether, no detrimental impact has been identified for the lack of sound wave propagation in MTBSim. If a shock occurs in which sound wave effects are significant, it will usually be a contingency situation. No important impact of sound waves or stick-slip processes on deployment dynamics has been recognized.

The irregularity of the deployment could be partially represented, in particular oscillations resulting from tether waves and the controller resonance with deployment velocity. It has been necessary to integrate the controller details into the simulator. The irregularity observed during the first hundred meters of deployment has not been recreated. It is therefore recommended to include endmass angular dynamics effects on the tether tension. The deployment tension model can be extended to include known cyclic effects due to criss-cross and parallel winding, as well as tether rubbing against the core at low velocity and the canister at high velocity.

Test vs. flight

Open and closed loop deployment testing for YES2 has provided results consistent with simulations (Chapter 5) and therefore has proved to be useful yet suffering from some of the same pitfalls. They have been adequate for characterization and verification of the overall hardware and controller performance. A stage transition like the transition from hold phase to second stage start is realistically reproduced. With calibration of the tether length sensors in both the winding and unwinding systems, it could eventually be established that a 0.1% deployed length determination accuracy is possible with the OLD system, determined from the congruence between the lengths measured by OLD and test rig. The attainable control accuracy both in test and in Monte Carlo simulation is better than 1%, where 3% is considered acceptable. YES2 mission analysis has shown that with the YES2 flight system as operated in space a length measurement accuracy of about 0.3% is obtained, whereas a control accuracy of 0.6% could be achieved.

However, the ground preparation activities have not alerted the team in advance for the irregularities observed in flight, specifically in early deployment, nor to the high value of T_0. It is necessary for now to treat such irregularities as a given and provide algorithmic robustness.

The system test should be as representative to the flight as possible. This seems trivial, but when test costs and demands on the timeline are traded-off against potential gains, compromises are easily made. For YES2, despite a large number of partial deployment tests with the flight hardware subsystems, full closed-loop deployment tests have been

performed only on the engineering model, with an external power supply and at room temperature. The full extent of the issue with the OLD patch has only been recognized post-flight, but would have surfaced in a test in a fully flight representative situation, including thermal vacuum. A similar conclusion holds for the tether stickiness on the spool, T_0, which during the YES2 mission was significantly higher than expected. Again, despite a large number of ground tests, including thermal cycling, due to time constraints the flight tether itself has only been deployed in ambient conditions, without the necessary *a priori* thermal cycling exposure (Section 8.5.1).

The hardware emulator

The hardware emulator has proven particularly helpful to test the deployer system's electrical and algorithmic performance without deploying an actual tether (Sections 5.2.3, 8.1). For this system, as used for YES2, one of the main limitations has turned out to be the level of realism of the OLD pulses. The pulses come quite regularly, giving the OBC velocity filter a rather straight-forward job. The limitation can be overcome by introducing artificial noise in the simulated pattern. The possibility to introduce such noise makes the emulator test set-up probably more suitable to test e.g. the dynamic interaction between endmass oscillations and tether deployment velocity than the actual hardware-in-the-loop closed-loop deployment test.

8.5.4 Fotino and the SpaceMail potential

There is no confirmation yet that Fotino has been delivered to the ground as intended and its integrity and exact whereabouts are unknown (Figure 273).

In an effort to determine the likely position of Fotino, a first uncertainty to be dealt with is the exact timing of its release from MASS and the tether. Although there is direct evidence for the tether release from Foton, it proves much more difficult to determine whether Fotino has released successfully from MASS at the nominal time. For this to happen, the tether should not be wrapped around the Fotino/MASS endmass. In other words, the endmass should have remained relatively stable at the end of the tether despite the stick-slip behavior, slackness and multiple shocks that the system experienced. The mission design includes an interval of 20 s between Fotino release and tether cut to allow for confirmation of release by GPS or tension measurements, but this interval has proven hardly sufficient due to the highly dynamic circumstances after the endshock. No steady-state measurements could be made (Figure 255).

There are some indications that Fotino might have released successfully however, albeit circumstantial at best:

- The tension drops deeply in the 20 s after the release of Fotino, similarly to deployment matching simulations that include a nominal Fotino release. The deployment matching simulations for the case of release failure show mostly a rise of tension (sometimes preceded by a small drop). However the particular deployment simulation that features the best-fit bouncing pattern to the flight data provides no clear insight (Figure 264).

- Simulation of endmass dynamics based on the measured tension profile and the initial angular dynamics (Section 8.3.3) shows that MASS/Fotino did not significantly tumble at the end of the tether, but remained largely stabilized by the tether force.
- DIMAC tension data (Figure 255) shows that the timing of the actual release was coincidentally optimal, at the peak of tension - tending to separate Fotino from MASS - at a level better than nominal, comparable to the best cases tested in parabolic flight [YES2 2006] .
- Detailed analysis of the end-shock tension pulse shows that as the shock of the halted tether reaches MASS/Fotino, a clear and brief drop in tension can be distinguished, compatible with a braking and unfolding of the 15 m ripstitch tether part. As this ripstitch part is included in the tether (for shock damping) at only 9 meters from the MASS/Fotino, the system could not be heavily wrapped at this time (Figure 265).

If release at the nominal time has failed, Fotino and MASS have entered the atmosphere together, and release has occurred at about 110 km altitude due to melting of any entangled tether as well as the small Kevlar cable restraining Fotino to MASS. Although the tether in such a case provides some initial stabilization [Kruijff 2003.I], the landing zone for this case is widely spread out due to the large amount of unknowns, covering most of the Foton-M3 ground track throughout the Kazakh/Russian landing zone, or a total area the size of The Netherlands. Also for this case the survivability probability of Fotino may be reduced due to possible violent interaction with the MASS structure.

If release has been nominal or close to nominal, a much better estimate can be made of Fotino's whereabouts using MTBSim. The atmospheric conditions were close to average on the 25th of September 2007. The Foton-M3 has landed the next day within 5% of its 3σ landing dispersion range. Note that the Fotino atmospheric dispersion estimator uses the same models as the Foton-M3 and its trajectory calculation and dispersion estimation has been verified against that of Foton-M3 [Stelzer 2006, TsSKB 2006]. The deployment match simulation #2 with nominal Fotino release (Section 8.4.1) has been used to determine the most likely actual landing site of Fotino. An error ellipse around this has been determined based on the error sources listed in Table 75. Most effects translate into several tens of kilometers in landing site dispersion.

The simulations show that re-entry conditions for Fotino would have just fallen within the nominal windows for entry angle, heat flux and angular rate. The increase in entry angle from 1.4° nominal to 1.5° actual results in about a 4-10% heatflux increase. Plasma chamber qualification level was 7-15% above nominal [Asma 2008].

For simulation of Fotino angular rates, the initial conditions have been taken from the MASS sensors (Section 8.3.2) and propagated by MTBSim using simulated tether tension. With the worst case initial angular rate of 30°/s as occurring around the time of release (Figure 275), response to the aerodynamic torques during re-entry has been calculated by YESSim. A

perfectly spherical capsule should have sufficiently stabilized at about 50° maximum angle attack to allow the peak heat flux to strike primarily the more heavily protected front of the capsule (Figure 276). The more sensitive capsule sides would however be significantly exposed as well. Note that more advanced simulations performed by Samara State Aerospace University, including (realistic) capsule asymmetries of 1 cm indicate that Fotino most likely has been tumbling during the peak heat flux. In such a tumble, the thinner back-side heat shield or the glue layer on the equator may have been exposed to the full heat flux [De Pascale 2006]. On the other hand, the heat may have been distributed over a greater surface [Kruijff 2003.II].

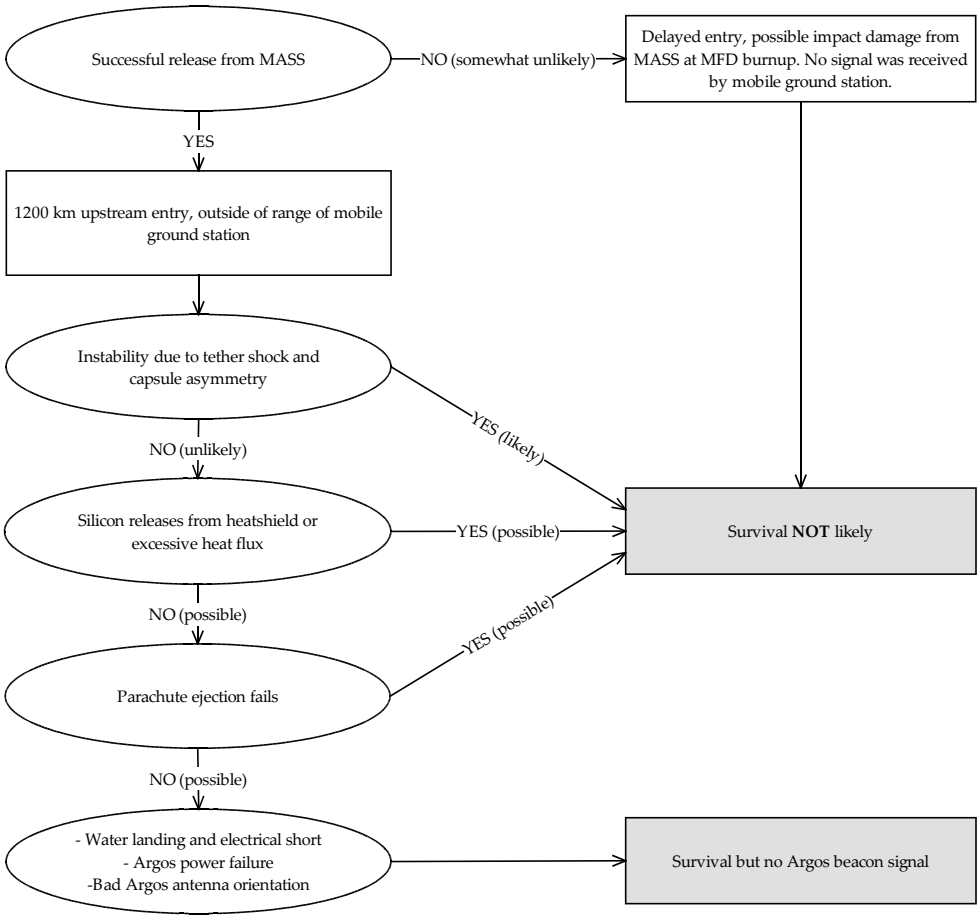

Figure 273. *Fate of Fotino*

Disturbed parameter	Comment
Actually achieved deployment profile	A variety of deployment profiles is selected to represent extreme cases (i.e. barely matching the data), and including release at different phases in the transverse wave oscillation.
Deployment completion time	A 3 s variation is used to take into account the speed of sound effect.
Fotino release timing	Max. 10 s delay in release is assumed, e.g. due to unwrapping from tether or orientation from Fotino.
Foton attitude control system	Simulated Foton attitude control (along the established control laws) is switched on and off to obtain maximum error contribution.
Atmospheric drag in orbit	Effect of about 1 degree on in-plane angle is conservatively taken into account as full uncertainty
Foton-M3 orbital parameters	Uncertainty in reconstructed parameters as provided by TsSKB and USSTRATCOM.
Tether dynamic model	Error estimated by comparison between various model results, number of beads etc.
Tether properties	Possible extremes of stiffness and damping.
Capsule properties	Capsule mass (uncertain ablation of heatshield), drag coefficient, possible lift due to asymmetries.
Atmospheric landing area	A 150x20 km uncertainty due to atmospheric density/horizontal wind uncertainty during entry, as determined by Monte Carlo runs using 1σ errors on the environmental model wind predictions and 1.5σ errors on density.

Table 75. *Disturbed parameters resulting in error estimate for Fotino landing site estimation*

Figure 274 shows the resulting reconstructed landing area, about 1250 km upstream of the nominal landing point. The area dimensions are 250x30 km. The area appears wild and uninhabited, in the border region of Kazakhstan, Uzbekistan and Turkmenistan, and covered with salty canyons, dry riverbeds, wet and dry lakes. Note that a wet landing would explain why no Argos beacon signal has been obtained from Fotino (Section 7.4.5). Fotino floats but the electronics are not water resistant. Alternative reasons could be a failure in heatshield, parachute or beacon (Figure 273).

Hypothetical landing site

Although the exact location of Fotino cannot be determined with certainty, the YES2 deployment is sufficiently understood such that credible extrapolations can be made to assess the hypothetical performance of the YES2 mission and answer the enthralling “what if” question. This simulation may serve as a confirmation of the sufficiently successful YES2 tether deployer hardware performance.

The simulation match versus flight data indicates that the Fotino trajectory insertion error can be attributed almost fully to the interface electronics power failure occurring around t_{eject}+6260 s. When the deployment matching simulation is performed with the same deployer hardware modeling yet without the artificial introduction of the electrical failure at t_{eject}+6260, deployment recovers smoothly from the troubled first stage and landing would still be within the nominal landing ellipse, about 150 km downstream from the nominal landing site (Figure 261, Figure 277). Strikingly (but coincidentally), this location happens to be only about 10 km from the position of the (inofficial) recovery team.

The filter resonance that has created the velocity oscillations in the first stage has a noticeable impact on the landing site. In Figure 277 is also visible the extrapolated landing site if the filter resonance problem would have been resolved as well. This site happens to nearly coincide with the nominal landing point. This result puts a number on the benefit of avoiding transverse wave excitation.

8.5.5 Lessons learned

The problems identified during YES2 are listed with their proposed, often straightforward, solutions in Table 76 and Table 78. Tension levels in the first stage deviated from ground test values. A hypothesis has been defined but needs further testing. Software/controller parameter issues led to over-braking in the first tens of seconds and unwanted resonance between controller and deployment velocity. Various simple solutions to these problems have been identified. Also, stability of the endmass at the end of the tether must be looked into carefully in the planning-stages.

Figure 274. *Reconstructed Fotino landing area. The ellipse is 250 km long.*

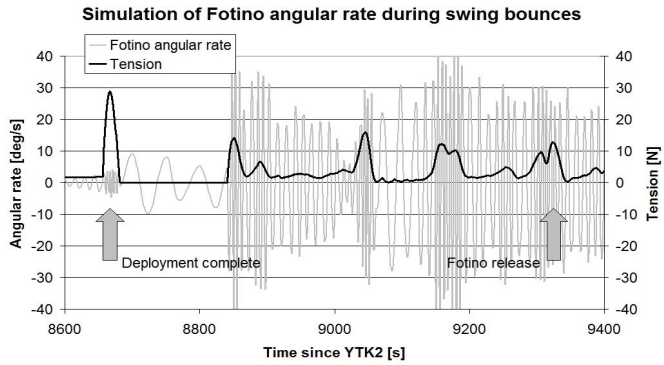

Figure 275. *Fotino angular rate simulation during swing bounce*

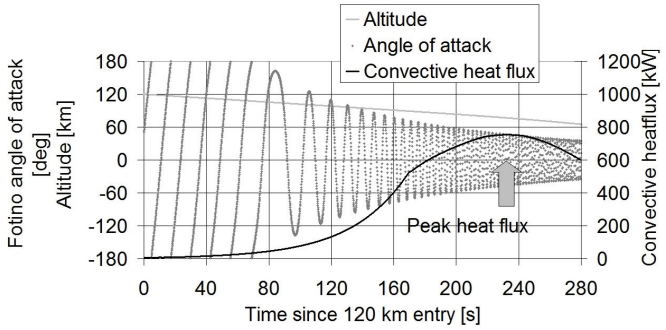

Figure 276. *Fotino simulated entry conditions*

Figure 277. *Nominal landing area including, the hypothetical landing site of Fotino resulting from extrapolation of mission data assuming no electrical failure at t = 6260 s. The ellipse is 380 km long.*

Programmatic issue	Cause	Suggested approach
Changing requirements	Change of ESA responsibles during project.	Start only after clear and full definition (this may not be sufficient). Reduce project duration by sufficient initial funding.
Lack of/staged funding	Insufficient broad support at start of project.	Start only once full funding is secured. This will however make the project more unlikely to start.
Missing internal deadlines	Insufficient know-how initially available in the team.	Involve senior experts from the early stages.

Table 76. *Analysis of programmatic issues occurring during YES2 and proposed approach*

Data sources	Description	Attainable accuracy
	Deployer performance	
DIMAC	Derived tension	10–25%
OLD plus DIMAC	Deployment reconstruction	10–25%
OLD plus DIMAC plus MTBSim Simulator	Deployment matching	10–25%
MASS tensiometer	Brake friction coefficient	~15%
	Tether properties	
DIMAC	Derived tension	——

Table 77. Data sources used: deployer and tether properties

Technical Problem	**Cause**	**Further work/Solution**
Tether more sticky than expected, makes it more difficult to control the deployment in the first stage.	Possibly due to 11 days of tether in thermal vacuum of space before deployment.	Confirm hypothesis by test with remaining flight tether. Future approach: test tether before and after full-scale exposure to representative environment. Preferably also during (though costly).
Velocity filter overestimates the velocity in the first minute after ejection, leading the controller to command additional braking, which leads to a decrease of velocity.	Software filter parameter not properly adjusted to real-flight condition.	- Remove the particular filter feature (it concerns a feature to cover for the unlikely double-channel OLD failure case), or - adjust parameter based on YES2 mission data.
Software controller responds poorly to first transverse wave and amplifies the waves by resonance. Effect decreases landing accuracy potential (by about 150 km).	Software velocity filter has a delay due to averaging and low-pass filtering, which can lead (in particular circumstances) to resonance between velocity and brake control.	- Increase stepper motor speed by a factor two, - decrease friction coefficient of brake pole (now it is sandblasted for higher friction), - decrease tether stickiness (see above), - improve low-pass filter, - improve feedback gains, - perform a sensitivity analysis to demonstrate controller robustness.
Electrical failure in OLD-OBC interface, leasd to open-loop control at end of second stage and bouncing of endmass on tether after completion, 1250 km landing error.	Failure on Central Processing Unit (CPU) board at the location of the OLD1 signal input (IRQ). The failure occurred before delivery of YES2 and was patched, but could not be sufficiently tested anymore. It was the patch that turned out faulty during flight.	Confirm hypothesis by further OLD data analysis. Investigation of the CPU board failure, possibly selection of a more robust CPU board.
Failure to receive signal from Fotino.	Possibly failure to release properly from MASS (due to possible endmass rotation), heatshield failure or beacon failure.	Improve endmass simulation (include effect of endmass attitude on tension in early deployment), perform a sensitivity analysis to demonstrate robustness with respect to control. Include (passive) oscillation damping in endmass. Confirm release: telemetry, simpler capsule (no heatshield sensors, focus on redundant beacon with robust monopole antenna's). Avoid tether entanglement by center of mass position. More robust heatshield.

Table 78. *Analysis of technical problems occurring during YES2 and proposed solutions*

Table 79. *Overview of mission parameters and results; Data sources used I - ejection and end mass dynamics*

Mission parameter	Nominal value	Acceptable range	Result
Ejection speed	2.2 m/s after tie-downs	1.2–3 m/s	Nominal: 2.2 m/s after tie-downs
Subsatellite initial dynamics around center of mass	10 deg /s initially	——	Nominal: 1.55 deg /s initially
Subsatellite continued dynamics around center of mass	Max 90 deg amplitude oscillation	Max 90 deg amplitude oscillation	Offnominal: subsatellite appears to be tumbling as a result of slackness
Deployment speed $t < 6260$ s	0–6 m/s	——	Acceptable: initially too much braking, due to temporary bad filtering
First-stage length profile	——	——	Nominal
First-stage length	3390 m	3100–3700 m	Nominal: 3380 m
Deployment speed 6260–8626 s	5–13 m/s	——	Offnominal: 5–16 m/s, due to OLD registration failure
Second-stage length profile	30,000 m	29,000–31,000 m	Offnominal: 31,700 m, due to OLD registration failure
In-plane angle	0–50 deg	——	Acceptable
Out-of-plane angle	0 deg	5 deg	Nominal: 0 deg
Fotino release	Release at $t = 9364$ s, 6 deg before vertical, entry angle 1.4 deg	20 s release error, 0.2 deg entry angle error	Acceptable: release $t = 9364$ s, entry angle 1.5 deg
Fotino landing site	Near Tasty Taldy, 66.3E 50.6N, Kazakhstan	200 km error	Offnominal: ~1250 km upstream, approx 55.7E 41.6N
Deployer performance	See Section 8.1.1	About a factor 3, and 50% on friction	Nominal: friction (10–15%), dynamic effect (15%); acceptable: stickiness (factor 2.7–4)
Tether properties	$EA = 5000$, $a = 10$ km/s, $\zeta = 0.08$	About a factor 3	Nominal: $EA = 5000$–$10,000$ N $a = 8.8$ km/s, $\zeta = 0.14$–0.16

Data sources	Description	Attainable accuracy
	Ejection speed	
OLD	Initial OLD rate	0.1 m/s
MASS tensiometer plus OLD	Integration of acceleration derived from MASS tensiometer, fit to OLD rate development	0.1 m/s
DIMAC plus OLD	Integration of DIMAC accelerations, fit to OLD rate development	0.1 m/s
	Subsatellite initial dynamics around center of mass	
MASS gyroscope	Direct measurement (1 axis)	0.2 deg /s
	Subsatellite continued dynamics around center of mass	
MASS magnetometers	3-axis derivatives	1 deg /s
MTBSim Simulator + DIMAC	Simulation using tension data fit to initial MASS data	——

Table 80. Data sources used: deployment length and velocity; Data sources used: deployment angle and capsule trajectory

Data sources	Description	Attainable accuracy
	Deployment speed $t < 6260$ s	
OLD	Rate data	~0.05 cm/s
DIMAC (plus OLD)	Confirmation by comparison of DIMAC derived tension to OLD reconstructed tension [Eq. 2.16]	1%
	First-stage length profile	
OLD	Loop count	20 m
	First-stage length	
OLD (plus statistical analysis)	Loop count, time interval/statistical analysis to estimate error	20 m
DIMAC	Gravity-gradient tension from DIMAC for hanging tether	~100 m
	Deployment speed 6260–8626 s	
DIMAC	Spectrograph rate profile	0.2–0.7 m/s
OLD	Rate data (interpolated over last 400 s)	1 m/s
	Second-stage length profile	
DIMAC	Integration of spectrograph rate profile	100 m
DIMAC	3 transition points in winding turns per cycle setting from spectrograph, end of deployment from tension spike	100 m
OLD	Reconstruction using rate data	~200 m

Data sources	Description	Attainable accuracy
	In-plane angle	
OLD (plusDIMAC, MTBSim)	Reconstruction using rate data with Eq. (2) or MTBSim. Better if amended with DIMAC spectrograph rate data.	2 deg
DIMAC	From ratio of x-axis and y-axis measurements combined with Foton orientation from magnetometer and horizon sensor.	5 deg
GPS	Determine vector to system center of mass. Not performed yet.	~1–5 deg (estimate)
	Out-of-plane angle	
DIMAC	z-axis acceleration	~1 deg
	Fotino release	
OLD plus DIMAC plus MTBSim simulator	Continuation of dynamics after deployment completion by simulation. Measured tension drop at tether cut.	1%
NORAD ground-based radar	NORAD measurement of Foton orbit after release evidencing momentum transfer.	6%
	Fotino landing site	
Fotino Beacon	Argos Beacon signal (failed)	350 m
OLD plus DIMAC plus MTBSim simulator	Simulation based on match of DIMAC tension profile during swing.	125 km

9 Discussion

Despite the promise of space tethers for essentially propellantless, sustainable space transportation, it has proven difficult to move beyond theory towards a first tether application, or even -after some (partial) in-orbit failures in the 1990s- to move towards a further concept demonstration.

In order to understand the programmatic and technical challenges currently faced by tether initiatives and to respond to them where possible, in this work, a broad approach of analyses and developments has been implemented. The MTBSim/ETBSim tool has been developed and used to analyze a range of candidates for tether applications, selected primarily for a perceived near-term suitability, i.e. based on a anticipated potential for system simplicity and mission safety. Focusing on the SpaceMail application, a safe tether and tether deployment system has been developed and evaluated with the help of a winding facility and unwinding test rig. Two flight systems, the Young Engineers' Satellites YES and YES2, have been developed and launched into Earth orbit, through involvement of a large number of highly motivated students and young engineers. The YES2 resulted in an in-orbit demonstration of a two-stage tether deployment and momentum transfer.

A review of this effort may shed some light on the questions posed and provide recommendations towards the development of further in-orbit demonstrations and applications. This discussion is organized according to four major insights obtained:

1. Tether applications face a rather particular developmental challenge.
2. In the near-term the use of tethers is limited to niche applications.
3. Tether applications can be sufficiently predictable and safe.
4. Tether applications can be affordable but further development may depend on an educational context.

1. Tether applications face a rather particular developmental challenge.

Due to their nature, space tether systems are not very suitable for on-ground validation, as compared to other systems whose performance may be sufficiently demonstrated in vacuum chambers or in parabolic flights. Any development of a new system requires a cycle of testing, failing and learning. The problem for tether systems is that much of this cycle typically takes place in orbit. Tethers seem simply too long and too non-linear in behavior to fully explore on-ground. Their dynamics depend on very low force levels that are difficult to replicate reliably over the full tether length of multiple kilometers, if not in orbit. Historical failures of in-orbit tether system tests are easily misjudged when compared to alternative solutions that have been exposed to ample ground testing before they have been brought to operate in orbit.

The cost of in-orbit demonstration is still a limiting factor for tether systems. One particular aspect that drives up the minimal system mass or its complexity, and that thus drives up the minimal demonstration cost, is the need to achieve sufficient initial vertical separation of tether endmasses. This separation is required such that gravity gradient forces can further drive deployment. Actively driven reel systems and cold gas systems can provide the required separation but increase complexity compared to a spring based separation system. Spring based separation systems rely on provision of sufficient initial kinetic energy and momentum to overcome the dissipative effect of deployment friction. At the same ejection energy, a larger endmass offers a more robust deployment. Note that the deployment friction also has advantages. It creates tension in the tether that keeps the tether taught and can be utilized to control deployment and stabilize the endmass attitude. It is for this reason that, although frictionless solutions for tether deployment may be devised, they have not been explored within this work. For the spool-type deployer and a 0.5-mm Dyneema tether as evaluated here, about 12 kg is required as a minimum endmass to secure successful deployment. Such constraints put a significant price tag on any tether system in-orbit test cycle.

In-orbit testing can be reduced if confidence is increased in the applicability of computer simulations. MTBSim/ETBSim has also been developed for this reason. Increase in simulator confidence for mechanical tether dynamics has been one objective of the YES2 mission analysis. In addition, it is recommended that future tether missions should continue to collect extensive data, through differential GNSS, ground observations and/or sensitive three-axis accelerometers to fill in the gaps left after the YES2 mission. These gaps are in particular related to stick-slip behavior during deployment of the tether from the spool, interaction between endmass oscillation and tension, as well as resonance between control and deployment. The DIMAC three-axis accelerometer data has proven to be invaluable for YES2 providing information on in-plane dynamics, tether transverse waves, longitudinal waves, spring-mass behavior, damping coefficient, deployer platform attitude thruster operation and, through Fourier analysis, even deployment rate. Electrodynamic tether behavior is significantly more complex, and a thorough evaluation is advised of the measurements required to credibly validate simulators such as ETBSim against flight data.

Furthermore, a need has been identified for improved ground-based deployment testing. For this reason, a test facility has been developed that provides an unprecedented potential for on-ground evaluation of tether deployment. The unwinding test rig described in this work integrates a real-time version of the MTBSim simulator and can evaluate in closed-loop the performance of deployer hardware, software and controller algorithms, as well as interactions with in-orbit dynamics. The level of realism of ground testing with respect to tether dynamics is limited by that of the simulator. Nevertheless these tests provide as solid a confirmation of system performance as can be achieved on-ground. They help to appreciate the time-scale of unwinding, brake and control system dynamics. The closed-loop tests enable visual inspection of the interrelationships between unwinding tether, operation of the brake system and, dynamic behavior of the tether as it finds it way through the deployer. Anomalies can be identified this way that otherwise would escape the eye

and hypotheses are more readily generated. Thresholds and offsets in control software can be empirically evaluated and selected. Although a full deployment test typically requires about a week to set-up, execute and evaluate, such tests do not need to be performed often. It is found that full system simulation and emulator tests that use a subset of deployer hardware but no tether, can provide much of the required information. Closed-loop full deployment demonstration is particularly of interest for initial system evaluation and final confirmation.

2. In the near-term the use of tethers is limited to niche applications.

The tether applications that have been investigated in this work are considered near-term for several reasons. In case of the proposed MARS-g artificial gravity demonstrator, the tether system is particularly enabling. No major technical show-stoppers have been identified. Concerning the other, more modest applications, the required technologies build heavily on those of systems already developed so far, as well as on successful in-flight demonstrations. It is judged that application demonstrations can be readily performed within the context of low-cost experiments akin to YES, YES2 and T-REX. The investigated near-term applications can indeed provide benefits compared to conventional alternatives but are as yet limited in their potential, when considering risk mitigation, programmatic and technological aspects.

Any tether mission planned today should take into account the off-nominal case that the tether or part thereof will be, or may have to be, separated from its endmass(es). Such a disconnected tether may result in a significant probability of collision with active satellites; measures should thus be taken to limit criticality. The most secure measure is to limit orbital altitude of the tether in the first place and rely on mechanisms such as atmospheric drag, possibly in combination with solar pressure, and electrodynamic drag. For both mechanical and electrodynamic tethers, a rough recommended altitude regime has been provided in this work, as a function of inclination, to be verified by analysis on a case-by-case basis.

Those applications investigated that are based on expendable mechanical tethers take place within this safe altitude regime, e.g. sample return/deorbit from LEO (SpaceMail), launch assist (T-Series) and short-duration lower thermosphere investigation. They have been found technically feasible and competitive to conventional alternatives. It is then unfortunate that the current International Space Station (ISS) is neither set-up for, nor in need of, a frequent sample return, whereas the T-Series application is limited to a rather limited range of combinations of launcher, payload and target orbits. Isolated mission opportunities may well occur but their volume may not suffice to turn designers away from well-demonstrated existing solutions based on propellant expulsion.

End-of-life deorbit for satellites by a bare electrodynamic tether is another application with potential for mass and cost advantage over the retro-rocket alternative. However, the deorbit performance is limited by the need to avoid tether slackness as a result of dynamic instability. Care must furthermore be taken that the tether's own contribution to collision probability does not worsen, rather than improve, both the threat to and the (costly) need for collision avoidance by third party active satellites. For this reason it is recommended to

make a critical case-by-case analysis. It is also advised to use a bare tether, as it will experience a Lorentz drag force even when disconnected from a cathode, to apply ground control of the deorbit rate and to release the tether from the endmasses as soon as a 25-year lifetime orbit has been achieved.

For some applications there seems to exist no credible alternative to a tether solution. A concept has been proposed in this work to provide comfortable artificial gravity for research in Low Earth Orbit that seems rather attractive, from a point of view of its favorable mass and system simplicity. Further, particularly promising and enabling applications exist for electrodynamic tethers. A space station's orbit could be cost-effectively maintained, even at a lower, more accessible, altitude than the current ISS (with a METS-type system). To clear LEO from the large population of left-behind spent stages, tether systems such as EDDE seem to be the only candidate.

Again however, there are considerable obstacles. In the absence of solid funding for interplanetary manned missions, there is little urgency for a manned artificial gravity laboratory. Also tether systems for orbit maintenance such as the METS, developed for the MIR station, have no immediate application available. The current ISS is not as well configured as the MIR station for attachment of a tether system. More importantly, also for orbit maintenance purpose, the continued use of the Progress and Autonomous Transfer Vehicles is likely to be preferred. Finally there are technical limitations, even if not directly related to tethers. The implementation of any system for removal of existing orbital debris for example, be it tethered or untethered, is hampered by the lack of a proven and suitable grappling system for that debris.

On the positive side, the international call to take action towards the orbital debris issue is gaining in strength today. The cards are being laid favorably here for a tether solution. Another promising near-term application is lower thermospheric in-situ research. It is hard to imagine an affordable alternative to atmospheric drag compensation by electrodynamic tether. Such a low-orbiting system would be intrinsically safe and could be a good, useful case for a application demonstrator.

In time, the situation is likely to improve further as new, critical, technologies become available. Examples are tether materials that are (even) lighter and stronger or that are self-degradable, systems for reliable tether retrieval and for in-orbit grappling of debris or payloads, as well as solutions to improve long-duration stability for electrodynamic tethers.

3. Tether applications can be sufficiently predictable and safe.

The results of the work reported here increase confidence in tether deployer hardware reliability, performance and safe usage. Logically following the SEDS missions, and adding to those in terms of complexity and challenge, the YES2 mission and subsequent data analysis has demonstrated that tether dynamics can be sufficiently predicted and controlled to enable an application such as SpaceMail. It is a persistent, open and responsive attitude towards a broad community of critics, that has covered most if not all of the *a priori* expressed worries, and that has finally led to a go-ahead for the YES2's in-orbit tether

deployment. Driving elements during this approach have been a focus on mechanical simplicity and commonality, comprehensive analysis and testing as well as attention to safety.

A choice has been made for a passive spool deployer and barberpole brake concept, that has been developed for controlled deployment of a mechanical, expendable tether. Passive deployers have a near-perfect flight record. The barberpole system has a low number of guides and provides minimal disturbance to the tether.

Nevertheless, such design simplicity comes at the price of non-linearity and behavioral complexity. A stepwise characterization and testing approach has therefore been defined as part of the mission preparation. The deployment test rig, already described above, benefits from equipment and insights derived from textile industry technology. It is highly compact and mobile so can be used in parabolic flights or other specific test environments. It is possible to reuse the tether that is under test. Extensive system characterization tests could therefore be performed, including investigations into e.g. qualitative spool cyclic tension patterns, friction on the brake, environmental impacts and tether twist impact. Some effort was put into the development of quantitative models, but this work is not concluded and further work here is recommended.

Regarding safety, key attention points have been identified for design of mission, system and tether. Mission design should include a responsible orbit selection, and simple but adequate ground control and abort options. To increase the likelihood of successful and controlled deployment from a spool, a minimal initial ejection energy and endmass is prescribed. The YES2 system design provides both commanded and autonomous tether release. Its tether deployment scheme has been segmented into intervals of deployed length, and each interval has been characterized by its particular contingency case. For each of those contingencies, relevant safety measures have been implemented, be it in the system or in the tether, such as the Prusik slipknot, the ripstitch damping and the automated tether cut. It is noted that one of the main properties of the tether design, its diameter, cannot be selected based on fiber strength considerations alone but should consider factors such as braiding and clamping effects, meteoroid/debris resistance and thermal heat input during friction braking.

Tether deployer technology, mission preparation methodology developed within the scope of this work, as well as related tools such as the test facility and the MTBSim simulation tool, can be used with only small modifications for future tethered re-entry missions and several other early tether applications, including launch assist akin to the T-Series concept and lower thermospheric in-situ research.

4. Tether applications can be affordable but may further depend on educational context.

Educational projects severely limited in funding and with limited professional guidance, such as YES, YES2 and recently T-Rex, the latter outside the scope of this work, have succeeded in creating complete flight systems and led to successful demonstration of innovative and controlled in-orbit deployment of both a mechanical and a bare conductive

tape tether. Still, the production of tether-related hardware has not been the major cost driver in these projects. The YES tether system for example was purchased from a small US company at a fraction of the total project cost. The YES2 experiment, including the tether deployer system, was developed from scratch according to rather comprehensive design and traceability standards. Virtually no commercially available subsystems were utilized. On the contrary, the project included multiple technology developments in addition to the tether deployer such as an ejection system and a (more experimental) light-weight re-entry capsule. Also, the YES2 effort featured a significant educational effort. The total project cost is estimated to be only about 1.5 MEuro. It has helped that no complex orientation system was required for the endmass and no special measures regarding personnel safety were required, as may be expected for the development of more conventional rocket-propelled spacecraft. These facts are testimony of the limited cost, limited complexity, and ease of dealing with tether systems. It seems therefore a credible claim that a tether system provides a cost-competitive solution.

However, space business is not yet commercial and often driven largely by other interests rather than technical and cost arguments. Through the educational context it has nevertheless been possible to develop and demonstrate innovative technology. In the near future, progress in the field of tethers may remain dependent on educationally driven projects such as YES, YES2 and T-REX.

Notably, the educational approach is not necessarily low-cost and certainly not without its particular challenges. Close and intense guidance and a proper traceability system are required to safeguard quality. Still, securing handover and continuity requires notable effort. Lack of experience (and funding) is compensated by perseverance and enthusiasm of the whole team, which can only be maintained by the maintaining of clear goals and by a generous distribution of responsibility. In order to secure progress, educational considerations can neither be leading in decision making nor for task definition. Critical phases of the project such as concept definition and testing, as well as overall system engineering, should however be closely steered and monitored, or better, handled by professionals. Despite application of these lessons learned, under the particular constraints and dynamics of such projects, it has proven hard to avoid occurrence of any flaw, be it in the process or in the system. It is then an additional challenge that, due to the openness typical for educational activities, such flaws are easily magnified in public perception.

Despite these reservations, educational projects have enabled significant progress that, in the case of tethers, would otherwise simply not have been made.

Concluding remark

To some extent, the above discussion may somewhat moderate expectations of the rate of implementation and the scope of tether applications in the near future. It is hoped that the results achieved and methods explored by this work can take away key concerns and obstacles to further demonstration missions and to early tether applications - both of which are needed for the acceptance of tethers as a credible design option on the road towards sustainable space transportation, and they are possible today.

References

Aerospatiale (1986), Space Mail, study report, Col-TN-AS-0050.

Alenia Spazio (1994). TMM&M, final report for ESA/ESTEC, Noordwijk.

Alenia Spazio, RSC Energya (1995). TATS, ESA/ESTEC Contract 11439/95/NL.

Andreopoulos, A. G., Theophanides, T . (1994). Degradable Plastics: A Smart Approach to Various Applications. *Journal of Elastomers and Plastics* 26, (1994) 308.

Anselmo, L., Rossi, A., Pardini, C. (1999.I). Updated results on the long-term evolution of the space debris environment. *Advances in Space Research*, Vol. 23 No. 1., pp. 201-211.

Anz-Meador, P.D., (2001). Tether-Debris Interactions in Low Earth Orbit, Space Technology and Applications International Forum, AIP Conference Proceedings, Volume 552, pp. 525-531

APEX Programme Ariane 5 Steering Committee Decision (1997), YES Review on the Space Debris Aspect, Paris 11 June 1997.

Artsutanov, Y.N. (1960). *V Kosmos na Elektrovoze. Komsomolskaya Pravda.* (Into space with the help of an electric locomotive, contents described in Lvov 1967 *Science* 158:946)

Asma C., De Pascale F., Kruijff M. (2008). Heatshield Qualification for the SpaceMail Re- Entry Capsule "Fotino" in the VKI Plasmatron, AIAA-2008-6561.

Bade, A., Eichler, P. (1993). The improved TERESA-concept for the removal of large space debris objects. In *Proceedings of the 1st European Conference on Space Debris*, Darmstadt, Germany, ESA SD-01.

Barnds, J., e.a. (January 1998). TiPS: Results of a Tethered Satellite System. *Tether technology Interchange Meeting*, NASA/CP-1998-206900, NASA Marshall.

Beletski, V.V., Levin, E.M. (1993). Dynamics of Space Tether Systems. Vol. 83 *Advances in the Astronautical Sciences*.

Belokonov (2003). *Proceedings of the Russian-European Summer Space School* "Future Space Technologies and Experiments in Space", 30 June-11 July, Samara State Aerospace University, Russia, ESA WPP-229.

Belokonov, I.V. (2008) Improvement of navigational tracking instrumentation and methods of tether system deployment on an example of experiment YES2 on space vehicle Foton-M3. IAC-08-B2.1.10

Benetti (2004) e.a.Development and testing of an inflatable capsule for the YES2 project, IAC-04- I.7.05.

Bergamaschi, S., Morgana, M. (1987). Order of Magnitude Evaluation of the Lifetime of a Free Tether in Orbit. In *Proceedings of the 2nd International Conference on Tethers in Space,* Societa Italiana de Fisica, Italy.

Betto, M., Jørgensen, J.L., Riis, T. and Thuesen, G.G. (2000). The determination of the attitude and attitude dynamics of TeamSat. *Acta Astronautica,* volume 46, issues 2-6, January-March 2000, Pages 423-432.

Beuselinck T., Bavinckhove C. Van, Abrashkin V.A., Sazonov V.V. (2008). Attitude Motion of the Foton-M3 Spacecraft and Quasi-steady Accelerations on its Board. In *Proceedings of SPEX-2008*, Samara, Russia.

Biesbroek, R and Crellin, E. (1999). On the validity of a simple bead model for tethered systems. In *50th Congress of the International Astronautical Foundation*. IAF Press, IAF-99-A.5.02.

Biesbroek, R. (1996). Evolution in a microchip, a brief study into genetic algorithms, ESTEC Working Paper 1870.

Bilitza, D. (1997), International Reference Ionosphere - Status 1995/96, *Advances in Space Research*. 20, #9, 1751-1754.

Blanksby C. (2000). Non-Linear Modelling of Space Tethers and Application to Deployment, Retrieval and Electrodynamic Operations. *4th Engineering Mathematics & Applications Conferenence*, Melbourne.

Blumer, J.H., Benjamin, B., Donahue, Michal, E. Bangham. (2001). Practicality of using a Tether for Electrodynamic Reboost of the International Space Station, CP552 STAIF-2001.

Bonnal, C., Missonnier, S., Malnar, B. and Bullock, M. (2005). Optimization of tethered deorbitation of spent upper stages: The mailman process. In *Proceedings of the 4th European Conference on Space Debris SP-587.*

Bortolami, S.B., Lorenzini, E.C., Rupp, C.C. and Angrilli, F. (1993). Control Law for the deployment of SEDS II. *AAS/AIAA Astrodynamics Specialist Conference*, Victoria, Canada.

Bradford, E.A., Hedqvist, E.A. (1997). Mechanical Testing of TEAMSAT. In *Proceedings of the 3rd International Symposium on Environmental Testing for Space Programmes*, ESTEC, 24-27 June 97, SP-408 August 1997.

Brinza, D.E., Stiegman, A.E., Staszak, P.R., Laue, E.G., Liargh, R.H. (1991). Vacuum Ultraviolet (VUV) Radiation-Induced Degradation of Fluorinated Ethylene Propylene (FEP) Teflon Aboard The Long Duration Exposure Facility (LDEF). In *Proceedings NASA, LDEF 69 Months in Space*, Part 2, (1991) 817.

Calzada, S. (2004). Re-entry simulation and landing area minimization for YES2, Master Thesis Report, Oulu University, Finland.

Camps, C. (2005). Tether winding for space applications, the development of YES2 CHAMPS, Bachelor Thesis report, Delta-Utec & Fontys Hogeschool Venlo.

Carroll, J.A. (1987). The Small Expendable Deployment System (SEDS). Presented at the PSN/NASA/ESA Second International Conference on Tethers in Space, Venice, Italy.

Carroll, J.A. (1995.II). A General-Purpose Tether Deboosted Reentry Capsule. *AIAA Space Programs and Technologies Conference*, Huntsville, AL, AIAA 95-4072.

Carroll, J.A. (2002). Space Transport Development Using Orbital Debris Final Report on NIAC Phase I, Research Grant No. 07600-087, Tether Applications, Inc.

Carroll, J.A. (September 1993). SEDS Deployer Desigh and Flight performance. *AIAA Space Programs and Technologies Conference and Exhibit*, Huntsville, AIAA-93-4764.

Carroll, J.A., Oldson, J.C. (1995.I). SEDS characteristics and capabilities. In *Proceedings of the 4th International Conference on Tethers in Space*, pp. 1079-1090.

Cartmell, M.P. and D.J. McKenzie. (2008). A review of space tether research. Review Article in *Progress in Aerospace Sciences*, Volume 44, Issue 1, Pages 1-21.

Castillejo G., Cichocki A., Burla M. (2008). Development, test and flight results of the RF systems for the YES2 Tether Experiment, IAC-08-E2.3.6.

Castronuovo, M.M, G. Laneve and C. Ulivieri. (2002). An Electrodynamic Tether System for Propulsion and Power Generation in a Jovian Mission. *Space Technology and Applications International Forum-STAIF 2002.*

Cefola, P., Volkov, I. I., Suevalov, V. V. (2004). Description of the Russian Upper Atmosphere Density Model GOST-2004, *Proceedings of 37th COSPAR Scientific Assembly*. Held 13-20 July 2008, in Montréal, Canada., p.476

Chobotov, V.A., Mains, D.L. (1999). Tether Satellite System Collision Study, , Acta Astronautica, Vol 44, Nos. 7 – 12, pp 543 – 551, 1999.

Clark, C., Hardy, J. (1960). Gravity Problems in Manned Space Stations. *Proceedings of the Manned Space Stations Symposium*, April 20-22, 1960, pp. 104-113, Institute of the Aeronautical Sciences.

Cook, G.E. (1962). Luni-Solar Perturbations of the orbit of an Earth satellite. *Geophysical Journal of the Royal Astronomical Society,* pp 261-291.

Cosmo, ML, and Lorenzini, E.C. (1997). Tethers In Space Handbook. Third Edition, prepared for NASA/MSFC by Smithsonian Astrophysical Observatory, Cambridge, MA.

Cramer, B. (1985). Physiological Considerations of Artificial Gravity. *Applications of Tethers in Space,* vol. 1, p. 3·95-3·107.

Crellin, E., Jansens, F. (1996). Some properties of the In-Plane motion of a dumbbell in elliptic orbit, ESTEC Working Paper 1888.

Crellin, E.B., Baldoni, C. (1994). An improved simple model of tethered satellite systems and some aspects of control. ESTEC Working Paper 1779.

Cross, J.B., Koontz, S.L. (1994), Ground-based simulation of LEO environment: investigations of a select LDEF material – FEP Teflon. In: A.F. Whitaker and J. Gregory, Editors, NASA CP-3257, *Proceedings of a NASA conference on LDEF materials results for spacecraft applications*, Oct. 27–28. Huntsville, Alabama (1994), pp. 379–389.

De Pascale, F. (2008). Fotino: Systems Engineering of the Re-entry Capsule of the Second Young Engineers' Satellite (YES2). Master Thesis TU Delft.

De Pascale, F., Kruijff, M. (2006). Fotino: design, manufacturing, testing of the capsule for the second Young Engineers Satellite, IAC-06-E1.1.05, Valencia.

Delta-Utec. (2001). Design of a Stable and Efficient Electrodynamic Tether for Deorbiting and/or Propulsion Applications, Report for ESA ARCOP contract.

Dijk, A. van, Kruijff, M., Heide, E.J. van der, Lebreton, J.-P. (2003.I). LeBRETON: a Lightweight Bare Rotating Electrodynamic Tether for jOvian eNtry, IAC-03-S.P.05, Bremen.

Dijk, A. van, Kruijff,M., Heide, E.J. van der (2003.II). LeBRETON Le Bare Rotating Electrodynamic Tether for jOvian eNtry Delta-Utec DU-SATAJ-1103, 2003, ESA/ESTEC study 17239/03/NL/HB

Divine, N. and H.B. Garrett. (1983). Charged Particle Distribution in Jupiter's Magnetosphere. *Journal of Geophysical Research*, Vol. 88, No. A9, pp. 6889-6903.

Dobrowolny M. (2002.I). Linear stability of electrodynamic tethers, *Il Nuovo Cimento* 2002 no. 25C, pag. 369-391.

Dobrowolny, M. (2002.II). Lateral oscillations of an electrodynamic tether. *Journal of the astronautical sciences 2002,* no. 50, pag. 125-147.

Dobrowolny, M., Colombo G., Grossi M.D. (1976). Electrodynamics of long tethers in near-Earth environment. *Smithsonian Astrophysical Observatory Reports in Geoastronomy No. 3.*

Dobrowolny, M., Stone, N.H. (1994). A Technical Overview of TSS-1: the First Tethered Satellite System Mission, *Il Nuovo Cimento*, Vol. 17C, N.1, p. 1-12.

Dobrowolny, M., Vannaroni, G., De Venuto, F. (2000). Electrodynamic deorbiting of LEO satellites, *Il Nuovo Cimento*, 23C, pp.85.

Drob, D. P., Picone, M. J., Le Pichon, A., Garces, M. (2007), Developing, Applying, and Refining Comprehensive Measurement Based Specifications of Upper Atmospheric Neutral Winds, Presented at American Geophysical Union, Fall Meeting 2007.

Durin, C., Alet, I. (1991). Results of the "Post-Flight" Analyses on System Materials for the "L.D.E.F.-FRECOPA" Experiment. *Materials in Space*.

Edwards, B. C. (2000). *Design and Deployment of a Space Elevator. Acta Astronautica, 47 no. 10: 735-74.*

Edwards, B.C. (2003). The Space Elevator NIAC Phase II Final Report, March 2003.

ESA (1999), Space Debris Mitigation Handbook, Release 1.0.

ESA (2000), European Space Debris Safety and Mitigation Standard.

ESA (2005), Foton Retrievable Capsules", European User Guide to Low Gravity Platforms, UIC-ESA-UM-0001.

Estes, R.D., Lorenzini, E.C. (2000.IV). Performance and Dynamics of an Electrodynamic Tether, *Proceedings of the 38th Aeropspace Sciences Meeting & Exhibit,* AIAA 2000-0440.

Estes, R.D., Lorenzini, E.C., Sanmartin, J., Pelaez, J., Martinez-Sanchez, M. and Johnson, C.L. (2000.III). Bare Tethers for Electrodynamic Spacecraft Propulsion. *Journal of Spacecraft and Rockets*, Vol. 37, No. 2, 205-211.

Estes, R.D., Sanmartin, J. (2000.II). Cylindrical Langmuir probes beyond the orbital-motion-limited regime. *Physics of Plasmas*, Volume 7, Issue 10, pp. 4320-4325.

Estes, R.D., Sanmartin, J. and Martinez-Sanchez, M. (2000.I). Performance of Bare-Tether Systems under Varying Magnetic and Plasma Conditions. *Journal of Spacecraft and Rockets*, Vol. 37, No. 2, 197-204.

Forward R.L. , Hoyt, R.P. (1995). Failsafe Multiline Hoytether Lifetimes. In *AIAA 95-2890 31st AIAA/SAE/ASME/ASEE Joint Propulsion Conference*, San Diego, CA, July 1995.

Forward, R.L., Hoyt, R.P. (1998). Application of the Terminator Tether Electrodynamic Drag Technology to the Deorbit of Constellation Spacecraft, AIAA-98-3491.

Forward, R.L., Nordley, G. (1999). MERITT: Mars-Earth Rapid Interplanetary Tether Transport System - Initial Feasibility Study. AIAA 99-2151.

Fujii, H.A., e.a. (2009). Sounding rocket experiment of bare electrodynamic tether system. *Acta Astronautica*, vol. 64, p.313-324.

Fujii, H.A., Miyahara, Y., Ichiki, W., (1996), Optimal trajectories for deployment/retrieval of tethered subsatellite, ISTS 96-c-10.

Gallagher, D.L. et al. (1998). Electrodynamic Tether Propulsion and Power Generation at Jupiter, NASA/TP-1998- 208475.

Gavira, J., Rozemeijer, H., Muencheberg, S. (2000). The Tether System Experiment. *ESA Bulletin 102*, ESA/ESTEC.

George, P.E., Hill, S.G. (1991). Results from Analysis of Boeing Composite Specimens Flown On LDEF Experiment M0003.

Gilchrist, B., et. al. (1998). Enhanced electrodynamic tether currents due to electron emission from a neutral gas discharge: Results from the TSS-1R mission. *Geophysical Research Letters*, Vol. 25, No. 4, pp. 437-440, February 15, 1998.

Gilchrist, B.E., Bilen, S., Choiniere, E., Gallimore, A.D. and Smith, T.B. (2002). Analysis of Chamber Simulations of Long Collecting Probes in High-Speed Dense Plasmas. *IEEE Transactions on Plasma Sciences*, Vol. 30, No. 5, 2023-2034.

Gilruth, R. (1969). Manned Space Stations - Gateway to our Future in Space. *Manned Laboratories in Space*, pp. 1-10.

Glaese J. (1994). Small Expendable Tether Deployer System, Analysis of SEDS-1 Flight Results. *NASA contract report*, NAS8-39873, April 1994.

Glaese, J. R. (1995). A Comparison of SEDS-2 Flight and Dynamics Simulation Results. In *Proceedings of the Fourth International Conference on Tethers in Space.*

Glaese, J., Issa, R., Lakshmanan, P. (1993). Comparison of SEDS-1 Pre-Flight Simulations and Flight Data. In *AIAA Space Programs and Technologies Conference*, AIAA 93-4766, Huntsville.

Gläßel, H. , Zimmermann, F., Brückner, S., Schöttle, U., Rudolph, S. (2004). Adaptive neural control of the deployment procedure for tether-assisted re-entry. *Aerospace Science and Technology* 8, p.73-81.

Graczyk, R., Kruijff, M., Spiliotopoulos, I. (2008). Design And Qualification Of A Smallsat Stepper Motor Driver: Flight Results On-Board The YES2 Satellite. *Small Satellite Systems and Services (4S) Symposium Rhodes.*

Grossman, E., Noter, Y., Lifshitz, Y. (1997). Oxygen and VUV Irradiation of Polymers: Atomic Force Microscopy (AFM) and Complementary Studies. *7th International Symposium on Materials in Space Environment.* SP-399.

Guyt, J., (2001). Combined Micro-VCM and VBQC testing on degradable tethers for Delta-Utec, TOS-QMC 2001/084, Draft, 21 May 2001

Habinc, S. e.a. (1998). TEAMSAT's Data-Handling Systems. *ESA Bulletin 95*, August 1998.

Hall, T. (1997). Artificial Gravity and the Architecture of Orbital Habitats. In *1st International Symposium on Space Tourism*, Bremen.

Hambloch, P., De Pascale, F., Kruijff, M. (2007). ALBATROS – A Space System Engineering Tool. IAC-07-D5.1.05, Hyderabad.

Hartley, G.H., Guillet, J.E. (1968). Photochemistry of Ketone Polymers I. Studies of Ethylene-Carbon Monoxide Copolymers, *Macromolecules*, Vol. I, pp. 165-170.

Hausmann, G., De Pascale, F., Kruijff, M., Mironov, M. (2008). Design, development and testing of a compact lightweight capsule recovery system, IAC-08-D2.3.5.

Hedin, A.E., e.a. (1996). Empirical wind model for the upper, middle and lower atmosphere, *J. Atmos. Terr. Phys.* 58, 1421-1447, 1996.

Heelis, R. (1998). Tethered satellite investigations of the ionosphere and lower thermosphere. In *Proceedings of the*

Tether Technology Interchange Meeting, Huntsville, University of Texas.

Heide, E.J. van der, Carroll, J., Kruijff, M. (2001.I). Options for coordinated multi-point sensing in the lower thermosphere, *Phys. Chem. Earth*, Vol. 26, No. 4, pp. 285-291.

Heide, E.J. van der, Kruijff, M. (1996.I). StarTrack: a swinging tether assisted re-entry for the International Space Station. ESA/ESTEC, WP 1883, March 1996.

Heide, E.J. van der, Kruijff, M. (1999). DU-TSE-DD-E-1015 Deployment Algorithm Design Report. Tether System Experiment (TSE) Phase B PDR/BDR Data Package, Kayser-Threde.

Heide, E.J. van der, Kruijff, M. (2001.II). Tethers and debris mitigation. *Acta Astronautica* Vol. 48/5-12, pp. 503-516.

Heide, E.J. van der, Kruijff, M., Avanzini A., Liedtke, V., Karlovsky, A. (2003.I). Thermal Protection Testing of the Inflatable Capsule for YES2, IAC-03-I.3.05, Bremen.

Heide, E.J. van der, Kruijff, M., Raitt, D., Hermanns, F. (2003.II). Space Spin-in from Textiles: Opportunities for Tethers and Innovative Technologies. IAC-03-U.2.b.09, Bremen.

Heide, E.J. van der. (1996.II). Comparison of Tether Simulators. IRS Stuttgart, 1996.

Hill, P., Schnitzer, E. (1962). Rotating Manned Space Stations. *Astronautics*, vol. 7, no. 9, p. 14-18, American Rocket Society.

Hoyt R. , Uphoff, C. (1999.I). Cislunar Tether Transport System, AIAA 99-2690.

Hoyt R., Twiggs, R. (2003). The Multi-Application Survivable Tether (MAST) Experiment. AIAA Paper 2003-5219.

Hoyt, Forward. (1995). Failsafe Multistrand Tether SEDS Technology, *Proceedings of 4th International Conference on Tethers In Space*, Washington.

Hoyt, R. (2000). Design and Simulation of a Tether Boost Facility For LEO GTO Transport. AIAA 2000-3866.

Hoyt, R. (2000.I). Tether Systems for Satellite Deployment and Disposal. IAF-00-S.6.04.

Hoyt, R.P., Forward, R.L. (1999.II). Performance of the Terminator Tether for Autonomous Deorbit of LEO Spacecraft, AIAA-99-2839.

Hyslop, A., Heide, E.J. van der, Kruijff, M., Bonnal, C., Talbot, C., Espinosa, A. (2006). Designing a micro-launcher with tethered upper stage. IAC-06-D2.3.03.

Hyslop. A., Kruijff, M., Menon, C. (2005). Simulating Space Tether Deployment on Earth for the YES2 satellite. IAC-05-A2.1.09, Fukuoka.

IADC (2002), Space Debris Mitigation Guidelines, Inter-Agency Space Debris Coordination Committee, IADC-02-10.

Ishkov, S.A., Naumov, S.A., Sheinikov, I.V. (2007). Problems of tether system deployment safety and possible ways of their solution. (pp. 165-169). In *Proceedings Control and guidance of flying vehicles,* Samara, part 1. (In Russian).

Ishkov, S.A., Naumov, S.A. (2006). Deployment control of orbital tether system for the problem of providing prescribed separation conditions. (pp. 71-75). In *Proceedings Control and guidance of flying vehicles,* Samara. (in Russian).

Ishkov, S.A., Shejnikov, I.V. (2006). Experimental study of mechanical properties of tether (pp. 76-79). In *Proceedings Control and guidance of flying vehicles,* Samara. (in Russian).

Jablonsky, A.M. (2008). Deorbiting of microsatellites in Low Earth Orbit (LEO). An Introduction, Defence R&D, Ottawa, Canada. TM 2008-097.

Johnson, L. e.a. (2003). Propulsive Small Expendable Deployer System (ProSEDS) Experiment Mission Overview and Status. In *39th AIAA ASME SAE ASEE Joint Propulsion Conference.*

Johnson, L., Estes, R.D., Lorenzini, E. C., Martinez-Sanchez, M., Sanmartin, J., Vas, I. (1998). Electrodynamic Tethers for Spacecraft Propulsion. In *36th Aerospace Sciences Meeting & Exhibit*, AIAA 98-0983.

Jones, M., Melton, B., Bandecchi, M. (1998). TEAMSAT's Low-Cost EGSE and Mission Control Systems. *ESA Bulletin 95*, August 1998.

Klinkrad, H. (2006). Space Debris – Models and Risk Analysis. *Springer and Praxis*, Chichester, UK.

Kromm, F.X., Lorriott, T., Coutand, B., Harry, R., Quenisset, J.M. (2003). Tensile and creep properties of ultra high molecular weight PE, *Polymer Testing* 22 (2003) 463–470

Kruijff M., (2009.III), YES2 flight analysis and definition for a re-flight, TN1 and TN2, Delta-Utec report FM0100-YES2R v1.3, ESA Contract 22154/08/NL/PA

Kruijff M., Heide E.J. van der, Ockels W.J. (2009.I). Data Analysis of a Tethered SpaceMail Experiment. In *Journal of Spacecraft and Rockets*, Vol. 46, No. 6, pp. 1272-1287. (presented as AIAA-2008-7385).

Kruijff M., Stelzer M. (2007.II), YES2 Preliminary Mission & Failure Analysis, Delta-Utec report TN0113 under contract 16156/02/NL/PA, version 1.4, 24 October 2007.

Kruijff, M. (1999.III). The Young Engineers' Satellite: Flight results and critical analysis of a super-fast hands-on project. IAF-99-P.1.04, Amsterdam.

Kruijff, M., Gijsman, P., Heide, E.J. van der. (1999.II). Opening the Way for Large, Light and Non-Hazardous Space Structures: Report of a search for a UV-degradable material, IAF-99-I.3.05, Amsterdam, 1999.

Kruijff, M., Hambloch, P., Heide, E.J. van der, Stelzer, M. (2007). The Second Young Engineers' Satellite. IAC-07-

D2.3.04, Hyderabad.

Kruijff, M., Heide, E. J. van der. (2009.II). Qualification and In-flight Demonstration of a European Tether Deployment System on YES2. In *Acta Astronautica*, vol. 64, p.882-905.

Kruijff, M., Heide, E.J. van der (2003.IV). YES2-PDR-DU-01, 2003, YES2 Preliminary Design Review documentation package, Delta-Utec.

Kruijff, M., Heide, E.J. van der, Calzada, S. (2003.I). YES2 Inherently-safe Tethered Re-entry Mission and Contingencies. IAC-03-IAA.6.2.02, Bremen.

Kruijff, M., Heide, E.J. van der, Dragoni, E., Ferretti, S., Castagnetti, D. (2003.II). Concept Selection and Design of the Inherently-Safe Re-Entry Capsule for YES2. IAC-03-V.3.08, Bremen.

Kruijff, M., Heide, E.J. van der, Ockels, W.J. (1996). Braking of a flexible and deploying tether: the Flex End Brake. In *Proceedings of Workshop on Advanced Mathematical Methods in the dynamics of flexible bodies.* WPP-113, ESA, June 1996.

Kruijff, M., Heide, E.J. van der, Stelzer, M., Ockels, W.J., Gill, E. (2008). "First Mission Results of the YES2 Tethered SpaceMail Experiment", AIAA-2008-7385

Kruijff, M., Heide, E.J. van der. (1998). The YES satellite: a tethered momentum transfer in the GTO orbit. In *Proceedings of Tether Technology Interchange Meeting*, NASA/CP-1998-206900, January 1998.

Kruijff, M., Heide, E.J. van der. (1999.I). DU-TSE-RP-E-1023 Tether Prestretch Effects Test Report. Tether System Experiment (TSE) Phase B PDR/BDR Data Package, Kayser-Threde.

Kruijff, M., Heide, E.J. van der. (2001.II). Integrated Test Rig For Tether Hardware, Real-Time Simulator And Control Algorithms: Robust Momentum Transfer Validated. In *Proceedings of STAIF*, Albuquerque.

Kruijff, M., Heide, E.J. van der. (2001.III). DU-TSE-RP-E-1035, Analysis of Breadboard Test Set-up, Hardware and Control algorithms. Tether System Experiment (TSE) Phase B CDR Data Package, Kayser-Threde.

Kruijff, M., Heide, E.J. van der. (2002). YES2, the second Young Engineers' Satellite, A Tethered Inherently-safe Re-entry Capsule. IAC-02-P.P.01, Houston.

Kruijff, M., Heide, E.J. van der. (2003.III). YES2 Education and Outreach. IAC-03-P.P.01, IAF Bremen.

Kruijff, M., Heide, van der E.J., De Venuto, F., Dobrowolny, M., Vannaroni, G. (2001.I). Long Term Stability Of Bare Conductive Tethers: Combined Results From Plasma Chamber Tests And Advanced Simulations. *Presented at STAIF*, Albuquerque.

Lansdorp, B. (2003.I). MARS-g: Manned Antecedent for Reduced and Simulated Gravity. Preliminary Study Report, Delta-Utec.

Lansdorp, B., Kruijff, M. (2006). Space Tethers: Read instructions before use. IAC-06-D4.3.02.

Lansdorp, B., Kruijff, M., Heide, E.J. van der. (2003.II). MARS-g: Manned Antecedent for Artificial Gravity. IAC-03-IAA-10.1.05, Bremen.

Lansdorp, B., Soemers, H.M.J.R., Heide, E.J. van der, Kruijff, M. (2004). Design of a high-tension elastically deforming space tether deployer. IAC-04-IAA-3.8.2, Vancouver.

Letton, A., Rock, N.I., Williams, T.W. Strganac, T.W., Farrow, A. (1991). Characterization of polymer films retrieved from LDEF. In *Proceedings NASA*, LDEF 69 Months in Space, Part 2, (1991) 705.

Levin, E. M. (1987). Stability of the Stationary Motions of an Electrodynamic Tether System in Orbit. In *Kosmicheskie Issledovaniya (Space explorations)*, Vol. 25, No. 4, pp. 491-501, July-August, (1987).

Levin, E.M. (2007). Dynamic Analysis of Space Tether Missions. *Advances in the Astronautical Sciences*, vol. 126.

Licata, R., Gavira, J.M. (1995). ESA development on expendable tether mechanism technology. In the *Fourth International Conference on Tethers in Space*, Washington D.C.

Lorenzini, E.C. , Bortolami, S.B., Rupp, C.C., and Angrilli, F. (1996). Control and flight performance of tethered satellite small expendable deployment system-II. In *Journal of Guidance, Control and Dynamics*, Vol. 19, No.5.

Lorenzini, E.C. , Mowery, D.K., Rupp, C.C. (1995). SEDS-II deployment control law and mission design. In *Proceedings of the Fourth International Conference on Tethers*, Washington, April 1995.

Lorenzini, E.C., Estes, R. D., Cosmo, M.L. and Pelaez, J. (1999.I). Dynamical, electrical and thermal coupling in a new class of electrodynamic tethered systems. *In Spaceflight Mechanics 2000*, Vol. 102, Advances in the Astronautical Sciences, ed. By R.H. Bishop, D.L. Mackison, R:D: Culp, M:J: Evans, 1999, paper AAS99-192.

Lorenzini, E.C., Mowery, D.K., Rupp, C.C. (1995). Dynamics and Control of SEDSAT Deployment. In *Proceedings of the Fourth International Conference on Tethers in Space*, pp. 551-561, 10-14 April 1995, Smithsonian Institution, Washington, DC., p.551.

Lyaskin, A. (2004), Численное моделирование теплового состояния спускаемой капсулы проекта YES2, *Control and guidance of flying vehicles*. Proceedings. Samara.

Matcham, J.S. (1998). Exposure of Alenia Dyneema tether samples to UV radiation, QMC 98/003, ESA/ESTEC.

McBride, N., Taylor, E.A. (1997). The Risk to Satellite Tethers from Meteoroid and Debris Impacts. In *Second European Conference on Space Debris*, edited by B. Kaldeich-Schiirmann and B. Harris, European Space Agency, pp. 643-648.

McCoy, J.E., e.a. (1995). Plasma Motor-Generator (PMG) Flight Experiment Results. In *the fourth Conference On Tethers in Space*, pp. 57-82.

McKenna,H.A., Hearle, J. W. S., O'Hear N. (2004). Handbook of fibre rope technology, Textile Institute, Manchester, England.

Menon, C., Kruijff, M., Vavouliotis, A. (2007). Design and Testing of a Space Mechanism for Tether Deployment. In *Journal of Spacecraft and Rockets*, Vol. 44, No. 4, July-August 2007.

Misra, A.K., Modi, V.J. (1986). A survey on the dynamics and control of tethered satellite systems, AAS 86-246.

Morel, Q., Hobbs, S., Kruijff, M., (2003). Cranfield's inherently safe re-entry capsule design for YES2, IAC-03-U.1.07, Bremen.

Morris, D., Gilchrist, B., Gallimore, A., Jensen, K. (2000). Developing field emitter array cathode systems for electrodynamic tether propulsion. In *the 36th AIAA/ASME/SAE/ASEE Joint Propulsion Conference*, AIAA 2000-3867, Huntsville, AL, July 16-20, 2000.

Muylaert, J., Reinhard, R., Asma, C.O. (2010). QB50: An International Network of 50 CubeSats for Multi-Point, In-Situ Measurements in the Lower Thermosphere and Re-Entry Research. In *Proceedings of the 4S Symposium*, 31 May - 4 June 2010.

NASA (1967). Gemini XII Program Mission Report, Manned Spacecraft Center, Houston, USA, January 1967.

NASA (1991). *Proceedings LDEF 69 Months in Space*, Part 2, (1991) 817.

NASA (1995). Guidelines and Assessment Procedures for Limiting Orbital Debris, NASA Safety Standard 1740.14.

NASA (1997). Human Exploration of Mars, Reference Mission v3.0, NASA SP 6107.

NASA (2001). Space Life Sciences Research Highlights, December 2001.

NASA (2007). Technical Standard, Process for Limiting Orbital Debris, NASA-STD-8719.14, 28. August 2007 (Initial Release).

Newlands, R. (1994). Lunar observations and direct lunar surface analysis through orbiting tethers. *Master Thesis report*, TU Delft.

Nicolini, D., Ockels, W.J. (2003). Coupled Electrodynamic Tether/Electrostatic Propulsion System, IEPC-03-306. Presented at *the 28th International Electric Propulsion Conference*, Toulouse, France, 17-21 March 2003.

Noteborn, R.M.H. (1997). Small satellites are fun! Delta-Utec, July 1997.

O'Rourke, L. (1997). Space Applications For Micro- & Nano-technologies with flight demonstration of 3-axis accelerometer units, ESA/ESTEC/QCT, April 1997.

Ockels, W.J, Biesbroek, R.G.J., Verduijn, D.F. (1996). Enhanced Efficiency of GEO Transfer and Lunar Missions by Using the Upperstage Momentum Transferred by Tether, IAF-96-A.2.01.

Ockels, W.J, Heide, E.J. van der, Kruijff, M. (1995). Space Mail and tethers, sample return capability for Space Station Alpha, IAF-95-T.4.10, Oslo.

Ockels, W.J. (1987). Absorptive tethers - a first test in space, ESTEC Noordwijk.

Ockels, W.J. , Nicolini, D., Jainandunsing, S. (2004). Combined propulsion system intended for a spacecraft, US Patent 6732978, 2004. Coupled Electrodynamic Tether/Electrostatic Propulsion System, European Space Agency patent ESA/PAT/466.

Ohtsuka, T. (1997). Stabilizing Receding Horizon Control of a Tethered Satellite, *Proceedings of ISAS 7th Workshop on Astrodynamics and Flight Mechanics*, Sagamihara, Japan.

Pearson, J. (1975). The Orbital tower: a spacecraft launcher using the Earth's rotational energy. *Acta Astronautica* 2:785.

Pearson, J., Carroll J., Levin E. (2010). Active Debris Removal: EDDE, The Electrodynamic Debris Eliminator. IAC-10-A6.4.9.

Pearson, J., Levin, E., Oldson, J., Carroll, J. (2001). The ElectroDynamic Delivery Experiment (EDDE), CP552, Space Technologies and Applications International Forum.

Pelaez, J., Lorenzini, E.C., Lopez-Rebollal, O., Ruiz, M. (2000.II). A new kind of dynamic instability in electrodynamic tethers. AAS/AIAA Space Flight Mechanics Meeting, ClearWater, Florida, January 2000, Paper AAS 00-190.

Pelaez, J., Ruiz, M., Lopez-Rebollal, O., Lorenzini, E.C. and Cosmo, M.L. (2000.I). A two bar model for the dynamics and stability of electrodynamic tethers. AAS/AIAA Space Flight Mechanics Meeting, ClearWater, Florida, January 2000, Paper AAS 00-188.

Pelt, M. van. (2009). Space Tethers and Space Elevators, Copernicus Books.

Penson, J. S. G., Burchell, M. (2003). Hypervelocity Impact Studies on Space Tethers. IAC-03-I.5.4.

Picone, J.M., Hedin, A.E., Drob, D.P., A.C. Aikin, A.C. (2002). NRLMSISE-00 empirical model of the atmosphere: Statistical comparisons and scientific issues, *J. Geophys. Res.*, 107(A12), 1468, doi: 10.1029/2002JA009430, 2002.

Pol, M. van de. (1998). The implementation of a GPS subsystem on TEAMSAT. Master Thesis report, Delft University of Technology, January 1998.

Rivaton, A. (1993). Photochemistry of poly(butyleneterephthalate): 1—Identification of the IR-absorbing photolysis products, *Polymer Degradation and Stability*. Vol. 41, Issue 3, pp. 283-296.

Rolo, L. (2005). A large hexagonal loop antenna with a metallic core for the YES2 space-tethered satellite, IAC-05-B3.6.07.

Rothwell, N. (2001). Technical Information on the Principles of Spooling, white paper,Double R Controls, Heywood, England.

Sabath D. (1996.I). Chancen und Probleme des Seilunterstuetzten Wiedereintritts. PhD Dissertation Technical University of Munich, April 1996.

Sabath, D., Kast, W., Kowalczyk, M., Krischke, M., Kruijff, M., Heide, E. van der. (1997). Results of the parabolic flight tests of the RAPUNZEL deployer. *IAF 1996, Acta Astronautica* Vol. 41, Issue 12, pp. 841-845.

Sabath, D., Paul, K.G. (1996.II). Hypervelocity Impact Experiments on Tether Materials, TU Munich.

Saccoccia, G., Gonzalez del Amo J., Estublier, D. (2000). *ESA Bulletin 101*, February 2000.

Sanmartín, J.R., Lorenzini, E.C. (2003). A 'Free-Lunch' Tour Of The Jovian System. In *Proceedings of the 8th Space Charging Technology Conference*, NASA/CP-2004-213091, Huntsville, Alabama.

Sanmartin, J. R. e.a. (2008). Electrodynamic tether mission to a Low Jovian Orbit, Vol. 3, EPSC 2008-A-00322.

Sanmartin, J.R., Estes, R.D. (1999). The Orbital-Motion-Limited Regime of Cylindrical Langmuir Probes. *Physics of plasmas*, Vol. 6, No. 1, pp. 395-405.

Sanmartin, J.R., Lorenzini, E.C. (2005). Exploration of outer planets using tethers for power and propulsion. *Journal pulsion and Power*, Vol. 21, No. 3, 573-576.

Sanmartin, J.R., Martinez-Sanchez, M., Ahedo, E. (1993). Bare Wire Anodes for Electrodynamic Tethers. *Journal of Propulsion and Power*, Vol. 9, No. 3, pp. 353-360.

Sasaki, S., e.a. (1987). Results from a Series of Tethered Rocket Experiments. AIAA, USA.

Sasaki, S., Oyama, K.I. (1994). Space Tether Experiments in Japan. *2nd International Workshop on the Application of Tethered Systems in Space*, Kanagawa, Japan, ISAS, May 1994.

Schagerl, M., Steiner W., Troger H. (1998). On numerical problems in the simulation of tethered satellite systems. *Workshop Proceedings Advanced Mathematical Methods in the Dynamics of Flexible Bodies*, 3-5 June 1996, ESA WPP-113, January 1998.

Schonenborg, R.A.C. (2000). Solid propellant de-orbiting for constellation satellites. Delft University of Technology, June 2000.

Schott, L. (1968). Electric Probes. In *Plasma Diagnostics*, ed. by W. Lochte-Holtgreven, North-Holland Publishing Co., Amsterdam.

Smirnov, N.N., Demyanova, Yu. A., Zvyaguina, A.V., Malashina A.A. and Luzhina, A.A. (2010). Dynamical simulation of tether in orbit deployment. *Acta Astronautica*, Volume 67, Issues 3-4, Pages 324-332, August-September 2010.

Sorensen, K. (2005). A Tether-Based Variable-Gravity Research Facility Concept, JANNAF.

Sorensen, K.F. (2001). Conceptual Design and Analysis of an MXER Tether Boost Station, AIAA 2001-3915.

Spiliotopoulos, I., Kruijff, M., Mirmont, M. (2008). Development and Flight Results of a PC104/QNX-Based On-Board Computer and Software for the YES2 Tether Experiment. In *Proceedings of Small Satellite Systems and Services (4S) Symposium Rhodes.*

Stadler, J.H. (1995). SEDS End Mass Payload Magnetometer Engineering Performance and Rotational Data Analysis Results. In *Proceedings of the Fourth International Conference on Tethers*, Washington, April 1995.

Stelzer, M. (2005). YESSim User Manual, Delta-Utec report CDR-E0205.

Stelzer, M. (2006). YES2 Mission Analysis – Phase C, Delta-Utec report CE0201.

Stimler, F.J. (1968). Advanced Orbiting Grid Sphere Spacecraft, TR 68-17, AF APL.

Stone, R. (1973). An Overview of Artificial Gravity. *Fifth Symposium on the Role of the Vestibular Organs in Space Exploration*, pp. 23-33.

Trivailo, P. M., Blanksby, C. (1997). Interactive 3D Dynamic Simulator for the Space Shuttle - Deployed Tethered Satellite Systems. In *Proceedings of Australian MATLAB Conference*, Sydney, Australia, 23-24 October 1997.

Tsiolkovsky, K.E. (1895). Speculations about Earth and Sky, and on Vesta. Akademiia Nauk SSSR, Moscow, 1895, p.35; reprinted in 1959.

TsSKB Progress (2006). YES2 Mission Feasibility Study for Launch on space craft FOTON-M3, Technical Notes TN1-TN7, 31-03-2006

Tsyganenko N. A. (1995). Modeling the Earth's magnetospheric magnetic field confined within a realistic magnetopause, *J. Geophys. Res.*, 100, 5599-5612.

Tyc, G., Han, R.P.S. (1995). Attitude Dynamics Investigation of the OEDIPUS-A Tethered Rocket Payload. *Journal of Spacecraft and Rockets*, Vol. 32, No. 1, p. 133-141, February 1995.

Tyc, G., Han, R.P.S. (2001). On the dynamics of spinning tethered space vehicles. Phil.Trans.R.Soc. Lond. A359, pp. 2161-2190.

U.S. Standard Atmosphere(1976). U.S. Government Printing Office, Washington, D.C. NOAA-S / T 76-1562.

Vannaroni et al. (1998). Current-voltage characteristics of the TSS-1R satellite: comparison with isotropic and unisotropic models. *Geophysical Research Letters*, Vol. 25, No. 5, 749-752.

Vannaroni, G. et al. (1999). Electrodynamic Tethers For Deorbiting Applications. *50th International Astronautical Congress*, Amsterdam.

Vas, I. E., Kelly, T. J. and Scarl, E. A. (2000). Space Station Reboost with Electrodynamic Tethers. *Journal of Spacecraft*

and Rockets (AIAA), Volume 37, Number 2, Virgina.

Vaughn, J.A., Curtis, L., Gilchrist, B.E., Bilen, S.G. and Lorenzini, E.C. (2004). Review of the ProSEDS Electrodynamic Tether Mission Development. *AIAA 40th Joint Propulsion Conference*, Paper AIAA 2004-3501, Fort Lauderdale, FL, July 2004.

Vigneron, F.R., Jablonski, A.M., et al. (1997). Comparison of Analytical Modeling of OEDIPUS Tethers with Data from Tether Laboratory. *Journal of Guidance, Control and Dynamics*, Vol. 20, No. 3, pp.471-478, May-June, 1997.

VSO (Visual Satellite Observer's Homepage), http://www.satobs.org/noss.html, last accessed November 2010.

Wallace, B.K. (1995). SEDS Tether Deployment Ground Tests. In *Proceedings of the Fourth International Conference on Tethers*, Washington, April 1995.

Warnock, T. W., Cochran, J. E. (1993). Orbital Lifetime of Tethered Satellites. *The Journal of the Astronautical Sciences*, 41(2), 165–188.

Wertz, J.R., Larson, W.J. (1993). Space Mission Analysis and Design, 2nd Edition.

Williams, J. D. and Wilbur, P. J. (1992). Electron Emission from a Hollow Cathode-Based Plasma Contactor. *Journal of Spacecraft and Rockets*, Vol. 29, No. 6, pages 820-829, November-December 1992.

Williams, P., Hyslop, A., Kruijff, M. (2006). Deployment control for the YES2 tether-assisted re-entry mission, *dvances in the Astronautical Sciences* (AAS 05-322), vol. 123, Part 2, pages 1101-1120.

Williams, P., Hyslop, A., Stelzer, M., Kruijff, M. (2009). YES2 Optimal trajectories in presence of eccentricity and aerodynamic drag. *Acta Astronautica* (IAC-06-D2.3.04), volume 64, Issues 7-8, April-May 2009, pages 745-769.

Williams, P., Stelzer, M., Hyslop, A., Kruijff, M. (2007). Evolutionary computation of tether deployment trajectories with application to YES2. *Spaceflight Mechanics*, volume 128, AAS 07-192, p.1351-1372.

Yamagiwa, Y., Takegahara, H., Nakajima, A. (1999). Quick Descent of HII Upper Stage by Electrodynamic Tether. IAF-99-V.2.05.

YES2 (2003), PDR Data Package, Delta-Utec.

YES2 (2006), CDR Data Package, Delta-Utec.

Yost S.A. (2002). The Effect of Spring Mass on the Oscillation Frequency. *University of Tennesee*, February 2002.

Zedd, M.F. (1998). Experiments in Tether Dynamics Planned for ATEx's Flight. *Tether technology Interchange Meeting*, NASA/CP-1998-206900, NASA Marshall, January 1998.

Zimmermann, F., Schoettle, U.M., Messerschmid, E. (2005). Optimization of the tether-assisted return mission of a guided re-entry capsule. *Aerospace science and technology*, vol. 9, no. 8, pp. 713-721.

Summary

Tether applications

Space tethers offer a myriad of possibilities. Futuristic, reusable concepts have been proposed that may create a paradigm shift towards sustainable and ubiquitous space travel.. The most graphic example is the Space Elevator. Yet, even today's single-use expendable tethers can provide significant advantages over conventional alternatives. They can maintain space stations in low orbits essentially without propellant, provide end-of-life deorbit for satellite constellations, or enable an accelerated scientific progress by providing a frequent return of samples from space to Earth. Tethers can uniquely provide artificial gravity to prepare for mission to the Moon and Mars, as well as coordinated multipoint sensing without the need for propellant-hungry formation-keeping infrastructure. Tether systems for such applications demand smart but typically not very complex solutions.

The principles behind those applications have been demonstrated in orbit already. Still, no tether application is in use today. (Partial) failures of the past appear to have damaged the image of tethers. A small step forward, a demonstration of a true application, may be able to repair the confidence, and thus could be of great consequence. Yet, as things have been, support for any demonstration in orbit is in short supply. For lack of opportunities there may be a temptation to gather many objectives within a single mission. Then again, a project that is very ambitious can well lead to a high-visibility failure and become counterproductive. Alternatively, success can be achieved by small steps, based on previous experiences.

In this thesis, developments are being detailed surrounding two projects that have followed the approach of small steps: the Young Engineers' Satellites. YES and YES2 have been made into reality and have yielded some new insights about tethers. They have benefited from a dedicated yet low-cost approach and from the attraction of their sympathetic educational aspects.

The driving thought behind the YES and YES2 projects has been to bring forward the case of tethers by improving and making accessible the general understanding of in-orbit tether behavior as well as tether mission aspects, related technologies and experimental knowledge and including the highly relevant issue of safety and predictability. In the context of YES and YES2, a sample return application has served as a technological focal point. The projects' public and open approach has allowed a large community of experts and decision makers to raise any concerns, over the full breadth of the issue. These concerns have been welcomed and responded to, such that obstacles have finally been surpassed and relevant lessons have been learned.

The legacy of the YES project – possibilities and limitations of a new approach

The first Young Engineers' Satellite, YES, has triggered a focus on responsible use of tethers in space - partly as a result of the unconventional approach that made it possible in the first place. The YES mission is to deploy and operate a 35-km rotating tether in Geostationary Transfer Orbit (GTO). Conceived in October 1996, YES is developed and launched within the course of only one year (1996-1997). It is produced by students and yung engineers assisted by ESA experts, collocated at ESTEC in Noordwijk, The Netherlands. YES exploits a free launch opportunity offered by the Ariane 502 qualification flight. Much of its hardware is donated by ESTEC, some components being new developments, offered for a maiden flight, others originating from previous ESA projects. The YES project has been particularly low on documentation and bureaucracy. The downside of this opportunistic approach has become apparent. The mission design is complex, development time is short and finances are severely limited. The system is thus insufficiently tested. As a result, the probability of at least a partial experiment failure is considered significant. In addition, the high perigee altitude and orientation of the Ariane 5 GTO orbit, as it is finally planned, translates into an unacceptable probability of tether collision with operational satellites. Although YES has been launched in October 1997, and its secondary experiments have been performed, it has been decided not to deploy the tether itself.

To avoid such problems in the future, several initiatives have been taken in the course of this work. Safe orbital domains and operational recommendations have been defined for both mechanical and electrodynamic tether applications. A search for an intrinsically safe tether system has resulted in the idea of "evaporating" tethers and the subsequent study of UV-degradation mechanisms in potential tether materials. A closed-loop deployment testing facility has been developed to mimic tether deployment on the ground as realistically as possible. An advanced tether and mission simulator, MTBSim/ETSim, has also been developed.

The YES2 project – taking in the lessons from YES

The YES2 project is conceived in 2001, and this time, safety and predictability have become prime concerns. The development takes six years. Similar to YES, YES2 has been built with help of highly motivated students and young engineers. However, based on the YES experience, significantly more time is reserved for understanding of the system by analysis, development and testing. Multiple generations of students are required and there is an increased need for documentation. A thorough system understanding and traceability is required as European and Russian officials need to be repeatedly convinced of the mission safety. A carefully selected orbit, extensive attention to mission simulation and a safe tether and system design are further elements that led to the final acceptance of the YES2 mission. The additional effort is not in vain: one decade after the YES flight, on September 25th 2007, YES2 succeeds in deploying a record-breaking 32 km tether from the Russian microgravity platform "Foton".

The YES2 system and tether deployment have demonstrated a number of technological novelties. YES2 has the SpaceMail application as its main theme. SpaceMail is a concept to

provide a frequent sample return capability for the International Space Station. In analogy, the YES2 is mounted on Foton as a massive platform, whereas the tether is used to deorbit a small re-entry capsule with scientific payload, Fotino. A tether deployer has been developed, as well as tether winding and testing technology and the necessary subsystems, such as the control electronics and an ejection system. In order to achieve high deorbit accuracy, the tether is deployed in two stages. The Fotino capsule is largely designed and built by students. It can be simple and light-weight, exactly because the tether provides both accurate deorbit and attitude stabilization.

YES2 technology development

The key elements of the YES2 tether deployer are the tether and spool, with ideally a passive, predictable unwinding behavior, and the friction brake, which provides the active deployment control capability. This concept has been first used in the Small Expendable Deployer System (SEDS) missions and has resulted in three successful deployments so far. Due to International Traffic in Arms Regulations (ITAR) it has unfortunately not been possible to obtain the SEDS hardware from the United States and the YES2 tether deployer had thus been developed from scratch (Section 5.4.2). The YES2 technology itself is publicly available and it is hoped that new parties, also from beyond the European Union, can benefit and build on the gained experience with low investment costs.

Both tether and spool have been extensively characterized and their design and manufacturing procedures adjusted accordingly.

The tether material was characterized for pole friction, outgassing, stiffness, damping and break strength. The tether was equipped with a system for shock damping tuned for maximum mission safety, based on deployment and jam analysis, combined with passive and active tether release mechanisms. The tether design was verified for survivability in case of shocks, particle impact and heating by friction. The latter requirement was found to be a significant design parameter.

Both a tether winding machine and an unwinding test rig have been developed. The unwinding rig recovers the deployed tether for reuse after testing. More tests can be held and a better understanding of usage dependent effects has been achieved, such as shrinkage and twist. The final system can estimate tether length with an error of about 0.1%, an improvement by about a factor ten with respect to the initial system.

The winding machine design has been optimized to achieve reproducible, stable and compact tether spools. A partly empirical and partly mathematical approach has been followed to design spool shape and winding pattern, with the objective to improve stability and uniformity. The spool's unwinding tension is characterized in tests and fitted to an approximation inherited from the SEDS projects. Spool properties and behavior have been quantified under a wide range of conditions, including various deployment velocities, zero-g environment, post-storage, after thermal vacuum exposure and at extreme temperatures. A level of predictability has been obtained matching requirements for flight.

The brake system is based on the “barberpole” concept, which originates from textile industry. The tether is guided around a capstan following a tortuous (helical) path to accumulate friction. The amount of friction is controlled by the amount of wrappings of the tether around the pole. The wrapping itself is effectuated by means of a worm gear.

To help improve understanding and performance of the barberpole concept, a mathematical model has been developed that predicts the generated tether tension and the path followed by the tether on the pole. A simple form of the model predicts a helical path and shows that contact between tether and pole is guaranteed for the deployment of a non-stiff tether from a spool. From this model recommendations for geometry and target level of friction can be derived. A more developed model approximates also the observed deviation from such a helical path, by introduction of a “stiction” coefficient. The contribution of tether diameter, wrapping direction and tether twist to this stiction effect has been qualitatively verified but could as yet be only partly quantified. During deployment tests, the tether path is instable, a behavior which is as yet not fully understood. The level of instability appears to depends at least on incoming tension level.

The final YES2 design for the barberpole system takes into account the model results, but has undergone further iterations after mechanical, thermal and performance testing. The brake's mechanical performance has been verified over a wide range of mechanical frequencies and temperatures. The gear includes a flexible coupling and its fixtures are specifically designed to reduce loss of driving torque in the presence of misalignment and thermal expansion effects. The pole's high heat capacity and good thermal conduction allows for operation also at high tension and velocities. An off-cylindrical shape for the pole has been introduced to guarantee spacing between the tether loops and gear. The resulting pole design has been verified to maintain exponential behavior at least until six turns. Since each additional turn represents a tension increase of about a factor three, this guarantees a large dynamic range of control. Finally, tests on the unwinding rig have been defined and performed to systematically determine the pole's friction coefficient and to verify effectiveness and reliability of deployment control and feedback.

YES2 mission

The flight plan of YES2 features a downward ejection of the tethered endmass consisting of the Fotino capsule and a Mechanical and data Acquisition Support System (MASS). The tether is deployed from the Foton vehicle in two stages, separated by a hold phase. The first stage is a deployment to the vertical, similar to that of SEDS-2 - albeit at a shorter and more challenging length. The second stage deploys the remainder of the tether to a large forward angle and is followed by a swing back to the vertical, much like the swing of the 20-km long tether of SEDS-1. When the tether passes through the local vertical, the Fotino capsule and tether are released. The actual YES2 mission has successfully demonstrated these steps.

The first stage has been successfully controlled to the target length of 3.4 km, with an error under 20 m. The deployment control algorithm compares length measurements to a predetermined reference table that contains the target length profile as well as feedback gains. It then determines the required barberpole brake position. Deployment control of this

first stage with such a short tether is a challenge. At these tether lengths there is a significant risk of premature deployment stop: the gravity gradient force that drives deployment is comparable to the spool friction, which tends to slow deployment down.

Over two stages finally 31.7 km of tether has been deployed, achieving the longest structure in orbit so far. The maximum velocity of 16 m/s also exceeds that of earlier tether experiments. The available YES2 dataset includes length and deployment rate measurements, detailed tension data, information on endmass dynamics sufficient to reconstruct initial conditions, and orbital data in the form of Two-Line Element (TLE) sets.

The YES2 deployment reveals some problems too. The initial tens of meters of deployment are irregular - presumably due to oscillation of the endmass. As a consequence, the length sensor filter briefly overestimates the velocity. Over a period of several seconds too much braking is applied. By itself such a brief deviation does not lead to any lasting effects. In addition however, the tether's stickiness to the spool is larger than expected -apparently as a result of a mechanical settling due to thermal cycles- and this impedes recovery of the deployment velocity. The combination of these two effects leads to an extended period of underdeployment. When the deployment velocity finally increases again as a result of the increasing gravity gradient, the controller attempts to return to the nominal profile by overcompensation and causes a transverse wave in the tether. In the remainder of the first stage, heavy oscillations in deployment velocity can be observed. During the hold phase between the two stages the transverse waves continue and leave a clear tension signature.

A more significant problem occurs during the second stage of deployment. This stage starts off promising. The tether accelerates cleanly out of the hold phase and the impact of the transverse oscillations diminishes. However, due to a faulty electrical patch, unforeseen electrical noise appears on the control computer's signal lines leaving the controller without length measurement. As a result, the final 40 minutes of the deployment is uncontrolled. A free deployment follows and results in a 40-N shock as it reaches the end of the tether, which is attached to the spool core. The shock is followed by some minutes of slackness and a complex recovery of tension during the swing to the vertical. At the vertical, the Fotino capsule is released into a slightly steeper trajectory than planned, probably however with a significant spin rate, as a consequence of the tether shock. From Fotino no beacon signal has been received, so it may not have survived the re-entry. If any, the exact landing location is unknown.

YES2 data analysis

From a point of view of tether deployment, tether dynamics analysis and demonstration of tether control capability, the mission can be declared a success. Tether length, deployment velocity, deployment angle and tension have all been successfully reconstructed for the full duration of the mission. The impact of tether tension on initial endmass dynamics has also been determined. Save for minor deviations, data analysis has demonstrated that the ejection system, deployer hardware and controller software performed nominally and in line with the SpaceMail requirements. Tether stickiness to the spool has been somewhat out of limits and must be better controlled. The tether length measurement filter has been

overoptimized, and as such has proven sensitive to deployment irregularities. It can better be simplified. The friction behavior of brake and spool dynamical behavior have been found close to nominal, validating the deployer hardware's performance. Tether swing underneath Foton, release at the nominal time and momentum transfer have all been confirmed by from analysis of Foton disturbances. The shock tension measurement has been used to determine independently tether braid stiffness and speed of sound in the fibers, they are in line with *a priori* expectations.

The observed tether dynamics have been matched closely by the MTBSim simulator. This match has multiple purposes.

- In order to create the match, the deployer parameter settings have been adjusted as necessary to reconstruct the observed deployment velocity profile. The fact that the values required for a match are within 10-20% from both those measured on-ground and the in-flight measurements, provides support for the applicability of simulation tools for mission planning.
- Also observed tether behavior that was not used to obtain the match is nevertheless well reproduced, in particular the in-plane deployment angle and the occurrence of transversal waves.
- The tether's damping coefficient could be estimated from the matching exercise and compared against ground measurements. Damping appears to have been higher in-flight than predicted. The deviation may be related to ground test limitations, in particularly with respect to tether length.
- The matched simulation has been used to propagate Fotino's supposed trajectory and estimate its possible landing point.
- Finally, with increased confidence, the simulations have been used to create credible hypotheses for the cause of the observed transverse oscillations and to propose preventive measures. The transverse oscillations were apparently reinforced by a controller resonance with the deployment velocity due to the delay in the velocity estimate as introduced by a low pass filter. Effective solutions derived from simulations remain to be confirmed by testing. They include a faster operating brake mechanism and a barberpole with lower friction coefficient. A pre-flight sensitivity analysis by simulation is recommended to verify selected feedback control parameters.

YES2 as an independent data point reinforces the conclusion by the SEDS team that mechanical tether deployment and behavior is both sufficiently predictable and controllable with regards to the applications considered, whereas system and simulation limitations can be spelled out more concretely. YES2 has demonstrated the validity of closed-loop ground testing and simulation of deployment in order to understand hardware performance and tether deployment behavior in space. A perhaps not so surprising finding following the analysis of failures occurring during the YES2 mission is that, before such tests, the tether should be exposed to realistic environmental conditions, presumably to obtain a representative level of settling of the tether on the spool. In addition, the YES2 data

demonstrates that for the more complex dynamics, such as resonance, shocks and other adverse effects, simulations can provide valuable qualitative insight that can be used for selection of hardware and controller parameters. Such selection should still take into account generous margins, to be based on a sensitivity analysis, as absolute performance for such complex dynamics cannot be reliably predicted, e.g. due the non-linearity and measurement uncertainty for various properties of tether, friction and spool. Some should additional effects should be taken into account in future simulations. In particular, unexpected deployment irregularities have been observed during the first minute of deployment, that are thought to arise from an interaction between endmass oscillation and deployment tension, specifically excluded from simulations so far.

Conclusions, recommendations and outlook

Despite the promise of space tethers for essentially propellantless, sustainable space transportation, it has proven difficult to move beyond theory towards a first tether application, and -following some (partial) failures in the 1990s- even to move towards a further concept demonstration.

In order to understand the programmatic and technical challenges currently faced by tether initiatives and to respond to them where possible, a broad approach has been followed. This approach includes tether simulation development and preliminary analysis of a range of potential tether applications, primarily from a perspective of potential for a small demonstration mission, technology availability and mission safety. Focusing on the SpaceMail application as an example, a safe tether and tether deployment system has been developed and extensively tested with the use of both a winding facility and an unwinding test rig. Through involvement of a large number of highly motivated young engineers, two complete flight systems have been developed and launched. Of those two systems, the YES2 resulted in an innovative in-orbit demonstration and evaluation of a two-stage tether deployment and momentum transfer.

Firstly it is found from this approach that tether applications face a particular developmental challenge, as due to their sheer size, they are not very suitable for testing on-ground. Much of the testing needs to take place in orbit. This constraint puts a significant price tag on any tether system test cycle and makes any failures occurring highly visible, even if they are in fact a normal part of the development cycle for any complex system. For this reason, it is relevant to increase confidence in the applicability of computer simulations. The MTBSim simulator and the YES2 mission have provided progress for the case of mechanical tethers, although future tether missions should continue to collect data to fill in the gaps identified in this work. Complementary to such simulations, ground-based closed-loop deployment testing as explored in this work provides as solid a confirmation of system performance as can be achieved on-ground.

Secondly, it is concluded that in the near-term the use of tethers is limited to niche applications, for considerations of risk reduction as well as programmatic and technological reasons. For both mechanical and electrodynamic tethers, a rough recommended safe altitude regime has been provided in this work. For applications based on expendable

mechanical tethers such as sample return and deorbit from LEO (SpaceMail), launch assist (T-Series) and short-duration lower thermosphere investigation, isolated mission opportunities may be identified. End-of-life deorbit for satellites can be achieved with some advantage by bare electrodynamic tethers, particularly if the deorbit rate is controlled. It is advised to release the conductive tether from the payload as soon as a 25-year lifetime orbit has been achieved. Design and control measures have been identified that help to prevent tether slackness resulting from dynamic instability as experienced by electrodynamic tether applications.

For some applications there seems to be hardly an alternative except for tethers, although they may be more far-off or as yet dependent on further technological advances. Examples are comfortable artificial gravity with the help of a mechanical tether, and in case of electrodynamic tethers, orbit maintenance of a space station and cleaning of LEO from left-behind upper stages. A promising and safe near-term application is long-term lower thermospheric in-situ research.

Thirdly, the case of the YES2 mission and the analysis of its deployment have made plausible the claim that a tether application such as SpaceMail can be sufficiently predictable and safe. A persistent, open and responsive attitude towards a broad community of critics has finally enabled the YES2 in-orbit tether deployment to take place. A key element of the YES2 approach has been simplicity and commonality based on the passive deployment and SEDS control hardware concept. Since mechanical design simplicity here comes at the price of non-linearity and behavioral complexity, a stepwise characterization and testing approach has therefore been defined as a compensation measure. Regarding safety, key factors have proven to be: a responsible orbit selection, a mission design providing basic but adequate ground control and abort options, as well as a system design that provides an adequate response for each of the identified critical phases of deployment, particularly regarding staging subsystems and tether design. Tether deployer technology and mission preparation methodology developed within the scope of this work can be used with only small modifications for near-future tethered momentum transfer missions and other early tether applications.

Finally, the success of a low-budget development and demonstration project like YES2 suggests that tether hardware is affordable in the sense that it is straightforward to build and qualify and can be handled without particular precautions. However, space business is not yet commercial and is often driven by special interests that bypass technical and even cost arguments. The well-recognized need for removal of pre-existing debris may prove to drive an exception, as no reasonable alternative is available. Unfortunately, such application is pending the development of critical technologies such as in-orbit debris grappling. In the mean time, upcoming demonstration missions may further depend on an educational context. Notably, the educational approach is not necessarily low-cost and certainly not without its particular challenges. Whereas it has proven hard to avoid occurrence of any type of flaw, be it in the process or in the system, the YES2 project has demonstrated that the challenges can indeed be met - largely. The educational approach has enabled significant progress that would otherwise simply not have been made.

Epilogue – Towards Sustainable Space Transportation

The promise of tethers for sustainable space transportation

Will all of us be astronauts one day? Will we find it normal to use the vacuum that surrounds Earth for travels to our daily destinations, or for prolonged stays in weightlessness? And will we leave our home planet to travel to the Moon or Mars or even beyond? First perhaps we'd go as businessmen to mine resources that are rare on Earth or as scientists to practice astronomy, life science and geology - later it'd be also as tourists and as settlers. If we could we probably would.

But the cost of space travel today is forbidding and the ecological burden on our planet's fragile equilibrium may not allow for such unrestricted freedom. The need for expulsion of large quantities of rocket propellant to accelerate spacecraft is to blame for this high cost. All this propellant has to be carried on-board and accelerated along. Moreover, once expelled, its kinetic energy is no longer available to the spacecraft.

In contrast, tether applications often require no propellant at all. Exploiting the mechanical link that space tethers provide, they can make it possible to conserve energy and momentum almost completely, and utilize those to achieve required changes in spacecraft motion. Furthermore, electrodynamic tethers can convert solar power into thrust. The tether mass is not a showstopper either. Modern fiber materials or tapes allow for single-use solutions lighter than rocket engines can provide. On top of that the tether hardware can be designed to be largely reusable. The concept of space tethers therefore holds a promise of a widespread and sustainable access to space. Eventually tethers could alter profoundly the way we lead our lives, as they would redefine the boundaries to our world.

Imagine for a moment such a reality. Using a suborbital space-plane as a spring board, moving, say, at 5 km/s, we would hook onto the end of a hundred kilometer long tether as it rotates around its center of mass, several hundreds of kilometers above the Earth's surface. A five-minute swing brings us above the system's center of mass, and here it releases us in forward direction at a velocity relative to Earth several kilometers per second higher than that of the spaceplane. Once in orbit, we can adjust our trajectory to fit our needs. Velocity increments of a few kilometers per second are sufficient for any transfer between Earth, Moon and Mars orbit, or between the surface of the Moon or Mars and an orbit around it. Let us opt to be hurled into an orbit around the Moon. A few days later, upon arrival, we'd be picked up by another rotating system and dropped off close to the Moon's surface with just a little bit of left-over velocity helping us to maneuver towards our target.

In this future, several small spinning electrodynamic tethers move from orbit to orbit to collect and clear space of those upper stages and defunct satellites that were left behind during mankind's first century of space-faring. These vehicles are powered by solar energy

and steered through ingenious modulation of the current in the tether. Rockets are becoming more and more in disuse, in anticipation of what is now being constructed. It is the Space Elevator, a giant tower made from a tape-like web of carbon nanotubes, held taught by the centrifugal force of the Earth's own rotation and by Earth's gravity pull as it diminishes with distance. As a first step in its construction, an ultra-thin carbon-nanotube tape has been lowered towards the Earth where it has eventually been connected to the ground. This connection has since been used to carry up materials, meant to reinforce the tower and to position intermediate stations. Once the elevator will be complete, lifts with cargo and passengers will be moving both up and down, exchanging energy amongst each other. Additional energy is provided by solar cells integrated in the elevator as well as by laser that is beamed from elsewhere. In the lower regions of the tower one can release satellites that will end up in an elliptic orbit around Earth, and that use tethers or drag sails for further transportation. From the orbital center one can simply place satellites into the geostationary ring. From the top of the tower, one can schedule a release to be hurled towards Mars. Where do you want to go?

No other technology than tethers is known today that could achieve such a paradigm shift in space infrastructure and space travel sustainability. The energy gap that separates a 1000-kg module in low orbit around Earth from one standing on the ground is equivalent to that of about a year's worth of gasoline for an average commuter. This may seem like a lot, but it should be affordable for anyone in the developed world. Unfortunately, the conventional rocket is notoriously inefficient at transferring energy to the module that is to be launched. It propels not only the module but also itself and all its fuel to high velocities. A significant fraction of this propellant -often toxic, reactive or acting as a greenhouse gas- would end up in the stratosphere, where each launch causes measurable differences in particle and aerosol abundance. The pollution and chemical impact is long-lived, typically stretching for decades and spreading worldwide. To raise one 1000-kg module, a rocket would consume about as much energy as is burnt away during a full career of commuting. Even if a space-plane is used to bring the rocket into a suborbital trajectory as a starting point, all the necessary propellant to accelerate from there into orbit has to be carried along by the space-plane, in addition to the module itself, and the energy cost will still equal several years worth of gasoline.

A rotating tether in Low Earth Orbit on the other hand can fully benefit from the principle of energy exchange and momentum transfer. The energy taken from one module that is about to land on Earth or to be lowered in orbit, is provided to another, that is just taking off or moving to a higher orbit. The suborbital space-plane can operate much more efficiently now as it only needs to carry the manned module, and not any propellant for the module's further acceleration. A conductive tether part that converts solar power into orbital energy can compensate any orbital losses of the tether system, e.g. resulting from the action of atmospheric drag or from an unbalance between the payload masses launched by the tether and those returned to Earth. Still it is true that at least the initial infrastructure for such a rotating system will have to be brought into orbit the conventional way, by rockets. In order to be effective, the tether system should also be at least an order of magnitude heavier than

the targeted payload. This represents a significant investment, but it is one that creates a solution for multiple, sustainable use. Note also that, once a first small-scale system is operational, it can be utilized to bring up materials and tools to help expand its own dimension and performance. The cost of the tether system mass that was conventionally launched into orbit can be largely distributed over the total payload mass that the system will launch over its lifetime. Suppose at least some hundred payloads can be launched, each with a mass about one tenth of that of the initial operational tether system, then significant benefits can be obtained. In this manner (depending on the exact space-plane cost) the launch cost per 1000 kg module can approach and eventually also dip below the one year's worth of gasoline that was used as the reference for a 100% efficiency.

Tether systems portrayed in this manner may seem too good to be true. Indeed, space elevators that let us climb directly into space, rotating tethers that send us on interplanetary trajectories: they are likely to be many decades away, pending for example development of in-orbit construction and grappling techniques as well as of revolutionary materials such as carbon-nanotubes. By that time, other innovative technological concepts yet unknown may have well surpassed the tether's projected capabilities.

Yet, even today's single-use expendable tethers can provide significant advantages over conventional alternatives. They can maintain space stations in low orbits essentially without propellant, provide end-of-life deorbit for satellite constellations, or enable an accelerated scientific progress by providing a frequent return of samples from space to Earth. Tethers can uniquely provide artificial gravity to prepare for mission to the Moon and Mars, as well as coordinated multipoint sensing without the need for propellant-hungry formation-keeping infrastructure. Tether systems for such applications demand smart but typically not very complex solutions.

The gap of skepticism, and crossing it

No such tethers are in use at the moment. There have been noticeable technology demonstrations in the past, including several 20 km tether deployments, and demonstrations of the concepts of artificial gravity, momentum transfer, electrodynamic thrust and power generation. Since the accidental cut of the TSS-1R tether in 1996 and the failed deployment of the ATeX tape tether in 1998, progress has been slow. Projects such as SEDSAT and ProSEDS have been cancelled for safety concerns. In the following decade, until 2007, there have been no tether deployments.

Space culture has become increasingly bureaucratic and more and more distanced from its experimental and bold origins. Sound unambiguous predictions and demonstrated performance are a prerequisite before new technologies are tried. But tethers cannot be fully demonstrated on the ground. They also have complex dynamics, both when under tension and when slack. This uncertainty feeds skepticism and lowers the appeal of tethers in the face of other interests.

Sizeable interests are behind the conventional technologies and their settled, often extensive infrastructures. A parallel may be drawn here with the oil industry in the face of emerging

sustainable energy technologies. Large players face an intrinsic conflict of interest between the huge investments in conventional technology and organizational structures done today and the developments of tomorrow. The leading technologies of the future may actually at this very moment be carried forward by still obscure, small parties, not yet of commercial interest.

When targeting space tether development in this type of environment, it is a challenging undertaking to obtain funds for substantial in-orbit demonstration, i.e. demonstration of a system of representative function and complexity. Yet such a demonstration seems required to obtain the desired credibility.

The "gap of skepticism" is to be bridged between the conceptual demonstrations done so far and a first convincing application. This could trigger development of other low-risk applications, such as lower-thermosperic coordinated measurements. With confidence gained, investments could be made in the development of more complex applications, e.g. to get more value out of the International Space Station or to remove debris from orbit. In a next step, space infrastructure may actually be designed with the use of tethers in mind, think of a next generation of Space Stations or a artificial gravity facility. Only that would finally open up the way for truly revolutionary tether applications and an interplanetary transport infrastructure.

In this context, the YES2 mission has only provided a step to bring back rationality into the discussion. Even if a small and imperfect step, YES2 has demonstrated responsibility and predictability of the approach and readiness and availability of the technology. The step has been taken not by the established industry but by rather inexperienced yet eager young people. We narrowed the gap, now, will you cross it?

Samenvatting

De toepassing van tethers

Tethers, kabels in de ruimte, hebben een breed scala aan mogelijke toepassingen. Futuristische, herbruikbare en energie-efficiënte concepten zijn voorgesteld, zoals een lift van het aardoppervlak naar de ruimte. Dat soort toepassingen zou ons beeld van ruimtereizen grondig veranderen. Maar zelfs de hedendaagse tethers kunnen voordelen bieden ten opzichte van conventionele alternatieven. Zonder significant stuwstofverbruik kunnen ze ruimtestations in een lage baan houden, in onbruik geraakte satellietconstellaties uit hun omloop halen, of een regelmatige aanvoer bieden van samples uit de ruimte naar de Aarde (SpaceMail). Buiten tethers zijn er geen haalbare alternatieven die comfortabele kunstmatige zwaartekracht kunnen leveren voor missies naar Mars. Dergelijke toepassingen van tethersystemen vragen om intelligente, maar meestal niet erg complexe oplossingen.

De principes achter deze ideeën zijn reeds gedemonstreerd, doch echte toepassingen laten op zich wachten. (Gedeeltelijke) mislukkingen uit het verleden lijken het vertrouwen in tethers geschaad te hebben. Een kleine stap voorwaarts, een demonstratie van een echte toepassing, zou dit vertrouwen kunnen herstellen en dus van groot belang zijn, maar juist zo'n missie is nu zeer moeilijk te bewerkstelligen. Met zo weinig mogelijkheden voor een demonstratie is het verleidelijk om met een enkele missie zoveel mogelijk vernieuwingen te demonstreren. Echter, hoe ambitieuzer het project, hoe groter de zichtbaarheid en hoe groter de kans op falen en een contraproductief resultaat. Een alternatieve aanpak is het nemen van kleine stappen, bouwend op eerdere successen.

In dit proefschrift wordt de aanpak van kleine stappen toegepast. Twee in-orbit experimenten worden ontworpen: de Young Engineers' Satellites YES en YES2. Dankzij een low-cost aanpak en mede door de sympathiek-educatieve invalshoek kunnen deze experimenten worden gebouwd en gelanceerd. Het doel van de YES projecten is het verkrijgen van een beter inzicht in tetherdynamica en tethermissie-aspecten, zoals veiligheid en voorspelbaarheid. De eerdergenoemde SpaceMail-toepassing dient als case-study. Een brede en open benadering wordt gevolgd, waarbij studenten, deskundigen en besluitvormers inspraak krijgen. Aan hun bezwaren en bedenkingen wordt systematisch tegemoetgekomen, een aanpak die heeft geholpen om het systeem en het begrip ervan te verbeteren.

YES - mogelijkheden en beperkingen van een nieuwe aanpak

De eerste Young Engineers' Satellite, YES, is mogelijk gemaakt door een onconventionele, opportunistische aanpak. Deze methode is inspirerend gebleken, maar niet zonder problemen en heeft geleid tot meer aandacht voor verantwoord gebruik van tethers in de ruimte. De YES-missie behelst een 35-km lange, draaiende tether in een langgerekte baan om de Aarde (Geostationary Transfer Orbit of GTO). Het idee voor YES wordt voorgesteld in oktober 1996 - precies een jaar later wordt YES al gelanceerd. YES wordt ontworpen en

gebouwd door studenten en jonge ingenieurs, bijgestaan door deskundigen van de European Space Agency (ESA) bij ESA's technische afdeling ESTEC in Noordwijk. YES maakt gebruik van een gratis lancering op de Ariane 502 kwalificatievlucht. Veel van de YES hardware is geschonken door ESTEC, sommige onderdelen afkomstig uit vorige ESA-projecten, andere zijn prototypes die in de ruimte getest moeten worden. Het YES project schuwt documentatie en bureaucratie. De missie echter is complex, de ontwikkeltijd is kort en de financiën zijn zeer beperkt. Het systeem wordt pas laat, en vrij minimaal, getest. Als gevolg daarvan wordt een (gedeeltelijke) mislukking van het tetherexperiment waarschijnlijk geacht. De door Ariane geselecteerde baanhoogte en -oriëntatie vergroten nog verder de kans op een botsing van de tether met andere satellieten. YES wordt gelanceerd in oktober 1997, en alhoewel de secundaire experimenten worden uitgevoerd, is besloten de tether zelf niet af te wikkelen.

Dit werk rapporteert ook de maatregelen die hierop zijn genomen om zulke problemen in de toekomst te voorkomen. Banen om de Aarde die veilig zijn voor tethertoepassingen worden geidentificieerd. Operationele aanbevelingen worden gedefinieerd voor zowel mechanische als elektrodynamische tethertoepassingen. In reaktie op het idee van een veilige, na gebruik "verdampende" tether wordt de degradatie van mogelijke tether materialen, in vacuum en onder ultraviolette straling, in kaart gebracht. Een testfaciliteit wordt ontwikkeld die een tether zo realistisch als mogelijk op Aarde kan afwikkelen. Ook wordt een geavanceerde tether- en missiesimulator, MTBSim/ETSim, ontwikkeld.

Het YES2 project - bouwen op de lessen van de eerste YES

Het YES2 project is bedacht in 2001. Deze keer zijn veiligheid en voorspelbaarheid de belangrijkste aandachtspunten. De ontwikkeling ervan duurt zes jaar. Net als YES wordt YES2 gebouwd met behulp van zeer gemotiveerde studenten en jonge ingenieurs. Echter aanzienlijk meer tijd wordt nu gereserveerd om het systeem beter te begrijpen door middel van systematische analyse, ontwikkeling en testen. De langere projektduur vereist meerdere generaties van studenten en een grondige documentatie. Een goedgedefinieerde methodiek en traceerbaarheid is vereist, daar de vaak skeptische functionarissen van de Europese en Russische ruimtevaartagentschappen dienen te worden overtuigd van de veiligheid van de missie. Ook een zorgvuldig baankeuze, uitgebreide missiesimulatie en een veilig ontwerp van tether en afwikkelsysteem hebben bijgedragen tot de definitieve acceptatie van de YES2 missie. Deze extra inspanning is niet tevergeefs: vrijwel exact een decennium na de YES vlucht, op 25 september 2007, slaagt YES2 er in om een recordbrekende 32 km lange tether af te wikkelen van het Russische microzwaartekrachtplatform "Foton".

Het YES2 systeem en de afwikkeling van de tether demonstreren een aantal technologische nieuwigheden. YES2 heeft de SpaceMail-toepassing als thema. Zoals gezegd, SpaceMail is een concept om regelmatig wetenschappelijke monsters naar Aarde te vervoeren vanuit bijvoorbeeld het International Space Station. YES2 wordt gemonteerd op Foton, dat dienstdoet als representatie van zo'n ruimtestation. De tether wordt gebruikt om Fotino, een kleine terugkeercapsule met wetenschappelijke lading, terug naar Aarde te sturen. Een tetherafwikkelsysteem is ontwikkeld, inclusief de benodigde elektronica en software en de

benodigde mechanieken om de verschillende elementen op de juiste tijd los te koppelen. De tether wordt afgewikkeld in twee nauwkeurig gecontroleerde fasen, zodat Fotino nauwkeuriger losgelaten kan worden en dichter bij de bedoelde landingsplaats op Aarde zal landen. De Fotino-capsule is zelf ook behoorlijk innovatief en grotendeels ontworpen en gebouwd door studenten. Ze is volledig uitgerust met meetapparatuur, een baken en telemetriesysteem en een parachuutsysteem. Desondanks heeft de capsule een massa van slechts 6 kg en een diameter van 40 cm. Dit is alleen mogelijk dankzij het gebruik van een tether die de capsule niet alleen in een nauwkeurige baan plaatst, maar ook de oriëntatie ervan zeker stelt.

YES2 technologie-ontwikkeling

De belangrijkste onderdelen van het YES2 tetherafwikkelsysteem zijn de tether, de spoel en de rem. De tether wikkelt af van de (stilstaande) spoel, idealiter met een voorspelbaar gedrag. De rem is gebaseerd op het "barberpole"-concept, waarbij de hoeveelheid wrijving, die optreedt bij het afwikkelen van de tether, door een simpel mechanisme geregeld kan worden over een zeer groot bereik. Het concept voor de combinatie van deze systemen is eerder toegepast in de Small Expendable Deployer System (SEDS) experimenten, resulterend in drie succesvolle missies. Vanwege de International Traffic in Arms Regulations (ITAR) is het voor YES2 helaas niet mogelijk geweest om de SEDS hardware uit de Verenigde Staten te importeren. Een nieuw systeem wordt daarom ontwikkeld, met de bijkomende voordelen dat hierdoor ook een beter begrip van het ontwerp en gedrag verkregen wordt, terwijl het ontwerp bovendien nu publiek toegankelijk is, zodat ook derden in toekomstige projecten ervan kunnen profiteren.

Het gedrag van zowel tether als spoel zijn uitgebreid in kaart gebracht. Ontwerp en fabricageprocedures zijn iteratief verder ontwikkeld. Eigenschappen van het tethermateriaal zijn gemeten, waaronder wrijvingscoëfficiënt, stijfheid en sterkte. In de tether is een systeem aangebracht om schokken te absorberen die tijdens het afwikkelen zouden kunnen optreden. Als het nodig is kan de tether, zowel passief als aktief, van de eindmassa's worden losgekoppeld. Ook moet het ontwerp berekend zijn op inslag van micrometeoroïdes en mag de tether niet smelten onder de te verwachten wrijvingshitte.

Testopstellingen zijn ontwikkeld voor zowel het wikkelen als het afwikkelen. De afgewikkelde tether wordt op een tijdelijke spoel opgeslagen voor hergebruik. Zo kunnen meer tests worden uitgevoerd en de effecten van gebruik worden bestudeerd, waaronder krimp en twist. Na verschillende iteraties kan de afgewikkelde tetherlengte met een nauwkeurigheid tot 0.1% worden bepaald, tegen 1.0% voor de eerste versie van het systeem.

De wikkelmachine is ontworpen om reproduceerbare, stabiele en compacte tetherspoelen te maken. Door een combinatie van analyse en experiment wordt stabiliteit en uniformiteit van de spoel verbeterd. Om voldoende voorspelbaarheid te verkrijgen voor de missie, wordt de voor het afwikkelen benodigde kracht gemeten en/of gemodelleerd, als functie van onder andere afwikkelsnelheid, zwaartekracht, opslagduur, blootstelling aan vacuum en extreme temperaturen.

Het remsysteem maakt gebruikt van het "barberpole"-concept dat afkomstig is uit de textielindustrie. De tether wordt langs een spiraalvormig pad rond een cylinder geleid waarbij wrijving zich opbouwt. Het aantal windingen om de cylinder bepaalt de totale wrijving en spanning in het touw. Met behulp van een electrisch aangedreven wormwiel kan dit aantal windingen worden gecontroleerd.

Een model is ontwikkeld dat de door de barberpole verkregen spanning in het touw voorspelt, alsmede het door de tether gevolgde pad over de cylinder. Het contact tussen tether en paal is gegarandeerd als een flexibele tether met eindige massadichtheid van een spoel afwikkelt en een spiraalvormig pad volgt. Het model kan worden gebruikt om geometrie van de cylinder en wrijvingscoëfficiënt te kiezen. Een gedetailleerder model voorspelt een afwijking van de spiraalvorm als een zogenaamde "stictie"-coëfficiënt wordt geïntroduceerd. Zo'n afwijking is inderdaad waargenomen en hangt af van van tether diameter, spiraalrichting en tetherverdraaiïng. Deze afhankelijkheden zijn nog niet volledig gekwantificeerd. Tijdens het afwikkelen is het gevolgde tetherpad ook niet volledig stabiel, afhankelijk van de spanning in de tether waar deze de "barberpole" binnenkomt. Dit gedrag is nog niet volledig begrepen.

Het uiteindelijke ontwerp voor de YES2 barberpole houdt rekening met de modelresultaten, metingen aan de spanning in het touw en met de resultaten van verdere mechanische en thermische testen. De as van het wormwiel is voorzien van een flexibele koppeling en de tandwiel-as heeft een aangepaste behuizing zodat in geval van verkeerde uitlijning en thermische expansie de wrijving in het mechanisme beperkt blijft. De paal heeft een hoge warmtecapaciteit en een goede thermische geleiding zodat de tether koel kan blijven bij hoge snelheid en grote remkracht. Het paaloppervlak is enigszins concaaf zodat de tether wikkelingen minder makkelijk over elkaar heenlopen. Het resulterende ontwerp blijft dicht bij het ideale exponentieel wrijvingsgedrag tot minimaal zes windingen om de cylinder. Aangezien elke extra winding een toename veroorzaakt in de kracht in de tether met ongeveer een factor drie, staat dit garant voor een groot dynamisch controle-bereik. Afwikkeltests gekoppeld aan een real-time tethersimulatie worden tenslotte gebruikt om de effectiviteit van de feedback en controle met behulp van de barberpole te verifiëren.

YES2 missie

De YES2 missie voorziet in het loskoppelen en neerlaten van een aan de tether gebonden eindmassa, bestaande uit de Fotino capsule en de MASS subsatelliet (Mechanical and Data Acquisition Support System). De tether wordt vanaf de Foton afgewikkeld in twee fasen, gescheiden door een zogenaamde "hold phase". Tijdens de eerste fase wordt de tether tot 3.4 km lengte op zo'n manier afgewikkeld dat Fotino/MASS recht onder Foton komt te hangen. Deze fase is vergelijkbaar met de SEDS-2 missie. De kortere tetherlengte bij YES2 maakt een nauwkeurige controle echter een uitdaging. Tijdens de tweede fase wordt de tether onder een hoek naar voren afgewikkeld tot een lengte van 30 km, waarna deze terugslingert naar de verticaal onder Foton. Deze tweede fase is vergelijkbaar met de SEDS-1 missie. Als de tether de verticaal nadert worden eerst de Fotino capsule en dan ook de

tether met MASS losgekoppeld. De eigenlijk YES2 missie verloopt grotendeels volgens dit plan.

De eerste fase wordt met succes gecontroleerd en bereikt de gewenste lengte van 3.4 km, met een fout van minder dan 20 m. Het afwikkelen wordt gecontroleerd met behulp van een feedbackalgoritme dat lengtemetingen vergelijkt met een vooraf vastgesteld referentieprofiel. Het bepaalt vervolgens de gewenste barberpole positie. Controle van de afwikkelsnelheid tijdens deze eerste fase, met een dergelijke korte tether, is een uitdaging. Bij deze tetherlengtes kan het makkelijk gebeuren dat het afwikkelen vroegtijdig stopt: de gradiënt in zwaartekracht is nog te klein om te dienen als drijvende kracht achter het afwikkelen, en is kleiner dan of vergelijkbaar met de wrijving in de spoel. Er is dus een risico dat het afwikkelen komt te vertragen.

Tijdens de tweede fase wordt de volledige tether van 31.7 km afgewikkeld, de langste structuur in de ruimte tot nog toe, met een maximale afwikkelsnelheid van 16 m/s. Data is beschikbaar van tetherlengte en afwikkelsnelheid, spankracht in het touw, de beweging van de eindmassa kort na de loskoppeling van Foton, en gegevens over de baan om de aarde in de vorm van Two Line Elements (TLE).

Een aantal problemen treden op tijdens het afwikkelen. De eerste tientallen meters van de afwikkeling zijn onregelmatig - vermoedelijk als gevolg van de oscillatie van de MASS/Fotino eindmassa. Als gevolg daarvan wordt de afwikkelsnelheid kortdurig overschat door de boordcomputer. Over een periode van enkele seconden wordt te veel geremd. Normaal gesproken zou dit geen probleem moeten zijn. Echter, de tether gedraagt zich ietwat plakkerig en komt moeilijker van de spoel dan verwacht, waarschijnlijk als gevolg van een soort inklinking van de tether in de spoel door thermische cycli. Met deze plakkerigheid kan de afwikkelsnelheid zich maar moeilijk herstellen. De combinatie van deze twee effecten zorgt ervoor dat de tetherlengte lange tijd achterblijft bij de referentie. Wanneer de afwikkelsnelheid eindelijk weer groeit, in navolging van de toename in tetherlengte en de hiermee samenhangende toenemende zwaartekrachtsgradiënt, overcompenseert het feedbackalgoritme en veroorzaakt een transversale golf in de tether. Deze golf duurt voort tijdens de rest van de eerste fase en is ook duidelijk aanwijsbaar tijdens de “hold phase” tussen de twee afwikkelfases.

Een belangrijker probleem doet zich voor tijdens de tweede afwikkelfase. Deze fase begint veelbelovend. De tether versnelt netjes uit de “hold phase” en het effect van de transversale trillingen vermindert. Echter, als gevolg van een foutief uitgevoerde elektronische reparatie, doet zich elektrische ruis voor op het signaal van de afwikkelsensoren. Het ruisfilter aktiveert en de computer kan niet langer de afwikkeling van de tether meten. De laatste 40 minuten van de afwikkeling zijn daarom ongecontroleerd en ongeremd. Zodra met hoge afwikkelsnelheid het einde van de spoel wordt bereikt resulteert een 40-N schok. De schok wordt gevolgd door enkele minuten van slapheid in de tether waarop op complexe wijze de spankracht terugkeert tijdens de slingerbeweging naar de verticaal. De Fotino capsule wordt op de verticaal losgelaten en gaat waarschijnlijk de atmosfeer iets steiler in dan gepland, wellicht met een forse rotatie als gevolg van de schok in de tether. Van Fotino wordt geen

bakensignaal ontvangen, vermoedelijk heeft deze de terugkeer in de atmosfeer of de landing niet overleefd. Hoe dan ook, de exacte huidige locatie van Fotino of zijn fragmenten is onbekend.

YES2 data-analyse

De YES2 missie kan als succesvol worden beschouwd wat betreft demonstratie van tether-afwikkeling en controle daarvan, alsmede het verkrijgen van inzichten in tetherdynamica. Tetherlengte, afwikkelsnelheid, afwikkelhoek en spankracht zijn met succes gemeten of gereconstrueerd voor de volledige duur van de missie. Ook de beweging van de Fotino/MASS eindmassa is in kaart gebracht, met name tijdens het begin van de afwikkeling. Het afwikkelsysteem en de besturingssoftware hebben zich grotendeels nominaal gedragen. Een soort plakkerigheid van de spoel is waargenomen en moet verder worden onderzocht. De software die de tetherlengte berekent is te complex bevonden, en daardoor gevoelig voor afwikkelonregelmatigheden. De wrijving van zowel rem als spoel gedragen zich nominaal, waarmee het afwikkelsysteem positief gekwalificeerd is. Ook de afwikkeling in twee fases, de slingerbeweging, de loskoppeling van tether en Fotino en de hierdoor veroorzaakte baanverandering zijn bevestigd. Metingen aan de opgetreden schok zijn gebruikt om stijfheid van de tether en snelheid van het geluid erin te bepalen.

De resultaten kunnen nauwkeurig door de MTBSim simulator gereproduceerd worden. Deze reproductie heeft meerdere doelen.

• Parameterwaardes van het spoelwrijving en remmodel in de simulator zijn zodanig aangepast dat het waargenomen snelheidsprofiel precies gevolgd wordt. De hiervoor benodigde aanpassingen wijken slechts 10-20% af van de op de grond en in-flight gemeten parameterwaardes. Dit resultaat geeft aan met welke marge simulaties voorspellend kunnen zijn voor de missieplanning.

• Ook waargenomen tethergedrag dat niet is gebruikt voor de reproductie is toch goed gereproduceerd, in het bijzonder de voorwaartse hoek met de verticaal waaronder de tether afwikkelt en het verschijnen van transversale golven.

• De tether viscositeit kan worden geschat op basis van de reproductie. Deze blijkt in-flight hoger te zijn geweest dan voorspeld op basis van metingen op aarde. Dit kan te maken hebben met de beperkte lengte van het stuk tether dat gebruikt is voor de aardse testen.

• De simulatie is gebruikt om het veronderstelde traject van Fotino te propageren en het mogelijke landingspunt te schatten.

• Tot slot kunnen nu, met meer vertrouwen, de simulaties gebruikt worden om geloofwaardige hypothesen te stellen voor waargenomen onverwacht gedrag tijdens het afwikkelen, zoals de transversale oscillaties. Op basis hiervan kunnen ook, in verdere simulaties, diverse mogelijke preventieve maatregelen uitgeprobeerd worden. Het blijkt dat de transversale oscillaties versterkt worden door een resonantie van de controller met de afwikkelsnelheid als gevolg van de vertraagde snelheidsinschatting door de on-board computer. Oplossingen die uit simulaties worden afgeleid moeten nog wel worden bevestigd in verdere testen. Mogelijke oplossingen zijn een snellere aansturing van het

remmechanisme en het gebruik van een gladdere barberpole, met een lagere wrijvingscoëfficiënt. Als het systeem aangepast is, en de feedpackparameters gekozen, is het aan te raden om nog een gevoeligheidsanalyse uit te voeren door middel van simulatie, om de onzekerheden in nauwkeurigheid van de simulatie te dekken en zeker te zijn van de robuustheid van de oplossing.

De YES2 missie kan gezien worden als een onafhankelijk datapunt dat de eerdere conclusie van het SEDS-team ondersteunt dat, tenminste voor de onderhavige toepassing, het afwikkelgedrag van een tether zowel voldoende voorspelbaar alsook controleerbaar is. De beperkingen van het afwikkelsysteem en van de tethersimulatie zijn nu concreter gedefinieerd. Een belangrijke beperking vloeit voort uit de nauwkeurigheid waarmee tetherhardware gemodelleerd kan worden, en die is niet beter dan 10-20%. Onregelmatigheden in het afwikkelen op een schaal van secondes worden vooralsnog ook nog maar minimaal gesimuleerd. Zulke onregelmatigheden zijn in de eerste minuut van het afwikkelen waargenomen, mogelijk als gevolg van oscillaties van de eindmassa. De op de grond uitgevoerde "closed-loop" afwikkeltesten en simulaties kunnen desondanks goed gebruikt worden om het afwikkelsysteem en het afwikkelen van een tether in de ruimte beter te begrijpen. De analyse van de problemen die tijdens YES2 zijn opgetreden onderstreept dat, voor zulke testen betekenisvol kunnen worden uitgevoerd, de tether aan een representatieve omgeving moet worden blootgesteld. Simulaties zijn nuttig om een kwalitatief inzicht te krijgen in de complexere dynamiek van tethers, waaronder effecten als schokken, resonantie en oscillaties. Met deze inzichten kunnen, binnen voldoende marge, geschikte hardware- en controller-parameters worden geselecteerd.

Conclusies, aanbevelingen en vooruitzichten

Ondanks de belofte die tethers bieden voor in essentie stuwstofvrij, duurzaam vervoer in de ruimte, is het moeilijk gebleken om verder te komen dan louter conceptdemonstraties. Sinds de mid-jaren 90 zijn er zelfs helemaal geen experimenten meer geweest.

Om beter te begrijpen met welke programmatische en technische uitdagingen nieuwe tetherinitiatieven worden geconfronteerd, en om hier beter op te reageren is, waar mogelijk, een brede benadering gevolgd. Deze aanpak omvat de ontwikkeling van een geavanceerde tethersimulator, de analyse van een aantal tethertoepassingen, voornamelijk geselecteerd met het oog op een kleine demonstratiemissie, de beschikbare technologie, en de veiligheid ervan. Het SpaceMail concept wordt als case-study gebruikt, waarvoor een veilige tether en afwikkelsysteem is ontwikkeld. Het systeem is uitgebreid getest met behulp van zowel een wikkel- als een afwikkelmachine. Met behulp van een groot aantal zeer gemotiveerde jonge ingenieurs zijn twee complete vluchtsystemen ontwikkeld en gelanceerd, YES en YES2. YES2 heeft geresulteerd in een demonstratie en evaluatie van een afwikkeling van de tether in twee fases, gevolgd door een impulsuitwisseling die de Fotino capsule de atmosfeer heeft ingeslingerd. De resultaten van deze aanpak kunnen worden samengevat in de volgende vier punten.

Ten eerste is het voor tethers in het bijzonder een uitdaging om een toepassing te ontwikkelen - puur door hun lengte zijn ze niet erg geschikt voor het testen op de grond en

een or meerdere lanceringen zullen dus nodig zijn om het systeem uit te proberen. Deze beperking brengt een aanzienlijke prijskaartje met zich mee voor elke testcyclus. Eventuele problemen die zich in een baan om de aarde voordoen beinvloeden de publieke opinie sterker dan problemen in een testruimte, ookal vormen zulke problemen een normaal onderdeel van de ontwikkelingscyclus van een complex systeem. Het is daarom van belang om in computersimulaties te kunnen vertrouwen. De MTBSim simulator en de YES2 missie hebben dit vertrouwen gesterkt, niet alleen door het overeenkomstige gedrag, maar ook door een beter begrip van de beperkingen. Het niveau van realisme kan op Aarde verder worden uitgebreid met behulp van een afwikkeltest inclusief closed-loop controller, en gekoppeld aan een real-time tether simulator, als gedemonstreerd in dit werk.

In de tweede plaats wordt geconcludeerd dat op de korte termijn tethers toepassingen slechts een niche vormen, vanwege risicovermindering maar ook om programmatische en technische redenen. Voor zowel mechanische als elektrodynamische tethers is ruwweg een algemeen veilige baanhoogte aan te wijzen. Sample return uit Low Earth Orbit (SpaceMail), lanceerassistentie (T-series) en kleinschalig onderzoek van de lagere thermosfeer zijn voorbeelden van beperkte doch zinvolle mechanische tethertoepassingen op korte termijn. Met elektrodynamische “bare” (niet-geïsoleerde) tethers kunnen uitgewerkte satellieten uit hun baan worden gehaald. Om het risico van botsingen van andere satellieten met de tether te voorkomen is het hierbij aan te raden om de tether van de satelliet los te koppelen zodra een baanhoogte, equivalent met een 25-jarige levensduur, is bereikt. Een probleem voor electrodynamische toepassingen is de inherente dynamische instabiliteit. Een aantal mogelijkheden om hier mee om te gaan is in kaart gebracht, maar dient voor specifieke gevallen verder uitgewerkt te worden.

Voor sommige tether toepassingen is er nauwelijks een geschikte alternatieve technologie voorhanden. Kunstmatige zwaartekracht bijvoorbeeld kan alleen comfortabel zijn als deze met behulp van een tether wordt verkregen, omdat alleen tethers de benodigde kilometer-lange structuur kunnen bieden. Electrodynamische tethers zijn bij uitstek geschikt om bijvoorbeeld een ruimtestation in een lage, toegankelijke, baan om de aarde te houden en de daar ondergane luchtweerstand te compenseren. Dankzij eenzelfde toepassing (electrodynamische compensatie van luchtweerstand) kan thermosferisch onderzoek ook in een lage baan om de aarde (van 150-250 km hoogte) in-situ uitgevoerd worden. Electrodynamische tethers lijken ook ook het enige haalbare concept te bieden om een groot deel van het bestaande ruimteafval in LEO te verwijderen.

Ten derde hebben de YES2 missie en de bijbehorende data analyse aannemelijk gemaakt dat een toepassing als SpaceMail voldoende voorspelbaar en veilig kan worden uitgevoerd. De YES2 missie heeft plaats kunnen vinden dankzij een open en dynamische houding, waarbij tegemoet gekomen is aan de zorgen en wensen van een brede gemeenschap van (potentiële) critici. Het YES2 systeem dankt zijn betrouwbaarheid aan de passieve (stilstaande) spoel waarvan het touw afwikkelt het mechanisch simpele SEDS remsysteem. Eenvoud komt hier tegen de prijs van niet-lineariteit in het afwikkel en remgedrag. Rem en spoel zijn daarom, ter compensatie, uitgebreid getest en gekarakteriseerd. Belangrijke ingrediënten voor een veilige missie zijn: een zorgvuldig geselecteerde baanhoogte, opties om het afwikkelen af te

breken, automatisch of per telecommando, en een systeemontwerp dat voor elk van de kritieke missiefasen een passende, veilige, uitweg biedt als er iets misgaat. Zowel het afwikkelsysteem zelf als de methodologie ter voorbereiding van de missie kan met slechts kleine wijzigingen gebruikt worden voor andere tethertoepassingen in de nabije toekomst.

Ten slotte kan worden vastgesteld dat het YES2 systeem ontwikkeld en in de ruimte gekwalificeerd is tegen zeer lage kosten. Dit is mede mogelijk gemaakt doordat het systeem eenvoudig te bouwen is en (grond)testen kunnen worden uitgevoerd zonder bijzondere voorzorgsmaatregelen. Lage kosten zijn echter niet per se voldoende om een technologische doorbraak te forceren. Ruimtevaart is nog niet commerciëel - beslissingen worden nog regelmatig gedreven door andere belangen dan technische of financiële. Wellicht immuun voor deze paradoxale situatie is de toepassing voor het verwijderen van reeds bestaand ruimtepuin. Hiervoor is geen redelijk alternatief beschikbaar, en tethers maken dus een goede kans. Helaas zal deze toepassing niet concretiseren voordat er een goede oplossing beschikbaar is om een tether (of ander soort systeem) in een baan om de aarde aan een willekeurige stuk afval te koppelen. Tot dan toe, of in elk geval tot het scepticisme is verdwenen, is het goed mogelijk dat verdere tetherontwikkelingen afhangen van een educatieve context, die als een soort sympathieke “dekmantel” kan blijven dienen en die het enthusiasme van jonge mensen beschikbaar kan stellen. Hierbij moet worden vermeld dat de educatieve benadering niet per definitie gelijk staat aan goedkoop en zeker zijn onvolkomenheden heeft. In deze benadering is het zeer moeilijk volledig foutloos te werk te gaan. Niettegenstaande heeft het YES2 project aangetoond dat aan de uitdagingen grotendeels tegemoetgekomen kan worden. De educatieve aanpak heeft wel degelijk aanzienlijke vooruitgang mogelijk gemaakt voor de toepassing van tethers

List of Author's Publications

Below a list of the relevant journal and conference papers published in the context of the thesis activities. Those papers to which the author contributed as main author or as key contributor of content, presentation and/or research work are specifically indicated. Papers to which the author has contributed as coordinator or by providing supportive input have been mentioned separately. Key reports with significant author contribution providing complementary content (i.e. not provided in the papers or in this thesis) are listed as well.

Journal Papers (key contribution)

1. Sabath, D., Kast, W., Kowalczyk, M., Krischke, M., Kruijff, M., Heide, E. van der, Results of the parabolic flight tests of the RAPUNZEL deployer, IAF 1996, Acta Astronautica Vol. 41, Issue 12, pp. 841-845, 1997.
2. Heide, E.J. van der, Carroll, J., Kruijff, M., Options for coordinated multi-point sensing in the lower thermosphere, Phys. Chem. Earth, Vol. 26, No. 4, pp. 285-291, 2001.
3. Heide, E.J. van der, Kruijff, M., Tethers and debris mitigation, Acta Astronautica Vol. 48/5-12, pp. 503-516, 2001.
4. Menon, C., Kruijff, M., Vavouliotis, A., Design and Testing of a Space Mechanism for Tether Deployment, Journal of Spacecraft and Rockets, Vol. 44, No. 4, July-August 2007.
5. Kruijff, M., Heide, E.J. van der, Qualification and In-Flight Demonstration of a European Tether Deployment System on YES2, Acta Astronautica 64 (2009), pp. 882-905.
6. Kruijff, M., Heide, E.J. van der, Qualification and In-Flight Demonstration of a European Tether Deployment System on YES2, Acta Astronautica 64 (2009), pp. 882-905.Kruijff M., Heide E.J. van der, Ockels W.J., Data Analysis of a Tethered SpaceMail Experiment, Journal of Spacecraft and Rockets, Vol. 46, No. 6, pp. 1272-1287, presented as AIAA-2008-7385.
7. Fujii, H.A., Kruijff, M., Heide, E.J. van der, Watanabe, T., Ockels, W.J., "The Second Young Engineers' Satellite: Innovative Technology Through Education," 2009-g-29, 27th International Symposium on Space Technology and Science", *Transactions of Japan Society for Aeronautical and Space Sciences, Space Technology Japan*, to be published (Vol. 8, 2010).

Further co-authored Journal Papers

8. H. A. Fujii, T. Watanabe, H. Kojima, K-I. Oyama, T. Kusagaya, Y. Yamagiwa, H. Ohtsu, M. Cho, S. Sasaki, K. Tanaka, J.Williams, B. Rubin, C. L. Johnson, G. Khazanov, J. R. Sanmartin, J-P. Lebreton, E. J. van der Heide, M. Kruijff, F. De Pascale, P. M. Trivailo, "Sounding rocket experiment of bare electrodynamic tether system," Acta Astronautica, Journal of the International Academy of Astronautics, Vol.64, No.2-3, Jan./Feb. 2009, 313-324.
9. Williams, P., Hyslop, A., Stelzer, M., Kruijff, M., YES2 optimal trajectories in presence of eccentricity and aerodynamic drag, IAC-06-D2.3.04, Valencia, 2006 and Acta Astronautica Volume 64, Issues 7-8, April-May 2009, Pages 745-769.

Conference Papers (key contribution)

10. Asma C., De Pascale F., Kruijff M., "Heatshield Qualification for the SpaceMail Re- Entry Capsule "Fotino" in the VKI Plasmatron", AIAA-2008-6561.
11. Dijk, A. van, Kruijff, M., Heide, E.J. van der, Lebreton, J.-P., LeBRETON: a Lightweight Bare Rotating Electrodynamic Tether for jOvian eNtry, IAC-03-S.P.05, Bremen, 2003.

12. Graczyk, R., Kruijff, M., Spiliotopoulos, I., Design And Qualification Of A Smallsat Stepper Motor Driver, Flight Results On-Board The YES2 Satellite, Small Satellite Systems and Services (4S) Symposium Rhodes, 2008.

13. Hambloch, P., De Pascale, F., Kruijff, M., ALBATROS – A Space System Engineering Tool, IAC-07-D5.1.05, Hyderabad, 2007.

14. Heide Erik J. van der, Michiel Kruijff, Wubbo J. Ockels, The YES2 Experience: Towards Sustainable Space Transportation using Tethers, IAC-08-E2.3.6, 2008.

15. Heide, E.J. van der, Kruijff, M., Raitt, D., Hermanns, F., Space Spin-in from Textiles: Opportunities for Tethers and Innovative Technologies, IAC-03-U.2.b.09, Bremen, 2003.

16. Hyslop, A., Kruijff, M., Heide, E.J. van der, Camps, C., Timmermans, M., Spool winding and deployment testing for the YES2 tethered re-entry mission, 11th Australian International Aerospace Congress, Melbourne, 2005. Superseded by Hyslop. A., Kruijff, M., Menon, C., Simulating Space Tether Deployment on Earth for the YES2 satellite, IAC-05-A2.1.09, Fukuoka, 2005.

17. Kruijff, M. , Ockels, W.J, Heide, E.J. van der, Tethers as sustainable space transportation: implications from the YES2 tethered SpaceMail development and flight results, IAC 2008.

18. Kruijff, M. The Young Engineers' Satellite, Flight results and critical analysis of a super-fast hands-on project, IAF-99-P.1.04, Amsterdam, 1999.

19. Kruijff, M., Gijsman, P., Heide, E.J. van der, Opening the Way for Large, Light and Non-Hazardous Space Structures: Report of a search for a UV-degradable material, IAF-99-I.3.05, Amsterdam, 1999.

20. Kruijff, M., Hambloch, P., Heide, E.J. van der, Stelzer, M., The Second Young Engineers' Satellite, IAC-07-D2.3.04, Hyderabad, 2007.

21. Kruijff, M., Heide, E.J. van der, Calzada, S., YES2 Inherently-safe Tethered Re-entry Mission and Contingencies, IAC-03-IAA.6.2.02, Bremen 2003.

22. Kruijff, M., Heide, E.J. van der, Dragoni, E., Ferretti, S., Castagnetti, D., Concept Selection and Design of the Inherently-Safe Re-Entry Capsule for YES2, IAC-03-V.3.08, Bremen, 2003.

23. Kruijff, M., Heide, E.J. van der, Integrated Test Rig For Tether Hardware, Real-Time Simulator And Control Algorithms: Robust Momentum Transfer Validated, Proceedings of STAIF, Albuquerque, 2001.

24. Kruijff, M., Heide, E.J. van der, Ockels, W.J., Braking of a flexible and deploying tether: the Flex End Brake, Proceedings of Workshop on Advanced Mathematical Methods in the dynamics of flexible bodies, WPP-113, ESA, June 1996.

25. Kruijff, M., Heide, E.J. van der, Qualification and In-Flight Demonstration of a European Tether Deployment System and SpaceMail Technology on YES2, Small Satellite Systems and Services (4S) Symposium Rhodes, 2008.

26. Kruijff, M., Heide, E.J. van der, Stelzer, M., Applicability of tether deployment simulation and tests based on YES2 flight data, AIAA-2008-2136.

27. Kruijff, M., Heide, E.J. van der, The YES satellite: a tethered momentum transfer in the GTO orbit, Proceedings of Tether Technology Interchange Meeting, NASA/CP-1998-206900, January 1998

28. Kruijff, M., Heide, E.J. van der, YES2 Education and Outreach, IAC-03-P.P.01, IAF Bremen, 2003.

29. Kruijff, M., Heide, E.J. van der, YES2, the second Young Engineers' Satellite, A Tethered Inherently-safe Re-entry Capsule, IAC-02-P.P.01, Houston, 2002.

30. Kruijff, M., Heide, van der E.J., De Venuto, F., Dobrowolny, M., Vannaroni, G., Long Term Stability Of Bare Conductive Tethers: Combined Results From Plasma Chamber Tests And Advanced Simulations, Presented at STAIF, Albuquerque, 2001.

31. Kruijff, M., Heide, E.J. van der, Stelzer, M., Ockels, W.J., Gill, E., "First Mission Results of the YES2 Tethered SpaceMail Experiment", AIAA-2008-7385.

32. Kruijff, M., E.J. van der Heide, W.J. Ockels, Summary of Data Analysis of the YES2 Tethered SpaceMail Experiment, Proceedings of the SPEXP Symposium, Samara, Russia, 2-5 September 2008.

33. Lansdorp, B., Kruijff, M., Heide, E.J. van der, MARS-g: Manned Antecedent for Artificial Gravity, IAC-03-IAA-10.1.05, Bremen, 2003.

34. Lansdorp, B., Kruijff, M., Space tethers: Read instructions before use, IAC-06-D4.3.02, Valencia, 2006.

35. Ockels, W.J, Heide, E.J. van der, Kruijff, M., Space Mail and tethers, sample return capability for Space Station Alpha, IAF-95-T.4.10, Oslo, 1995.

36. Spiliotopoulos, I., Kruijff, M., Mirmont, M., Development and Flight Results of a PC104/QNX-Based On-Board Computer and Software for the YES2 Tether Experiment, Small Satellite Systems and Services (4S) Symposium Rhodes, 2008.

Further co-authored Conference Papers

37. Drakonakis, V., Miaris, A., Vavouliotis, A., Patricio R., Kruijff M., Kostopoulos, V., Thermal Modelling of ESA's Second Young Engineers' Satellite, IAC-06-C2.2.09, Valencia, 2006.

38. Fujii, H.A., e.a., A proposed bare-tether experiment on board a sounding rocket, 2nd IECEC, Rhode Island, AIAA 2004-5718.

39. Fujii, H.A., e.a., Space Experiment of Bare Tape-Tether Technology on the Sounding Rocket S520 the 25th, ISTS 2008. Duplicated by Fujii, H.A.,…, Heide, E.J. van der, Kruijff, M., Bare-Electric-Tether Experiment on a Sounding Rocket, Proceedings of Astronautical Conference, 28-29 July 2008 at ISAS/JAXA.

40. Hausmann, G., De Pascale, F., Kruijff, M., Mironov, M., Design, development and testing of a compact lightweight capsule recovery system, IAC-08-D2.3.5, 2008.

41. Heide, E.J. van der, Kruijff, M., Avanzini A., Liedtke, V., Karlovsky, A., Thermal Protection Testing of the Inflatable Capsule for YES2, IAC-03-I.3.05, Bremen 2003.

42. Hyslop, A., e.a.., Designing a micro-launcher with tethered upper stage, IAC-06-D2.3.03, 2006.

43. Hyslop, Heide, e.a., A Tethered Upper Stage for Small Launchers -Preliminary Analysis, Design and Test, 2nd European Conference for Aerospace Sciences (EUCASS), Brussels 2007.

44. Lansdorp, B., Soemers, H.M.J.R., Heide, E.J. van der, Kruijff, M., Design of a high-tension elastically deforming space tether deployer, IAC-04-IAA-3.8.2, Vancouver, 2004.

45. Morel, Q., Hobbs, S., Kruijff, M., Cranfield's inherently safe re-entry capsule design for YES2, IAC-03-U.1.07, Bremen, 2003.

46. Wijnans, A.S., Zandbergen, B.T.C., Kruijff, M., Heide, E.J. van der, Bare electrodynamic tape tether experiment onboard the Delfi-1 university satellite, Proceedings of the 4th International Spacecraft Propulsion Conference (ESA SP-555). 2-9 June, 2004, Chia Laguna, Italy.

47. Williams P., Stelzer, M., Hyslop, A., Kruijff, M., Evolutionary computation of tether deployment trajectories with application to YES2, AAS 07-192, Spaceflight Mechanics Volume 128, AAS, p.1351-1372, 2007.

48. Williams, P., Hyslop, A., Kruijff, M., Deployment control for the YES2 tether-assisted re-entry mission, AAS 05-322, Advances in the Astronautical Sciences, 2006, Vol. 123, Part 2, pages 1101-1120, duplicated by Williams, P., Hyslop, A., Kruijff, M., Trajectory Optimisation and Feedback Control for the YES2 Tether-Assisted Re-Entry Mission, 5th Australian Space Science Conference, Melbourne, 2005.

Key Publications and Technical Reports (selection)

49. Heide, E.J. van der, Kruijff, M., StarTrack, a swinging tether assisted re-entry for the International Space Station, ESA/ESTEC, WP 1883, March 1996.

50. Willekens, P., Dijk, A. van, Kruijff, M., Heide, E.J. van der, Young Engineers' Satellite, Educational Demonstration of SpaceMail, ESA's "on Station" no. 17, Aug. 2004.

Curriculum Vitae

Michiel Kruijf is born in Den Helder, The Netherlands on 8 May 1973. Starting from 1985, he attends the Murmellius Gymnasium in Alkmaar and graduates Cum Laude in 1991.

Michiel starts his studies at the Faculty of Aerospace Engineering at the Delft University of Technology in 1991. In 1994, he joins the European Space Research and Technology Centre (ESTEC) in Noordwijk, The Netherlands for an internship related to lunar landing site investigation. Here he meets his later colleague Erik Jan van der Heide, who is studying space tethers. Initially, Michiel finds tethers mainly appealing because the materials used are interesting to improve windsurf equipment. Soon however he is struck by the elegance of the tether and the interesting people within the tether community. He decides to join Erik in his research on a Swinging Tether Assisted Re-entry Through Robust Actively Controlled Kinetics (StarTrack). This becomes their joint Master thesis subject, under supervision of Prof. Dr. Wubbo J. Ockels. In 1996, Michiel obtains his Master's degree Cum Laude in Aerospace Engineering.

Following graduation he joins the European Space Agency as Young Graduate Trainee, and soon starts a company with Erik, Delta-Utec Space Research and Consultancy, with the aim to develop a space tether experiment. In response to a challenge set by Prof. Ockels, they initiate the Young Engineers' Satellite (YES) in October 1996. The project is supported by ESTEC staff and a large number of young engineers, as well as by tether pioneer Joseph A. Carroll from Tether Applications in San Diego. YES is launched in 1997 but the tether experiment is not performed for safety reasons. Finally in 2007, following continued developments in the field of tethers, Delta-Utec succeeds to deploy a 32-km tether in orbit, with the YES2 experiment on-board Foton-M3. Since then, Michiel has been documenting the experiments and results performed over the years, in the context of this PhD work for the chairs of AeroSpace for Sustainable Engineering and Technology (ASSET), led by Prof. Ockels and Space Systems Engineering (SSE), led by Prof. Dr. E.K.A. Gill, both at the Faculty of Aerospace Engineering at the Delft University of Technology.

Currently, Michiel works as a Feasibility Studies Manager at the Integrated Application Promotion group in ESTEC.

Acknowledgments

The work reported in this thesis has been performed between 1996 and 2008, since then I have been mostly compiling and refreshing the (now often outdated) papers. The results include a 32 km tether deployment by the YES2 experiment and, indeed, that deployed length happened to establish a world record. Once a tether deployer is in space however, deploying many kilometers of tether is not a large achievement. The YES2 but also missions such as SEDS-1 and SEDS-2 could have just as easily deployed *132 km*. I hope this thesis has made clear what *has* been the primary technical relevance and interest of the YES2 deployment.

Yet for me, the most important discovery has been something that is hardly sufficiently credited in this thesis. Tether experiments have been the inspiration but not the heart or soul of the YES and YES2 projects. Rather the true enabler of the projects has been the creation of a feeling of being part of an extraordinary joint effort and progressing towards a common goal with exceptional determination. After 12 years of work to finally bring back and analyze data from a tether deployment in space, what I have really discovered is the blessing of true team spirit.

Over 500 people have contributed to the activities and developments that led to the launch and operation of the YES and YES2 experiments. Some of them have worked intensely on the tether system development itself. I hope they are appropriately credited in this work, be it as (co-)authors in the references or in the remainder of this section.

Right here and now I need however to mention Erik Jan van der Heide, my colleague at Delta-Utec, who has put his whole self into our shared dream and who handled most of the contractual and programmatic work – plus a significant amount of technical work. I fear Erik is half the reason that the book you have in your hands has become such a long read. Thanks to Lidy & Jeroen, my friend Michan and my wife Maria, for their support.

I thank my supervisors. Prof. Wubbo Ockels has been the inspirator behind much of this work, he has provided the necessary continuity and context. Prof. Eberhard Gill has hosted me in the Space Systems Engineering chair and provided me with both enthusiastic and constructive commentary and thus safeguarded quality. Nana Saaneh must be credited for her patience and for keeping the administrative machine rolling.

As so many people have been involved in this work it may be necessary to define clearly my contribution. Generally I have tried to refer to external activities outside the scope of this work in the past tense. The other activities I have either been responsible for or at least contributed to significantly. Overall my role has been that of Lead Designer and Systems Engineer of the YES and YES2 satellites, and Prime Investigator of the YES and YES2 tether experiments. In these roles role I have instructed, guided, supported and supervised the approximately 100 students and staff at Delta-Utec over the years 1996-2007. I have been responsible for definition and coordination of all tether tests and performed the full YES2 flight data analysis. Furthermore I performed a significant fraction of preparatory tether tests and mission and data analyses referred to in this thesis, with the notable exceptions as detailed in below acknowledgments. To the T-REX experiment, a project led by Prof. H.A. Fujii, I have only participated as system engineering advisor and design reviewer.

Chapter 2. The MTBSim/ETBSim has been developed from Joe Carroll's BeadSim by Erik and myself. The YESSim extension includes a lot of contributions from my interns. This work owes to contributions from Marco Stelzer (attitude, mission analysis tools), Silvia Calzada (re-entry simulator) and Dr. Anton Lyaskin (heat flux models).

Chapter 3. StarTrack SpaceMail precedes this work, it is a joint effort of Erik and me, under supervision of Prof. Ockels. T-Series has been performed for CNES mostly by Andrew Hyslop at Delta-Utec. My contribution is limited to

task definition support and review and integration of the results. The debris mitigation and electrodynamic deboost studies have been performed by Erik and myself jointly. I developed the risk analysis approach and performed and analyzed many of the simulations. The bare tether as fail-safe concept is my idea. The plasma chamber tests at IFSI-CNR were performed and analyzed for us by F. de Venuto & G. Vannaroni. M. Dobrowolny provided a sneak preview into his dynamic models for comparison with our simulations. The multi-point sensing options are generated by Joe Carroll, Erik and myself. The deboost study was supported by ESA ARCOP contract 14621/00/NL/MV. Bas Lansdorp at Delta-Utec came up with the rimspeed as critical parameter for the artificial gravity comfort zone ("no tether no comfort"). He also made many of the MARS-g trade-offs and designed the HELD deployer. The self-accelerating rotating tether for stable deorbit (LeBRETON) is my idea, Alexander van Dijk at Delta-Utec worked out a lot the details for the Jupiter case. Overall it has been a joint effort including also Erik and Prof. Juan Sanmartin, funded by ESA/ESTEC contract 17239/03/NL/HB.

Chapter 4. Thanks to Martien Jacobs, Daan Tummers, Joyce Kersjens, Hans Plug at DSM High Performance Fibers and for their advise on Dyneema® and helpful discussions. All at ESTEC/QMC (Marc, Jacco, Andreas, Gerard, ...) & Antonio Araujo for providing and operating the test facilities and a lot of support. Prof. Guillet for the E/CO and MVK samples. Pieter Gijsman at DSM research provided chemistry advice and performed the GPC and FTIR tests. The degradable tether study was supported by ESA contract 13746/99/NL/MV. Andrew (break strength), Igor Sheynikov at Delta-Utec (damping, ripstitch) and Center of Expertise in Reggio Emilia (stiffness) were a great help with the material tests. Igor also helped me with the barberpole test in vacuum, performed at the SSAU. The YES2 Center of Expertise in Samara was led by Igor Belokonov. Chris Blanksby did the Foton-tether interaction simulations. Joep Breuer came up with the Prusik knot idea, it proved to be Columbus' egg.

Chapter 5. The Rapunzel deployer is a brainchild of Manfred Krischke and Dieter Sabath, built by Werner Kast and Mario Kowalchyk with whom Erik and I tested it in zero-g. The YES2 breadboard barberpole is designed by Carlo Menon at Delta-Utec, he also devised the conceptual trade-offs. The YES2 flight hardware by the YES2 Center of Expertise in Patras and our students in Delta-Utec. Bradford Engineering manufactured it. Marcel van Slogteren and colleagues at the ESTEC workshop helped out a lot. Thanks to Kayser-Threde and Christian Knueppel of the TSE team for the opportunity to do the deployment tests and for the TSE breadboard long-term loan afterwards. I often think back of the 21 day stay with Erik in a tent in Rostock. TSE was an ESA GSTP project. Prof. Ferdi Hermanns at the YES2 Center of Expertise in Remagen/Krefeld is the source of the great textile industry ideas in winding and unwinding rig. These rigs are truly an extensive effort, involving many of Hermanns' students. I am most indebted to the builders of the first version: Stefan Zwick, Joerg Malchus, Thomas Betz, David Schaefer, the builders of the second version: Mario Timmermanns and Christian Camps. Andrew again helped a lot and performed many of the YES2 unwinding tests. We even lived together in Krefeld for I do not know how many months to get these things running properly. I was particularly supported with the last-but-not-least improvements for the third and final version -and long nights of tether winding- by Florian Helling and Marco Stelzer (an ace on the "Winding machine DeLuxe"), at Delta-Utec and ESTEC. Thanks to Marco again and Paul Williams for the help with the control algorithms. Mathieu Mirmont programmed the flight model of the OBC (I was allowed to do only the breadboard). Ilias Spiliotopoulos and Rafal Graczyk programmed and built the flight stepper driver. The Chapter 5 early work and YES2 design phase were mostly funded by Delta-Utec. The brainstorm phase, the Centers of Expertise and the flight hardware development were funded by the ESA Education Office.

Chapter 6. I thank Erik, Prof. Ockels, the Delta-Utec students, the ESA staff, the ESA Young Graduates, Tether Applications, Arthur C. Clarke, TNO and Bradford Engineering for their help. ESA, NIVR & Delta-Utec funded YES.

Chapter 7. The FLOYD, MASS and Fotino have been designed, built and tested under my lead with the help of 100 Delta-Utec interns, and about 80 other students at the 4 YES2 Centers of Expertise, in Warsaw and scattered elsewhere around Europe. Thanks to Fabio De Pascale (the integration manager) and all ESA staff that supported us. Emxys in Elche, Spain supported the electronics development, as well as Bernard Ouwehand and Bradford Engineering.

Chapter 8. Thanks to the ESA Human Spaceflight microgravity department, the ESA Education Office and TsSKB to make the YES2 mission possible, in particular Antonio Verga and Ruedeger Reinhard for their genuine interest. Tom and Christophe at RedShift for providing the excellent DIMAC data.

Receiving data from your own space experiment is exhilarating, but that joyful moment may not by itself balance the efforts that needs to be invested to get it done. Having worked with so many dedicated young people so closely, and with a shared goal, certainly does.